Heung Sik Kang
Joong Mo Ahn
Yusuhn Kang

Oncologic Imaging
Bone Tumors

Springer

Oncologic Imaging: Bone Tumors

Heung Sik Kang • Joong Mo Ahn
Yusuhn Kang

Oncologic Imaging: Bone Tumors

Springer

Heung Sik Kang, MD
Department of Radiology
Seoul National University
College of Medicine
Seoul National University
Bundang Hospital
Seongnam
South Korea

Joong Mo Ahn, MD
Department of Radiology
Seoul National University
Bundang Hospital
Seongnam
South Korea

Yusuhn Kang, MD
Department of Radiology
Seoul National University
Bundang Hospital
Seongnam
South Korea

ISBN 978-981-287-702-4 ISBN 978-981-287-703-1 (eBook)
DOI 10.1007/978-981-287-703-1

Library of Congress Control Number: 2017931639

Printed on acid-free paper

This Springer imprint is published by Springer Nature
The registered company is Springer Nature Singapore Pte Ltd.
The registered company address is: 152 Beach Road, #21-01/04 Gateway East, Singapore 189721, Singapore

To my coauthors, Joong Mo Ahn and Yusuhn Kang, whose enthusiasm and hardwork enabled the publication of this book.

Heung Sik Kang

To my teacher, Dr. Heung Sik Kang, for his invaluable guidance and unwavering support.

Joong Mo Ahn

To my teacher, Dr. Heung Sik Kang, for his guidance, inspiration, and faith.
To my parents, husband, and kids, for their love, support, and understanding.

Yusuhn Kang

Preface

Radiologic imaging is an integral part of the diagnosis and staging of the bone tumors, the evaluation of the treatment outcome, and patient management. This book aims to provide radiologists, orthopedic surgeons, and surgical pathologists with understanding of the spectrum of radiologic appearances of bone tumors, which reflect histopathology, and the pattern analysis of the imaging findings.

The first part of this book is an overview of diagnostic considerations, including epidemiology and diagnostic parameters for bone tumors. It is intended to give basic concepts for approaching bone tumors: patients' demographics, lesion location, biological activity, periosteal reaction, MR characteristics, etc.

In the second part, typical and atypical radiologic features of bone tumors are addressed in detail, with an emphasis on the characteristic radiographic and MR imaging findings. Furthermore, pathologic or operative images in some selected cases are provided.

The third part is focused on problem solving for the cases encountered in real radiology practice and comprised of 18 categorical patterns, combining variables in radiographic and MR findings as well as lesion location.

Finally, 30 cases of bone tumors are shown with questions, answers, and commentary to recollect what the readers learned from this book. This part will help the readers hone their diagnostic reasoning skills as well as comprehensive radiological knowledge in their clinical practice.

The authors hope that this book may guide the readers to an organized understanding of the imaging findings of tumors and tumorlike lesions of the bone to arrive at a diagnosis.

Seongnam, South Korea

Heung Sik Kang
Joong Mo Ahn
Yusuhn Kang

Contents

Part I

Introduction

Basic Concepts and Diagnostic Parameters

1

Contents

Accurate radiological diagnosis of bone tumors is based on a systematic and organized analysis of the clinical and radiographic features. Factors to be considered include clinical factors such as the age and gender of the patient, and radiographic factors of the lesion including location, biological activity, matrix mineralization, periosteal and endosteal reaction, and size and number of lesions. Each of these features is discussed and illustrated in detail in this chapter.

1.1 Demographics

Age

The age of the patient is the single most important clinical data in establishing the diagnosis of a bone tumor. Certain bone tumors have a predilection for patients of certain age groups. For example, for an intramedullary osteolytic tumor involving the metaphysis and epiphysis of a long bone, chondroblastoma would be high up on the list of possible diagnoses, if the patient is 10–20 years old. However, in a patient aged 20–40 years, giant cell tumor would be moved high up on the list. Table 1.1 lists the benign and malignant tumors frequently encountered in each age group.

Gender

Most tumors are found equally in both genders, but some show predilection for a certain gender. Table 1.2 shows the predilection of some tumors for a certain gender.

H.S. Kang et al., *Oncologic Imaging: Bone Tumors*, DOI 10.1007/978-981-287-703-1_1

Table 1.1 Age predilection of bone tumors

Age	Benign	Malignant
<20	Chondroblastoma, chondromyxoid fibroma, osteoid osteoma, osteoblastoma, fibrous dysplasia, nonossifying fibroma, fibrous cortical defect, desmoplastic fibroma of bone, giant cell tumor of small bone, simple bone cyst, aneurysmal bone cyst, osteofibrous dysplasia, Langerhans cell histiocytosis	Osteosarcoma, Ewing's sarcoma
20–40	Giant cell tumor of bone, osteoid osteoma, osteoblastoma, fibrous dysplasia	Osteosarcoma (parosteal, periosteal, low-grade central), chondrosarcoma (periosteal) adamantinoma
>40		Metastasis, plasma cell myeloma, solitary plasmacytoma, chondrosarcoma, osteosarcoma (secondary, >60)
Wide age range	Chondromas, benign fibrous histiocytoma of bone, intraosseous lipoma, hemangioma	Fibrosarcoma, angiosarcoma, primary lymphoma of bone

Table 1.2 Gender predilection of bone tumors

Strong male predilection	Osteoblastoma (2.5:1), High-grade surface Osteosarcoma (2:1), Chondroblastoma (2:1), Clear cell Chondrosarcoma (3:1) Solitary plasmacytoma of bone (2:1) , Simple bone cyst (3:1)
Slight male predilection	Enostosis, Telangiectatic Osteosarcoma (1.5), Periosteal Osteosarcoma Osteochondroma, Chondromyxoid fibroma Conventional Chondrosarcoma, Dedifferentiated Chondrosarcoma Ewing's sarcoma(1.4:1) Angiosarcoma, Lymphoma(1.5:1)
Equally distributed	Osteoma, Chondromas (enchondroma, periosteal chondroma), Mesenchymal Chondrosarcoma, Fibrosarcoma of bone Plasma cell myeloma, Aneurysmal bone cyst, Fibrous dysplasia
Slight female predilection	Low-grade central Osteosarcoma, Small cell Osteosarcoma, Parosteal Osteosarcoma, Hemangioma (2:3)
Strong female predilection	Giant cell tumor of bone (1.5– 2:1)

1.2 Lesion Location

Bone tumors, both benign and malignant, have predilection for specific bones and certain locations within a specific bone. Table 1.3 shows the predilection sites of certain tumors within the skeleton. For example, for an osteolytic intracortical lesion at the anterior tibia, the most probable diagnosis would be osteofibrous dysplasia or adamantinoma. The location of a lesion within a specific bone can be specified along the longitudinal axis (i.e., epiphysis, metaphysis, and diaphysis) and the transverse plane (i.e., central intramedullary, eccentric intramedullary, cortical, juxtacortical) (Fig. 1.1). For example, a simple bone cyst is typically a central intramedullary lesion in the metaphysis of a long bone, with the most common site being the proximal humerus (Fig. 1.2a). Chondroblastomas are characterized by its intramedullary epiphyseal location in a long bone (Fig. 1.2b). Nonossifying fibroma appears as cortical lesions of the metaphysis of a long bone (Fig. 1.2c). Parosteal osteosarcoma is an example of a juxtacortical location of lesion, and has a predilection for the posterior aspect of the distal femur (Fig. 1.2d). Recognizing these site predilections of different bone tumors will aid in the differential diagnoses of bone tumors. Table 1.4 shows the predilection sites in summary.

It is also important to note that there are epiphyseal equivalent sites, called apophysis. Apophysis is defined as epiphysis that does not articulate with another bone. Examples of apophyses are greater and lesser tuberosities of the humerus, greater and lesser trochanter of the femur, tibial tubercle, iliac crest, carpal and tarsal bones, and calcaneus. Bone tumors that affect the epiphysis may involve these epiphyseal equivalents.

Table 1.3 Predilection for specific bone

Site	Common tumor
Tibia anterior cortex	Osteofibrous dysplasia, adamantinoma
Calcaneus	Simple bone cyst, intraosseous lipoma
Posterior cortex of distal femur	Parosteal osteosarcoma, periosteal desmoid
Distal phalangeal tuft	Epidermal inclusion cyst, glomus tumor
Short tubular bones of hand	Enchondroma
Great toe	Subungual exostosis
Calvarium	Osteoma
Mandible	Desmoplastic fibroma of bone, giant cell lesion (giant cell reparative granuloma)

Table 1.4 Predilection for specific locations within a bone

	Intramedullary		Cortical	Juxtacortical
	Central	Eccentric		
Epiphysis	Chondroblastoma (immature skeleton)[a] Giant cell tumor (mature skeleton)[a] Aneurysmal bone cyst[a] Osteomyelitis (<18 months old, Tb and fungus in adult) Clear cell chondrosarcoma			
Metaphysis	Fibrous dysplasia Enchondroma Chondrosarcoma Simple bone cyst	Giant cell tumor Chondromyxoid fibroma Osteosarcoma Aneurysmal bone cyst Osteomyelitis Langerhans cell histiocytosis	Nonossifying fibroma Fibrous cortical defect Osteoid osteoma	Juxtacortical chondroma Periosteal osteosarcoma Parosteal osteosarcoma Osteochondroma
Diaphysis	Fibrous dysplasia Enchondroma Simple bone cyst	Ewing's sarcoma Langerhans cell histiocytosis	Adamantinoma Osteofibrous dysplasia Osteoid osteoma	

[a]Epimetaphyseal location

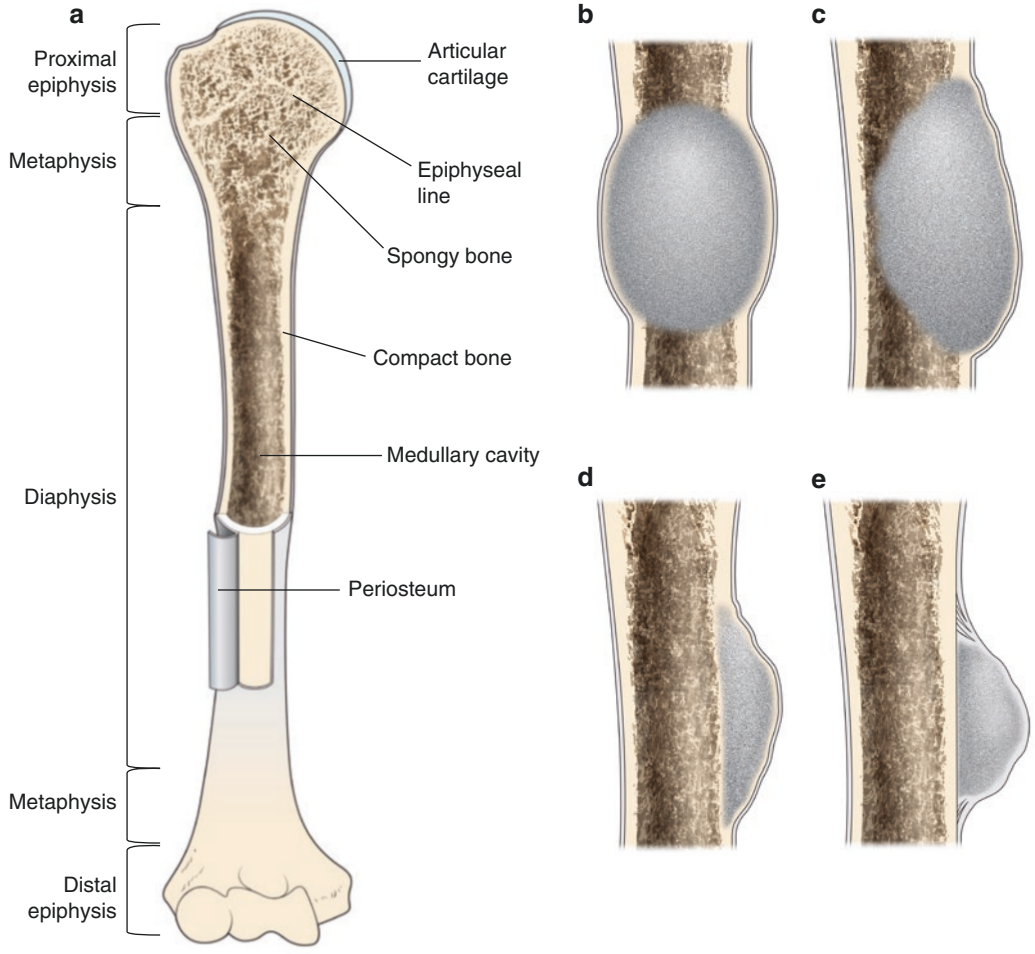

Fig. 1.1 Lesion location. (**a**) The location of a lesion within a specific bone can be specified along the longitudinal axis: epiphysis, metaphysis, and diaphysis. The epiphysis is the rounded end portion of a long bone, where it forms a joint with adjacent bones. The diaphysis is the tubular shaft portion of a long bone, and the metaphysis is the wide portion of a long bone located between the diaphysis and epiphysis. In the transverse plane, lesions can be either (**b**) central intramedullary, (**c**) eccentric intramedullary, (**d**) cortical, or (**e**) juxtacortical in location

Fig. 1.2 Predilection sites of lesion. (**a**) Simple bone cysts are located at the metaphysis of a long bone with a central intramedullary location, and the most common site is the proximal metaphysis of humerus. (**b**) Chondroblastomas are located at an intramedullary epiphyseal location within a long bone. (**c**) Nonossifying fibromas appear as cortical lesions at the metaphysis of a long bone. (**d**) Parosteal osteosarcoma is a juxtacortical lesion with a strong predilection for the posterior aspect of the distal femur

1.3 Biological Activity (Pattern of Destruction)

The margin or border of the lesion indicates the biological activity of the bone tumor. A well-defined border, in other words, a narrow zone of transition between the lesion and adjacent bone, indicates a slow growth rate, and in turn a higher probability of benignity. On the other hand, an ill-defined infiltrative border, a broad zone of transition, implies a fast growth rate, and hence a greater risk of malignancy.

Bone tumors can be categorized into several groups according to their pattern of destruction and margin (Fig. 1.3). A geographic lesion (type I) is characterized by a uniformly destroyed area within a sharply defined border. Geographic lesions are further divided into three groups according to their margins: geographic lesion with sclerotic margin (IA), geographic lesion with well-defined border but without sclerotic rim (IB), and geographic lesion with an ill-defined border (IC). The term "moth-eaten (type II)" is used to describe lesions with clustered multiple small osteolytic areas. Finally, permeative lesions (type III) are those with ill-defined areas of lytic bone destruction. Table 1.5 lists tumors that may show each pattern of destruction.

As discussed above, a narrow zone of transition generally indicates a benign lesion, and a broad zone of transition a malignant lesion. However, it is important to note that this is not always true; benign lesions may have aggressive appearances and malignant lesions may appear nonaggressive. Recognizing these exceptions is important to avoid misleading diagnoses. Examples are listed in Table 1.6.

Table 1.6 Exceptions: benign lesions with aggressive appearance and malignant lesions with nonaggressive appearance

Benign lesions with aggressive appearance	Malignant lesions with nonaggressive appearance
Langerhans cell histiocytosis Osteoblastoma Chondroblastoma Giant cell tumor Osteomyelitis	Telangiectatic osteosarcoma Chondrosarcoma

Table 1.5 Pattern of bone destruction

Type IA **Geographical lesion with sclerotic margin**	*Type IB* **Geographical lesion with well-defined border but without sclerotic rim**	*Type IC* **Geographical lesion with an ill-defined border**
Simple bone cyst Chondroblastoma Fibrous dysplasia Intraosseous lipoma Nonossifying fibroma Brodie abscess	Aneurysmal bone cyst Giant cell tumor Myeloma Metastasis	Chondrosarcoma
Type II **Moth-eaten**	*Type III* **Permeative**	
Ewing's sarcoma Langerhans cell histiocytosis Osteosarcoma Myeloma	Small round cell tumors (lymphoma) Ewing's sarcoma Acute osteomyelitis	

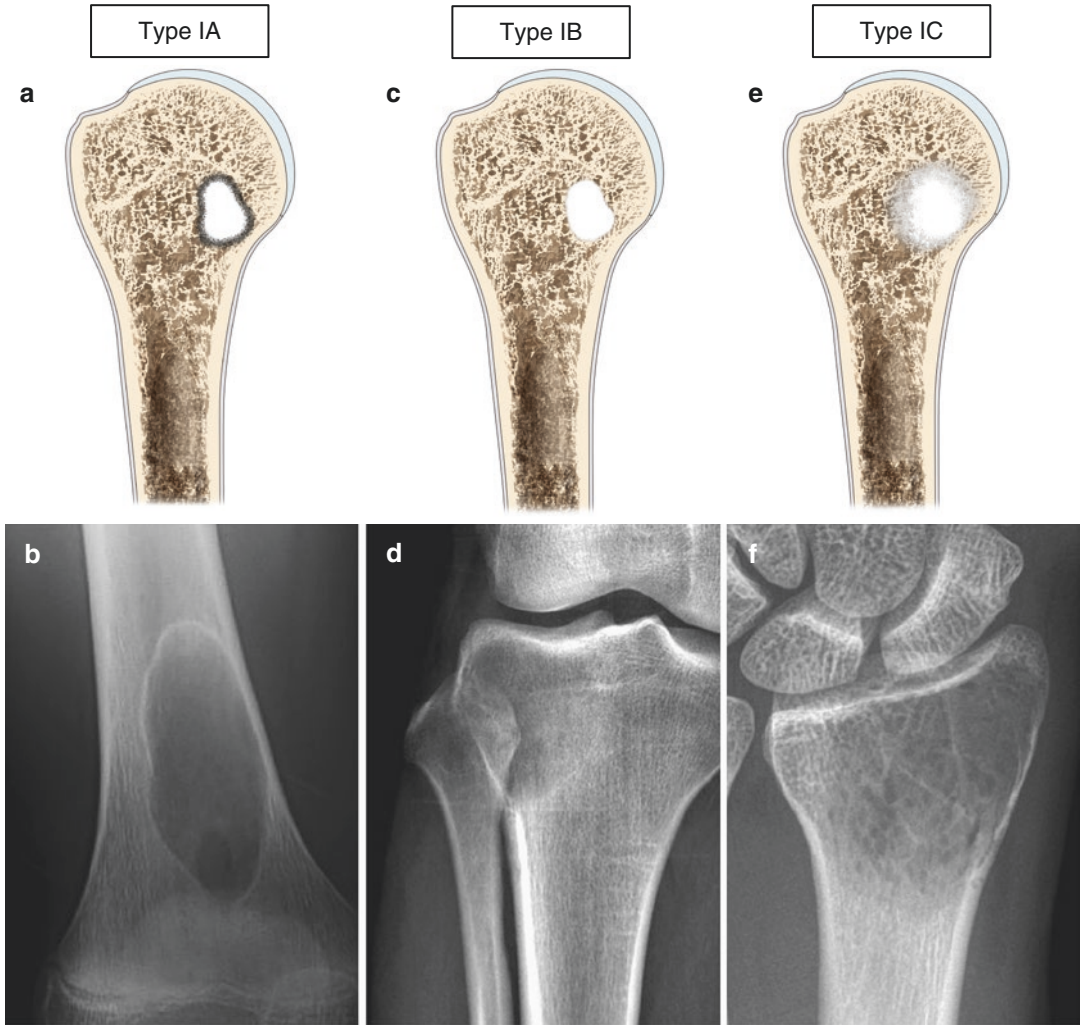

Fig. 1.3 Pattern of bone destruction. (**a**) Type IA, geographical lesion with sclerotic rim. (**b**) Fibrous dysplasia exhibiting type IA pattern of destruction. (**c**) Type IB, geographical lesion with well-defined border but without sclerotic rim. (**d**) Giant cell tumor with type IB pattern of destruction. (**e**) Type IC, geographical lesion with an ill-defined border. (**f**) Giant ell tumor with type IC pattern of destruction. (**g**) Moth-eaten lesion, clustered multiple small osteolytic areas. (**h**) Metastatic lesion from hepatocellular carcinoma, exhibiting moth-eaten pattern of destruction. (**i**) Permeative lesion, ill-defined areas of lytic bone destruction. (**j**) Ewing's sarcoma of bone showing a permeative pattern of destruction

Fig. 1.3 (continued)

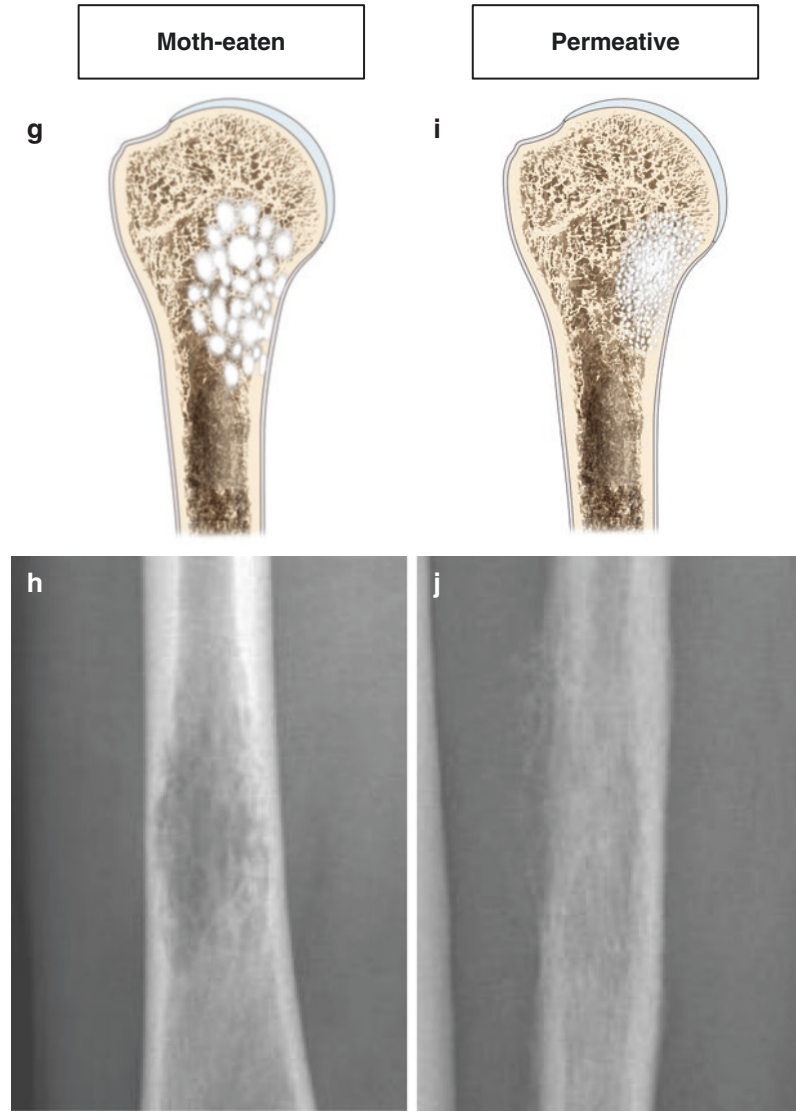

1.4 Opacity of Lesion and Matrix Mineralization

Opacity of Lesion

Bone tumors may appear lucent or sclerotic, relative to the surrounding bone, or may be a mixture of lucent and sclerotic areas. The radiographic opacity of a bone tumor is determined by (i) the alteration in osteoclastic or osteoblastic activity and (ii) the mineralization of tumor matrix. Osteoid osteoma appears sclerotic due to its osteoblastic activity, whereas enchondromas may appear sclerotic due to the mineralization of its matrix. Table 1.7 lists the possible differential diagnoses according to the opacity of the lesion.

Tumor Matrix

Matrix refers to the intercellular material produced by mesenchymal cells, and may consist of chondroid, osteoid, collagenous, myxoid, and adipose tissue. Chondroid and osteoid matrix undergo mineralization or calcification, and typical mineralization patterns may aid in narrowing in the differential diagnoses. Chondroid matrix mineralization has various appearances that may be described with the following terms: stippled, flocculent, popcorn-like, or ring-and-arc (Fig. 1.4). The presence of chondroid pattern of mineralization would suggest a chondrogenic tumor, such as enchondroma, chondrosarcoma, chondroblastoma. Osteoid matrix mineralization appears as cloud-like, amorphous, and cottony densities within the tumor (Fig. 1.4).

Although radiographs remain the mainstay for initial assessment and diagnosis of bone tumors, magnetic resonance imaging may aid in further characterizing nonmineralized matrix of the tumor. Collagenous stroma appears hypointense on both T1-weighted and T2-weighted images; myxoid stroma appears hypointense on T1-weighted image and markedly hyperintense on T2-weighted images; adipose stroma appears markedly hyperintense on T1-weighted images, moderately high on T2-weighted images, and hypointense on fat-suppressed images (Fig. 1.5). For example, desmoplastic fibroma of bone is histologically characterized by its abundant collagenous stroma and little cellularity, resulting in hypointensity on both T1-weighted and T2-weighted images, and lucent on radiographs.

Table 1.7 Differential diagnoses according to the opacity of the lesion

Lucent	Sclerotic	Mixed
Most benign and malignant bone tumors	Bone island (enostosis), osteoma Osteoid osteoma, osteoblastoma Osteosarcoma Osteoblastic metastasis Densely mineralized enchondroma Healed benign lesions (nonossifying fibroma, simple bone cyst)	Lymphoma Fibrous dysplasia Osteomyelitis

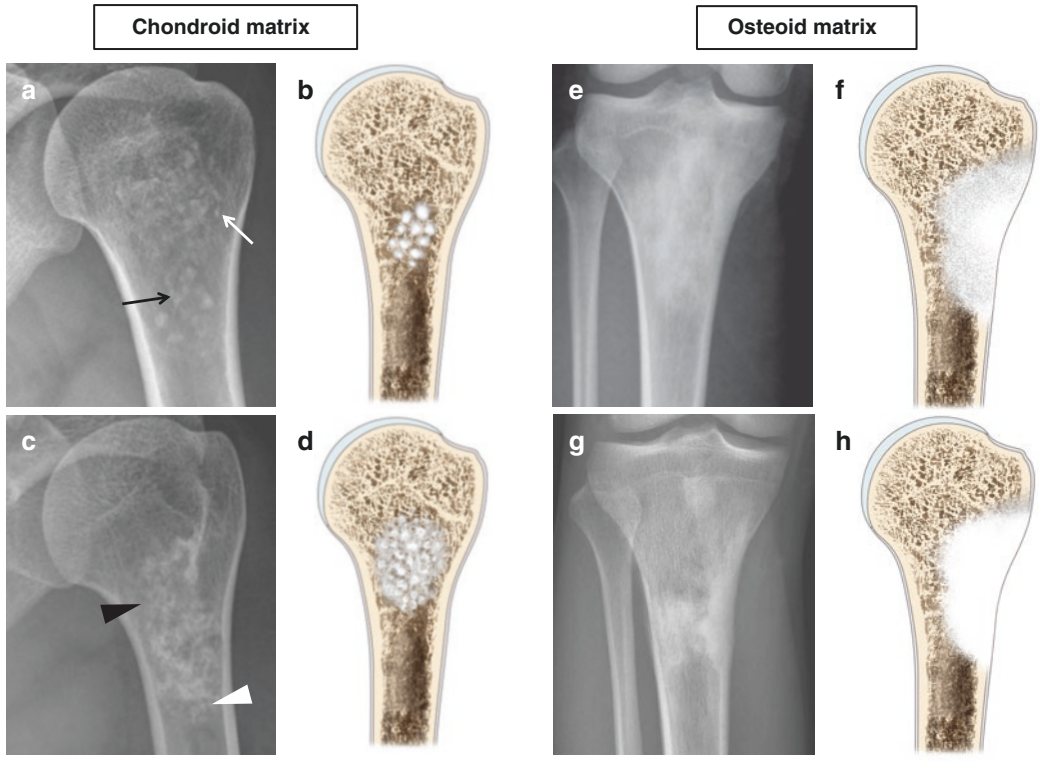

Fig. 1.4 Tumor matrix – chondroid and osteoid matrix mineralization. (**a**–**d**) Chondroid matrix. Chondroid matrix mineralization appears as stippled (*white arrow*), flocculent (*black arrow*), popcorn-like (*white arrowhead*), or ring-and-arc densities (*black arrowhead*). (**e–h**) Osteoid matrix. Osteoid matrix mineralization appears as cloud-like, amorphous, and cottony densities within the tumor

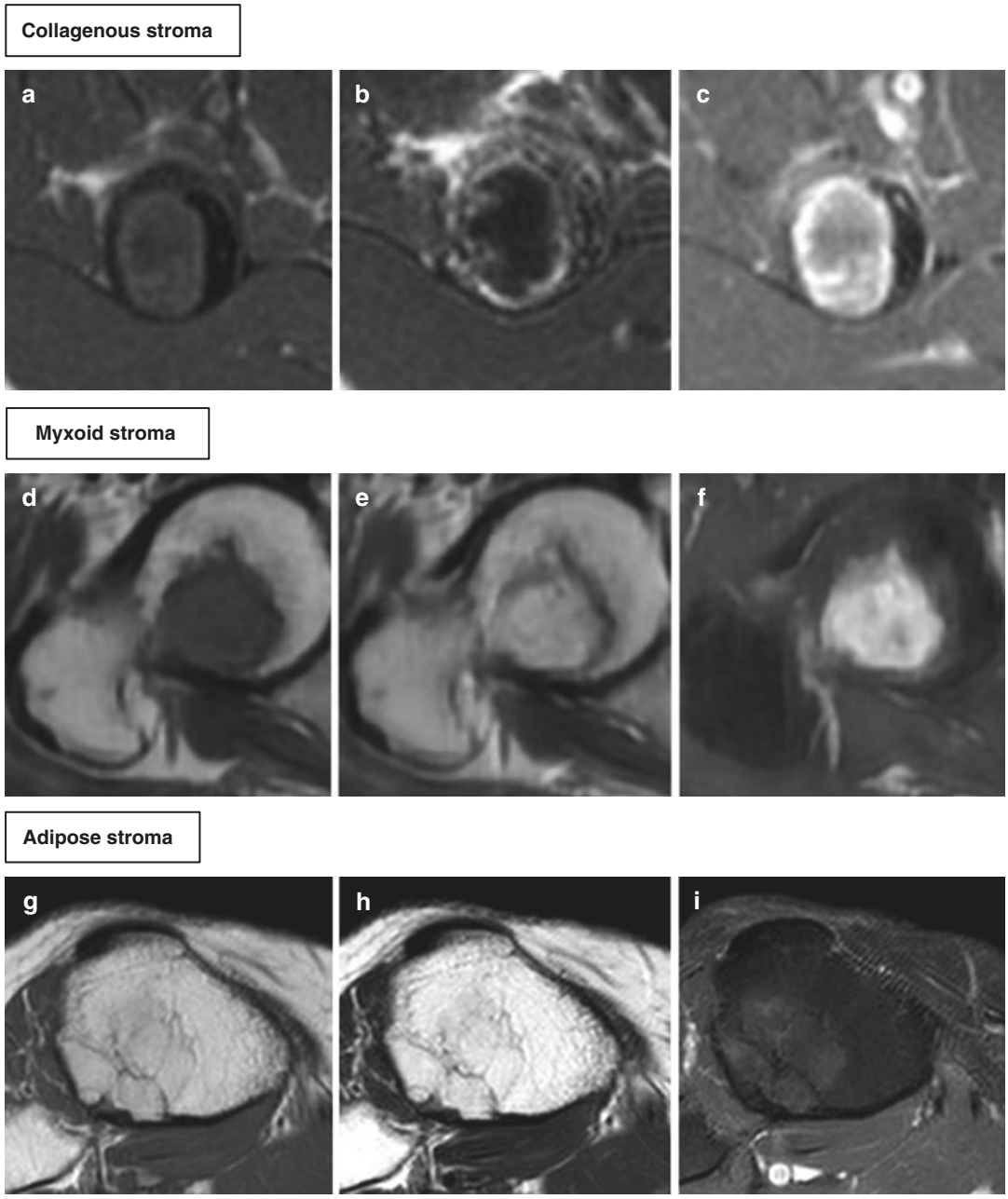

Fig. 1.5 Magnetic resonance imaging of nonmineralized matrix of bone tumors. Images are T1-weighted images (**a**, **d**, **g**), T2-weighted images (**b**, **e**, **h**) and contrast-enhanced T1-weighted fat-suppressed images (**c**, **f**, **i**). (**a**–**c**) Collagenous stroma appears hypointense on both T1-weighted and T2-weighted images, and exhibits mild enhancement. (**d**–**f**) Myxoid stroma appears hypointense on T1-weighted image and markedly hyperintense on T2-weighted images. Delayed strong enhancement is noted after the intravenous injection of contrast media. (**g**–**i**) Adipose stroma appears markedly hyperintense on T1-weighted images, moderately high on T2-weighted images, and hypointense on fat-suppressed images

1.5 Periosteal and Endosteal Reaction

The presence and pattern of periosteal reaction is an important clue in assessing the biological activity of bone lesions. The periosteum is a membranous structure covering the bone, consisting of two distinct layers, an outer fibrous layer and an inner cambium layer with osteoblastic potential. Pathological processes of the bone, including tumor and infection, can elevate the periosteum from the cortex, resulting in subperiosteal deposition of new bone, which we call "periosteal reaction." According to the biological activity of the lesion, various periosteal reactions can be seen (Fig. 1.6 Table 1.8). A slow-growing bone lesion would result in a nonaggressive, solid form of periosteal reaction, whereas rapidly growing lesions will produce more aggressive, multilamellated, or spiculated periosteal reactions or Codman's triangles.

Table 1.8 Types of periosteal reaction

Nonaggressive	Solid-type Single-layer lamellated
Aggressive	Multilamellated (Onion skin) Spiculated Hair-on-end Sunburst Codman's triangle

Bone tumors may evoke changes, not only along the periosteal surface, but also along the endosteal side. Endosteal scalloping refers to the erosion of the inner surface of the cortex due to the expansion of a medullary process. If the bone lesion is less aggressive and grows slowly, endosteal scalloping is accompanied by periosteal new bone formation, resulting in an expansion or ballooning of the bone. On the contrary, in aggressive bone lesions with a rapid growth rate, endosteal erosion would eventually lead to cortical breaching and extraosseous extension of the lesion, as there is not enough time to lay down new bone on the periosteal side.

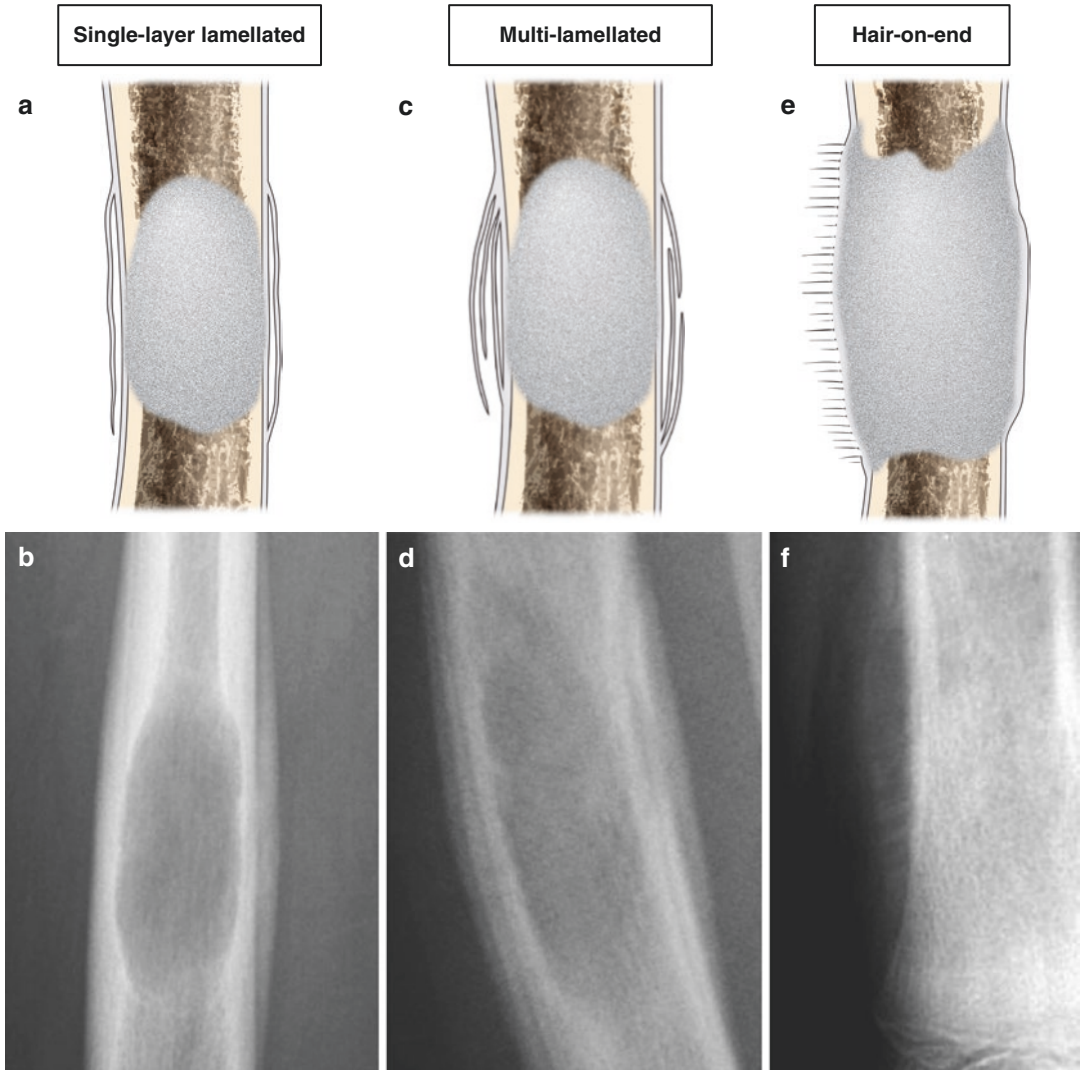

Fig. 1.6 Periosteal reactions. (**a**) Single-layer lamellated periosteal reaction is a nonaggressive pattern of periosteal reaction, indicating a slow growing lesion. (**b**) A simple bone cyst complicated with a pathological fracture exhibiting a single-layer lamellated periosteal reaction. (**c**) Multilamellated periosteal reaction suggests an intermediate aggressive process. (**d**) Langerhans cell histiocytosis accompanying a multilamellated periosteal reaction. (**e**) Hair-on-end periosteal reaction refers to parallel bony spicules, perpendicularly oriented along the cortical surface. (**f**) An osteosarcoma showing hair-on-end periosteal reaction. (**g**) Sunburst periosteal reaction is the divergent pattern of bony spicules fanning out from the bone. (**h**) Sunburst periosteal reaction noted in a case of osteosarcoma. (**i**) Codman's triangle refers to the triangle area of subperiosteal new bone formation noted when the periosteum is elevated away from the cortex by an aggressive lesion. (**j**) Codman's triangle is noted in a case of osteosarcoma

Fig. 1.6 (continued)

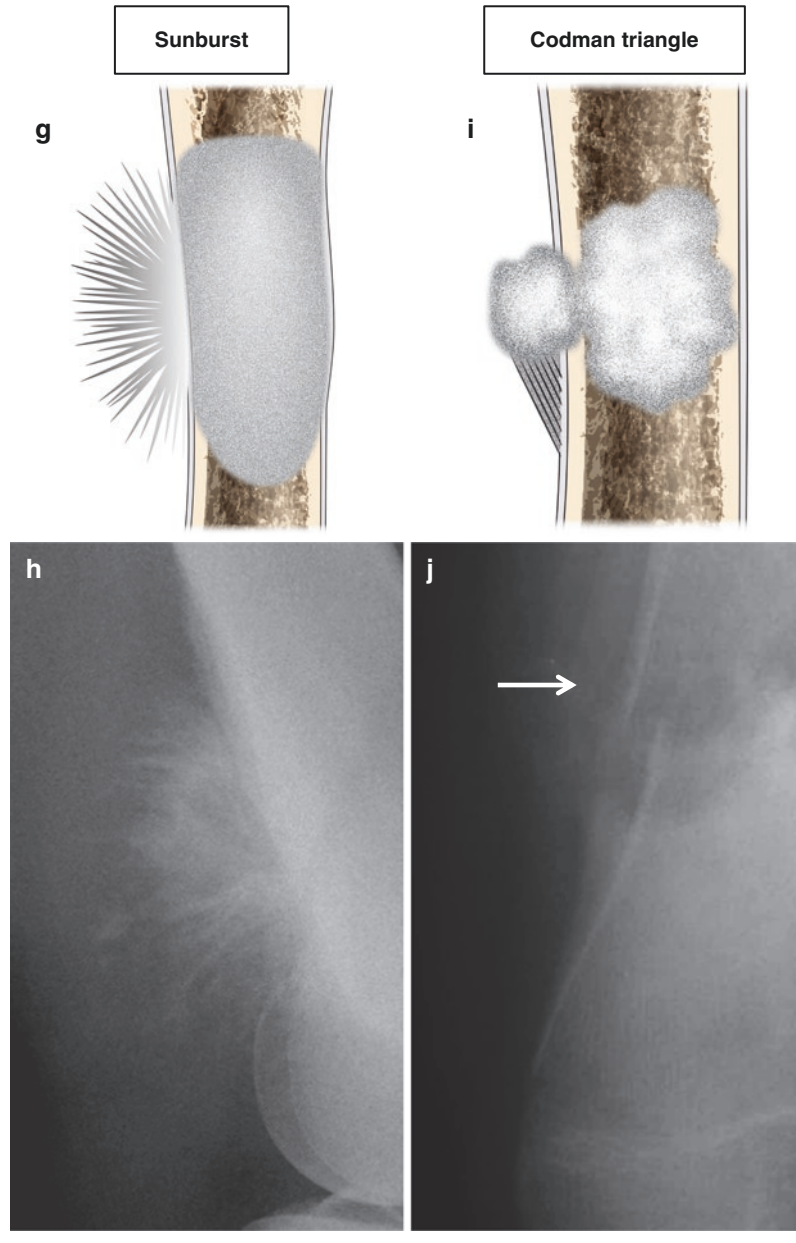

1.6 Number of the Lesions

Most primary bone tumors occur as solitary lesions, but some may present with multiplicity. In an adult, over the age of 40 years, multiple osteolytic lesions would suggest the diagnoses of metastasis, multiple myeloma, and lymphoma. In a pediatric age group, Langerhans cell histiocytosis, enchondromatosis, hereditary exostosis, and angiomatosis may present with multiplicity. Metabolic bone lesions such as brown tumors or hemophilic pseudotumors may also present with multiple lesions.

Suggested Reading

Fletcher CDM, World Health Organization. International Agency for Research on Cancer. WHO classification of tumours of soft tissue and bone. 4th ed. Lyon: IARC Press; 2013.

Greenspan A, Borys D. Radiology and pathology correlation of bone tumors: a quick reference and review. Philadelphia: Wolters Kluwer; 2016.

Greenspan A, Jundt G, Remagen W, Greenspan A. Differential diagnosis in orthopaedic oncology. 2nd ed. Philadelphia: Lippincott Williams & Wilkins; 2007.

Hakim DN, Pelly T, Kulendran M, Caris JA. Benign tumours of the bone: a review. J Bone Oncol. 2015;4: 37–41.

Madewell JE, Ragsdale BD, Sweet DE. Radiologic and pathologic analysis of solitary bone lesions. Part I: internal margins. Radiol Clin N Am. 1981;19: 715–48.

Miller TT. Bone tumors and tumorlike conditions: analysis with conventional radiography. Radiology. 2008;246: 662–74.

Ragsdale BD, Madewell JE, Sweet DE. Radiologic and pathologic analysis of solitary bone lesions. Part II: periosteal reactions. Radiol Clin N Am. 1981;19: 749–83.

Resnick D. Diagnosis of bone and joint disorders. 4th ed. Philadelphia: Saunders; 2002.

Part II

Tumor Classification and Specific Radiologic Features

Osteogenic Tumors

2

Contents

2.1 Osteoma

Overview

Osteoma is a benign slow-growing tumor composed entirely of osteoid tissue, representing a focal exaggeration of intramembranous bone formation, resulting in juxtacortical lesion. Histologically, an osteoma is usually a mixture of woven bone and dense lamellar bone, arising strictly from the cortex of the bone. Osteoma may or may not have Haversian systems.

Osteomas are usually small, and patients frequently have no symptoms. Lesions are often discovered as incidental findings on radiographs. Multiple osteomas are commonly associated with Gardner syndrome, which is a familial autosomal-dominant disorder characterized by multiple osteomas, intestinal polyposis, dentigerous cysts, epidermoid cysts, desmoid tumors, and skin fibromas.

Epidemiology

Osteomas occur twice as frequently in males as in females, and reported most frequently in the third and fourth decades.

Common Locations

An osteoma is most commonly found within the paranasal sinuses and the skull. However, it may also be found in the long bones, and has been described as appendicular osteoma. This rare entity is also termed parosteal osteoma or surface osteoma.

H.S. Kang et al., *Oncologic Imaging: Bone Tumors*, DOI 10.1007/978-981-287-703-1_2

Imaging Features

Radiograph

An osteoma is a small, round, well-defined, homogeneous, bony surface lesion arising from the cortex (Fig. 2.1) and does not demonstrate the corticomedullary continuity seen in an osteochondroma. It demonstrates a density identical to cortex. Osteomas become more lobulated with increasing size. When an osteoma is composed primarily of compact bone, it will appear as a contour deformity of the cortex that blends with the surrounding cortical bone. When composed primarily of trabecular bone and marrow, the interface between the osteoma and adjacent bone will be more distinct.

Magnetic resonance imaging

Osteomas follow the persistent low signal intensity characteristics of cortex on all MR pulse sequences (Fig. 2.1).

Differential Diagnoses

1. Parosteal osteosarcoma

   Differentiation of an appendicular osteoma from a parosteal osteosarcoma can be difficult both radiographically and histologically, because both lesions appear as ivory-like masses attached to bone surface. Osteomas have usually smooth borders and well-circumscribed, intensely homogeneous sclerotic appearance. In contrast, parosteal osteosarcoma may show a zone of decreased density at the periphery and usually appears less dense and homogeneous than osteoma.
2. Osteochondroma

   Osteochondroma can be differentiated by its corticomedullary continuity and cartilaginous cap.
3. Myositis ossificans

   A well-matured focus of myositis ossificans may occasionally mimic osteoma. Myositis ossificans shows a zonal phenomenon, characterized by a radiolucent area in the center of the lesion and a dense zone of mature ossification at the periphery.

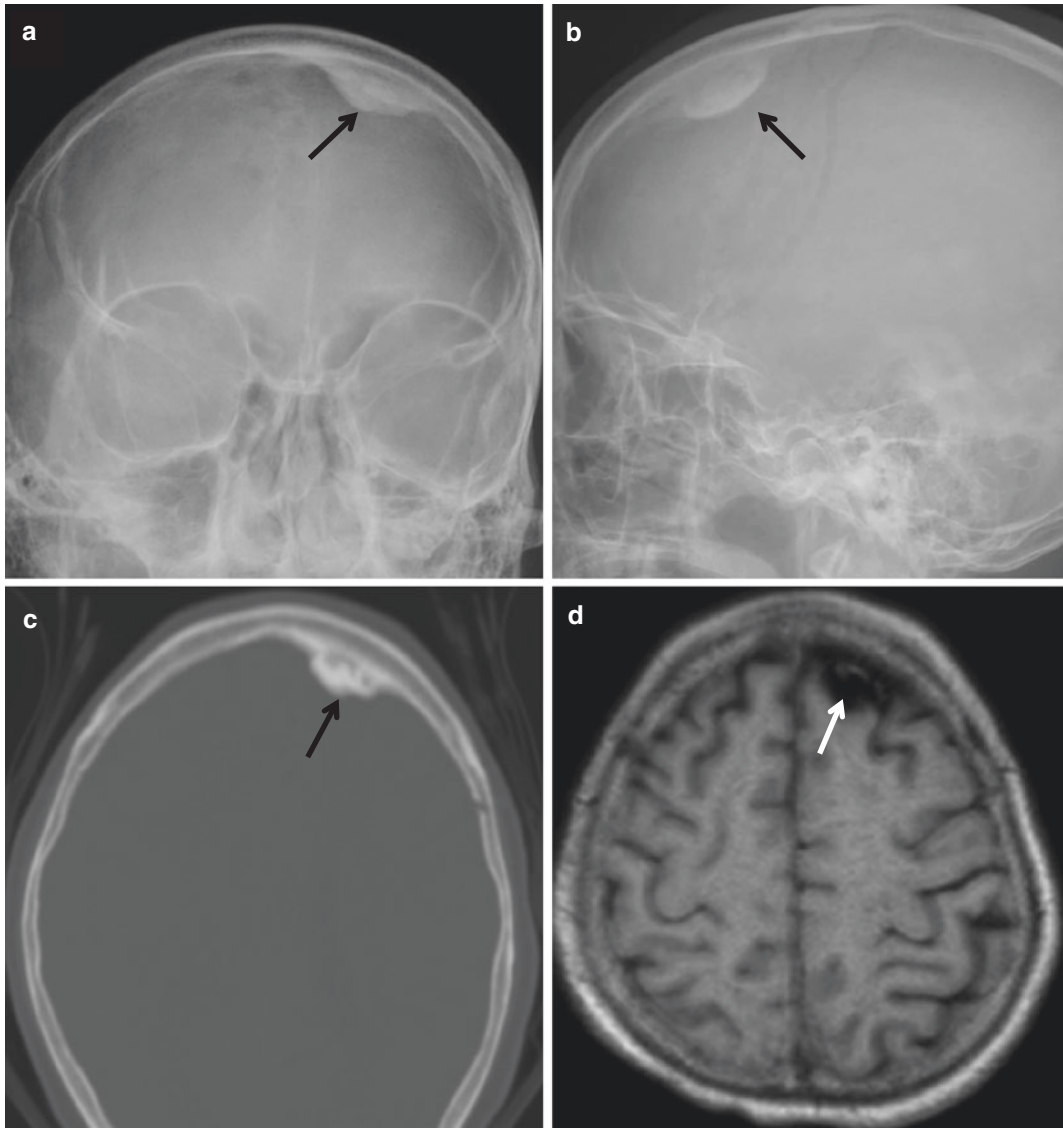

Fig. 2.1 Osteoma. (**a**) Anteroposterior radiograph of the skull shows a well-defined, homogeneous, bony surface lesion arising from the inner table of the left frontal bone (*arrow*). (**b**) Lateral radiograph of the skull shows a well-defined, homogeneous, bony surface lesion arising from the left frontal bone (*arrow*). (**c**) Corresponding axial CT scan shows an osteoma arising from the inner table of the left frontal bone (*arrow*). (**d**) Corresponding axial T1-weighted MR image demonstrates a hypointense osteoma from the inner table of the left frontal bone (*arrow*). (**e**) Corresponding axial T2-weighted MR image demonstrates a persistent hypointense osteoma from the inner table of the left frontal bone (*arrow*)

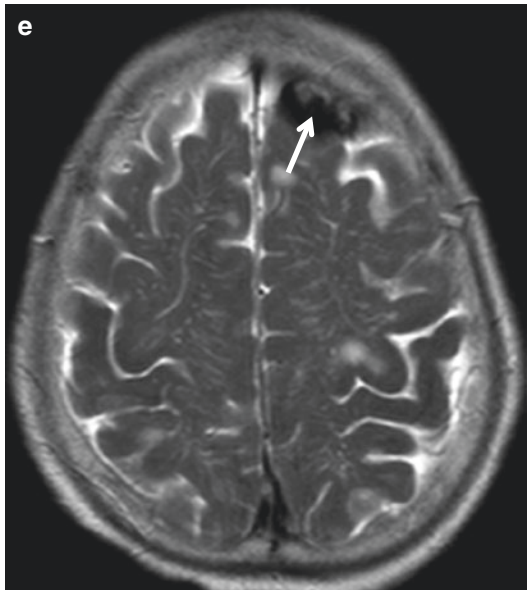

Fig. 2.1 (continued)

2.2 Bone Islands

Overview

Bone island (enostosis) is defined as a focus of mature compact bone within the spongiosa. The lesion is typically asymptomatic and often an incidental finding on radiographs. Histologically, bone islands consist of dense intramedullary lamellar bone with normal Haversian canals, which blend in with the normal surrounding trabecular bone. A bone island may slightly fluctuate in size, but a growth of >25 % over 6 months is unusual. While the majority of bone islands range in size from 1 mm to 2 cm, the term giant bone island is given to those lesions larger than 2 cm.

Epidemiology

Although there is no gender or age preference, bone islands are unusual in children.

Common Locations

Bone islands are most commonly found in the axial skeleton, spine, pelvis, and ribs. In the long bones, they are usually located in the epiphysis or metaphysis.

Imaging Features

Radiograph

A bone island characteristically appears on conventional radiography and CT scan as densely sclerotic intramedullary focus (Fig. 2.2). Bone islands are round to oval, with the long axis of oval lesions paralleling the long axis of the affected bone. The surrounding cancellous bone which blends imperceptibly with the surface of the bone island provides a brush-like, spiculated, or thorny margin.

Magnetic resonance imaging

On MR imaging, a hypointense focus (Fig. 2.2) on all pulse sequences with a normal surrounding bone marrow is noticed. A bone island is usually inactive on bone scan. Further work-up is rarely necessary, and biopsy is generally not indicated.

Differential Diagnoses

1. Osteoblastic metastasis

   Metastatic lesion shows increased activity on bone scan (Fig. 2.3), and may demonstrate a halo of surrounding fluid-filled gap secondary to destruction of trabeculae on fluid-sensitive MR sequences.
2. Sclerosing bone dysplasias

   Multiple bone islands may be associated with sclerosing bone dysplasia such as osteopoikilosis (Fig. 2.4), osteopathia striata (Fig. 2.5), or melorheostosis. Osteopoikilosis consists of numerous circular or ovoid bone islands. Melorheostosis is characterized by long segments of cortical hyperostosis (Fig. 2.6).

Fig. 2.2 Bone island. (**a**) Anteroposterior radiograph of the left femur shows a densely sclerotic intramedullary focus with thorny margin (*arrow*). The long axis of this focus is paralleling the long axis of the affected bone. (**b**) Lateral radiograph again shows a densely sclerotic focus with thorny margin (*arrow*). The long axis of this focus is paralleling the long axis of the affected bone. (**c**) Corresponding axial CT scan demonstrates a round sclerotic intramedullary focus (*arrow*). (**d**) Bone scan demonstrates increased uptake in the left distal femur (*arrow*). (**e**) Sagittal T1-weighted MR image shows low signal intensity (*arrow*). (F) Sagittal proton density-weighted MR image shows low signal intensity (*arrow*). (**g**) Coronal T2-weighted MR image again reveals low signal intensity (*arrow*). (**h**) Sagittal fat-suppressed contrast-enhanced T1-weighted MR image shows persistent low signal intensity

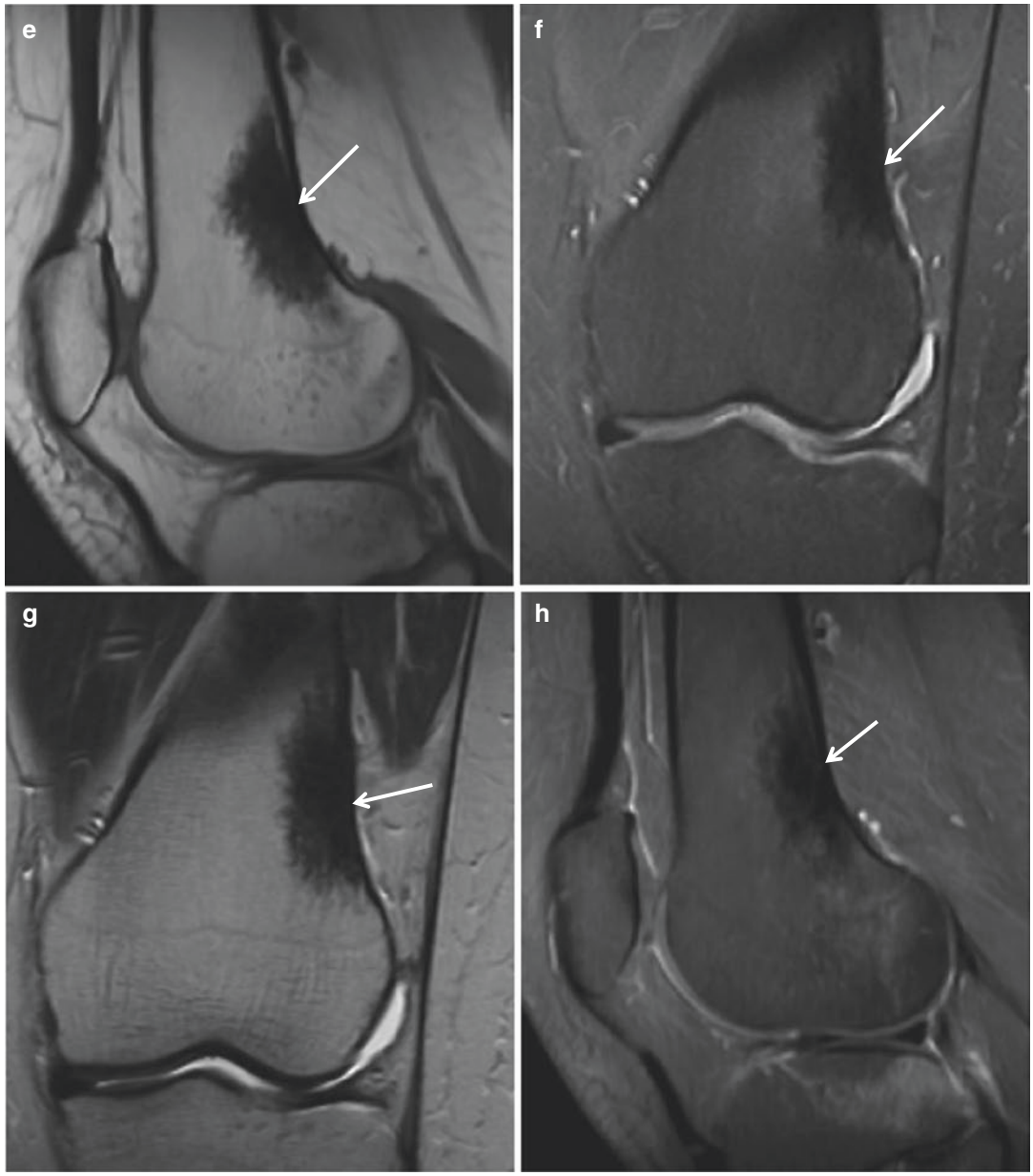

Fig. 2.2 (continued)

Fig. 2.3 Metastasis. (**a**) Anteroposterior radiograph of the pelvis shows sclerotic lesions in the right ilium (*arrow*). (**b**) Bone scan shows increased uptake in the right ilium (*arrow*)

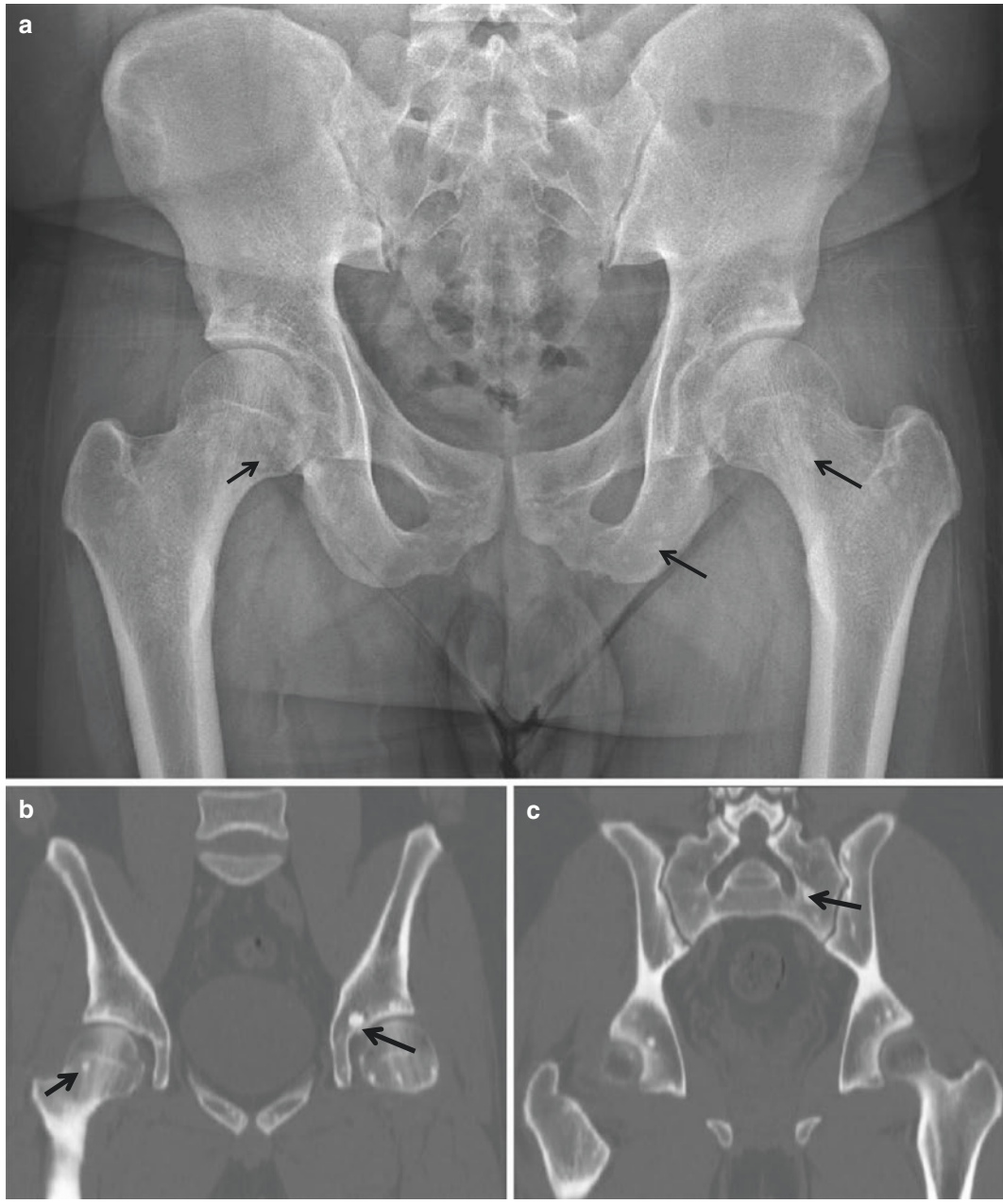

Fig. 2.4 Osteopoikilosis. (**a**) Anteroposterior radiograph of the pelvis shows multiple scattered sclerotic foci in the bony pelvis and bilateral proximal femurs (*arrows*). (**b**) Coronal reformatted CT scan shows scattered sclerotic foci in the bony pelvis, sacrum, and bilateral proximal femurs (*arrows*). (**c**) Coronal reformatted CT scan shows scattered sclerotic foci in the bony pelvis, sacrum (*arrow*), and bilateral proximal femurs. (**d**) Axial T1-weighted MR image reveals multiple scattered hypointense foci (*arrow*). (**e**) Axial T2-weighted MR image shows multiple scattered foci of persistent hypointensity (*arrow*)

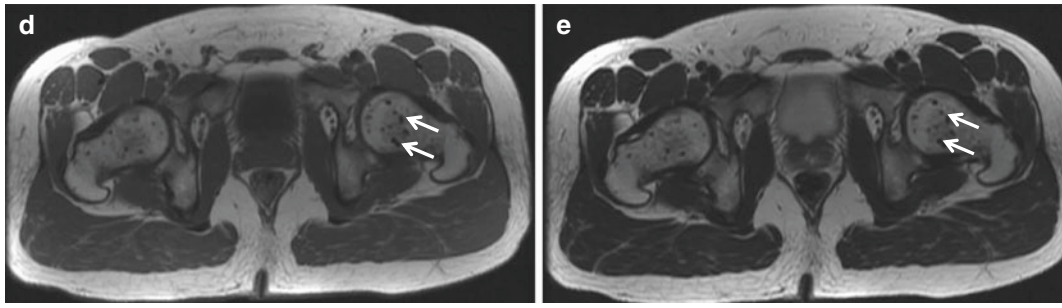

Fig. 2.4 (continued)

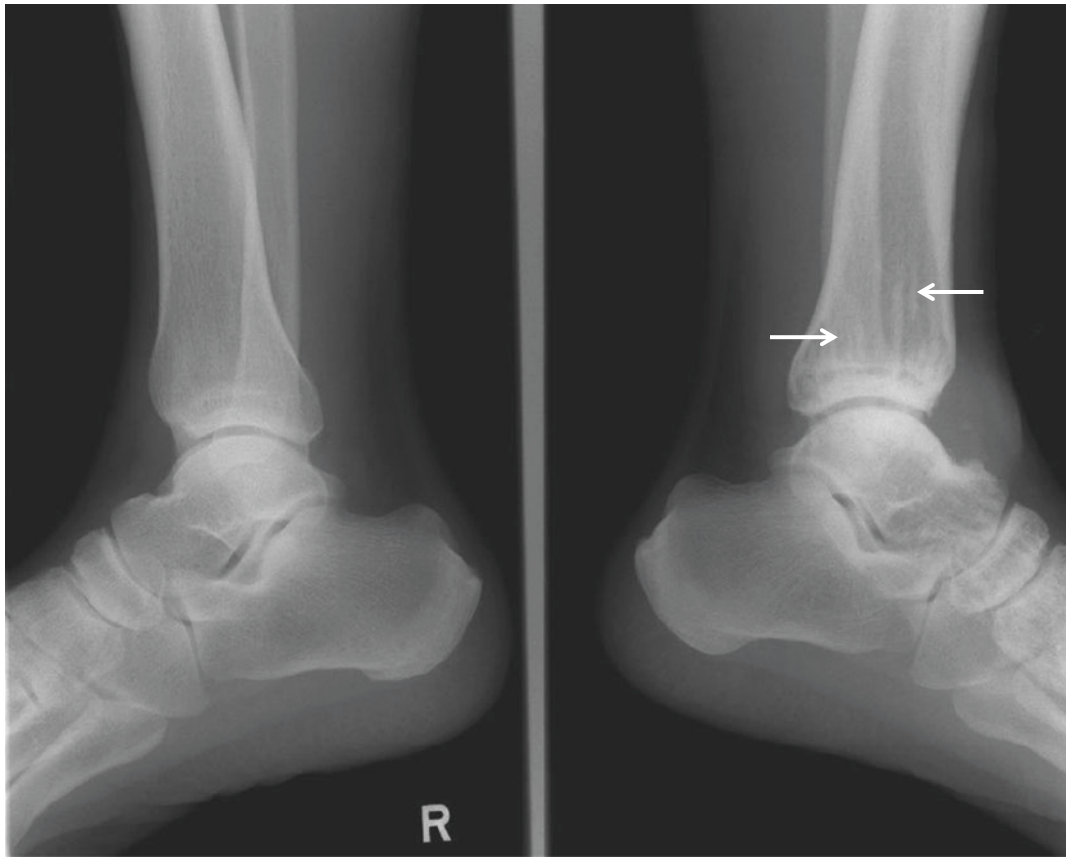

Fig. 2.5 Osteopathia striata. Lateral radiographs of the bilateral ankles show dense linear striations (*arrows*) in the diaphysis and metaphysis of the left tibia

Fig. 2.6 Melorheostosis. (**a**) Lateral radiograph of the right ankle shows cortical and medullary hyperostosis in the right fibula and right calcaneus (*arrows*). (**b**) Standing anteroposterior radiograph of the right foot shows hyperostosis in the calcaneus, metatarsal, and phalanges of the right ankle and foot (*arrows*). A flowing dripping candle wax appearance is noted. (**c**) Bone scan shows increased uptake (*arrow*) in the right foot. (**d**) Sagittal reformatted CT scan shows hyperostosis in the tarsal bones (*arrow*). (**e**) Sagittal reformatted CT scan shows hyperostosis in the metatarsal. (**f**) Sagittal T1-weighted MR image reveals hypointense hyperostosis in the calcaneus (*arrow*). Thickening of the plantar fascia is also identified. (**g**) Sagittal fat-suppressed T2-weighted MR image again demonstrates hypointense hyperostosis in the calcaneus (*arrow*). Thickening of the plantar fascia is also identified

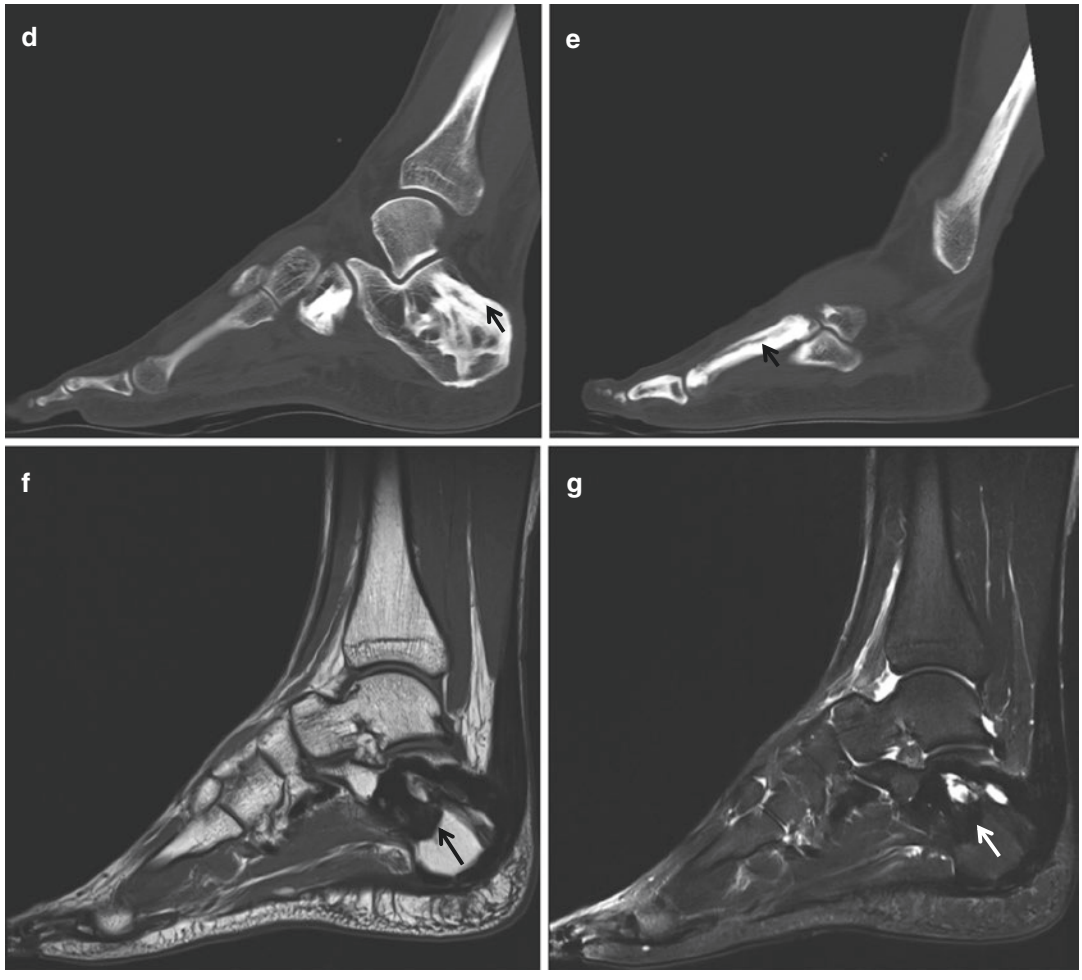

Fig. 2.6 (continued)

2.3 Osteoid Osteoma

Overview

Osteoid osteoma is a painful bony lesion of unknown cause. Pain, which can be worse at night, is usually relieved with nonsteroidal anti-inflammatory medication. The "nidus," representing the actual lesion, is round to oval, and usually <1 cm in diameter, although its diameter ranges from 1 mm to 2 cm. The nidus is composed of osteoid and woven bone on a background of highly vascularized fibrous connective tissue. The nidus is usually a radiolucent focus, but may be calcified to a varying degree, and may be surrounded by sclerosis depending on the location within or along the bone. Very rare cases of multicentric or multifocal osteoid osteoma have been described.

Epidemiology

Osteoid osteoma is more common in males (2–3:1) and mostly affects patients between 5 and 25 years of age.

Common Locations

The cortical osteoid osteoma is the most common, and is usually located in the shaft of the long bones. Many osteoid osteomas arise in a tubular bone, possibly originate in a subperiosteal site, and later appear as an intracortical lesion. This site of origin appears to relate principally to continual remodeling of bone with subperiosteal deposition and endosteal erosion.

Imaging Features

Radiograph

The radiographic characteristics of osteoid osteoma depend on its location. The nidus appears as an osteolucent focus (Fig. 2.7), which may or may not have a dense central focus of mineralization (Fig. 2.8). In long bones, surrounding extensive fusiform sclerosis (Fig. 2.7) is the characteristic finding, representing both cortical and periosteal reaction. Intra-articular lesions may have no or only limited surrounding sclerosis, due to the inability of the intracapsular periosteum to produce proliferative and sclerotic new bone. Radiographs could be diagnostic of osteoid osteoma if the nidus can be identified. Thin section CT is best suited to depict the nidus (Fig. 2.9)

Magnetic resonance imaging

The intense bone marrow edema (Fig. 2.8) adjacent to the nidus is typical finding. The nidus may easily be overlooked with MR imaging depending on its size and the degree of mineralization. An intra-articular lesion may be masked by reactive changes in the surrounding tissue (Fig. 2.10).

Differential Diagnoses

1. Stress fracture

   When the nidus cannot be seen on radiographs, the differential diagnosis includes the lesions that can be associated with intense, benign-appearing new bone formation, such as stress fracture. The radiolucency associated with a stress fracture is usually more linear than in osteoid osteoma, and it runs perpendicular or at an angle to the cortex rather than parallel to it.
2. Brodie abscess

   Although a bone abscess may have a similar radiographic appearance to osteoid osteoma, bone abscess can usually be differentiated by a linear, serpentine tract extending from the abscess cavity toward the closest growth plate.
3. Toxic and inflammatory synovitis

   Toxic and inflammatory synovitis can be considered in the differential diagnosis for the intra-articular lesions.

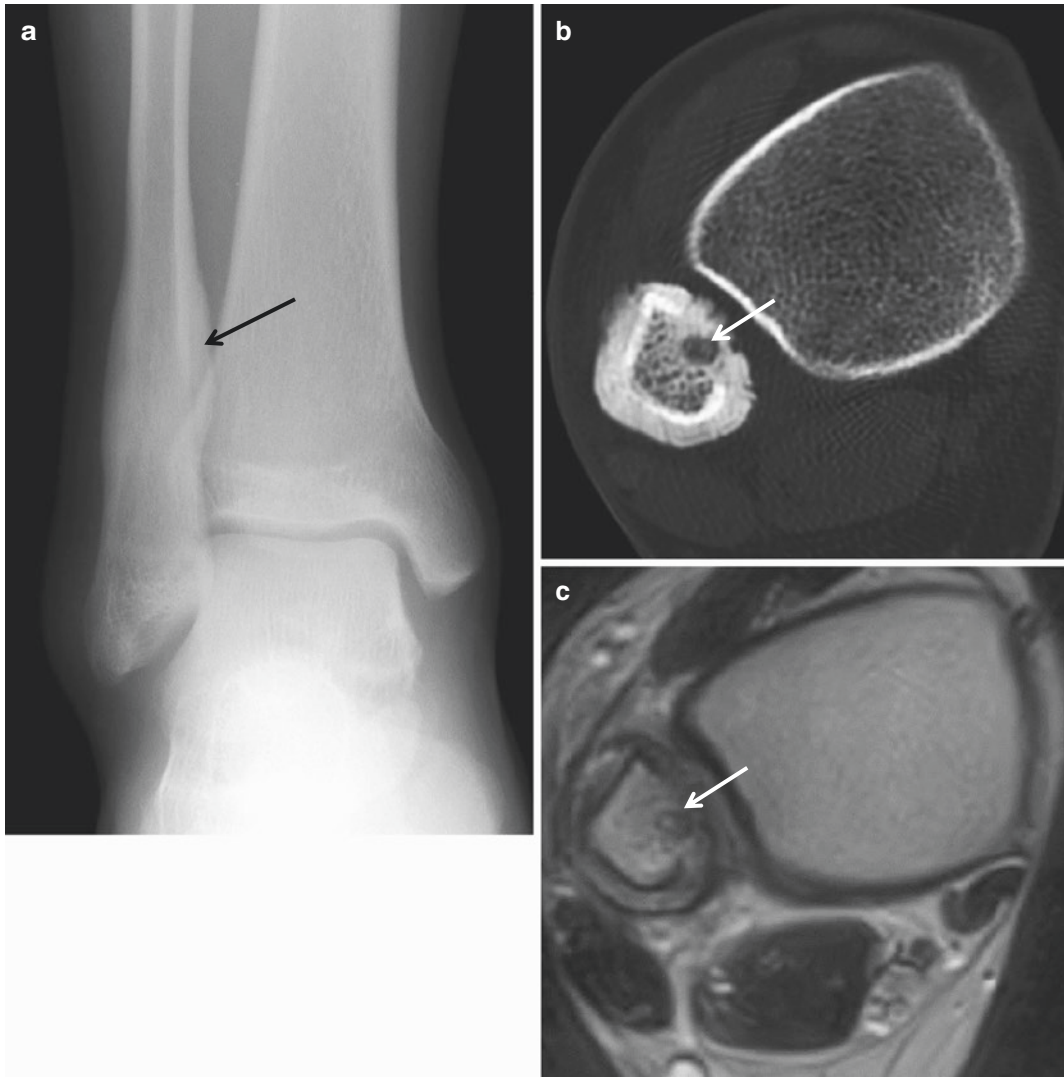

Fig. 2.7 Osteoid osteoma. (**a**) Anteroposterior radiograph of the right ankle shows thick solid periosteal reaction in the right distal fibula (*arrow*). (**b**) Corresponding axial CT scan demonstrates a round radiolucent focus (*arrow*) in the cortex of the right distal fibula. Periosteal reaction is also identified. (**c**) Axial T2-weighted MR image reveals increased signal intensity of the nidus (*arrow*)

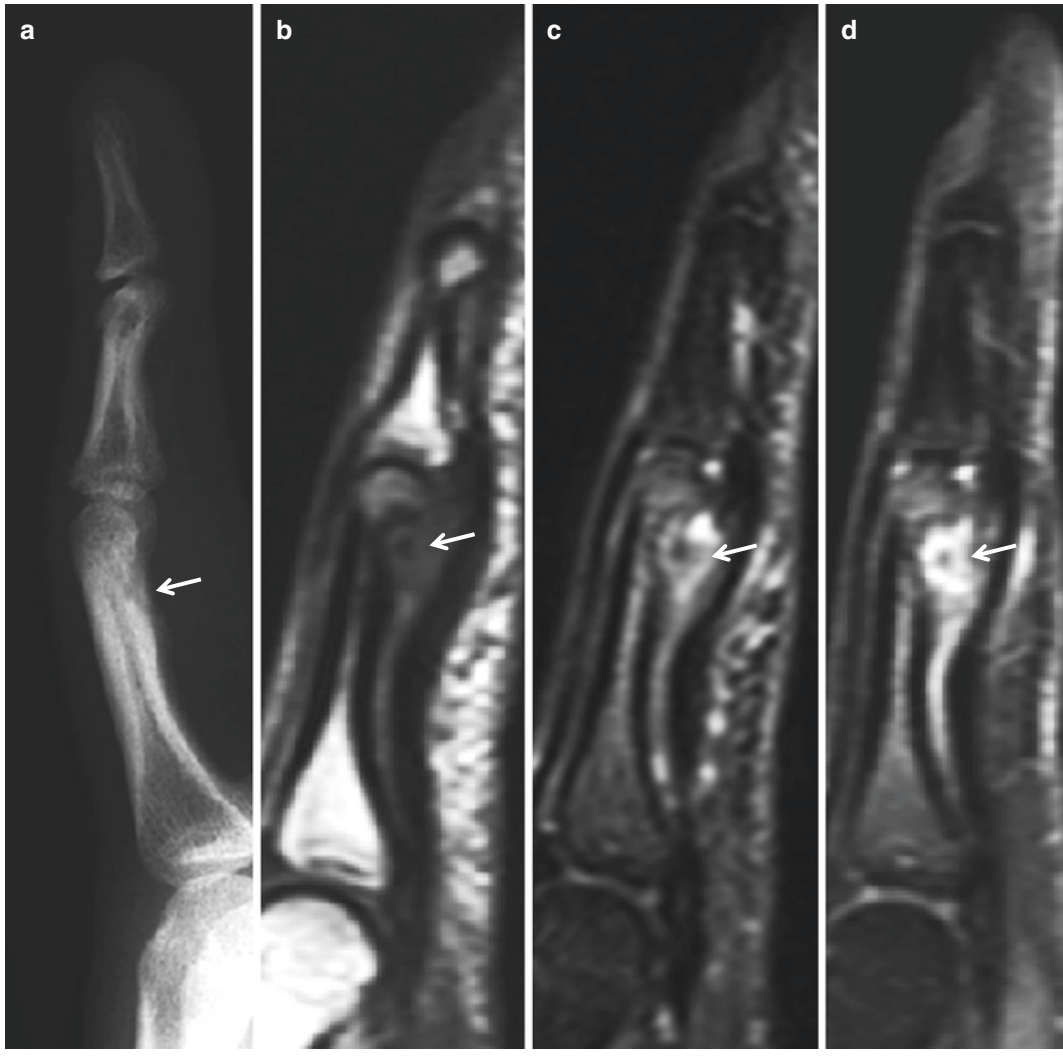

Fig. 2.8 Osteoid osteoma. (**a**) Lateral radiograph of the right index finger shows a juxtacortical osteolytic lesion with a mineralized focus (*arrow*) in the volar portion of the proximal phalanx. (**b**) Sagittal T1-weighted MR image shows a nidus with intermediate signal intensity and central hypointense focus (*arrow*) in the volar aspect of the middle phalanx. (**c**) Sagittal T2-weighted MR image reveals a hyperintense nidus with a central hypointense focus correlating to the mineralization noted within the nidus (*arrow*). Edema is noted in the surrounding soft tissue and bone marrow. (**d**) Sagittal fat-suppressed contrast-enhanced T1-weighted MR image shows the intensely enhancing nidus with central hypointensity due to mineralization (*arrow*)

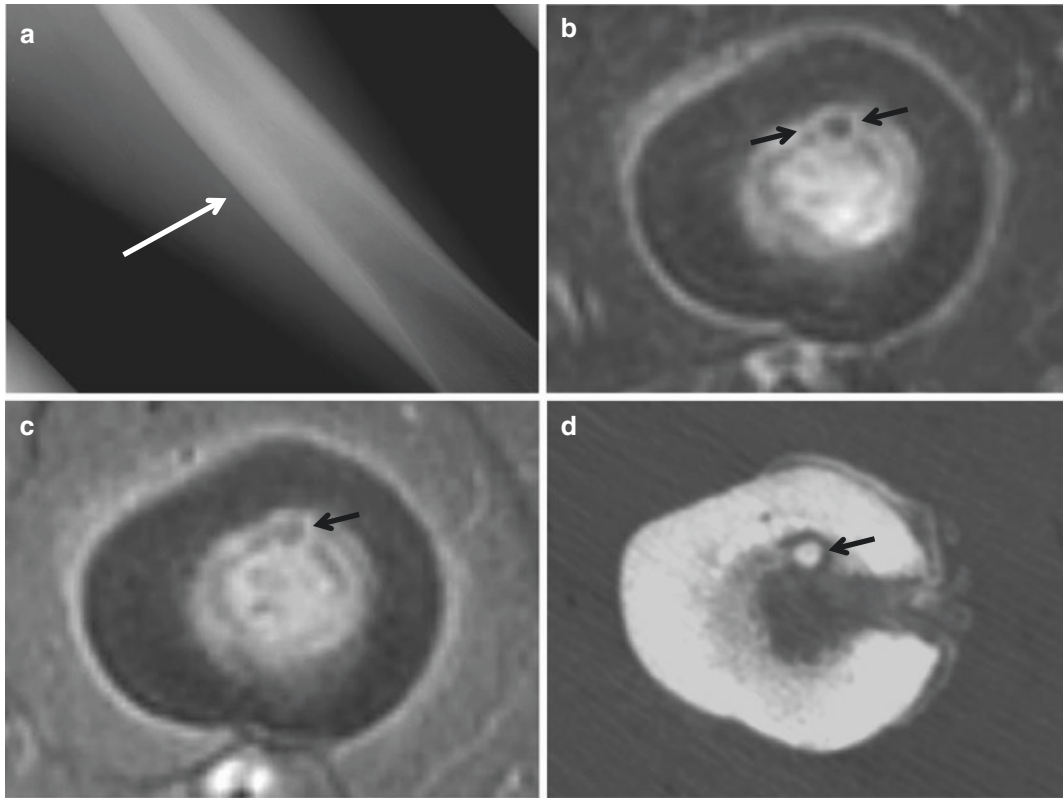

Fig. 2.9 Osteoid osteoma. (**a**) Anteroposterior radiograph of the left femur shows cortical thickening (*arrow*). (**b**) Axial T2-weighted MR image shows a hyperintense nidus (*arrow*) with central mineralization noted as a focus of hypointensity. (**c**) Axial fat-suppressed contrast-enhanced T1-weighted MR image shows a minimal enhancement of the nidus (*arrow*). (**d**) Corresponding axial CT scan demonstrates mineralized nidus (*arrow*)

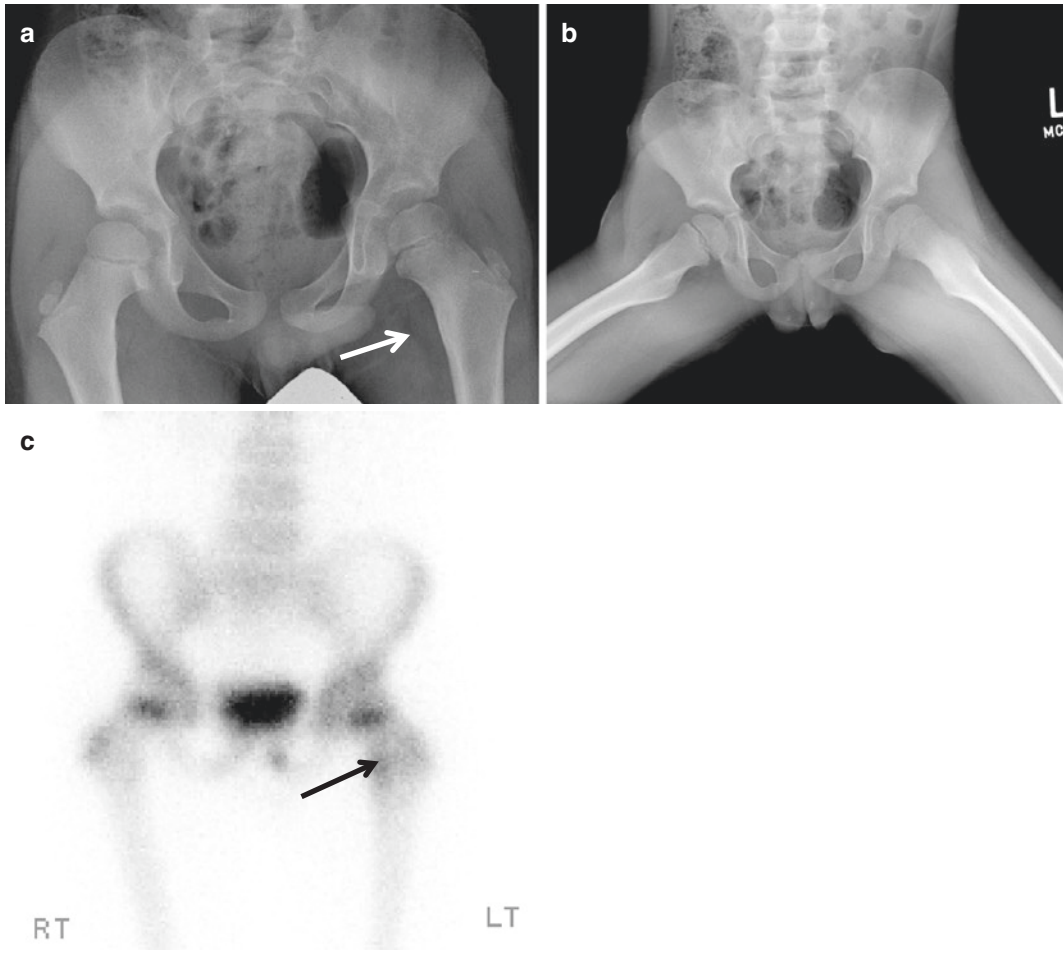

Fig. 2.10 Osteoid osteoma. (**a**) Anteroposterior radiograph of the pelvis shows an area of subtle sclerosis (*arrow*) about the lesser trochanter of the left femur. (**b**) Frog leg lateral view shows a similar finding. (**c**) Bone scan shows increased uptake (*arrow*) in the medial portion of the left proximal femur. (**d**) Axial T1-weighted MR image shows a focus of intermediate signal intensity (*arrow*). (**e**) Axial T2-weighted fat-suppressed MR image shows an increased signal intensity of nidus with surrounding edema (*arrow*). (**f**) Axial contrast-enhanced T1-weighted fat-suppressed MR image demonstrates an enhanced nidus (*arrow*) with pronounced surrounding edema. (**g**) Coronal fat-suppressed contrast-enhanced T1-weighted MR image again reveals an enhanced nidus (*arrow*) with pronounced surrounding edema

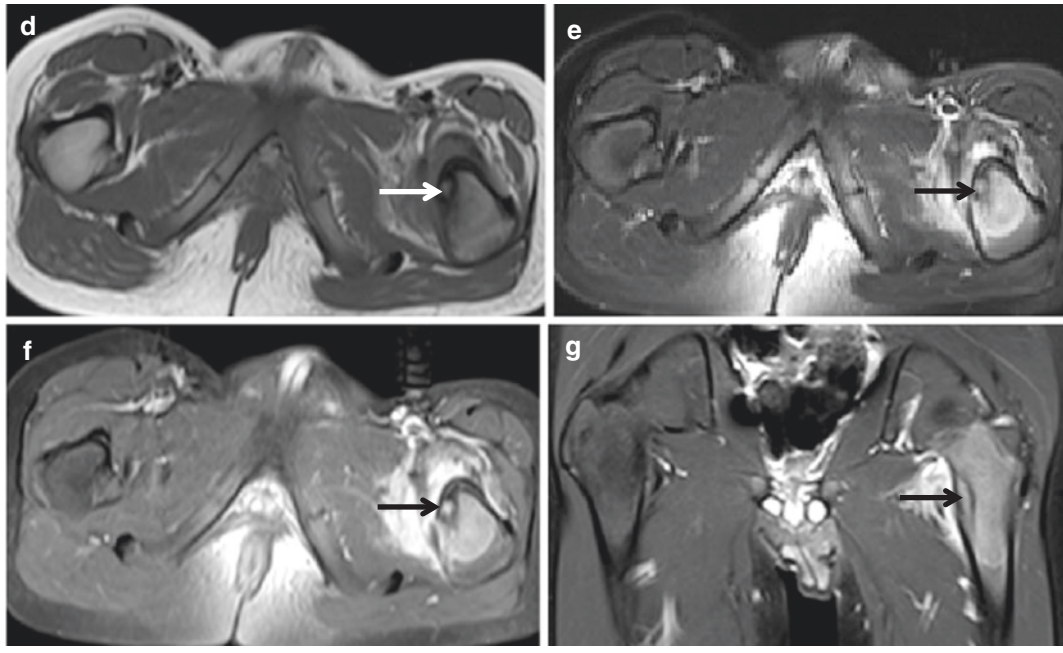

Fig. 2.10 (continued)

2.4 Osteoblastoma

Overview

Osteoblastoma is a rare osteoid-forming tumor, which is indistinguishable from the osteoid osteoma on routine histological analysis, and is differentiated from osteoid osteoma on the basis of the tumor size (2 cm or larger) and a lack of response to nonsteroidal anti-inflammatory drugs. Osteoblastoma presents with a dull ache and possible swelling that may not be worse at night.

Approximately 16 % of osteoblastomas have components of aneurysmal bone cyst. Aggressive-appearing inflammatory variants have been described. A malignant transformation into an osteosarcoma is rare.

Epidemiology

The patients are usually younger than 30 years of age, and the lesion is twice as common in males as females.

Common Locations

The common locations are the spine, particularly the posterior elements, and long bones. In most cases in long bones, an eccentric location in the diaphysis or metaphysis is noted. Although osteoblastomas are usually intramedullary lesions, an intracortical location is not uncommon.

Imaging Features

Radiograph

Three distinct types of osteoblastomas can be identified on radiographs.

Osteoblastoma may be similar to osteoid osteoma, although much larger in size, greater than 1.5–2 cm in diameter. This is termed a giant osteoid osteoma. This type occasionally exhibits less reactive sclerosis than osteoid osteoma, but the periosteal reaction is possibly more prominent.

Osteoblastoma may appear as a blow-out expansive lesion with small central calcification and peripheral sclerotic rim similar to an aneurysmal bone cyst. This pattern is particularly common in spinal osteoblastoma.

Osteoblastoma may also appear as an aggressive lesion with osseous expansion, partial cortical disruption, and soft tissue infiltration, simulating a malignant neoplasm. This is more common in long bones. Aggressive osteoblastomas belong to this group.

Magnetic resonance imaging

MR imaging may show reactive marrow edema in the surrounding bone, usually less than with osteoid osteoma, with a variable degree of increased T2 signal intensity depending on matrix mineralization and cellularity of the lesion. MR imaging optimally depicts the effects of the tumor on adjacent structures and surrounding soft tissues. The extensive peritumoral edema-like signal can be helpful in suggesting the diagnosis in equivocal case.

Differential Diagnoses

1. Osteoid osteoma

   Distinction of osteoid osteoma from osteoblastoma can be very difficult.
2. Bone abscess

   Bone abscess can usually be differentiated by a linear, serpentine tract extending from the abscess cavity toward the closest growth plate.
3. Osteosarcoma

   Aggressive osteoblastoma should be differentiated from osteosarcoma. CT and MR imaging are helpful in making the distinction by demonstrating the soft tissue component of osteosarcoma.

2.5 Osteosarcoma

Osteosarcoma is histologically composed of mesenchymal stem cells and characterized by production of osteoid matrix. Osteosarcoma is the most common primary nonhematological bone malignancy and is the most common primary bone malignancy in children and adolescents. There are various subtypes of osteosarcoma, and can be classified as intramedullary (low-grade, conventional, telangiectatic, small cell), juxtacortical (parosteal, periosteal, high-grade surface), or secondary lesions. Juxtacortical (surface) osteosarcoma refers to osteosarcoma originating from the surface of bone, and is classified into three main subtypes – parosteal, periosteal, and high-grade surface osteosarcoma. Juxtacortical osteosarcoma accounts for 4–10 % of all osteosarcomas. Conventional osteosarcoma and secondary osteosarcoma are histologically indistinguishable.

2.5.1 Low-Grade Central Osteosarcoma

Overview

Low-grade central osteosarcoma is composed of a microtrabecular osseous matrix in a bland fibrous stroma with a variable amount of bone production. The prognosis for patients with low-grade central osteosarcoma is substantially better than that for patients with conventional osteosarcoma.

Epidemiology

Low-grade central osteosarcoma (well-differentiated, sclerosing) accounts for 1–2 % of all osteosarcomas. This condition occurs in the third and fourth decades of life and is seen equally in men and women.

Common Locations

Low-grade central osteosarcoma commonly occurs within the medullary canal of the distal femur and proximal tibia.

Imaging Features

Radiograph

Low-grade central osteosarcoma may show well-defined margins, a sclerotic rim (Fig. 2.11), prominent internal trabeculation, and diffuse sclerosis (Fig. 2.12), and it may cause expansile remodeling of bone. However, radiographic evidence of a more aggressive process, such as associated bone lysis, focally indistinct margins, cortical destruction, and soft tissue mass can be seen.

The radiographic findings mimic those of fibrous dysplasia, often resulting in erroneous radiographic diagnosis. Any bone tumor with the appearance of fibrous dysplasia that also shows cortical effacement or destruction or a soft tissue mass should be considered a low-grade osteosarcoma.

Magnetic resonance imaging

Cortical disruption and soft tissue extension are common on MR imaging.

Differential Diagnoses

1. Fibrous dysplasia

   Fibrous dysplasia can usually be recognized by its distinctly nonaggressive appearance on radiographs. The presence of cortical destruction, soft tissue extension, and periosteal reaction are clue for differentiation of low-grade central osteosarcoma from benign fibro-osseous lesions.
2. Desmoplastic fibroma

   Desmoplastic fibroma is devoid of tumor bone components, although it may contain reactive bone at its periphery.

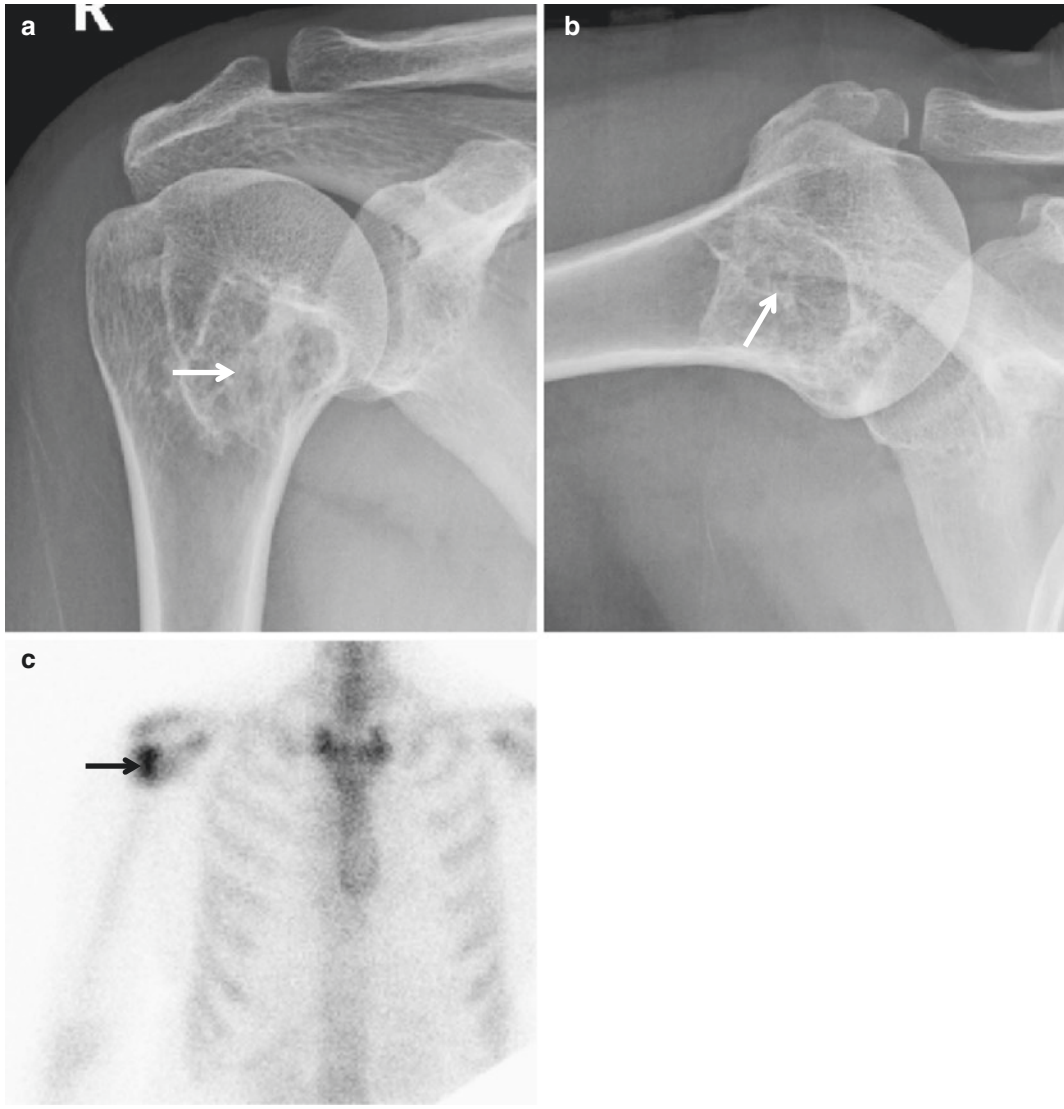

Fig. 2.11 Low-grade osteosarcoma. (**a**) Anteroposterior radiograph of the right humerus shows an osteolytic lesion with sclerotic rim, internal trabeculation, and areas of osteoid matrix (*arrow*). (**b**) Lateral view again shows an osteolytic lesion with sclerotic rim, internal trabeculation, and areas of osteoid matrix (*arrow*). (**c**) Bone scan shows increased uptake (*arrow*) in the right proximal humerus. (**d**) Sagittal T1-weighted MR image shows focal low signal intensity (*arrow*) with adjacent areas of intermediate signal intensity. (**e**) Axial T2-weighted MR image demonstrates focal low signal intensity (*arrow*), representing osteoid matrix, and adjacent areas of slightly increased signal intensity. (**f**) Coronal proton density-weighted MR image demonstrates focal low signal intensity with adjacent areas of slightly increased signal intensity (*arrow*). (**g**) Coronal proton density-weighted fat-suppressed MR image demonstrates high increased signal intensity portion (*arrow*) within the lesion

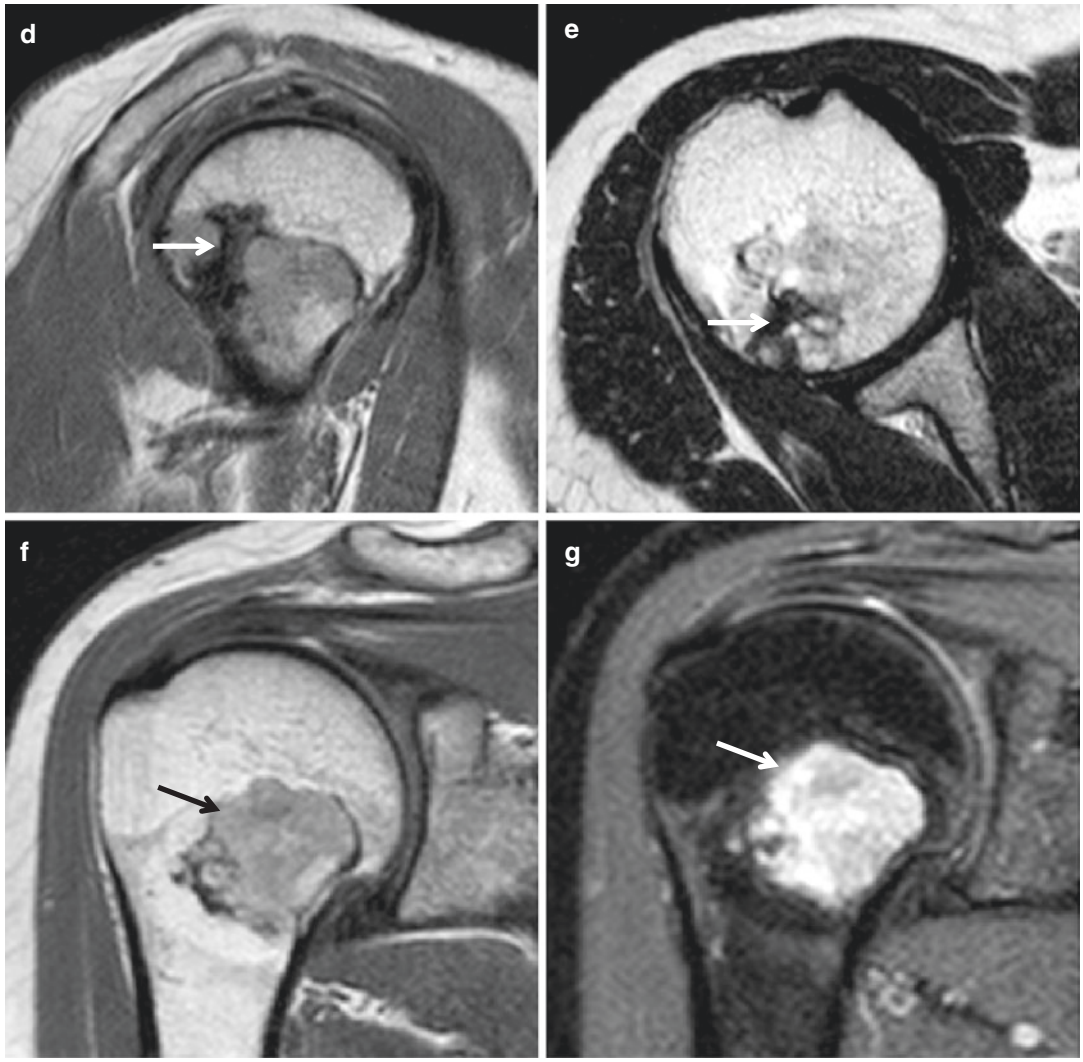

Fig. 2.11 (continued)

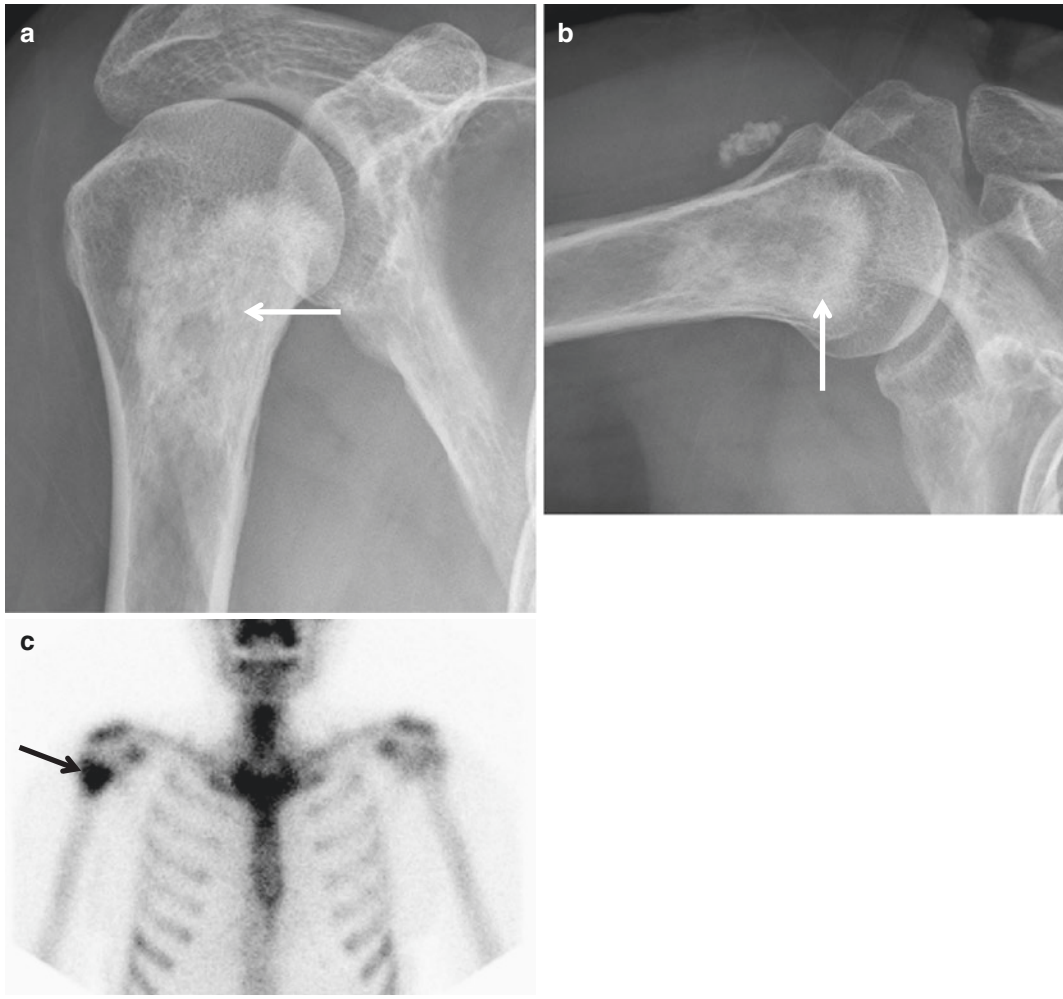

Fig. 2.12 Low-grade osteosarcoma. (**a**) Anteroposterior radiograph of the right humerus shows an intramedullary lesion with areas of diffuse sclerosis (*arrow*). (**b**) Lateral view again shows an intramedullary lesion with areas of diffuse sclerosis (*arrow*). (**c**) Bone scan shows increased uptake (*arrow*) in the right proximal humerus. (**d**) Axial T1-weighted MR image demonstrates diffuse low signal intensity (*arrow*) within the lesion, representing osteoid matrix. (**e**) Coronal T1-weighted MR image again demonstrates diffuse low signal intensity (*arrow*) within the lesion. (**f**) Coronal fat-suppressed proton density-weighted MR image shows subtle increased signal intensity (*arrow*) within the lesion. (**g**) Coronal T2-weighted MR image again shows subtle increased signal intensity (*arrow*) within the lesion

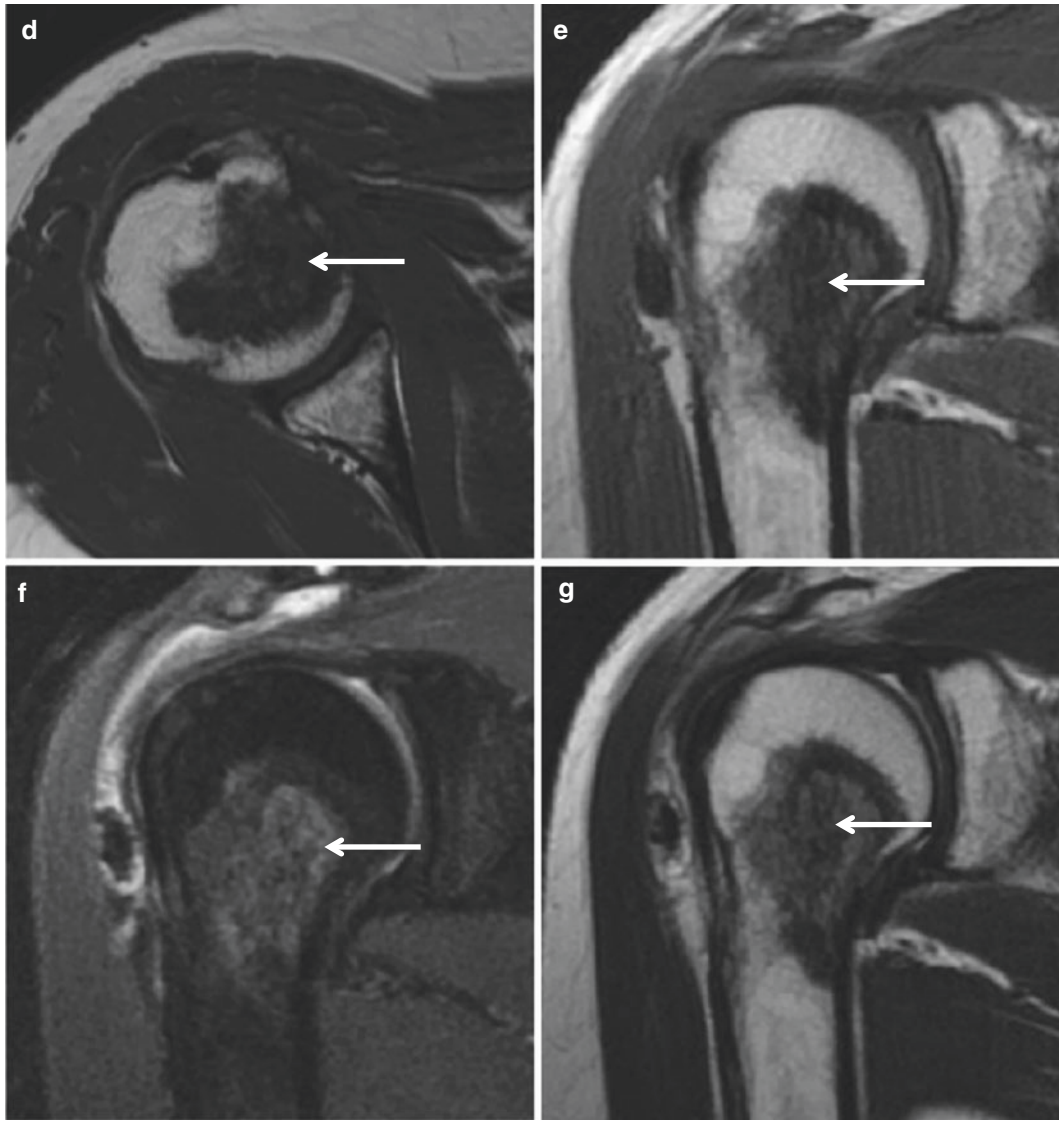

Fig. 2.12 (continued)

2.5.2 Conventional Osteosarcoma

Overview

Conventional osteosarcoma is the most common subtype of osteosarcoma, accounting for 75 % of all cases. Conventional osteosarcoma is a high-grade intramedullary form of osteosarcoma that is pathologically characterized by the production of tumor osteoid that originates centrally within the bone and involves the entire width of the bone. Conventional osteosarcoma is often pleomorphic and can produce variable amounts of cartilage, fibrous tissue, or other components. Depending on the dominant cell type, it can be classified as osteoblastic (50–80 %), fibroblastic-fibrohistiocytic (7–25 %), chondroblastic (5–25 %), telangiectatic (2.5–12 %), or small cell (1 %). Giant cells and osteoblastoma-like cells can also be seen. The lungs are the most common sites for metastatic osteosarcoma; lung metastasis often shows ossification and may be associated with spontaneous pneumothorax. Joint involvement is seen in 19–24 % of cases and is diagnosed when hyaline cartilage is penetrated. Synovial involvement is rare.

Epidemiology

Conventional osteosarcoma is more common in the second and third decades of life, peaking when patients are aged 10–15 years. Conventional osteosarcoma is uncommon in patients younger than 6 years or older than 60 years, and is more common in white patients and men.

Common Locations

Conventional osteosarcoma is seen in the long bones (70–80 %), most commonly near the knee, in the femur, tibia, and humerus. This lesion originates in the metaphysis, with extension to the epiphysis. Primary involvement of the diaphysis or epiphysis is uncommon. Osteosarcoma distal to the wrist and ankle is very rare.

Skip metastases are defined as discontinuous tumors in the primary bone site and represent foci of tumor occurring in the same bone anatomically as the primary lesion, but which show no continuity with the primary lesion, being separated by normal marrow. Skip metastasis occurs in about 5 % of patients. The identification of skip metastases is important not only for defining the extent of disease, but also for directing treatment. Patients with skip metastases have been traditionally been thought to have an extremely poor prognosis; however, a recent report has identified prolonged survival in this group following aggressive multimodality therapy.

Imaging Features

Radiograph

Conventional osteosarcoma is identified as an intramedullary mass with immature cloudlike osteoid matrix in the metaphyses of long bones. It is characterized by an aggressive periosteal reaction (Fig. 2.13) and a soft tissue mass. Although the most common pattern is mixed lytic and sclerotic, purely lytic (fibroblastic) (Fig. 2.14) or sclerotic (osteoblastic) types may also be seen.

Magnetic resonance imaging

MR imaging is the examination of choice for local staging and for planning biopsies or surgery. The lytic areas show low signal intensity on T1-weighted images and high signal intensity on T2-weighted images, whereas the mineralized matrix shows low signal intensity on both T1-weighted and T2-weighted images (Figs. 2.15 and 2.16). Foci of central hemorrhage have high signal intensity with all MR pulse sequences. Area of necrosis has low signal intensity on T1-weighted images and high signal intensity on T2-weighted images. Foci of central hemorrhage and necrosis are common in both the intraosseous and soft tissue tumor components.

A diagnosis of joint involvement by tumor on MR images is difficult, but is suggested when the hyaline cartilage is penetrated, or more commonly, when tumor extends through the capsule, such as into the suprapatellar bursa anteriorly or posteriorly, to encompass the cruciate ligaments. Fat-suppressed T1-weighted gadolinium-enhanced images are helpful for delineating extension of tumor into the joint, but enhancing synovium may mimic tumor spread. Although invasion of the joint is unlikely in the absence of an effusion, the

presence of an effusion does not allow an accurate prediction of intra-articular invasion.

Skip metastases are best identified with MR imaging, and a study of the entire length of an affected bone should be performed at the time of primary evaluation.

MR imaging provides the backbone for monitoring disease response to therapy. The clinical significance of a change in size depends on the primary tumor type. Osteosarcoma decreases a little in size during therapy, due to the dense osteoid. Improved demarcation of the soft tissue component may indicate a favorable therapeutic response.

Differential Diagnoses

1. Ewing's sarcoma

   Ewing's sarcoma appears as a highly aggressive diaphyseal lesion, but may be metaphyseal. Ewing's sarcoma may elicit prominent reactive bone formation, mimicking osteosarcoma. Cortical thickening and cortical saucerization may allow differentiation of Ewing's sarcoma from osteosarcoma. Calcifications rarely occur in Ewing's sarcoma.
2. Metastasis

   Osseous metastases may present as lucent or sclerotic lesions, mimicking osteosarcoma.
3. Osteoblastoma

   Osteoblastoma occasionally appears highly aggressive and may mimic osteosarcoma.
4. Undifferentiated high-grade pleomorphic sarcoma

   Undifferentiated high-grade pleomorphic sarcoma appears as a permeative aggressive metaphyseal lesion and may mimic lytic osteosarcoma.

Fig. 2.13 Conventional osteosarcoma. (**a**) Anteroposterior radiograph of the left femur shows ill-defined osteolytic lesion with osteoid matrix, interrupted periosteal reaction, and cortical breaching (*arrow*). (**b**) Lateral radiograph of the left femur shows osteoid matrix (*arrow*). (**c**) Bone scan shows increased uptake (*arrow*) in the left distal femur. (**d**) Axial T1-weighted MR image demonstrates intramedullary mass of low signal intensity (*arrow*) with cortical breaching and soft tissue extension. (**e**) Coronal T2-weighted MR image demonstrates intramedullary mass of heterogeneous signal intensity (*arrow*) with cortical breaching and soft tissue extension. (**f**) Coronal fat-suppressed contrast-enhanced T1-weighted MR image demonstrates heterogeneous enhancement (*arrow*) with soft tissue extension. (**g**) Corresponding gross photograph shows the intramedullary mass with soft tissue extension

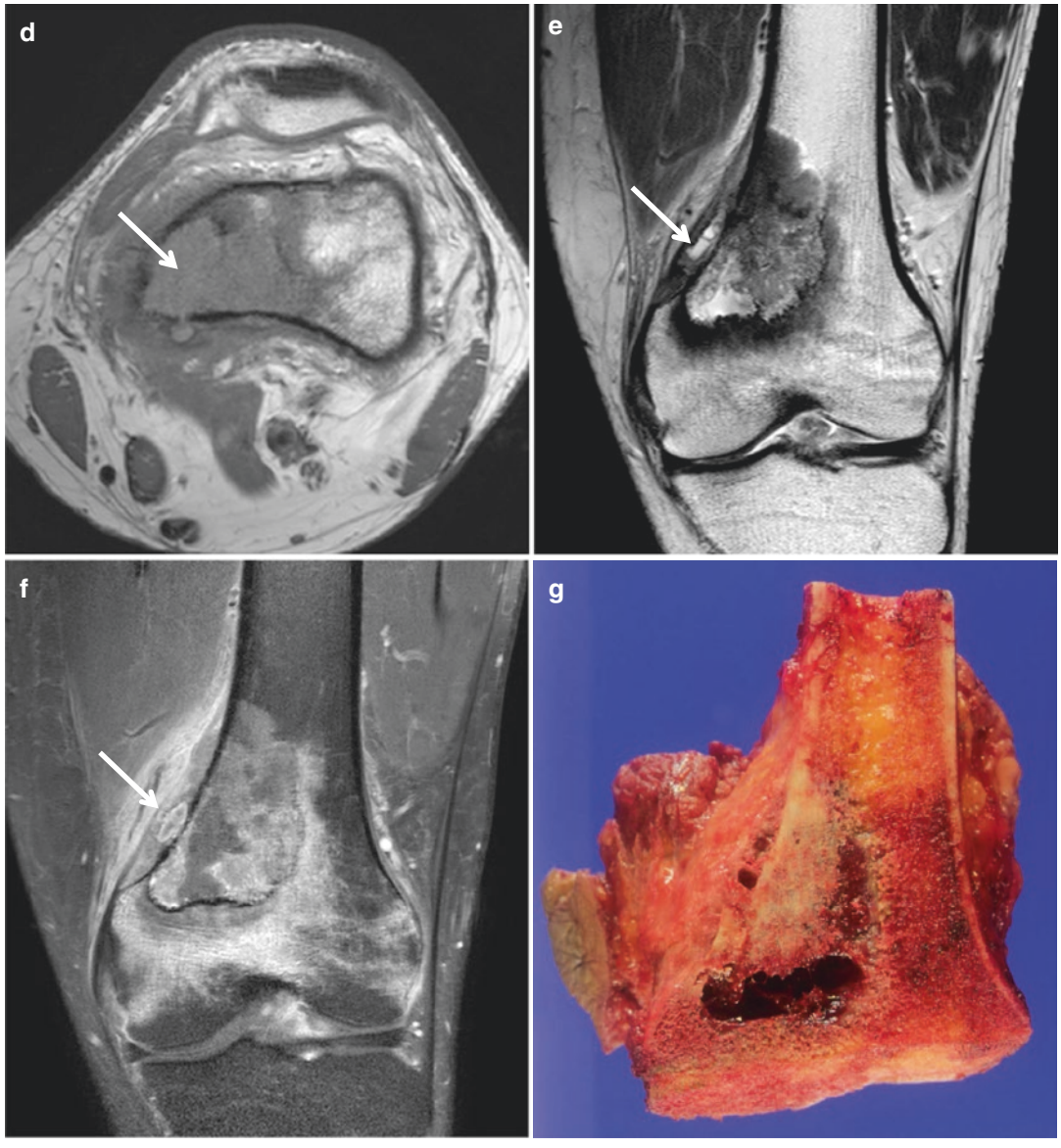

Fig. 2.13 (continued)

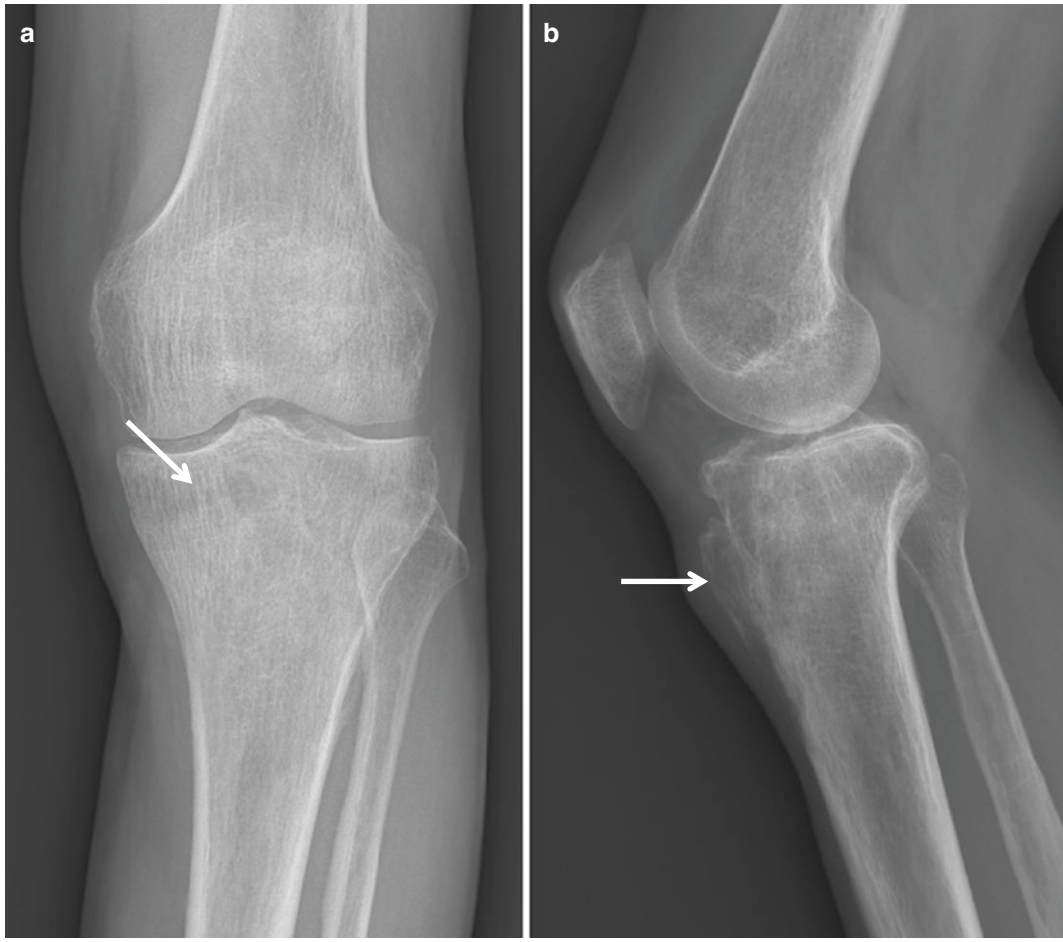

Fig. 2.14 Conventional osteosarcoma. (**a**) Anteroposterior radiograph of the left knee shows ill-defined osteolytic lesion (*arrow*) in the left proximal tibia. (**b**) Lateral radiograph of the left knee again shows osteolytic lesion with indistinct anterior cortex (*arrow*) of the left proximal tibia. (**c**) Coronal proton density-weighted MR image demonstrates intramedullary mass of low signal intensity (*arrow*). (**d**) Sagittal T2-weighted MR image demonstrates intramedullary mass of low signal intensity (*arrow*) with extraosseous soft tissue mass. (**e**) Sagittal fat-suppressed contrast-enhanced T1-weighted MR image demonstrates enhancing intramedullary mass (*arrow*) with soft tissue extension. (**f**) Corresponding gross photograph shows the intramedullary mass with soft tissue extension

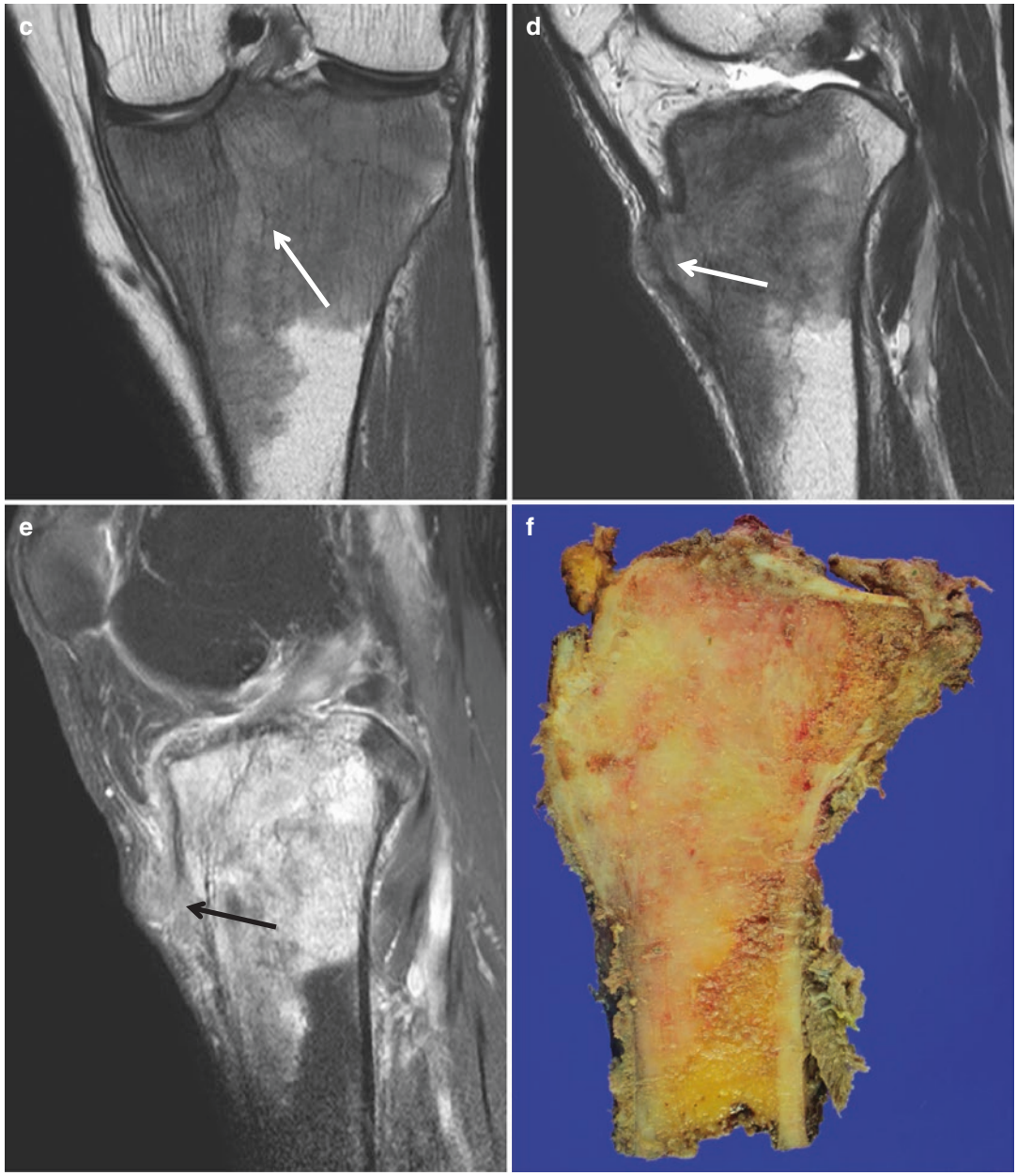

Fig. 2.14 (continued)

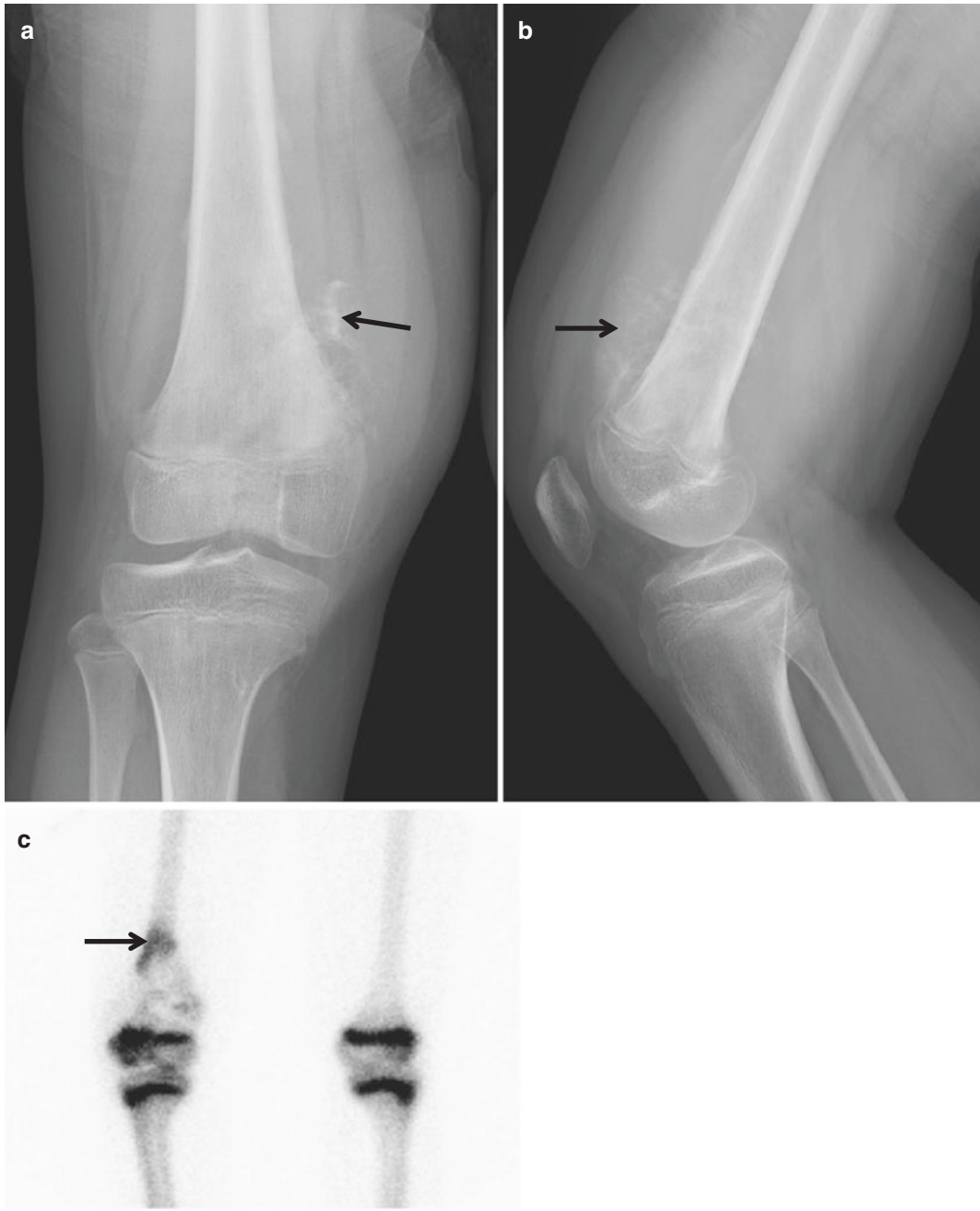

Fig. 2.15 Conventional osteosarcoma. (**a**) Anteroposterior radiograph of the right knee shows extraosseous mineralization (*arrow*) with interrupted periosteal reaction in the right distal femur. (**b**) Lateral radiograph of the right knee again shows extraosseous mineralization (*arrow*) with interrupted periosteal reaction. (**c**) Bone scan shows increased uptake (*arrow*) in the right distal femur. (**d**) Coronal T1-weighted MR image demonstrates intramedullary mass of low signal intensity (*arrow*) with soft tissue extension. (**e**) Coronal T2-weighted MR image demonstrates intramedullary mass of heterogeneous signal intensity (*arrow*) with extraosseous soft tissue mass. (**f**) Coronal contrast-enhanced T1-weighted fat-suppressed MR image demonstrates peripheral enhancement (*arrow*) with soft tissue extension. (**g**) Corresponding gross photograph shows the intramedullary mass with soft tissue extension

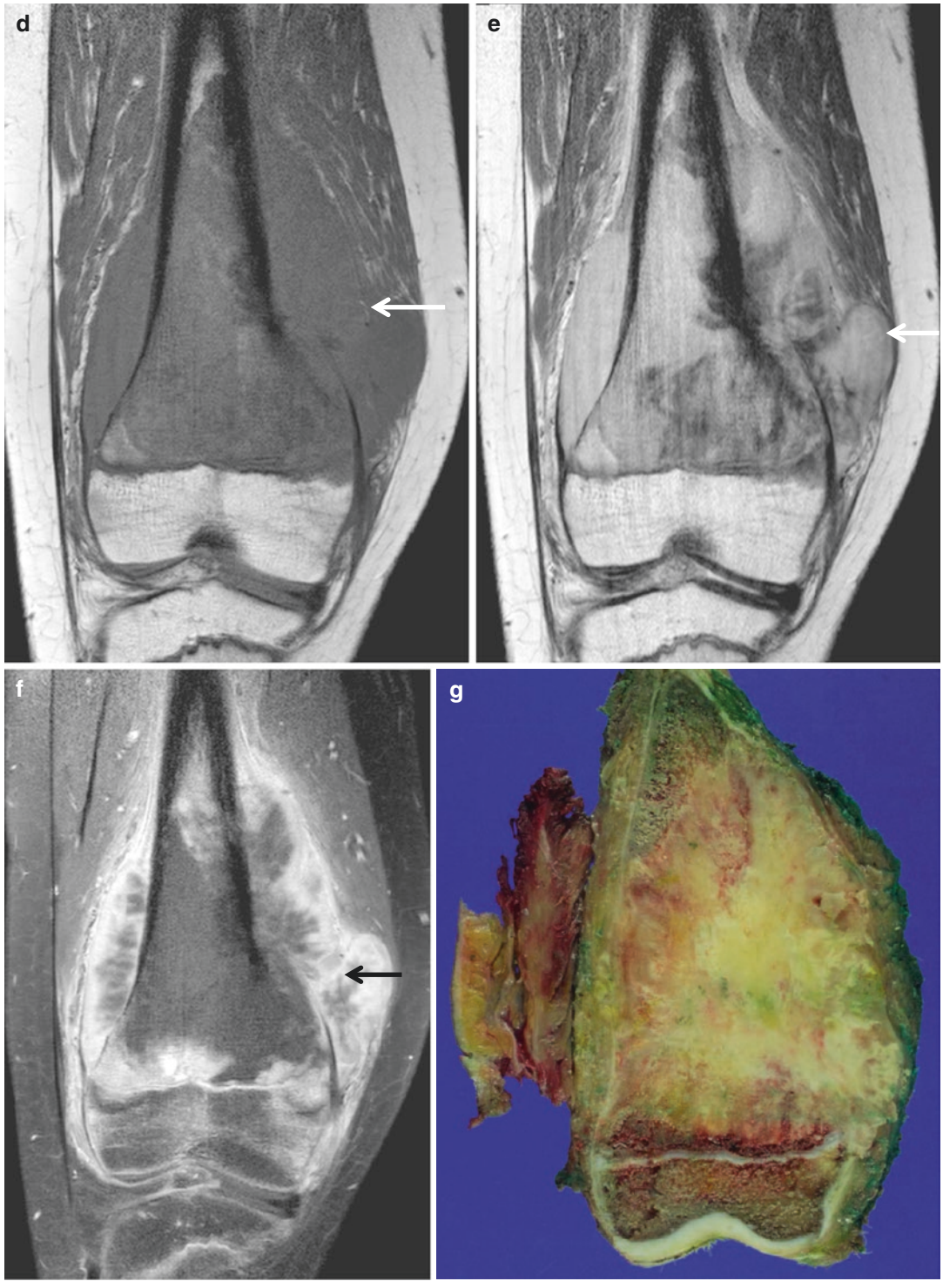

Fig. 2.15 (continued)

Fig. 2.16 Conventional osteosarcoma. (**a**) Anteroposterior radiograph of the right knee shows an expansive osteolytic lesion (*arrow*) involving the right proximal fibula. (**b**) Lateral radiograph of the right knee again shows expansive osteolytic lesion (*arrow*). (**c**) Bone scan shows increased uptake (*arrow*) in the right proximal fibula. (**d**) Corresponding axial CT scan shows an expansive osteolytic lesion with cortical breaching. (**e**) Sagittal T1-weighted MR image demonstrates an expansive mass of heterogeneous signal intensity (*arrow*). (**f**) Coronal fat-suppressed T2-weighted MR image demonstrates cystic components within the mass (*arrow*). (**g**) Coronal fat-suppressed contrast-enhanced T1-weighted MR image demonstrates enhancing mass (*arrow*) with areas of rim enhancement, representing cystic components. (**h**) Corresponding gross photograph shows the intramedullary mass with internal cystic components

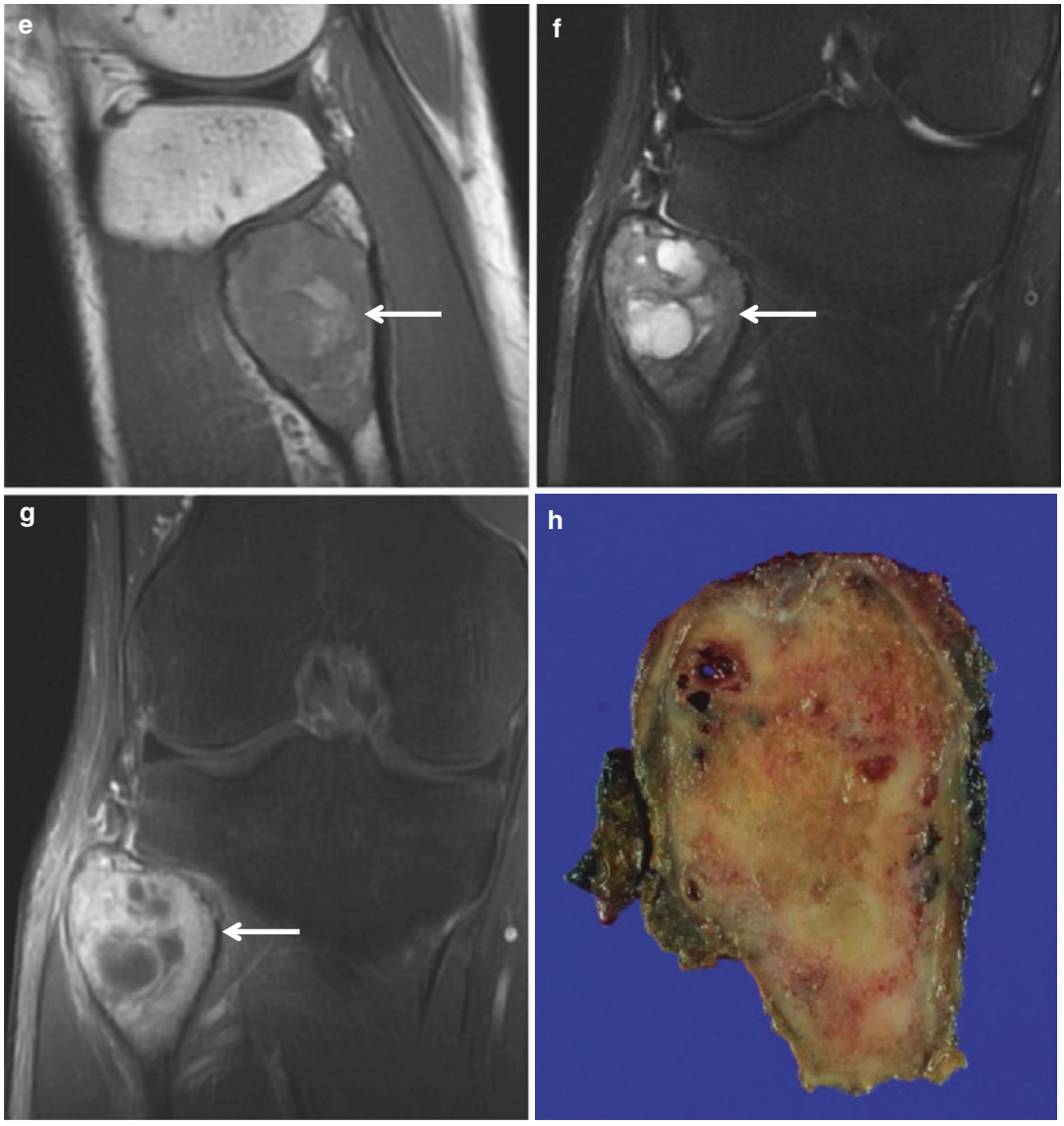

Fig. 2.16 (continued)

2.5.3 Telangiectatic Osteosarcoma

Overview

Telangiectatic osteosarcoma is pathologically characterized by dilated cavities filled with blood and septa and a rim that contains high-grade osteosarcomatous cells. The favorable response for telangiectatic osteosarcoma to chemotherapy may be related to the increased growth fraction of tumor cells compared with that in conventional osteosarcoma. Pathologically, hemorrhagic, cystic, or necrotic spaces occupy more than 90 % of the tumor, with only a small fraction of solid tissue.

Epidemiology

Telangiectatic osteosarcoma accounts for 1.2–12 % of osteosarcomas, and most commonly occurs in the first and second decades of life.

Common Locations

Telangiectatic osteosarcoma occurs most often in the metaphysis of long bones, with the femur being the most common site.

Imaging Features

Radiograph

Radiographic appearances of the telangiectatic osteosarcoma include geographical osteolytic pattern of bone destruction, with ill-defined margins, asymmetric expansion, cortical destruction, periosteal reaction, and soft tissue mass (Fig. 2.17). Matrix mineralization may be subtle.

Magnetic resonance imaging

Hemorrhage and fluid–fluid levels are frequently identified. Enhancing thick, nodular, solid tissue within or around the cystic spaces (Fig. 2.18), best seen on contrast-enhanced MR images, corresponds to variable high-grade sarcomatous tissue in hemorrhagic or necrotic spaces.

Differential Diagnoses

1. Aneurysmal bone cyst

   Similar to telangiectatic osteosarcoma, aneurysmal bone cyst can be hypervascular and show progressive osteolytic bone expansion and hemorrhage with fluid–fluid levels. However, aneurysmal bone cyst typically shows only an enhancing thin peripheral rim and septa without nodularity or osteoid matrix mineralization. The pattern of growth in aneurysmal bone cyst is frequently less aggressive, with marked ballooning and a well-defined encapsulated margin, in contrast to the cortical destruction and infiltrative margins seen in telangiectatic osteosarcoma.
2. Giant cell tumor

   Giant cell tumor is hemorrhagic tumor with an expansile osteolytic appearance that can be confused with telangiectatic osteosarcoma. Giant cell tumor is usually located at the end of bone, close to the subchondral bone, and is a solid mass with intermediate signal intensity on T2-weighted MR images.
3. Metastasis

   Osteolytic metastasis may mimic telangiectatic osteosarcoma on radiography, but can readily be distinguished at cross-sectional imaging, which demonstrates the presence of soft tissue without fluid–fluid levels.

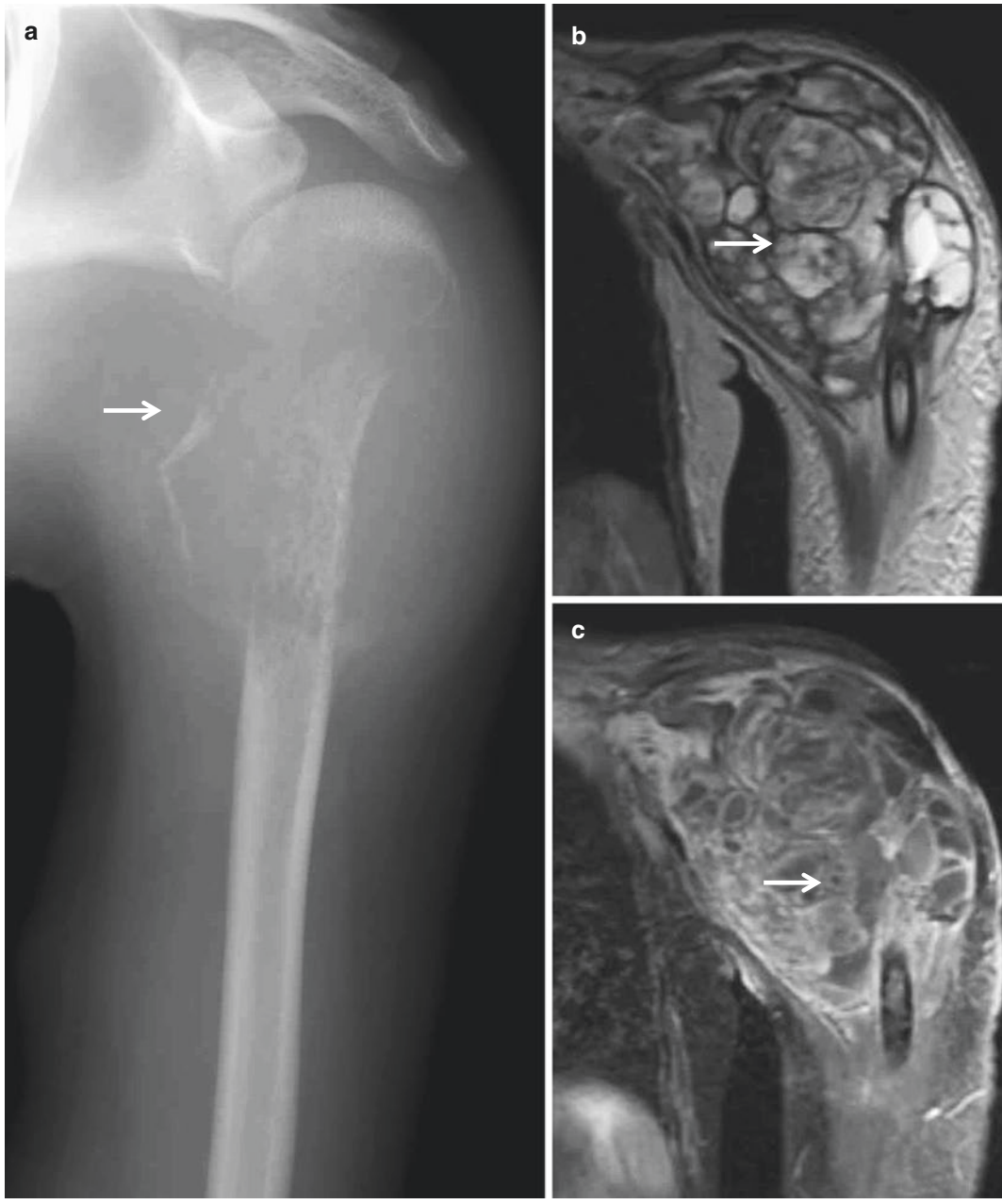

Fig. 2.17 Telangiectatic osteosarcoma. (**a**) Radiograph of the left humerus shows osteolytic pattern of bone destruction with ill-defined margins and cortical destruction (*arrow*). (**b**) Coronal T2-weighted MR image demonstrates expansive mass with cystic spaces (*arrow*). (**c**) Coronal fat-suppressed contrast-enhanced T1-weighted MR image demonstrates expansive and cystic mass with rim and nodular enhancement (*arrow*)

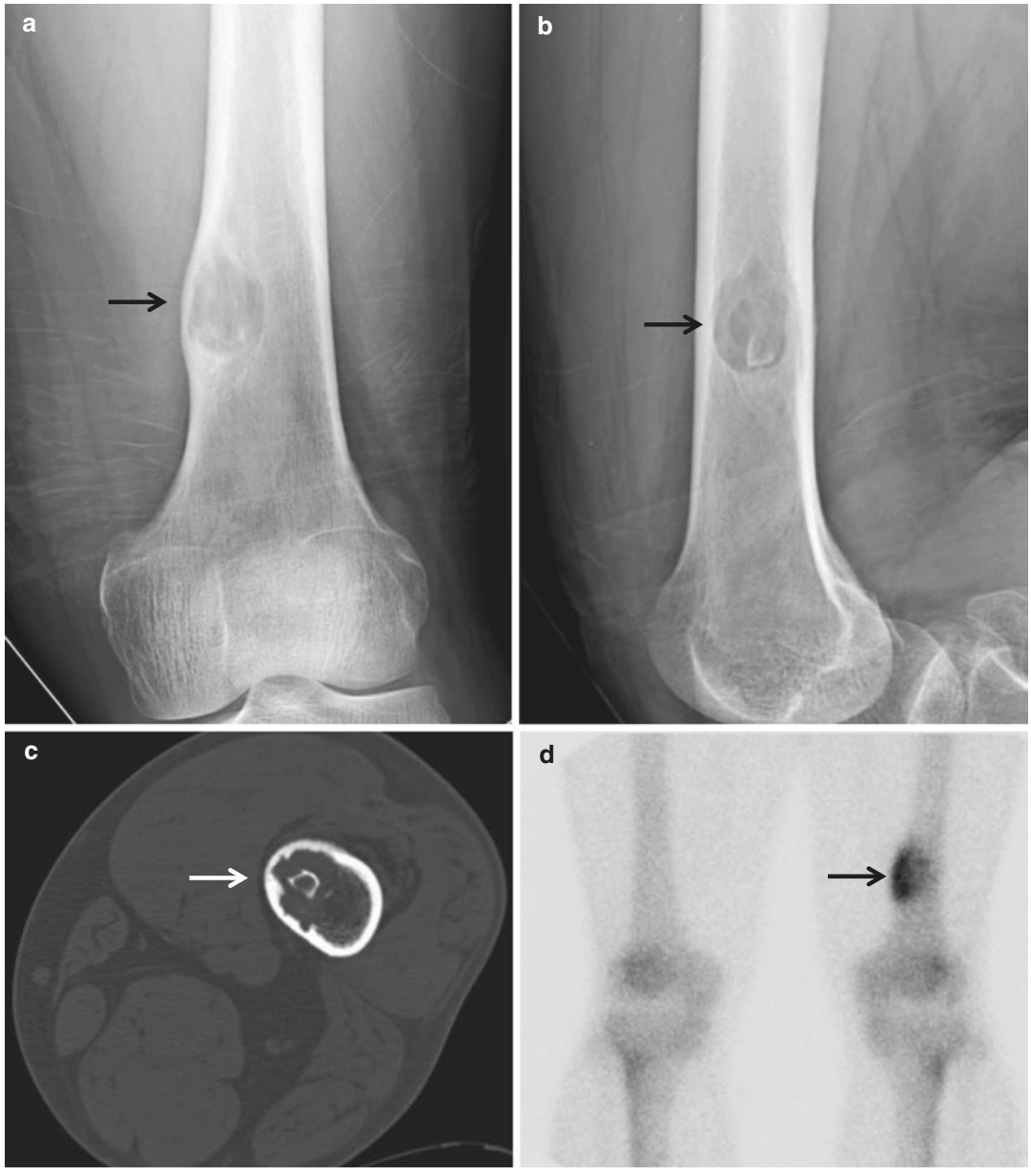

Fig. 2.18 Telangiectatic osteosarcoma. (**a**) Anteroposterior radiograph of the left femur shows eccentric expansive osteolytic lesion (*arrow*) in the left distal femur. (**b**) Lateral radiograph of the left femur shows eccentric expansive osteolytic lesion (*arrow*) internal mineralization. (**c**) Corresponding axial CT scan shows an expansive osteolytic lesion (*arrow*) with internal mineralization. (**d**) Bone scan shows increased uptake (*arrow*) in the left distal femur. (**e**) Coronal T1-weighted MR image demonstrates an eccentric mass of heterogeneous signal intensity (*arrow*). (**f**) Coronal T2-weighted MR image demonstrates cystic components of the mass (*arrow*). (**g**) Coronal fat-suppressed contrast-enhanced T1-weighted MR image demonstrates enhancing mass (*arrow*) with areas of rim and solid enhancement. (**h**) Corresponding gross photograph shows the intramedullary mass with internal cystic and nodular components

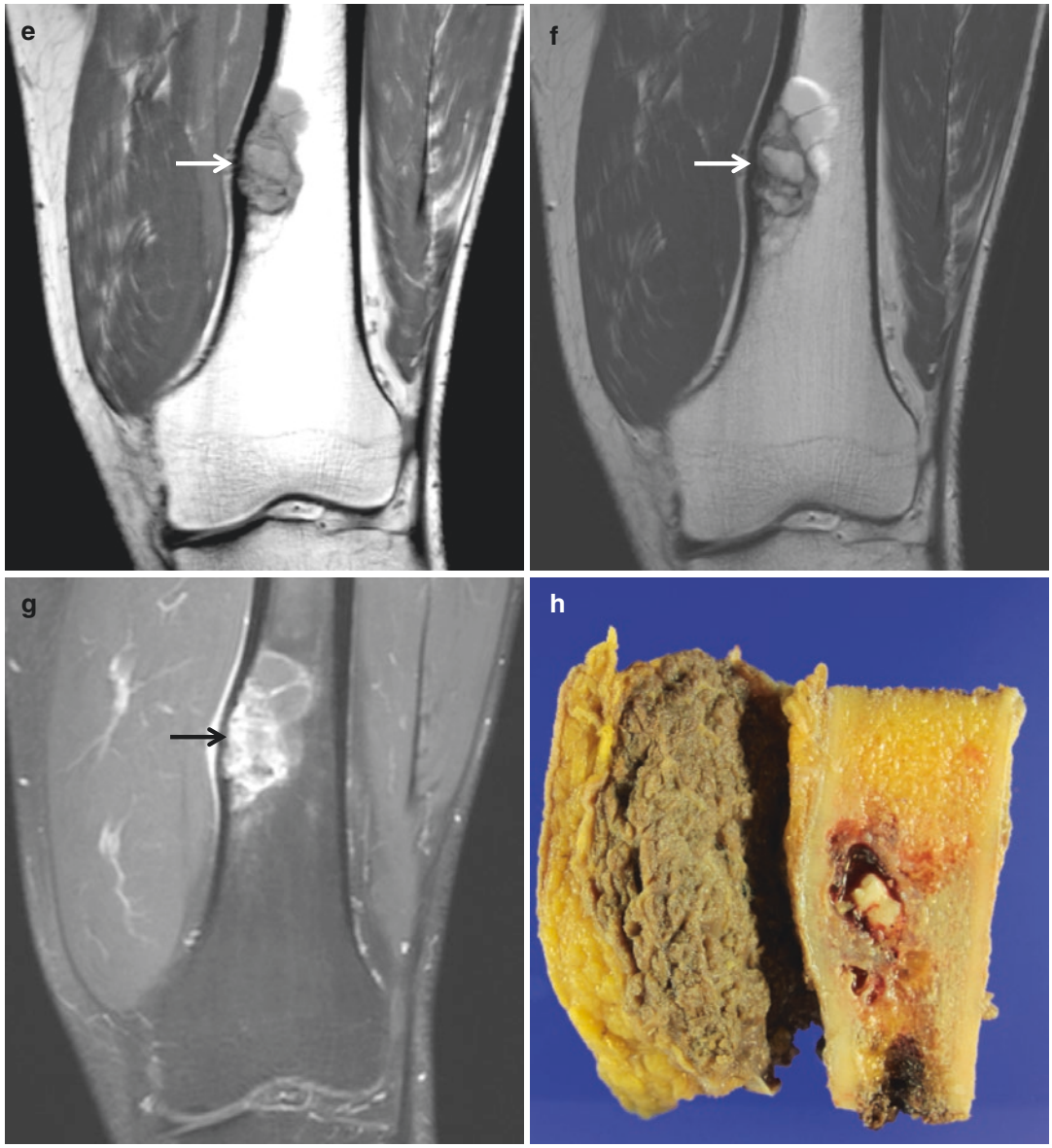

Fig. 2.18 (continued)

2.5.4 Small Cell Osteosarcoma

Overview

Small cell osteosarcoma is a distinct subtype of conventional osteosarcoma, composed of small, round, blue cells. On pathological examination, small cell osteosarcoma may be mistaken for Ewing's sarcoma or primitive neuroectodermal tumor, because its cells are small and have round, hyperchromatic nuclei.

Epidemiology

Small cell osteosarcoma accounts for only 1–4 % of osteosarcomas, and most often affects patients in the second and third decades of life. There is no gender predilection.

Common Locations

The lesions are most commonly seen in the metaphysis of long bones and most frequently involve the femur, with occasional extension to the epiphysis, but they are isolated to the diaphysis in 15 % of cases.

Imaging Features

Radiograph

Small cell osteosarcoma is an intramedullary, permeative lytic lesion with ill-defined margins that is associated with cortical destruction, aggressive periosteal reaction, and soft tissue mass (Fig. 2.19). Purely lytic lesions may occur in up to 40 % of cases. Calcification in the intramedullary cavity or an associated extraosseous soft tissue mass is frequent.

Magnetic resonance imaging

MR images may show an intramedullary tumor with circumferential extraosseous soft tissue mass.

Differential Diagnoses

1. Ewing's sarcoma

   Cortical thickening and cortical saucerization may allow differentiation of Ewing's sarcoma from small cell osteosarcoma. Cortical saucerization is caused by local periosteal destruction by tumor and surrounding periosteal reaction. Calcifications rarely occur in Ewing's sarcoma.
2. Lymphoma

   Lymphoma of bone is a permeative osteolytic lesion commonly associated with extraosseous masses. Lymphoma may spread outside of bone without osseous destruction.
3. Conventional osteosarcoma

   Conventional osteosarcoma is identified as an intramedullary mass with aggressive periosteal reaction and a soft tissue mass.

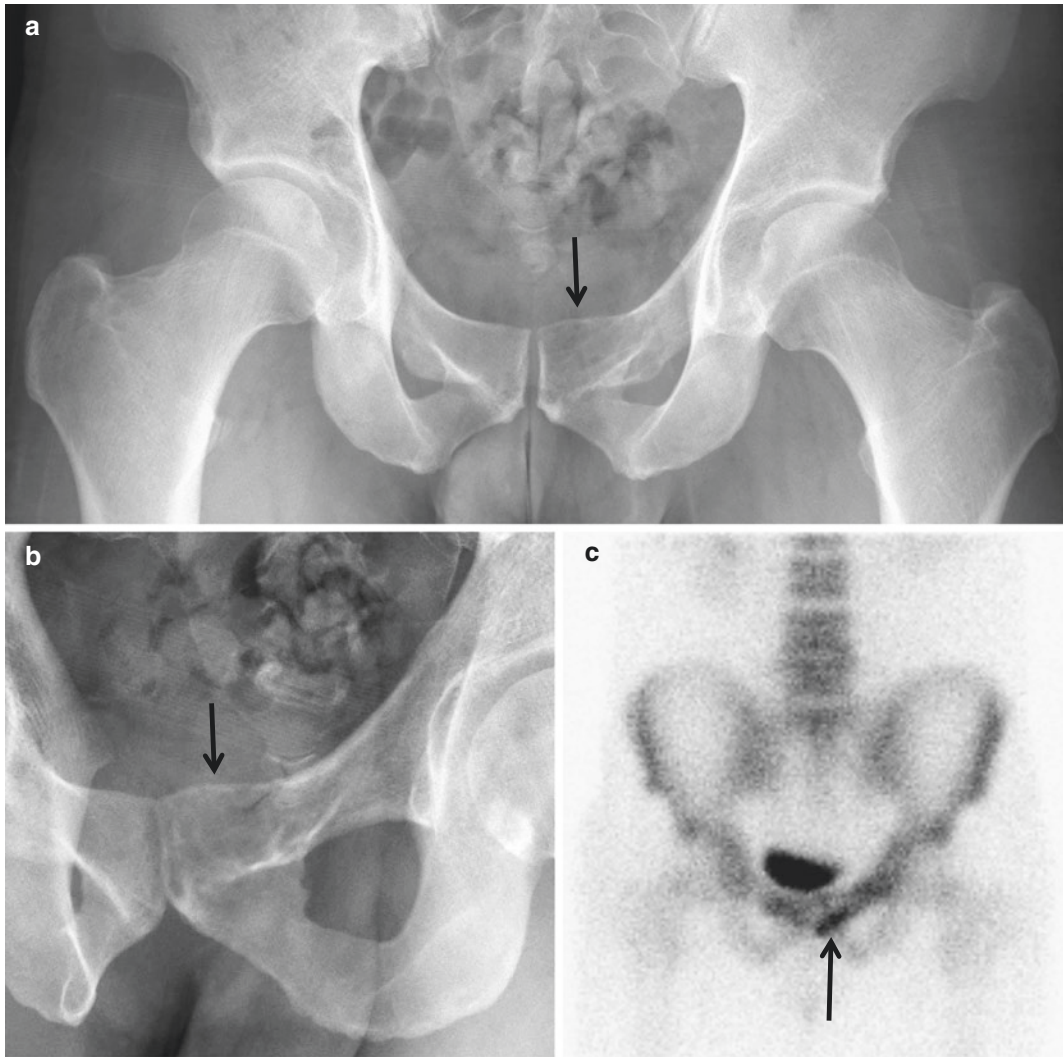

Fig. 2.19 Small cell osteosarcoma. (**a**) Anteroposterior radiograph of the pelvis shows an osteolytic lesion (*arrow*) involving the left pubic body. No obvious mineralization is noticed. (**b**) Oblique radiograph of the pelvis shows an osteolytic lesion (*arrow*) with no obvious mineralization. (**c**) Bone scan shows increased uptake (*arrow*) in the left pubic bone. (**d**) Corresponding axial CT scan shows an osteolytic lesion (*arrow*) with no internal mineralization. (**e**) Coronal T1-weighted MR image demonstrates an intramedullary mass of intermediate signal intensity (*arrow*). (**f**) Coronal fat-suppressed proton density-weighted MR image demonstrates increased signal intensity of the mass (*arrow*) with extraosseous extension. (**g**) Coronal T2-weighted MR image demonstrates increased signal intensity of the mass (*arrow*) with extraosseous extension

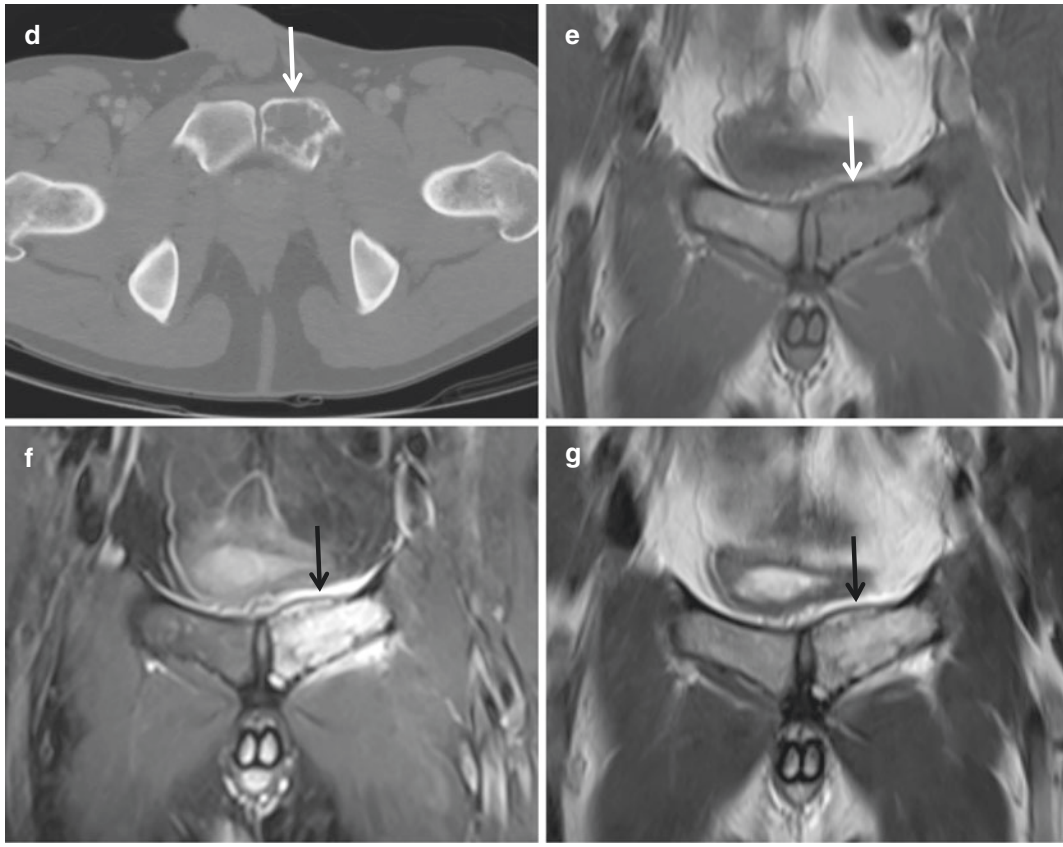

Fig. 2.19 (continued)

2.5.5 Parosteal Osteosarcoma

Overview

Anatomically, parosteal osteosarcoma originates from the outer layer of the periosteum. Most parosteal osteosarcomas are of low grade, but high-grade foci can be seen in 22–64 % of cases. The prognosis for parosteal osteosarcoma is better than that for conventional osteosarcoma. It has a tendency to wrap around the bone.

Lesions of higher grade have been called dedifferentiated parosteal osteosarcoma, although the term dedifferentiation is generally reserved for those lesions that contain a second cell line. Dedifferentiation of low-grade parosteal osteosarcoma to high-grade disease has been reported in 16–43 % of cases.

Epidemiology

Parosteal osteosarcoma is the most common subtype of juxtacortical osteosarcoma, accounting for approximately 65–75 % of all juxtacortical osteosarcomas. Parosteal osteosarcoma is typically seen in the second to fourth decades of life and is more common in women.

Common Locations

Parosteal osteosarcoma usually occurs in the metaphyses of long bones. The posterior aspect of the distal femoral shaft is the most common site, followed by the tibia, fibula, and the proximal humerus.

Imaging Features

Radiograph

The typical appearance is a lobulated and exophytic juxtacortical ossific mass (Figs. 2.20 and 2.21), which in its early stages is separated by a radiolucent cleavage plane (string sign) from the remaining cortical bone; in the later stages of growth, this plane may be obliterated. This cleavage plane corresponds histologically to the periosteum interposed between the cortex and the tumor mass. The tumor is densely ossified at the center and relatively lucent at the periphery. Cortical thickening without aggressive periosteal reaction may also be seen. Extension into the medullary cavity may be seen in both low-grade and high-grade lesions, and its effect on prognosis is controversial. Knowledge of this extension is important before the performance of complete surgical resection.

Dedifferentiation correlates with increased lysis and the presence of a soft-tissue mass without ossification.

Magnetic resonance imaging

The ossified tumor is predominantly hypointense (Fig. 2.20) on both T1-weighted and T2-weighted images, owing to lack of mobile protons that produce MR signal. When there is an unmineralized soft tissue mass larger than 1 cm^3 or the lesion is predominantly hyperintense on T2-weighted images, the tumor is more likely to be of high grade.

Differential Diagnoses

1. Myositis ossificans

   Myositis ossificans is a benign ossified soft tissue mass within the muscle, and is not attached to the cortex. This condition is located in the paraosseous compartment within the skeletal muscle. It is the soft tissue counterpart of periostitis ossificans. Gradual ossification of the lesion from the periphery toward the center of the mass is a characteristic radiographic finding of myositis ossificans. Histologically, this progressive maturation from central osteoid foci to peripheral lamellar mature bone is known as the zoning pattern of ossification.
2. Osteochondroma

   The diagnostic feature of osteochondroma is corticomedullary continuity of a juxtacortical bone lesion with the adjacent bone, with or without a hyaline cartilage cap. The cartilage cap of the osteochondroma demonstrates high signal intensity on fluid-sensitive sequences owing to

its high water content. In contrast to osteochondroma, parosteal osteosarcoma lacks corticomedullary continuity between the tumor and the medullary canal. Although parosteal osteosarcoma occasionally demonstrates cartilage tissue with a cap-like appearance on MR images, it is often irregular, incomplete, and thick, in contrast to the smooth, continuous, and relatively thin cartilage cap of an osteochondroma.

3. Periostitis ossificans

Periostitis ossificans shows variable degrees of periosteal reaction on radiographs. The cortex is usually intact. It does not wrap or encircle the entire bone, as does parosteal osteosarcoma. Periostitis ossificans shows the zoning pattern of ossification, which is usually more radiodense at the periphery and lucent at the center.

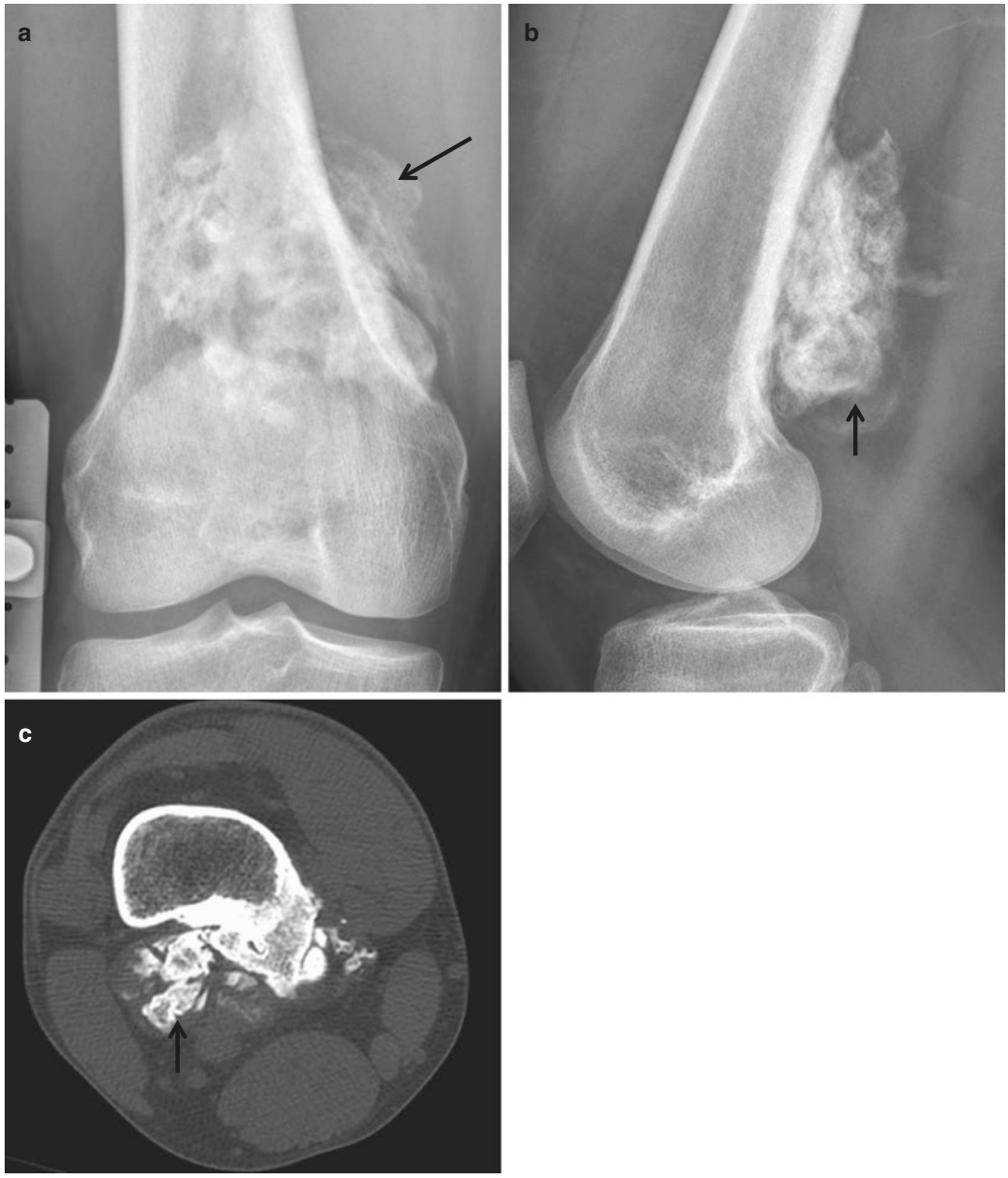

Fig. 2.20 Parosteal osteosarcoma. (**a**) Anteroposterior radiograph of the right knee shows a lobulated and exophytic juxtacortical ossific mass (*arrow*). (**b**) Lateral radiograph of the right knee shows a lobulated and exophytic juxtacortical ossific mass (*arrow*), which is separated by a radiolucent cleavage plane from the remaining cortical bone. (**c**) Corresponding axial CT scan shows a lobulated and exophytic juxtacortical ossific mass (*arrow*). (**d**) Axial T1-weighted MR image shows a lobulated and exophytic juxtacortical mass with heterogeneous signal intensity (*arrow*). (**e**) Axial T2-weighted MR image demonstrates increased signal intensity in the unmineralized portion of the mass (*arrow*). (**f**) Axial fat-suppressed contrast-enhanced T1-weighted MR image demonstrates enhancement in the unmineralized portion of the mass (*arrow*). (**g**) Corresponding gross photograph shows the juxtacortical mass

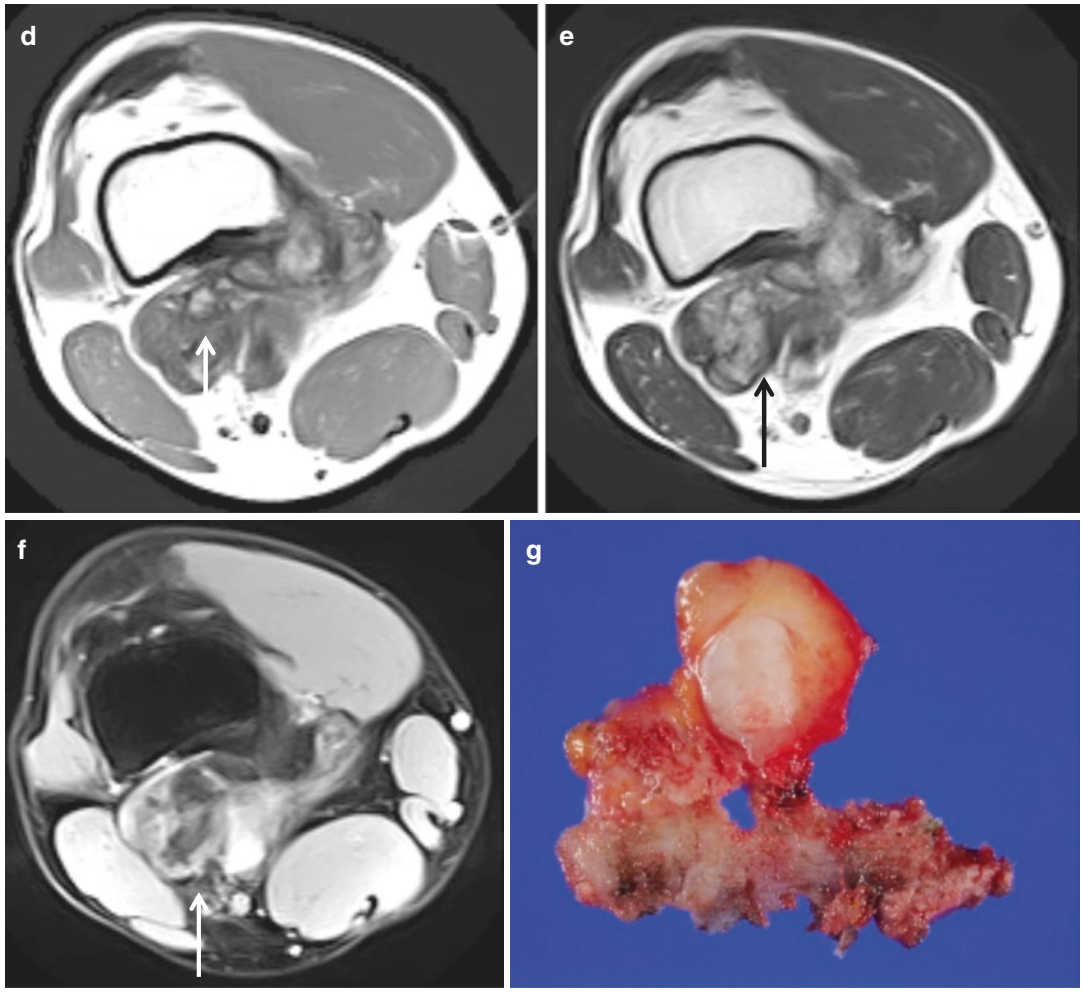

Fig. 2.20 (continued)

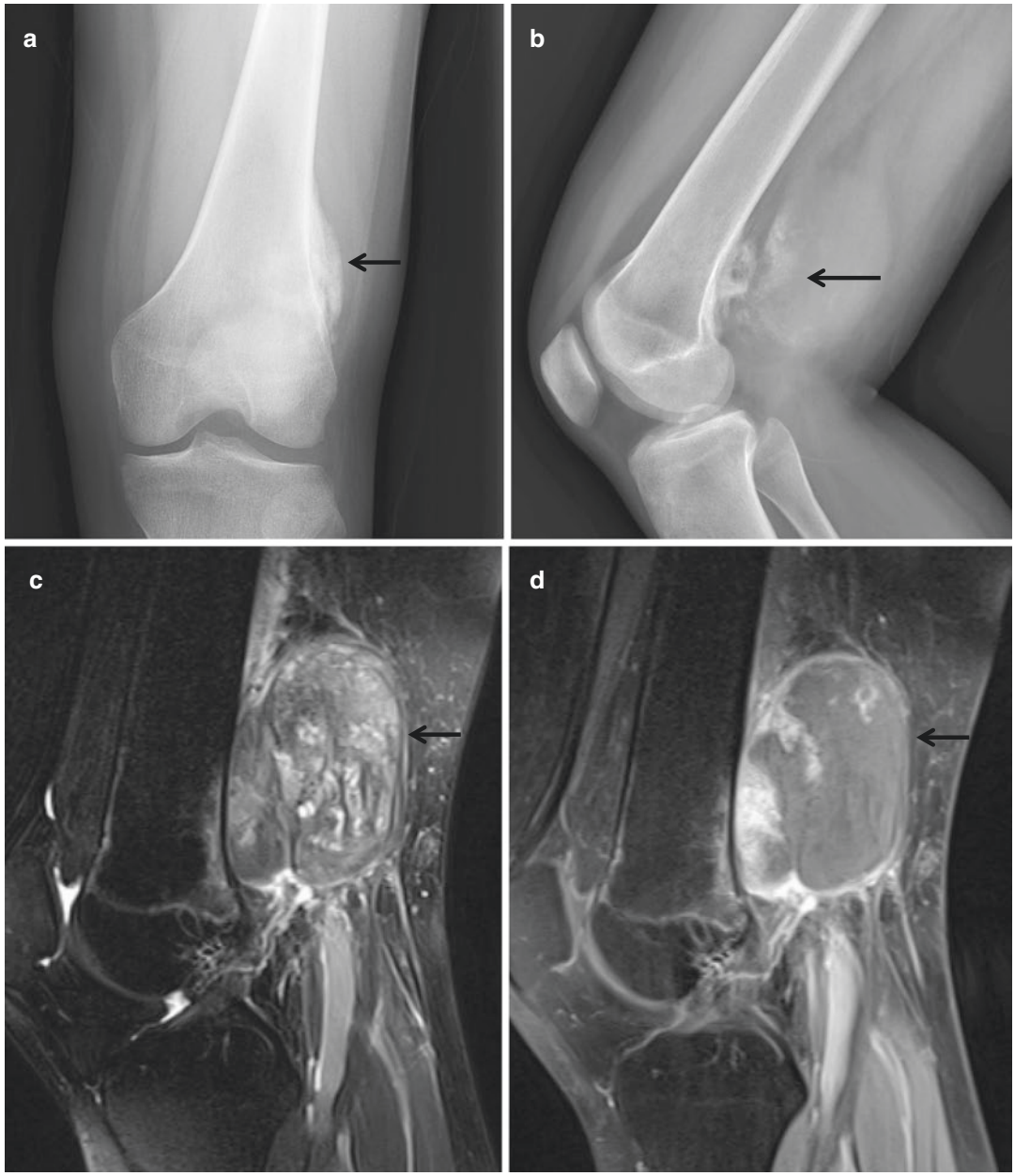

Fig. 2.21 Parosteal osteosarcoma. (**a**) Anteroposterior radiograph of the left femur shows a juxtacortical ossific mass (*arrow*). (**b**) Lateral radiograph of the left femur shows a lobulated and exophytic juxtacortical ossific mass (*arrow*). (**c**) Sagittal fat-suppressed T2-weighted MR image demonstrates exophytic mass with heterogeneous signal intensity (*arrow*). (**d**) Sagittal fat-suppressed contrast-enhanced T1-weighted MR image demonstrates peripheral enhancement of the mass (*arrow*). (**e**) Axial fat-suppressed T1-weighted MR image demonstrates exophytic mass with heterogeneous intermediate signal intensity (*arrow*). (**f**) Axial fat-suppressed T2-weighted MR image demonstrates heterogeneous signal intensity of the mass with scattered hypointense foci representing mineralized components (*arrow*). (**g**) Axial fat-suppressed contrast-enhanced T1-weighted MR image demonstrates exophytic mass with peripheral enhancement (*arrow*). (**h**) Corresponding gross photograph shows the exophytic mass with fibrous capsule and whirling pattern

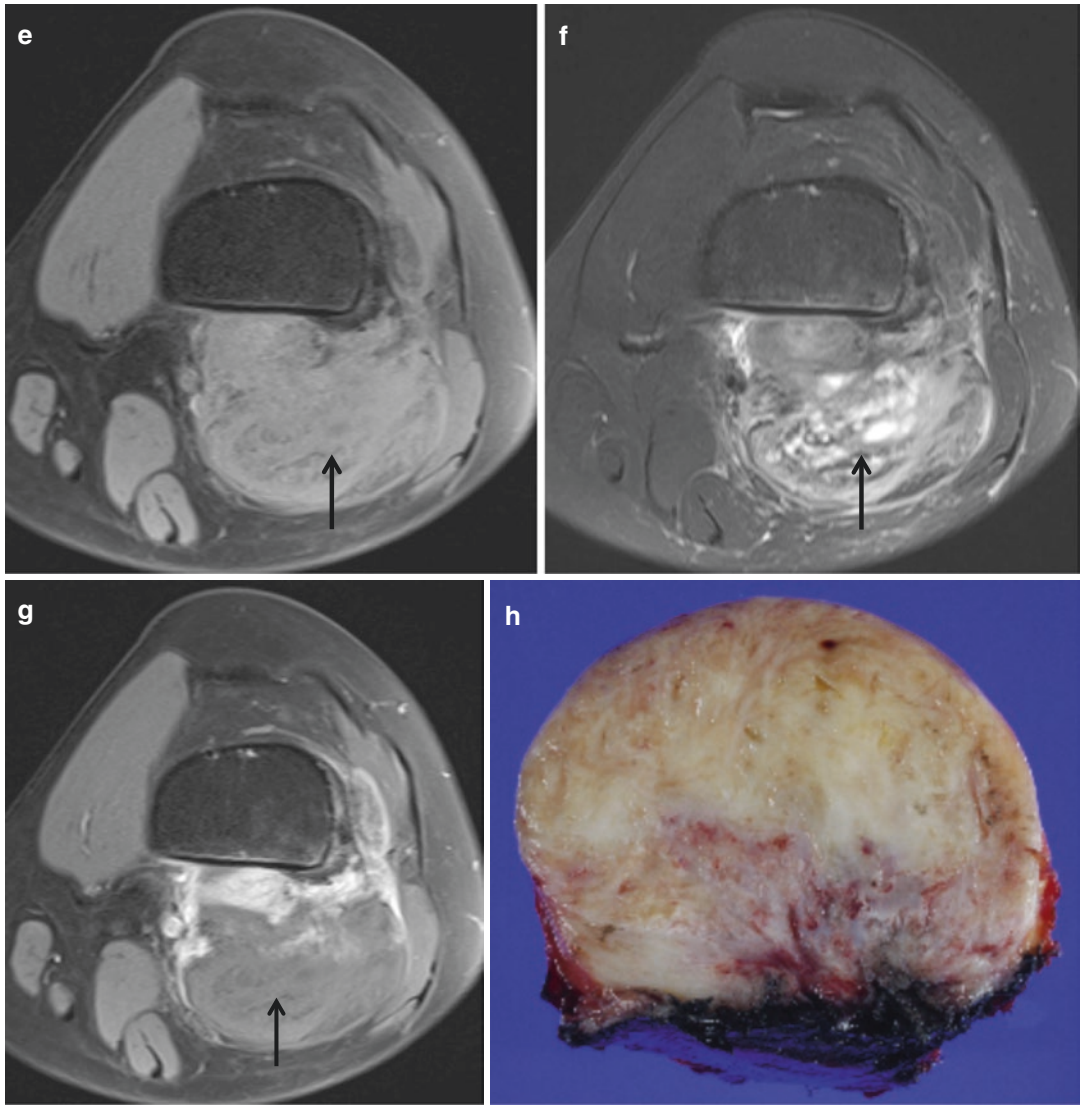

Fig. 2.21 (continued)

2.5.6 Periosteal Osteosarcoma

Overview

Periosteal osteosarcoma is an intermediate-grade tumor that originates from the deep periosteal layer. Periosteal osteosarcoma is predominantly chondroblastic with small areas of osteoid. The prognosis for periosteal osteosarcoma is better than that for conventional osteosarcoma, but worse than that for parosteal osteosarcoma.

Epidemiology

Periosteal osteosarcoma, which accounts for 25 % of juxtacortical osteosarcomas, is commonly seen in the second and third decades, and has a slight male preponderance.

Common Locations

Periosteal osteosarcoma most commonly occurs in the diaphysis or metadiaphysis and involves 50 % of the osseous circumference. This condition most commonly affects the tibia and femur, followed by the ulna and humerus. Femoral periosteal osteosarcoma is usually located in the anterior, lateral, or medial portion of the bone.

Imaging Features

Radiograph

A broad-based soft tissue mass with perpendicular periosteal reaction is seen on the surface of the bone (Fig. 2.22), with cortical scalloping, cortical thickening, and Codman triangle occurring at the upper or lower margins. Because these lesions are pathologically chondroblastic, matrix ossification is not distinctly seen. Periosteal osteosarcoma involves 50 % of the osseous circumference.

Magnetic resonance imaging

The predominantly chondroid matrix of this tumor shows low signal intensity on T1-weighted images and high signal intensity on T2-weighted images, with smaller foci of low signal intensity representing calcified matrix. Perpendicular periosteal reaction is seen as rays of low signal intensity on all MR imaging sequences. Invasion of the marrow is rare; when seen, it is contiguous with the surface mass. However, reactive changes in the marrow occur in more than 50 % of cases, appearing as low signal intensity on T1-weighted images and as high signal intensity on T2-weighted images.

Differential Diagnoses

1. Parosteal osteosarcoma

   Parosteal osteosarcoma is a densely ossified juxtacortical mass that lies outside the cortex and occurs in metaphyses, whereas periosteal osteosarcoma is usually more lytic in appearance, causing cortical erosion and periosteal reaction, and occurs in diaphyses.
2. High-grade surface osteosarcoma

   High-grade surface osteosarcoma often involves the entire circumference of the cortex and is more likely to show medullary invasion.

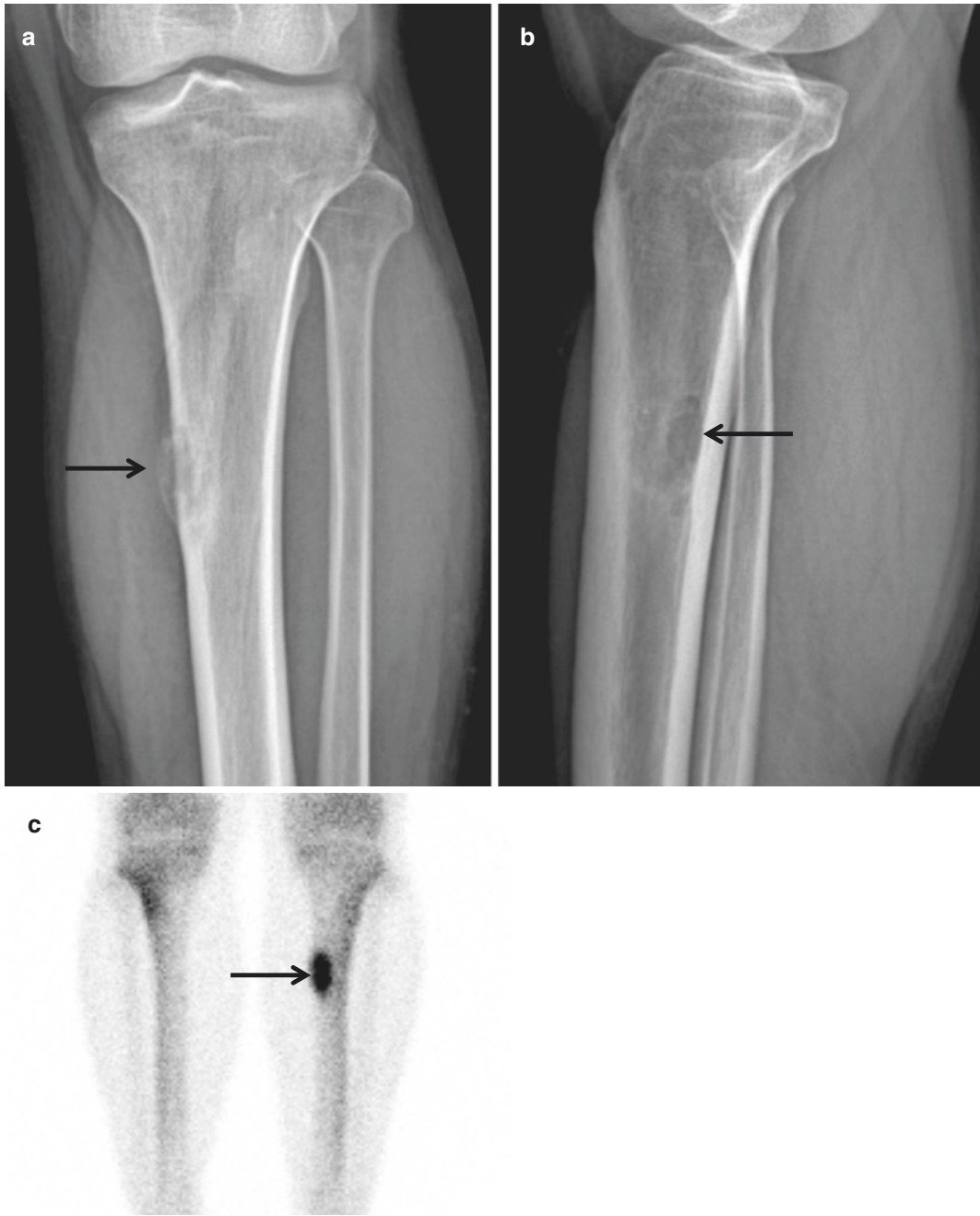

Fig. 2.22 Periosteal osteosarcoma. (**a**) Anteroposterior radiograph of the left lower leg shows an osteolytic lesion with cortical scalloping and periosteal reaction (*arrow*) in the left tibia. (**b**) Lateral radiograph of the left lower leg again demonstrates an osteolytic lesion (*arrow*). (**c**) Bone scan shows a focal increased uptake (*arrow*) in the left tibia. (**d**) Axial T1-weighted MR image demonstrates a juxtacortical mass with intramedullary extension (*arrow*). (**e**) Axial fat-suppressed T2-weighted MR image demonstrates a heterogeneous signal intensity (*arrow*) of the lesion. (**f**) Axial fat-suppressed contrast-enhanced T1-weighted MR image demonstrates an enhancing juxtacortical mass with intramedullary extension (*arrow*). (**g**) Coronal T1-weighted MR image demonstrates a juxtacortical mass with intramedullary extension (*arrow*). (**h**) Coronal T2-weighted MR image demonstrates a heterogeneous signal intensity (*arrow*) of the lesion. (**i**) Coronal fat-suppressed contrast-enhanced T1-weighted MR image demonstrates an enhancing juxtacortical mass with intramedullary extension (*arrow*). (**j**, **k**) Corresponding gross photographs show a hemorrhagic and necrotic juxtacortical mass with intramedullary extension

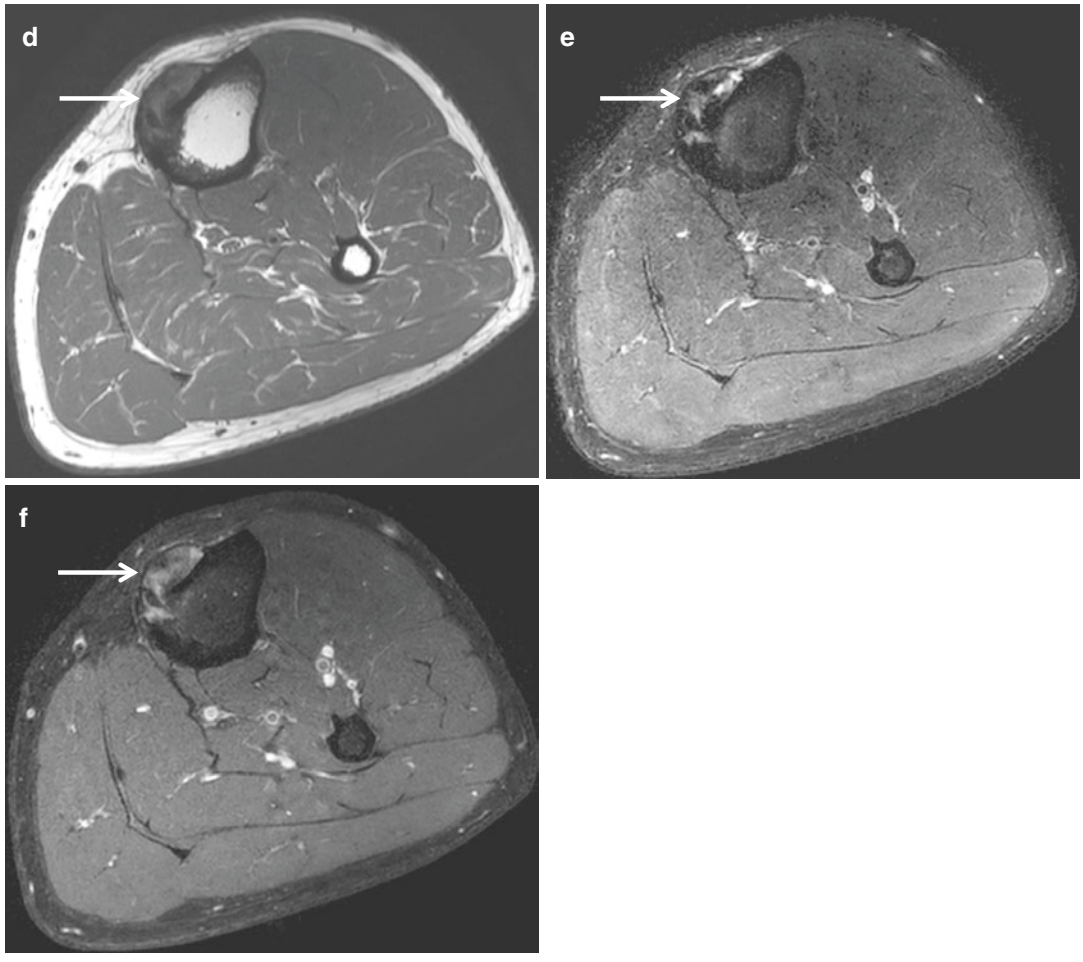

Fig. 2.22 (continued)

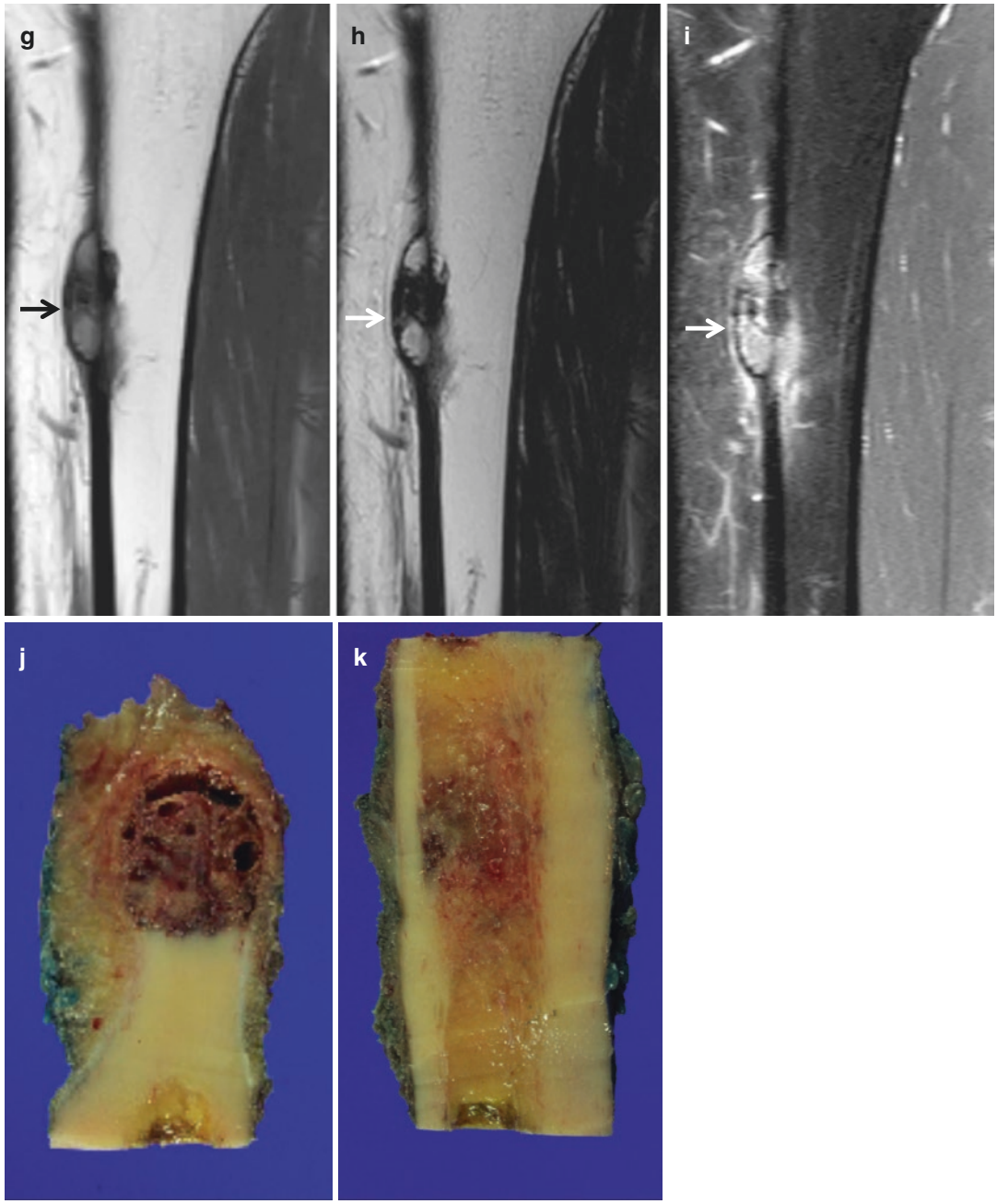

Fig. 2.22 (continued)

2.5.7 High-Grade Surface Osteosarcoma

Overview

High-grade surface osteosarcoma is pathologically similar to conventional intramedullary osteosarcomas. The tumor is usually large, ranging from 4.5 to 22 cm. The prognosis for high-grade surface osteosarcoma was initially considered worse than that for other types of juxtacortical osteosarcomas and similar to that for conventional osteosarcoma; however, more recent studies have shown an improved prognosis that is better than that for conventional osteosarcoma, probably due to aggressive chemotherapy and surgical resection.

Epidemiology

High-grade surface osteosarcoma is less frequently encountered than parosteal and periosteal osteosarcoma, and accounts for 10 % of juxtacortical osteosarcomas. High-grade surface osteosarcoma is more common in the second and third decades, and has a male predominance.

Common Locations

High-grade surface osteosarcoma affects the diaphysis and metaphysis of long bones, such as the femur, humerus, and fibula, with the femur being the most common site.

Imaging Features

Radiograph

High-grade surface osteosarcoma appears similar to periosteal osteosarcoma, but involves the entire circumference of the bone and may invade the medullary cavity. Dense ossification and periosteal reaction are seen in the majority of cases. Cortical erosion and thickening are also seen frequently.

Magnetic resonance imaging

The predominantly chondroid matrix of this tumor shows low signal intensity on T1-weighted images and high signal intensity on T2-weighted images, with smaller foci of low signal intensity representing calcified matrix. Perpendicular periosteal reaction is seen as rays of low signal intensity on all MR imaging sequences. Invasion of the marrow is rare; when seen, it is contiguous with the surface mass. However, reactive changes in the marrow occur in more than 50 % of cases, appearing as low signal intensity on T1-weighted images and as high signal intensity on T2-weighted images.

Differential Diagnoses

1. Juxtacortical osteosarcomas including parosteal osteosarcoma, periosteal osteosarcoma

   Circumferential bone involvement can be more extensive in high-grade surface osteosarcoma than in other forms of juxtacortical osteosarcomas.
2. Conventional osteosarcoma

   When medullary invasion is a prominent feature, it may be difficult to distinguish this tumor from conventional osteosarcoma with a large extraosseous component.

Suggested Reading

Osteoma

Gardner EJ, Richards RC. Multiple cutaneous and subcutaneous lesions occurring simultaneously with hereditary polyposis and osteomatosis. Am J Hum Genet. 1953;5:139–47.

Greenspan A. Benign bone-forming lesions: osteoma, osteoid osteoma, and osteoblastoma. Clinical, imaging, pathologic, and differential considerations. Skelet Radiol. 1993;22:485–500.

Kransdorf MJ, Murphey MD. Osseous tumors. In: Davies AM, Sundaram M, James SLJ, editors. Imaging of bone tumors and tumor-like lesions: techniques and applications. 1st ed. Berlin: Springer; 2009. p. 251–306.

Motamedi K, Seeger LL. Benign bone tumors. Radiol Clin N Am. 2011;49:1115–34.

Resnick D, Kyriakos M, Greenway GD. Enostosis, hyperostosis, and periostitis. In: Resnick D, editor. Diagnosis of bone and joint disorders. 4th ed. Philadelphia: Saunders; 2002. p. 4844–919.

Seeger LL, Yao L, Eckardt JJ. Surface lesions of bone. Radiology. 1998;206:17–33.

Sundaram M, Falbo S, McDonald D, Janney C. Surface osteomas of the appendicular skeleton. AJR Am J Roentgenol. 1996;167:1529–33.

Bone Islands

Cerase A, Priolo F. Skeletal benign bone-forming lesions. Eur J Radiol. 1998;27(Suppl 1):S91–-7.

Greenspan A. Bone island (enostosis): current concept: a review. Skelet Radiol. 1995;24:111–5.

Ihde LL, Forrester DM, Gottsegen CJ, Masih S, Patel DB, Vachon LA, White EA, Matcuk Jr GR. Sclerosing bone dysplasias: review and differentiation from other causes of osteosclerosis. Radiographics. 2011;31:1865–82.

Kransdorf MJ, Murphey MD. Osseous tumors. In: Davies AM, Sundaram M, James SLJ, eds. Imaging of bone tumors and tumor-like lesions: techniques and applications. 1st ed. Berlin: Springer; 2009. p. 251–306.

Motamedi K, Seeger LL. Benign bone tumors. Radiol Clin N Am. 2011;49:1115–34.

Schweitzer ME, Levine C, Mitchell DG, Gannon FH, Gomella LG. Bull's-eyes and halos: useful MR discriminators of osseous metastases. Radiology. 1993;188:249–52.

Osteoid Osteoma

Cerase A, Priolo F. Skeletal benign bone-forming lesions. Eur J Radiol. 1998;27(Suppl 1):S91–7.

Kayser F, Resnick D, Haghighi P, Pereira Edo R, Greenway G, Schweitzer M, Kindynis P. Evidence of the subperiosteal origin of osteoid osteomas in tubular bones: analysis by CT and MR imaging. AJR Am J Roentgenol. 1998;170:609–14.

Kenan S, Abdelwahab IF, Klein MJ, Hermann G, Lewis MM. Lesions of juxtacortical origin (surface lesions of bone). Skelet Radiol. 1993;22:337–57.

Kransdorf MJ, Murphey MD. Osseous tumors. In: Davies AM, Sundaram M, James SLJ, editors. Imaging of bone tumors and tumor-like lesions: techniques and applications. 1st ed. Berlin: Springer; 2009. p. 251–306.

Motamedi K, Seeger LL. Benign bone tumors. Radiol Clin N Am. 2011;49:1115–34.

Nichols RE, Dixon LB. Radiographic analysis of solitary bone lesions. Radiol Clin N Am. 2011;49:1095–114.

Seeger LL, Yao L, Eckardt JJ. Surface lesions of bone. Radiology. 1998;206:17–33.

Osteoblastoma

Crim JR, Mirra JM, Eckardt JJ, Seeger LL. Widespread inflammatory response to osteoblastoma: the flare phenomenon. Radiology. 1990;177:835–6.

Greenspan A. Benign bone-forming lesions: osteoma, osteoid osteoma, and osteoblastoma. Clinical, imaging, pathologic, and differential considerations. Skelet Radiol. 1993;22:485–500.

Kransdorf MJ, Murphey MD. Osseous tumors. In: Davies AM, Sundaram M, James SLJ, eds. Imaging of bone tumors and tumor-like lesions: techniques and applications. 1st ed. Berlin: Springer; 2009. p. 251–306.

Motamedi K, Seeger LL. Benign bone tumors. Radiol Clin N Am. 2011;49:1115–34.

Nichols RE, Dixon LB. Radiographic analysis of solitary bone lesions. Radiol Clin N Am. 2011;49:1095–114.

Malignant

Czerniak B. Osteosarcoma. In: Czerniak B, ed. Dorfman and Czerniak's bone tumors. 2nd ed. Philadelphia: Elsevier Saunders; 2016. p. 200–355.

Kransdorf MJ, Murphey MD. Osseous tumors. In: Davies AM, Sundaram M, James SLJ, eds. Imaging of bone tumors and tumor-like lesions: techniques and applications. 1st ed. Berlin: Springer; 2009. p. 251–306.
Nichols RE, Dixon LB. Radiographic analysis of solitary bone lesions. Radiol Clin N Am. 2011;49:1095–114.
Rajiah P, Ilaslan H, Sundaram M. Imaging of primary malignant bone tumors (nonhematological). Radiol Clin N Am. 2011;49:1135–61.
Yarmish G, Klein MJ, Landa J, Lefkowitz RA, Hwang S. Imaging characteristics of primary osteosarcoma: nonconventional subtypes. Radiographics. 2010;30: 1653–72.

Conventional Osteosarcoma

Czerniak B.. Osteosarcoma. In: Czerniak B editor. Dorfman and Czerniak's bone tumors. 2nd ed. Philadelphia: Elsevier Saunders; 2016. p. 200–355.
Greene FL, Page DL, Fleming ID, Fritz AG, Balch CM, Haller OG, Morrow M. AJCC cancer staging manual. Berlin Heidelberg New York: Springer; 2002.
Kager L, Zoubek A, Kastner U, Kempf-Bielack B, Potratz J, Kotz R, Exner GU, Franzius C, Lang S, Maas R, Jürgens H, Gadner H, Bielack S. Skip metastases in osteosarcoma: experience of the Cooperative Osteosarcoma Study Group. J Clin Oncol. 2006;24:1535–41.
Kaste SC. Imaging pediatric bone sarcomas. Radiol Clin N Am. 2011;49:749–65.
Kransdorf MJ, Murphey MD. Osseous tumors. In: Davies AM, Sundaram M, James SLJ, eds. Imaging of bone tumors and tumor-like lesions: techniques and applications. 1st ed. Berlin: Springer; 2009. p. 251–306.
Nichols RE, Dixon LB. Radiographic analysis of solitary bone lesions. Radiol Clin N Am. 2011;49:1095–114.
Rajiah P, Ilaslan H, Sundaram M. Imaging of primary malignant bone tumors (nonhematological). Radiol Clin N Am. 2011;49:1135–61.
Schima W, Amann G, Stiglbauer R, Windhager R, Kramer J, Nicolakis M, Farres MT, Imhof H. Preoperative staging of osteosarcoma: efficacy of MR imaging in detecting joint involvement. AJR Am J Roentgenol. 1994;163:1171–5.
Yarmish G, Klein MJ, Landa J, Lefkowitz RA, Hwang S. Imaging characteristics of primary osteosarcoma: nonconventional subtypes. Radiographics. 2010;30:1653–72.

Telangiectatic Osteosarcoma

Czerniak B. Osteosarcoma. In: Czerniak B, ed. Dorfman and Czerniak's bone tumors. 2nd ed. Philadelphia: Elsevier Saunders; 2016. p. 200–355.
Kransdorf MJ, Murphey MD. Osseous tumors. In: Davies AM, Sundaram M, James SLJ, eds. Imaging of bone tumors and tumor-like lesions: techniques and applications. 1st ed. Berlin: Springer; 2009. p. 251–306.
Rajiah P, Ilaslan H, Sundaram M. Imaging of primary malignant bone tumors (nonhematological). Radiol Clin N Am. 2011;49:1135–61.
Yarmish G, Klein MJ, Landa J, Lefkowitz RA, Hwang S. Imaging characteristics of primary osteosarcoma: nonconventional subtypes. Radiographics. 2010;30:1653–72.

Small Cell Osteosarcoma

Czerniak B.. Osteosarcoma. In: Czerniak B, ed. Dorfman and Czerniak's bone tumors. 2nd ed. Philadelphia: Elsevier Saunders; 2016. p. 200–355.
Kransdorf MJ, Murphey MD. Osseous tumors. In: Davies, AM, Sundaram M, James, SLJ, eds. Imaging of bone tumors and tumor-like lesions: techniques and applications. 1st ed. Berlin: Springer; 2009. p. 251–306.
Rajiah P, Ilaslan H, Sundaram M. Imaging of primary malignant bone tumors (nonhematological). Radiol Clin N Am. 2011;49:1135–61.
Yarmish G, Klein MJ, Landa J, Lefkowitz RA, Hwang S. Imaging characteristics of primary osteosarcoma: nonconventional subtypes. Radiographics. 2010;30:1653–72.

Parosteal Osteosarcoma

Bertoni F, Bacchini P, Staals EL, Davidovitz P. Dedifferentiated parosteal osteosarcoma: the experience of the Rizzoli Institute. Cancer. 2005;103:2373–82.
Czerniak B.. Osteosarcoma. In: Czerniak B, ed. Dorfman and Czerniak's bone tumors. 2nd ed. Philadelphia: Elsevier Saunders; 2016. p. 200–355.
Kenan S, Abdelwahab IF, Klein MJ, Hermann G, Lewis MM. Lesions of juxtacortical origin (surface lesions of bone). Skelet Radiol. 1993;22:337–57.
Kransdorf MJ, Murphey MD. Osseous tumors. In: Davies AM, Sundaram M, James SLJ, eds. Imaging of bone tumors and tumor-like lesions: techniques and applications. 1st ed. Berlin: Springer; 2009. p. 251–306.
Rajiah P, Ilaslan H, Sundaram M. Imaging of primary malignant bone tumors (nonhematological). Radiol Clin N Am. 2011;49:1135–61.
Seeger LL, Yao L, Eckardt JJ. Surface lesions of bone. Radiology. 1998;206:17–33.
Yarmish G, Klein MJ, Landa J, Lefkowitz RA, Hwang S. Imaging characteristics of primary osteosarcoma: nonconventional subtypes. Radiographics. 2010;30:1653–72.

Periosteal Osteosarcoma

Czerniak B.. Osteosarcoma. In: Czerniak B, ed. Dorfman and Czerniak's bone tumors. 2nd ed. Philadelphia: Elsevier Saunders; 2016. p. 200–355.

Kenan S, Abdelwahab IF, Klein MJ, Hermann G, Lewis MM. Lesions of juxtacortical origin (surface lesions of bone). Skelet Radiol. 1993;22:337–57.

Kransdorf MJ, Murphey MD. Osseous tumors. In: Davies AM, Sundaram M, James SLJ, eds. Imaging of bone tumors and tumor-like lesions: techniques and applications. 1st ed. Berlin: Springer; 2009. p. 251–306.

Rajiah P, Ilaslan H, Sundaram M. Imaging of primary malignant bone tumors (nonhematological). Radiol Clin N Am. 2011;49:1135–61.

Seeger LL, Yao L, Eckardt JJ. Surface lesions of bone. Radiology. 1998;206:17–33.

Yarmish G, Klein MJ, Landa J, Lefkowitz RA, Hwang S. Imaging characteristics of primary osteosarcoma: nonconventional subtypes. Radiographics. 2010;30: 1653–72.

High-Grade Surface Osteosarcoma

Czerniak B. Osteosarcoma. In: Czerniak B, ed. Dorfman and Czerniak's bone tumors. 2nd ed. Philadelphia: Elsevier Saunders; 2016:200–355.

Kenan S, Abdelwahab IF, Klein MJ, Hermann G, Lewis MM. Lesions of juxtacortical origin (surface lesions of bone). Skelet Radiol. 1993;22:337–57.

Kransdorf MJ, Murphey MD. Osseous tumors. In: Davies AM, Sundaram M, James SLJ, editors. Imaging of bone tumors and tumor-like lesions: techniques and applications. 1st ed. Berlin: Springer; 2009. p. 251–306.

Rajiah P, Ilaslan H, Sundaram M. Imaging of primary malignant bone tumors (nonhematological). Radiol Clin N Am. 2011;49:1135–61.

Seeger LL, Yao L, Eckardt JJ. Surface lesions of bone. Radiology. 1998;206:17–33.

Yarmish G, Klein MJ, Landa J, Lefkowitz RA, Hwang S. Imaging characteristics of primary osteosarcoma: nonconventional subtypes. Radiographics. 2010;30: 1653–72.

Chondrogenic Tumors

3

Contents

3.1 Osteochondroma

Overview

Osteochondroma is a surface lesion composed of lamellar bone covered by a cartilage cap (Fig. 3.1). Clinically, it presents most commonly as painless swelling and cosmetic deformity. Further clinical presentation may include neurovascular impingement, fracture, overlying bursal or pseudoaneurysm development, and malignant transformation (Fig. 3.2). The younger the patient, the closer the lesion will be to the growth plate. Osteochondroma ceases to grow by the time the physis closes, and the cartilage cap usually involutes after skeletal maturity. This lesion is usually classified as a neoplasm, but it is generally believed that it occurs as a result of physeal cartilage displacement onto the bone surface. If the lesion is asymptomatic, it can be followed radiographically and clinically until cessation of growth.

A benign osteochondroma may become painful for a number of reasons, including fracture through the stalk, development of an overlying bursa, or compression of adjacent neurovascular bundle.

Epidemiology

Osteochondroma is the most common benign bone tumor. There is a male predominance, and 75 % of patients are younger than 20 years of age.

H.S. Kang et al., *Oncologic Imaging: Bone Tumors*, DOI 10.1007/978-981-287-703-1_3

Common Locations

Osteochondroma can arise from any bone undergoing enchondral maturation, but it is most common in tubular bones and in particular around the knee. The ilium and scapula are the two most commonly affected flat bones. In long bones, it is located at the metaphysis and grows away from the joint.

Imaging Features

Radiograph

Osteochondroma is a surface lesion that demonstrates corticomedullary continuity (Fig. 3.3). It may be on a stalk (pedunculated) (Fig. 3.4) or broad based (sessile) (Fig. 3.5). The osteochondroma can usually be diagnosed with radiography alone.

Magnetic resonance imaging

MR imaging may demonstrate a cartilage cap. After skeletal maturity, the cartilage cap should not be thicker than 2 cm; if it is, then transformation to chondrosarcoma should be considered. MR imaging aids in distinguishing bursa formation over the cap from the actual cap. Cartilage cap growth after skeletal maturity and pain are worrisome for malignant transformation.

Differential Diagnoses

1. Parosteal osteosarcoma

   Osteochondromatous lesions in the popliteal fossa should be differentiated from parosteal osteosarcoma. Round-shaped parosteal osteosarcoma may mimic a densely calcified osteochondroma.

2. Osteoma

   Osteoma is a small, round, well-defined, homogeneous, bony surface lesion arising from the cortex and does not demonstrate the corticomedullary continuity seen in an osteochondroma.

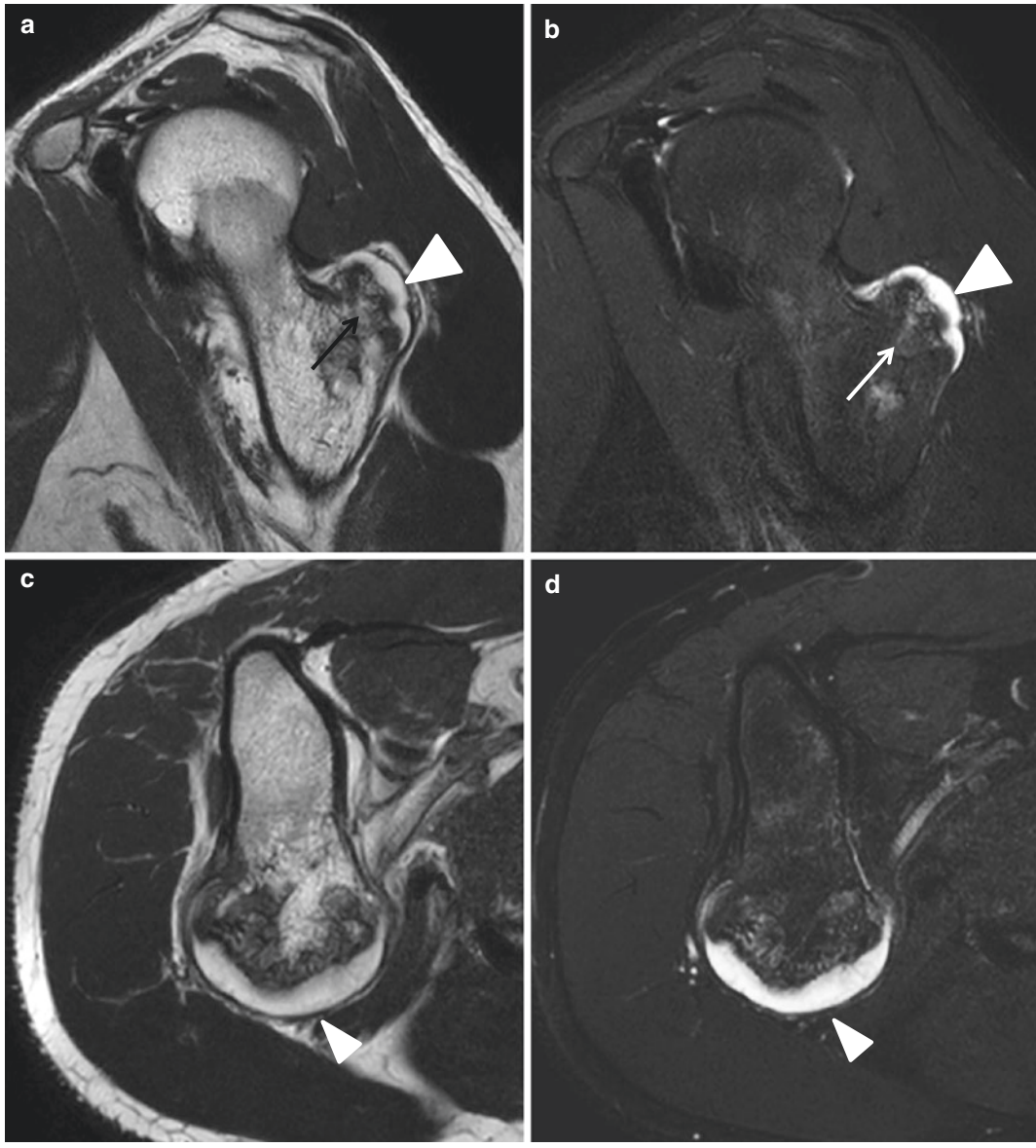

Fig. 3.1 Osteochondroma. (**a**) Sagittal T2-weighted MR image shows a surface lesion composed of lamellar bone (*arrow*) covered by a cartilage cap (*arrowhead*). (**b**) Sagittal fat-suppressed T2-weighted MR image demonstrates a surface lesion composed of lamellar bone (*arrow*) covered by a cartilage cap (*arrowhead*). (**c**) Axial T2-weighted MR image shows an osteochondroma with hyperintense cartilage cap (*arrowhead*). (**d**) Axial fat-suppressed T2-weighted MR image demonstrates an osteochondroma with hyperintense cartilage cap (*arrowhead*)

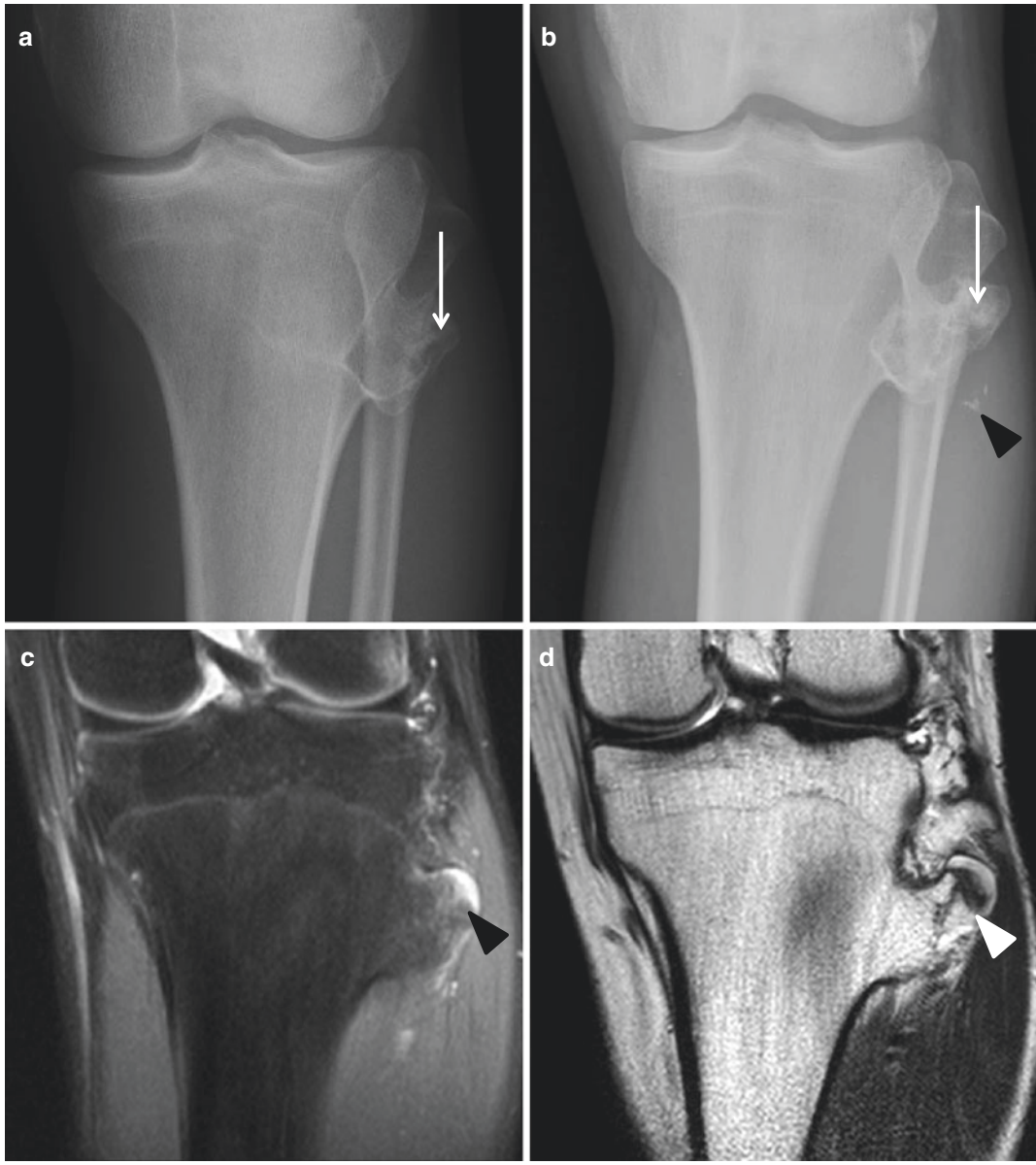

Fig. 3.2 Malignant transformation of osteochondroma. (**a**) Anteroposterior radiograph of the left knee shows a pedunculated bony protrusion (*arrow*) arising from the left proximal tibia, representing an osteochondroma. (**b**) Four-year follow-up anteroposterior radiograph shows slightly increased size of the osseous protrusion (*arrow*) with adjacent soft tissue mineralization (*arrowhead*). (**c**) Coronal fat-suppressed proton density-weighted MR image shows an osseous protrusion with hyperintense cartilage cap (*arrowhead*). (**d**) Coronal T2-weighted MR image again demonstrates an osseous protrusion with hyperintense cartilage cap (*arrowhead*). (**e**) Axial fat-suppressed proton density-weighted MR image shows an osseous protrusion with hyperintense cartilage cap (*arrowhead*). (**f**) Axial T2-weighted fat-suppressed MR image shows an osseous protrusion with hyperintense cartilage cap (*arrowhead*). (**g**) Corresponding gross photograph shows an osseous mass with thick cartilage cap. Histopathology showed a chondrosarcoma, grade 1

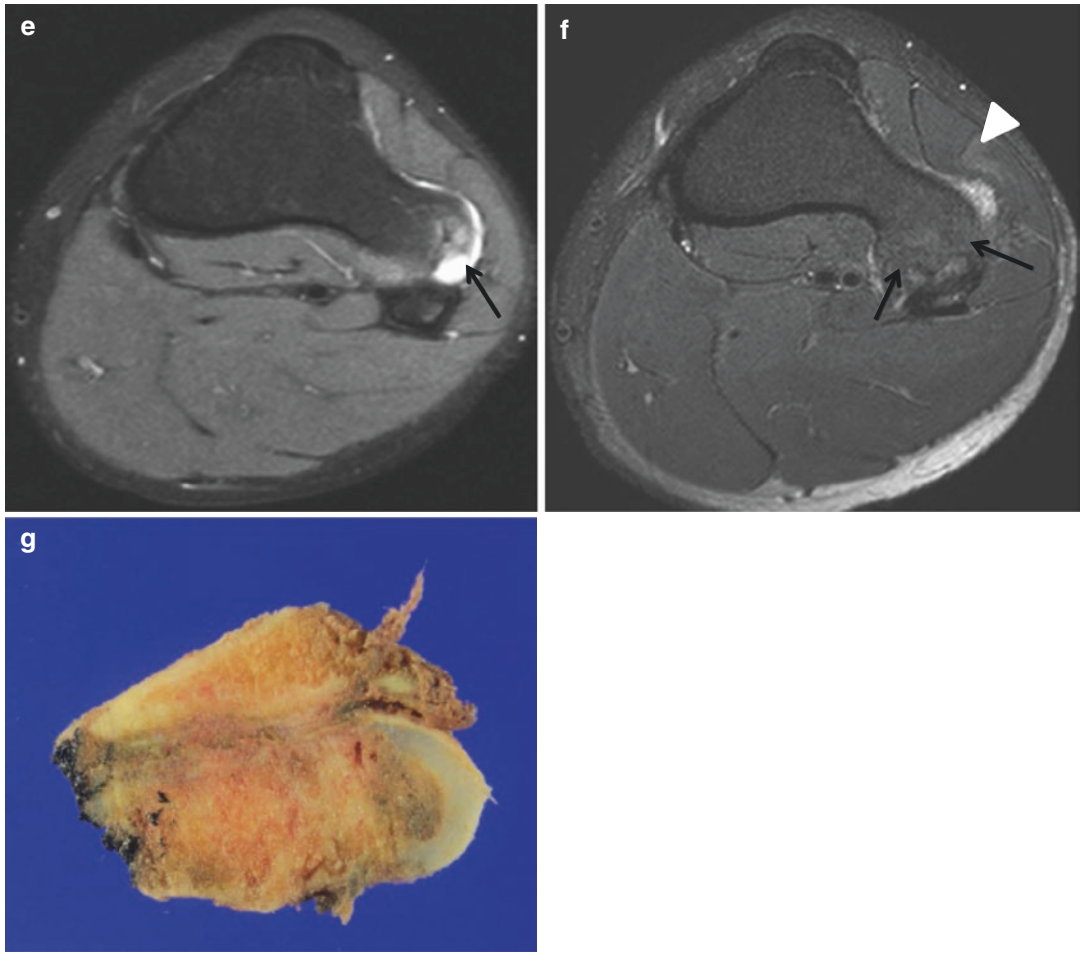

Fig. 3.2 (continued)

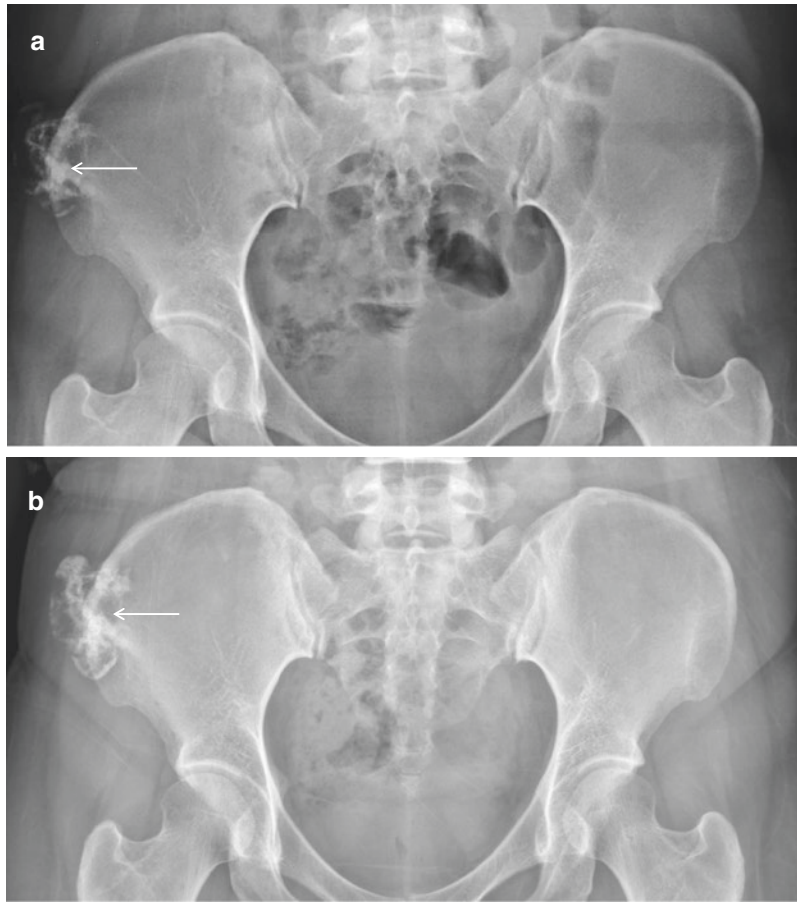

Fig. 3.3 Osteochondroma. (**a**) Anteroposterior radiograph of the pelvis shows a pedunculated osseous mass (*arrow*) with corticomedullary continuity, arising from the right ilium. (**b**) Four-year follow-up anteroposterior radiograph of the pelvis shows slightly increased size of the osteochondroma (*arrow*). Surgical resection was performed, and histopathology showed features of an osteochondroma without evidence of malignant transformation

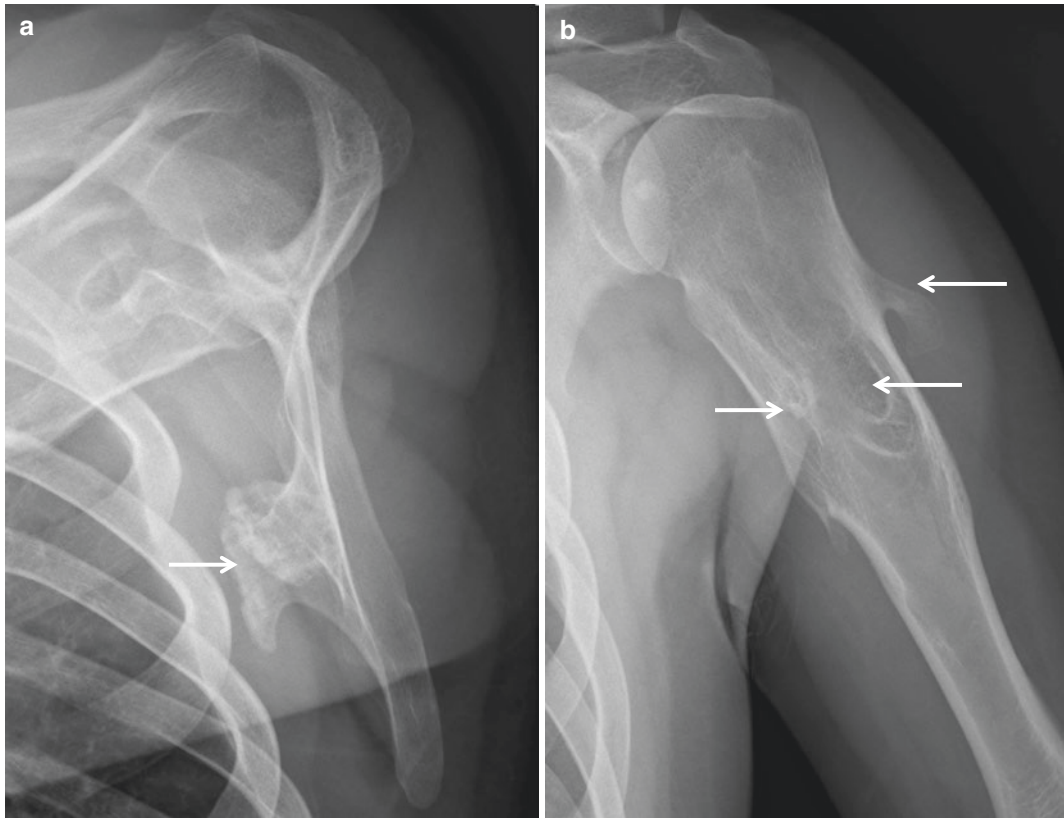

Fig. 3.4 Osteochondroma. (**a**) Lateral radiograph of the left scapula shows a pedunculated osseous mass (*arrow*) with corticomedullary continuity, representing osteochondroma. (**b**) Lateral radiograph of the left humerus demonstrates multiple osteochondromas (*arrows*). The osteochondromas point toward the diaphysis

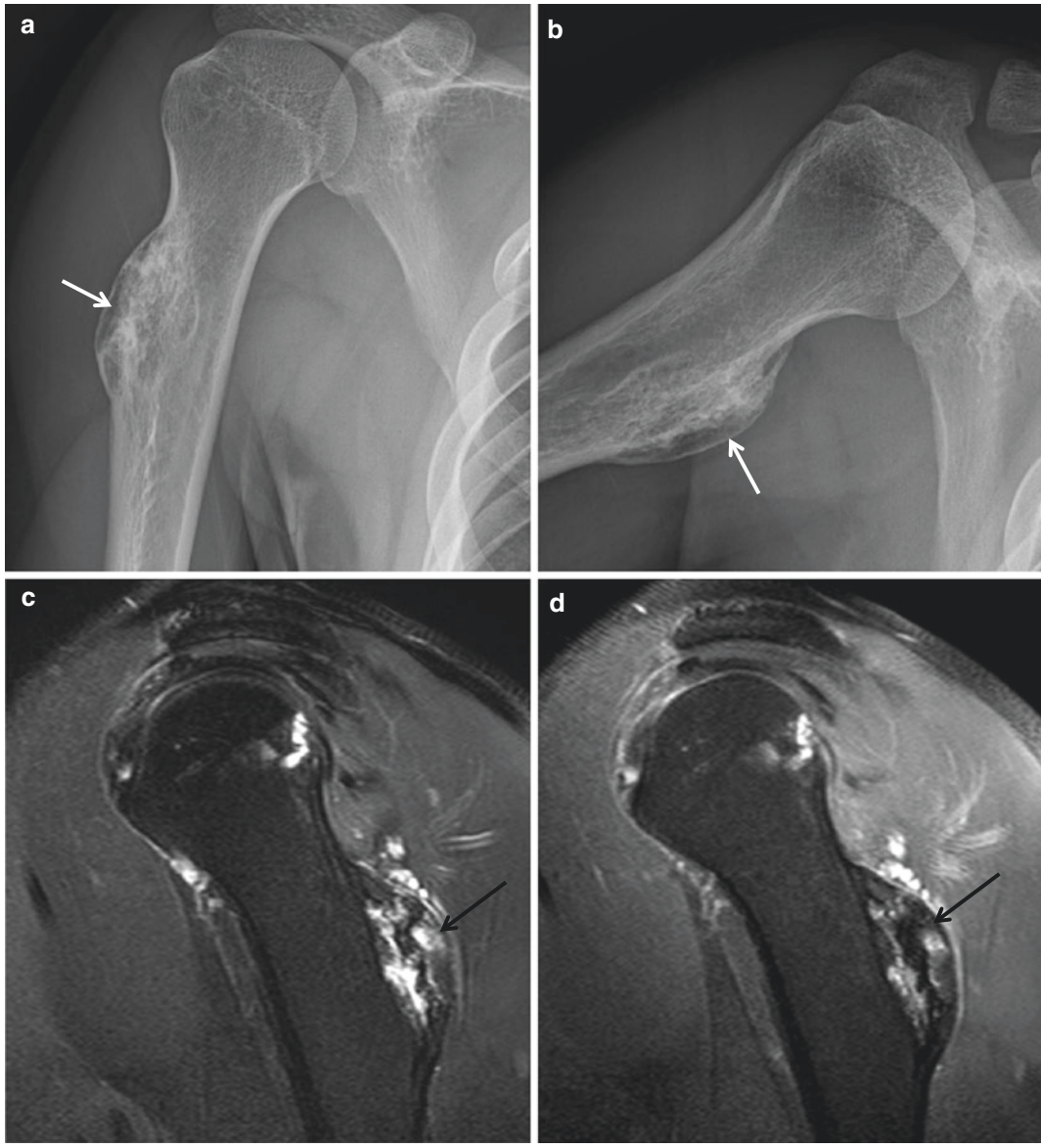

Fig. 3.5 Osteochondroma. (**a**) Anteroposterior radiograph of the right humerus shows sessile osteochondroma (*arrow*). (**b**) Lateral radiograph of the right humerus again shows sessile osteochondroma (*arrow*). (**c**) Sagittal T2-weighted fat-suppressed MR image shows a broad-based osseous protrusion (*arrow*) with hyperintense areas. (**d**) Sagittal fat-suppressed contrast-enhanced T1-weighted MR image shows a broad-based osseous protrusion (*arrow*) with areas of nodular enhancement

3.2 Enchondroma

Overview

Enchondroma is a benign cartilaginous tumor and is usually discovered either incidentally in long bones or when a pathological fracture occurs. Histologically, it is characterized by rests of hyaline cartilage within the medullary bone intermixed at times with a myxoid matrix.

Enchondroma may have a variable degree of amorphous matrix mineralization. These lesions may undergo a chondrosarcomatous transformation, presenting with a more destructive lytic lesion with a soft tissue mass. Multiple enchondromas can be seen in various syndromes. Ollier disease refers to multiple enchondromas in the appendicular skeleton, particularly the hands. Multiple hemangiomas and enchondromas are present in Maffucci syndrome. Both of these syndromes are associated with an increased rate of malignant transformation of enchondromas.

Epidemiology

Enchondroma is the second most common benign neoplasm of the bone and comprises 3–5 % of biopsied primary bone lesions. Enchondroma is encountered equally in men and women and has a peak incidence in the third decade.

Common Locations

It is common in the bones of the hand and feet and in long bones. Enchondroma occurs mostly as a central lesion in the metaphysis.

Imaging Features

Radiograph

Enchondroma appears as a well-marginated expansile lucent lesion (Fig. 3.6) arising in the medullary cavity, usually near the epiphysis. Chondroid mineralization (Fig. 3.7), including stippling, rings, and arcs calcification, develops in the matrix. Enchondroma is included in the differential diagnosis of lucent lesions, because it lacks matrix mineralization in the hands, where it most commonly occurs. The hand lesions are usually centrally located and can be expansile with associated cortical thickening and endosteal scalloping. This may lead to pathological fracture with minimal trauma. Enchondromas outside of the hands and feet often have a different, distinctive radiographic appearance because of the calcified chondroid matrix.

Magnetic resonance imaging

MR imaging can show typical lobular morphology and high signal intensity of the hyaline cartilage within the lesion on the fluid-sensitive sequences and scattered low signal intensity of chondroid mineralization (Fig. 3.7). Rings and arcs pattern of enhancement represents the fibrovascular septae between the cartilage lobules.

Differential Diagnoses

1. Bone infarct

   Unlike enchondroma, bone infarct has a well-defined shell-like peripheral sclerosis and does not show endosteal scalloping.
2. Chondrosarcoma

   Enchondromas are rare in the axial skeleton, talus, and calcaneus, whereas chondrosarcomas are rare in the short tubular bones. Large size, lesser extent of matrix mineralization within the lesion, greater depth and extent of endosteal scalloping, cortical penetration, periosteal reaction, cortical remodeling, soft tissue extension, and high uptake on bone scan can be suggestive of a chondrosarcoma.
3. Intraosseous ganglion

   An intraosseous ganglion appears radiographically as a well-defined lucency with a sclerotic margin adjacent to the articular surface. It most commonly involves the proximal tibia, proximal femur, and the medial malleolus.
4. Skeletal sarcoidosis

   Perivascular granulomatous infiltration of sarcoidosis in the Haversian canals of bone may destroy the fine trabeculae and produce a mottled or lacelike coarsely trabeculated pattern. This appears as single or multiple sharply circumscribed, punched-out areas of lucency, primarily involving the small bones of the hands and feet. There may be cortical thinning, expansion, or destruction.

Fig. 3.6 Enchondroma. (**a**) Posteroanterior radiograph of the right hand shows a lucent lesion with chondroid mineralization (*arrow*) in the proximal phalanx of the right third finger. (**b**) Oblique radiograph again demonstrates an intramedullary lesion with chondroid mineralization (*arrow*)

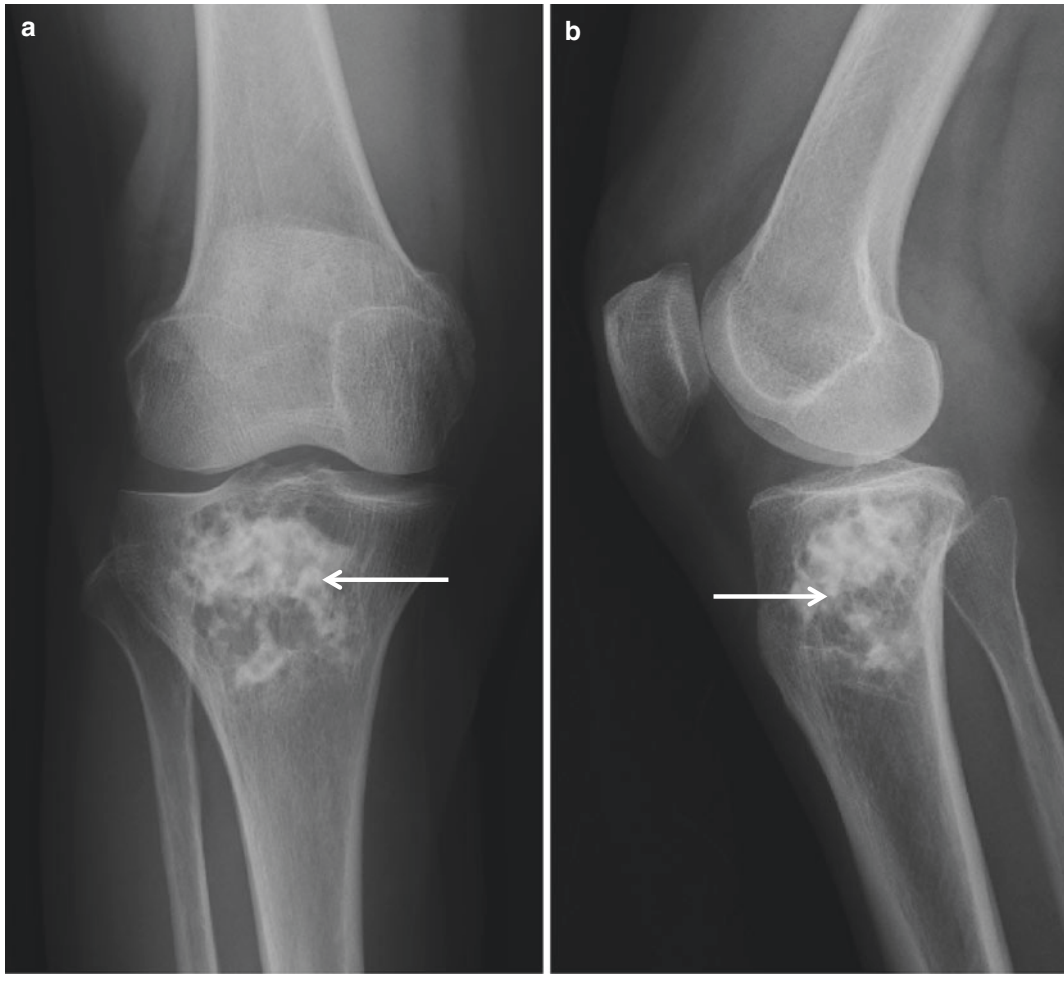

Fig. 3.7 Enchondroma. (**a**) Anteroposterior radiograph of the right knee shows a lucent lesion with stippled and flocculent mineralization (*arrow*) in the proximal tibia. (**b**) Lateral radiograph again demonstrates an intramedullary lesion with chondroid mineralization (*arrow*). (**c**) Sagittal T1-weighted MR image shows an intramedullary lesion with hypointense foci (*arrow*). (**d**) Coronal T2-weighted MR image again shows an intramedullary lesion with hypointense foci (*arrow*). (**e**) Coronal fat-suppressed contrast-enhanced T1-weighted MR image shows peripheral and nodular enhancement and persistent hypointense foci (*arrow*)

Fig. 3.7 (continued)

3.3 Periosteal Chondroma (Juxtacortical Chondroma)

Overview

Periosteal or juxtacortical chondroma represents the surface variant of an enchondroma and believed to originate from the periosteum. Periosteal or juxtacortical chondroma presents as focal swelling. Histologically, periosteal chondroma demonstrates lobules of hyaline cartilage limited to the cortex and beneath the periosteum without an extension into the medullary cavity. It grows slowly and ranges from 1 cm to 7 cm in size at presentation. Periosteal chondroma is usually a solitary lesion. Patients with more than one periosteal chondroma should be suspected of having Ollier disease.

Epidemiology

Periosteal chondroma is a lesion of children and young adults, and most patients are in their second through fourth decades of life. It is more prevalent among males.

Common Locations

Periosteal chondroma occurs in the surface of tubular bones, characteristically in the metaphysis. It is most common in the proximal humerus followed by the femur, tibia, short tubular bones of the hands and feet. Pelvis and ribs are uncommon sites.

Imaging Features

Radiograph

Periosteal chondromas present as lesions scalloping the cortex from the periosteal side and eventually forming a sclerotic rim separating them from the medullary cavity of the parent bone (Fig. 3.8). Saucerization or a well-defined depression of the adjacent cortex with a soft tissue mass can be seen. The lesion is sharply circumscribed by a solid buttress of reactive bone or overhanging cortical edges which may entirely cover the lesion. Periosteal chondromas may be purely lytic or may show internal chondroid mineralization.

Magnetic resonance imaging

Periosteal chondroma is typically multilobulated and shows a low signal intensity rim on MR imaging. MR imaging shows the high water content of the cartilage tissue (Fig. 3.8). Peritumoral edema is typically absent. Administration of contrast depicts peripheral enhancement. MR imaging also confirms the lack of communication of this lesion with the medullary canal.

Differential Diagnoses

1. Periosteal chondrosarcoma

   Periosteal chondrosarcoma usually presents later in life and demonstrates invasion of the medullary cavity and peritumoral edema. Periosteal chondrosarcomas are generally larger (>3 cm), may contain hazy windblown densities, and do not show an endosteal border of sclerosis.
2. Juxtacortical osteosarcoma

   Juxtacortical osteosarcoma is usually more aggressive, frequently with a pattern resembling a sunburst-type periosteal reaction, and may have an osteogenic matrix.
3. Chondromyxoid fibroma

   Chondromyxoid fibroma generally appears as an eccentric expansile metaphyseal osteolytic lesion with cortical expansion, coarse trabeculation, endosteal scalloping, and scalloped sclerotic medullary border.
4. Aneurysmal bone cyst

   Surface aneurysmal bone cysts show predominantly extraosseous extension with varying amounts of preservation of the inner cortex. Typically, a thin layer of inner cortex remains, and the lesion is surrounded by a radiographically visible shell of periosteal new bone.

Fig. 3.8 Periosteal chondroma. (**a**) Anteroposterior radiograph of the right fifth finger shows a well-defined osteolytic lesion (*arrow*) in the proximal phalanx with adjacent soft tissue mass (*arrowhead*). (**b**) Lateral radiograph demonstrates a saucerization of the volar cortex and a soft tissue mineralization (*arrow*). (**c**) Axial T1-weighted MR image shows a cortical-based periosteal mass that has intermediate signal intensity (*arrow*). (**d**) Axial T1-weighted MR image shows a cortical-based periosteal mass with increased signal intensity (*arrow*). (**e**) Axial fat-suppressed contrast-enhanced T1-weighted MR image demonstrates a cortical-based periosteal mass that shows heterogeneous enhancement (*arrow*). (**f**) Additional axial fat-suppressed contrast-enhanced T1-weighted MR image demonstrates a cortical-based periosteal mass that shows heterogeneous enhancement (*arrow*). (**g**) Coronal T1-weighted MR image shows a lobulated mass with intermediate signal intensity (*arrow*). (**h**) Coronal fat-suppressed contrast-enhanced T1-weighted MR image demonstrates a lobulated mass with peripheral enhancement (*arrow*). (**i**) Sagittal fat-suppressed contrast-enhanced T1-weighted MR image demonstrates a juxtacortical mass with heterogeneous enhancement (*arrow*). (**j**) Additional sagittal fat-suppressed contrast-enhanced T1-weighted MR image demonstrates a juxtacortical mass with heterogeneous enhancement (*arrow*)

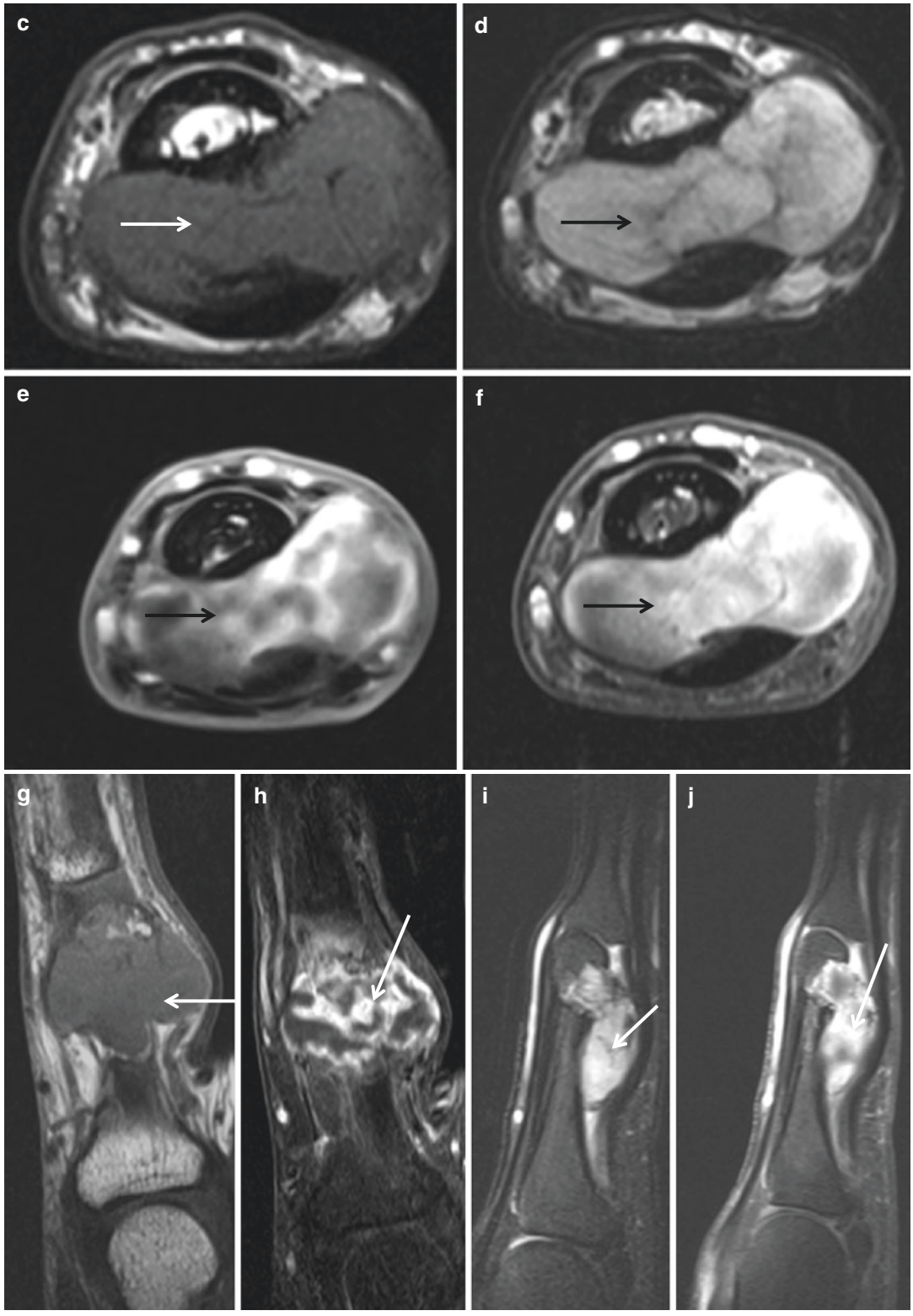

Fig. 3.8 (continued)

3.4 Chondromyxoid Fibroma

Overview

Chondromyxoid fibroma is composed of varying degrees of cartilaginous, fibrous, and myxoid components. It presents with swelling and may occasionally be painful.

Epidemiology

Chondromyxoid fibroma is the least common benign tumor of chondroid origin and <1 % of primary bone tumors. It has a slight male predilection. Most cases occur younger than age of 30, although it affects a wide range of age between 3 and 70 years.

Common Locations

It arises most often around the knee, with the proximal tibia as the single most common location. The foot and pelvic bones also are common sites. Chondromyxoid fibroma is usually located in the metaphysis of the long bones as an eccentric lesion, and it is often cortical.

Imaging Features

Radiograph

Chondromyxoid fibroma generally appears as an eccentric expansile metaphyseal osteolytic lesion with cortical expansion, coarse trabeculation, endosteal scalloping, and scalloped sclerotic medullary border on radiographs (Fig. 3.9). Calcification is infrequent, unlike chondroblastoma and other cartilaginous lesions. Inner narrow zone of transition with the adjacent normal bone and a thinned or absent outer margin may simulate a more aggressive lesion. Larger lesion may show destruction of the cortex resulting in a hemispherical osseous defect or "bite" without periosteal reaction. In the foot and flat bones, it presents as a central expansile lesion.

Magnetic resonance imaging

MR imaging may demonstrate a lobulated margin. The MR signal intensity of this lesion is variable (Fig. 3.9).

Differential Diagnoses

1. Periosteal chondroma

   Periosteal chondroma may be purely lytic or may show internal chondroid mineralization, saucerization, or a well-defined depression of the adjacent cortex with a soft tissue mass.
2. Aneurysmal bone cyst

   Aneurysmal bone cyst can be found in the metaphysis or diaphysis of long bone and show morphological signs of slow growth. Matrix calcifications detected radiographically or by CT exclude this entity. MR imaging is able to differentiate a solid lesion like chondromyxoid fibroma from cystic lesions.
3. Giant cell tumor

   Giant cell tumor is more likely than chondromyxoid fibroma to reach the subchondral bone in the epiphysis, and more frequently penetrates the cortex without neocortex formation.
4. Enchondroma in the short bones

   Enchondroma in the short bones is much more frequent than chondromyxoid fibroma, but can show a similar radiographic pattern.
5. Nonossifying fibroma

   Larger nonossifying fibroma can be radiographically indistinguishable from chondromyxoid fibroma.

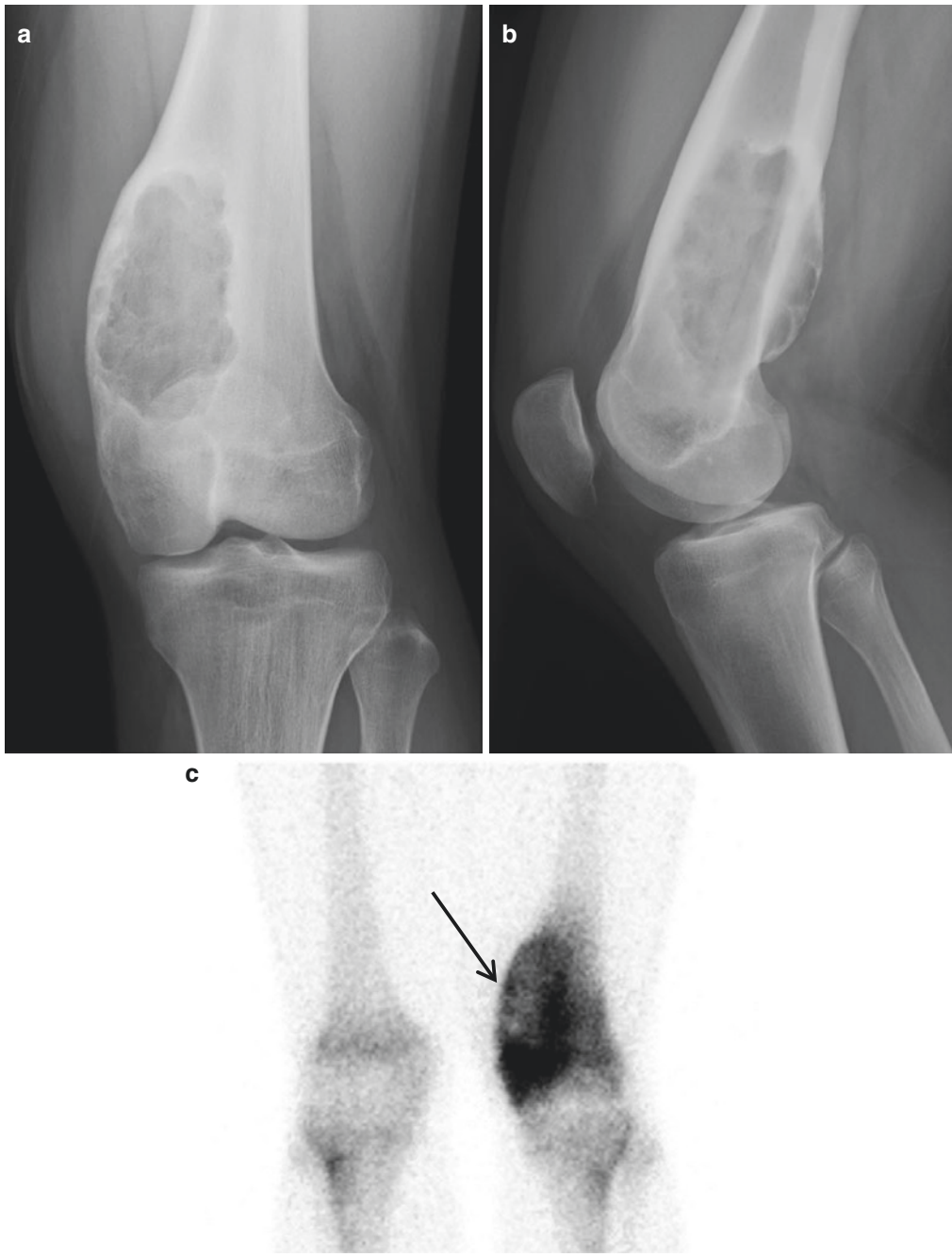

Fig. 3.9 Chondromyxoid fibroma. (**a**) Anteroposterior radiograph of the left knee shows an eccentric expansile metaphyseal osteolytic lesion with cortical expansion, coarse trabeculation, endosteal scalloping, and scalloped sclerotic medullary border. (**b**) Lateral radiograph of the left knee demonstrates an expansile osteolytic lesion with cortical expansion and endosteal scalloping. (**c**) Bone scan shows an increased uptake (*arrow*) with photon defect in the central portion in the left distal femur. (**d**) Coronal T1-weighted MR image demonstrates a lobulated mass with intermediate signal intensity (*arrow*). (**e**) Axial fat-suppressed proton density-weighted MR image demonstrates a lobulated mass with increased signal intensity (*arrow*). (**f**) Coronal fat-suppressed T2-weighted MR image demonstrates a lobulated mass with high signal intensity (*arrow*). (**g**) Sagittal fat-suppressed contrast-enhanced T1-weighted MR image demonstrates a lobulated enhancing mass with central nonenhancing component (*arrow*)

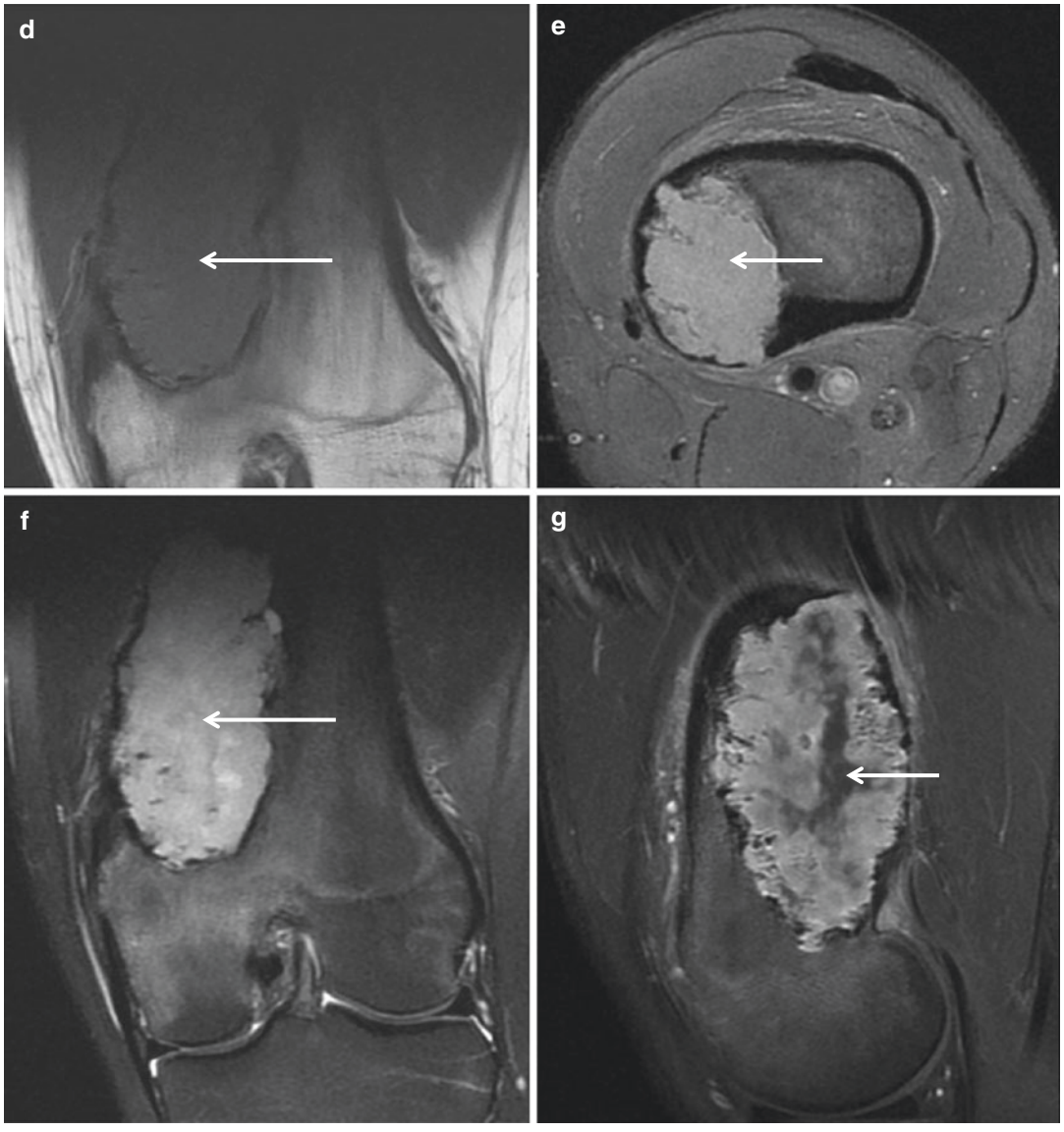

Fig. 3.9 (continued)

3.5 Subungual Exostosis

Overview

Subungual exostosis is a reactive nonneoplastic growth characterized by proliferating fibroblasts and cartilage metaplasia, which progresses to mature ossification. The cartilage cap is typically larger than the base and may be either indistinct or well demarcated.

Subungual exostosis shares some radiographic features with osteochondroma, but pathologically represents a distinct entity. The etiology is uncertain, although trauma, irritation, inflammation, and infection have been proposed. The term "subungual" may be misleading, as in some cases the growth is not subungual, but in the periungual region.

Epidemiology

Subungual exostosis occurs in the second and third decades of life. Both sexes are equally affected.

Common Locations

Subungual exostosis most commonly arises from the dorsal or dorsomedial aspect of the distal phalanx of the great toe, with a variable relationship to the nail bed. This location may be related to the loose periosteum in this area, as opposed to the tightly adherent periosteum in the volar aspect of the toe and finger pads. The distal phalanges of the fingers, thumb, and index are affected in 10 % of cases, usually in the dominant hand.

Imaging Features

Radiograph

Radiographs show an ossific mass protruding from the bone without corticomedullary continuity to the underlying bone (Fig. 3.10).

Magnetic resonance imaging

MR images show projection of trabecular bone covered by fibrocartilaginous cap (Fig. 3.11). MR images also depict adjacent connective tissue including the nail matrix.

Differential Diagnoses

Unlike most osteochondromas in this region, subungual exostoses arise distal to the physeal scar, manifest in older patients, and are not associated with growth deformities.

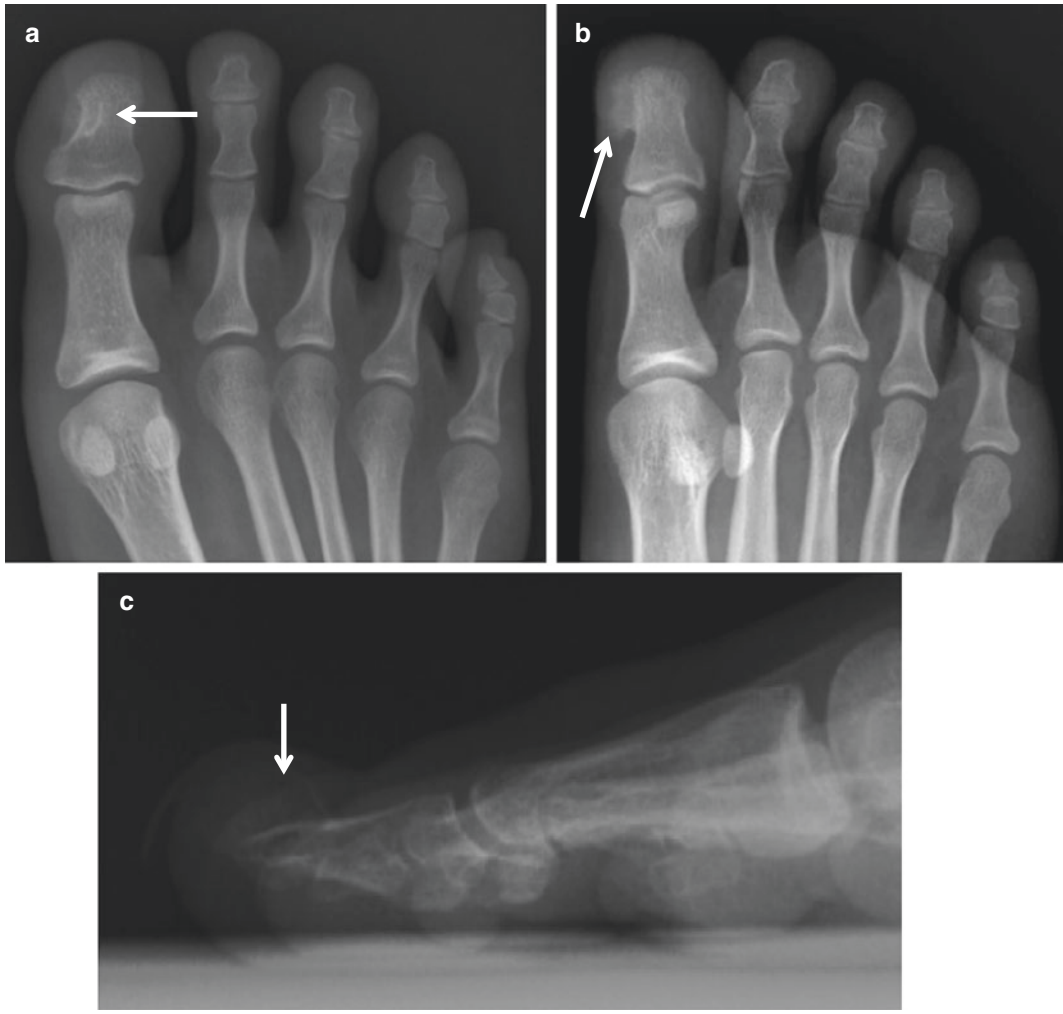

Fig. 3.10 Subungual exostosis. (**a**) Anteroposterior radiograph of the right foot shows an ossific mass arising from the distal phalanx of the right great toe (*arrow*). (**b**) Oblique radiograph shows the mass protruding from dorsomedial aspect of the distal phalanx of the right great toe (*arrow*). (**c**) Lateral radiograph again demonstrates an ossific mass arising from the dorsomedial aspect of the distal phalanx of the right great toe (*arrow*)

Fig. 3.11 Subungual exostosis. (**a**) Lateral radiograph of the left foot shows an ossific mass arising from the dorsal aspect of the distal phalanx of the left great toe (*arrow*). (**b**) Oblique radiograph demonstrates an ossific mass arising from the dorsal aspect of the distal phalanx of the left great toe (*arrow*). (**c**) Sagittal T2-weighted MR image demonstrates a projection of trabecular bone covered by fibrocartilaginous cap (*arrow*). (**d**) Coronal T2-weighted MR image shows a projection of trabecular bone (*arrow*). (**e**) Sagittal fat-suppressed contrast-enhanced T1-weighted MR image demonstrates a protruding bony mass with fibrocartilaginous cap (*arrow*)

3.6 Bizarre Parosteal Osteochondromatous Proliferation

Overview

Bizarre parosteal osteochondromatous proliferation is a rare entity and also known as a Nora lesion. It is unclear whether this lesion may either represent a periostitis ossificans with organizing hematoma and ossification, or may have a neoplastic origin.

Epidemiology

There is no gender predilection.

Common Locations

Bizarre parosteal osteochondromatous proliferation occurs most commonly in the small bones of the hands and feet.

Imaging Features

Radiograph

Bizarre parosteal osteochondromatous proliferation appears as a mass of mineralization within the soft tissues, with no clear osseous attachment in early stage. When mature, radiographs may show a bony pedicle attached directly to the outer cortical surface with no communication to the medullary cavity (Fig. 3.12). The underlying cortex is intact.

Magnetic resonance imaging

MR images demonstrate a mass arising from the cortical surface (Fig. 3.12), which shows low signal intensity on T1-weighted images and high signal intensity on fluid-sensitive sequences (Fig. 3.13). The lesions may show a mushroom-shaped cartilaginous cap on MR images. In particular, the lack of soft tissue, cortical and medullary abnormality is a useful sign in helping to define the nature of this lesion.

Differential Diagnoses

1. Osteochondroma

   The bony protuberance and the shape of the cartilage cap of the bizarre parosteal osteochondromatous proliferation give a resemblance to an osteochondroma. However, bizarre parosteal osteochondromatous proliferation can be differentiated from osteochondroma by the lack of corticomedullary continuity with the underlying bone.
2. Parosteal osteosarcoma

   Bizarre parosteal osteochondromatous proliferation can be differentiated from parosteal osteosarcoma by the absence of soft tissue abnormality, cortical destruction, and medullary involvement.

Fig. 3.12 Bizarre parosteal osteochondromatous proliferation. (**a**) Anteroposterior radiograph of the left hand shows mineralization (*arrow*) within the soft tissues attached to the outer cortical surface with no communication to the medullary cavity. (**b**) Oblique radiograph again demonstrates osseous lesion (*arrow*) with no communication to the medullary cavity. (**c**) Oblique coronal T1-weighted MR image shows an ossifying mass arising from the cortical surface of the first metacarpal (*arrow*). (**d**) Oblique coronal fat-suppressed contrast-enhanced T1-weighted MR image again demonstrates an ossifying mass (*arrow*) with minimal nodular enhancement. (**e**) Axial T1-weighted MR image demonstrates a lobulated juxtacortical mass (*arrow*) with adipose signal intensity. (**f**) Axial fat-suppressed contrast-enhanced T1-weighted MR image demonstrates a lobulated juxtacortical mass (*arrow*) with minimal enhancement

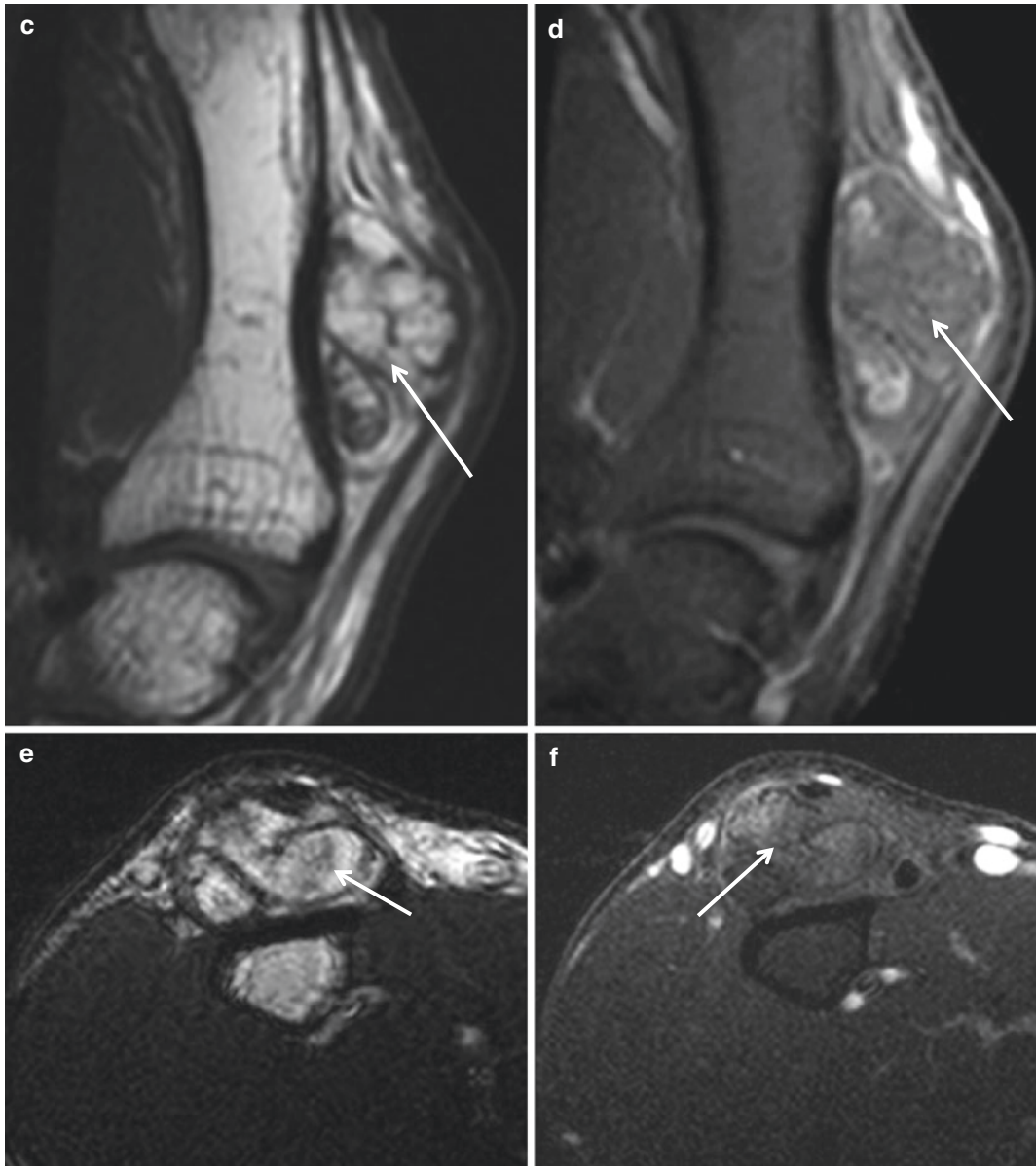

Fig. 3.12 (continued)

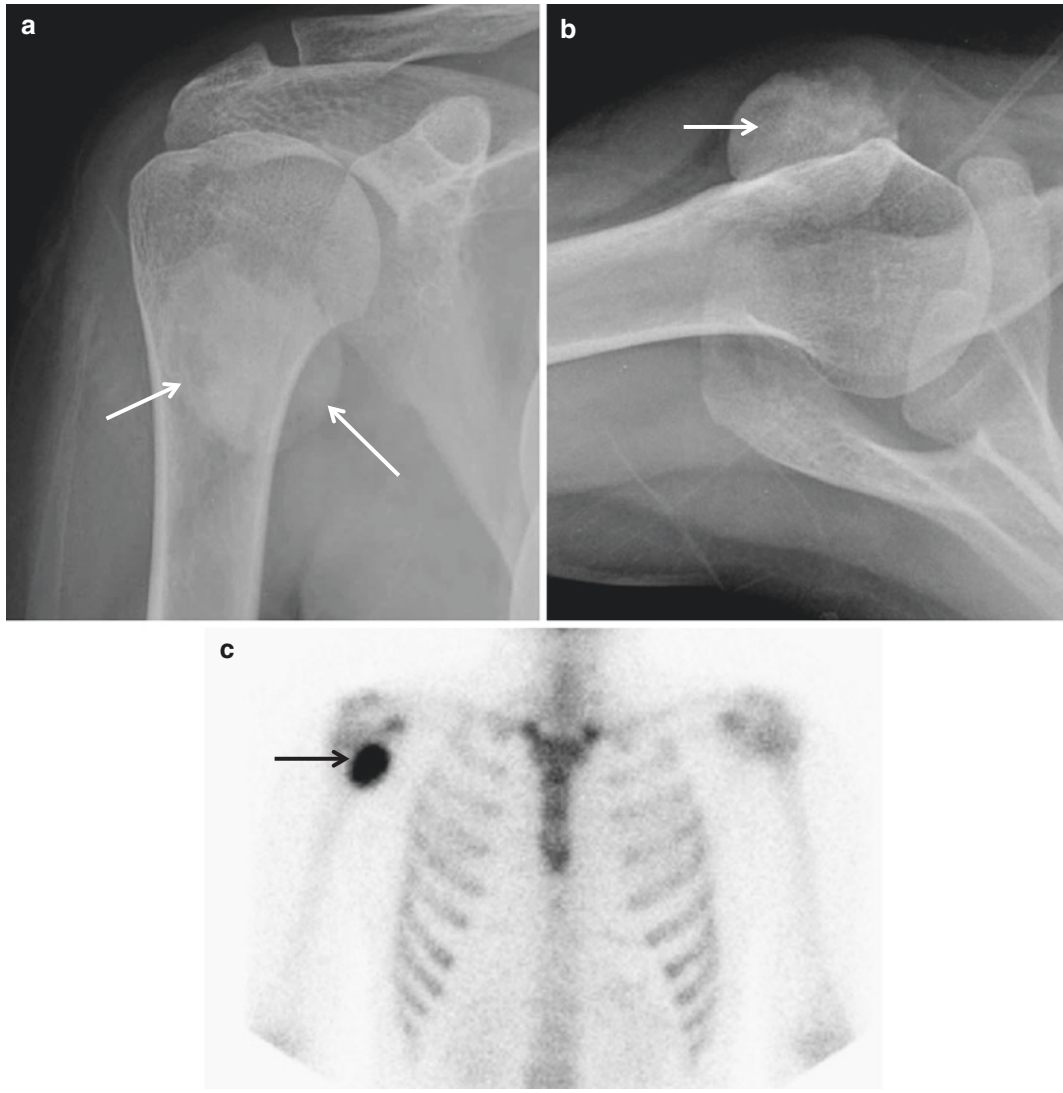

Fig. 3.13 Bizarre parosteal osteochondromatous proliferation. (**a**) Anteroposterior radiograph of the right shoulder shows a mineralized mass (*arrow*). (**b**) Lateral radiograph again shows a mineralized mass (*arrow*) with no communication to the medullary cavity. (**c**) Bone scan shows an increased uptake (*arrow*) in the right proximal humerus. (**d**) Sagittal T1-weighted MR image demonstrates a lobulated juxtacortical mass (*arrow*) with low signal intensity. (**e**) Sagittal contrast-enhanced T1-weighted MR image demonstrates a lobulated juxtacortical mass (*arrow*) with heterogeneous enhancement. (**f**) Axial fat-suppressed T2-weighted MR image demonstrates a lobulated juxtacortical mass (*arrow*) with heterogeneous areas of high signal intensity. (**g**) Axial contrast-enhanced T1-weighted MR image demonstrates a lobulated juxtacortical mass (*arrow*) with heterogeneous enhancement

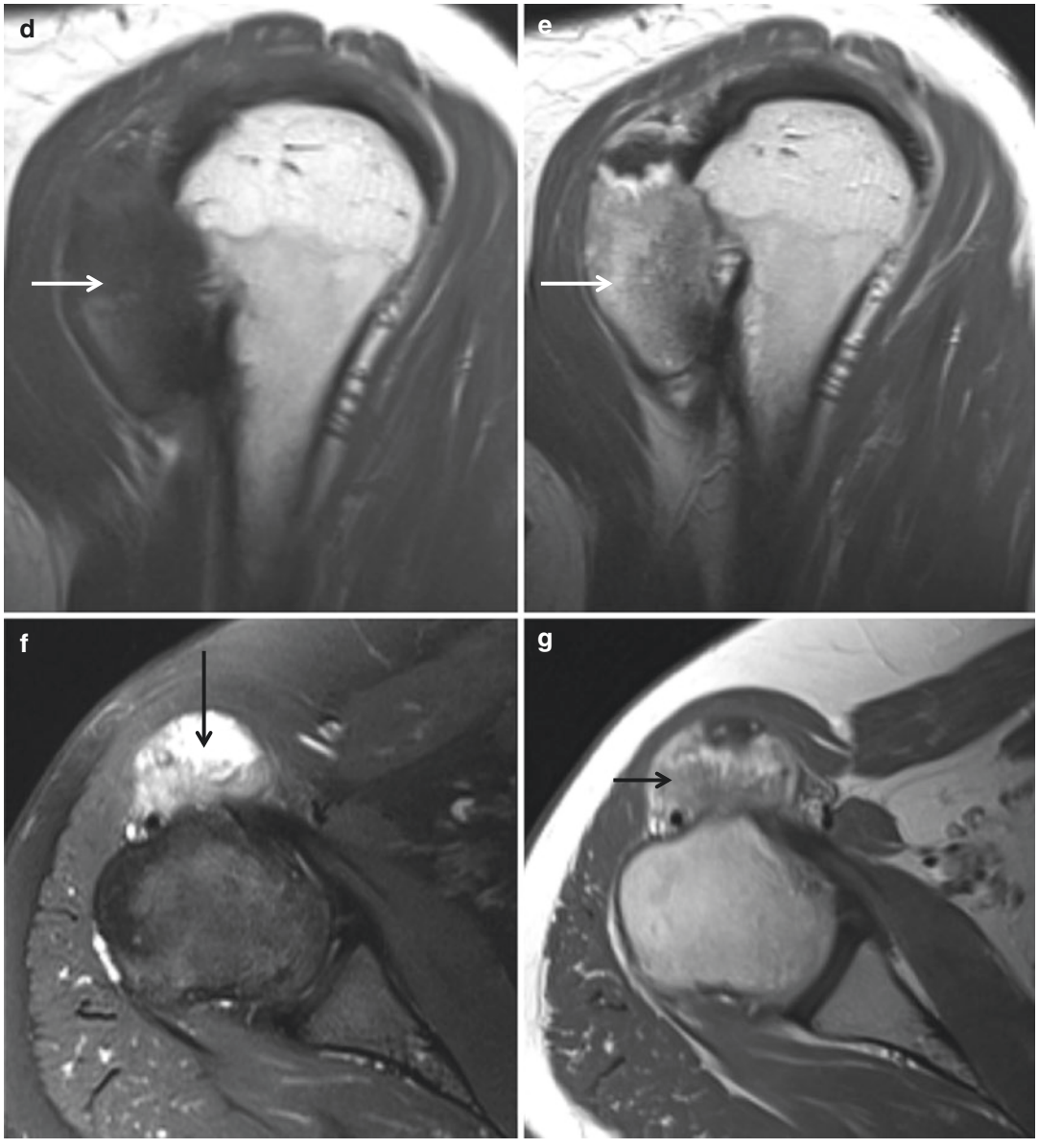

Fig. 3.13 (continued)

3.7 Chondroblastoma

Overview

Chondroblastoma is a benign chondrogenic tumor with a strong predilection for the epiphysis of long tubular bones. Histologically, it presents as a sharply marginated and lobulated lesion containing chondroblasts, occasional giant cells, and abundant chondroid matrix. Aneurysmal bone cyst components may be present in up to 15 % of cases, and matrix mineralization occurs in a lace-like pattern with a histological appearance similar to chicken wire.

Epidemiology

Chondroblastoma is an uncommon lesion compromising < 2 % of benign primary bone neoplasms. It is twice as common in males as females, and most cases occur between the ages of 5 and 25 years.

Common Locations

Chondroblastoma is the classic epiphyseal lesion, which occurs predominantly in the epiphysis or epiphysis equivalents such as apophyses and sesamoids, close to joints, and may present with some loss of joint function. It is most commonly seen in the proximal tibia, the proximal humerus, the distal femur, and the apophysis of the greater trochanter. Interestingly, the proximal epiphysis of the femur is not a very frequent location. Extension in the metaphysis is reported in up to 50 % of chondroblastomas.

Imaging Features

Radiograph

Chondroblastoma typically appears as an eccentric, round, or oval epiphyseal lucency with a thin sclerotic rim (Fig. 3.14). It may have a subtle chondroid matrix (Fig. 3.15) or contain flocculent calcification. It may appear more expansile depending on the size of the associated aneurysmal bone cyst. A more aggressive appearance may be encountered, featuring cortex destruction (Fig. 3.16) and invasion of the surrounding soft tissues or the joint space. Lack of a sclerotic rim does not exclude the diagnosis of a chondroblastoma.

Magnetic resonance imaging

MR imaging readily demonstrates the intense surrounding marrow edema (Figs. 3.14 and 3.15) and the typical low-to-intermediate signal intensity of the tumor on fluid-sensitive sequences. This is a distinguishing feature of the chondroblastoma, which has been attributed to the high hemosiderin content or highly cellular matrix. Sometimes, cystic regions within the chondroblastoma can be seen.

Differential Diagnoses

1. Giant cell tumor

   Giant cell tumors are located metaepiphyseally, are more aggressive in terms of cortex penetration, and prefer a slightly older age group.
2. Intraosseous ganglion

   Intraosseous ganglion, frequently located in the epiphyseal area of long bones, does not show matrix mineralization, is more frequent in higher age groups. Intraosseous ganglion can mostly be distinguished from the chondroblastoma by the fluid signal on MR imaging.
3. Infection

   Bone abscesses have a wider sclerotic rim, but can occur in a metaepiphyseal location and produce a profound peritumoral edema as well. MR imaging can help in the differentiation from bone abscess in which it shows a ring enhancement around a liquid center in contrast to the solid tissue of a chondroblastoma.
4. Clear cell chondrosarcoma

   Clear cell chondrosarcoma is a rare low-grade malignant lesion that can be morphologically indistinguishable from chondroblastoma. Its most frequent location is the proximal epiphysis of the femur, a site that is infrequent in chondroblastoma.
5. Chondromyxoid fibroma

   Chondromyxoid fibromas usually arise in the metaphysis. If they extend into the epiphysis, differentiation from a chondroblastoma with extension into the metaphysis can be difficult.

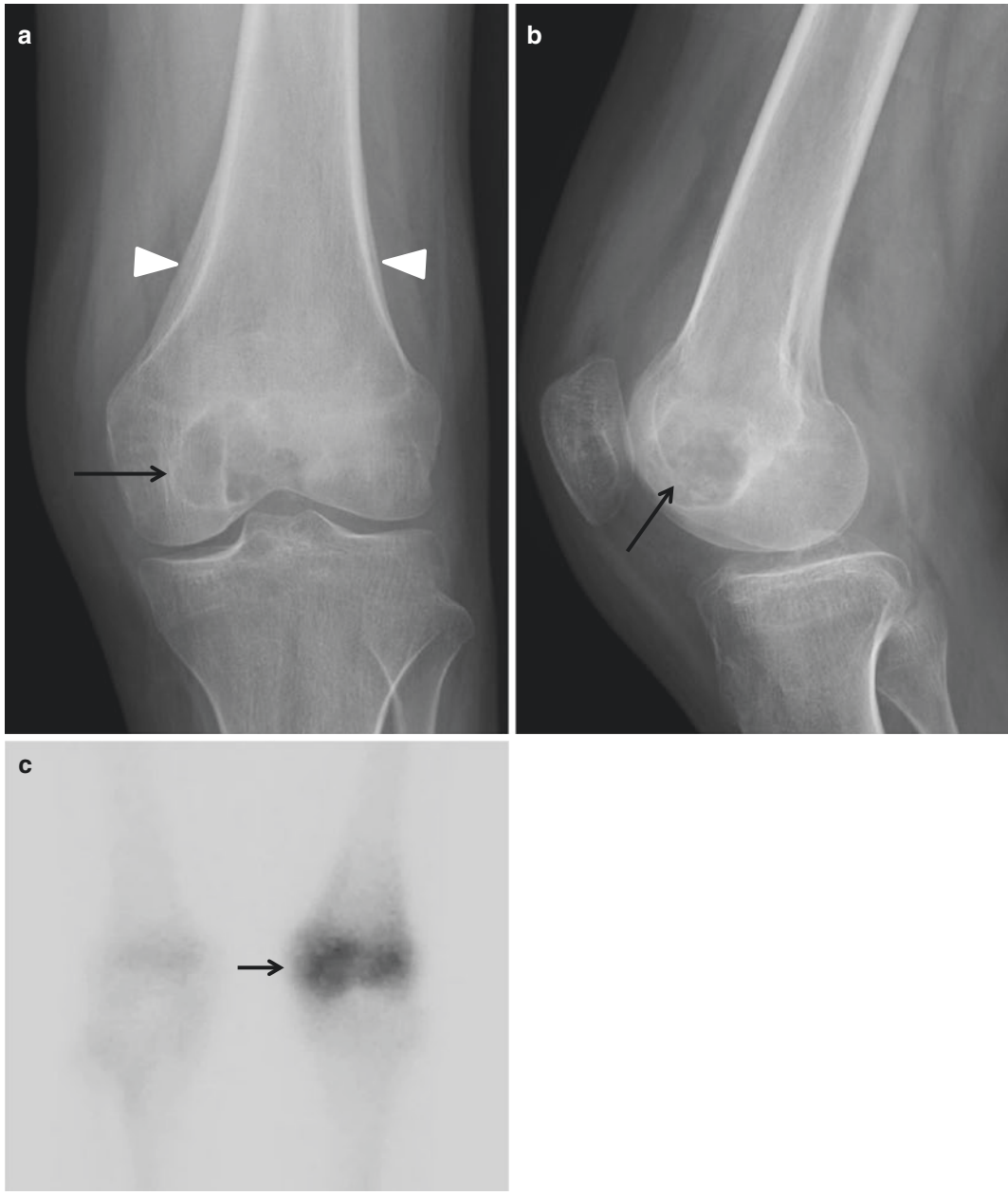

Fig. 3.14 Chondroblastoma. (**a**) Anteroposterior radiograph of the left knee shows an eccentric round epiphyseal lucency (*arrow*) with a thin sclerotic rim in the left distal femur. Periosteal reaction is noticed in the metaphysis of the left distal femur (*arrowheads*). (**b**) Lateral radiograph again shows a round epiphyseal lucency (*arrow*) with a thin sclerotic rim. (**c**) Bone scan shows an increased uptake (*arrow*) in the left distal femur. (**d**) Sagittal T1-weighted MR image demonstrates a round epiphyseal lesion (*arrow*) with a thin hypointense rim. (**e**) Sagittal fat-suppressed proton density-weighted MR image demonstrates a round epiphyseal lesion (*arrow*) with heterogeneous areas of high signal intensity and fluid–fluid level. (**f**) Coronal fat-suppressed proton density-weighted MR image demonstrates a round lesion (*arrow*) with surrounding reactive bone marrow edema. (**g**) Axial T2-weighted MR image shows a round lesion (*arrow*) with fluid–fluid level

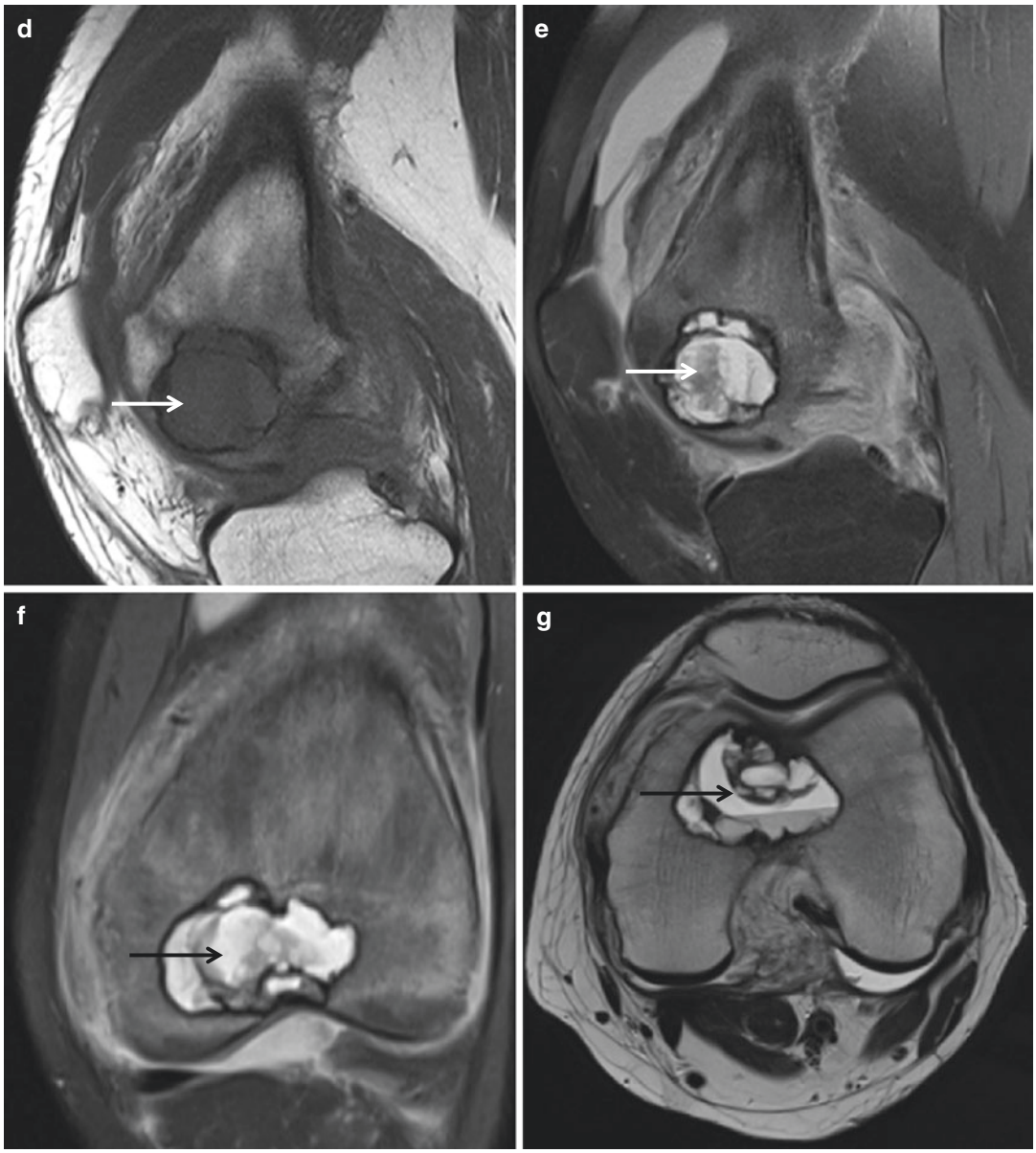

Fig. 3.14 (continued)

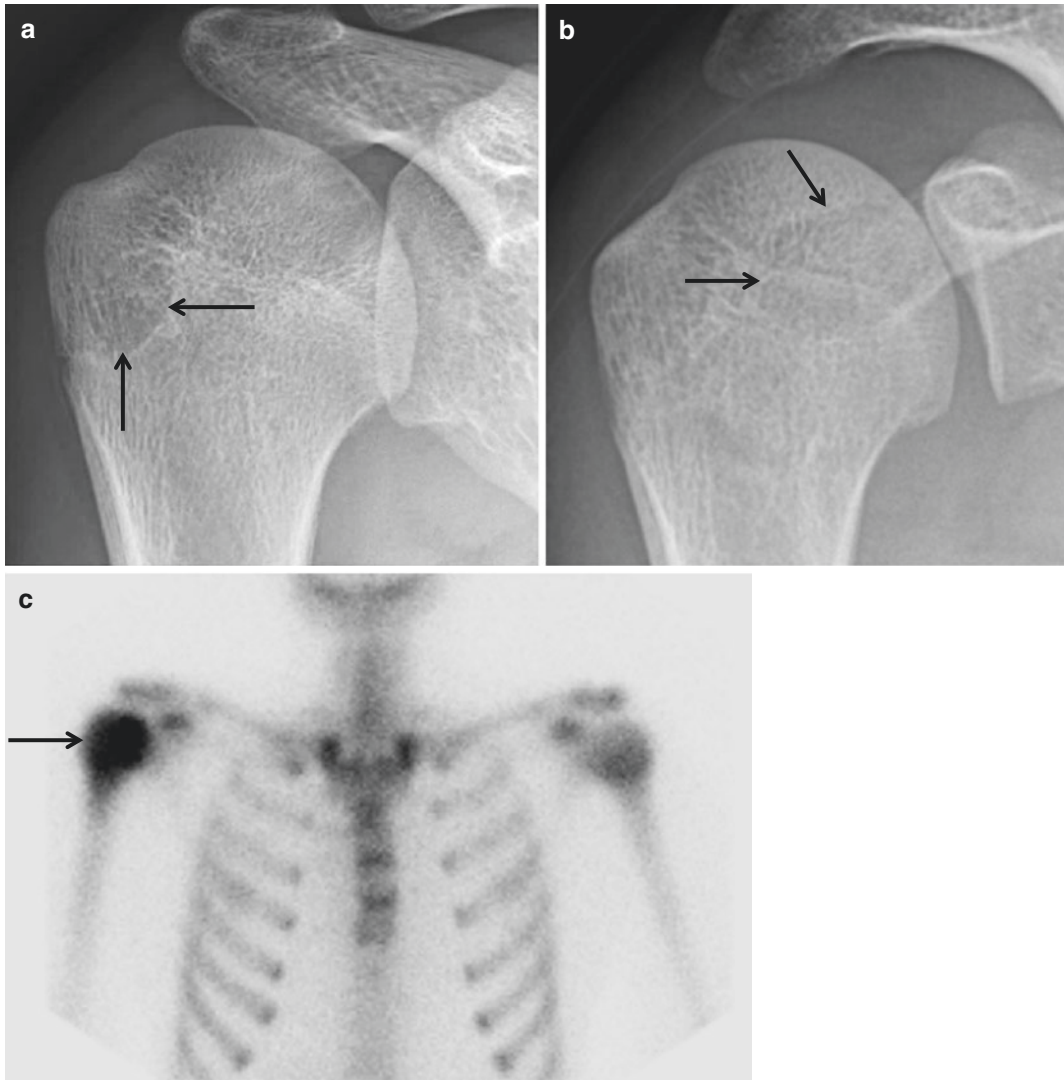

Fig. 3.15 Chondroblastoma. (**a**) Anteroposterior radiograph of the right shoulder shows an eccentric round epiphyseal lucency (*arrows*) with a thin sclerotic rim in the right proximal humerus. (**b**) Grashey view of the right shoulder shows an eccentric round epiphyseal lucency (*arrows*) with a thin sclerotic rim in the right humerus head. (**c**) Bone scan shows an increased uptake (*arrow*) in the right proximal humerus. (**d**) Coronal T1-weighted MR image demonstrates a round epiphyseal lesion (*arrow*) with intermediate signal intensity. (**e**) Coronal fat-suppressed proton density-weighted MR image demonstrates a round lesion (*arrow*) with intermediate signal intensity. Surrounding reactive bone marrow edema is noticed. (**f**) Coronal T2-weighted MR image demonstrates a round lesion (*arrow*) with intermediate-to-intermediate signal intensity. (**g**) Coronal fat-suppressed contrast-enhanced T1-weighted MR image demonstrates an enhancing epiphyseal lesion (*arrow*) with surrounding reactive bone marrow edema

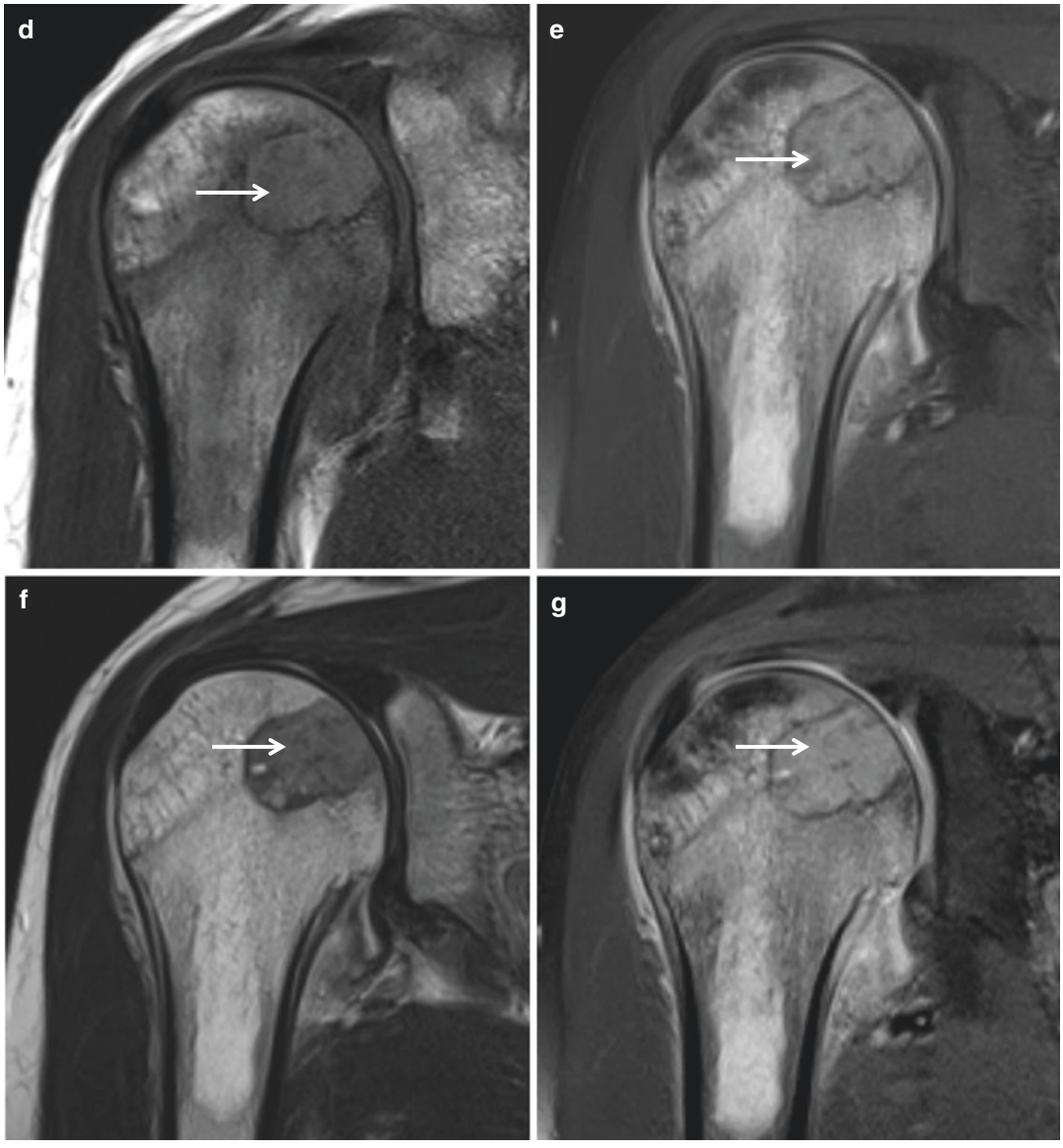

Fig. 3.15 (continued)

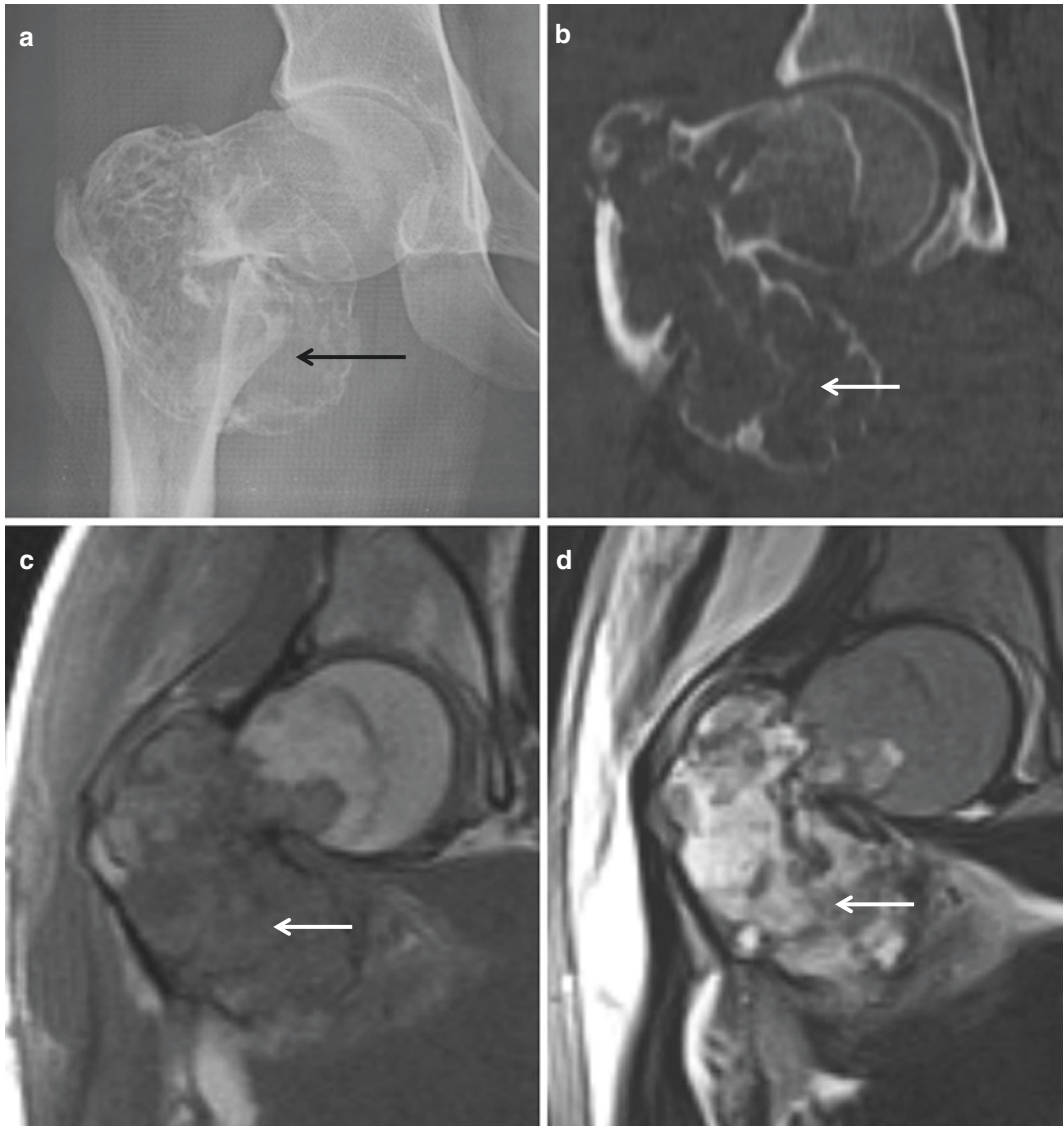

Fig. 3.16 Chondroblastoma. (**a**) Anteroposterior radiograph of the right hip shows an expansile osteolytic lesion (*arrow*) in the right femoral neck extending into the apophyses of the greater and lesser trochanters. Pathological fracture is noticed in the greater and lesser trochanters. (**b**) Coronal reformatted CT scan shows an expansile osteolytic lesion (*arrow*) with endosteal scalloping. (**c**) Coronal T1-weighted MR image demonstrates an intermediate intense expansile lesion (*arrow*) in the right femoral neck extending into the apophyses of the greater and lesser trochanters. (**d**) Coronal T2-weighted MR image shows mixed low-to-intermediate and high signal intensity within the lesion (*arrow*). (**e**) Axial T2-weighted MR image again shows heterogeneous low-to-intermediate and high signal intensity within the lesion (*arrow*)

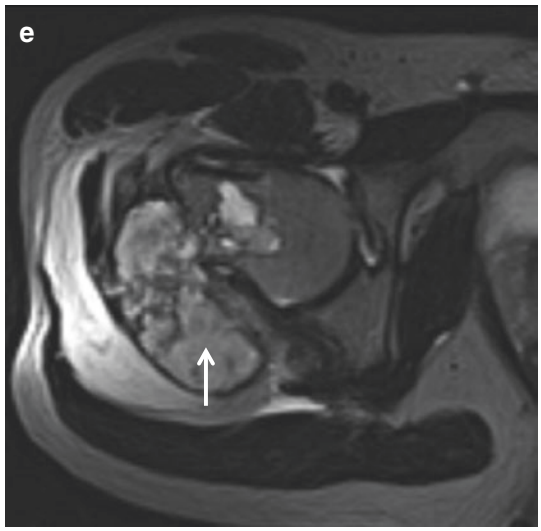

Fig. 3.16 (continued)

3.8 Chondrosarcoma

Chondrosarcoma is a malignant tumor of chondroid origin that accounts for 25 % of malignant bone tumors. It is the third most common malignant bone tumor after myeloma and osteosarcoma. Chondrosarcomas are classified as grade 1–3, based on clinical behavior and likelihood of metastasis.

Primary chondrosarcoma is a chondrosarcoma without evidence of a precursor lesion, and secondary chondrosarcoma is a chondrosarcoma which develops out of an enchondroma or osteochondroma.

The most frequent histological type is conventional intramedullary (central) chondrosarcoma. Rare histological varieties are clear cell chondrosarcoma and mesenchymal chondrosarcoma. Dedifferentiated chondrosarcoma is an entity that consists of two different components: a well-differentiated chondrogenic component, enchondroma, low-grade chondrosarcoma or osteochondroma, and a high-grade, noncartilaginous component, frequently undifferentiated high-grade pleomorphic sarcoma, fibrosarcoma, or osteosarcoma.

A rare subtype defined by location is periosteal or juxtacortical chondrosarcoma.

3.8.1 Conventional Intramedullary Chondrosarcoma

Overview

Microscopically, most of the conventional intramedullary chondrosarcomas are further classified as grade 1 or 2 (low or intermediate grade), and behave in an indolent manner with low potential to metastasize. The remaining 5–10 % of conventional intramedullary chondrosarcomas are classified as grade 3 lesions, and possess high metastatic potential.

Epidemiology

Conventional intramedullary chondrosarcoma is the most common type of chondrosarcoma, accounting for 90 % of chondrosarcomas. Conventional intramedullary chondrosarcoma is most commonly seen in the sixth decade, and is more common in men.

Common Locations

Conventional intramedullary chondrosarcoma typically occurs in or close to the trunk, particularly in the pelvis, proximal femur, proximal humerus, distal femur, and ribs. In the long bones, conventional intramedullary chondrosarcoma is located in the metaphysis or metadiaphysis.

Imaging Features

Radiograph

The imaging appearance of conventional intramedullary chondrosarcoma depends on the grade of the lesion and ranges from a well-defined lucent lesion with chondroid matrix indistinguishable from an enchondroma to an aggressive, moth-eaten tumor with ill-defined margins, cortical destruction, aggressive periosteal reaction, and soft tissue mass (Fig. 3.17). Conventional intramedullary chondrosarcoma most commonly appears as a large geographical expansile osteolytic lesion with cortical scalloping, cortical penetration and/or thickening, mild periosteal reaction, and chondrogenic calcification (Fig. 3.18).

Magnetic resonance imaging

Conventional intramedullary chondrosarcoma has a lobular pattern with low signal intensity on T1-weighted images and high signal intensity on T2-weighted images secondary to the high water content of cartilage. Conventional intramedullary chondrosarcoma also demonstrates a ring-and-arcs pattern of enhancement of fibrovascular septae (Fig. 3.19). Tumors with a ring-and-arcs pattern of fibrovascular septal enhancement are usually of grade 2 in histology.

Differential Diagnoses

1. The differential diagnosis for lesions with chondroid calcification includes enchondroma.

   Distinguishing an enchondroma from a low-grade chondrosarcoma can be challenging, as enchondromas have malignant potential and the borderline between enchondroma and low-grade chondrosarcoma is not well defined. Enchondromas are rare in the axial skeleton, talus, and calcaneus, whereas chondrosarcomas are rare in the short tubular bones. Progressive radiographic changes in the mature skeleton, large size (>5 cm), lesser extent of matrix mineralization within the lesion (within less than two-thirds of the lesion as seen on radiographs), depth and extent of endosteal scalloping (greater than two-thirds of the cortical thickness and along more than two-thirds of the lesion), cortical penetration, periosteal reaction, cortical remodeling, soft tissue extension, and high uptake on bone scan (typically more than that of anterior iliac crest) can be suggestive of a chondrosarcoma.
2. The differential diagnosis for lesions without chondroid calcification includes metastasis, osteolytic secondary osteosarcoma, undifferentiated high-grade pleomorphic sarcoma, and fibrosarcoma.

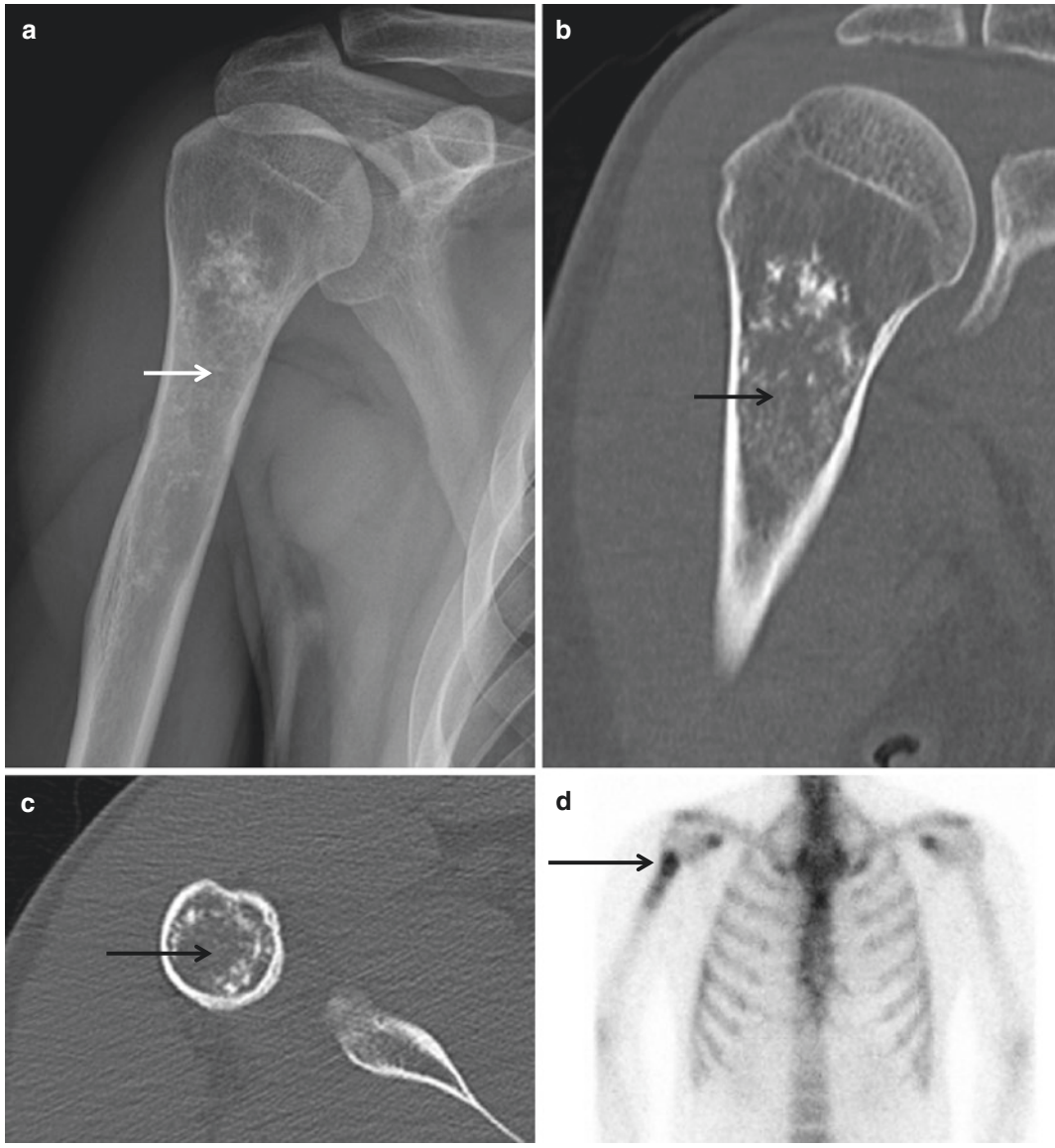

Fig. 3.17 Conventional chondrosarcoma. (**a**) Anteroposterior radiograph of the right humerus shows an ill-defined intramedullary radiolucent lesion with chondrogenic matrix calcification (*arrow*). (**b**) Coronal reformatted CT scan again shows an ill-defined intramedullary radiolucent lesion with chondrogenic matrix calcification (*arrow*). (**c**) Corresponding axial CT scan demonstrates chondrogenic matrix calcification (*arrow*). (**d**) Bone scan shows an increased uptake (*arrow*) in the right proximal humerus. (**e**) Coronal T1-weighted MR image shows a lobular pattern of the lesion with low signal intensity (*arrow*). (**f**) Coronal T2-weighted MR image shows a lobular pattern of the lesion with high signal intensity (*arrow*). (**g**) Coronal fat-suppressed contrast-enhanced T1-weighted MR image demonstrates a rings-and-arcs pattern of enhancement (*arrow*). (**h**) Axial fat-suppressed contrast-enhanced T1-weighted MR image also demonstrates a rings-and-arcs pattern of enhancement (*arrow*)

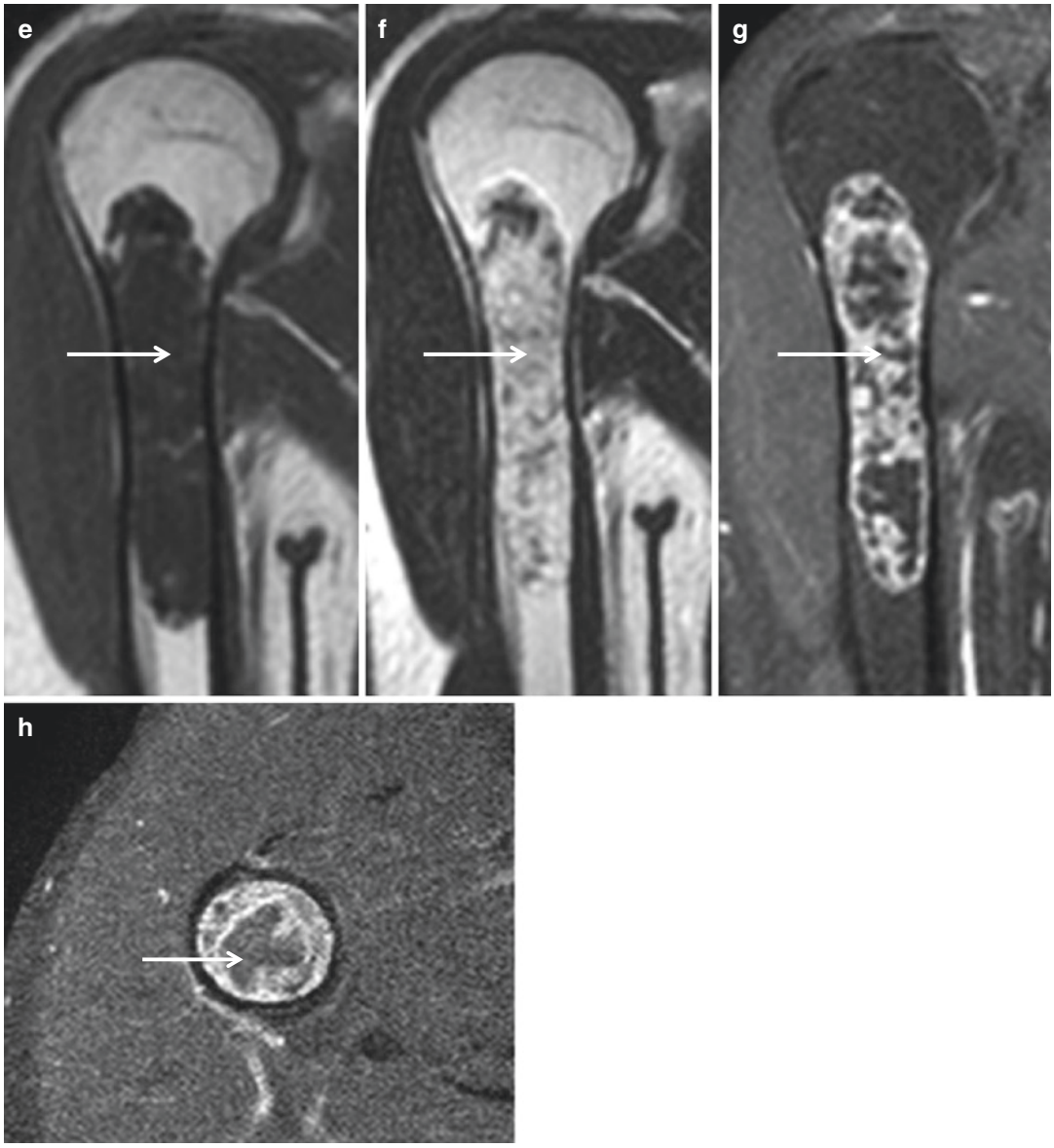

Fig. 3.17 (continued)

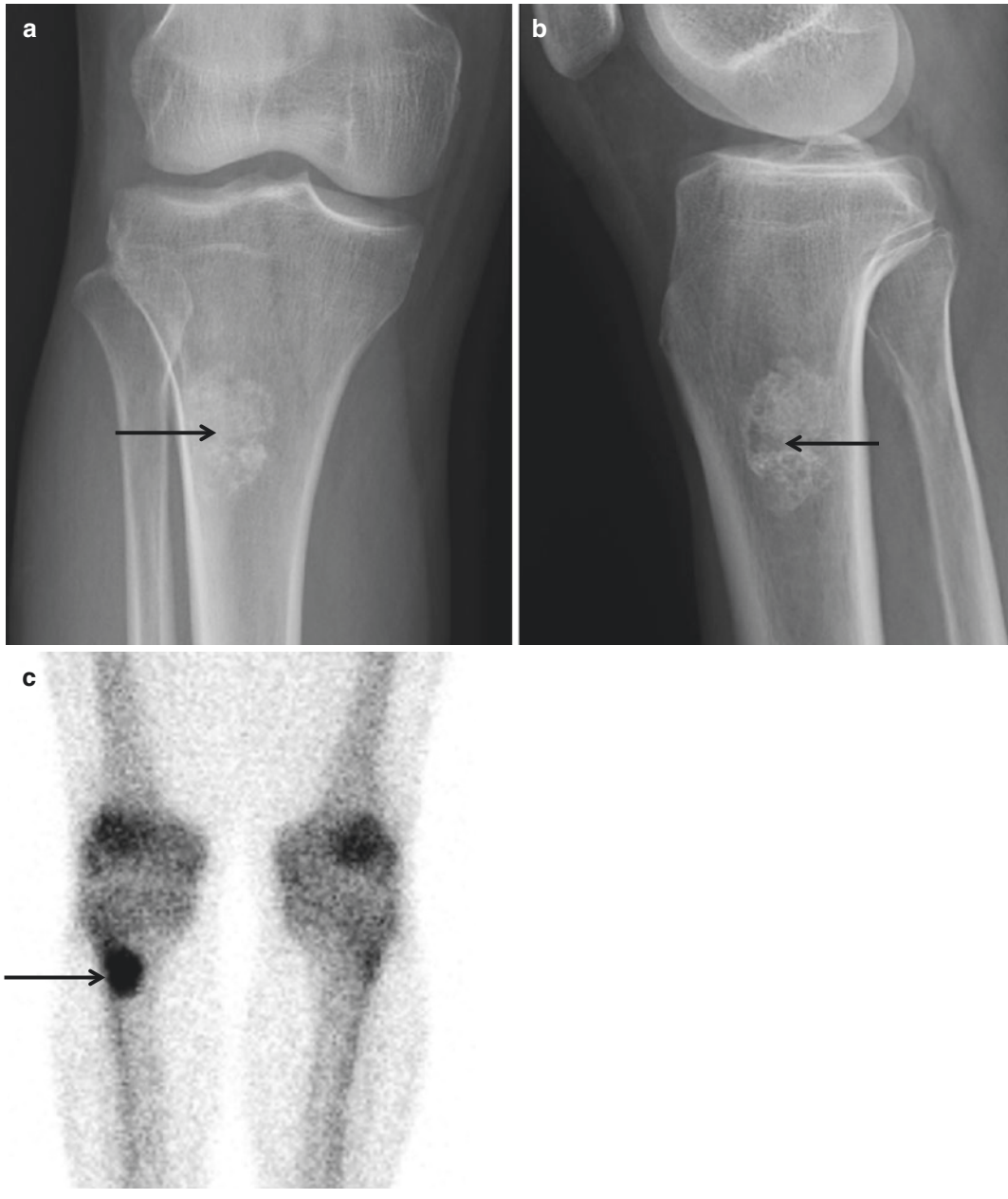

Fig. 3.18 Conventional chondrosarcoma. (**a**) Anteroposterior radiograph of the right knee shows intramedullary chondrogenic matrix calcification (*arrow*) in the right proximal tibia. (**b**) Lateral radiograph again demonstrates intramedullary chondrogenic matrix calcification (*arrow*) in the right proximal tibia. (**c**) Bone scan shows a focal increased uptake (*arrow*) in the right proximal tibia. (**d**) Coronal T1-weighted MR image shows a lobular pattern of the lesion with low signal intensity (*arrow*). (**e**) Coronal T2-weighted MR image shows a lobular pattern of the lesion with scattered areas of high signal intensity (*arrow*). (**f**) Coronal fat-suppressed contrast-enhanced T1-weighted MR image demonstrates a rings-and-arcs pattern of enhancement (*arrow*). (**g**) Axial fat-suppressed contrast-enhanced T1-weighted MR image also demonstrates a rings-and-arcs pattern of enhancement (*arrow*)

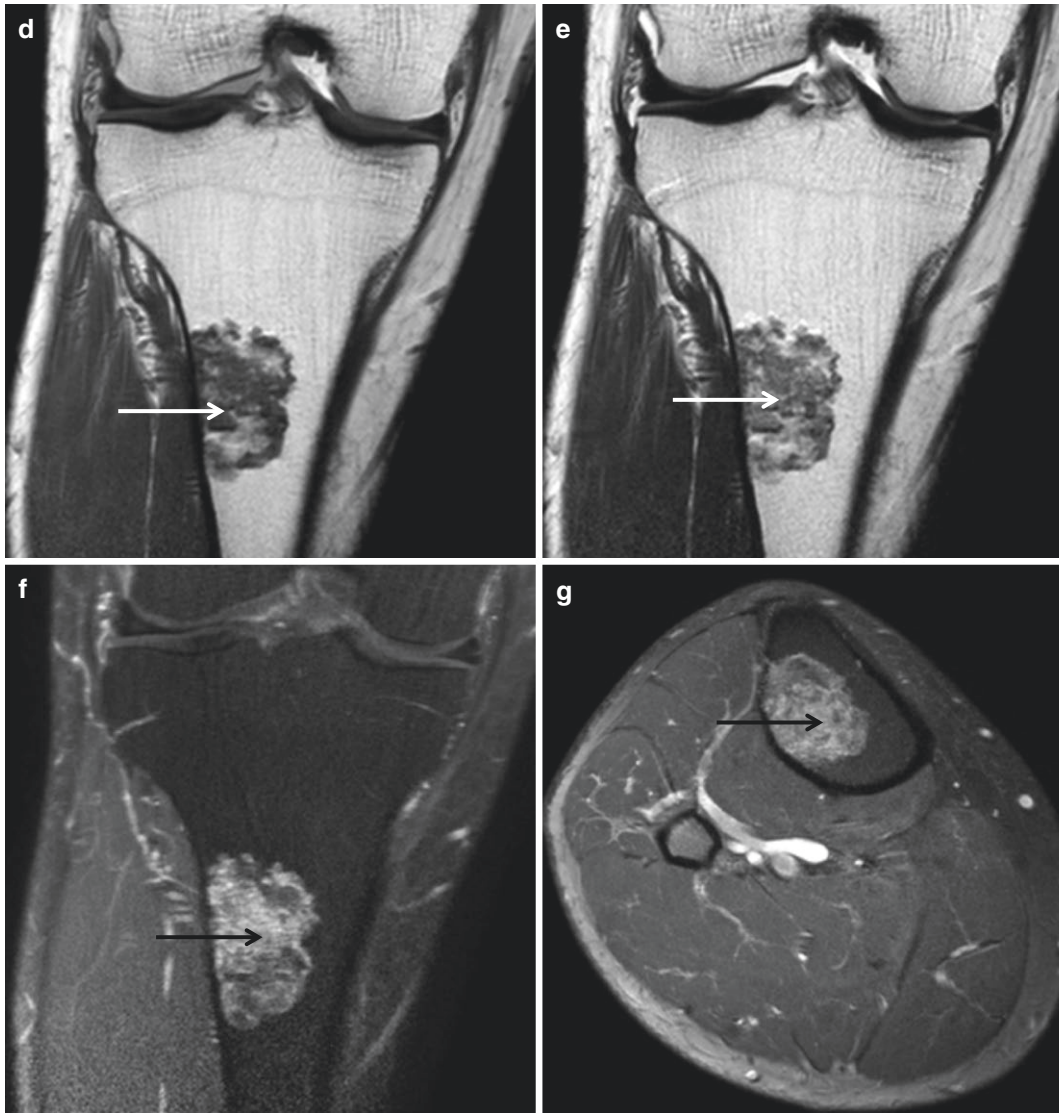

Fig. 3.18 (continued)

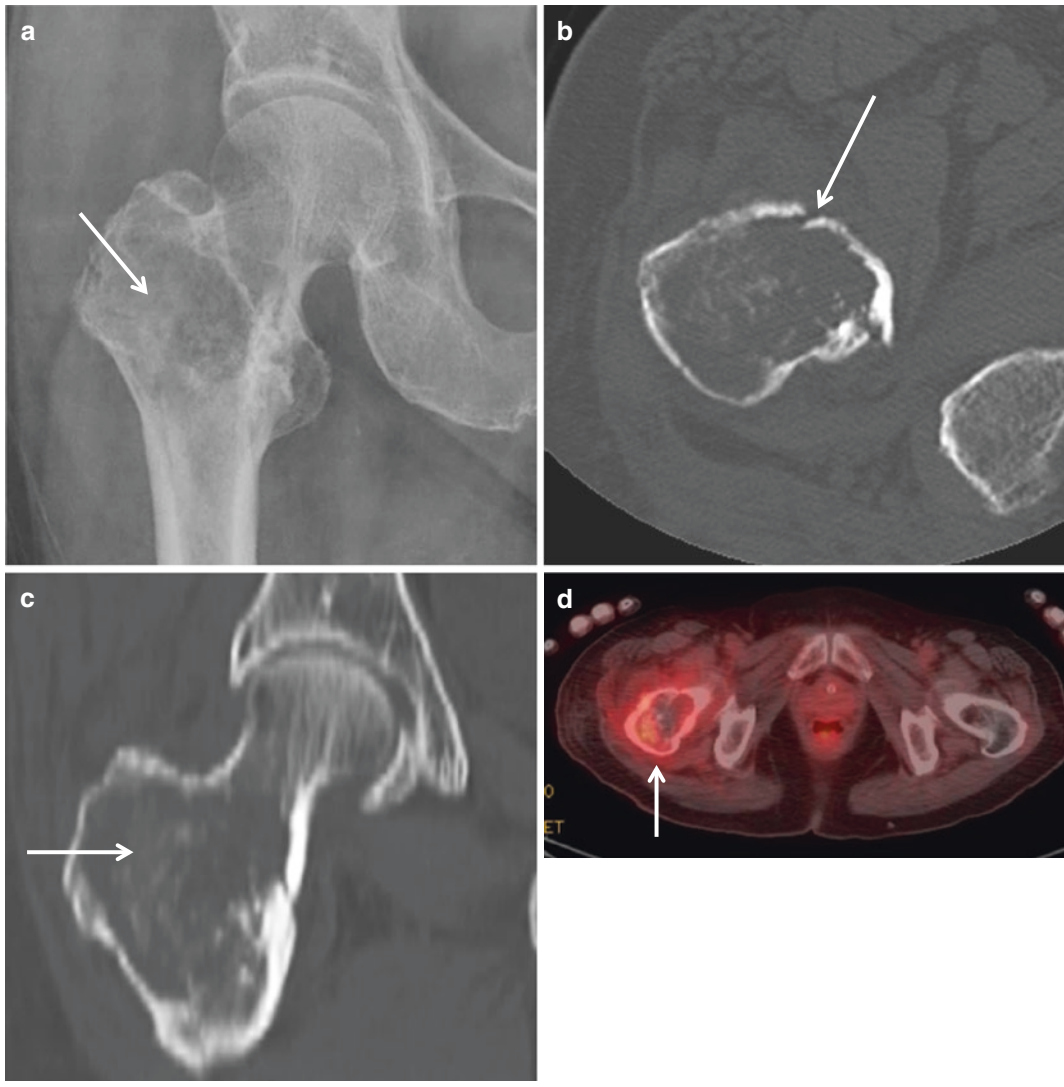

Fig. 3.19 Conventional chondrosarcoma. (**a**) Anteroposterior radiograph of the right hip shows an ill-defined osteolytic lesion (*arrow*) in the intertrochanteric region of the right femur with chondrogenic matrix calcification and pathological fracture. (**b**) Corresponding axial CT scan shows an ill-defined osteolytic lesion (*arrow*) and pathological fracture. (**c**) Coronal reformatted CT scan shows an ill-defined osteolytic lesion with chondrogenic matrix calcification (*arrow*) in the right femoral neck and the proximal shaft. (**d**) PET scan demonstrates a hypermetabolic lesion (*arrow*) in the right proximal femur. (**e**) Coronal T1-weighted MR image shows a lobular hypointense lesion (*arrow*) involving the right proximal femur. (**f**) Coronal fat-suppressed proton density-weighted MR image shows a lobular lesion (*arrow*) with high signal intensity. (**g**) Coronal fat-suppressed contrast-enhanced T1-weighted MR image demonstrates stippled pattern of enhancement (*arrow*). (**h**) Axial fat-suppressed contrast-enhanced T1-weighted MR image also demonstrates stippled pattern of enhancement (*arrow*)

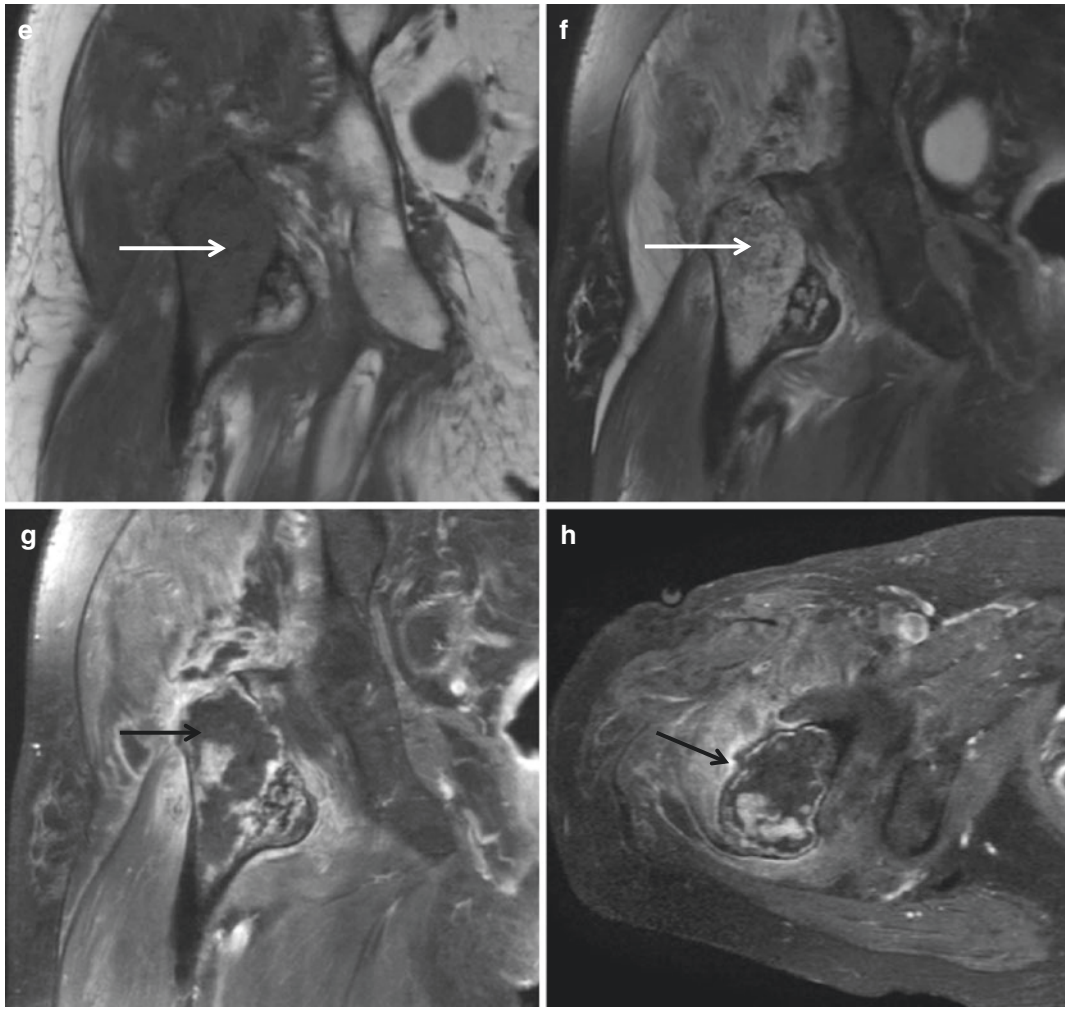

Fig. 3.19 (continued)

3.8.2 Periosteal/Juxtacortical Chondrosarcoma

Overview

Periosteal chondrosarcoma is a rare low-grade chondrosarcoma that originates on the surface of long bones.

Epidemiology

Periosteal chondrosarcoma is seen in patients aged 17–65 years, and is more common in women.

Common Locations

Periosteal chondrosarcoma occurs most commonly in the metaphyseal region of long bones, the distal femur and the proximal humerus being the most common sites. In the femur, it occurs usually in the distal posterior metaphysis.

Imaging Features

Radiograph

The lesion presents as a fusiform mass attached to the surface of the bone, producing saucerization (Fig. 3.20). In most cases, it does not communicate with the medullary cavity. It may produce cortical thickening.

Magnetic resonance imaging

T2-weighted MR images may show hyperintense soft tissue mass based on the periosteal surface. The lesion has low signal intensity on T1-weighted images. Reactive marrow involvement may be seen on MR imaging.

Differential Diagnoses

1. Periosteal chondroma

   The radiographic appearance of periosteal chondrosarcoma resembles that of a periosteal chondroma with a surface mass scalloping the cortex from the periosteal side. Compared with a periosteal chondroma, a periosteal chondrosarcoma is larger, has striated calcifications, and does not show an endosteal border of sclerosis.
2. Periosteal osteosarcoma

   Periosteal osteosarcoma is a more aggressive tumor and may demonstrate a sunburst periosteal reaction and osteoid matrix.

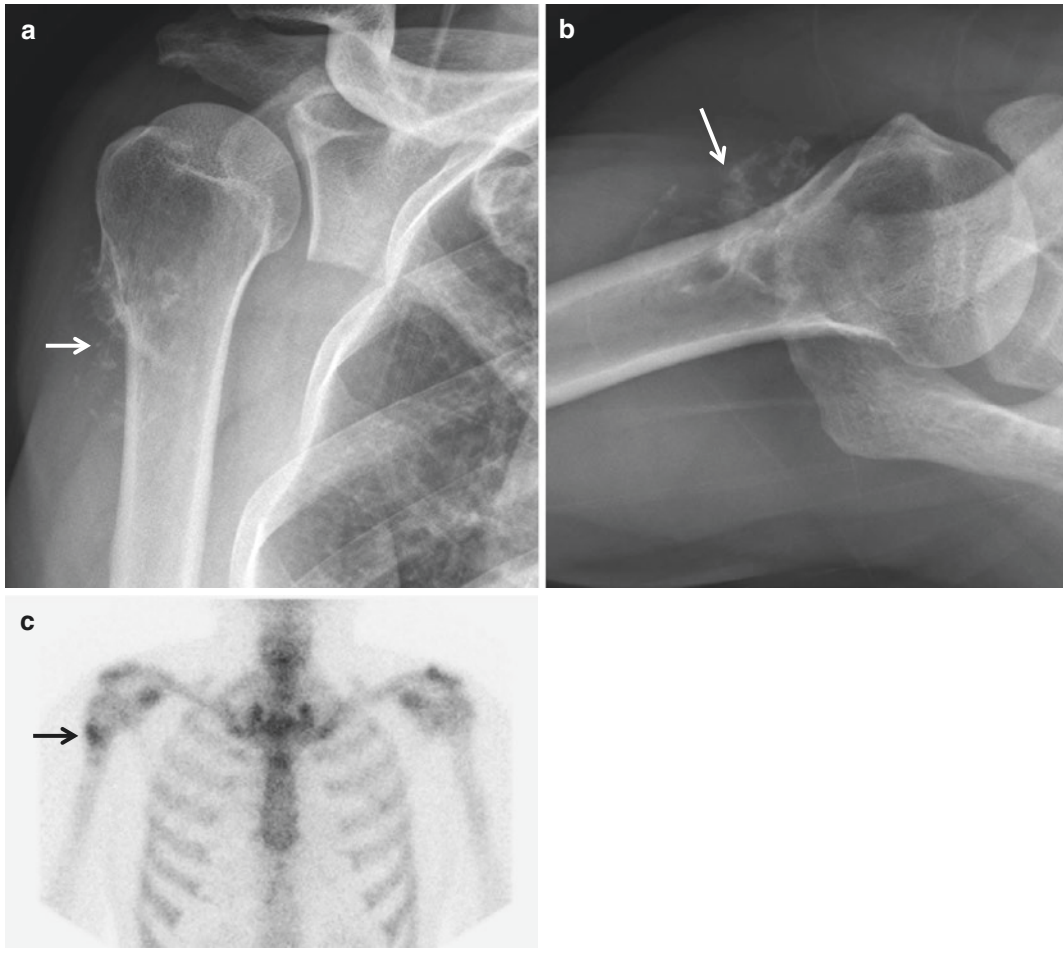

Fig. 3.20 Periosteal chondrosarcoma. (**a**) Anteroposterior radiograph of the right shoulder shows juxtacortical cartilaginous mineralization (*arrow*) and saucerization of the lateral cortex of the right proximal humerus. Also noted is mineralization perpendicular to the cortex. (**b**) Axillary radiograph of the right shoulder again shows juxtacortical cartilaginous mineralization (*arrow*). (**c**) Bone scan shows an increased uptake (*arrow*) in the right proximal humerus. (**d**) Coronal T1-weighted MR image demonstrates low-to-intermediate intense soft tissue mass based on the periosteal surface with osseous erosion (*arrow*). (**e**) Coronal fat-suppressed T2-weighted MR image shows a juxtacortical mass (*arrow*) with heterogeneous high signal intensity. (**f**) Coronal contrast-enhanced T1-weighted MR image demonstrates stippled and rings-and-arcs pattern of enhancement (*arrow*). (**g**) Corresponding gross photograph shows the juxtacortical cartilaginous mass

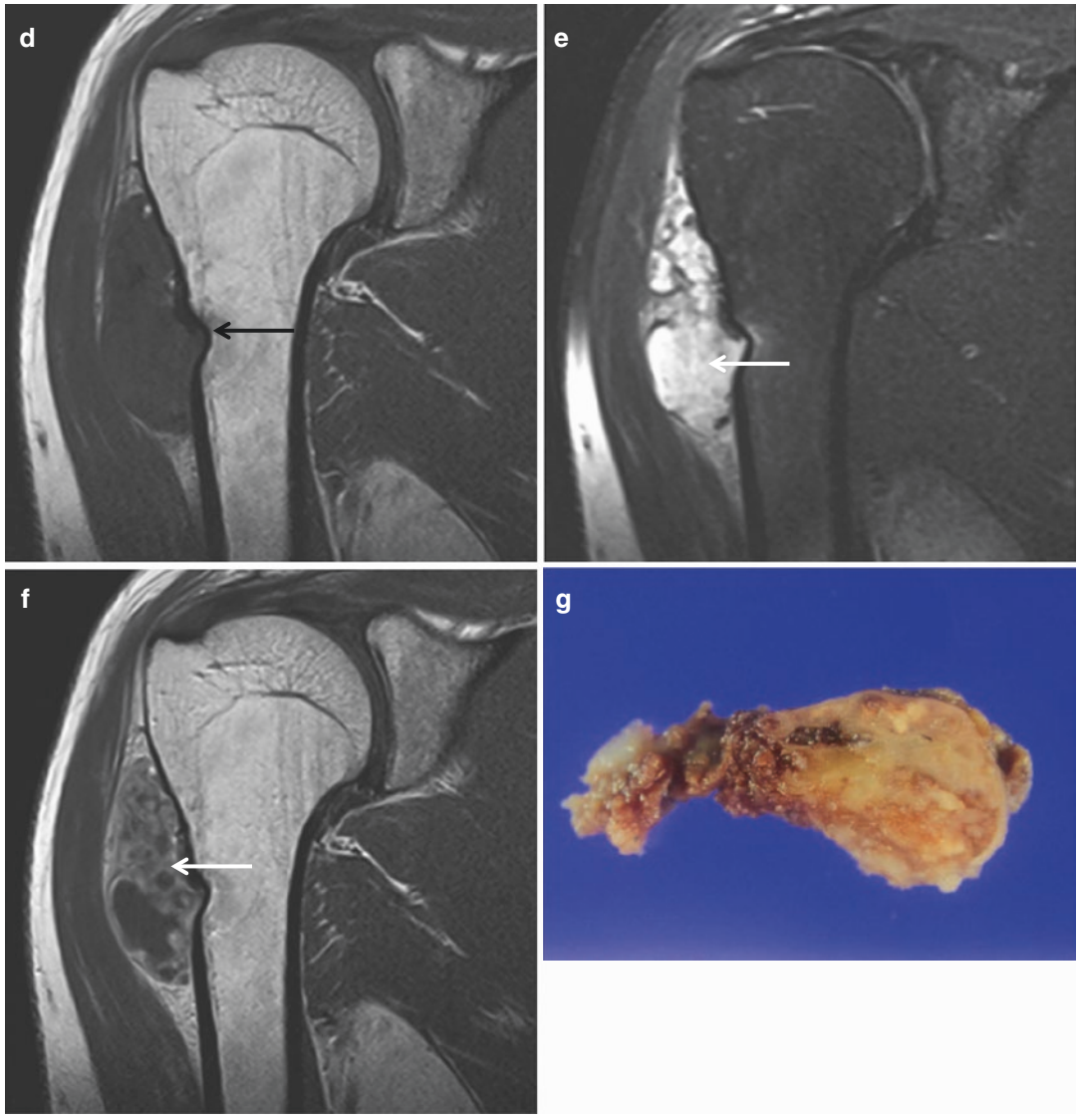

Fig. 3.20 (continued)

3.8.3 Mesenchymal Chondrosarcoma

Overview

Mesenchymal chondrosarcoma is a rare type of chondrosarcoma that consists of highly differentiated cartilage cells and undifferentiated small round cells.

Epidemiology

Mesenchymal chondrosarcoma accounts for about 3–10 % of primary chondrosarcomas. The incidence of mesenchymal chondrosarcoma peaks in the second and third decades, and is equally seen in men and women.

Common Locations

Osseous lesions are common in the craniofacial bones, ribs, ilium, and vertebrae. One-third of mesenchymal chondrosarcoma cases may originate in the soft tissues.

Imaging Features

Radiograph

Radiographic findings of the osseous mesenchymal chondrosarcoma are similar to those seen with conventional chondrosarcoma. Most cases show chondroid calcification.

Magnetic resonance imaging

MR findings of the osseous mesenchymal chondrosarcoma are also similar to those seen with conventional chondrosarcoma.

Differential Diagnoses

1. Dedifferentiated chondrosarcoma

   Dedifferentiated chondrosarcoma appears as an intramedullary tumor with two different components, including a cartilaginous component and a highly aggressive, noncartilaginous osteolytic component.
2. Ewing's sarcoma

   Cortical thickening and cortical saucerization may be seen. Calcifications rarely occur in Ewing's sarcoma.
3. Lymphoma

   Lymphoma appears as a permeative osteolytic lesion commonly associated with extraosseous masses. Lymphoma may spread outside of bone without osseous destruction.
4. Small cell osteosarcoma

   Small cell osteosarcoma appears as an intramedullary, permeative lytic lesion with ill-defined margins that is associated with cortical destruction, aggressive periosteal reaction, and soft tissue mass.

3.8.4 Clear Cell Chondrosarcoma

Overview

Clear cell chondrosarcoma is a low-grade, slow-growing variant of chondrosarcoma, and is characterized histologically by large neoplastic cells with clear and slightly eosinophilic cytoplasm.

Epidemiology

Clear cell chondrosarcoma is usually encountered in the third and fourth decades and is three times more common in men than in women.

Common Locations

Lesions are seen in long bones, such as the femur and humerus, mainly in the epiphyseal equivalent area, and less commonly in the ribs, skull, spine, hands, and feet.

Imaging Features

Radiograph

Radiography shows predominantly lytic lesion with well-defined thin sclerotic rim (Fig. 3.21), or may appear expansive with cortical thinning. Chondroid calcifications are seen in one-third of cases. Occasionally, endosteal scalloping is present. Periosteal reaction is rare.

Magnetic resonance imaging

MR imaging may show homogeneous intermediate signal intensity on T1-weighted images and heterogeneous high signal intensity on fluid-sensitive sequences (Fig. 3.22), which is related to hyaline matrix. Peritumoral bone marrow edema, periosteal reaction, and soft tissue reaction can be seen (Fig. 3.23).

Differential Diagnoses

1. Chondroblastoma

   Chondroblastoma occurs in younger patients with an open growth plate, is smaller than clear cell chondrosarcoma, and is more confined to the epiphysis. The overlap of signal intensity patterns on MR does not allow a reliable differentiation of chondroblastoma and clear cell chondrosarcoma. Chondroblastomas are typically associated with bone marrow edema, periosteal reaction, and soft tissue reaction.
2. Intraosseous ganglion

   Intraosseous ganglion does not have chondroid calcification, but may have a sclerotic rim.
3. Metastasis

   Metastasis may appear more aggressive than clear cell chondrosarcoma and does not show chondroid calcification.
4. Giant cell tumor

   Giant cell tumor does not have chondroid calcification and is typically eccentric.

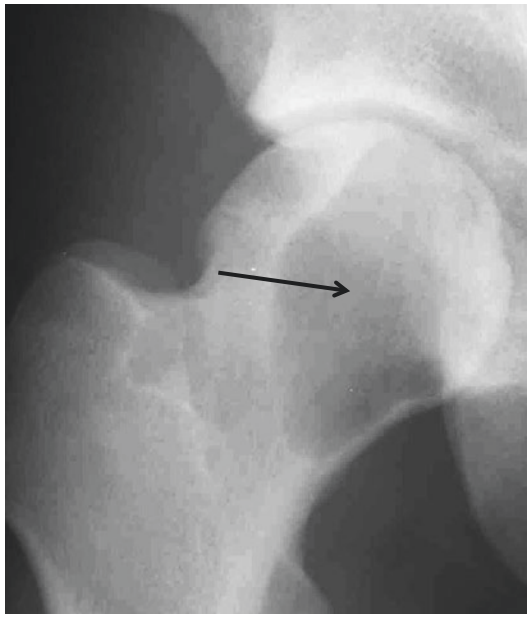

Fig. 3.21 Clear cell chondrosarcoma. Anteroposterior radiograph of the right hip shows a well-defined osteolytic lesion (*arrow*) with no mineralization in the epiphyseal location of the proximal femur

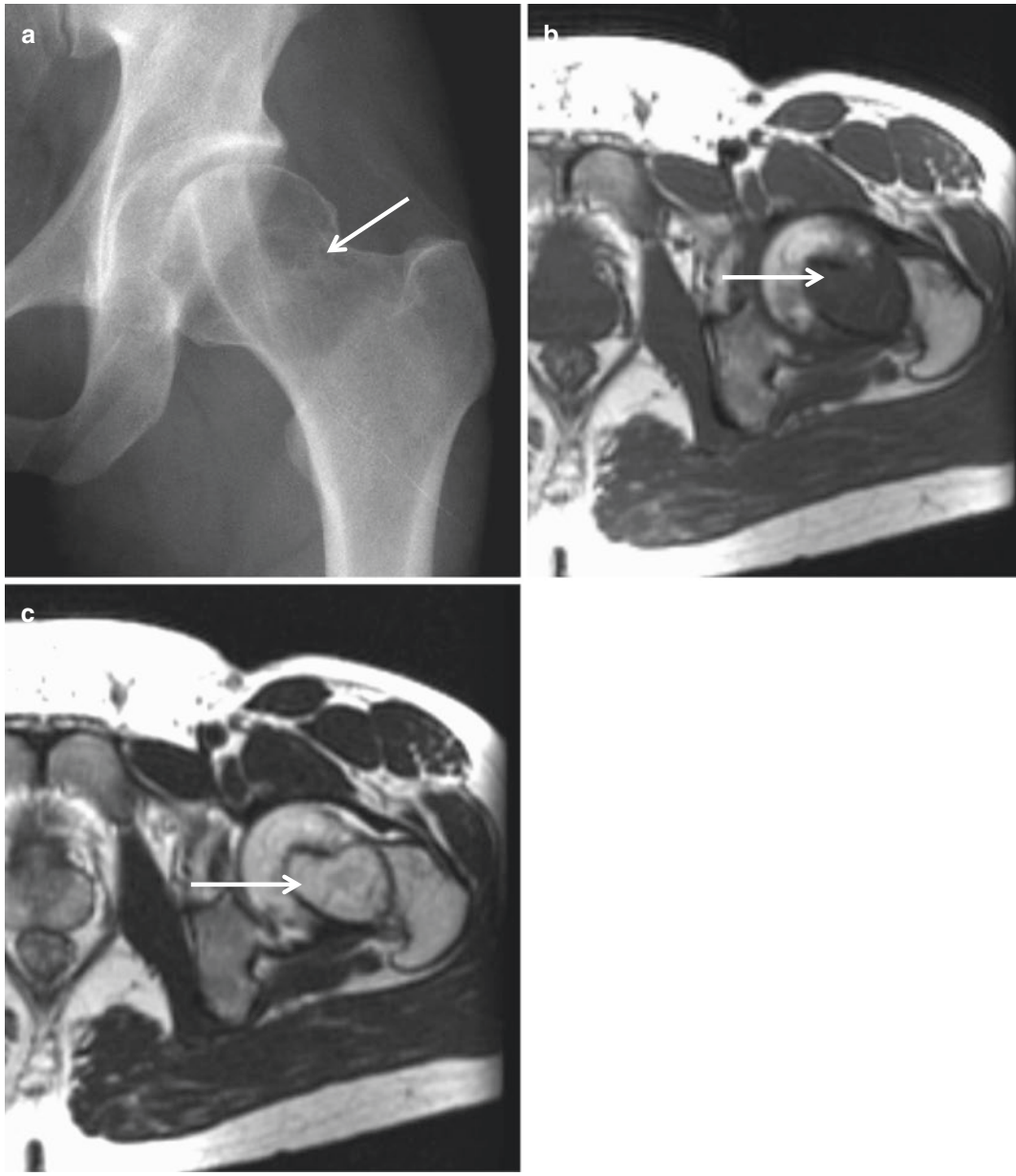

Fig. 3.22 Clear cell chondrosarcoma. (**a**) Anteroposterior radiograph of the left hip shows a well-defined osteolytic lesion (*arrow*) with no mineralization in the epiphyseal location of the proximal femur. (**b**) Axial T1-weighted MR image demonstrates a well-defined lesion with relatively homogeneous intermediate signal intensity (*arrow*). (**c**) Axial T2-weighted MR image demonstrates a well-defined lesion with heterogeneous high signal intensity (*arrow*). (**d**) Coronal T1-weighted MR image demonstrates a well-defined lesion with relatively homogeneous intermediate signal intensity (*arrow*). (**e**) Coronal T2-weighted MR image demonstrates a well-defined lesion with heterogeneous high signal intensity (*arrow*)

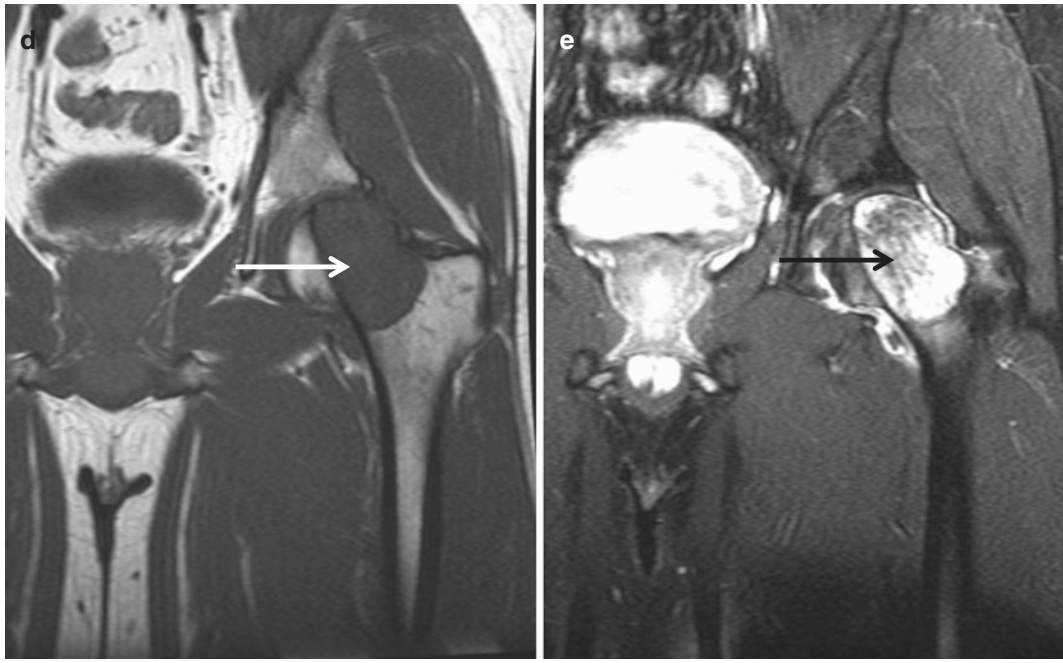

Fig. 3.22 (continued)

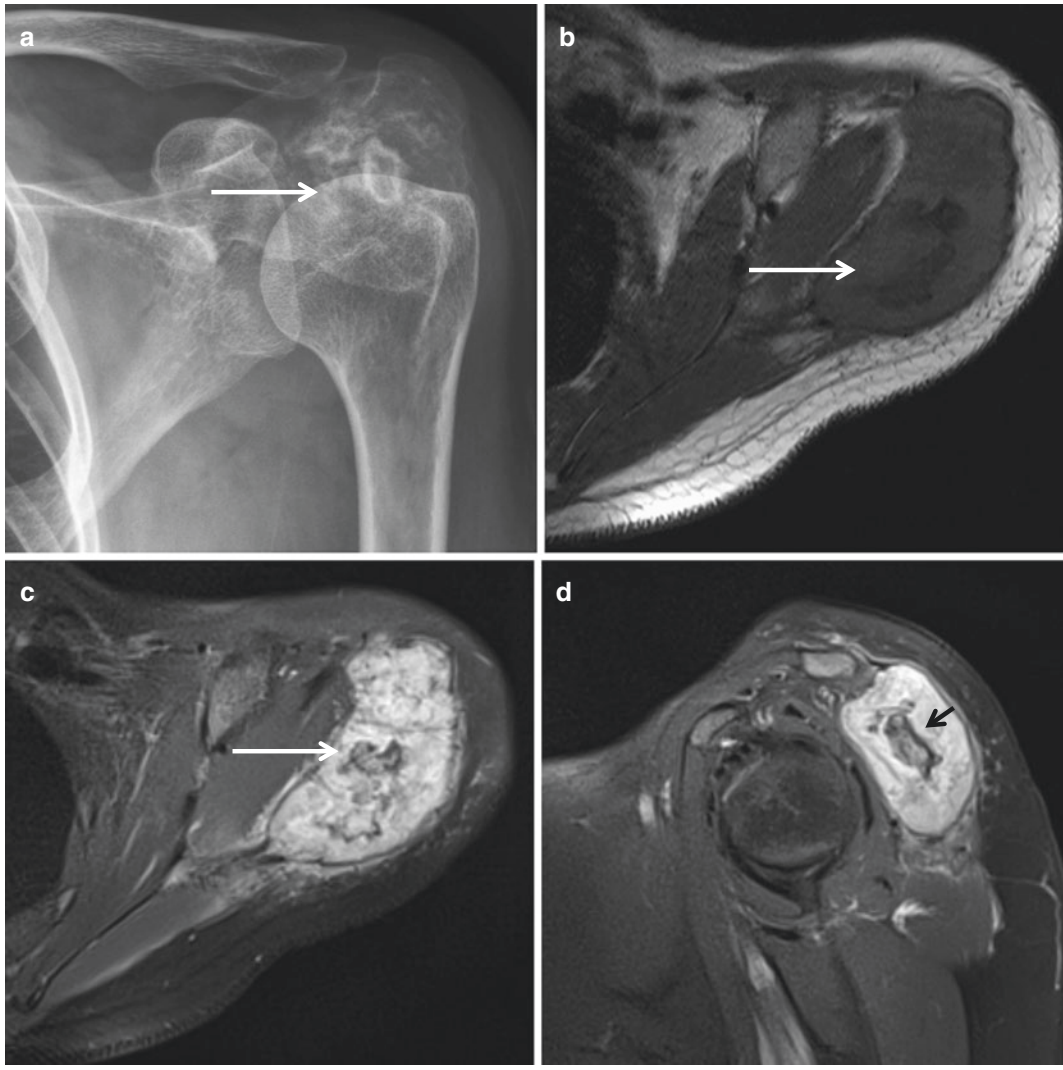

Fig. 3.23 Clear cell chondrosarcoma. (**a**) Anteroposterior radiograph of the left shoulder shows a lobulated expansile osteolytic lesion (*arrow*) with chondroid mineralization in the acromion and scapular spine. (**b**) Axial T1-weighted MR image demonstrates a lobulated mass with heterogeneous low-to-intermediate signal intensity (*arrow*). (**c**) Axial fat-suppressed T2-weighted MR image demonstrates a lobulated mass with heterogeneous high signal intensity (*arrow*) with stippled, rings-and-arcs pattern of low signal intensity. (**d**) Sagittal fat-suppressed T2-weighted MR image again shows a lobulated mass with heterogeneous high signal intensity (*arrow*) with stippled, rings-and-arcs pattern of low signal intensity

3.8.5 Dedifferentiated Chondrosarcoma

Overview

Dedifferentiated chondrosarcoma, which accounts for 10 % of chondrosarcomas, is composed of a well-differentiated chondrogenic lesion (low-grade chondrosarcoma, enchondroma, or osteochondroma) and a high-grade noncartilaginous lesion (undifferentiated high-grade pleomorphic sarcoma, fibrosarcoma, or osteosarcoma).

Epidemiology

Dedifferentiated chondrosarcoma most commonly occurs in the fifth to ninth decades, and has a slight male predominance.

Common Locations

The femur is the most frequently involved bone, followed by the pelvis, humerus, ribs, and scapula.

Imaging Features

Radiograph

Radiographs may show an intramedullary tumor with two different components, including a cartilaginous component showing chondroid calcifications and a highly aggressive, noncartilaginous osteolytic component with ill-defined margins, cortical penetration, and soft tissue mass.

Magnetic resonance imaging

Fluid-sensitive sequences may show two distinct areas of signal intensity, with the low-grade chondrosarcoma appearing hyperintense but the high-grade dedifferentiated component having relatively reduced signal intensity.

Differential Diagnoses

1. High-grade conventional chondrosarcoma

   High-grade conventional chondrosarcoma does not show the biphasic character of the dedifferentiated chondrosarcoma with sharp demarcation of the two components.
2. Mesenchymal chondrosarcoma

   Mesenchymal chondrosarcoma shows a more gradual transition between the regions of chondroid elements and the undifferentiated round-cell or spindle-cell components than that seen in dedifferentiated chondrosarcoma.
3. Metastatic high-grade spindle-cell sarcoma

   Metastatic high-grade spindle-cell sarcoma in bone, including leiomyosarcoma and rhabdomyosarcoma, can mimic dedifferentiated chondrosarcoma.

Suggested Reading

Benign: Osteochondroma

Kenan S, Abdelwahab IF, Klein MJ, Hermann G, Lewis MM. Lesions of juxtacortical origin (surface lesions of bone). Skelet Radiol. 1993;22:337–57.
Ludwig K. Cartilage tumours. In: Davies AM, Sundaram M, James SLJ, editors. Imaging of bone tumors and tumor-like lesions: techniques and applications. 1st ed. Berlin: Springer; 2009. p. 225–50.
Motamedi K, Seeger LL. Benign bone tumors. Radiol Clin N Am. 2011;49:1115–34.
Murphey MD, Choi JJ, Kransdorf MJ, Flemming DJ, Gannon FH. Imaging of osteochondroma: variants and complications with radiologic-pathologic correlation. Radiographics. 2000;20:1407–34.
Nichols RE, Dixon LB. Radiographic analysis of solitary bone lesions. Radiol Clin N Am. 2011;49: 1095–114.

Benign : Enchondroma

Currie JW, Davis KW, Lafita VS, Blankenbaker DG, De Smet AA, Rosas H, Lee KS. Musculoskeletal mnemonics: differentiating features. Curr Probl Diagn Radiol. 2011;40:45–71.
Eisenberg RL. Bubbly lesions of bone. AJR Am J Roentgenol. 2009;193:W79–94.
Ludwig K. Cartilage tumours. In: Davies AM, Sundaram M, James SLJ, editors. Imaging of bone tumors and tumor-like lesions: techniques and applications. 1st ed. Berlin: Springer; 2009. p. 225–50.
Motamedi K, Seeger LL. Benign bone tumors. Radiol Clin N Am. 2011;49:1115–34.
Nichols RE, Dixon LB. Radiographic analysis of solitary bone lesions. Radiol Clin N Am. 2011;49:1095–114.

Benign: Periosteal Chondroma (Juxtacortical Chondroma)

Kenan S, Abdelwahab IF, Klein MJ, Hermann G, Lewis MM. Lesions of juxtacortical origin (surface lesions of bone). Skelet Radiol. 1993;22:337–57.
Ludwig K. Cartilage tumours. In: Davies AM, Sundaram M, James SLJ, editors. Imaging of bone tumors and tumor-like lesions: techniques and applications. 1st ed. Berlin: Springer; 2009. p. 225–50.
Motamedi K, Seeger LL. Benign bone tumors. Radiol Clin N Am. 2011;49:1115–34.
Seeger LL, Yao L, Eckardt JJ. Surface lesions of bone. Radiology. 1998;206:17–33.

Benign: Chondromyxoid Fibroma

Ludwig K. Cartilage tumours. In: Davies AM, Sundaram M, James SLJ, editors. Imaging of bone tumors and tumor-like lesions: techniques and applications. 1st ed. Berlin: Springer; 2009. p. 225–50.
Motamedi K, Seeger LL. Benign bone tumors. Radiol Clin N Am. 2011;49:1115–34.

Benign: Subungual Exostosis

Higuchi K, Oiso N, Yoshida M, Kawada A. Preoperative assessment using magnetic resonance imaging for subungual exostosis beneath the proximal region of the nail plate. Case Rep Dermatol. 2011;3: 155–7.
Kenan S, Abdelwahab IF, Klein MJ, Hermann G, Lewis MM. Lesions of juxtacortical origin (surface lesions of bone). Skelet Radiol. 1993;22:337–57.
Ludwig K. Cartilage tumours. In: Davies AM, Sundaram M, James SLJ, editors. Imaging of bone tumors and tumor-like lesions: techniques and applications. 1st ed. Berlin: Springer; 2009. p. 225–50.
Murphey MD, Choi JJ, Kransdorf MJ, Flemming DJ, Gannon FH. Imaging of osteochondroma: variants and complications with radiologic-pathologic correlation. Radiographics. 2000;20:1407–34.
Seeger LL, Yao L, Eckardt JJ. Surface lesions of bone. Radiology. 1998;206:17–33.

Benign: Bizarre Parosteal Osteochondromatous Proliferation

Kenan S, Abdelwahab IF, Klein MJ, Hermann G, Lewis MM. Lesions of juxtacortical origin (surface lesions of bone). Skelet Radiol. 1993;22:337–57.
Seeger LL, Yao L, Eckardt JJ. Surface lesions of bone. Radiology. 1998;206:17–33.
Torreggiani WC, Munk PL, Al-Ismail K, O'Connell JX, Nicolaou S, Lee MJ, Masri BA. MR imaging features of bizarre parosteal osteochondromatous proliferation of bone (Nora's lesion). Eur J Radiol. 2001; 40:224–31.

Benign: Chondroblastoma

Kaim AH, Hügli R, Bonél HM, Jundt G. Chondroblastoma and clear cell chondrosarcoma: radiological and MRI characteristics with histopathological correlation Skeletal Radiol. 2002;31:88–95.

Ludwig K. Cartilage tumours. In: Davies AM, Sundaram M, James SLJ, editors. Imaging of bone tumors and tumor-like lesions: techniques and applications. 1st ed. Berlin: Springer; 2009. p. 225–50.
Motamedi K, Seeger LL. Benign bone tumors. Radiol Clin N Am. 2011;49:1115–34.

Malignant: Conventional Intramedullary Chondrosarcoma

Czerniak B. Malignant cartilage tumors. In: Czerniak B, editor. Dorfman and Czerniak's bone tumors. 2nd ed. Philadelphia: Elsevier Saunders; 2016. p.474–569.
Kaste SC. Imaging pediatric bone sarcomas. Radiol Clin N Am. 2011; 49:749–65.
Ludwig K. Cartilage tumours. In: Davies AM, Sundaram M, James SLJ, editors. Imaging of bone tumors and tumor-like lesions: techniques and applications. 1st ed. Berlin: Springer; 2009. p. 225–50.
Murphey MD, Flemming DJ, Boyea SR, Bojescul JA, Sweet DE, Temple HT. Enchondroma versus chondrosarcoma in the appendicular skeleton: differentiating features. Radiographics. 1998;18:1213–37
Rajiah P, Ilaslan H, Sundaram M. Imaging of primary malignant bone tumors (nonhematological). Radiol Clin N Am. 2011;49:1135–61.

Malignant: Periosteal/Juxtacortical Chondrosarcoma

Czerniak B. Malignant cartilage tumors. In: Czerniak B, editor. Dorfman and Czerniak's bone tumors. 2nd ed. Philadelphia: Elsevier Saunders; 2016. p.474–569.
Kenan S, Abdelwahab IF, Klein MJ, Hermann G, Lewis MM. Lesions of juxtacortical origin (surface lesions of bone). Skelet Radiol. 1993;22:337–57.
Ludwig K. Cartilage tumours. In: Davies AM, Sundaram M, James SLJ, editors. Imaging of bone tumors and tumor-like lesions: techniques and applications. 1st ed. Berlin: Springer; 2009. p. 225–50.
Rajiah P, Ilaslan H, Sundaram M. Imaging of primary malignant bone tumors (nonhematological). Radiol Clin N Am. 2011;49:1135–61.
Seeger LL, Yao L, Eckardt JJ. Surface lesions of bone. Radiology. 1998;206:17–33.

Malignant: Mesenchymal Chondrosarcoma

Czerniak B. Malignant cartilage tumors. In: Czerniak B, editor. Dorfman and Czerniak's bone tumors. 2nd ed. Philadelphia: Elsevier Saunders; 2016. p. 474–569.
Ludwig K. Cartilage tumours. In: Davies AM, Sundaram M, James SLJ, editors. Imaging of bone tumors and tumor-like lesions: techniques and applications. 1st ed. Berlin: Springer; 2009. p. 225–50.
Rajiah P, Ilaslan H, Sundaram M. Imaging of primary malignant bone tumors (nonhematological). Radiol Clin N Am. 2011;49:1135–61.

Malignant: Clear Cell Chondrosarcoma

Czerniak B. Malignant cartilage tumors. In: Czerniak B, ed. Dorfman and Czerniak's bone tumors. 2nd ed. Philadelphia: Elsevier Saunders; 2016. p. 474–569.
Kaim AH, Hügli R, Bonél HM, Jundt G. Chondroblastoma and clear cell chondrosarcoma: radiological and MRI characteristics with histopathological correlation Skeletal Radiol. 2002;31:88–95.
Ludwig K. Cartilage tumours. In: Davies AM, Sundaram M, James SLJ, editors. Imaging of bone tumors and tumor-like lesions: techniques and applications. 1st ed. Berlin: Springer; 2009. p. 225–50.
Rajiah P, Ilaslan H, Sundaram M. Imaging of primary malignant bone tumors (nonhematological). Radiol Clin N Am. 2011;49:1135–61.

Malignant: Dedifferentiated Chondrosarcoma

Czerniak B. Malignant cartilage tumors. In: Czerniak B, editor. Dorfman and Czerniak's bone tumors. 2nd ed. Philadelphia: Elsevier Saunders; 2016. p. 474–569.
Ludwig K. Cartilage tumours. In: Davies AM, Sundaram M, James SLJ, editors. Imaging of bone tumors and tumor-like lesions: techniques and applications. 1st ed. Berlin: Springer; 2009. p. 225–50.
MacSweeney F, Darby A, Saifuddin A. Dedifferentiated chondrosarcoma of the appendicular skeleton: MRI-pathological correlation. Skelet Radiol. 2003;32:671–8.
Rajiah P, Ilaslan H, Sundaram M. Imaging of primary malignant bone tumors (nonhematological). Radiol Clin N Am. 2011;49:1135–61.

Fibrogenic and Fibrohistiocytic Tumors

4

Contents

4.1 Desmoplastic Fibroma of Bone

Overview

Desmoplastic fibroma of bone is a rare, locally aggressive benign tumor, characterized by the presence of spindle cells and abundant collagen produced by the tumor cells. It is the intraosseous counterpart of the soft tissue desmoid tumor. It does not metastasize and is considered benign, but is locally aggressive, and recurrences are common after curettage.

Epidemiology

Desmoplastic fibroma of bone accounts for <0.1 % of primary bone tumors, and 0.3 % of benign bone tumors. It can be seen at any age, but it is common in adolescents and young adults, with most cases occurring in the second and third decades of life. It distributes equally in both genders.

Common Locations

Desmoplastic fibromas are most common in the mandible, followed by femur, pelvic bone, radius, and tibia. In the long bones, desmoplastic fibromas are usually located at the metadiaphysis (Fig. 4.1). They may extend to the epiphysis in patients with closed physis (Fig. 4.2).

H.S. Kang et al., *Oncologic Imaging: Bone Tumors*, DOI 10.1007/978-981-287-703-1_4

Imaging Features

Radiograph

Desmoplastic fibromas are well-defined osteolytic lesions noted at the metadiaphysis of a long bone. They may have a sclerotic border and usually expand the bone. The internal trabeculations or ridges within the lesion, along with bone expansion, give a soap-bubble appearance on radiograph (Fig. 4.2). Periosteal reaction is rarely seen with desmoplastic fibromas.

Magnetic resonance imaging

Desmoplastic fibromas usually appear hypointense on T1-weighted images, and heterogeneous isointense to hypointense on T2-weighted images, with heterogeneous enhancement. The signal intensity of desmoplastic fibroma on MR imaging is attributable to its collagen content, as for soft tissue desmoid tumors. Therefore, the signal intensity of the desmoplastic fibromas may vary according to the proportion of collagen content and cellular component. Acellular lesions with rich collagenous stroma exhibit hypointensity on T2-weighted images, whereas more cellular lesions with relatively small amount of collagenous stroma exhibit isointensity to hyperintensity on T2-weighted images (Fig. 4.3).

Differential Diagnoses

1. Aneurysmal bone cyst

   The radiographic appearance of desmoplastic fibromas and aneurysmal bone cysts may be similar; expansile osteolytic lesions with well-defined borders occur in the metadiaphysis. However, the two lesions are readily differentiated on MRI; aneurysmal bone cysts appear as multiloculated cystic lesions with multiple fluid–fluid levels.
2. Chondromyxoid fibroma

   Chondromyxoid fibromas exhibit soap-bubble appearance on radiograph, similar to desmoplastic fibromas. However, on MR imaging, chondromyxoid fibromas are distinguished from desmoplastic fibromas by their predominantly high signal intensity on T2-weighted imaging.
3. Other differentials may include fibrous dysplasia and giant cell tumor

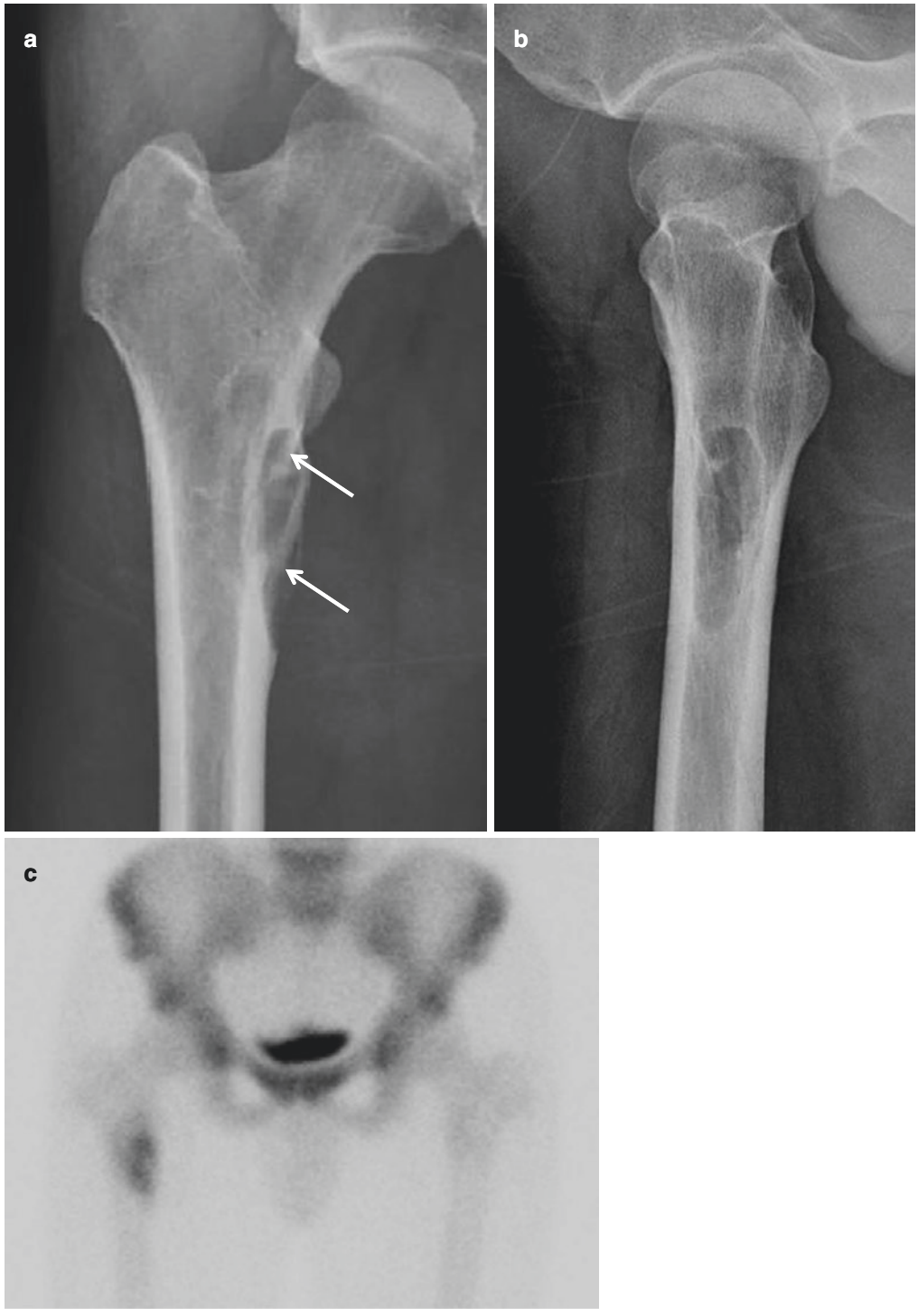

Fig. 4.1 Desmoplastic fibroma of bone. (**a**) Anteroposterior and (**b**) lateral radiographs show a well-defined osteolytic lesion at the proximal metadiaphysis of the femur. Intralesional trabeculations are seen within the lesion (*white arrow* in **a**). (**c**) The lesion shows increased uptake on bone scan

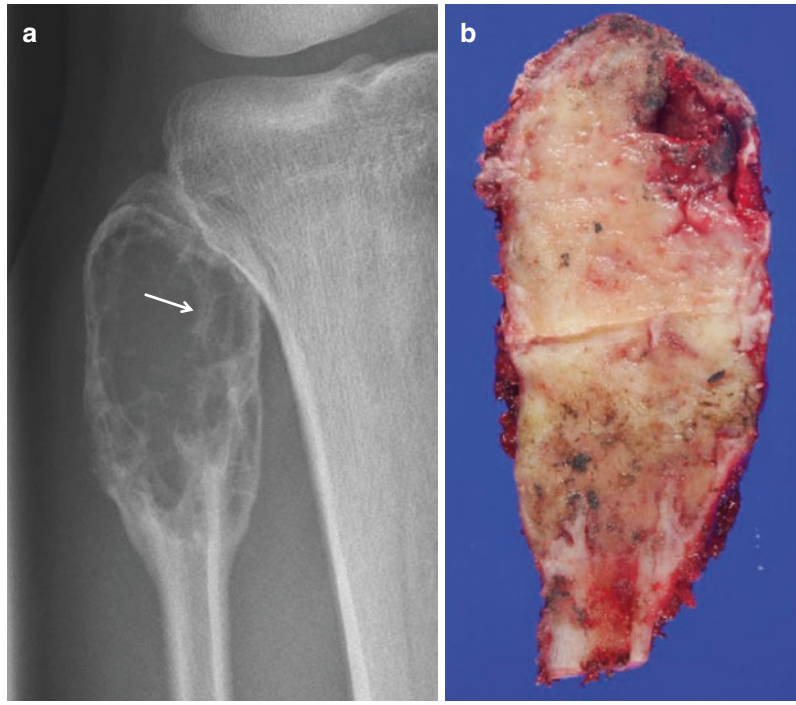

Fig. 4.2 Desmoplastic fibroma of bone. (**a**) A well-defined expansile osteolytic lesion is seen at the proximal epimetaphysis of the fibula on radiograph. Internal trabeculations or ridges (*white arrow*) are seen within the lesion, giving the lesion a soap-bubble appearance. (**b**) Section through the specimen of resected proximal fibula shows expansile lobulated solid fibrous tumor. The lesion appears isointense to adjacent muscle on T1-weighted images (**c**, **e**) and heterogeneous on T2-weighted images (**d**), and exhibits heterogeneous enhancement (**e**). Areas of hypointensity are noted on T2-weighted images due to the rich collagen content. Internal ridges are noted at the periphery of the lesion on axial images (*arrowheads* in **e**, **f**)

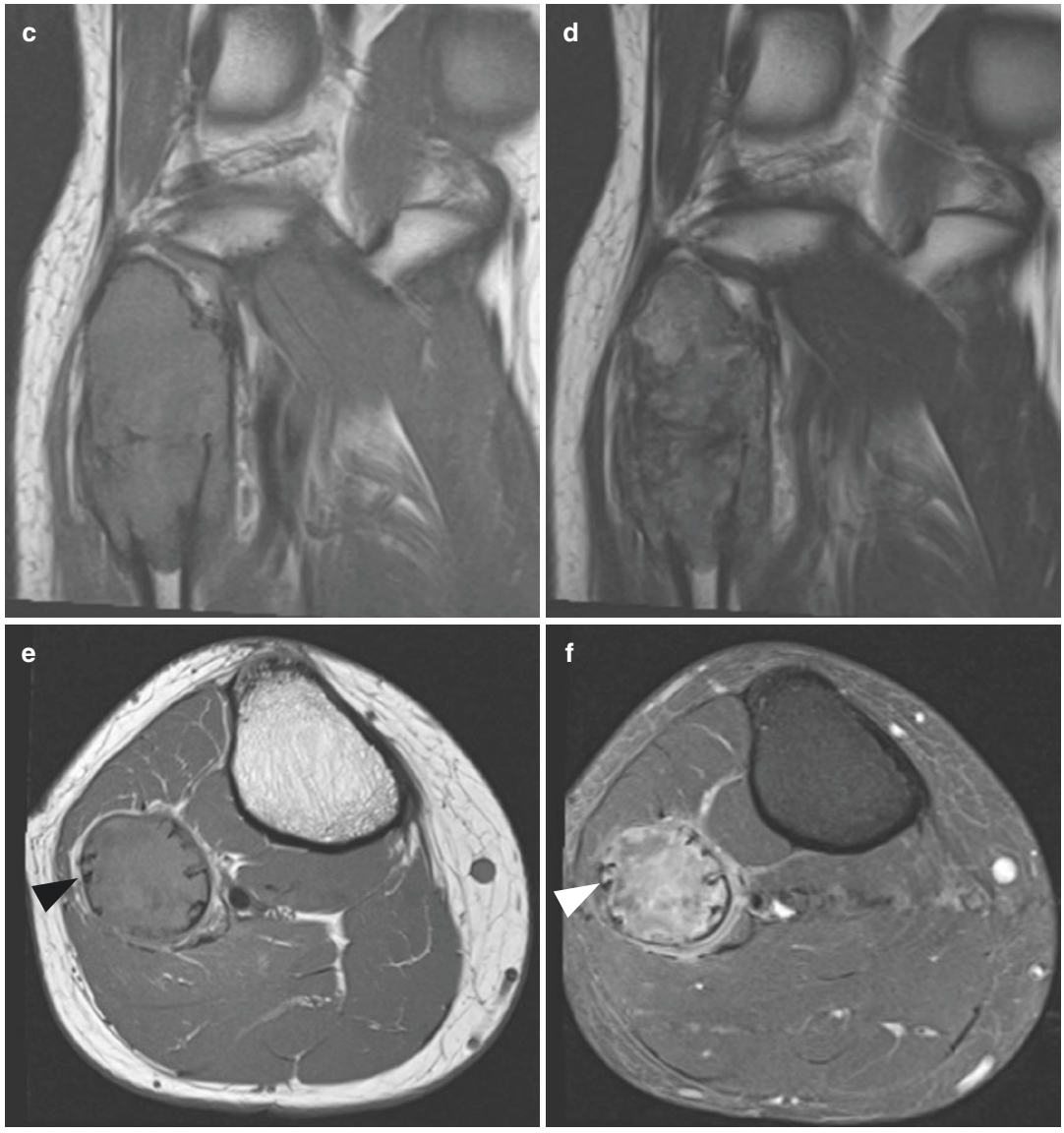

Fig. 4.2 (continued)

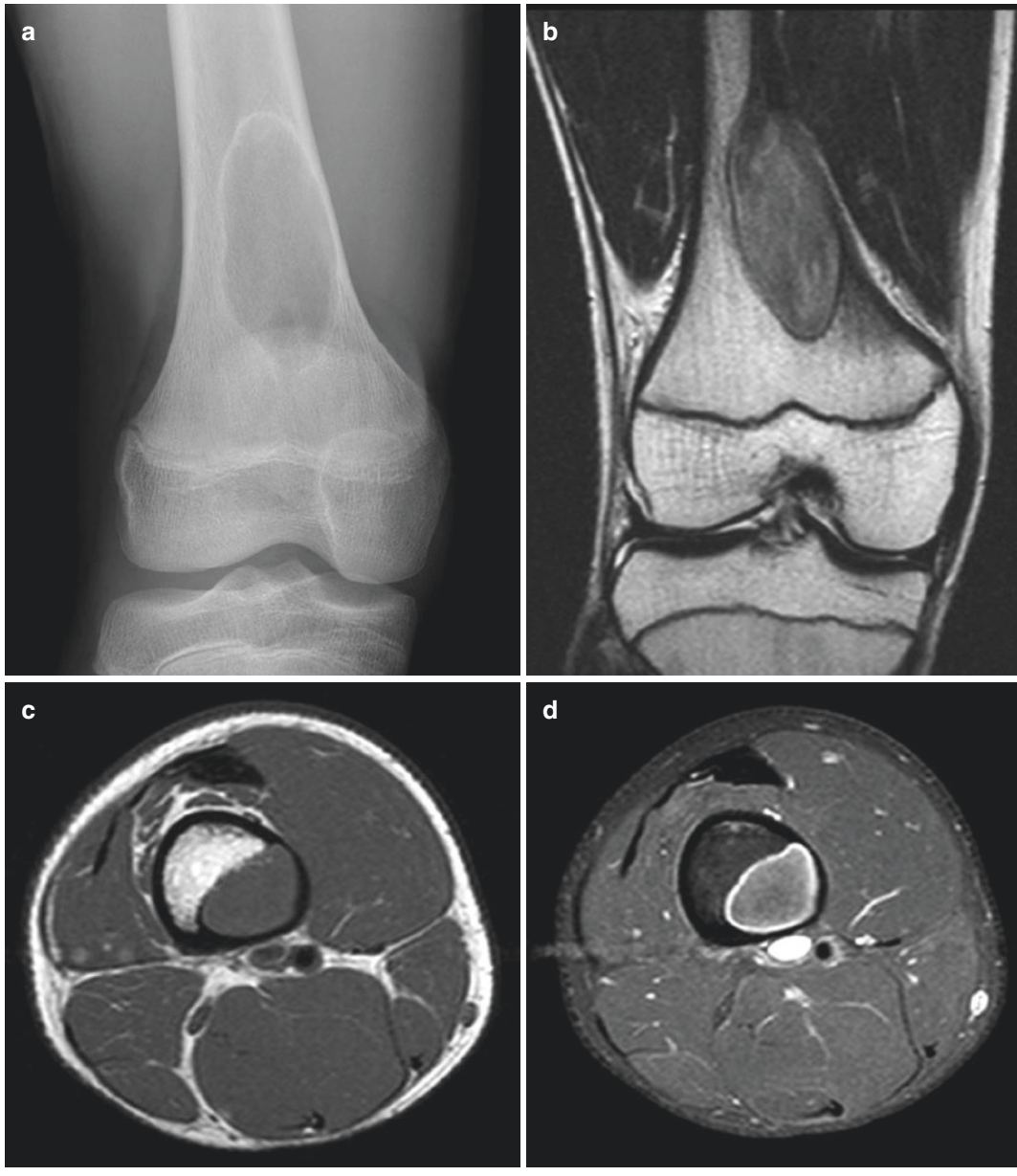

Fig. 4.3 Desmoplastic fibroma of bone. (**a**) A geographical osteolytic lesion with a thin sclerotic rim is noted at distal femoral metadiaphysis on anteroposterior radiograph. (**b**) The lesion appears heterogeneous on T2-weighted image with areas of hypointensity corresponding to the collagenous stroma. The lesion shows intermediate signal intensity on T1-weighted image (**c**) and shows mild enhancement on contrast-enhanced T1-weighted fat-suppressed image (**d**)

4.2 Fibrosarcoma of Bone

Overview

Fibrosarcoma of bone is a rare malignant spindle cell neoplasm of the bone. Fibrosarcomas were originally reported to show a characteristic histological appearance, "herringbone" pattern. However, more recent studies have revealed that the "herringbone" pattern is not a finding specific to fibrosarcoma and that it can be seen in a variety of other primary bone tumors. Moreover, the advances in immunohistochemistry and molecular genetic analysis have resulted in the reclassification of tumors previously diagnosed as fibrosarcomas, into other primary bone tumors. Nowadays, fibrosarcoma is less commonly used as a specific diagnostic category and is considered a diagnosis of exclusion.

Epidemiology

Fibrosarcoma of bone has been reported to account for <5 % of all primary malignant bone tumors. It usually occurs in the third to sixth decades of life and has an equal distribution between genders.

Common Locations

Fibrosarcoma is common in long tubular bone, and within a tubular bone, it has a metaphyseal or metadiaphyseal location. The femur is most commonly affected, followed by humerus, tibia, and pelvic bones.

Imaging Features

Radiograph

Fibrosarcomas are osteolytic lesions with a wide zone of transition exhibiting a moth-eaten or permeative pattern of bone destruction. They frequently destruct the cortex and extend to the surrounding soft tissue, but periosteal reactions are rare. Low-grade fibrosarcomas may exhibit more defined borders.

Magnetic resonance imaging

The MR imaging findings of fibrosarcoma are nonspecific. MR imaging cannot be used to distinguish fibrosarcomas from other tumors, but is rather used to determine the intramedullary extent of the lesion and the presence and extent of soft tissue extension (Fig. 4.4).

Differential Diagnoses

1. Differential diagnoses for low-grade fibrosarcoma
   - Desmoplastic fibroma, chondromyxoid fibroma, giant cell tumor
2. Differential diagnoses for high-grade fibrosarcoma
   - Metastasis, plasmacytoma, lymphoma

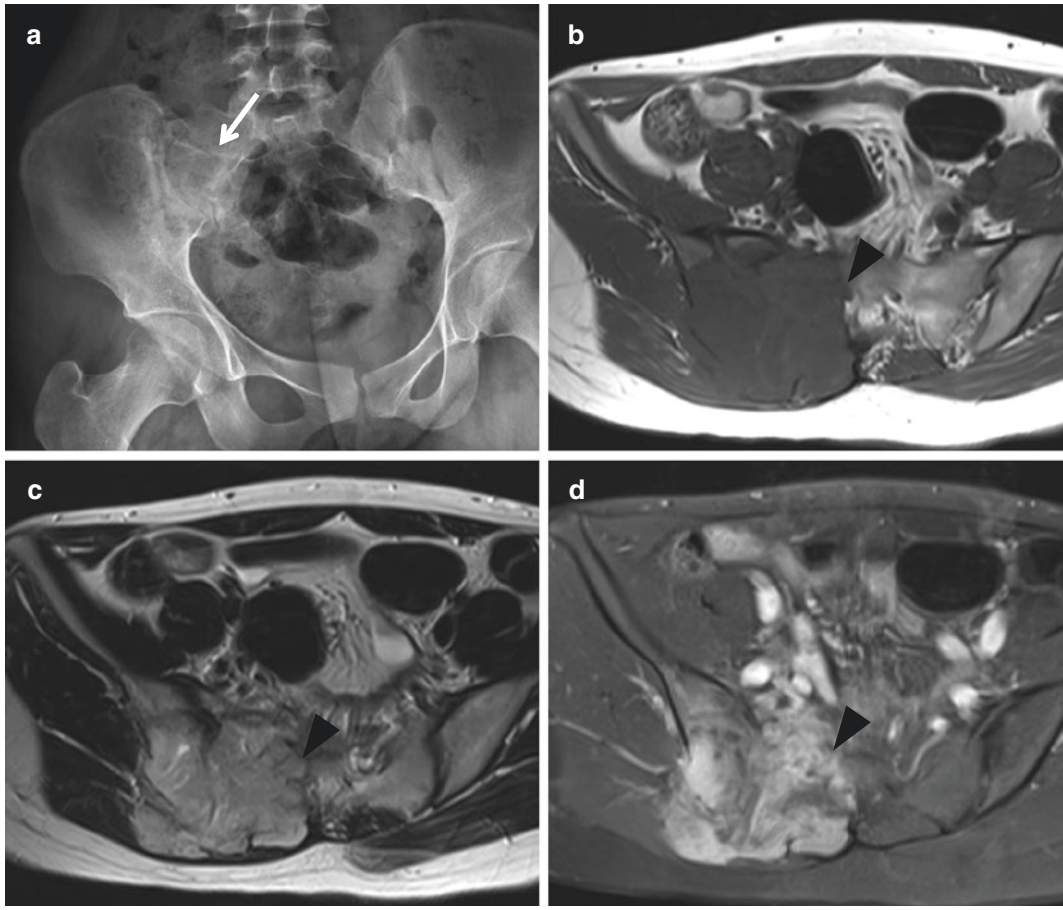

Fig. 4.4 Fibrosarcoma of bone. (**a**) The cortical margin of the right posterior ilium (*white arrowhead*) is blurred, compared to the contralateral side, due to the presence of a bone destructing mass. (**b**) Axial T1-weighted, (**c**) T2-weighted, and (**d**) contrast-enhanced T1-weighted fat-suppressed images show a large osteolytic mass involving the right posterior ilium and right sacral ala, with extraosseous extension to the paraspinal and gluteal muscles. The right S1 sacral neural foramen is encroached (*black arrowhead*). The MR imaging findings of fibrosarcoma are nonspecific and cannot be used to distinguish fibrosarcomas from other tumors

4.3 Nonossifying Fibroma/ Fibrous Cortical Defect

Overview

Nonossifying fibroma (NOF) and fibrous cortical defect (FCD) are common benign bone tumors consisting of benign fibroblastic proliferations intermingled with multinucleated osteoclast-type giant cells. Lesions that are confined to the cortex are called "fibrous cortical defects," and lesions that are larger and extend to the medullary cavity are called "nonossifying fibromas."

Epidemiology

The exact incidence of NOF/FCD is not known, as most lesions are asymptomatic, incidentally found, and undergo spontaneous resolution. The estimated incidence is around 30–40 % in asymptomatic children and teens.

Common Locations

NOFs/FCDs occur in the metaphysis of the long bone, with a cortical or eccentric corticomedullary location (Fig. 4.5). The most common site is the distal femur followed by the proximal and distal tibia. Among nontubular bones, the ilium is most commonly affected.

Imaging Features

Radiograph

NOFs/FCDs are seen as well-defined geographical radiolucent lesions with a sclerotic border, and are eccentrically located at the metaphysis or diaphysis of long bones. FCDs are limited within the cortex, whereas NOFs extend into the adjacent medullary cavity. They usually start at the metaphysis and migrate away from the epiphysis along with the bone growth, and may end up in a diaphyseal location. NOFs/FCDs are known for their natural course of spontaneous resolution. Along the course of evolution, lesions become sclerotic, and new bone formation gradually fills the lucent lesion, leading to its disappearance (Fig. 4.6).

Magnetic resonance imaging

NOFs/FCDs exhibit variable signal intensity according to the evolutional stage of lesion, but are generally isointense to hypointense to muscle on T1-weighted images, and intermediate to hyperintense on T2-weighted images (Fig. 4.7). Lesions may accompany a hypointense rim on both T1-weighted and T2-weighted images corresponding to the sclerotic border on radiograph (Fig. 4.8). They may show variable contrast enhancements.

Differential Diagnoses

1. Fibrous dysplasia

   Fibrous dysplasia has a central intramedullary location, whereas NOFs/FCDs are eccentrically located within the cortex with or without intramedullary extension. A typical fibrous dysplasia has ground-glass appearance on radiograph.
2. Osteofibrous dysplasia

   Osteofibrous dysplasia occurs as a cortical lesion, but is located in the diaphysis and commonly occurs at a typical location, the anterior cortex of the tibia.

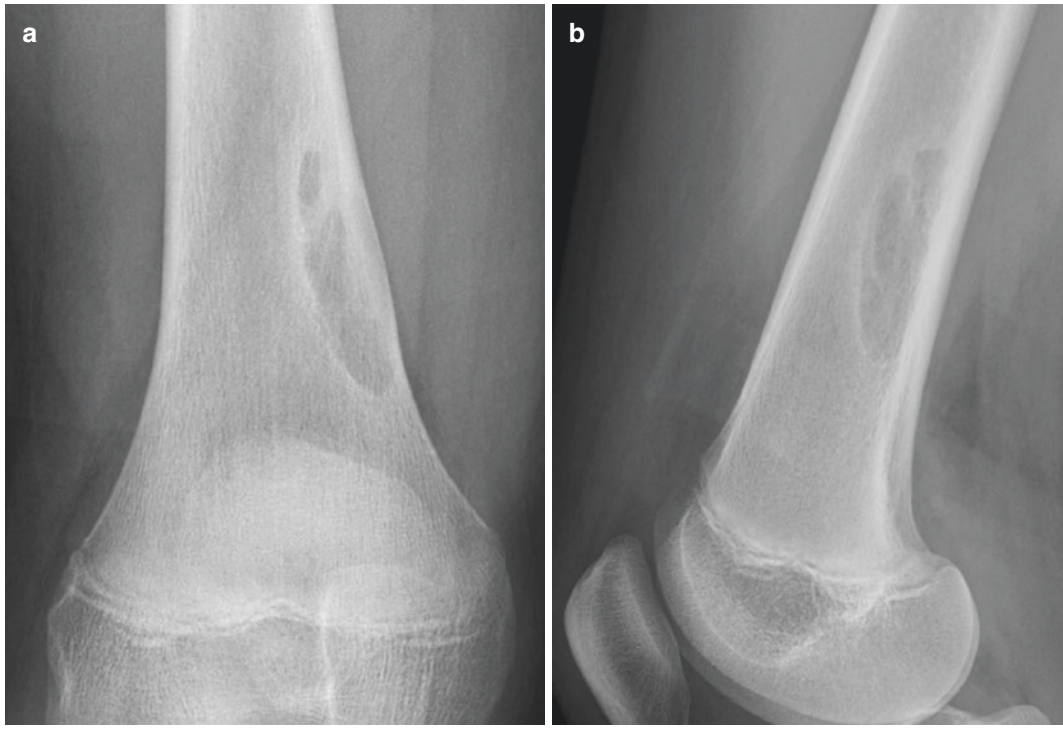

Fig. 4.5 Nonossifying fibroma. (**a**) Anteroposterior and (**b**) lateral radiographs of the femur show a well-defined osteolytic lesion with a thin sclerotic border at the distal metadiaphysis of the femur, with an eccentric intramedullary location, in a 15-year-old male

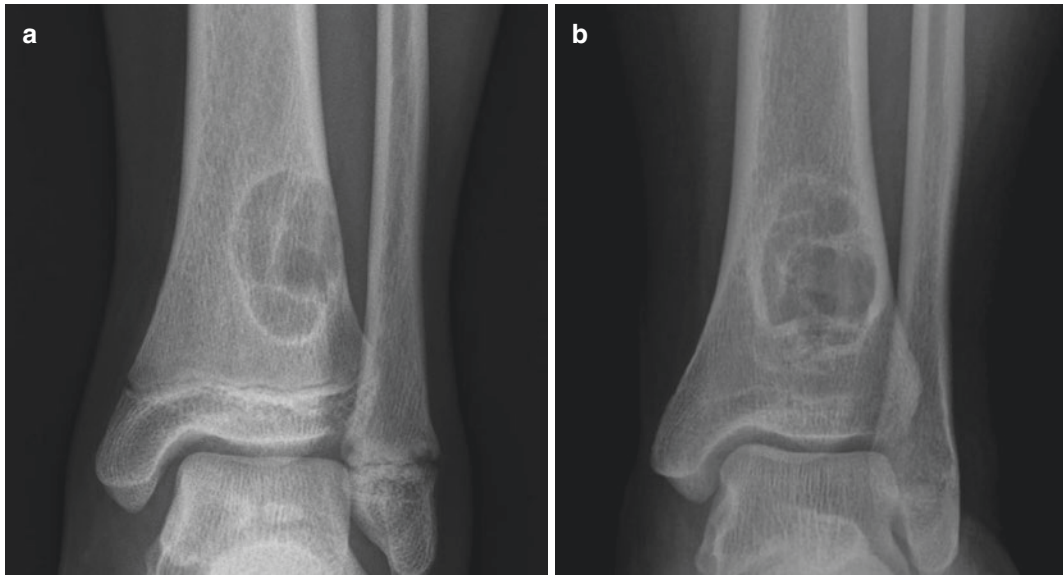

Fig. 4.6 Nonossifying fibroma. (**a**) A geographical osteolytic lesion with a thin sclerotic rim is eccentrically located at the distal metaphysis of the tibia in a 12-year-old female. (**b**) Follow-up radiograph taken 6 years later shows sclerotic change along the periphery of the lesion, indicating that the lesion is spontaneously healing

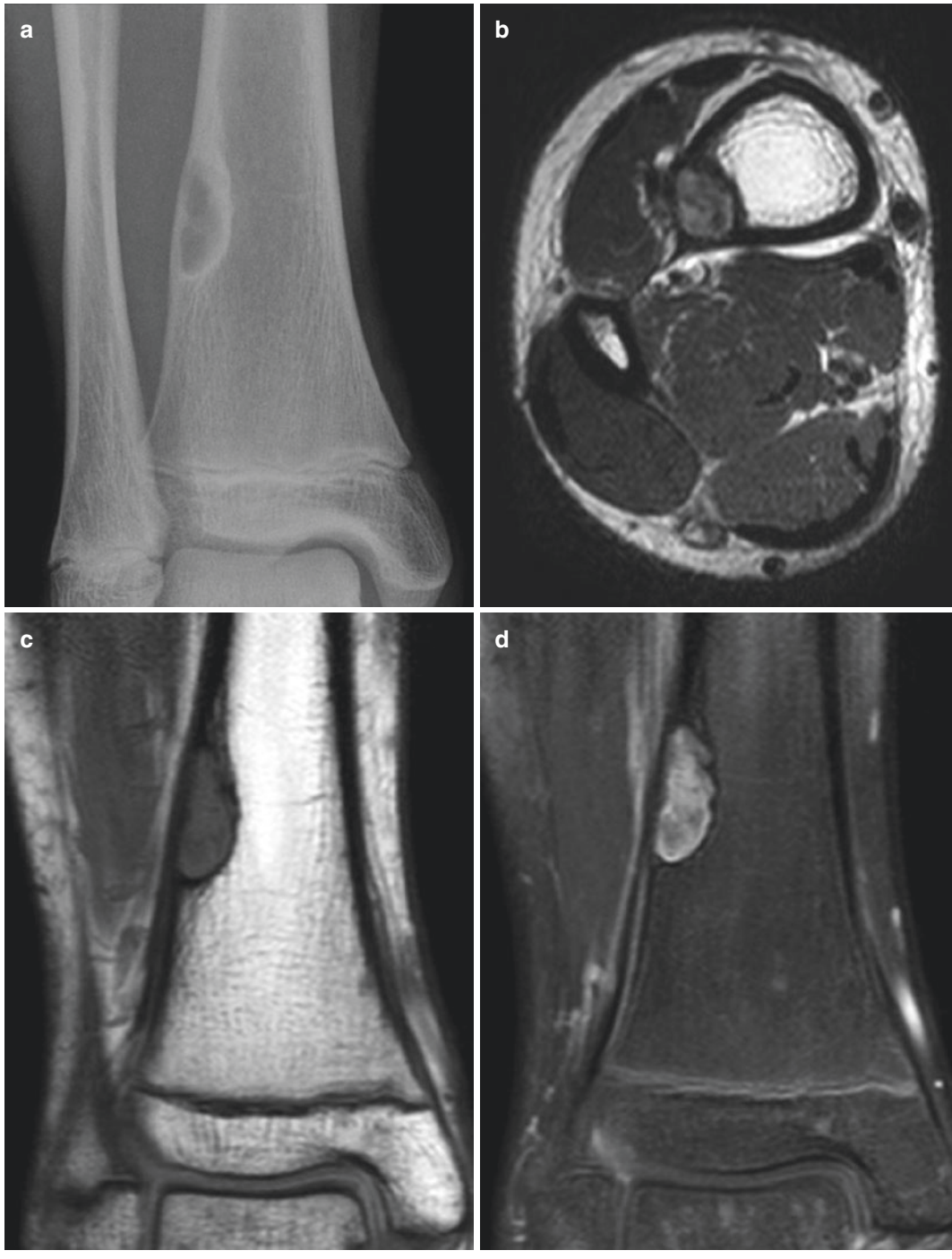

Fig. 4.7 Fibrous cortical defect. (**a**) A small well-defined osteolytic lesion with a sclerotic border is noted at the lateral aspect of the distal metadiaphysis of the tibia, in a cortical location. (**b**) This lesion exhibits heterogeneous signal intensity on T2-weighted image with predominantly hyperintensity compared to muscles. It is isointense to muscle on T1-weighted image (**c**) and shows fair enhancement on T1-weighted fat-suppressed images acquired after administration of gadolinium-based contrast agent (**d**)

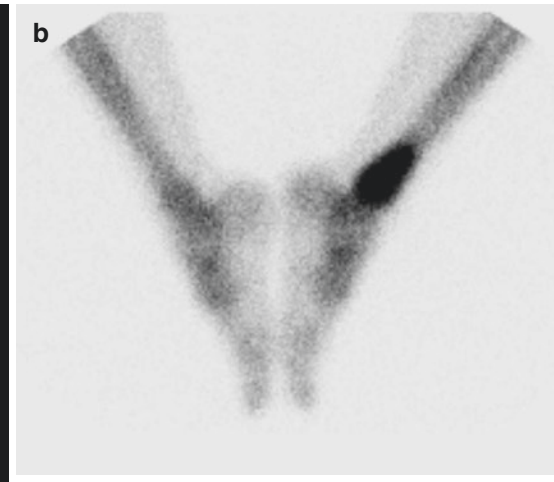

Fig. 4.8 Nonossifying fibroma. (**a**) A geographical osteolytic lesion with a sclerotic border is noted at the distal metaphysis of the tibia with an eccentric intramedullary location. (**b**) The lesion shows increased uptake on bone scan. The lesion is isointense on T1-weighted image (**c**), hypointense on T2-weighted image (**d**, **e**) compared to adjacent muscle and shows heterogeneous enhancement on T1-weighted fat-suppressed contrast-enhanced image (**f**). A hypointense rim is noted on both T1-weighted and T2-weighted images corresponding to the sclerotic border on radiograph (*black arrowheads* in **a**, **c**, **d**)

Fig. 4.8 (continued)

4.4 Benign Fibrous Histiocytoma of Bone

Overview

Benign fibrous histiocytoma (BFH) of bone is a benign bone tumor, which is categorized as a fibrohistiocytic tumor. It is also known as fibroxanthoma, fibrous xanthoma, xanthofibroma, and xanthogranuloma. It shares its histological features with NOFs/FCDs, the benign fibroblastic proliferations intermingled with multinucleated osteoclast-type giant cells. However, BFH differ from NOFs/FCDs in its clinical and radiographic features.

Epidemiology

BFH is a very rare benign tumor, with <100 cases reported in previous published literature. The reported patients have a wide age range from 5 to 75 years. However, most are older than 20 years of age. It has no gender predilection.

Common Locations

BFH is usually located at the epiphysis or diaphysis of the long bone, and within flat bones such as the pelvis and ribs.

Imaging Features

Radiograph

BFH presents as a well-defined, geographical radiolucent lesion with a sclerotic border at the epiphysis or diaphysis of a long bone (Fig. 4.9). It may accompany internal trabeculation or pseudoseptations, but matrix formation and periosteal reaction are usually absent.

Magnetic resonance imaging

The MR imaging features of BFH are similar to that of NOFs/FCDs; they are isointense to hypointense to muscle on T1-weighted images and intermediate to hyperintense on T2-weighted images, and may show variable contrast enhancement (Fig. 4.9).

Differential Diagnoses

1. Giant cell tumor

   Both giant cell tumors and BFH may appear as well-defined osteolytic lesions at the epimetaphysis of a long bone. However, giant cell tumors usually do not have a sclerotic border, whereas BFH shows a sclerotic border in two-thirds of the cases.
2. Nonossifying fibroma

   Nonossifying fibromas occur at a younger age compared to BFH. Nonossifying fibromas have a typical metaphyseal location, whereas BFH is located at nonmetaphyseal locations within a long bone.

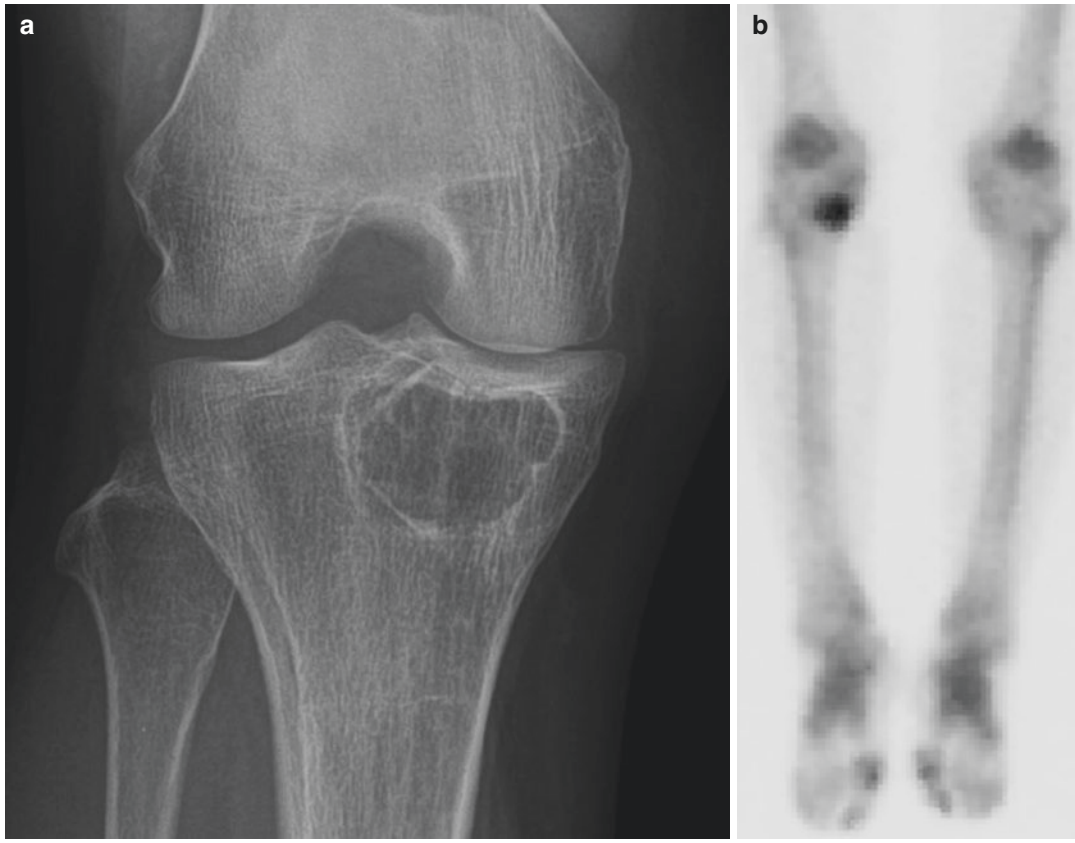

Fig. 4.9 Benign fibrous histiocytoma of bone. (**a**) A geographical osteolytic lesion with a thin sclerotic rim is noted at the proximal epiphysis of the tibia in a 58-year-old female. (**b**) The lesion exhibits increased uptake on bone scan. On magnetic resonance imaging, the lesion is isointense to hypointense to muscle on T1-weighted image (**c**) and isointense to hyperintense on T2-weighted image (**d**, **f**), and shows intense contrast enhancement on T1-weighted fat-suppressed contrast-enhanced image (**e**)

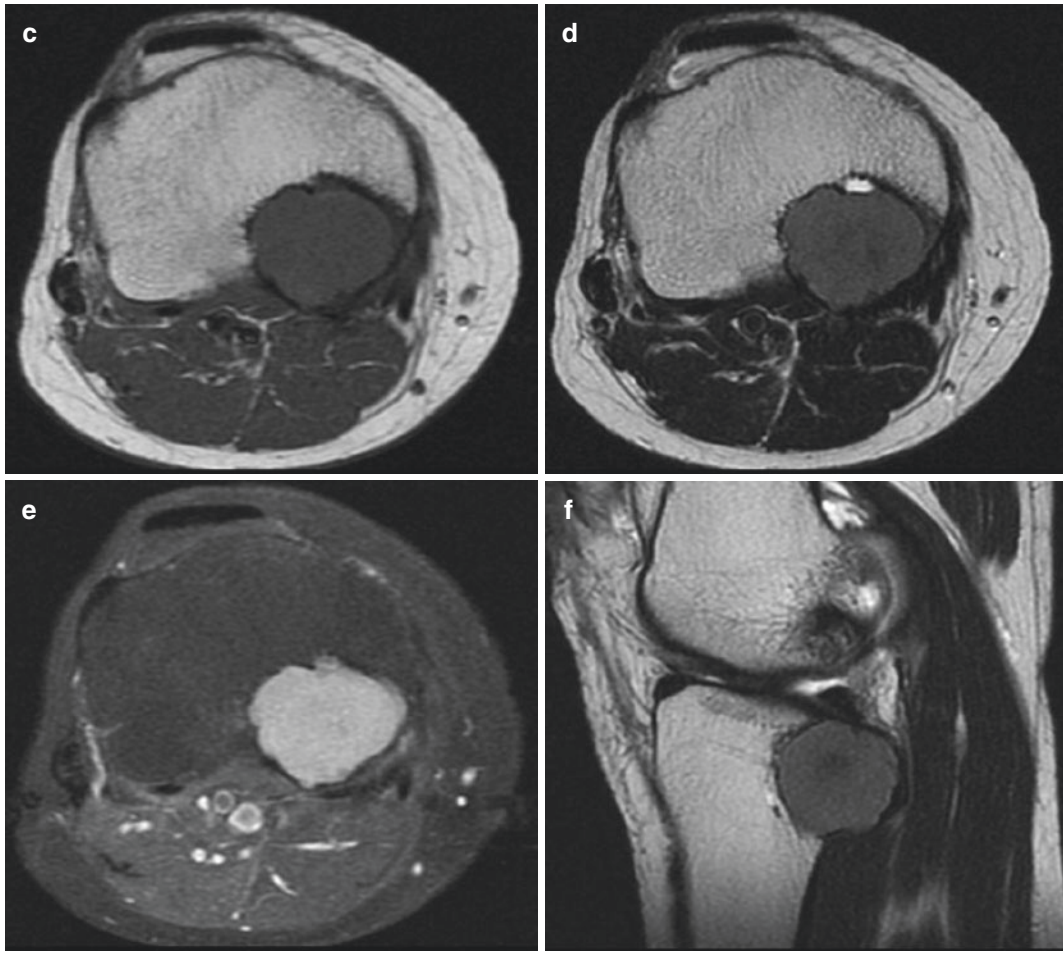

Fig. 4.9 (continued)

Suggested Reading

Desmoplastic Fibroma of Bone

Bohm P, Krober S, Greschniok A, Laniado M, Kaiserling E. Desmoplastic fibroma of the bone. A report of two patients, review of the literature, and therapeutic implications. Cancer. 1996;78:1011–23.

Crim JR, Gold RH, Mirra JM, Eckardt JJ, Bassett LW. Desmoplastic fibroma of bone: radiographic analysis. Radiology. 1989;172:827–32.

Haney J, Olson PN, Griffiths HJ. Radiologic case study. The clinical and radiologic features of desmoplastic fibroma of bone. Orthopedics. 1994;17:7780–5, 8.

Inwards CY, Unni KK, Beabout JW, Sim FH. Desmoplastic fibroma of bone. Cancer. 1991;68:1978–83.

Taconis WK, Schutte HE, van der Heul RO. Desmoplastic fibroma of bone: a report of 18 cases. Skelet Radiol. 1994;23:283–8.

Vanhoenacker FM, Hauben E, De Beuckeleer LH, Willemen D, Van Marck E, De Schepper AM. Desmoplastic fibroma of bone: MRI features. Skelet Radiol. 2000;29:171–5.

Fibrosarcoma of Bone

Antonescu CR, Erlandson RA, Huvos AG. Primary fibrosarcoma and malignant fibrous histiocytoma of bone – a comparative ultrastructural study: evidence of a spectrum of fibroblastic differentiation. Ultrastruct Pathol. 2000;24:83–91.

Papagelopoulos PJ, Galanis EC, Trantafyllidis P, Boscainos PJ, Sim FH, Unni KK. Clinicopathologic features, diagnosis, and treatment of fibrosarcoma of bone. Am J Orthop (Belle Mead NJ). 2002;31:253–7.

Papagelopoulos PJ, Galanis E, Frassica FJ, Sim FH, Larson DR, Wold LE. Primary fibrosarcoma of bone. Outcome after primary surgical treatment. Clin Orthop Relat Res. 2000;373:88–103.

Romeo S, Bovee JV, Kroon HM, et al. Malignant fibrous histiocytoma and fibrosarcoma of bone: a re-assessment in the light of currently employed morphological, immunohistochemical and molecular approaches. Virchows Arch. 2012;461:561–70.

Taconis WK, Mulder JD. Fibrosarcoma and malignant fibrous histiocytoma of long bones: radiographic features and grading. Skelet Radiol. 1984;11:237–45.

Nonossifying Fibroma/Fibrous Cortical Defect

Blau RA, Zwick DL, Westphal RA. Multiple nonossifying fibromas. J Bone Joint Surg Am. 1988;70A:299–304

Hetts SW, Hilchey SD, Wilson R, et al. Case 110:nonossifying fibroma. Radiology. 2007;243:288–92

Jee WH, Choe BY, Kang HS, et al. Nonossifying fibroma: characteristics at MR imaging with pathologic correlation. Radiology. 1998;209:197–202.

Kumar R, Madewell JE, Lindell MM, Swischuk LE. Fibrous lesions of bones. Radiographics. 1990;10:237–56.

Benign Fibrous Histiocytoma of Bone

Clarke BE, Xipell JM, Thomas DP. Benign fibrous histiocytoma of bone. Am J Surg Pathol. 1985;9:806–15.

Grohs JG, Nicolakis M, Kainberger F, Lang S, Kotz R. Benign fibrous histiocytoma of bone: a report of ten cases and review of literature. Wien Klin Wochenschr. 2002;114:56–63.

Hamada T, Ito H, Araki Y, Fujii K, Inoue M, Ishida O. Benign fibrous histiocytoma of the femur: review of three cases. Skelet Radiol. 1996;25:25–9.

Osteoclastic Giant Cell-Rich Tumors

5

Contents

5.1 Giant Cell Lesion of the Small Bones

Overview

Giant cell lesion of the small bone (GCLSB) is not a neoplastic condition, but a reactive process consisting of hemorrhage, fibroblasts, multinucleated giant cells, and reactive bone formation. It is more commonly known as *giant cell reparative granuloma (GCRG)*. The term *giant cell reparative granuloma* originates from a report by Jaffe (1953), in which he describes lesions of the jaw formed in response to traumatic intraosseous hemorrhage. The mandible and maxilla are known to be the most common locations of GCRG, but we will limit our discussion to lesions that occur in the small bones of hand and feet (GCLSB).

Epidemiology

GCLSB is most common in the first and second decades of life, and 74 % of the reported patients are under the age of 30 years at the time of presentation. It does not have a predilection for a certain gender and is equally distributed between the sexes.

H.S. Kang et al., *Oncologic Imaging: Bone Tumors*, DOI 10.1007/978-981-287-703-1_5

Common Locations

GCLSB affects the phalanges of the hand, metacarpal, metatarsal, carpal, and tarsal bones, in decreasing order of frequency. Within a given small bone, it most commonly involves the metaphysis with or without extension to the diaphysis. Unlike GCT, it rarely extends to the epiphysis.

Imaging Features

Radiograph

GCLSB typically appears as a meta(dia)physeal osteolytic lesion with expansile remodeling in the small bones of hands and feet. The cortex undergoes expansile remodeling and is thinned but not destroyed, and periosteal reaction is usually absent. It may accompany internal trabeculation and mineralization on radiography.

Magnetic resonance imaging

GCLSBs usually appear as solid lesions without cystic changes. It has been reported to exhibit intermediate signal intensity on T1-weighted images and heterogeneous hyperintensity on T2-weighted images.

Differential Diagnoses

1. Giant cell tumor

   Giant cell tumors rarely occur in the small bones of the hands and feet. They differ from GCLSB in that they extend to the epiphysis and lack intralesional mineralization.
2. Aneurysmal bone cyst

   GCLSBs are thought to be solid counterparts of aneurysmal bone cysts. The solid parts of aneurysmal bone cysts are histopathologically similar to GCLSB. On imaging, aneurysmal bone cysts can be differentiated from GCLSB, due to the presence of multiple fluid–fluid levels.
3. Enchondroma

   The most common bone tumor of the hands and feet is enchondroma. It may be differentiated from GCLSB by the presence of typical ring-and-arc pattern of chondroid mineralization.
4. Other osteolytic lesions such as glomus tumors and epidermal inclusion cysts that affect the distal phalanx may need to be considered for differential diagnoses.

5.2 Giant Cell Tumor of Bone

Overview

Giant cell tumor (GCT) of bone is generally a benign tumor that falls into the category of "osteoclastic giant cell-rich tumors." It is histologically characterized by the presence of multinucleated giant cells in a background of mononuclear stromal cells. It frequently occurs at the ends of long bones in skeletally mature patients. Although it is categorized as a benign lesion, GCT may be locally aggressive and may exhibit destructive features on imaging, may locally recur after surgical resection (15–50 % after curettage), and may also metastasize to the lung (2 % of cases). Malignant GCTs are rare, but do exist, accounting for approximately 2 % of all cases of GCT.

Epidemiology

GCT is a relatively common benign bone tumor, accounting for about 15–20 % of benign bone tumors and 3–5 % of all primary bone tumors. The peak age of presentation is the third decade, with most cases occurring between 20 and 40 years of age. They rarely occur in skeletally immature patients or in patients over the age of 50 years. GCTs have a slight female predilection with a male to female ratio of 1.5–2:1.

Common Locations

GCTs are most commonly found at the end of long bones (60 % of cases affect the long bone), with a majority of cases involving the distal femur, proximal tibia, distal radius, and proximal humerus. They originate in the metaphysis and extend into the epiphysis resulting in a metaepiphyseal location. GCT rarely occurs in the axial skeleton and flat bones, but among the vertebrae, the sacrum is most commonly affected. In flat bones, they appear at apophyses, which is an epiphyseal equivalent (refer to part 1 for more detail on apophyses). Giant cell tumors may occur secondary to Paget's disease, and in this case, they may exhibit multiplicity.

Imaging Features

Radiograph

A typical GCT appears as an eccentric osteolytic lesion with a nonsclerotic well-defined border at the metaepiphysis of a long bone that is skeletally mature (Fig. 5.1). It frequently expands the cortex, and usually does not accompany periosteal reaction (Fig. 5.2). Usually, little or no matrix mineralization is seen within the tumor. Infrequently, GCTs may show thickened trabeculation along the periphery of the lesion, exhibiting a soap-bubble appearance (Fig. 5.2). Atypical cases may show more aggressive features with a wide zone of transition and cortical destruction. These aggressive features are more frequently found in bones with a small caliber, such as the fibula or ulna. The radiograph findings of lesions arising from the apophyses are identical to those arising in long bones (Figs. 5.3 and 5.4).

Magnetic resonance imaging

The findings of GCTs on magnetic resonance imaging are nonspecific. They generally appear isointense to hypointense on T1-weighted image, and inhomogeneous hyperintense on fluid-sensitive sequences. Lesions may contain areas of low signal intensities on T1-weighted and T2-weighted images, and show blooming artifact on gradient-echo sequences; these areas correspond to the hemosiderin deposition related to the extravasated erythrocytes in the tumor and the phagocytic function of the tumor cells (Figs. 5.5, 5.7, and 5.8). GCTs may undergo secondary aneurysmal bone cyst formation, resulting in a multiloculated cystic appearance with fluid–fluid levels on T2-weighted imaging (Fig. 5.6).

Differential Diagnoses

1. Chondroblastoma

   Chondroblastoma usually occurs in skeletally immature patients, before the closure of growth plates. Chondroblastoma may have a metaepiphyseal location like GCTs, but chondroblastomas originate in the epiphysis, whereas GCTs originate in the metaphysis. Chondroblastomas usually have a sclerotic border and may accompany periosteal reaction. On MR imaging, chondroblastomas may be distinguished from GCTS by the presence of an extensive edema in the surrounding soft tissue and bone marrow.

2. Aneurysmal bone cyst

   GCTs may undergo secondary changes and include an aneurysmal bone cyst within the tumor. Aneurysmal bone cysts occurring without an underlying GCT are reported to occur at a younger age, and on imaging, they can be differentiated with GCT with secondary ABC formation by the absence of enhancing soft tissue component within the tumor.

3. Other differentials may include osteolytic bone metastases, plasmacytoma, telangiectatic osteosarcoma, giant cell-rich osteosarcoma, and clear cell chondrosarcoma.

Fig. 5.1 Giant cell tumor in the distal femur. (**a**) Anteroposterior and (**b**) lateral radiographs of the right knee show a geographical osteolytic lesion without a sclerotic rim (*arrowheads*) at the distal epimetaphysis of the femur in a 31-year-old male. (**c**) Bone scan shows increased uptake in the right distal femur. On magnetic resonance imaging, the lesion shows intermediate signal intensity on sagittal T1-weighted image (**d**), heterogeneous on coronal T2-weighted image (**e**), and enhances intensely on sagittal T1-weighted fat-suppressed image acquired after administration of gadolinium-based contrast agent (**f**). Low signal intensity areas noted on T2-weighted image (*arrow* in **e**) are attributable to the hemosiderin deposition related to the extravasated erythrocytes in the tumor and the phagocytic function of the tumor cells

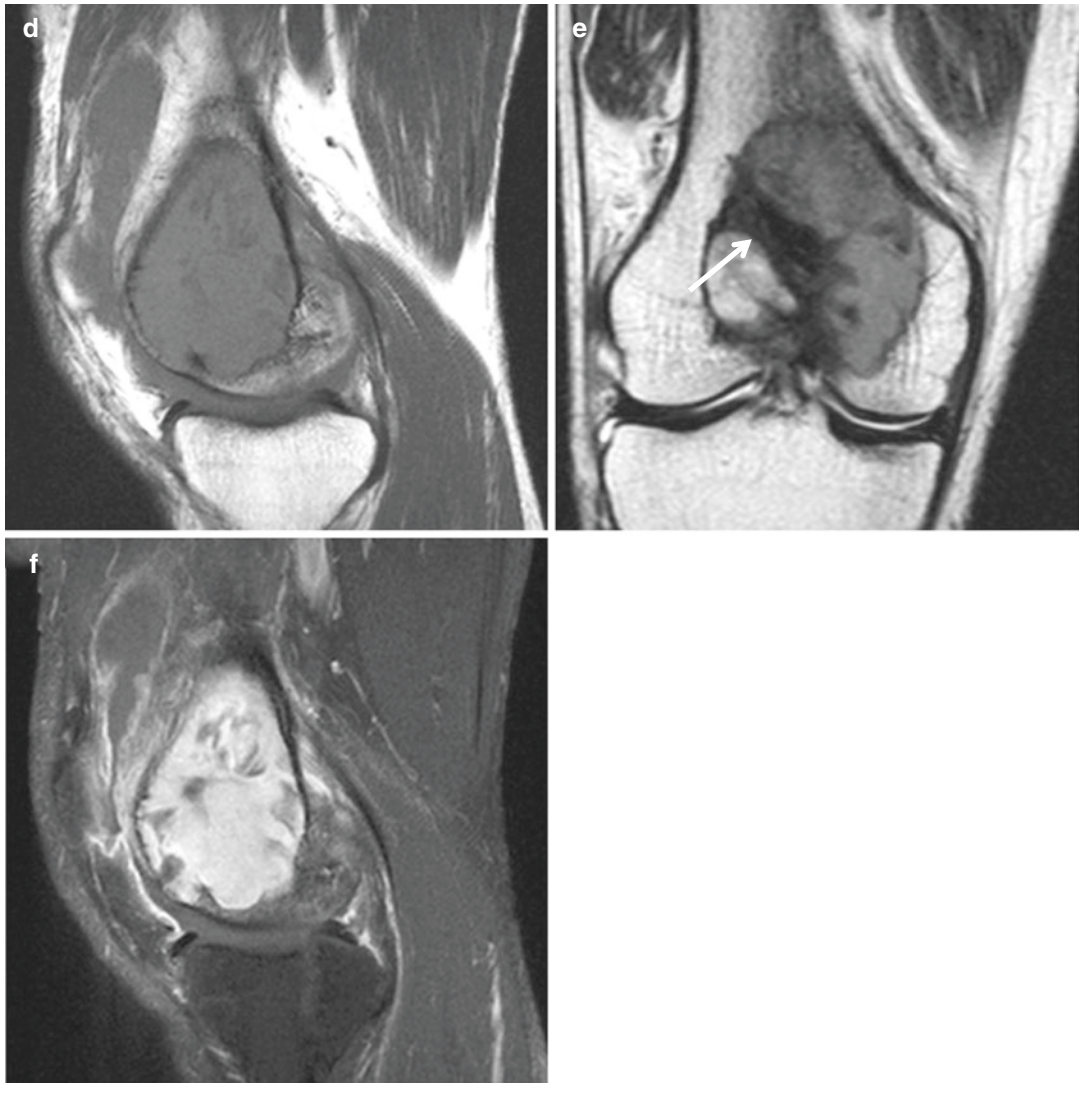

Fig. 5.1 (continued)

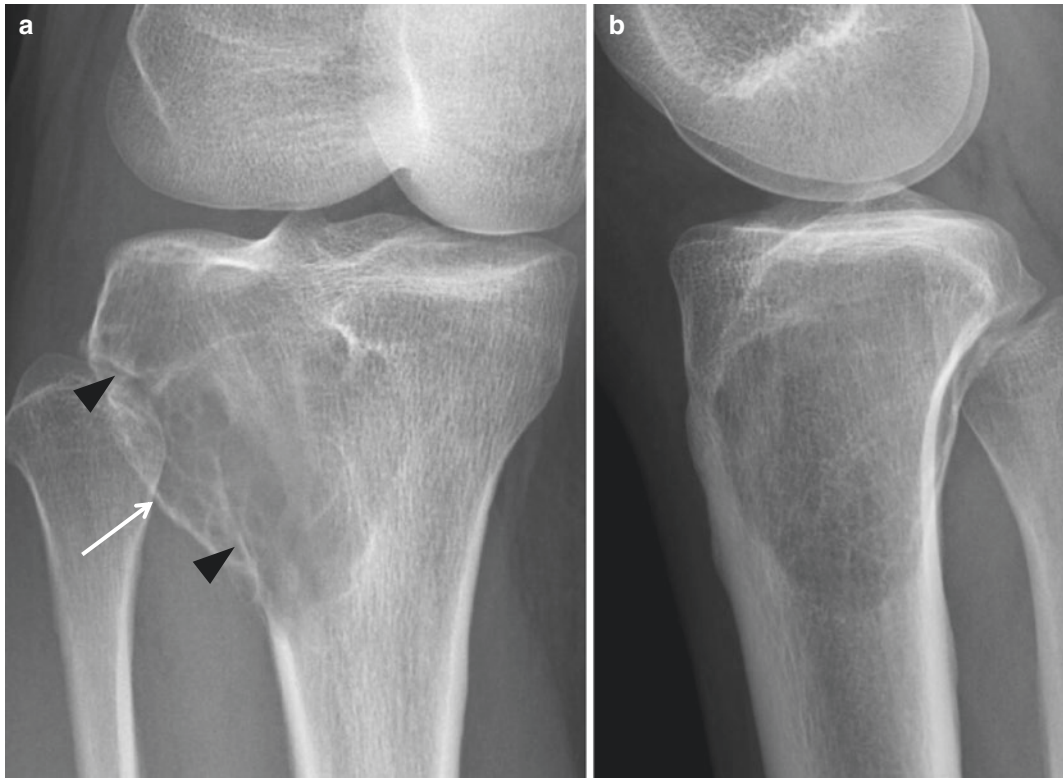

Fig. 5.2 Giant cell tumor in the proximal tibia. (**a**) Oblique and (**b**) lateral radiographs of the right knee in a 27-year-old female show a geographical osteolytic lesion without a sclerotic rim, eccentrically located at the proximal epimetaphysis of the tibia. The lesion expands the tibial cortex (*arrow*), but does not show periosteal reaction. Thickened trabeculations are noted along within the lesion (*black arrowheads*)

Fig. 5.3 Giant cell tumor in the greater trochanter of femur. (**a**) Radiograph shows a geographical osteolytic lesion without a sclerotic rim in the greater trochanter of the left femur. (**b**) Mildly increased uptake is noted at the corresponding region on bone scan. On magnetic resonance imaging, the lesions appear intermediate on axial T1-weighted image (**c**), hypointense on axial T2-weighted image (**d**), and shows mild enhancement on axial contrast-enhanced T1-weighted image (**e**)

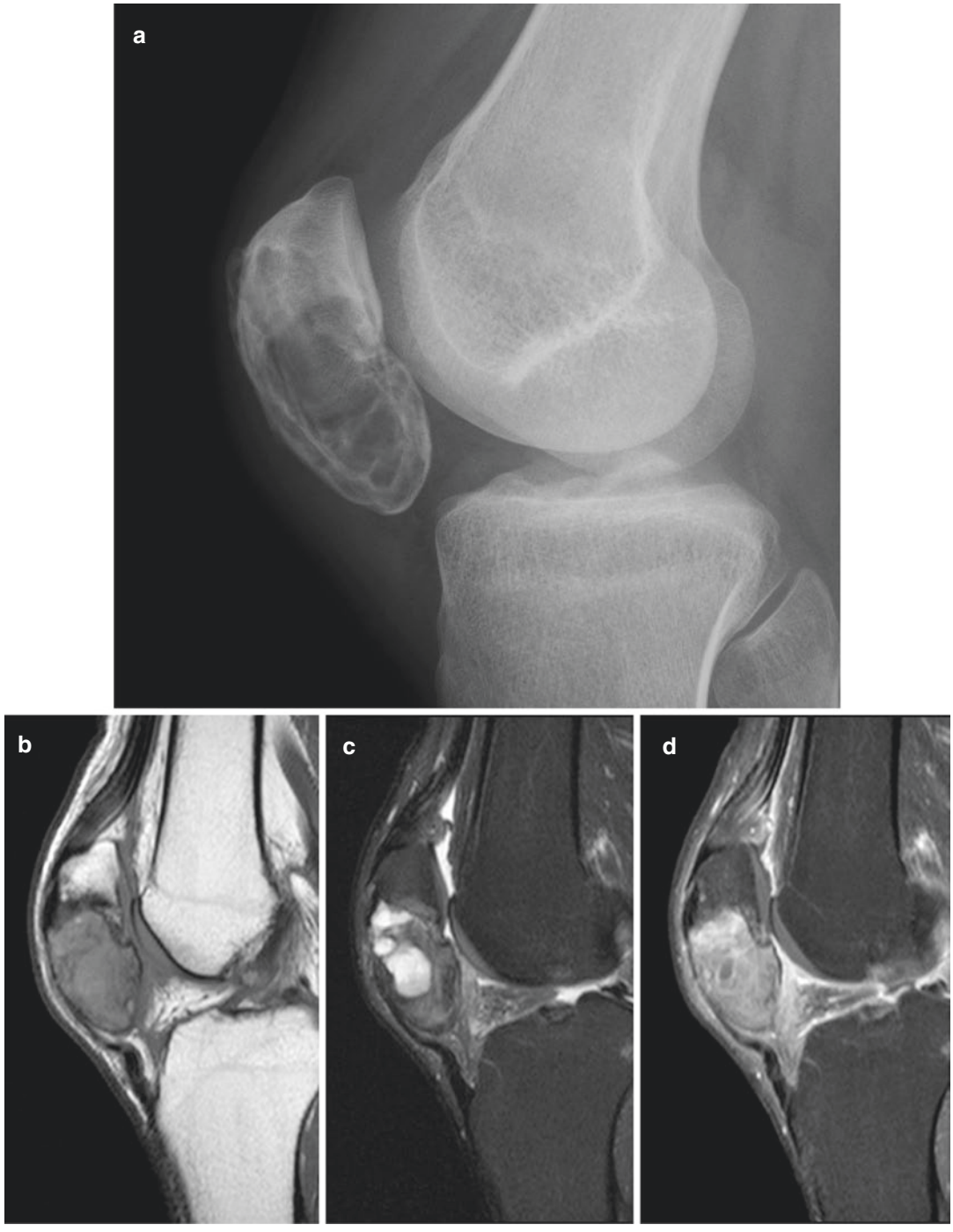

Fig. 5.4 Giant cell tumor in the patella. (**a**) Lateral radiograph of the knee in a 28-year-old male. A mildly expansile, geographical osteolytic lesion without a sclerotic rim is noted in the lower two-thirds of the patella. The lesion shows intermediate signal intensity on sagittal T1-weighted image (**b**), slightly hyperintense with cystic portions on T2-weighted fat-suppressed image (**c**), and shows heterogeneous enhancement on T1-weighted fat-suppressed image acquired after contrast administration (**d**)

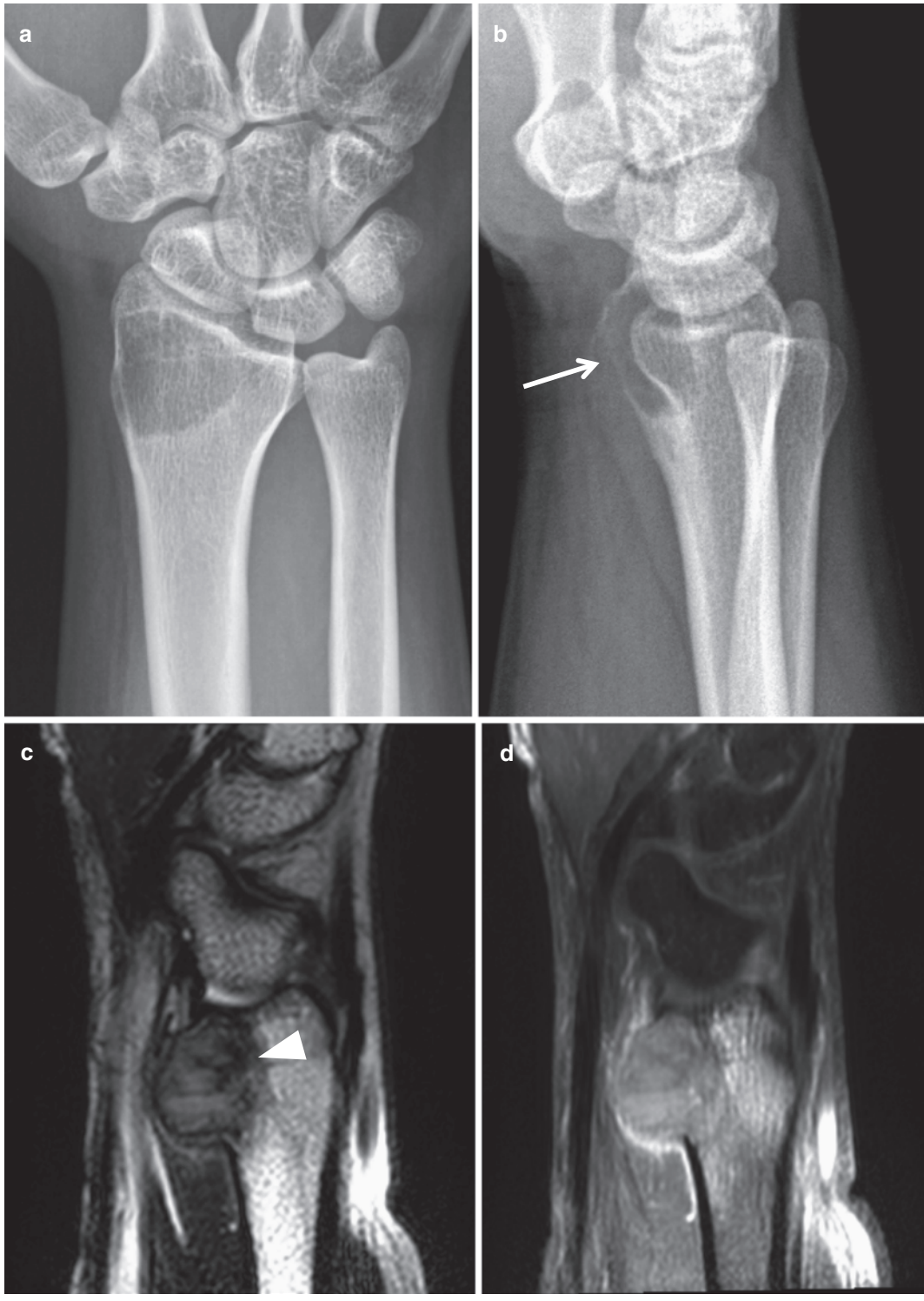

Fig. 5.5 Giant cell tumor in the distal radius. (**a**) Anteroposterior and (**b**) lateral radiographs of the left wrist in the 36-year-old male. A geographical osteolytic lesion without a sclerotic rim is noted at the distal epimetaphysis of the radius with mild expansion of the cortex (*white arrow*). (**c**) The lesion shows hypointense areas on sagittal T2-weighted image (*arrowhead*), probably corresponding to the hemosiderin deposition within the tumor. (**d**) The lesion exhibits moderate enhancement on sagittal contrast-enhanced T1-weighted fat-suppressed image.

Fig. 5.6 Giant cell tumor in the proximal tibia. (**a**) Anteroposterior and (**b**) lateral radiographs of the right knee show a geographical osteolytic lesion at the proximal epimetaphysis of the tibia. The lesion exhibits cortical ballooning at the posterior aspect of the tibia (*white arrows*). (**c**) The lesion shows increased uptake on bone scan. (**d**) On sagittal reformatted CT image, the ballooned posterior tibial cortex is well noted. (**e**) Sagittal T1-weighted, (**f**) sagittal T2-weighted, (**g**) sagittal contrast-enhanced T1-weighted fat-suppressed images show multiple fluid–fluid levels within the lesion which can be seen in aneurysmal bone cysts. (**h**) Axial T2-weighted fat-suppressed images show noncystic solid portion within the lesion (*white arrow*) favoring the diagnosis of secondary aneurysmal bone cysts over primary aneurysmal bone cyst

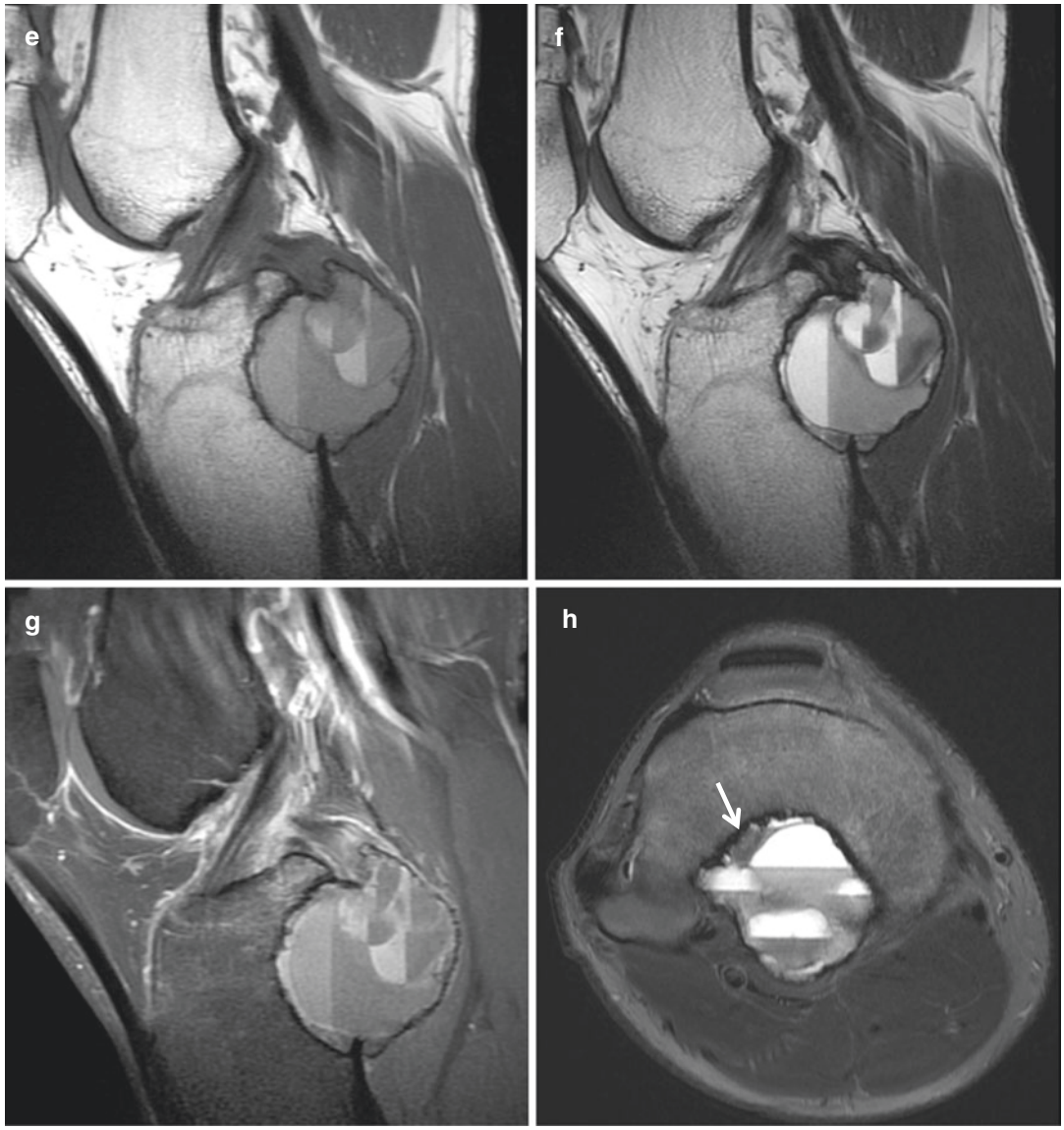

Fig. 5.6 (continued)

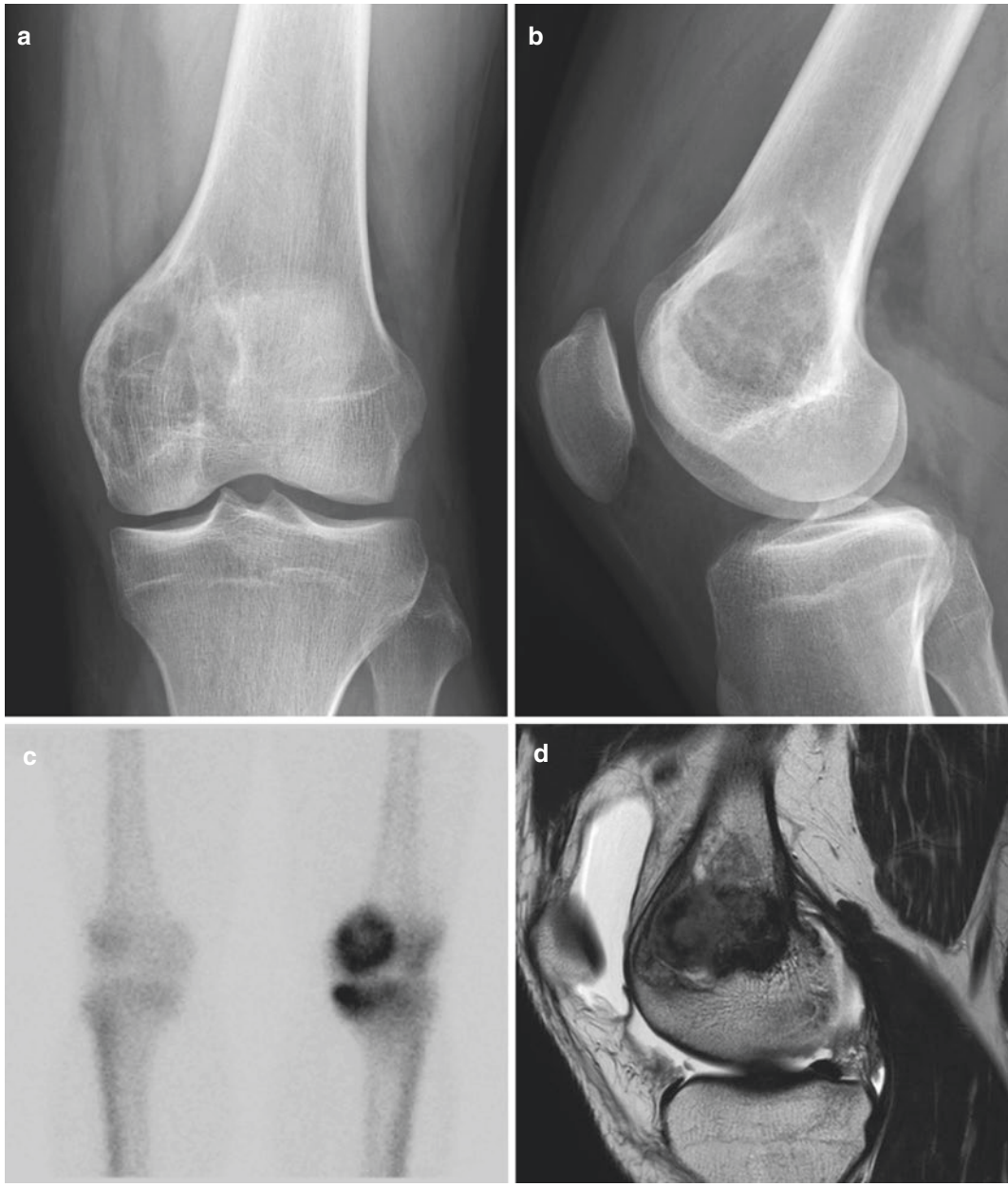

Fig. 5.7 Giant cell tumor in the distal femur. (**a**) Anteroposterior and (**b**) lateral radiographs of the left knee in a 52-year-old male are shown. A geographical osteolytic lesion with a thin sclerotic rim is noted at the distal femur. The lesion involves both the epiphysis and metaphysis, but the epicenter of the lesion is located at the metaphysis, indicating that it has originated from the metaphysis. (**c**) Bone scan shows increased uptake in the left distal femur. The lesion is hypointense on T2-weighted image (**d**), shows intermediate signal intensity on T1-weighted image (**e**), and shows heterogeneous strong enhancement (**f**). The lesion was treated with curettage and cancellous bone grafting. (**g**) Radiograph and (**h**) coronal T1-weighted fat-suppressed contrast-enhanced MR image taken 4 months after operation show normal appearance of the bone graft; the cancellous bone graft shows similar density to adjacent bone on radiograph, and shows peripheral enhancement with central nonenhancing portion with speckled hypointense foci.

Fig. 5.7 (continued)

Fig. 5.8 Giant cell tumor in the distal ulna. (**a**) An expansile osteolytic lesion with type IB pattern of destruction is noted at the distal epimetaphysis of the ulna on anteroposterior radiograph of the left wrist in a 33-year-old female. The lesion shows intermediate signal intensity on axial T1-weighted image (**b**), mildly hyperintense with hypointense areas on axial T2-weighted images (**c**), and intensely enhances on axial T1-weighted fat-suppressed image obtained after administration of gadolinium-based contrast agent (**d**). The patient was treated with curettage and cancellous bone graft. (**e**) Anteroposterior radiograph taken 10 days after operation shows the grafted cancellous bone filling the curettage site with a density similar to adjacent bone. (**f**) On follow-up radiograph taken 8 months after operation, well-defined osteolytic areas are noted at the graft site (*arrows*), suggesting the possibility of tumor recurrence. (**g**) Coronal T2-weighted image reveals hypointense nodular lesions at corresponding locations (*arrows*), which is differentiated from surrounding background of incorporated cancellous bone graft). (**h**) The distal ulna was resected, and recurrent lesions were found on histopathological examination

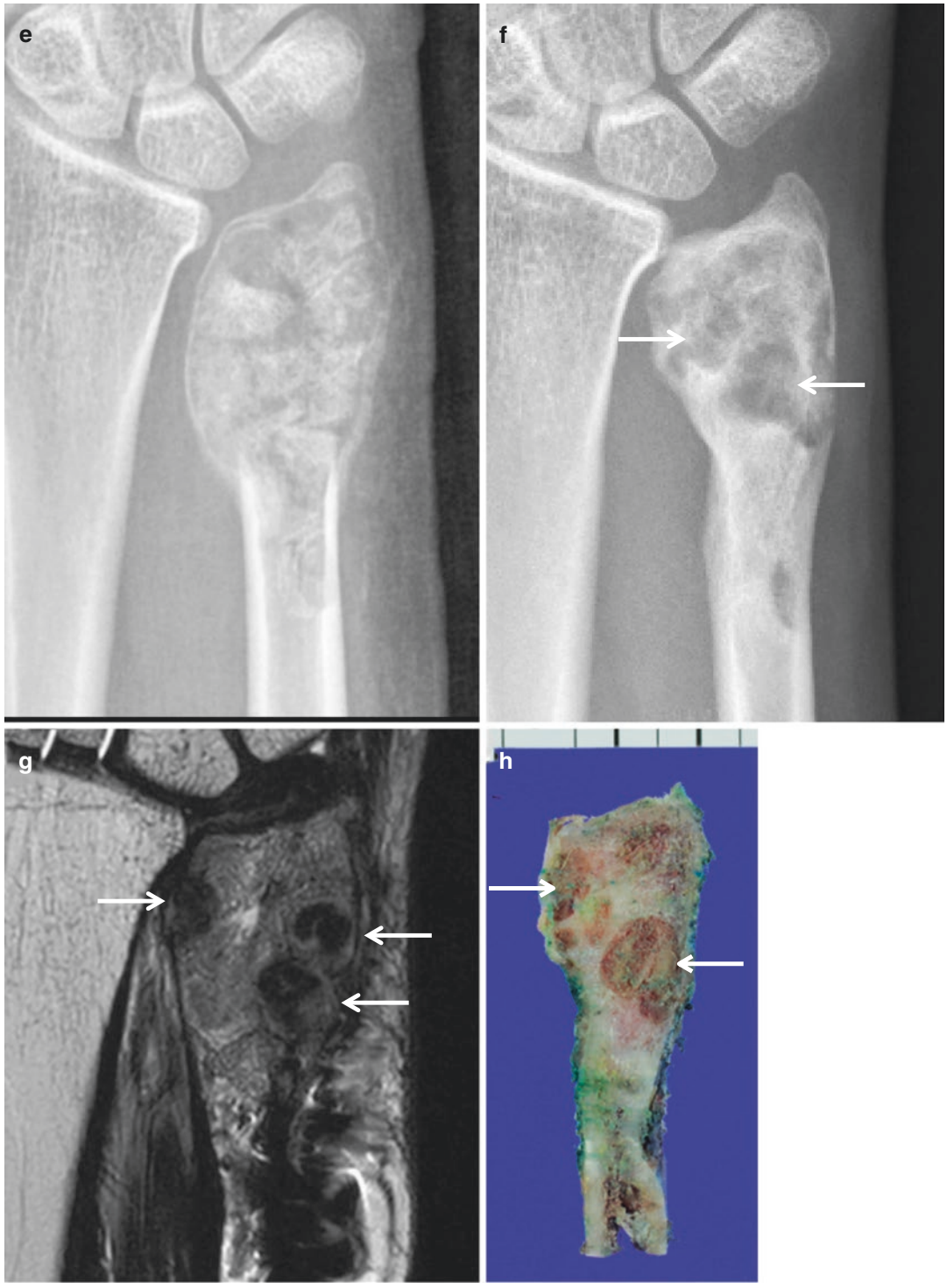

Fig. 5.8 (continued)

Suggested Reading

Giant Cell Lesion of the Small Bones

Glass TA, Mills SE, Fechner RE, Dyer R, Martin 3rd W, Armstrong P. Giant-cell reparative granuloma of the hands and feet. Radiology. 1983;149:65–8.

Jaffe HL. Giant-cell reparative granuloma, traumatic bone cyst, and fibrous (fibro-osseous) dysplasia of the jawbones. Oral Surg Oral Med Oral Pathol. 1953;6:159–75.

Lorenzo JC, Dorfman HD. Giant-cell reparative granuloma of short tubular bones of the hands and feet. Am J Surg Pathol. 1980;4:551–63.

Murphey MD, Nomikos GC, Flemming DJ, Gannon FH, Temple HT, Kransdorf MJ. From the archives of AFIP. Imaging of giant cell tumor and giant cell reparative granuloma of bone: radiologic-pathologic correlation. Radiographics. 2001;21:1283–309.

Picci P, Baldini N, Sudanese A, Boriani S, Campanacci M. Giant cell reparative granuloma and other giant cell lesions of the bones of the hands and feet. Skeletal Radiol. 1986;15:415–21.

Giant Cell Tumor of Bone

Aoki J, Tanikawa H, Ishii K, et al. MR findings indicative of hemosiderin in giant-cell tumor of bone: frequency, cause, and diagnostic significance. AJR Am J Roentgenol. 1996;166:145–8.

Chakarun CJ, Forrester DM, Gottsegen CJ, Patel DB, White EA, Matcuk Jr GR. Giant cell tumor of bone: review, mimics, and new developments in treatment. Radiographics. 2013;33:197–211.

Larsson SE, Lorentzon R, Boquist L. Giant-cell tumor of bone. A demographic, clinical, and histopathological study of all cases recorded in the Swedish Cancer Registry for the years 1958 through 1968. J Bone Joint Surg Am. 1975;57:167–73.

Lorentzon R, Lundstrom B, Larsson SE. Growth rate of giant-cell tumor of bone: radiographic and clinical considerations. Clin Orthop Relat Res. 1980;149:299–304.

Murphey MD, Nomikos GC, Flemming DJ, Gannon FH, Temple HT, Kransdorf MJ. From the archives of AFIP. Imaging of giant cell tumor and giant cell reparative granuloma of bone: radiologic-pathologic correlation. Radiographics. 2001;21:1283–309.

Raskin KA, Schwab JH, Mankin HJ, Springfield DS, Hornicek FJ. Giant cell tumor of bone. J Am Acad Orthop Surg. 2013;21:118–26.

Turcotte RE. Giant cell tumor of bone. Orthop Clin North Am. 2006;37:35–51.

Hematopoietic Neoplasms and Small Round Cell Tumors

6

Contents

6.1 Plasma Cell Myeloma/ Solitary Plasmacytoma of Bone

Overview

Plasma cell myeloma (multiple myeloma) and solitary plasmacytoma are clonal neoplastic proliferation of plasma cells of bone marrow derivation. Plasma cell myeloma is a multicentric disease with systemic manifestations, whereas solitary plasmacytoma is a unicentric disease, localized to a single bone. Multiple solitary plasmacytomas without evidence of multiple myeloma may occur.

Epidemiology

Plasma cell myeloma is the most common malignant primary bone tumor. It commonly occurs in patients in their sixth and seventh decades of life, and is rare under the age of 40 years. Solitary plasmacytomas tend to occur at a younger age, with a median age of 55 years at diagnosis. Plasma cell myeloma affect both genders equally, whereas solitary plasmacytomas are more common in males than in females (M:F = 2:1).

Common Locations

Plasma cell myelomas and solitary plasmacytomas are found in bones containing hematopoietic marrow, usually the axial skeleton. Solitary plasmacytomas have been reported most commonly

H.S. Kang et al., *Oncologic Imaging: Bone Tumors*, DOI 10.1007/978-981-287-703-1_6

in the vertebra, and other possible sites include ribs, skull, pelvis, and femur.

Imaging Features

Radiograph

Plasma cell myelomas may have various appearances according to the site of involvement and type of lesion. Typical plasma cell myelomas present with multiple well-demarcated osteolytic lesions with medullary location, often referred to as "punched-out" lesions (Fig. 6.1). In bones with small calibers, such as the rib, plasma cell myelomas may cause expansion of the bone (Figs. 6.2, 6.3, and 6.4). However, periosteal reactions are rare. Atypical cases may present with more aggressive features with either moth-eaten or permeative pattern of bone destruction (Fig. 6.5). Diffuse osteopenia in the spine with or without compression fractures may be the sole finding, making the diagnosis of myeloma difficult. Occasionally, myeloma may present with multiple sclerotic lesions, usually in the setting of POEMS syndrome (polyneuropathy, organomegaly, endocrinopathy, monoclonal gammopathy, skin changes) (Fig. 6.6).

Magnetic resonance imaging

Plasma cell myeloma and solitary plasmacytoma show nonspecific findings on MR imaging. MR may be useful in (i) detecting small lesions not readily seen on radiographs and (ii) evaluating the presence and extent of soft tissue extension.

Differential Diagnoses

1. Plasma cell myeloma: metastasis, lymphoma, Langerhans' cell histiocytosis, brown tumors of hyperparathyroidism
2. Solitary plasmacytoma: metastasis

Fig. 6.1 Solitary plasmacytoma in the left femur. (**a**) On radiograph, a geographical osteolytic lesion with a well-defined margin (punched-out lesion) is noted at the proximal metadiaphysis of the left femur in a 39-year-old female. The femoral cortex is thinned due to endosteal scalloping (*arrow*). (**b**) Increased uptake is noted at the left proximal femur on bone scan (*arrowhead*). (**c**) Axial and (**d**) coronal T1-weighted images, (**e**) coronal T2-weighted fat-suppressed image, and (**f**) coronal contrast-enhanced T1-weighted fat-suppressed images are shown. The lesion shows homogeneous signal intensity on all sequences. Endosteal scalloping is noted around the lesion, resulting in cortical thinning. Based on negative bone marrow biopsy results and other laboratory tests, the lesion was diagnosed as solitary plasmacytoma

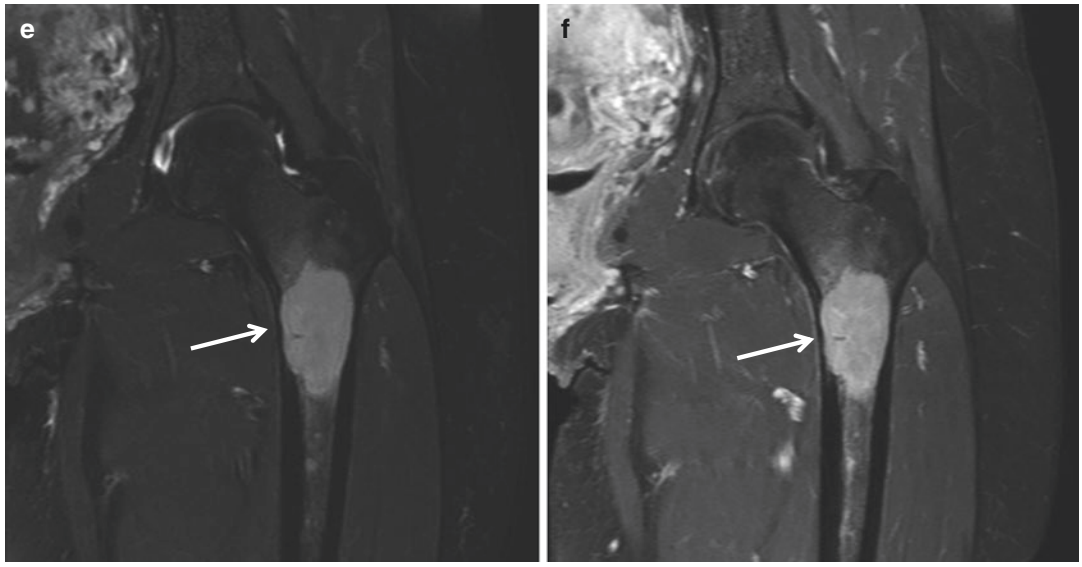

Fig. 6.1 (continued)

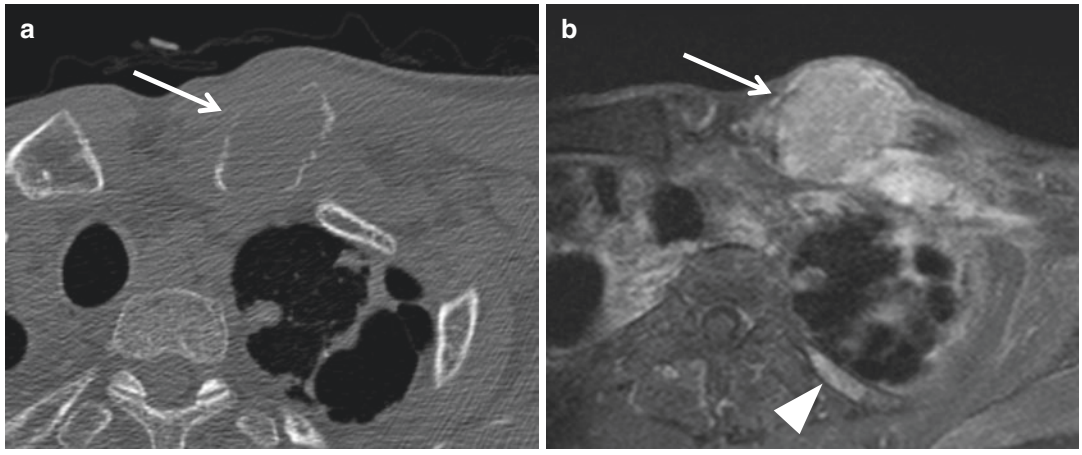

Fig. 6.2 Plasmacytoma in the left clavicle in a 58-year-old male with plasma cell myeloma. (**a**) Axial CT image shows an expansile osteolytic lesion at the proximal end of the left clavicle (*arrow*). (**b**) A homogeneously enhancing lesion is noted at the corresponding site on axial contrast-enhanced T1-weighted fat-suppressed image (*arrow*). Another enhancing lesion is noted at the posterior arc of the left third rib (*arrowhead*). Based on bone marrow biopsy results and other laboratory tests, the patient was diagnosed with plasma cell myeloma

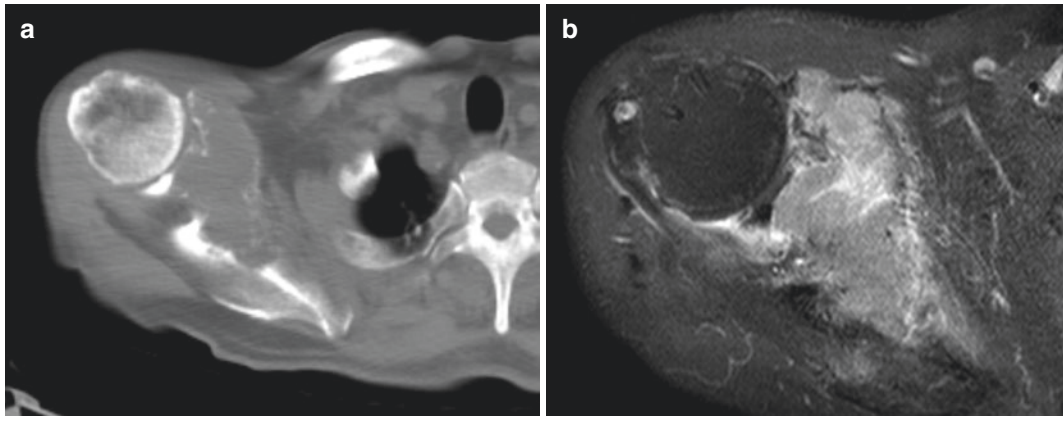

Fig. 6.3 Plasmacytoma in the right scapula in a 79-year-old male with plasma cell myeloma. (**a**) Axial CT image shows an expansile osteolytic lesion involving the right scapula, extending from the scapular body, glenoid to the coracoid process. (**b**) A homogeneous enhancing mass with extraosseous extension is noted on axial contrast-enhanced T1-weighted fat-suppressed image.

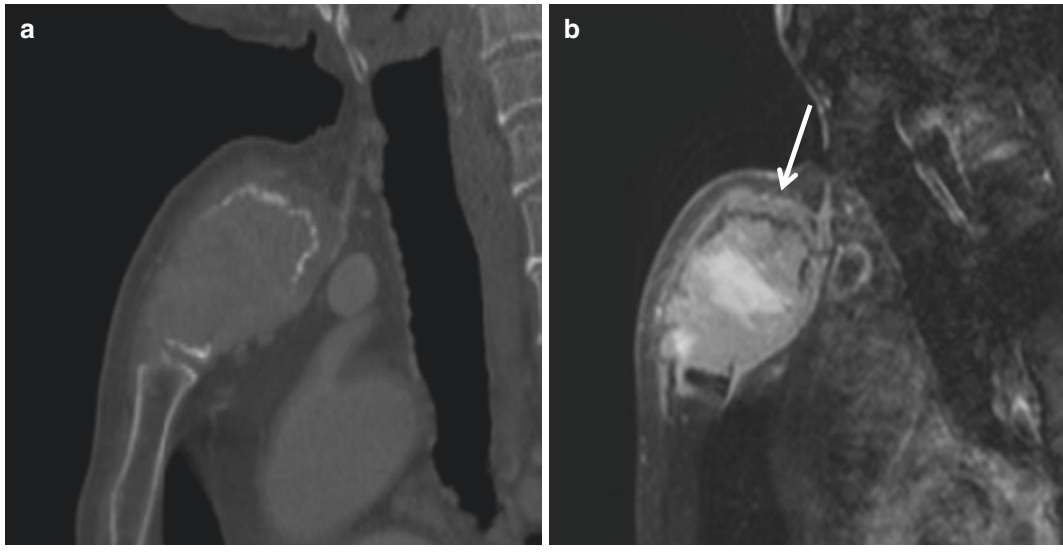

Fig. 6.4 Plasmacytoma in the sternal manubrium in an 87-year-old male with plasma cell myeloma. (**a**) Sagittal reformatted CT image shows an expansile osteolytic lesion with cortical breaching in the manubrium. (**b**) Sagittal contrast-enhanced T1-weighted fat-suppressed image shows an enhancing mass lesion in the manubrium. Extraosseous extension is noted without overt cortical breaching along the superior aspect of the manubrium (*arrow*), favoring the diagnosis of a round cell tumor.

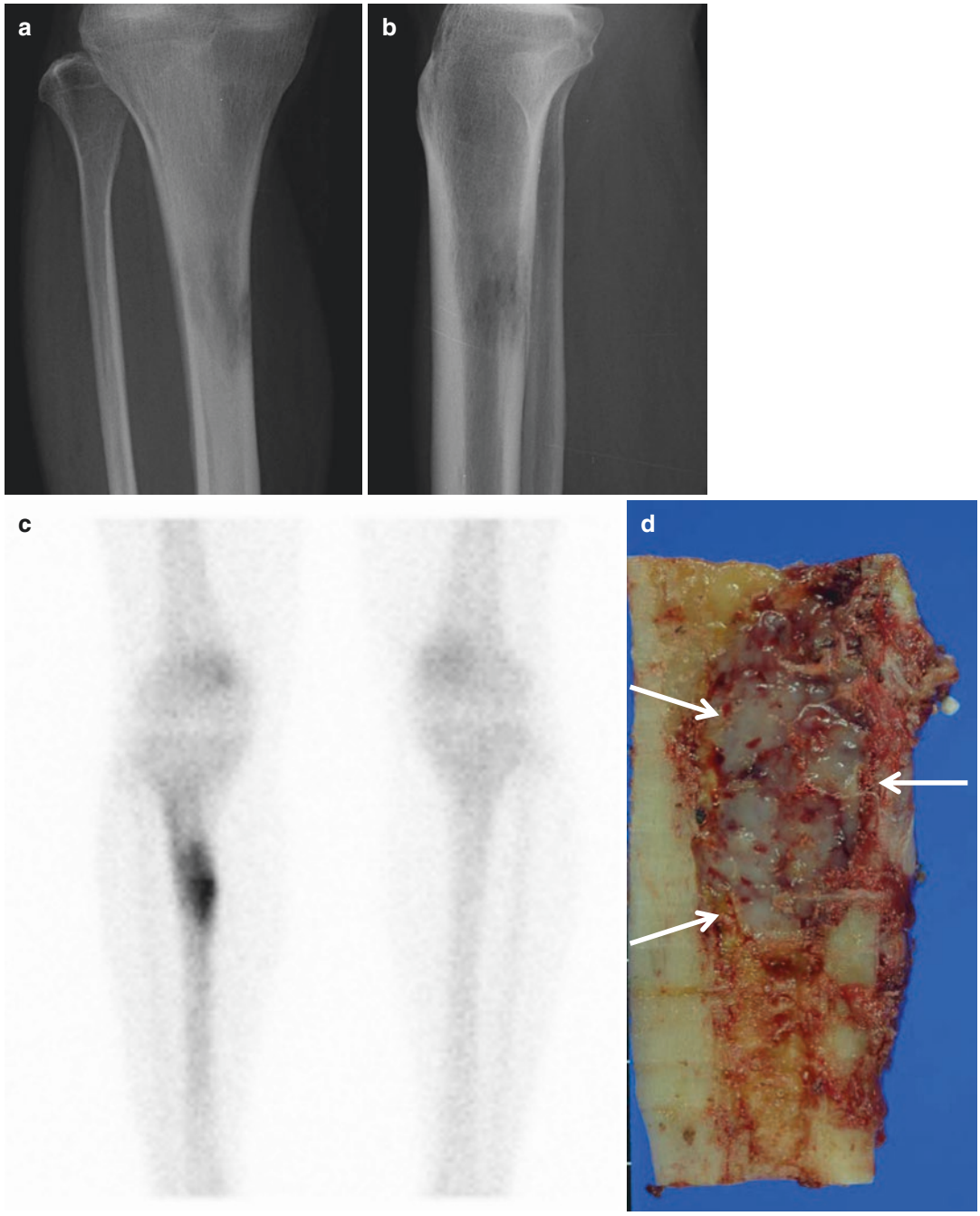

Fig. 6.5 Solitary plasmacytoma. (**a**) Anteroposterior and (**b**) lateral radiographs of the right lower leg show an ill-defined osteolytic lesion with a moth-eaten pattern of destruction in the proximal diaphysis of the tibia. (**c**) Bone scan exhibits an increased uptake at the corresponding site. (**d**) Sagittal section of the resected tibia shows a whitish glistening mass lesion in the medulla. (**e**) Axial T1-weighted image, (**f**) axial T2-weighted image. (**g**) Axial and (**h**) coronal contrast-enhanced T1-weighted images show an intramedullary mass lesion with endosteal scalloping (*arrowheads*) in the right tibia

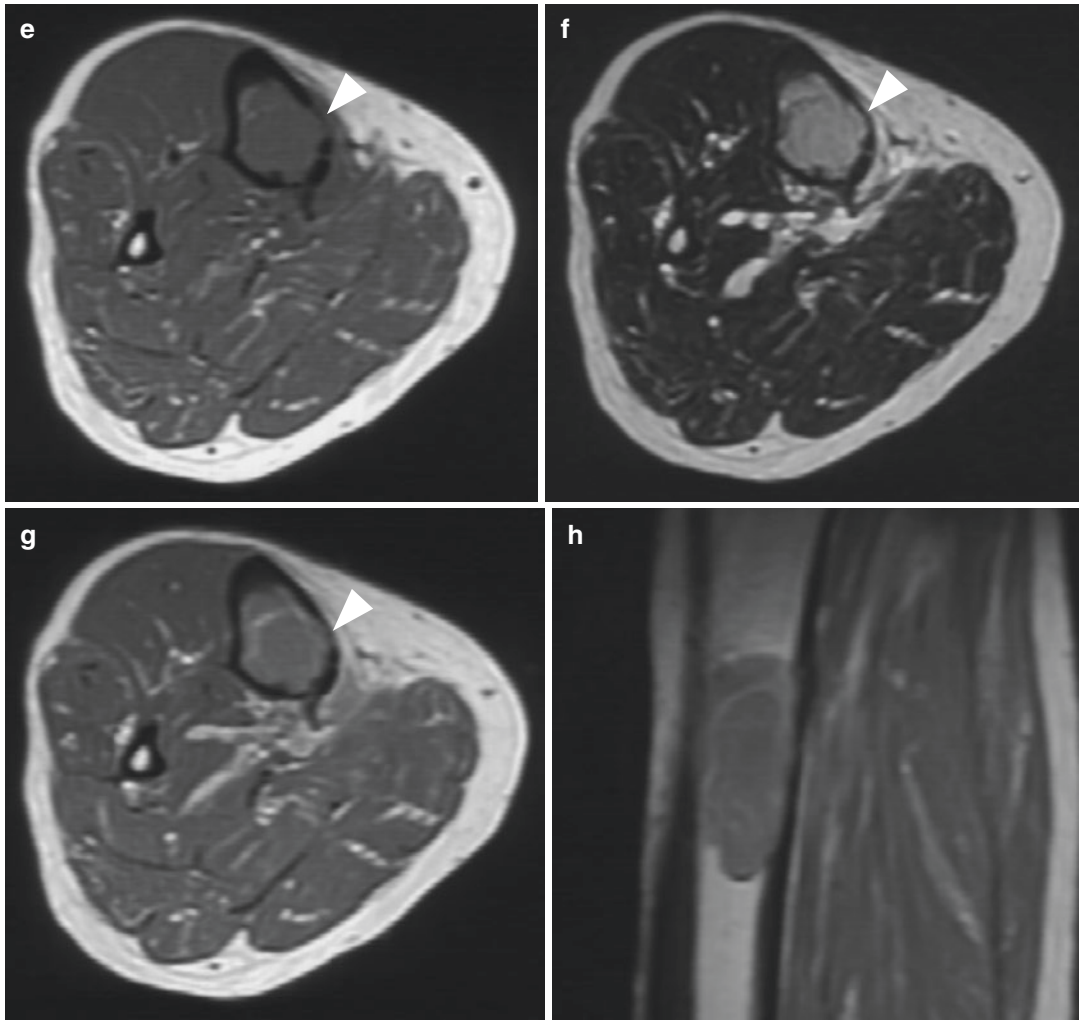

Fig. 6.5 (continued)

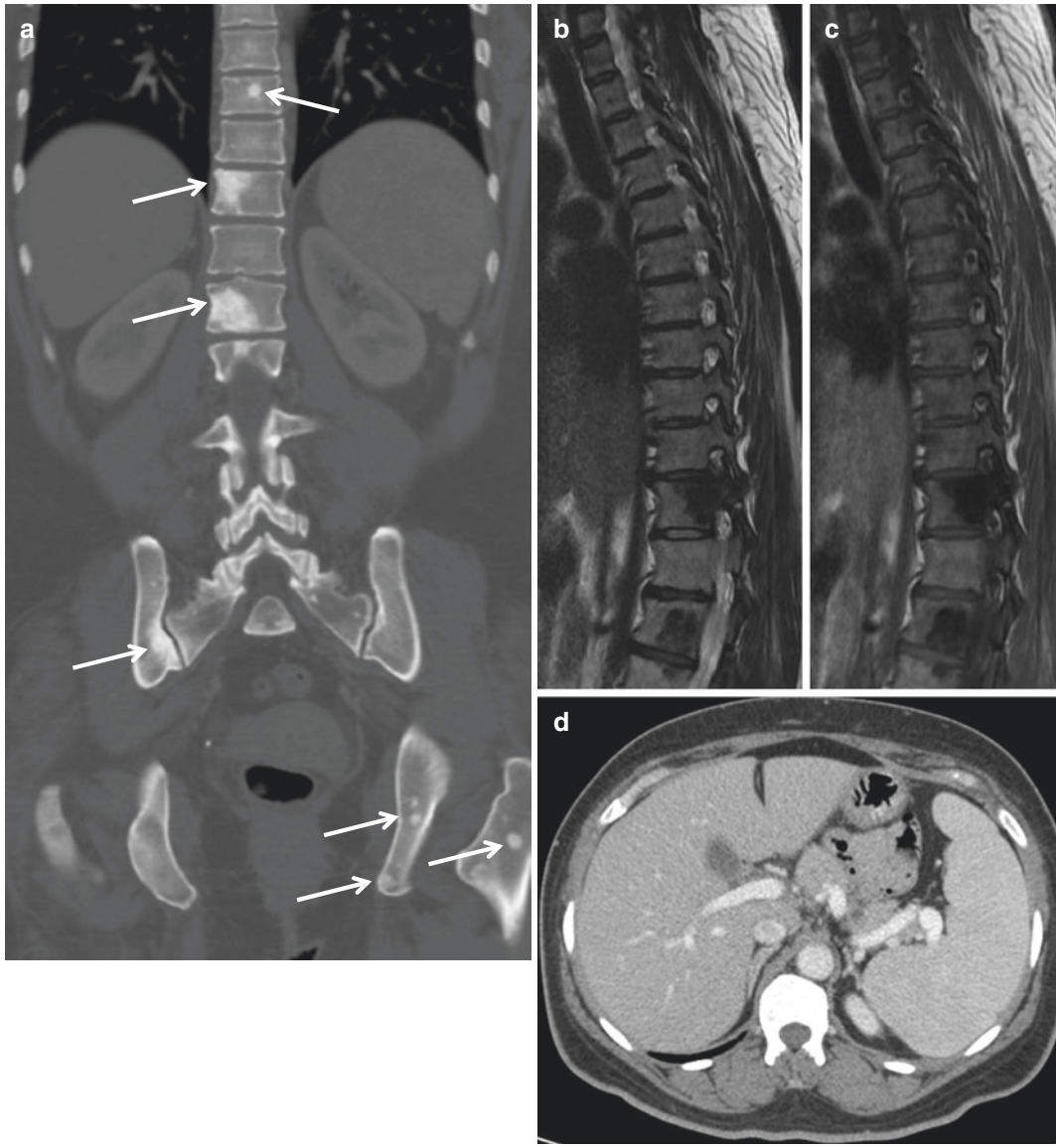

Fig. 6.6 POEMS syndrome. A 47-year-old female patient presented with tingling sensation and weakness in the lower extremities and numbness in the upper extremities. (**a**) Coronal reformatted CT image shows multiple sclerotic bone lesions scattered in the vertebral column, pelvic bones, and left proximal femur (*arrows*). (**b**) Sagittal T1-weighted and (**c**) T2-weighted images of the thoracic spine show lesions with dark signal intensity on both sequences. (**d**) Axial CT image of the upper abdomen shows splenomegaly

6.2 Lymphoma of Bone

Overview

Lymphoma is a disease histologically characterized by the proliferation of lymphocytes, histiocytes, and their precursors. Lymphoma of bone can be classified as primary lymphoma of bone or secondary bone lymphoma. Secondary bone lymphoma refers to the involvement of bone secondary to a systemic disease with nodal or other extranodal involvement, and is not uncommon. On the other hand, primary lymphoma of bone is defined as lymphoma confined to the bone or bone marrow without evidence of concurrent systemic disease, and is rare. The majority of primary bone lymphomas are non-Hodgkin lymphomas.

Epidemiology

Primary lymphoma of bone accounts for <5 % of primary bone tumors. It may occur in any age group, but has a peak prevalence in the sixth and seventh decades of life. It is slightly more common in males(male: female = 1.5:1).

Common Locations

The femur is the most commonly affected site, accounting for 25 % of the cases. Within the femur, the lesion is usually located in the metadiaphysis. The spine and pelvic bone, humerus, tibia, and head and neck are the other possible sites.

Imaging Features

Radiograph

A typical primary bone lymphoma appears as an osteolytic lesion with permeative or moth-eaten pattern of bone destruction, located at the diaphysis of a long bone (Fig. 6.7). Mixed areas of osteolysis and sclerosis may be noted in some lesions. More than half of the lesions accompany periosteal reaction, and aggressive lesions may lead to cortical destruction and soft tissue mass formation. Lesions confined to the medullary cavity without cortical destruction appear normal on plain radiograph.

Magnetic resonance imaging

The MR imaging findings of primary lymphoma of bone are variable. A typical lesion would appear isointense to slightly hypointense to muscle on T1-weighted images, and hyperintense on T2-weighted images or fluid-sensitive sequences, and show enhancement after injection of gadolinium-based contrast agents (Fig. 6.7). The extent of soft tissue involvement is readily evaluated on MR images (Fig. 6.8), and multiplicity may be found (Fig. 6.9). When an intramedullary lesion extends to the surrounding soft tissue without extensive cortical destruction, the diagnosis of small round cell lesions such as lymphoma, multiple myeloma, and Ewing's sarcoma should be considered.

Differential Diagnoses

1. In young patient: Ewing's sarcoma, leukemia, lytic osteosarcoma, osteomyelitis
2. In older patients: Plasma cell myeloma, metastasis

Fig. 6.7 Primary lymphoma of bone in a 70-year-old female. (**a**) An osteolytic lesion with permeative pattern of bone destruction is noted in the proximal metadiaphysis of the right humerus on anteroposterior radiograph of the right humerus. The lesion is complicated with a pathological fracture. (**b**) Axial T1-weighted, (**c**) axial T2-weighted, (**d**) coronal T1-weighted, (**e**) coronal contrast-enhanced T1-weighted fat-suppressed images reveal the true extent of the lesion. A large extraosseous soft tissue mass component is noted around the humerus (*arrows*) without overt cortical destruction, indicating the presence of a round cell tumor.

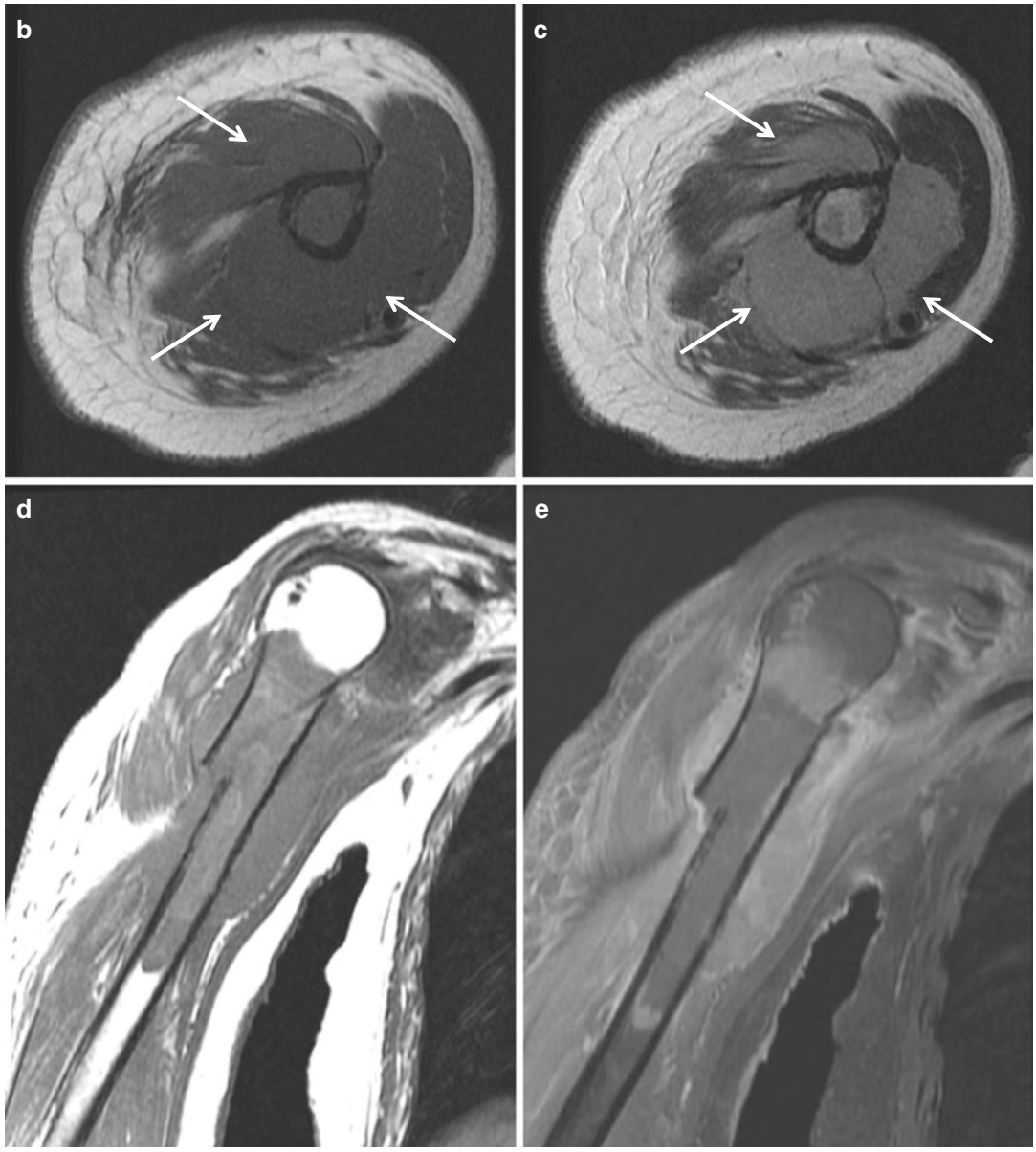

Fig. 6.7 (continued)

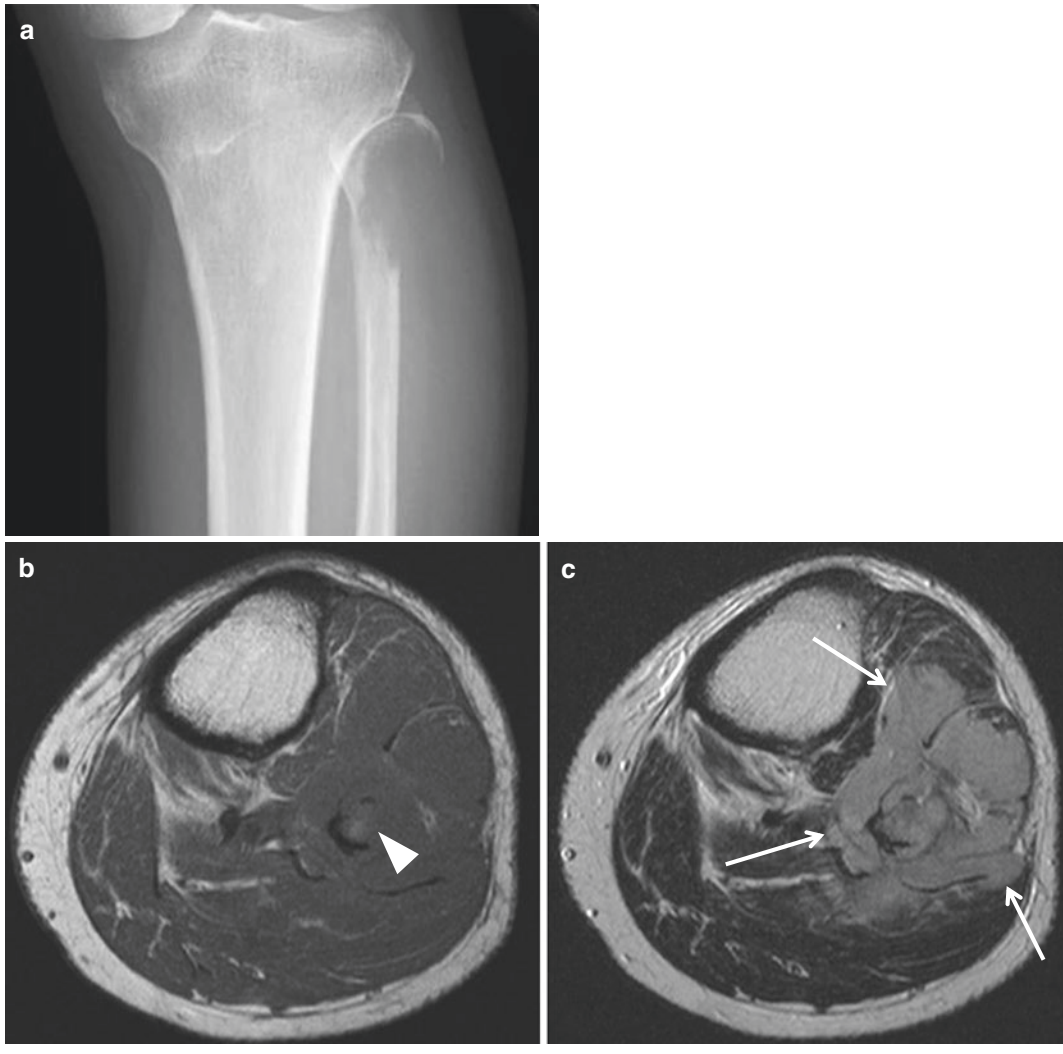

Fig. 6.8 Secondary bone lymphoma of bone in a 64-year-old male diagnosed with testicular lymphoma. (**a**) A geographical osteolytic lesion is noted at the proximal fibula on anteroposterior radiograph of the left knee. (**b**) Axial T1-weighted image, (**c**) axial T2-weighted image, (**d**) axial contrast-enhanced T1-weighted fat-suppressed image, and (**e**) coronal T2-weighted image of the left lower leg show the intramedullary mass in the fibula causing cortical destruction (*arrowhead*). A large soft tissue mass is surrounding the fibula (*arrows*), a finding consistently seen in round cell tumors

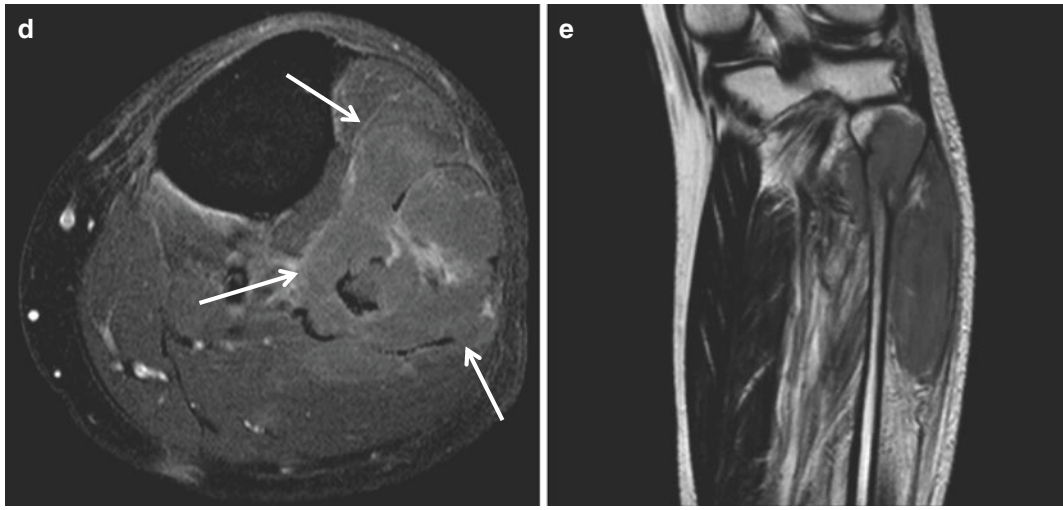

Fig. 6.8 (continued)

Fig. 6.9 Primary lymphoma of bone in an 83-year-old male. (**a**) Anteroposterior radiograph of the right lower leg shows multiple geographical osteolytic lesions in the right tibia. (**b**) PET scan image shows the hypermetabolic activity of these lesions. (**c**) Axial T1-weighted image, (**d**) axial contrast-enhanced T1-weighted fat-suppressed image, (**e**) sagittal T2-weighted image, and (**f**) sagittal contrast-enhanced T1-weighted fat-suppressed image of the right lower leg are shown. The lesion is intermediate on T1-weighted image, heterogeneously hypointense on T2-weighted image, and heterogeneously enhances after administration of gadolinium-based contrast agent

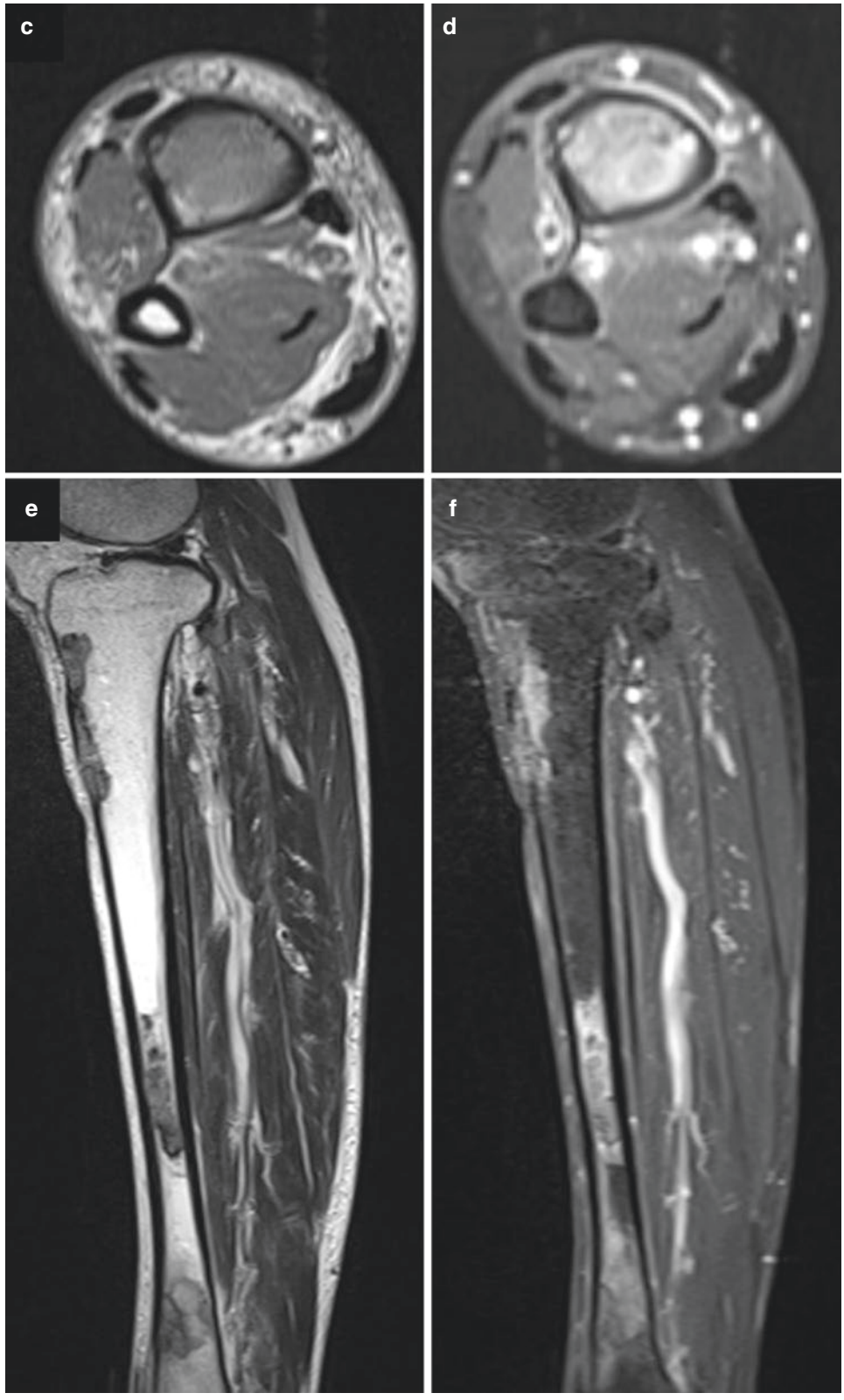

Fig. 6.9 (continued)

6.3 Ewing's Sarcoma

Overview

Ewing's sarcoma is a highly aggressive primary bone tumor that is composed of small round cells showing varying degrees of neuroectodermal differentiation. It is genetically characterized by a specific chromosomal translocation, involving the EWSR1 gene and a member of the ETS family of transcription factors. Primitive neuroectodermal tumor (PNET) was originally thought to be a distinct pathology, but the advent of cytogenetic evaluation has shown that the Ewing's sarcoma and PNET are a spectrum of the same disease, and is commonly referred to as "Ewing/PNET."

Epidemiology

Ewing's sarcoma accounts for 6–8 % of all primary malignant bone tumors. It is a common tumor in children, second only to osteosarcoma. It usually occurs in the first two decades of life, with 80 % of cases occurring within this age group. It has a slight predilection for males (male: female = 1.4:1). Ewing's sarcoma has an ethnic predilection, more commonly occurring in Caucasians.

Common Locations

The majority of Ewing's sarcomas occur in the bone (90 %), but around 10 % originate from the extraskeletal soft tissue. Ewing's sarcoma of bone can occur in both appendicular and axial skeletons, and has a wide distribution. However, the most common location is in the diaphysis or metadiaphysis of long tubular bones (femur, tibia, humerus), followed by the pelvis and ribs.

Imaging Features

Radiograph

Ewing's sarcomas present as osteolytic lesions in the diaphysis or metadiaphysis of long bones with a wide zone of transition, resulting in a moth-eaten or permeative pattern of bone destruction (Fig. 6.10). Periosteal reaction is frequently seen with an aggressive pattern: multilamellated (onion-skin) or spiculated (hair-on-end, sunburst). About one-third of the tumors have a sclerotic component (Fig. 6.11).

Magnetic resonance imaging

Ewing's sarcomas exhibit intermediate to low signal intensity on T1-weighted images, high signal intensity on T2-weighted images, and contrast enhancement is seen after intravenous gadolinium injection. As with other "small round cell tumors," Ewing's sarcoma may form large extraosseous soft tissue masses with only subtle cortical destruction, and the soft tissue masses are commonly disproportionally larger than their intraosseous components (Fig. 6.12).

Differential Diagnoses

1. Osteosarcoma

   Osteosarcomas commonly affect the same age group and may share similar radiographic appearances with Ewing's sarcoma: moth-eaten or permeative osteolytic lesions with aggressive periosteal reaction. However, (i) a metaphyseal location, (ii) the presence of osteoid pattern of mineralization, and (iii) Codman's triangle periosteal reaction may suggest the diagnosis of osteosarcoma.
2. Osteomyelitis

   Ewing's sarcoma may present with fever and elevated acute phase reactants, making it difficult to distinguish from osteomyelitis. On imaging, (i) penumbra sign on T1-weighted imaging (a rim of high T1 signal intensity along the periphery of the lesion corresponding to vascularized granulation tissue), (ii) a more infiltrative extraosseous soft tissue component would favor the diagnosis of osteomyelitis.

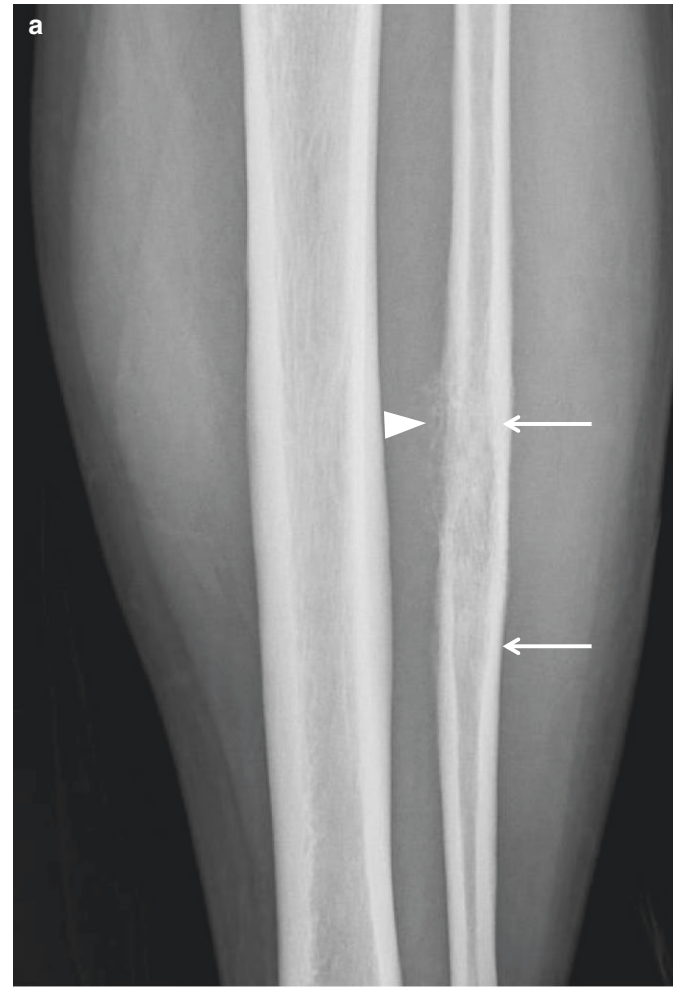

Fig. 6.10 Ewing's sarcoma in the left fibula in a 25-year-old male. (**a**) Anteroposterior radiograph of the left lower leg shows a permeative osteolytic lesion at the midshaft of the fibula (*arrow*). Aggressive interrupted pattern of periosteal reaction is noted along the cortical surface (*arrowhead*). The lesion shows intermediate to low signal intensity on T1-weighted image (**b**), high signal intensity on T2-weighted image (**c**), and contrast enhancement is seen after intravenous gadolinium-based contrast media injection (**d, e**). A large extraosseous mass is noted around the fibula (*arrows* in **b, c**, **d**)

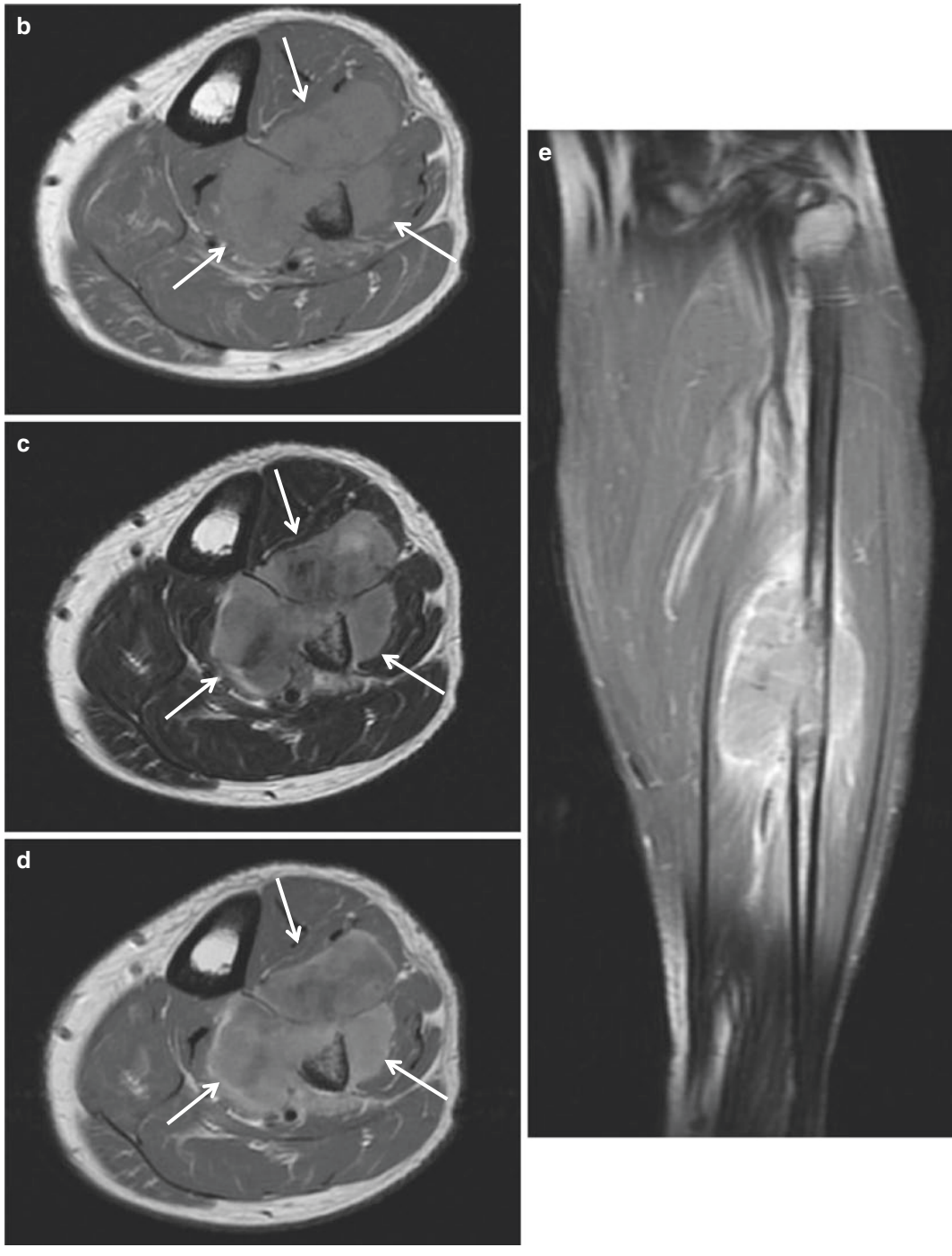

Fig. 6.10 (continued)

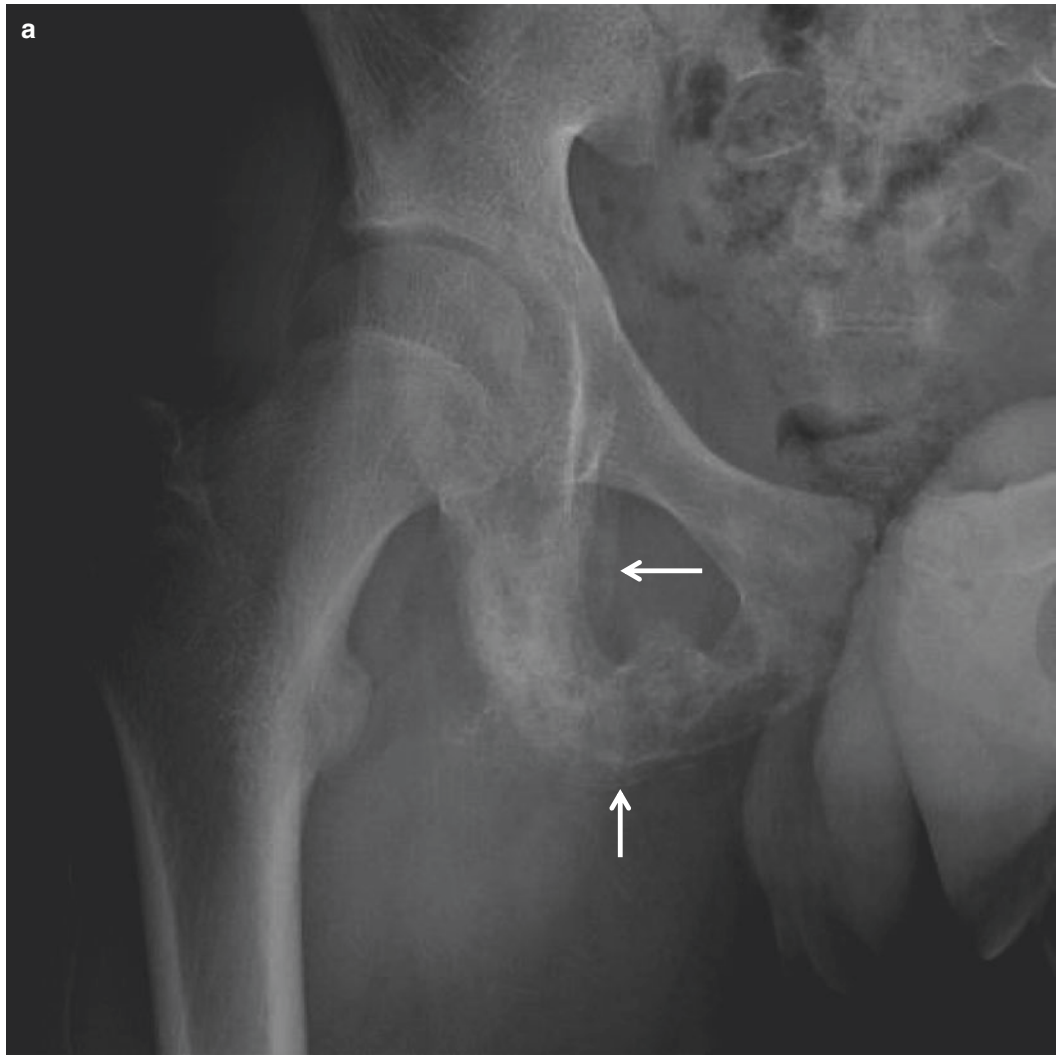

Fig. 6.11 Ewing's sarcoma in the right pelvic bone. (**a**) Anteroposterior radiograph of the hip shows ill-defined mixed osteolytic and osteosclerotic lesion noted in the right ischium and inferior pubic ramus in a 13-year-old male. Aggressive interrupted pattern of periosteal reaction is noted around the lesion (*arrows*). (**b**) Axial CT scan shows the mixed osteolytic and osteosclerotic lesion involving the inferior pubic ramus and ischium with periosteal new bone deposition. The extraosseous soft tissue mass exhibits irregular mineralization (*arrowhead*). (**c**) Axial fusion PET-CT images show a hypermetabolic mass in the corresponding area. (**d**) Axial T1-weighted image, (**e**) axial T2-weighted image, (**f**) axial contrast-enhanced T1-weighted fat-suppressed image, and (**g**) coronal T2-weighted images show the right pelvic bone lesion with large extraosseous soft tissue mass. The periosteum is elevated from the cortical bone, and subperiosteal extension of tumor is noted *(arrow* in **g**)

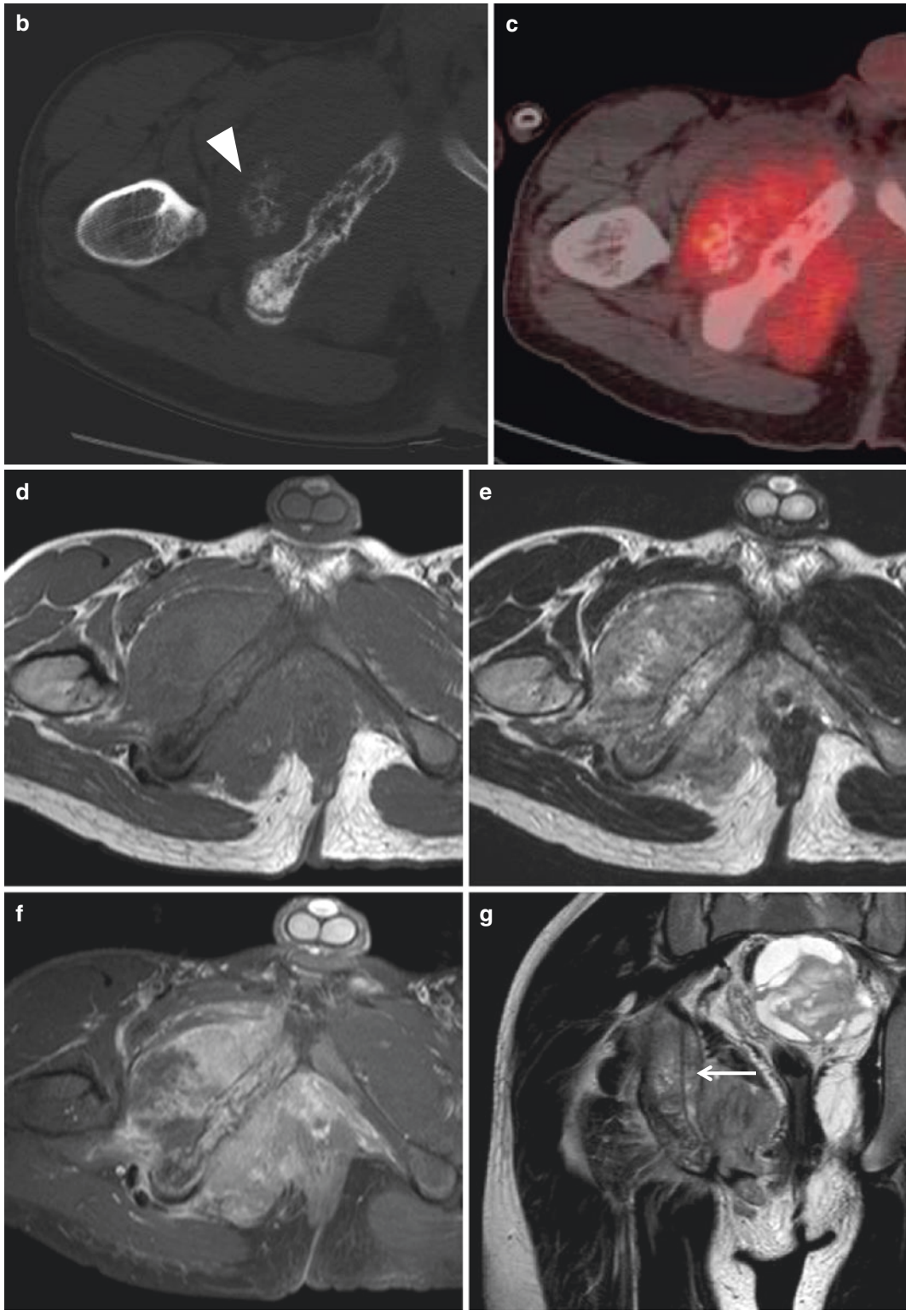

Fig. 6.11 (continued)

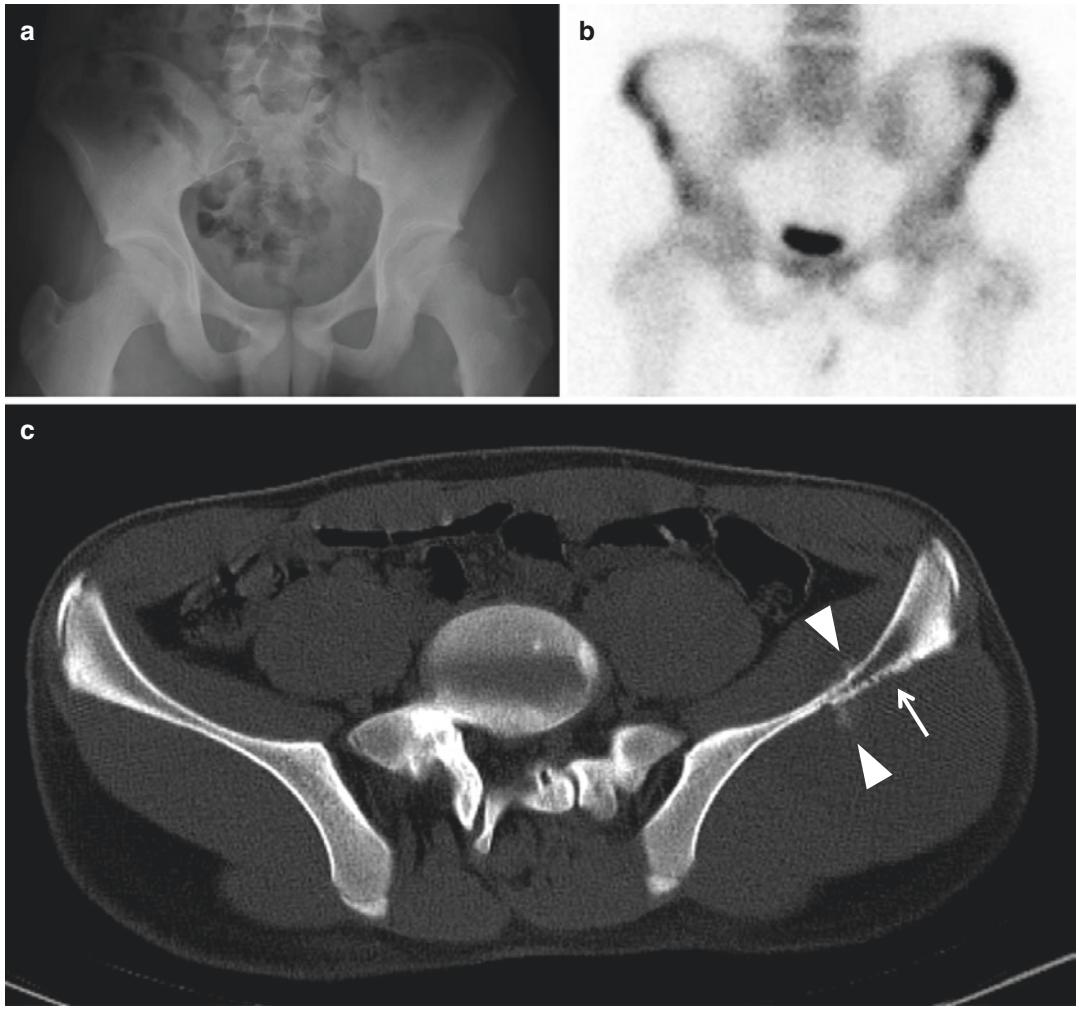

Fig. 6.12 Ewing's sarcoma in the left ilium. (**a**) No significant bony abnormality is detected on the anteroposterior radiograph of the pelvis. (**b**) On bone scan, increased uptake is noted in the left ilium. (**c**) On axial CT image, an osteolytic lesion with subtle cortical fenestration (*arrow*). Subtle periosteal bone deposition is noted around the lesion (*arrowheads*). (**d**) Axial T1-weighted image, (**e**) axial T2-weighted image, and (**f**) axial contrast-enhanced T1-weighted fat-suppressed image show intramedullary lesion involving the left iliac wing and a disproportionally large soft tissue mass involving the iliac fossa and gluteus muscles, which is a characteristic finding for small round cell tumors. (**g**) Fusion PET/CT image demonstrates the hypermetabolic activity of this lesion

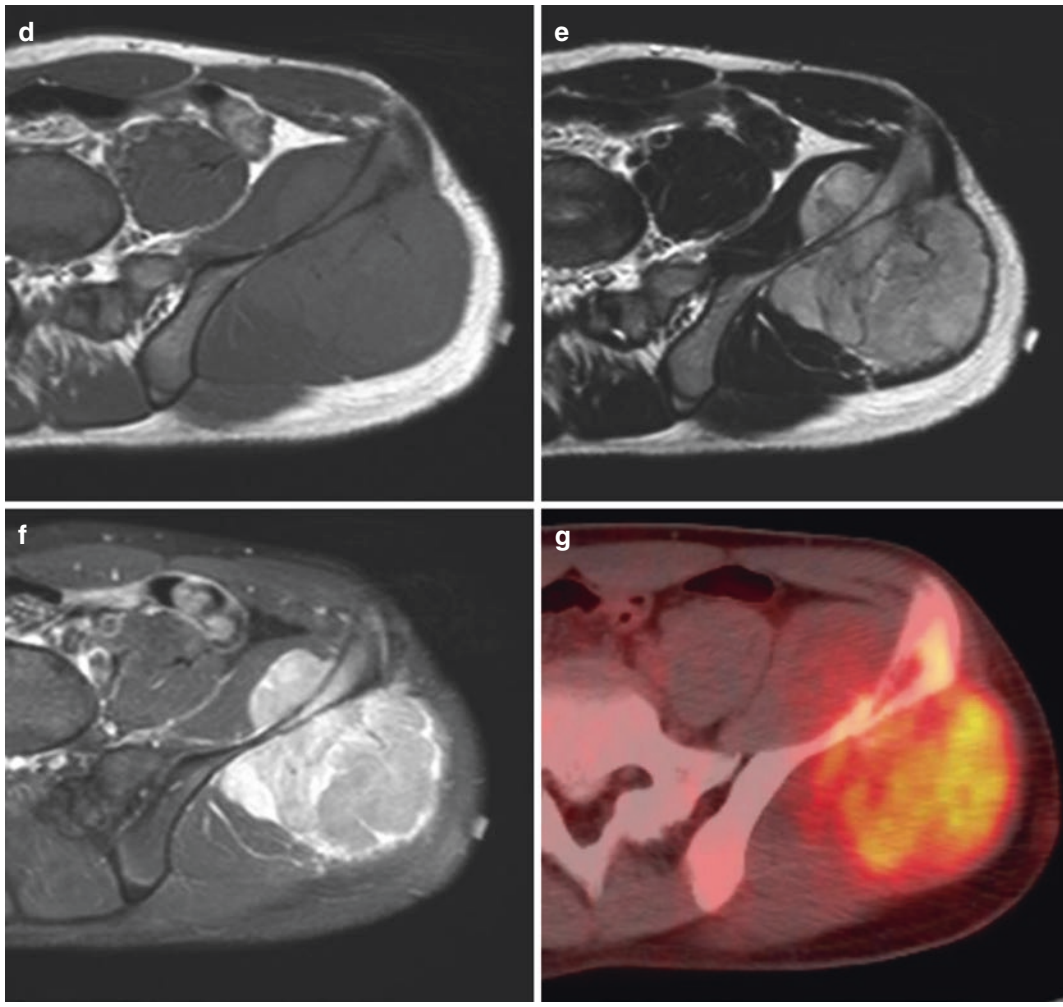

Fig. 6.12 (continued)

Suggested Reading

Plasma Cell Myeloma/Solitary Plasmacytoma of Bone

Angtuaco EJ, Fassas AB, Walker R, Sethi R, Barlogie B. Multiple myeloma: clinical review and diagnostic imaging. Radiology. 2004;231:11–23.

Dimopoulos MA, Moulopoulos LA, Maniatis A, Alexanian R. Solitary plasmacytoma of bone and asymptomatic multiple myeloma. Blood. 2000;96:2037–44.

Dispenzieri A, Kyle RA, Lacy MQ, et al. POEMS syndrome: definitions and long-term outcome. Blood. 2003;101:2496–506.

Moulopoulos LA, Dimopoulos MA, Weber D, Fuller L, Libshitz HI, Alexanian R. Magnetic resonance imaging in the staging of solitary plasmacytoma of bone. J Clin Oncol. 1993;11:1311–5.

Tong D, Griffin TW, Laramore GE, et al. Solitary plasmacytoma of bone and soft tissues. Radiology. 1980;135:195–8.

Lymphoma of Bone

Baar J, Burkes RL, Gospodarowicz M. Primary non-Hodgkin's lymphoma of bone. Semin Oncol. 1999;26:270–5.

Griffiths H, Conaway JR. Radiologic case study. Primary lymphoma of bone. Orthopedics. 1999;22:265–6. 72.

Haussler MD, Fenstermacher MJ, Johnston DA, Harle TS. MRI of primary lymphoma of bone: cortical disorder as a criterion for differential diagnosis. J Magn Reson Imaging. 1999;9:93–100.

Heyning FH, Kroon HM, Hogendoorn PC, Taminiau AH, van der Woude HJ. MR imaging characteristics in primary lymphoma of bone with emphasis on non-aggressive appearance. Skeletal Radiol. 2007;36:937–44.

Krishnan A, Shirkhoda A, Tehranzadeh J, Armin AR, Irwin R, Les K. Primary bone lymphoma: radiographic-MR imaging correlation. Radiographics. 2003;23:1371–83.

Mulligan ME, McRae GA, Murphey MD. Imaging features of primary lymphoma of bone. AJR Am J Roentgenol. 1999;173:1691–7.

Stiglbauer R, Augustin I, Kramer J, Schurawitzki H, Imhof H, Radaszkiewicz T. MRI in the diagnosis of primary lymphoma of bone: correlation with histopathology. J Comput Assist Tomogr. 1992;16(2):248–53.

White LM, Schweitzer ME, Khalili K, Howarth DJ, Wunder JS, Bell RS. MR imaging of primary lymphoma of bone: variability of T2-weighted signal intensity. AJR Am J Roentgenol. 1998;170(5):1243–7.

Ewing Sarcoma

Balamuth NJ, Womer RB. Ewing's sarcoma. Lancet Oncol. 2010;11:184–92.

Frouge C, Vanel D, Coffre C, Couanet D, Contesso G, Sarrazin D. The role of magnetic resonance imaging in the evaluation of Ewing sarcoma. A report of 27 cases. Skeletal Radiol. 1988;17:387–92.

Javery O, Krajewski K, O'Regan K, et al. A to Z of extraskeletal Ewing sarcoma family of tumors in adults: imaging features of primary disease, metastatic patterns, and treatment responses. AJR Am J Roentgenol. 2011;197:W1015–22.

Maheshwari AV, Cheng EY. Ewing sarcoma family of tumors. J Am Acad Orthop Surg. 2010;18:94–107.

Murphey MD, Senchak LT, Mambalam PK, Logie CI, Klassen-Fischer MK, Kransdorf MJ. From the radiologic pathology archives: ewing sarcoma family of tumors: radiologic-pathologic correlation. Radiographics. 2013;33:803–31.

Vascular Tumors

7

Contents

7.1 Hemangioma

Overview

Hemangioma is a common benign bone tumor, characterized by newly formed thin-walled capillary or cavernous type blood vessels.

Epidemiology

Hemangiomas may occur in any age, but most cases are diagnosed between the fourth and seventh decades of life. A slight female predilection has been reported (male: female = 2:3).

Common Locations

The vertebral bodies and craniofacial bones are the two most commonly affected sites. Multifocal involvement is frequent in the spine. When they occur in a long bone (femur, tibia, humerus), the metaphysis is commonly affected, and can occur with a medullary, intracortical, or periosteal location.

Imaging Features

Radiograph

Vertebral hemangiomas present as radiolucent lesions with coarse trabeculations or striations (corduroy pattern, polka-dot pattern). The mixed osteolytic and trabeculated appearance of hemangiomas may be found in flat bones and tubular bones, sometimes exhibiting a "honeycomb" pattern (Fig. 7.1). In flat bones, hemangiomas may

H.S. Kang et al., *Oncologic Imaging: Bone Tumors*, DOI 10.1007/978-981-287-703-1_7

cause significant expansion of the bone and may accompany radially oriented striations.

Magnetic resonance imaging

The classic appearance of hemangioma of the bone is hyperintense on T1-weighted images due to the presence of it within the lesion, but the signal may be variable depending on the amount of fat. Hemangiomas are hyperintense on T2-weighted images and fluid-sensitive sequences, due to the vascular channels within the mass (Fig. 7.2). The thickened trabeculation exhibits dark signal intensity on both T1-weighted and T2-weighted images. Most lesions show significant contrast enhancement after intravenous gadolinium injection.

Differential Diagnoses (for Lesions in Long Bone)

Aneurysmal bone cyst

Hemangiomas that exhibit expansile osteolytic appearance with striations may appear similar to aneurysmal bone cysts on radiograph.

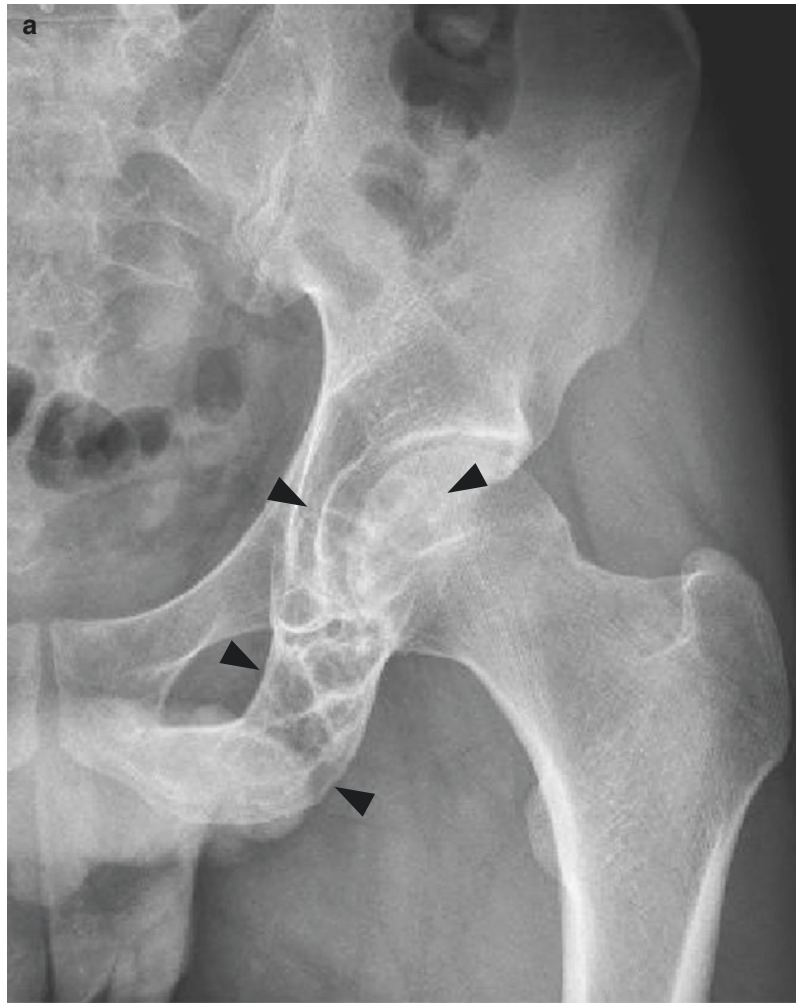

Fig. 7.1 Hemangioma in the left acetabulum and inferior pubic ramus. (**a**) Anteroposterior radiograph of the left hip shows an expansile osteolytic lesion in the left acetabulum and inferior pubic ramus (*black arrowheads*). Multiple thickened trabeculations are noted within the mass. (**b**) Axial T1-weighted image, (**c**) axial T2-weighted image, (**d**) axial contrast-enhanced T1-weighted fat-suppressed image, and (**e**) coronal T1-weighted image show a multilobulated septated intramedullary lesion in the left acetabulum and inferior pubic ramus. Some portions exhibit fluid-equivalent signal intensity and show thin peripheral rim enhancement (*arrows*), whereas some portions have fat-equivalent signal intensity (*white arrowheads*)

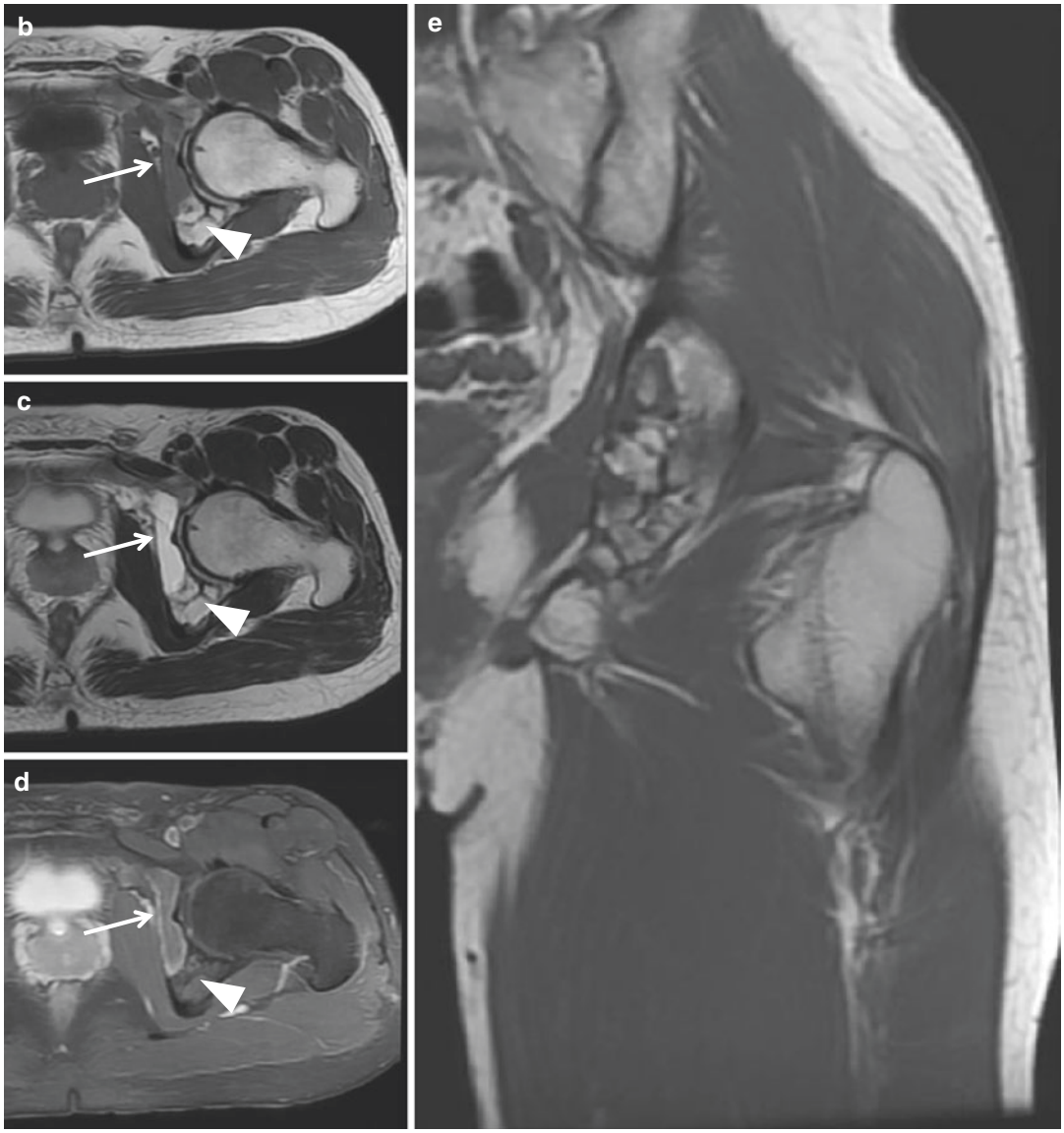

Fig. 7.1 (continued)

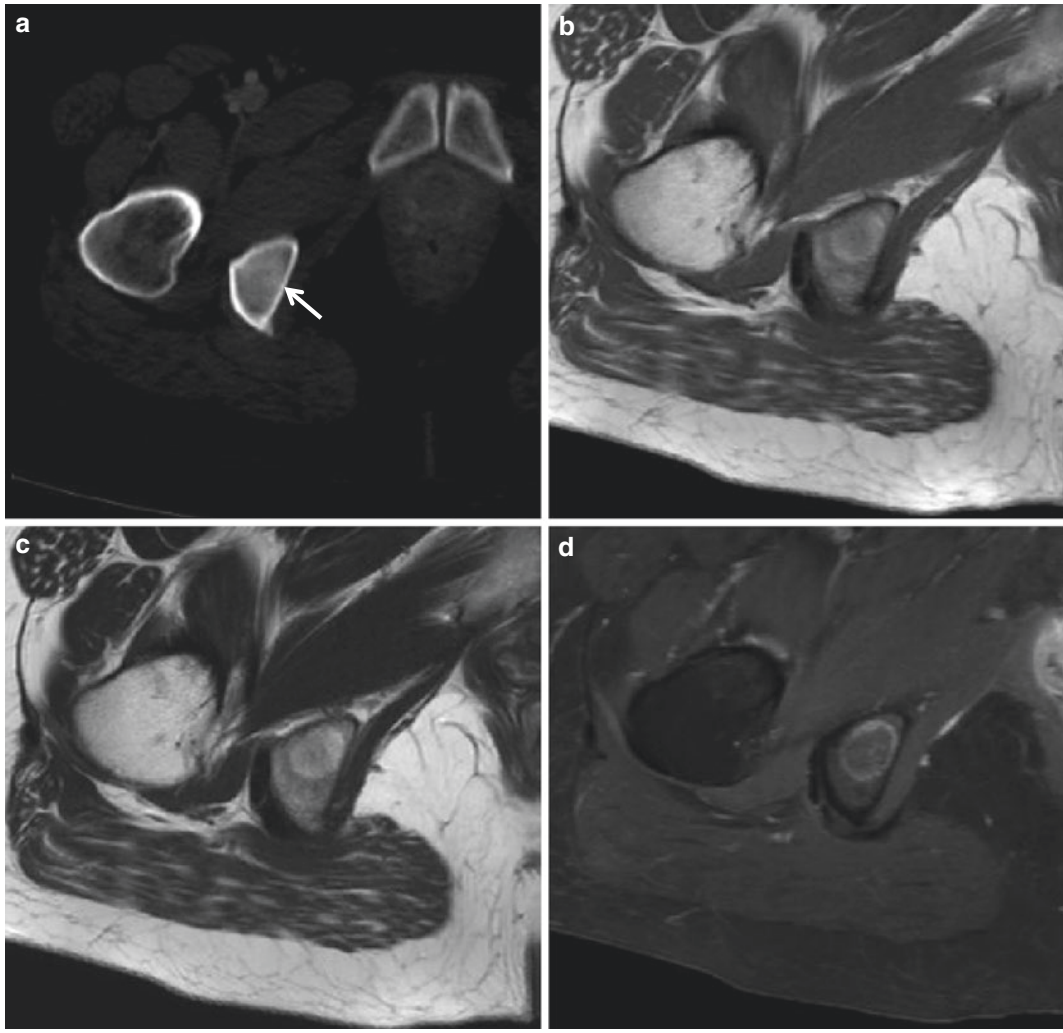

Fig. 7.2 Hemangioma in the right ischium. (**a**) Axial contrast-enhanced CT image shows a hyperattenuated lesion in the right ischium (*arrow*). This lesion is hyperintense on both (**b**) axial T1-weighted image and (**c**) axial T2-weighted images, and shows peripheral enhancement on (**d**) contrast-enhanced T1-weighted fat-suppressed image. Hyperintensity on both T1-weighted and T2-weighted images probably corresponds to the fat deposition within the hemangioma

7.2 Angiosarcoma

Overview
Angiosarcoma is a vascular tumor of high-grade malignancy, which is histologically characterized by cells showing endothelial differentiation.

Epidemiology
Angiosarcoma accounts for <1 % of primary malignant bone tumors. It has been reported to occur in patients between the third and ninth decades with a peak incidence in the third to fifth decades. It has a male predominance, with a male-to-female ratio of 2:1.

Common Locations
Angiosarcomas more commonly involve the skin and soft tissue, and rarely occur in the bone. It has a wide skeletal distribution, with a majority involving the long tubular bones (tibia, femur), pelvic bones, and spine.

Imaging Features
Radiograph

Angiosarcoma appears as an osteolytic lesion with a wide zone of transition, and cortical breaching with soft tissue extension is common (Fig. 7.3).

Magnetic resonance imaging

The MR imaging findings are nonspecific.

Differential Diagnoses
The list of differential diagnoses consists of osteolytic lesions with aggressive features: metastasis, plasmacytoma, lymphoma, fibrosarcoma.

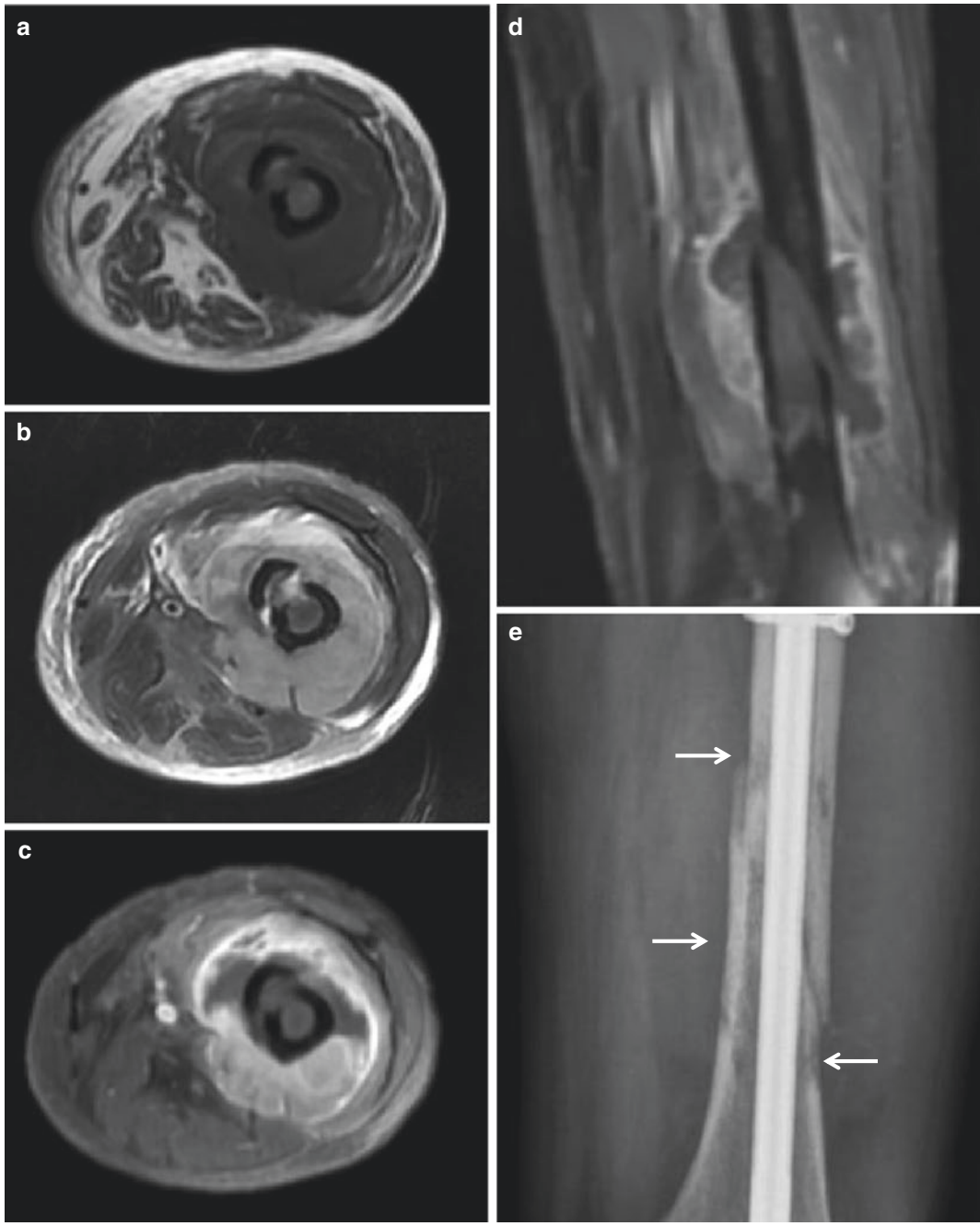

Fig. 7.3 Angiosarcoma in the left femur. A 79-year-old male patient presented with fracture of the left femur after a minor traumatic event. (**a**) Axial T1-weighted image, (**b**) axial T2-weighted fat-suppressed image, (**c**) axial and (**d**) coronal contrast-enhanced T1-weighted fat-suppressed image show a intramedullary lesion at the fracture site accompanied by a large extraosseous soft tissue mass. (**e**) The left femur was internally fixated with an intramedullary nail. A permeative osteolytic lesion is noted around the site of fracture (*arrow*)

7.3 Epithelioid Hemangioendothelioma

Overview

Epithelioid hemangioendothelioma is a rare low-to-intermediate grade malignant vascular neoplasm.

Epidemiology

Epithelioid hemangioendothelioma may occur at any age, but most frequently present in the second or third decade of life. It has been reported to have a male preponderance, with a male-to-female ratio of 2:1.

Common Locations

The most commonly affected sites are caldarium, axial skeleton, and lower limbs (tibia, femur). More than half of the patients present with multifocal disease. Multiple lesions may be noted in single bone, or polyostotic involvement may also be noted. Within a long bone, lesions may be metaphyseal, diaphyseal, or even epiphyseal.

Imaging Features

Radiograph

EH appear as osteolytic lesions with either a cortical or medullary location (Fig. 7.4). Matrix mineralization is usually not noted, and periosteal reaction is rare. Cortical disruption with extraosseous extension may be present.

Magnetic resonance imaging

There are no specific features of EH on MR imaging. Generally, lesions show low-to-intermediate signal intensity on T1-weighted image, high signal intensity on T2-weighted images, and homogeneous enhancement after intravenous contrast injection (Figs. 7.4 and 7.5).

Differential Diagnoses

The list of differential diagnoses includes skeletal angiomatosis, LCH, angiosarcoma, myeloma, metastasis, which can present as solitary or multiple osteolytic lesions.

Fig. 7.4 Epithelioid hemangioendothelioma involving the left lower extremity. Anteroposterior radiograph of the thigh (**a**) and lower leg (**b**) shows multiple geographical osteolytic lesions scattered in the distal femur, tibia, and fibula in a 37-year-old male. (**c**) Axial T1-weighted image, (**d**) axial T2-weighted fat-suppressed image, (**e**) axial and (**f**) coronal contrast-enhanced T1-weighted fat-suppressed images of the thigh show multiple bone destructing lesions with intramedullary and cortical involvement. The lesions are of intermediate signal intensity on T1-weighted image, slightly high signal intensity on T2-weighted images, and homogeneously enhance after intravenous contrast injection. (**g**) Axial contrast-enhanced T1-weighted fat-suppressed image of the lower leg also exhibits multiple round intracortical lesions with contrast enhancement

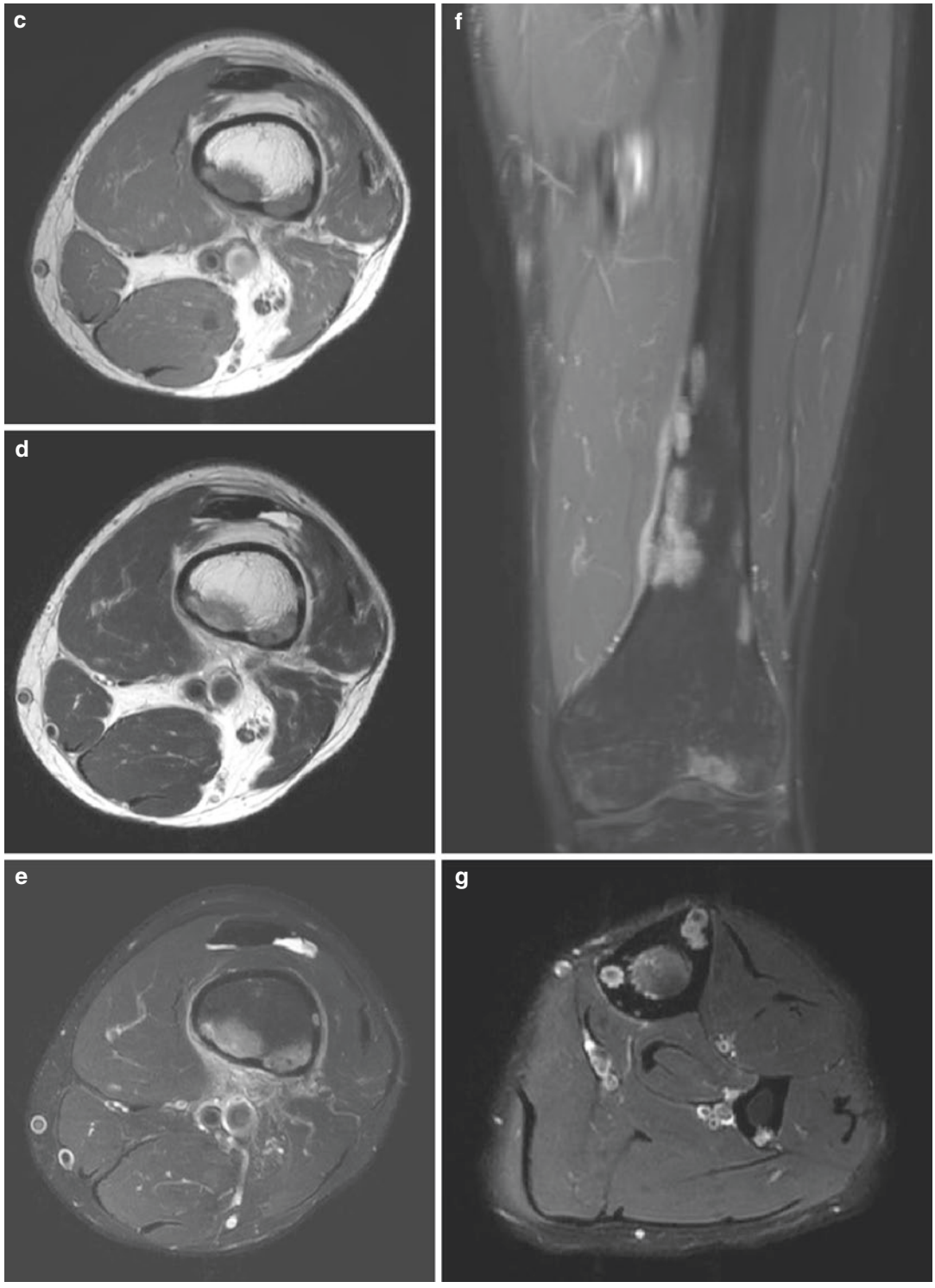

Fig. 7.4 (continued)

Fig. 7.5 Epithelioid hemangioendothelioma involving the right lower leg. (**a**) Anteroposterior and (**b**) lateral radiographs of the right lower leg in a 31-year-old male. Multiple intracortical osteolytic lesions are noted along the anterior cortex of the tibia. The lesions show intermediate signal intensity on axial T1-weighted image (**c**), slightly high signal intensity on axial T2-weighted image (**d**), and homogeneously enhance on axial contrast-enhanced T1-weighted fat-suppressed image (**e**)

Suggested Reading

Hemangioma

Chawla A, Singrakhia M, Maheshwari M, Modi N, Parmar H. Intraosseous haemangioma of the proximal femur: imaging findings. Br J Radiol. 2006;79: e64–6.

Greenspan AJG, Remagen W. Differential diagnosis of orthopaedic oncology. 2nd ed. Philadelphia: Lippincott Williams & Wilkins; 2007. p. 366–7.

Kaleem Z, Kyriakos M, Totty WG. Solitary skeletal hemangioma of the extremities. Skeletal Radiol. 2000;29: 502–13.

Levine SM, Lambiase RE, Petchprapa CN. Cortical lesions of the tibia: characteristic appearances at conventional radiography. Radiographics. 2003;23:157–77.

Murphey MD, Fairbairn KJ, Parman LM, Baxter KG, Parsa MB, Smith WS. From the archives of the AFIP. Musculoskeletal angiomatous lesions: radiologic-pathologic correlation. Radiographics. 1995;15: 893–917.

Simonetti S, Mignogna C, La Mantia V, Lanza F, Insabato L. Primary intraosseous cavernous hemangioma of the metacarpal bone: a very rare entity. Case report. Tumori. 2009;95:101–3.

Unni KK, Ivins JC, Beabout JW, Dahlin DC. Hemangioma, hemangiopericytoma, and hemangioendothelioma (angiosarcoma) of bone. Cancer. 1971;27:1403–14.

Verbeke SL, Bovee JV. Primary vascular tumors of bone: a spectrum of entities? Int J Clin Exp Pathol. 2011;4:541–51.

Angiosarcoma

Palmerini E, Maki RG, Staals EL, et al. Primary angiosarcoma of bone: a retrospective analysis of 60 patients from 2 institutions. Am J Clin Oncol. 2014;37:528–34.

Unni KK, Ivins JC, Beabout JW, Dahlin DC. Hemangioma, hemangiopericytoma, and hemangioendothelioma (angiosarcoma) of bone. Cancer. 1971;27:1403–14.

Verbeke SL, Bovee JV. Primary vascular tumors of bone: a spectrum of entities? Int J Clin Exp Pathol. 2011;4: 541–51.

Vermaat M, Vanel D, Kroon HM, et al. Vascular tumors of bone: imaging findings. Eur J Radiol. 2011;77:13–8.

Epithelioid Hemangioendothelioma

Abrahams TG, Bula W, Jones M. Epithelioid hemangioendothelioma of bone. A report of two cases and review of the literature. Skeletal Radiol. 1992;21:509–13.

Boutin RD, Spaeth HJ, Mangalik A, Sell JJ. Epithelioid hemangioendothelioma of bone. Skeletal Radiol. 1996;25:391–5.

Kleer CG, Unni KK, McLeod RA. Epithelioid hemangioendothelioma of bone. Am J Surg Pathol. 1996;20:1301–11.

Larochelle O, Perigny M, Lagace R, Dion N, Giguere C. Best cases from the AFIP: epithelioid hemangioendothelioma of bone. Radiographics. 2006;26:265–70.

Tsuneyoshi M, Dorfman HD, Bauer TW. Epithelioid hemangioendothelioma of bone. A clinicopathologic, ultrastructural, and immunohistochemical study. Am J Surg Pathol. 1986;10:754–64.

Other Tumor-Like Lesions and Soft Tissue Type Tumors

8

Contents

8.1 Simple Bone Cyst

Overview

Simple bone cyst is a benign nonneoplastic lesion of the bone, characterized by an intramedullary unilocular cystic lesion filled with serous or serosanguinous fluid.

Epidemiology

Simple bone cysts account for 3 % of all primary bone lesions. It is most common in the second decade of life, with the first two decades of life accounting for 80 % of the cases. It has a strong male predilection (male: female = 3:1).

Common Locations

Ninety percent of the cases occur in long bones; humerus, proximal femur, and proximal tibia are affected in decreasing order. Lesions arise in the metaphysis and tend to migrate away from the physis along with skeletal growth. They may end up with the metadiaphyseal or even diaphyseal location. In adults, simple bone cysts are commonly found in the ilium, calcaneus, and talus.

Imaging Features

Radiograph

A typical simple bone cyst appears as a well-defined geographical osteolytic lesion with a thin sclerotic rim. It may also exhibit a pseudotrabeculated appearance due to prominent endosteal

H.S. Kang et al., *Oncologic Imaging: Bone Tumors*, DOI 10.1007/978-981-287-703-1_8

bony ridges. Simple bone cysts may cause circumferential expansion of the bone, but periosteal reaction is usually absent. When simple bone cysts are complicated with a pathological fracture, "fallen fragment sign" (fractured bone fragment that moves to the dependent site with positional change) and periosteal reaction may be noted (Fig. 8.1).

Magnetic resonance imaging

MR imaging is useful in confirming the cystic nature of the lesion. It usually shows fluid-equivalent signal intensity, but the signal intensity may vary according to the amount and stage of blood products included in the lesion (Fig. 8.2). Lesions usually show thin peripheral rim enhancement after intravenous gadolinium injection (Fig. 8.3).

Differential Diagnoses

1. Aneurysmal bone cyst.

   Aneurysmal bone cysts are more expansile compared to simple bone cysts, and multiple fluid–fluid levels are noted on MR imaging.
2. Fibrous dysplasia.

   The "ground-glass" density within the lesion may favor the diagnosis of fibrous dysplasia over simple bone cyst on radiograph. Fibrous dysplasia may be readily differentiated from simple bone cyst on MR imaging, due to the presence of enhancing solid component.

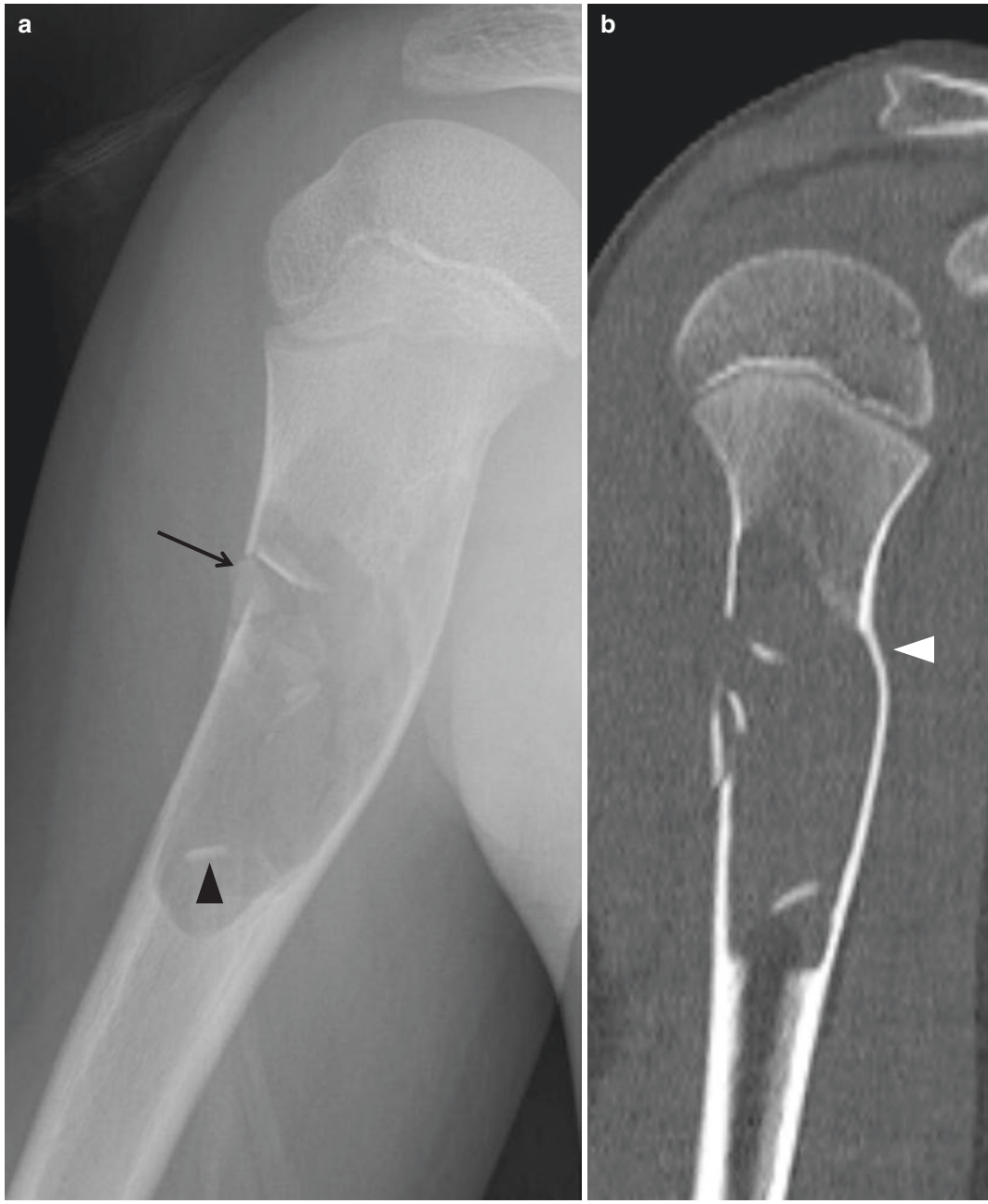

Fig. 8.1 Simple bone cyst in the right proximal humerus in an 11-year-old male. (**a**) An expansile, geographical osteolytic lesion with a nonsclerotic well-defined margin (type IB pattern of destruction) is noted at the proximal metadiaphysis of the right humerus. The lesion is complicated with a pathological fracture (*black arrow*), and the typical "fallen fragment sign" is noted (*black arrowhead*). (**b**) The cortical expansion is well noted on coronal reformatted CT image (*white arrowhead*)

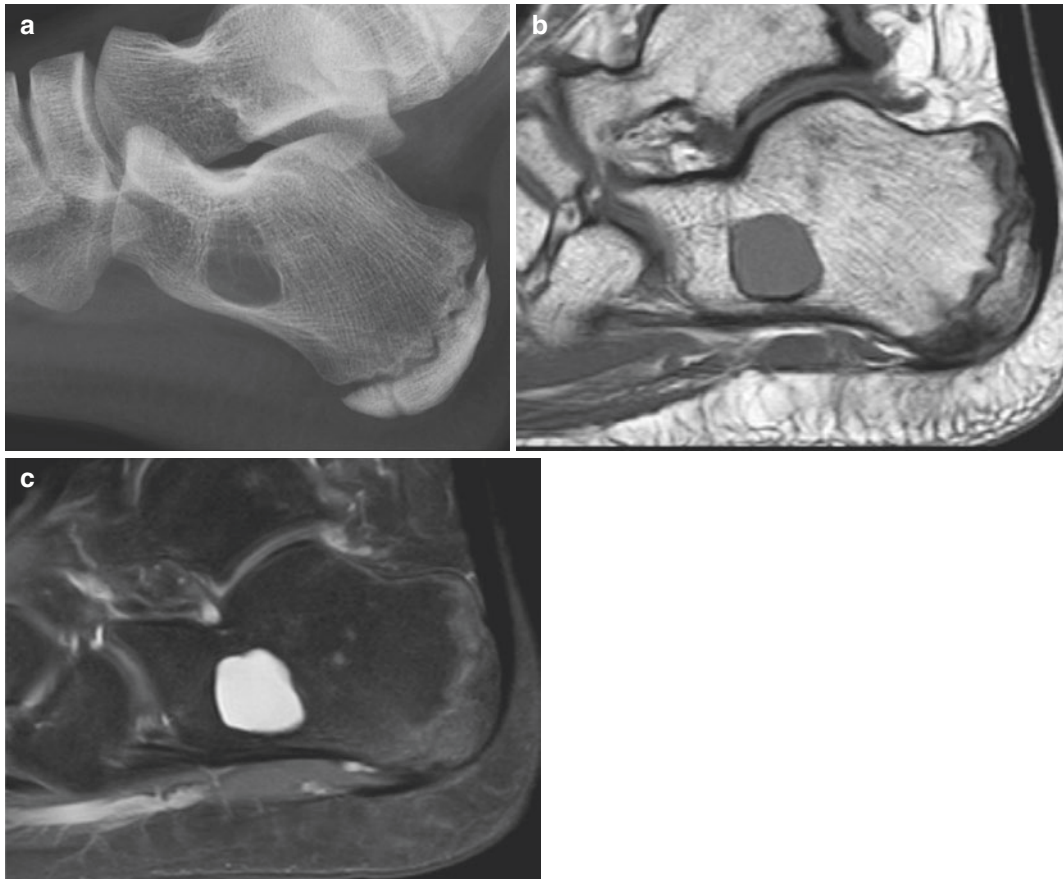

Fig. 8.2 Simple bone cyst in the calcaneus. (**a**) A geographical osteolytic lesion with a thin sclerotic border is noted in the calcaneus on lateral radiograph of the foot. The posterior ossification center of the calcaneus is present, and not yet fused in this 12-year-old patient. (**b**) Sagittal T1-weighted image and (**c**) sagittal T2-weighted fat-suppressed images show the fluid-equivalent signal intensity of the calcaneal lesion

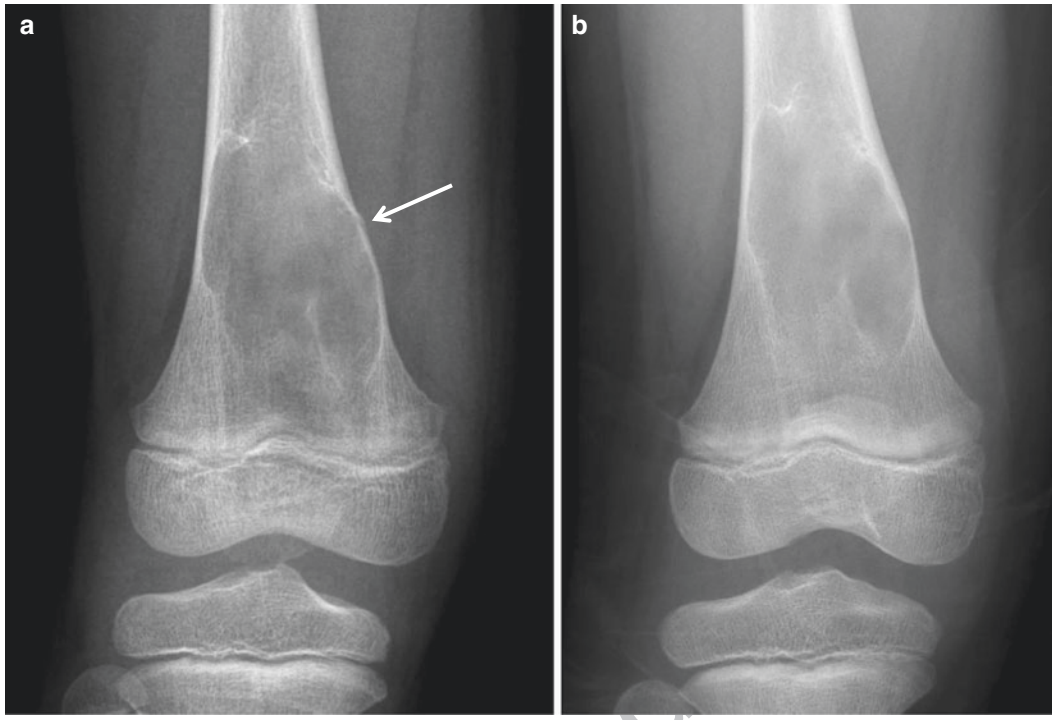

Fig. 8.3 Simple bone cyst in the right distal femur in a 7-year-old male. (**a**) Anteroposterior radiograph of the right thigh shows a mildly expansile geographical osteolytic lesion in the distal metaphysis of the right femur with a central intramedullary location. This lesion is associated with a pathological fracture (*white arrow*). (**b**) Follow-up radiograph taken 4 months later shows healing of the fracture site. (**c**) Axial T1-weighted image, (**d**) axial, and (**e**) sagittal T2-weighted fat-suppressed images show the mildly expansile central lesion in the distal femur with most of the lesion exhibiting fluid-equivalent signal intensity. However, a fluid–fluid level is seen within the lesion, and the dependent portion shows slight hyperintensity on T1-weighted image and shading on T2-weighted image, indicating the presence of blood products due to the associated fracture (*white arrows* in **c**–**e**). (**f**) A thin peripheral rim of enhancement is noted on axial contrast-enhanced T1-weighted fat-suppressed image

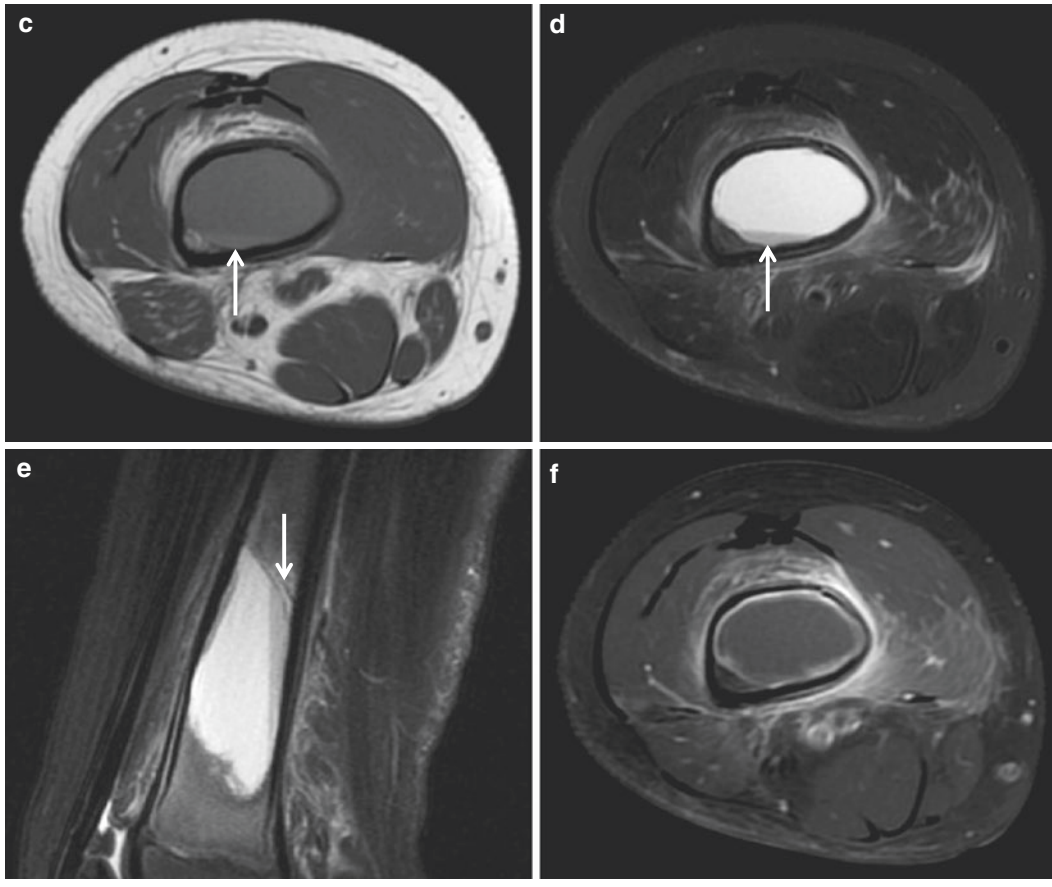

Fig. 8.3 (continued)

8.2 Aneurysmal Bone Cyst

Overview

Aneurysmal bone cyst (ABC) is a benign primary bone tumor composed of multiloculated blood-filled cystic spaces separated by connective tissue septae. It may occur as a primary lesion (70 %) or arise secondarily within a preexisting bone tumor (30 %).

Epidemiology

ABCs account for 1–2 % of primary bone tumors. ABC may occur in any age group, but is most common in the second decade of life, followed by the first decade. The first two decades of life account for 80 % of the cases. A slight female predominance has been reported in some studies, but there is no significant gender predilection.

Common Locations

ABCs have a predilection for the metaphysis of long bone. The distal femur, proximal tibia, and proximal femur are frequently affected. When it occurs in the spine, it is usually located in the posterior element.

Imaging Features

Radiograph

ABC presents as a well-defined, geographical osteolytic lesion with an eccentric intramedullary location at the metaphysis of a long bone (Fig. 8.4). It frequently accompanies a thin shell of cortical/periosteal bone along the surface of the lesion. Internal trabeculations may be seen within the lesion (Fig. 8.5). When the expansion of bone is associated with the internal trabeculations, lesions may exhibit a multiloculated "soap-bubble" appearance.

Magnetic resonance imaging

Multiple fluid–fluid levels are seen within the lesion on MR imaging (Fig. 8.6). MR imaging is useful in differentiating primary from secondary ABCs. The presence of a significant solid component within the tumor indicates an underlying lesion.

Differential Diagnoses

1. Simple bone cyst.

   SBC has a central intramedullary location and is a unilocular lesion. SBCs are less expansile, compared to ABCs. Septations and fluid–fluid levels can be seen in SBC when complicated with a fracture.
2. Telangiectatic osteosarcoma.

   Telangiectatic osteosarcoma is a purely osteolytic lesion on radiographs and exhibits more aggressive features, compared to ABCs.
3. Lesions that may accompany secondary ABCs: chondroblastoma, giant cell tumor, osteoblastoma, fibrous dysplasia, nonossifying fibroma, chondromyxoid fibroma.

Fig. 8.4 Aneurysmal bone cyst in the right tibia. (**a**) Anteroposterior radiograph shows an eccentric geographical osteolytic lesion with a sclerotic rim at the distal metaphysis of the right tibia. (**b**) On bone scan, a subtle increase in uptake is noted at the distal metaphysis of the right tibia compared to contralateral side (*black arrow*). The intense symmetric uptake noted in both tibiae is due to the open physes. The lesion shows intermediate signal intensity on axial T1-weighted image (**c**), and shows multiple fluid–fluid levels on axial T2-weighted image (**d**). A thin peripheral and septal enhancement is noted on (**e**) axial and (**f**) coronal contrast-enhanced T1-weighted fat-suppressed images. No definite solid component is noted within the tumor

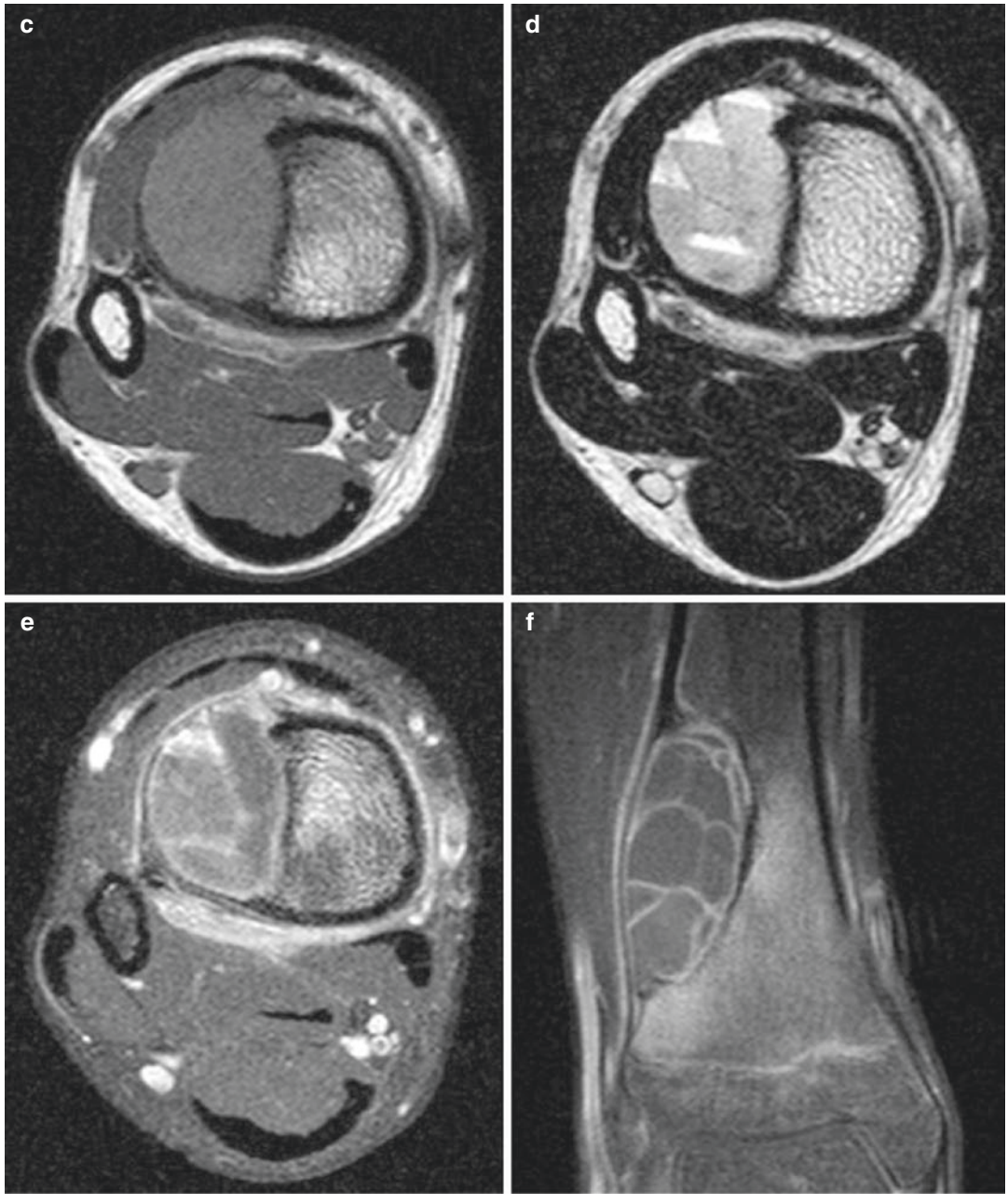

Fig. 8.4 (continued)

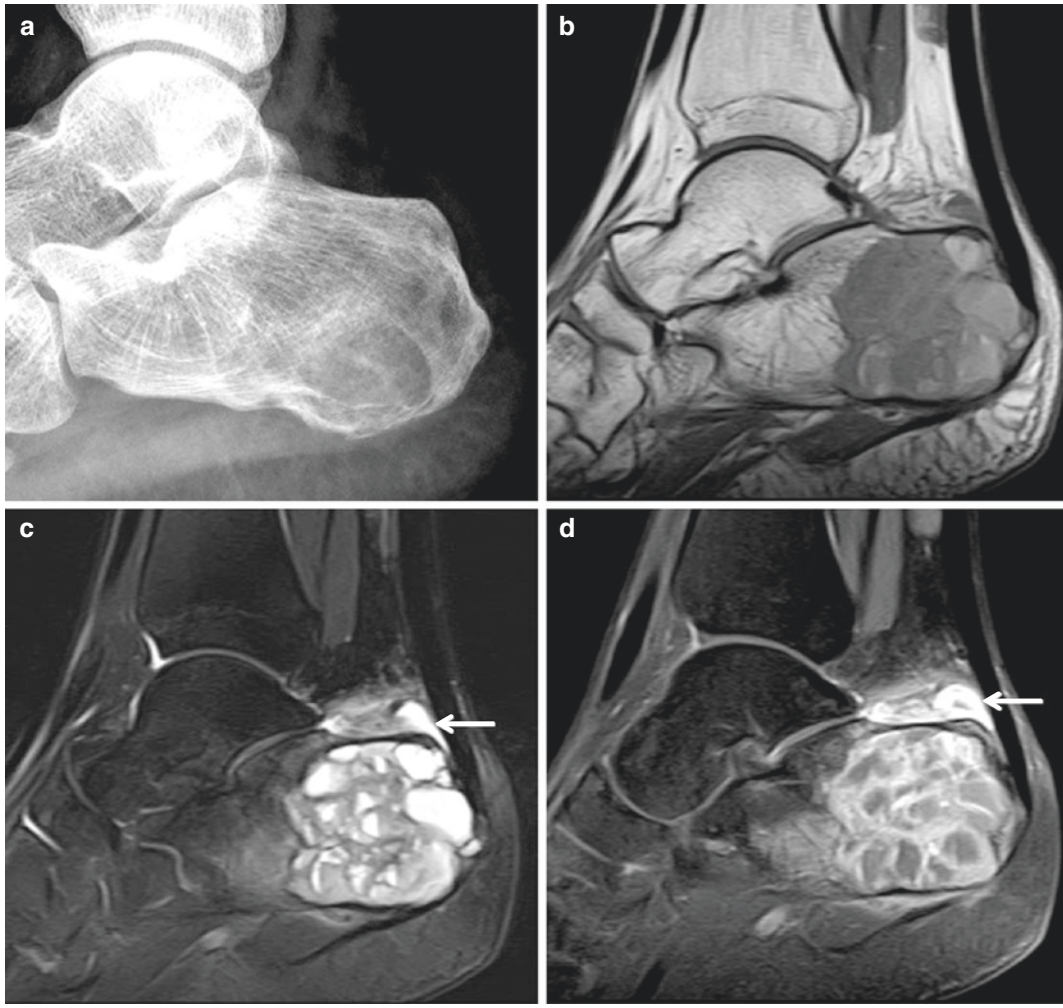

Fig. 8.5 Aneurysmal bone cyst in the calcaneus. (**a**) Lateral radiograph of the foot shows a geographical osteolytic lesion in the calcaneus, with internal trabeculations (*arrowhead*). (**b**) Sagittal T1-weighted image, (**c**) sagittal T2-weighted fat-suppressed image, and (**d**) sagittal contrast-enhanced T1-weighted fat-suppressed images show the multiloculated cystic lesion with multiple fluid–fluid levels in the calcaneus. Soft tissue lesion with hyperintensity on T2-weighted image and contrast enhancement (*white arrow*) noted at the superior aspect of the calcaneus is due to the presence of retrocalcaneal bursitis

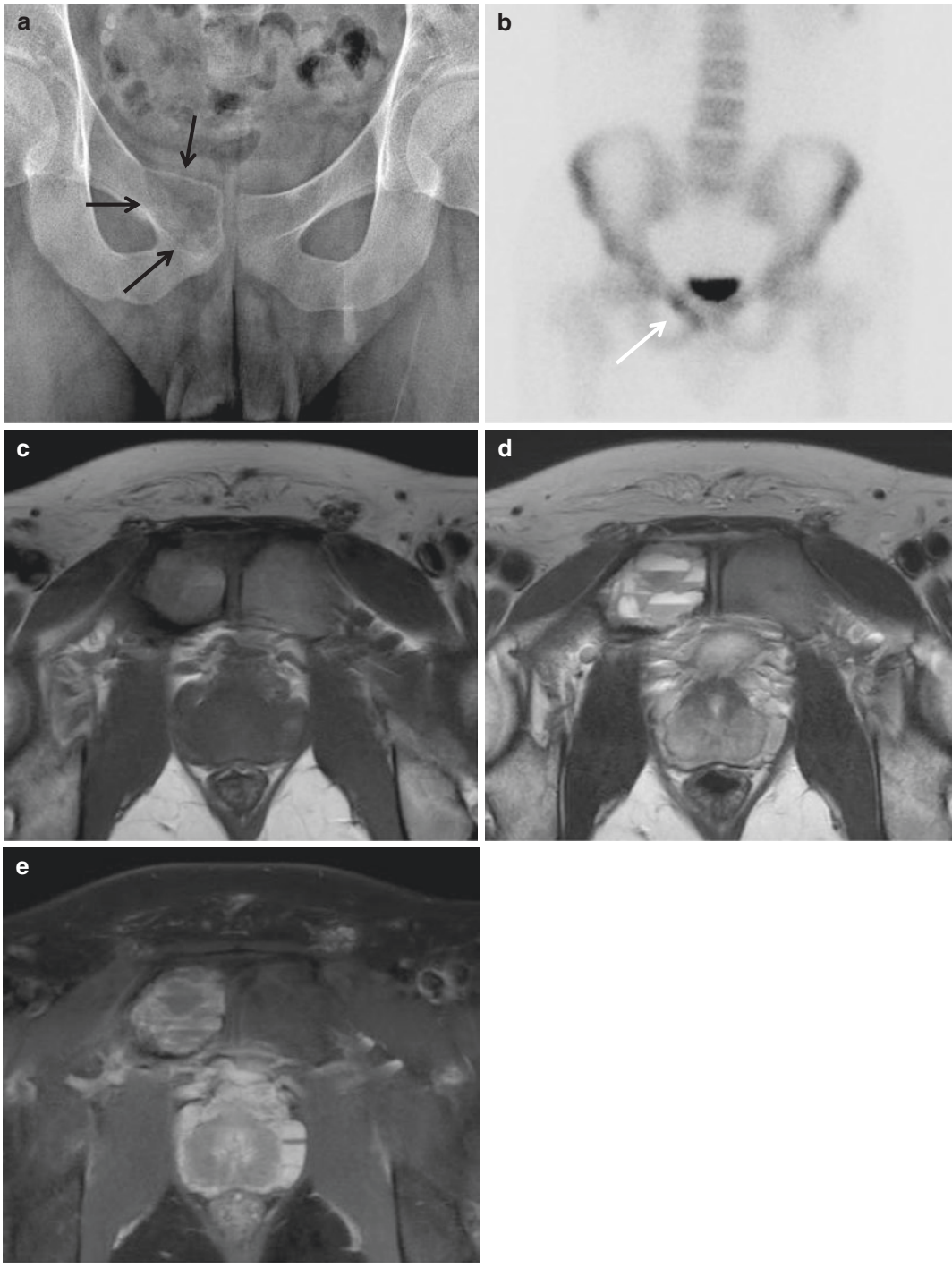

Fig. 8.6 Aneurysmal bone cyst in the right pubic bone. (**a**) Anteroposterior radiograph of the pelvis shows an expansile osteolytic lesion at the right pubic body (*black arrows*). (**b**) Mildly increased uptake is noted on bone scan (*white arrow*). (**c**) Axial T1-weighted image, (**d**) axial T2-weighted fat-suppressed image, and (**e**) axial contrast-enhanced T1-weighted fat-suppressed image reveal the cystic nature of the lesion, with multiple fluid–fluid levels

8.3 Fibrous Dysplasia

Overview

Fibrous dysplasia is a benign fibro-osseous lesion characterized by the presence of abnormal fibrous tissue and islands of immature woven bone. They may appear in either monostotic or polyostotic forms. In polyostotic forms, it can distribute in one extremity, one side of the body, or be diffusely distributed throughout the body.

Epidemiology

Fibrous dysplasia is a common benign lesion that affects both children and adults, and is equally distributed in both genders. Monostotic forms are more common than polyostotic forms.

Common Locations

Fibrous dysplasias are most common in the craniofacial bones and femur. The femur, skull, tibia, and ribs are the most commonly affected sites in the monostotic form. In the polyostotic form, the femur, pelvis, and tibia are frequently affected. Within a long bone, lesions are intramedullary and diaphyseal in location.

Imaging Features

Radiograph

Fibrous dysplasia has a wide spectrum of radiographic findings, ranging from radiolucent to radiopaque lesions. The typical fibrous dysplasia appears as a well-defined intramedullary lesion with ground-glass density (Fig. 8.7). The opacity of the ground-glass density is determined by the amount of bone trabeculae and fibrous component. Fibrous dysplasias commonly show a sclerotic rim (rind sign; characteristic in the proximal femur) (Fig. 8.8). Fibrous dysplasias usually expand the bone; endosteal scalloping and cortical thinning may be present. Periosteal reaction is usually absent, unless the lesion is complicated with a pathological fracture. Fibrous dysplasia causes bowing or deformity of the bone, especially in polyostotic forms (Fig. 8.9). When the proximal femur is affected, a coxa varus angulation may result in a "shepherd crook" deformity (Refer to Tumor syndromes, Fig. 9.7).

Magnetic resonance imaging

The MR imaging is useful in determining the extent of the disease, rather than in differentiating fibrous dysplasia from other entities. The MR imaging findings are nonspecific: intermediate to low signal intensity on T1-weighted imaging, high signal intensity on T2-weighted imaging, and contrast enhancement after intravenous gadolinium administration.

Differential Diagnoses

1. Osteofibrous dysplasia.

   Osteofibrous dysplasias are found at a typical site: the anterior cortex of tibial diaphysis. Osteofibrous dysplasias are intracortical in location, whereas fibrous dysplasias are intramedullary lesions.
2. Liposclerosing myxofibrous tumor of bone.

   Liposclerosing myxofibrous tumors (LSMFTs) occur at characteristic locations: the femoral neck and intertrochanteric region. At these locations, the differential diagnosis of LSMFT and fibrous dysplasia may be difficult. LSMFTs tend to have more osteosclerosis compared to fibrous dysplasia on radiographs.
3. Solitary bone cyst.

   Solitary bone cysts appear as well-defined intramedullary osteolytic lesion with a thin sclerotic rim at the metadiaphysis of a long bone, similar to fibrous dysplasia. The findings on MR imaging readily differentiate the two entities: solitary bone cysts are cystic in nature, whereas fibrous dysplasia is a solid lesion. However, areas of cystic degeneration may be found within fibrous dysplasia, making the diagnosis confusing.

Fig. 8.7 Monostotic fibrous dysplasia in the left femur. (**a**) Anteroposterior radiograph of the left hip shows a ground-glass opacity lesion in the proximal metaphysis of the left femur in a 9-year-old male. A thin sclerotic rim is noted around the lesion (*black arrows*). (**b**) The patient presented with a pathological fracture after a minor trauma event. (**c**) Axial CT image shows the typical ground-glass opacity of the lesion. The lesion shows intermediate to low signal intensity on axial T1-weighted image (**d**), slightly high signal intensity on axial T2-weighted image (**e**), and homogeneous enhancement after intravenous gadolinium administration (**f**, **g**)

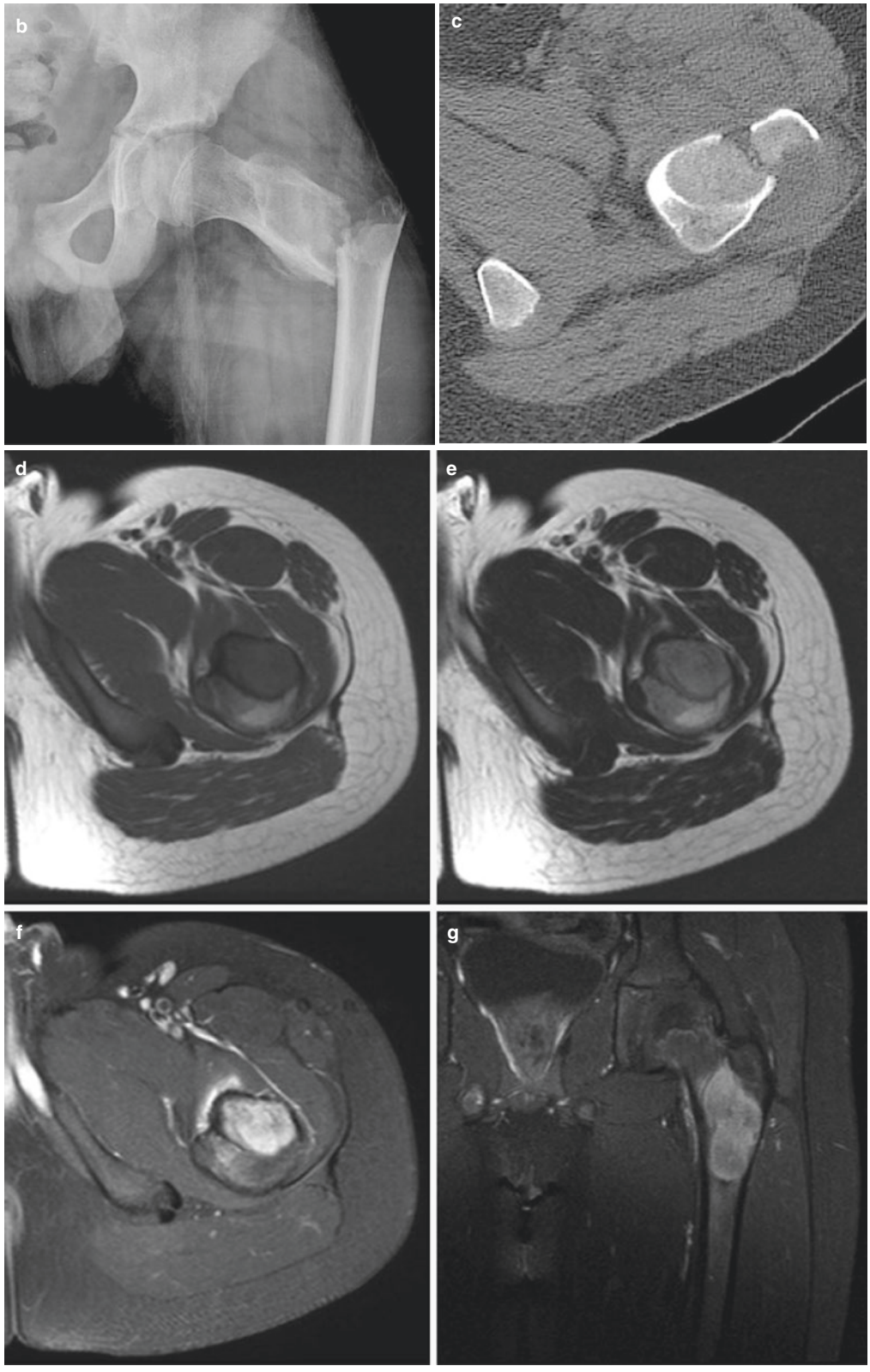

Fig. 8.7 (continued)

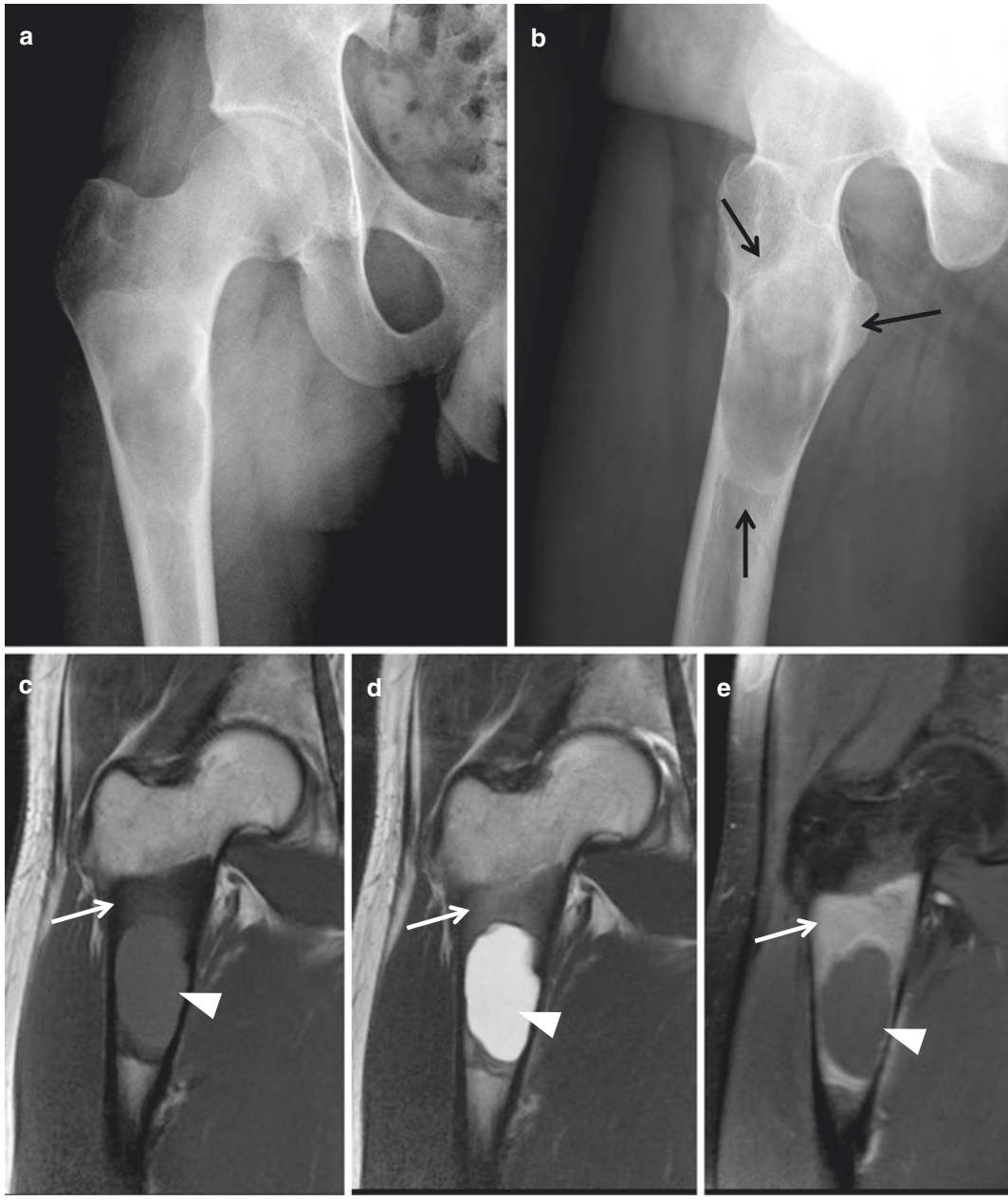

Fig. 8.8 Fibrous dysplasia in the right femur. (**a**) Anteroposterior and (**b**) lateral radiographs of the right hip show a ground-glass opacity lesion in the proximal metaphysis of the right femur. A sclerotic rim is noted around the ground-glass opacity lesion ("rind sign", *black arrows* in **b**). Coronal (**c**) T1-weighted image, (**d**) T2-weighted image, and (**e**) contrast-enhanced T1-weighted fat-suppressed images are shown. The solid portion of the lesion exhibits hypointensity on both T1-weighted and T2-weighted images and homogeneous enhancement (*white arrows*). A well-defined cystic portion is noted within the mass (*white arrowheads*), due to the cystic degeneration of fibrous dysplasia

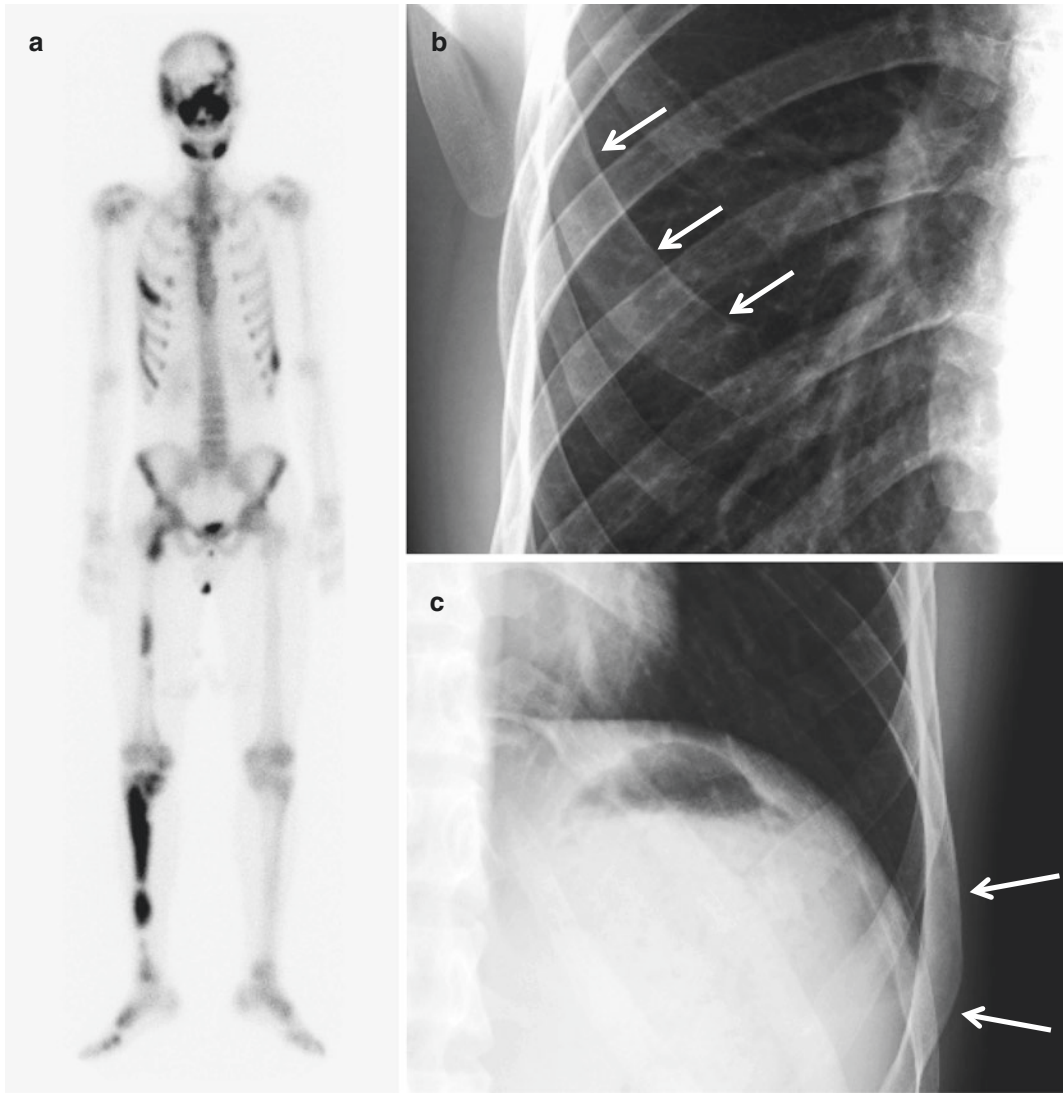

Fig. 8.9 Polyostotic fibrous dysplasia. (**a**) Bone scan shows multifocal increased uptake throughout the body: craniofacial bones, ribs, right femur, right tibia, and right foot. Expansion of the right fourth rib anterolateral arc (**b**) and left ninth lateral arc (**c**) is noted (*white arrows*), corresponding to the increased uptake on bone scan. Anteroposterior radiographs of the femur (**d**), tibia (**e**), and right foot (**f**) show multiple ground-glass opacity lesions (*arrows* in **d**–**f**). The tibial cortex shows undulation with deformity due to the presence of multiple fibrous dysplasias

Fig. 8.9 (continued)

8.4 Osteofibrous Dysplasia

Overview

Osteofibrous dysplasia is a benign fibro-osseous lesion of bone, typically found at the anterior tibial cortex. It is also referred to as ossifying fibroma or Kempson-Campanacci lesion.

Epidemiology

Osteofibrous dysplasias are rare lesions, accounting for <1 % of all bone tumors. It is usually noted in young children, and is rarely seen in patients over the age of 20 years, due to its self-limiting nature. It has been reported to have a male preponderance, but the exact male to female ratio is not known.

Common Locations

The characteristic location of osteofibrous dysplasia is the anterior cortex of the proximal or midshaft of tibia (Fig. 8.10). Another possible site of involvement is the fibular cortex. In 20 % of the patients with a tibial lesion, the ipsilateral fibular cortex is also involved (Fig. 8.11). Other long bones are rarely affected.

Imaging Features

Radiograph

Osteofibrous dysplasias are seen as well-defined intracortical osteolytic lesions along the anterior cortex of the tibia. Multifocal or confluent lesions oriented along the long axis of the tibia shaft are often encountered. Large lesions may appear expansile, with thinning of the cortex, resulting in a saw-toothed or bubbly multiloculated appearance. It may cause anterior bowing of the tibia.

Magnetic resonance imaging

Osteofibrous dysplasia appears of low to intermediate signal intensity on T1-weighted image, intermediate to high signal intensity on T2-weighted image, and typically show contrast enhancement (Fig. 8.12).

Differential Diagnoses

1. Adamantinoma.

   Adamantinoma and osteofibrous dysplasia both have a predilection for the anterior cortex of the tibial shaft. The differentiation between osteofibrous dysplasia and adamantinoma may be difficult due to the similarity of image findings. However, an older age of the patient and more aggressive features of cortical destruction with extension of lesion in the medulla or extraosseous soft tissue may favor the diagnosis of adamantinoma over osteofibrous dysplasia.
2. Fibrous dysplasia.

   Fibrous dysplasia is typically an intramedullary lesion, whereas osteofibrous dysplasias are intracortical lesions.

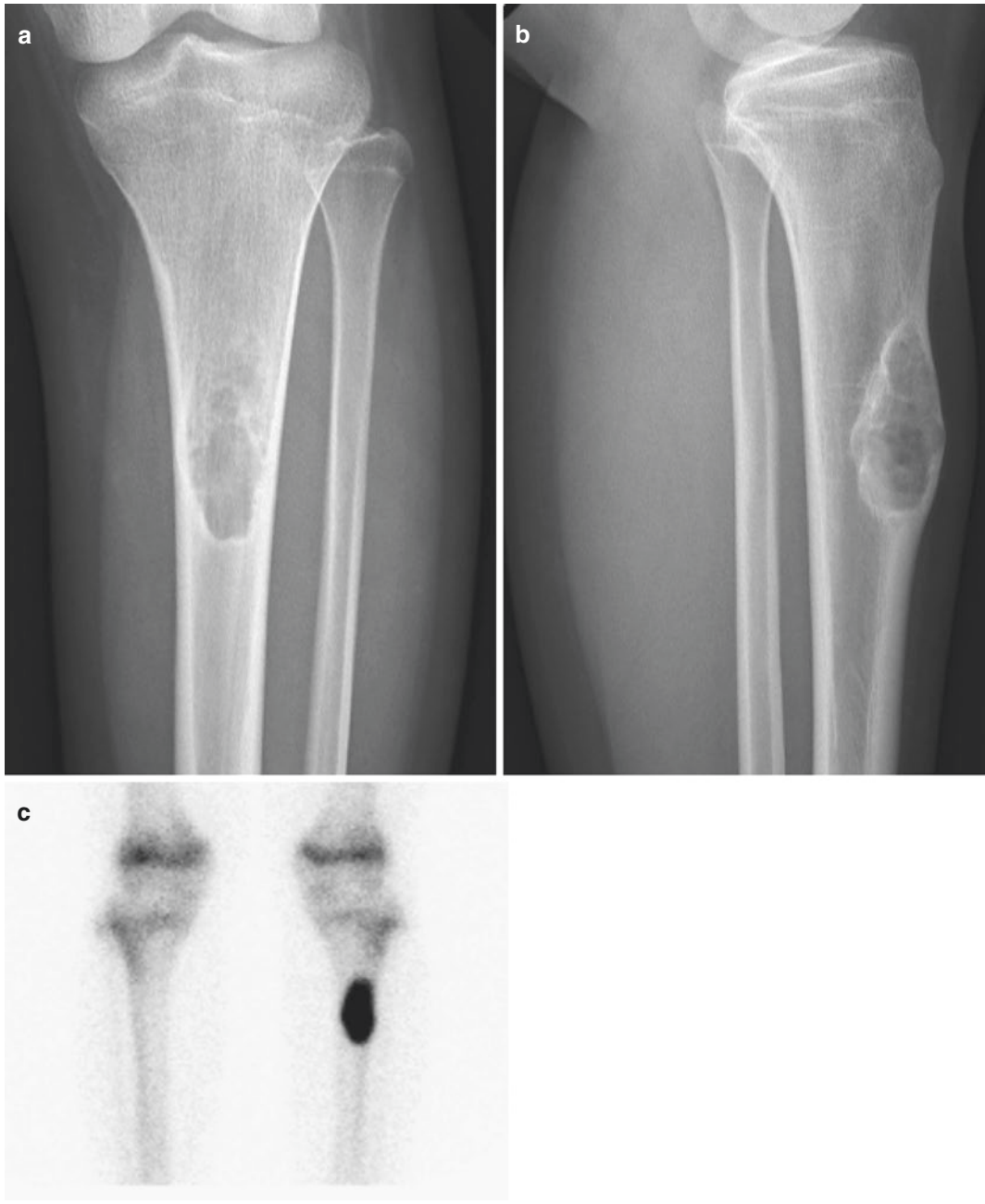

Fig. 8.10 Osteofibrous dysplasia. (**a**) Anteroposterior and (**b**) lateral radiographs of the left lower leg of a 15-year-old female are shown. A well-defined osteolytic lesion is noted at the anterior cortex of the proximal shaft of tibia with a predominantly cortical location. (**c**) Markedly increased uptake is noted on bone scan. (**d**) Axial and (**e**) sagittal T1-weighted images, (**f**) axial T2-weighted fat-suppressed image, and (**g**) axial contrast-enhanced T1-weighted fat-suppressed image are shown. The lesion shows intermediate signal intensity on T1-weighted image, high signal intensity on T2-weighted image, and shows intense contrast enhancement

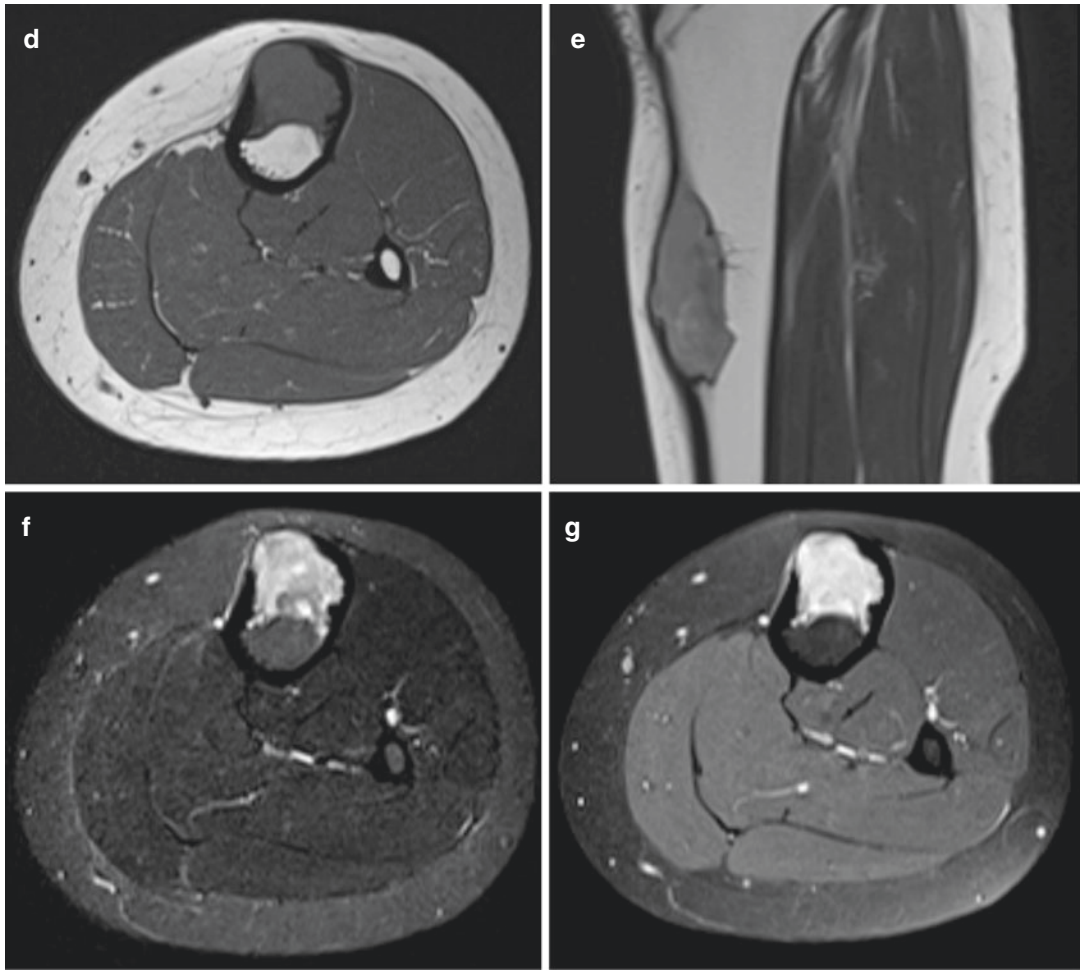

Fig. 8.10 (continued)

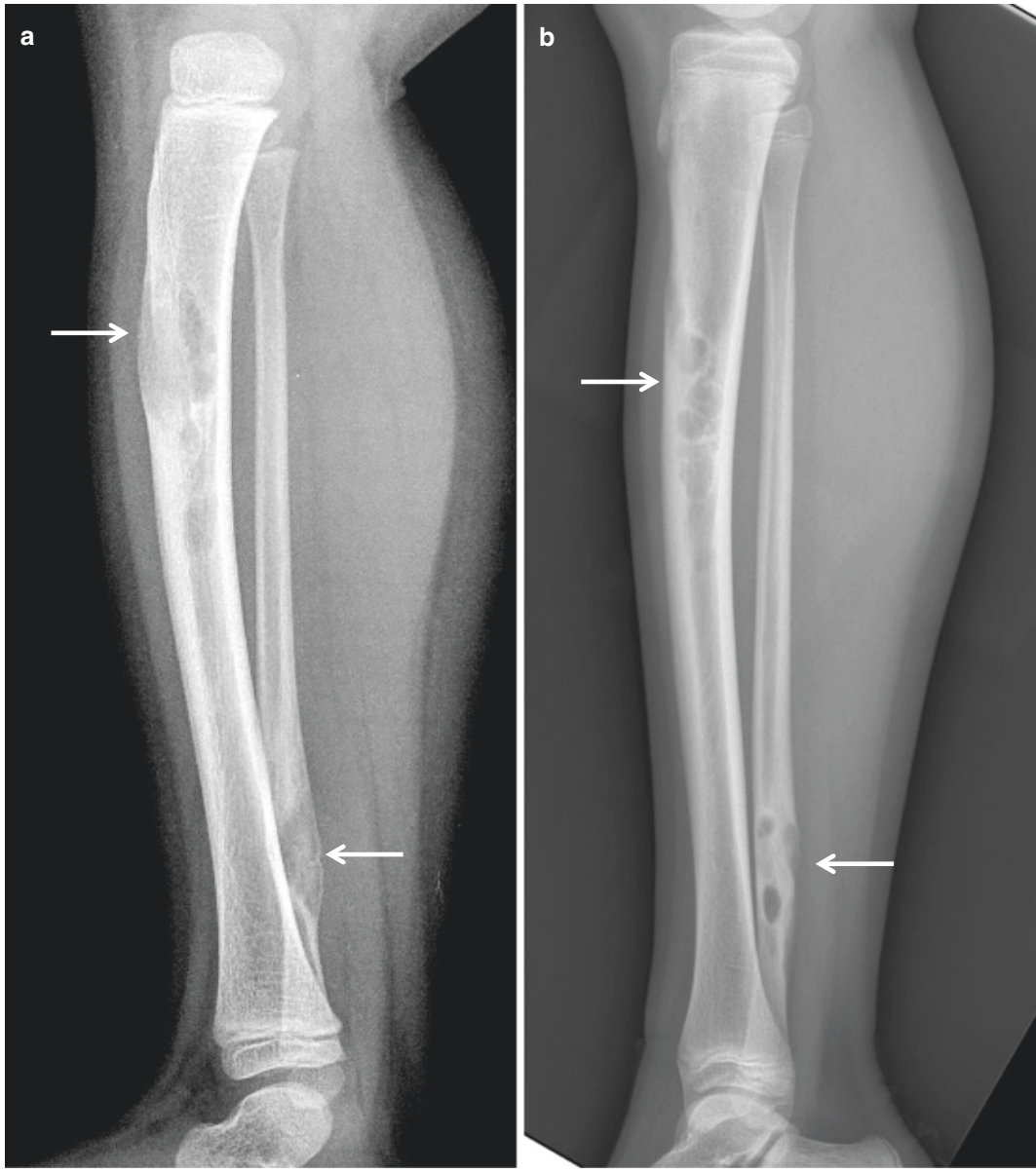

Fig. 8.11 Osteofibrous dysplasia in the tibia with ipsilateral fibular cortex involvement. (**a**) Lateral radiograph of the left lower leg in a 3-year-old female. Well-defined osteolytic lesions are noted not only at the proximal shaft of tibia but also at the distal shaft of fibula (*arrows*). (**b**) Lateral radiograph of the left lower leg taken 8 years later shows interval sclerotic change of the previously noted osteolytic lesions, indicating that spontaneous healing is in progress

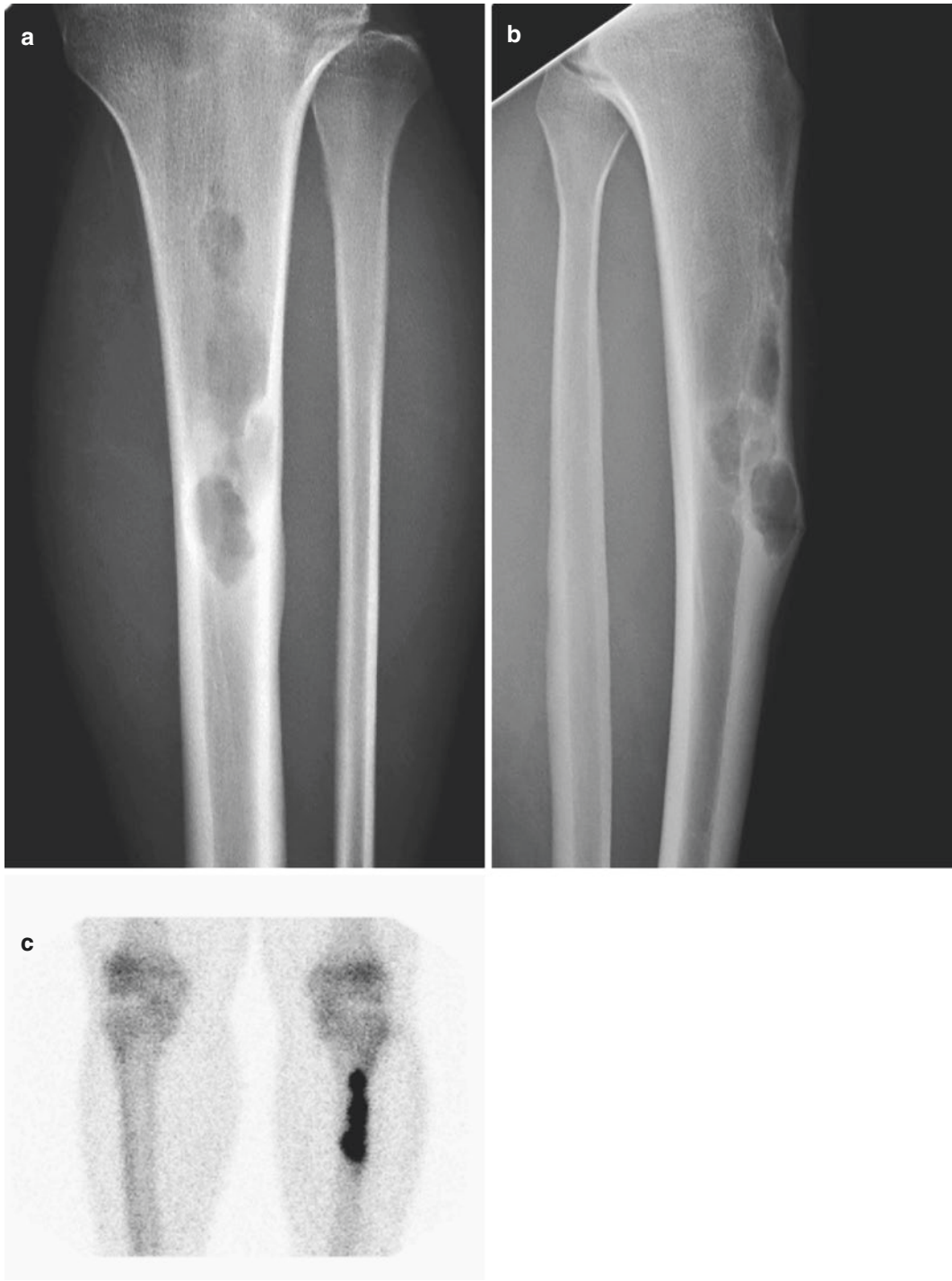

Fig. 8.12 Osteofibrous dysplasia. (**a**) Anteroposterior and (**b**) lateral radiographs show multiple well-defined osteolytic lesions along the anterior cortex of the tibia in a 17-year-old male. (**c**) Markedly increased uptake is noted on bone scan. (**d**) Axial T1-weighted image, (**e**) axial T2-weighted image, and (**g**) axial and (**g**) sagittal contrast-enhanced T1-weighted fat-suppressed images are shown. The lesion shows intermediate signal intensity on T1-weighted image, high signal intensity on T2-weighted image, and shows intense contrast enhancement. The lesion is predominantly intracortical in location, but minimal medullary extension is noted (*arrowheads* in **d**–**g**)

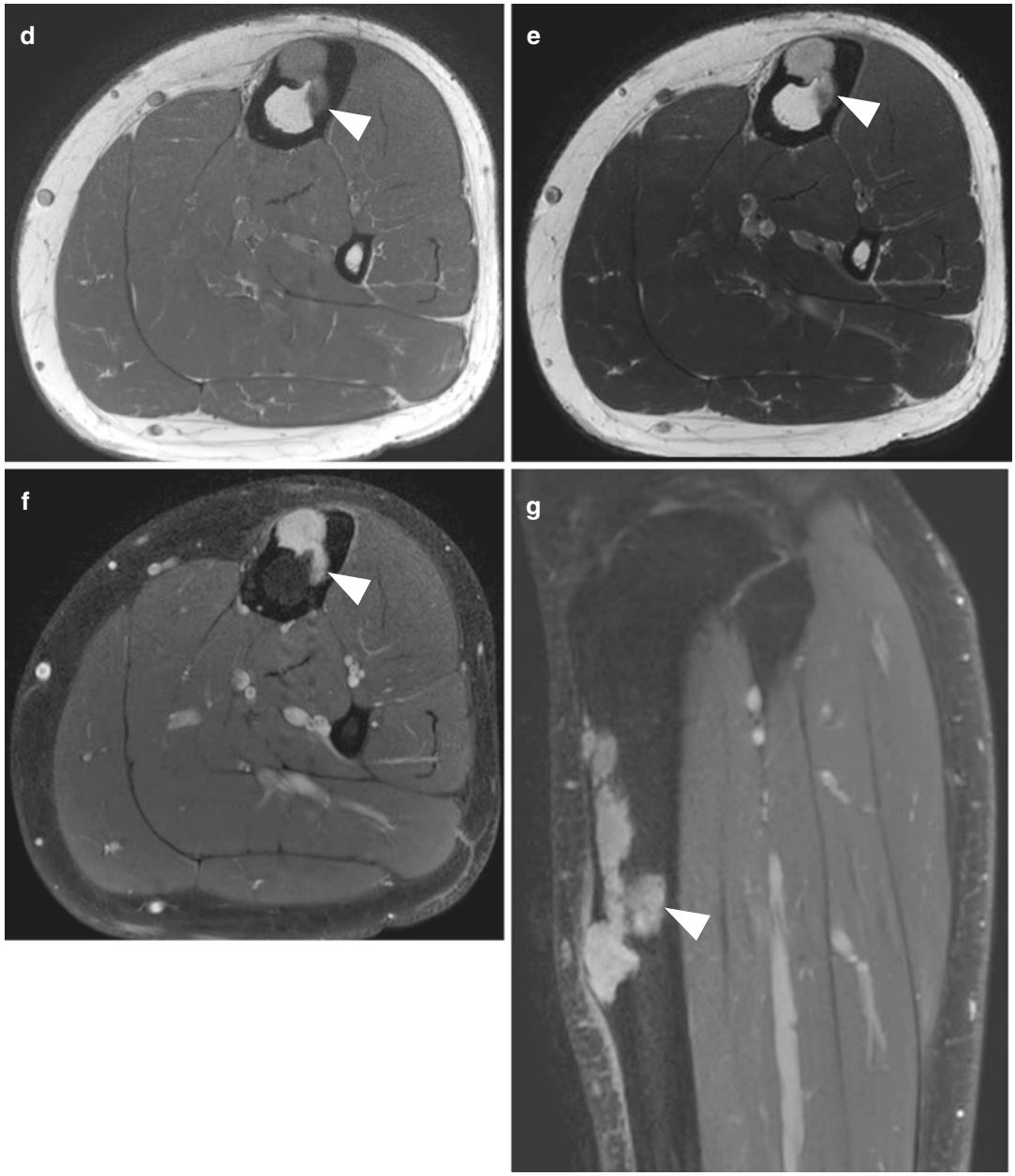

Fig. 8.12 (continued)

8.5 Langerhans Cell Histiocytosis

Overview

Langerhans cell histiocytosis (LCH) is a multisystem disease characterized by the proliferation of pathological Langerhans cells. The skeletal system is a commonly involved organ system in disseminated disease and is frequently the only organ system involved.

Epidemiology

LCH can occur in a wide age range, from the first to eighth decades of life. However, the mean age at presentation is 5–7 years, and most cases are seen in patients below the age of 30 years. LCH has a male preponderance with a male-to-female ratio of 2:1.

Common Locations

LCH can involve any bone throughout the body, but has a predilection for axial skeleton. More than 50 % of the lesions occur in flat bone, including skull, ribs, and pelvis. Among long bones, femur is the most common site of involvement, followed by the humerus and tibia.

Imaging Features

Radiograph

In the calvarium, LCH typically shows a well-defined osteolytic lesion with a "hole-in-hole" appearance; the hole-in-hole appearance is due to the unequal involvement of the inner and outer tables of the cranial vault. This corresponds to the "beveled edge" of the lesion on computed tomography (Fig. 8.13). In long bones, lesions usually appear as well-defined osteolytic lesions at an intramedullary location of the metaphysis or diaphysis. Endosteal scalloping is commonly found, and a solid type of periosteal reaction may accompany the lesion (Fig. 8.14). Some lesions may appear more aggressive, with a permeative type of bone destruction, wide zone of transition, and multilamellated periosteal reaction (Figs. 8.15 and 8.16).

Magnetic resonance imaging

The signal intensity of the lesion on MR imaging is nonspecific: intermediate signal intensity on T1-weighted imaging, high signal intensity on T2-weighted imaging, and significant enhancement of lesion after intravenous administration of gadolinium. Endosteal scalloping may lead to a "budding appearance" on MR imaging (Figs. 8.14 and 8.16). Usually, lesions accompany an extensive area of surrounding bone marrow and soft tissue edema.

Differential Diagnoses

1. Single lesion: Osteomyelitis and small round cell tumors including Ewing's sarcoma.

   LCH lesions exhibiting aggressive features may mimic osteomyelitis and Ewing's sarcoma, and tissue confirmation with biopsy may be necessary for differential diagnosis.
2. Multiple lesions.
   - Metastasis.
   - Multiple myeloma: Multiple osteolytic lesions may be seen in both LCH and multiple myeloma, but the different clinical features make the differentiation between the two diseases possible in most cases. LCH usually affects patients below the age of 30 years, whereas multiple myeloma is rare under the age of 40 years.
   - Brown tumors in hyperparathyroidism: Other radiographic features of hyperparathyroidism (decreased bone mineral density, subperiosteal or subchondral bone resorption, soft tissue calcifications) may aid in the differential diagnosis.

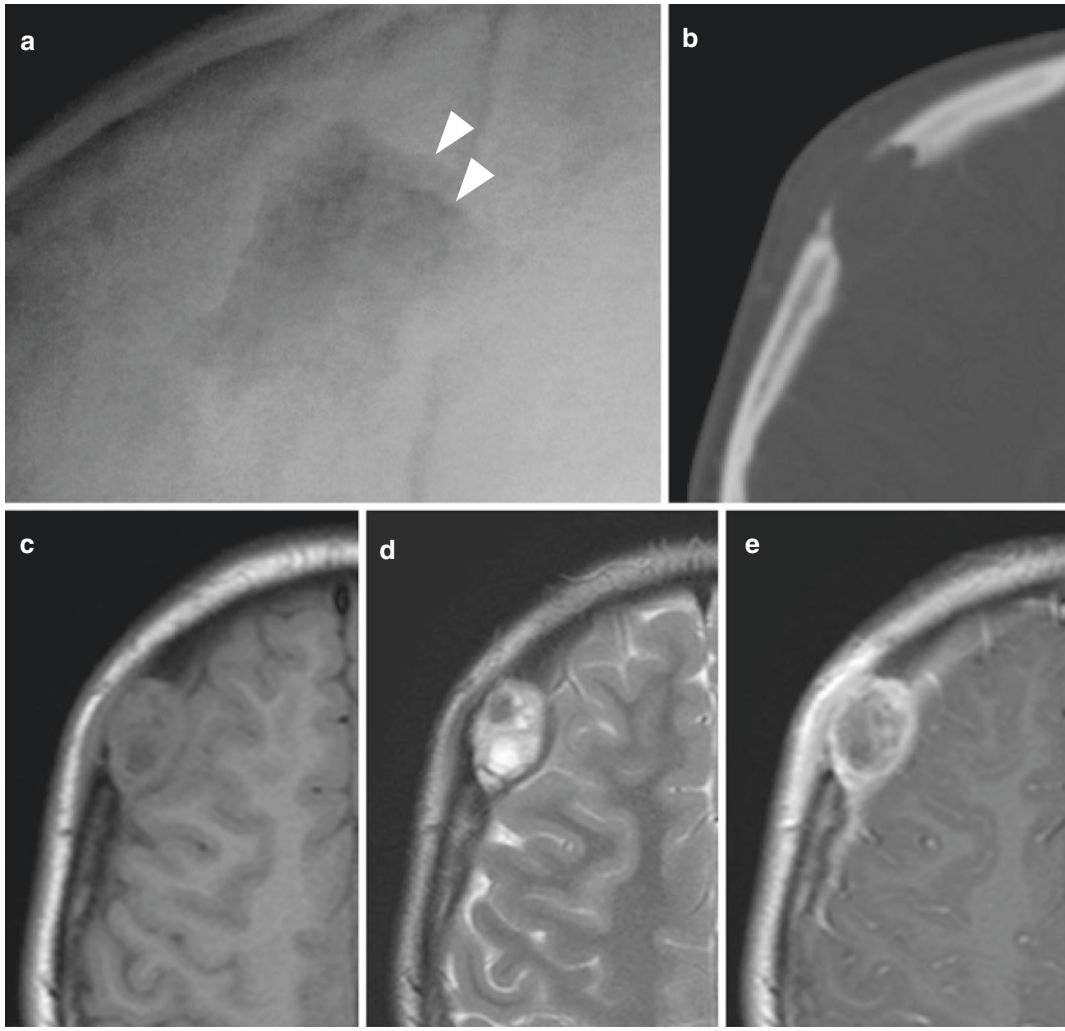

Fig. 8.13 Langerhans cell histiocytosis in the skull. (**a**) Lateral radiograph of the skull shows a well-defined osteolytic lesion with punched-out appearance. The lesion has double contour (*arrowheads*) resulting from the unequal involvement of the inner and outer tables of the cranial vault ("hole-in-hole" appearance). (**b**) The typical "beveled edge" is noted on computed tomography. (**c**) Axial T1-weighted, (**d**) axial T2-weighted, and (**e**) axial contrast-enhanced T1-weighted fat-suppressed images show a soft tissue mass lesion at this site. The lesion shows intermediate signal intensity on T1-weighted image, high signal intensity on T2-weighted image, and significant enhancement of lesion after intravenous administration of gadolinium

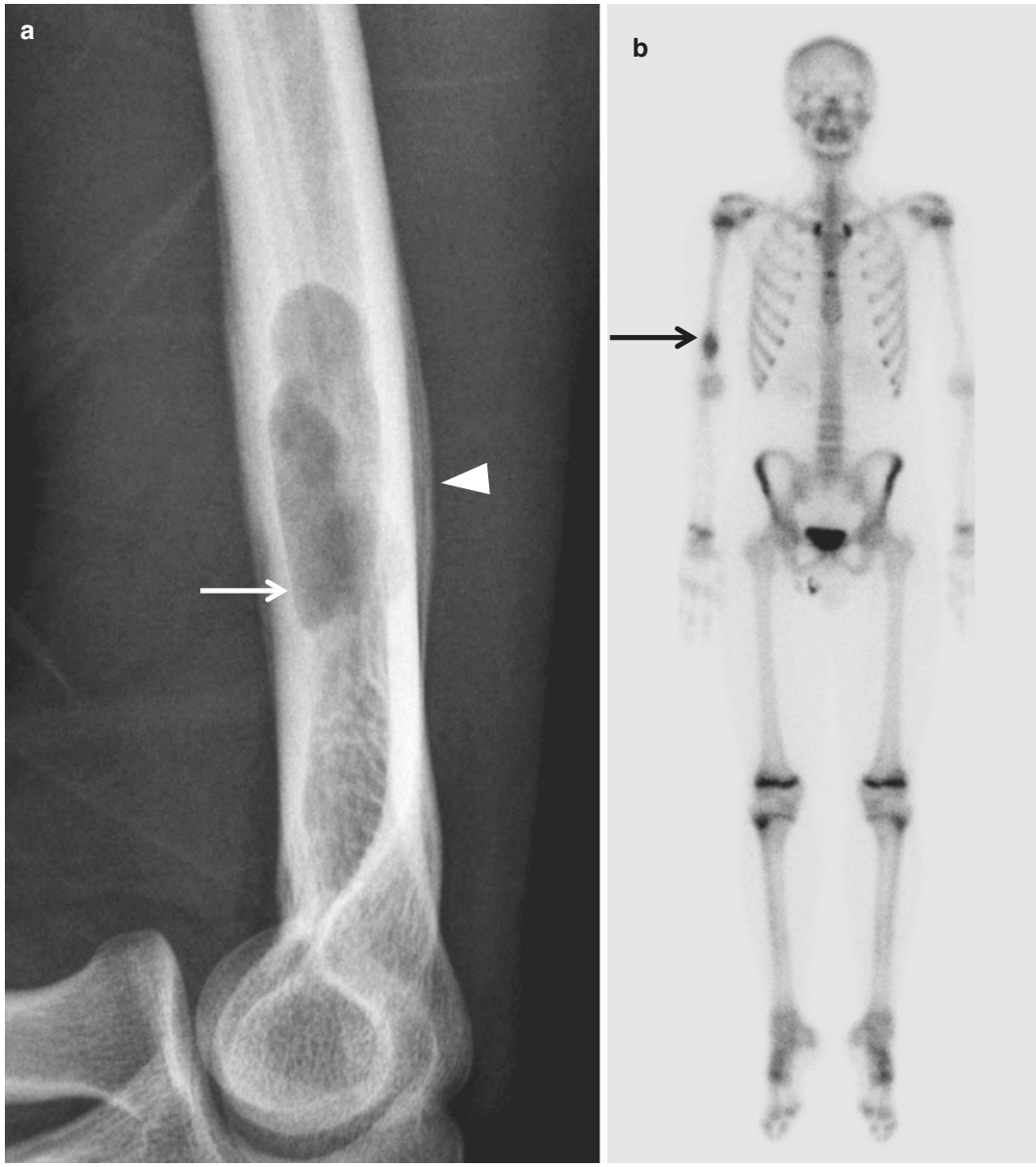

Fig. 8.14 Langerhans cell histiocytosis in the right humerus. (**a**) Lateral radiograph of the upper arm in a 15-year-old male shows a geographical osteolytic lesion with clearly defined margin in the distal diaphysis of the right humerus. The lesion shows endosteal scalloping (*white arrow*), and a solid or unilamellar pattern of periosteal reaction (white arrowhead) is noted. (**b**) On bone scan, the lesion shows increased uptake (*black arrow*). Coronal (**c**) T1-weighted image, (**d**) T2-weighted image, and (**e**) contrast-enhanced T1-weighted fat-suppressed images are shown. The lesion shows intermediate signal intensity on T1-weighted image, high signal intensity on T2-weighted image, and shows significant enhancement. An extensive area of surrounding bone marrow edema (*arrows* in **c**, **e**) and soft tissue edema (*arrowheads* in **d**, **e**) is noted. (**f**) Axial contrast-enhanced T1-weighted fat-suppressed images show the typical "budding appearance" of the lesion (*white arrow*) due to the erosion of the endosteal surface in a nodular configuration

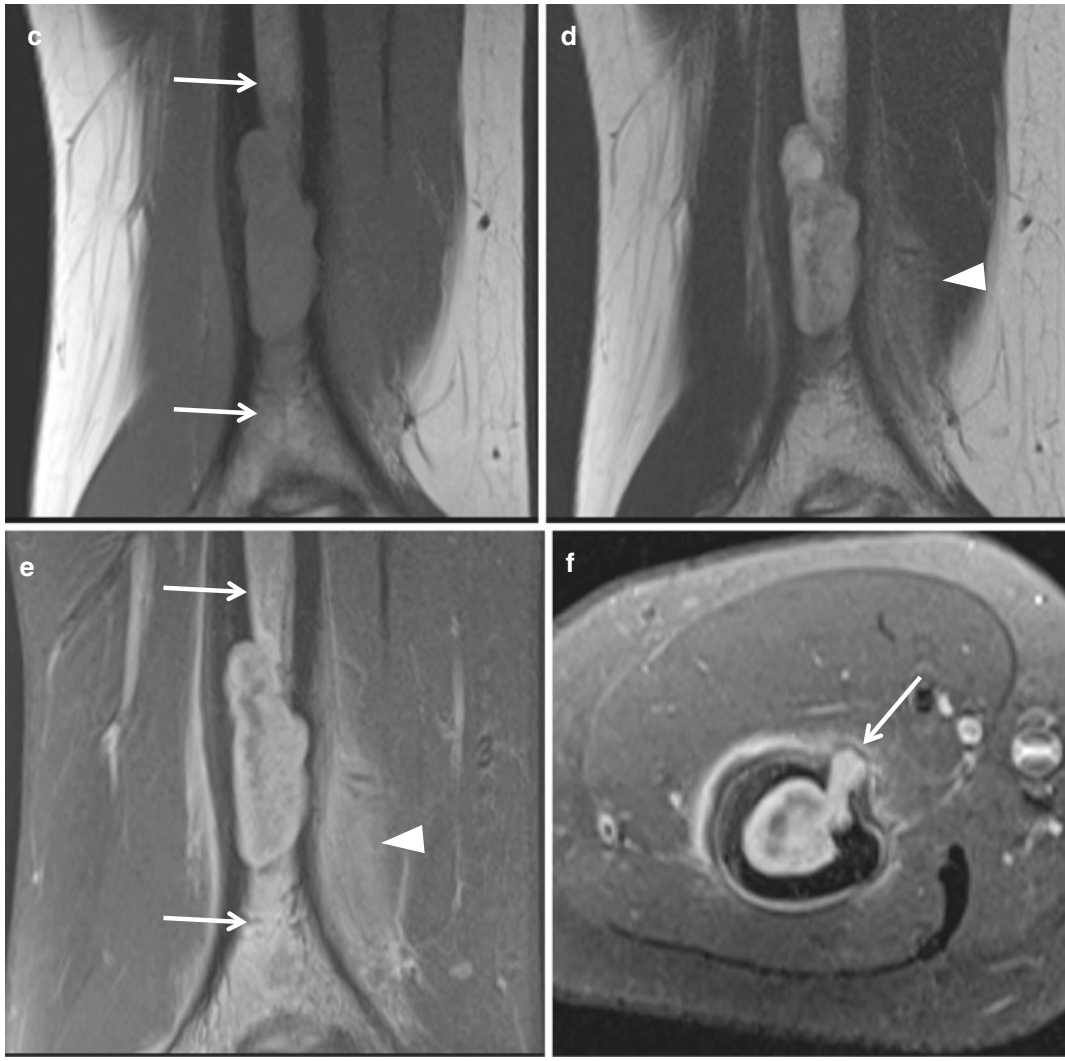

Fig. 8.14 (continued)

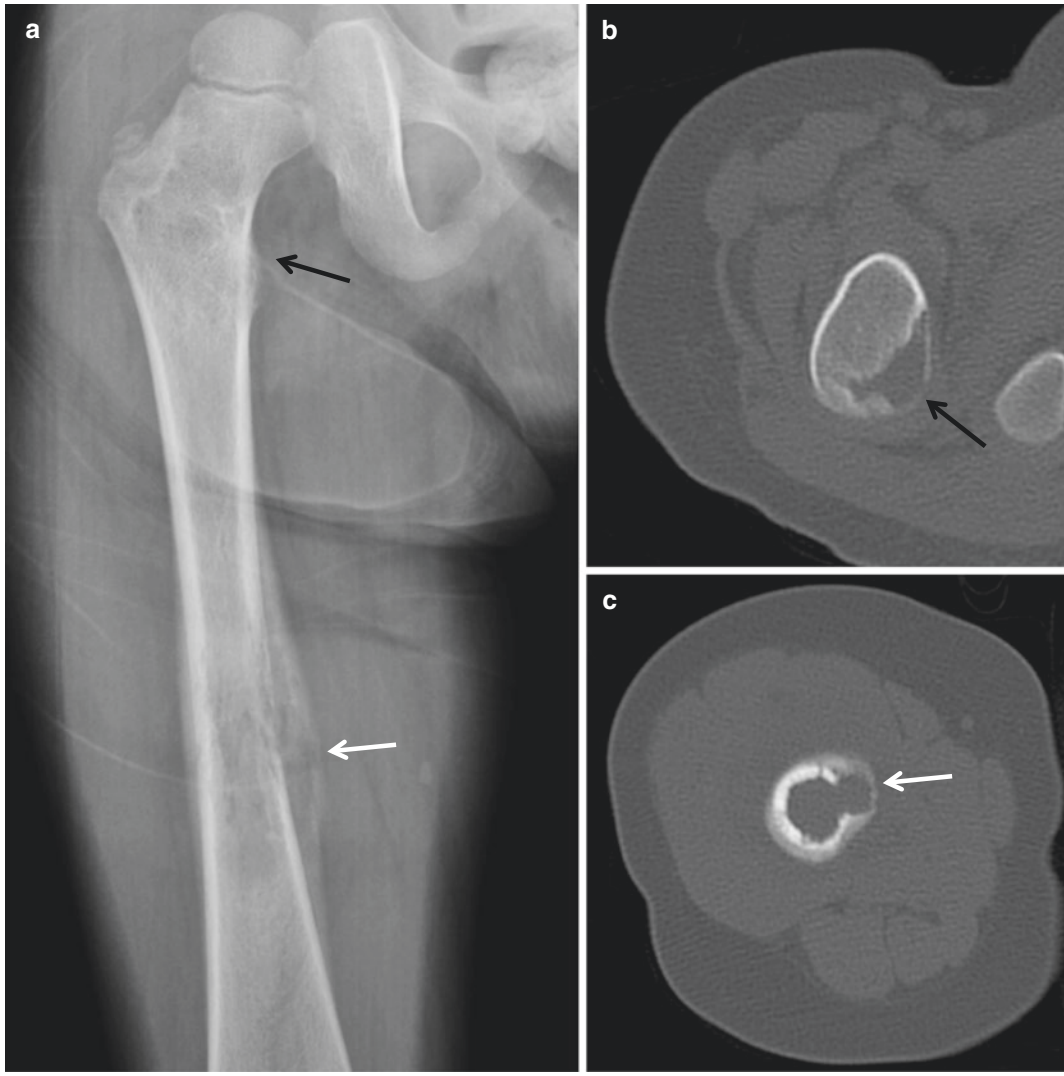

Fig. 8.15 Langerhans cell histiocytosis in the right femur. (**a**) Anteroposterior radiograph of the right femur exhibits an ill-defined osteolytic lesion with aggressive pattern of destruction and periosteal reaction in the diaphysis of the right femur (*white arrow*) in a 3-year-old female. Another ill-defined osteolytic lesion is suspected at the intertrochanteric region of the femur (*black arrow*). Axial CT images of the right femur at the intertrochanteric level (**b**) and mid-diaphysis level (**c**) reveal the osteolytic lesions The lesion has extended to and eroded the newly deposited bone (*white arrow* in **c**). The diaphyseal lesion shows intermediate signal intensity on axial T1-weighted image (**c**), heterogeneously hyperintense on axial T2-weighted image (**d**), and shows homogeneous enhancement on axial contrast-enhanced T1-weighted fat-suppressed image (**e**). An extensive area of soft tissue around the lesion shows T2-hyperintensity and contrast enhancement. (**f**) The proximal femoral lesion shows homogeneous intense enhancement on axial contrast-enhanced T1-weighted fat-suppressed image

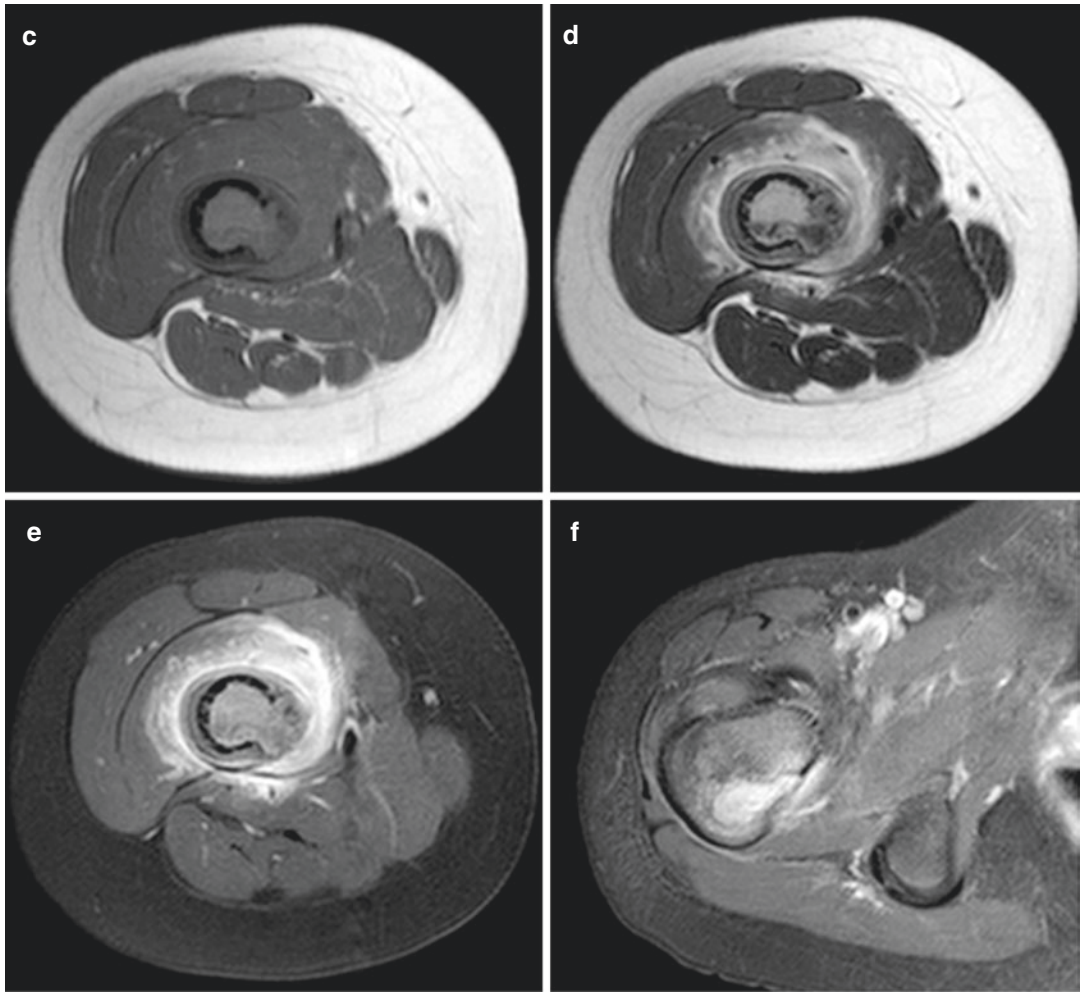

Fig. 8.15 (continued)

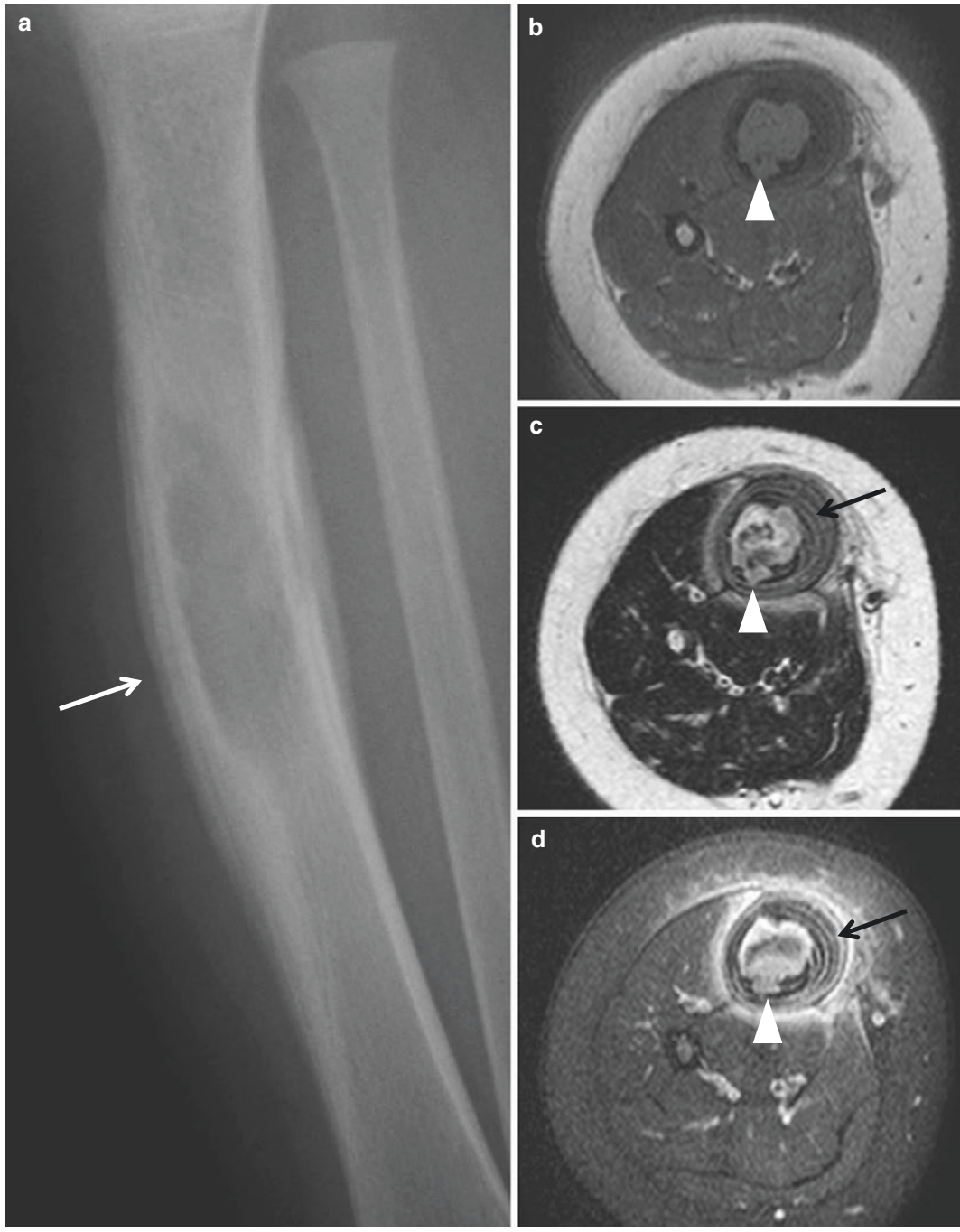

Fig. 8.16 Langerhans cell histiocytosis in the right tibia. (**a**) Lateral radiograph of the lower leg in a 13-month-old male shows a geographical osteolytic lesion accompanied by a multilamellated periosteal reaction. The budding appearance (*white arrowheads* in **b**–**d**) and multilamellated periosteal reaction (*black arrows*) are well demonstrated on magnetic resonance imaging; (**a**) axial T1-weighted image, (**b**) axial T2-weighted image, and (**c**) axial contrast-enhanced T1-weighted fat-suppressed image

8.6 Intraosseous Lipoma

Overview

Intraosseous lipoma is a benign lipomatous neoplasm that arises from the bone, either in the medullary cavity, cortex, or on the surface of the bone (parosteal lipoma).

Epidemiology

Intraosseous lipomas are rare, accounting for <0.1 % of all primary bone tumors. It has been reported to present at a wide age range, but most patients are 40–50 years of age at presentation. A slight male predominance has been reported (male: female = 4:3).

Common Locations

The most commonly affected sites are the metaphysis of long bone (femur, tibia, and fibula) and calcaneus. Less frequently affected sites include pelvic bones, vertebrae, and sacrum. Parosteal lipomas develop along the diaphysis of long tubular bones (femur, tibia, humerus, and radius).

Imaging Features

Radiograph

Typical lesions appear as well-defined osteolytic intramedullary lesions with a thin sclerotic rim, at the metaphysis of a long bone or within the calcaneus (Fig. 8.17). Commonly, a focus of ossification or calcification is seen within the mass (Fig. 8.18). Parosteal lipomas may appear as radiolucent mass at the juxtacortical location, with or without calcification.

Magnetic resonance imaging

The signal intensity of intraosseous lipoma follows that of fat: hyperintense on both T1-weighted and T2-weighted images, with absent contrast enhancement.

Differential Diagnoses

1. Long bone: simple bone cyst, bone infarct.
2. Calcaneus: simple bone cyst, pseudocyst of calcaneus.

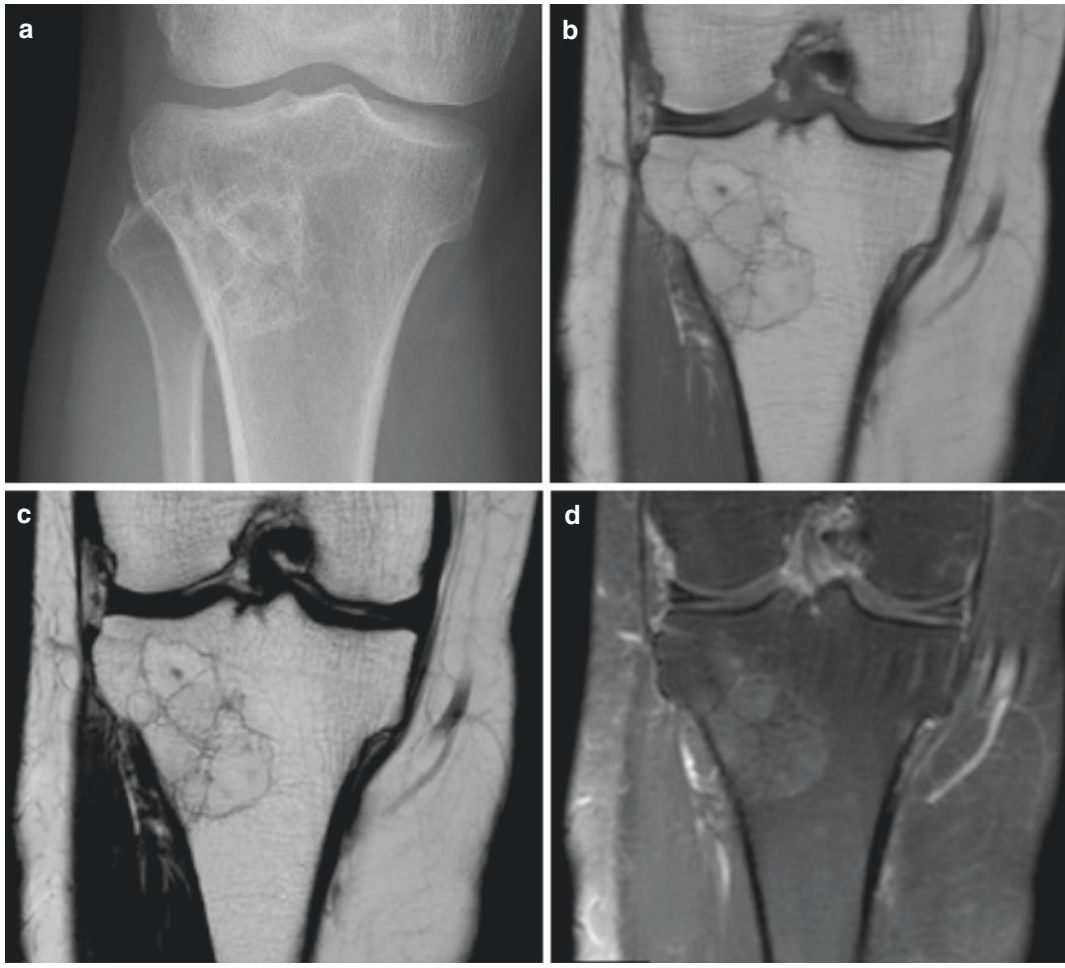

Fig. 8.17 Intraosseous lipoma in the tibia. (**a**) Anteroposterior radiograph of the right knee shows a multilobulated osteolytic lesion with a thin rim of sclerosis along the periphery and septa of the lesion. The lesion has signal intensity identical to the adjacent fatty marrow on coronal T1-weighted image (**b**) and T2-weighted image. The lesion is slightly hyperintense compared to adjacent marrow on coronal contrast-enhanced T1-weighted fat-suppressed image (**c**)

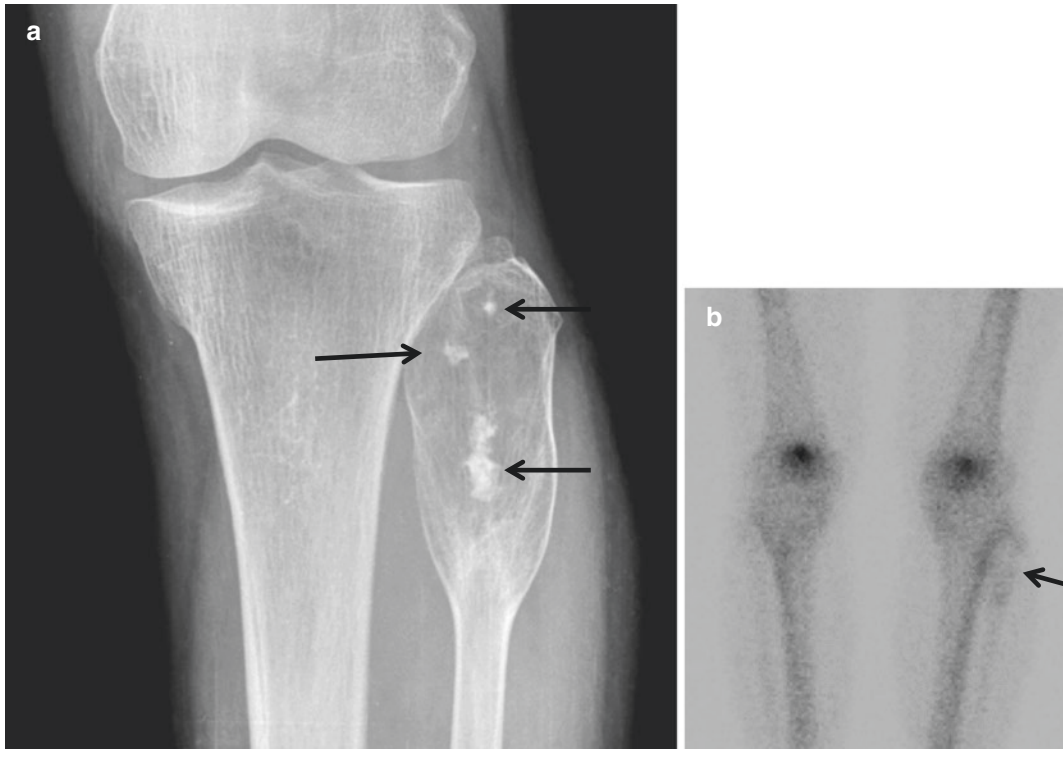

Fig. 8.18 Intraosseous lipoma in the fibula. (**a**) An expansile osteolytic lesion is noted at the proximal fibula on anteroposterior radiograph of the left knee. Calcification is noted within the mass (*arrows*). (**b**) On bone scan, an area of photon deficit is noted with mild increased uptake along the periphery of the deficit (*arrow*). The lesion has fat-equivalent signal intensity on axial (**c**) T1-weighted image, (**d**) T2-weighted image, and (**e**) axial contrast-enhanced T1-weighted fat-suppressed image. (**f**) Dark signal intensity foci are noted within the lesion corresponding to the mineralization noted on radiograph (*arrows*)

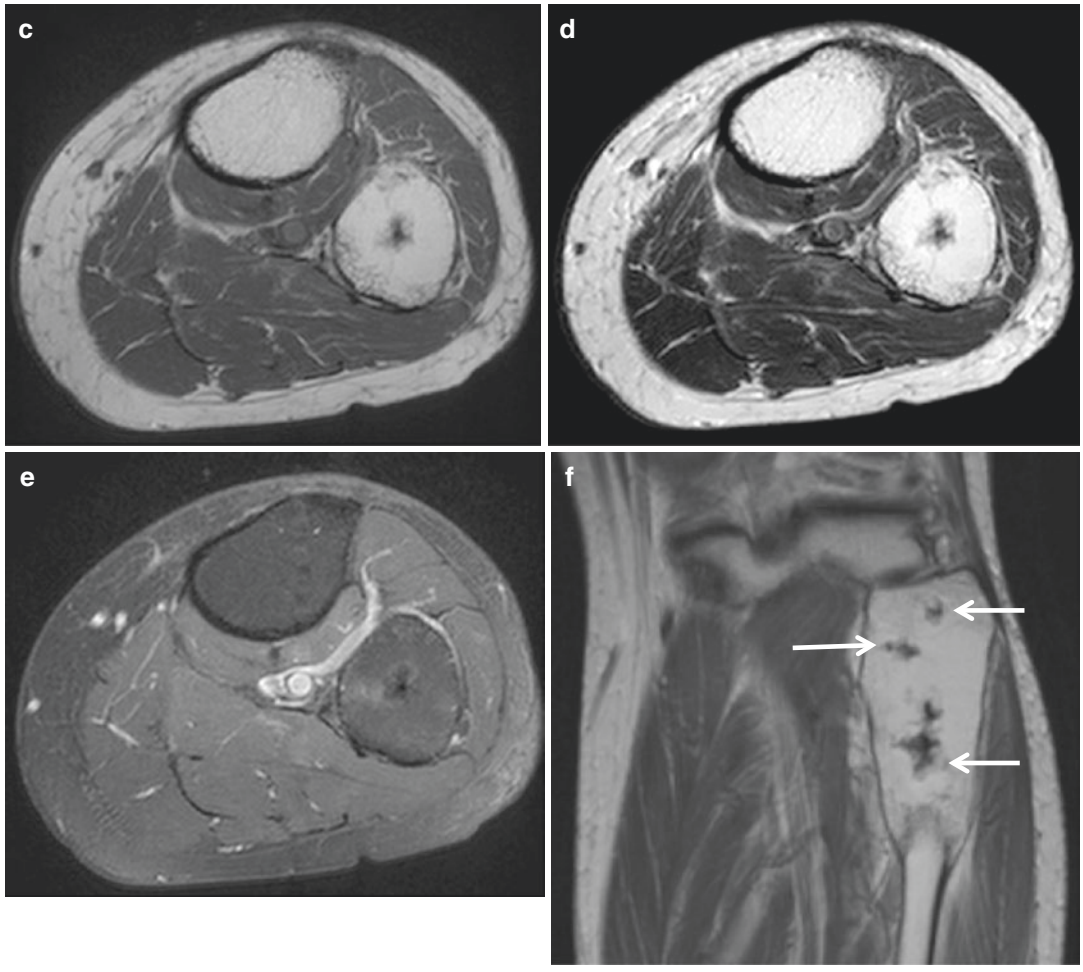

Fig. 8.18 (continued)

8.7 Liposclerosing Myxofibrous Tumor

Overview

Liposclerosing myxofibrous tumor (LSMFT) is a benign fibro-osseous lesion of the bone, which is also known as "polymorphic fibrocystic disease of bone" or "polymorphic fibro-osseous lesion of bone." It is histologically characterized by the wide mixture of various tissues, including lipomatous, fibroxanthomatous, myxomatous, and myxofibromatous components.

Epidemiology

LSMFT is a recently recognized, rare benign lesion of the bone. It has a reported age range of 15–80 years, with the majority presenting in the fourth decade of life. It does not have a gender predilection.

Common Locations

Typical lesions are located in the intertrochanteric region of the femur (80–90 %). Other sites of involvement include the tibia, humerus, ilium, and rib.

Imaging Features

Radiograph

LSMFT is noted as a well-defined, geographical osteolytic lesion with a sclerotic margin, at the intertrochanteric region of the femur (Fig. 8.19). The sclerotic margin of the tumor is often thick and coarse (Fig. 8.20). The contour of the bone is either normal or show mild expansile remodeling. Matrix calcification is found in up to 70 % of the cases.

Magnetic resonance imaging

Despite the name "LSMFT," evidence of macroscopic fat is usually not observed on MR imaging. The myxoid component within the tumor results in a signal intensity similar to skeletal muscles on T1-weighted image and high signal intensity on T2-weighted MR imaging (Fig. 8.21).

Differential Diagnoses

1. Intraosseous lipoma.

   Intraosseous lipomas exhibit high signal intensity on both T1-weighted and T2-weighted images due to the presence of macroscopic fat, whereas LSMFT usually does not show macroscopic fat on imaging.
2. Fibrous dysplasia.

   Fibrous dysplasia typically shows ground-glass opacity and a thin sclerotic margin, whereas LSMFT commonly has a thick and coarse sclerotic margin.

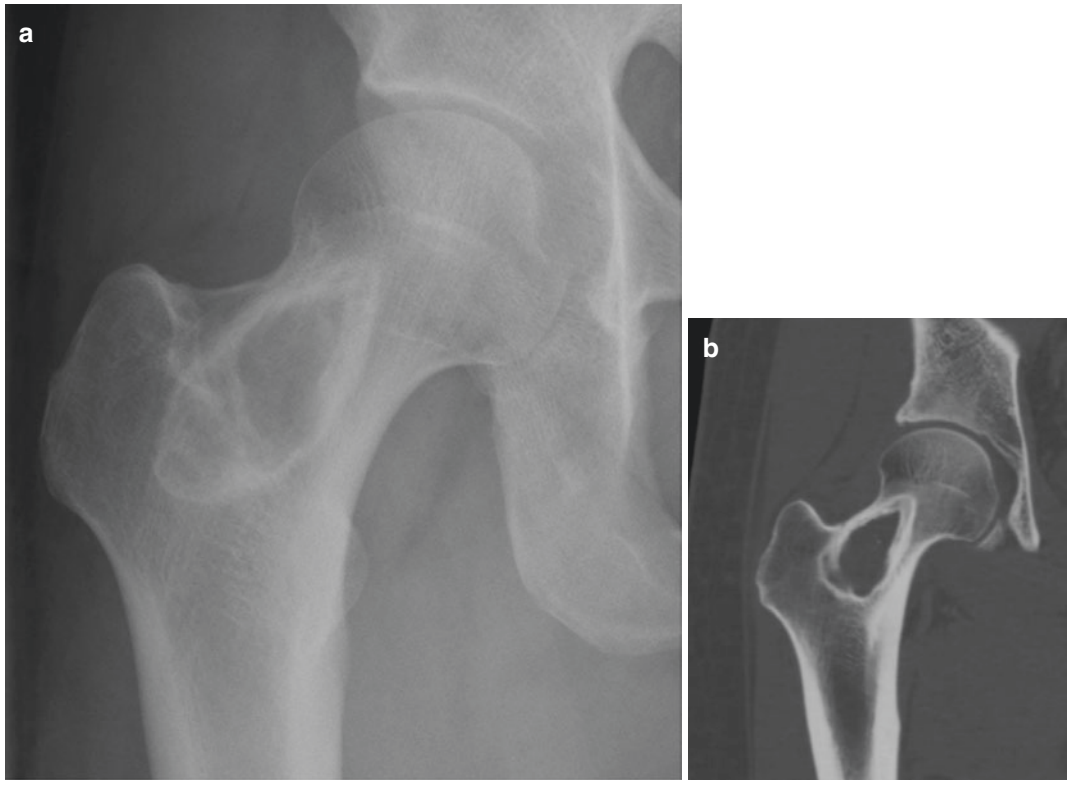

Fig. 8.19 Liposclerosing myxofibrous tumor in the proximal femur. (**a**) Anteroposterior radiograph of the right femur shows a geographical osteolytic lesion with a thick sclerotic rim involving the right femoral neck and intertrochanteric region. (**b**) Identical findings are noted on coronal reformatted CT image. (**c**) Coronal T1-weighted image, (**d**) axial T2-weighted image, (**e**) coronal and (**f**) axial contrast-enhanced T1-weighted fat-suppressed images are shown. The signal intensity of the lesion is similar to skeletal muscles on T1-weighted image and hyperintense on T2-weighted image, and gradually enhances on contrast-enhanced image due to the myxoid stroma within the lesion

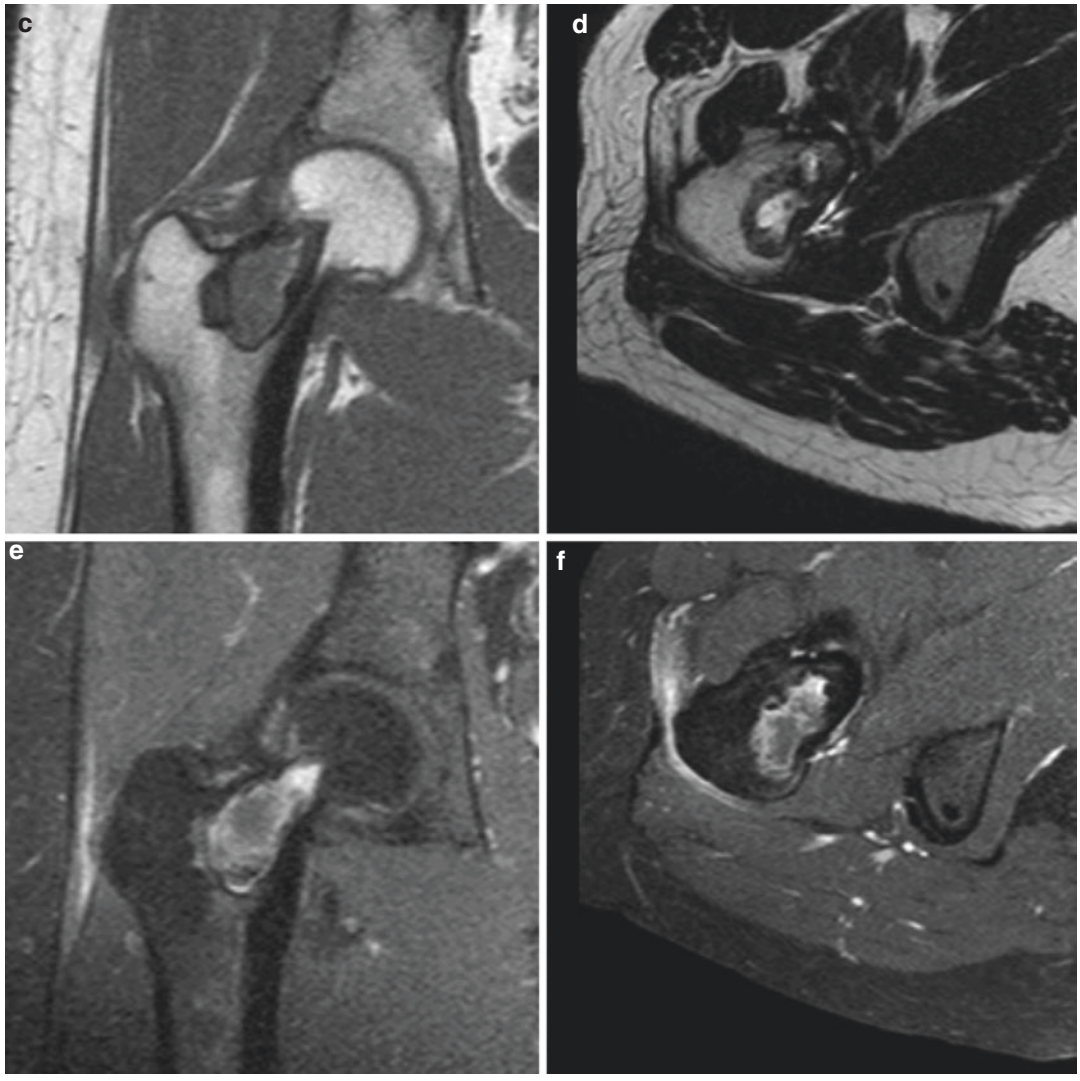

Fig. 8.19 (continued)

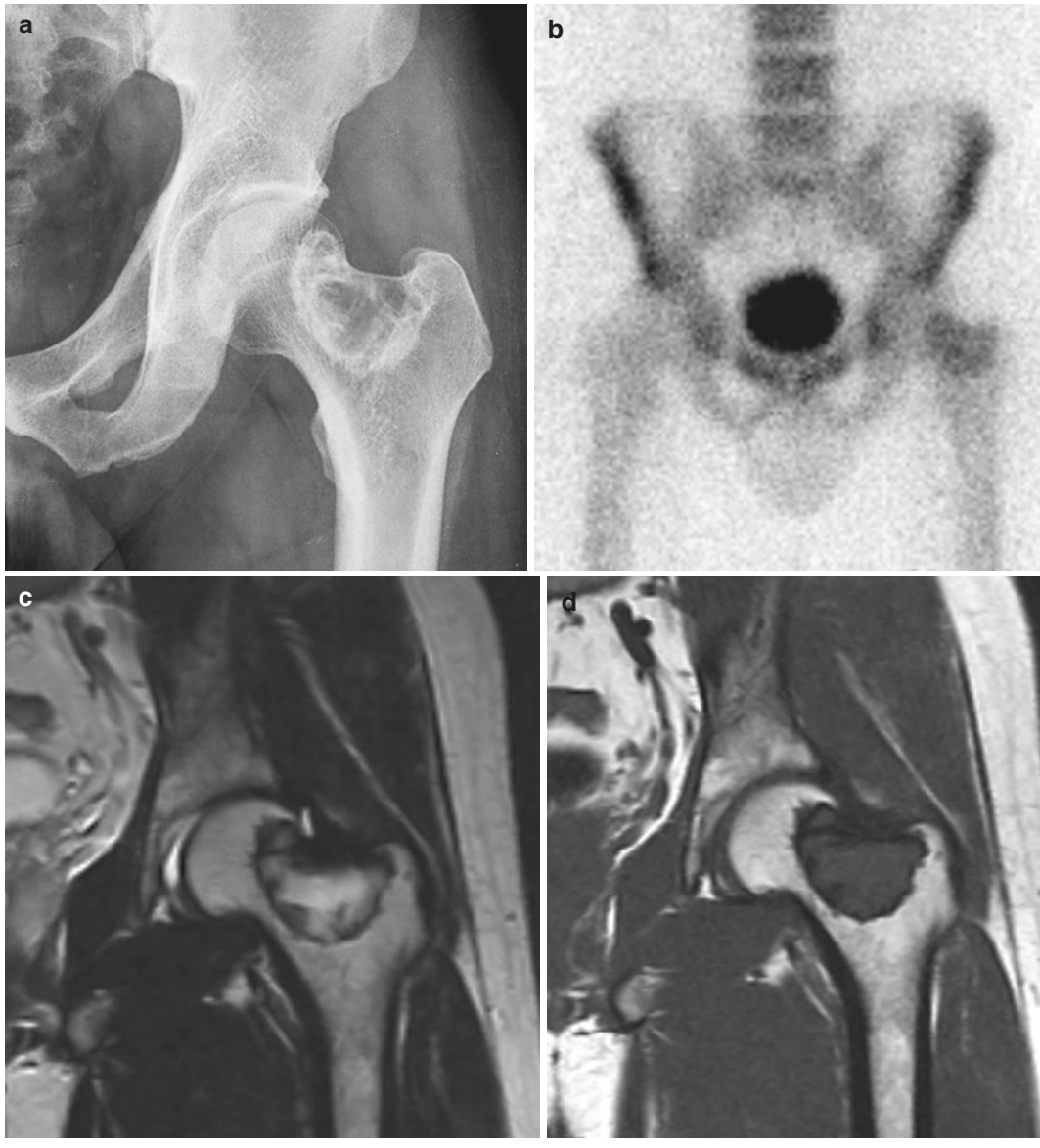

Fig. 8.20 Liposclerosing myxofibrous tumor in the proximal femur. (**a**) Anteroposterior radiograph of the left femur shows a well-defined, geographical osteolytic lesion with a thick sclerotic margin, at the femoral neck. (**b**) Bone scan exhibits increased uptake in the lesion. The lesion is hyperintense on (**c**) coronal T2-weighted image and isointense on (**d**) coronal T1-weighted image, compared to skeletal muscle. A rim of dark signal intensity is noted on both T1-weighted and T2-weighted images corresponding to the sclerotic rim noted on radiograph

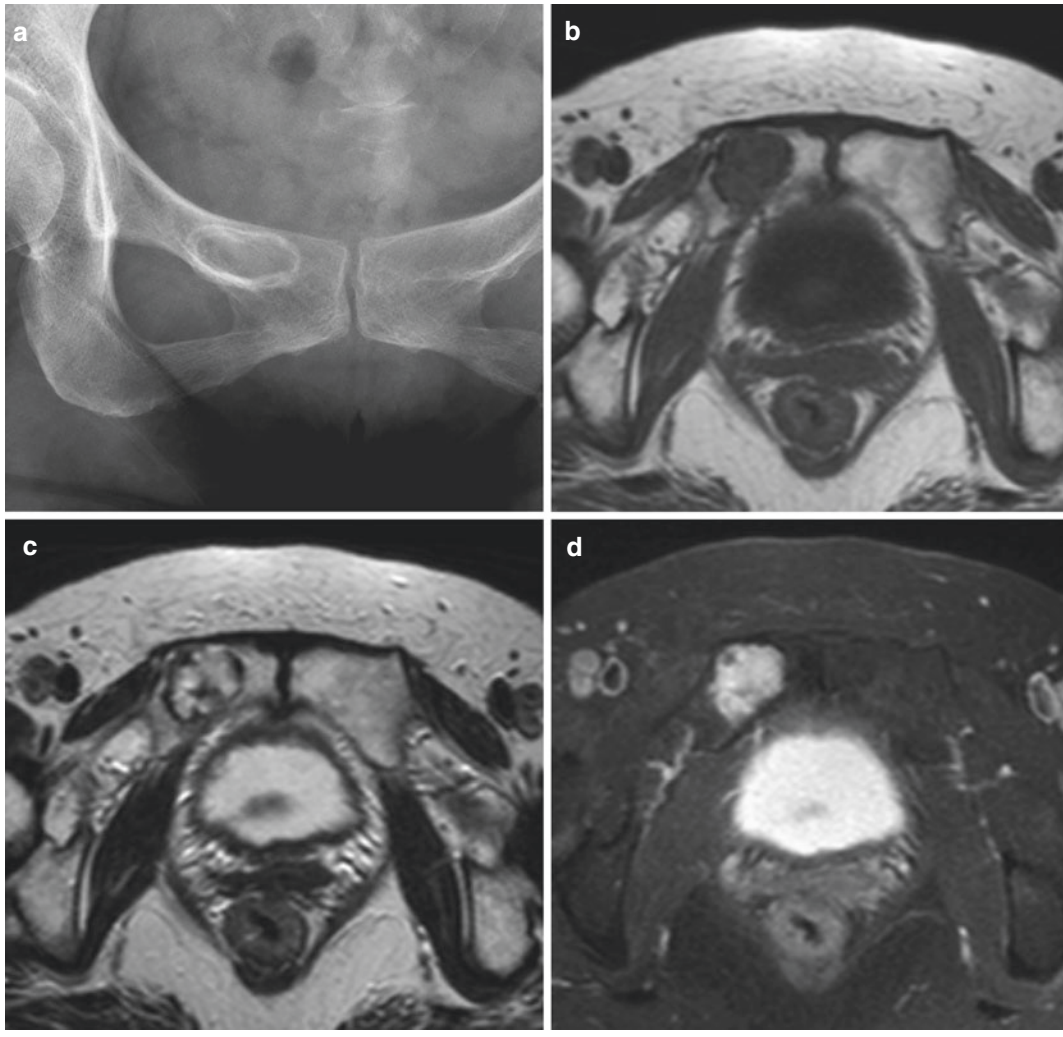

Fig. 8.21 Liposclerosing myxofibrous tumor in the right pubic body. (**a**) A well-defined osteolytic lesion with a sclerotic rim is noted at the right pubic body on anteroposterior radiograph of the pelvis. Axial (**b**) T1-weighted image, (**c**) T2-weighted image, and (**d**) contrast-enhanced T1-weighted fat-suppressed images are shown. The signal intensity of the lesion indicates the presence of myxoid stroma within the lesion

8.8 Adamantinoma

Overview

Adamantinoma is a low-grade malignant bone tumor characterized by mixed osteofibrous and epithelial components. Adamantinomas can be further divided into classic adamantinoma and osteofibrous dysplasia-like adamantinoma (differentiated adamantinoma).

Epidemiology

Adamantinomas are rare, accounting for 0.4 % of all primary bone tumors. It has a wide age range at presentation, from 3 to 86 years, but is usually around 30 years. There is a slight male predominance.

Common Locations

The anterior tibial metaphysis or diaphysis is the most common site of involvement (85–90 %). Multifocal involvement of the tibia is common, and ipsilateral fibula may be involved in 10 % of the cases. Involvement of ulnar and humerus has been rarely reported.

Imaging Features

Radiograph

Adamantinoma present as a well-defined intracortical osteolytic lesion at the anterior tibial cortex (Fig. 8.22). It extends longitudinally along the long axis of the tibia, and may accompany expansion, cortical destruction, and medullary extension. Occasionally, adamantinomas exhibit a "soap-bubble" appearance (Fig. 8.23). Multiple satellite osteolytic lesions may be found on radiograph.

Magnetic resonance imaging

Adamantinomas are hypointense on T1-weighted image and hyperintense on T2-weighted image, and may or may not show contrast enhancement. The findings on MRI are nonspecific, and MRI is more useful in evaluating the extent and multiplicity of the tumor, rather than making the specific diagnosis of adamantinoma.

Differential Diagnoses

1. Osteofibrous dysplasia.

   Osteofibrous dysplasia and adamantinoma both have a predilection for the anterior tibial cortex, often making the differential diagnosis difficult. Osteofibrous dysplasia exhibits less aggressive features; there is no medullary involvement or extraosseous soft tissue extension.
2. Fibrous dysplasia.

   Fibrous dysplasias are centered in the medullary cavity, whereas adamantinomas are intracortical lesions.

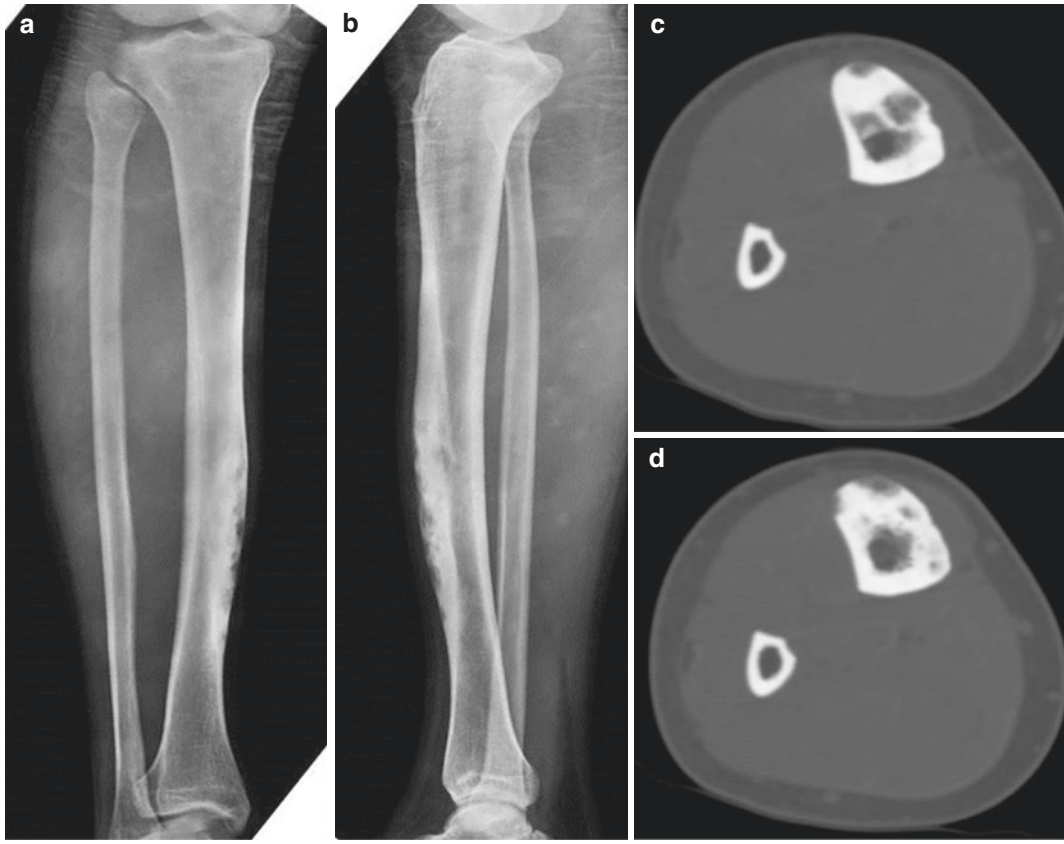

Fig. 8.22 Differentiated adamantinoma in the tibia. (**a**) Anteroposterior and (**b**) lateral radiographs of the lower leg show multilobulated osteolytic lesions involving the anterior cortex of the tibia. The lesions are expansile and cause mild anterior bowing of the tibia. (**c**, **d**) Axial CT images show cortical thickening in the tibia with well-defined osteolytic lesions within the thickened cortex. (**e**) Axial T1-weighted image, (**f**) axial T2-weighted fat-suppressed image, (**g**) axial contrast-enhanced T1-weighted fat-suppressed image, and (**h**) sagittal T2-weighted fat-suppressed image of the right lower leg are shown. The intracortical lesions are intermediate on T1-weighted image, hyperintense on fluid-sensitive sequences, and show enhancement (Courtesy of Jaehyuck Yi, Kyungpook National University Hospital, Korea)

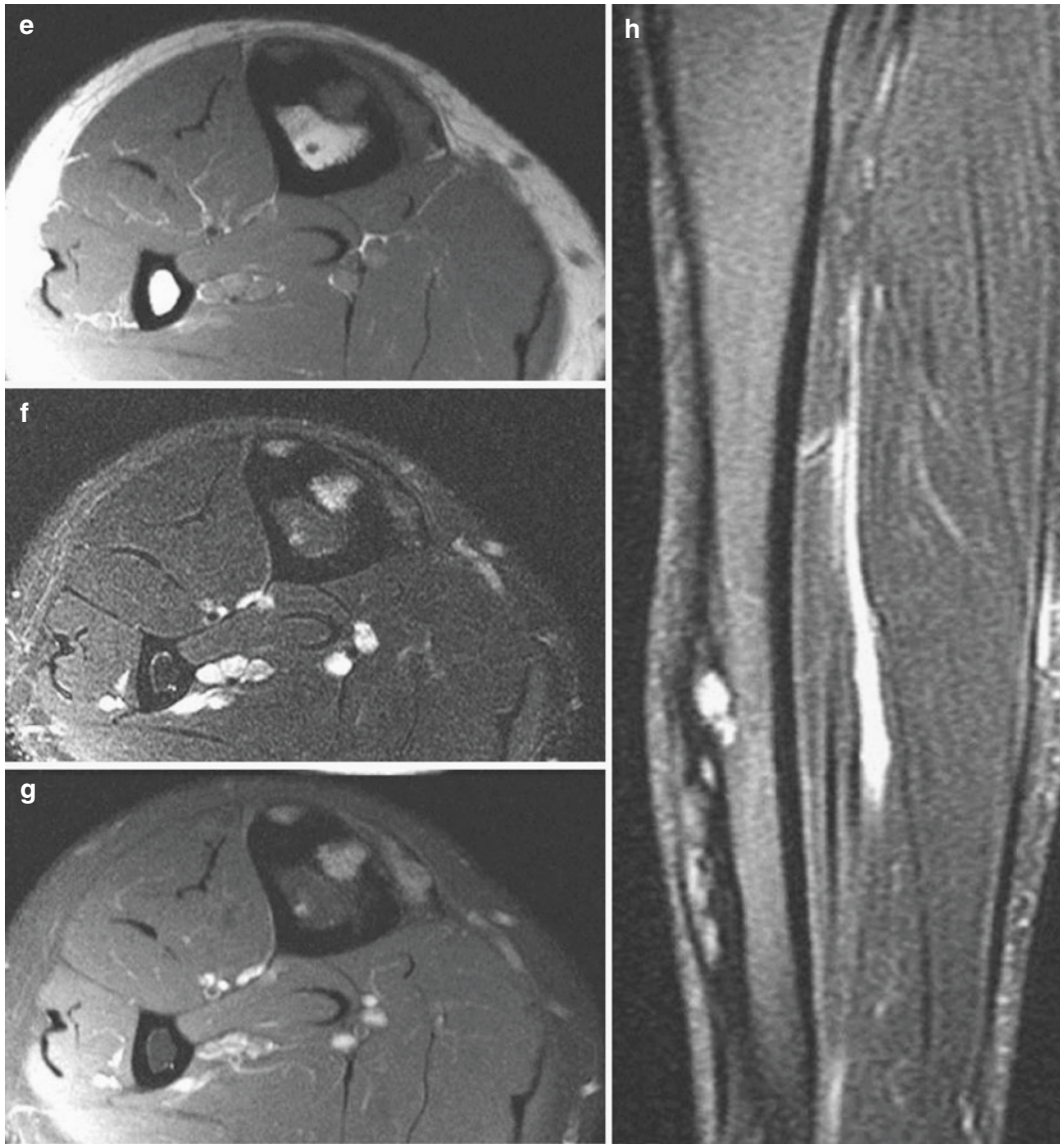

Fig. 8.22 (continued)

Fig. 8.23 Adamantinoma in the radius. (**a**) A multilobulated osteolytic lesion is noted at the mid-diaphysis of the radius. The lesion is mildly expansile and has internal trabeculations, resulting in a "soap-bubble" appearance. (**b**, **e**) T1-weighted image, (**c**) T2-weighted image, and (**d**, **f**) contrast-enhanced T1-weighted images are shown. The lesion is slightly hyperintense to muscle on T1-weighted image, hyperintense on T2-weighted image, and show strong enhancement. The lesion shows cortical breaching with extraosseous extension (*arrows* in **b**–**f**)

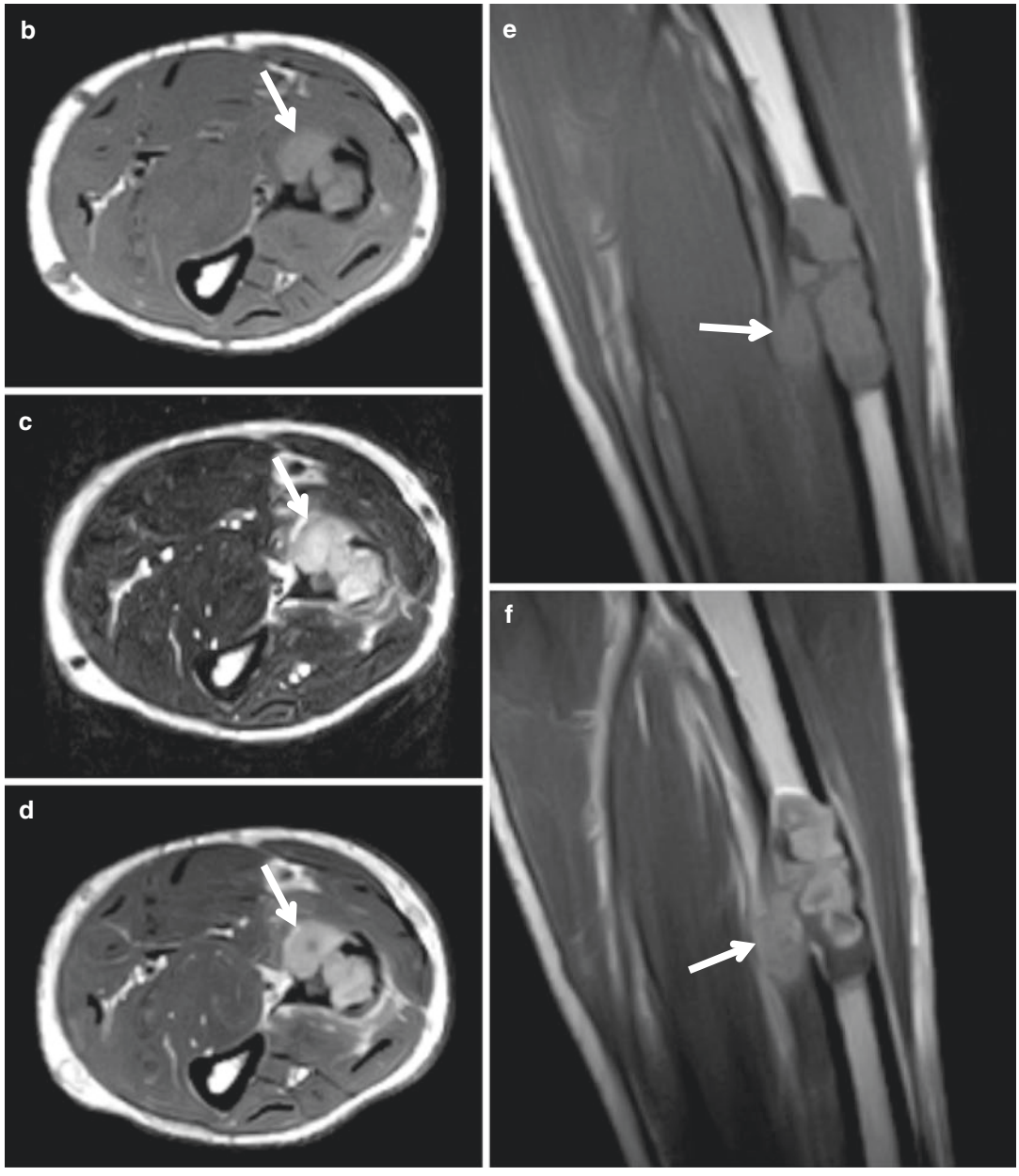

Fig. 8.23 (continued)

8.9 Brown Tumor

Overview

Brown tumor is a nonneoplastic lesion that occurs as a manifestation of hyperparathyroidism. It is also known as osteitis fibrosa cystica or osteoclastoma. The overproduction of parathyroid hormone leads to the increased osteoclastic resorption of bone. Localized areas of severe bone loss are filled with granulation tissue and vascularized fibrous tissue with hemosiderin deposition, resulting in "brown tumors." Brown tumors usually resolve with the treatment of hyperparathyroidism, and local treatment of the tumor itself is usually not necessary.

Epidemiology

Brown tumors tend to occur more frequently in patients with primary hyperparathyroidism (3 %) than those with secondary hyperparathyroidism (1.5–1.7 %). However, the overall incidence of secondary hyperparathyroidism is much more higher than primary hyperparathyroidism.

Common Locations

Brown tumors occur throughout the entire skeleton. Commonly involved sites include small tubular bones of hands, skull, pelvis, clavicle, rib, spine, and femur.

Imaging Features

Radiograph

Brown tumors occur as well-defined, geographical osteolytic lesions that are centrally located, and may be slightly expansile (Fig. 8.24).

Magnetic resonance imaging

Brown tumors can exhibit either a solid or cystic nature or a mixture of the two. Solid portions have been reported to show isointensity to hypointensity on T1-weighted and T2-weighted images, and cystic portions may exhibit fluid–fluid levels.

Differential Diagnoses

Solitary lesions: simple bone cyst, aneurysmal bone cyst, giant cell tumor, giant cell reparative granuloma.

Multiple lesions: metastasis, multiple myeloma, Langerhans cell histiocytosis.

The characteristic laboratory findings and other characteristic skeletal manifestations of hyperparathyroidism on radiography may aid in the differential diagnoses of brown tumor.

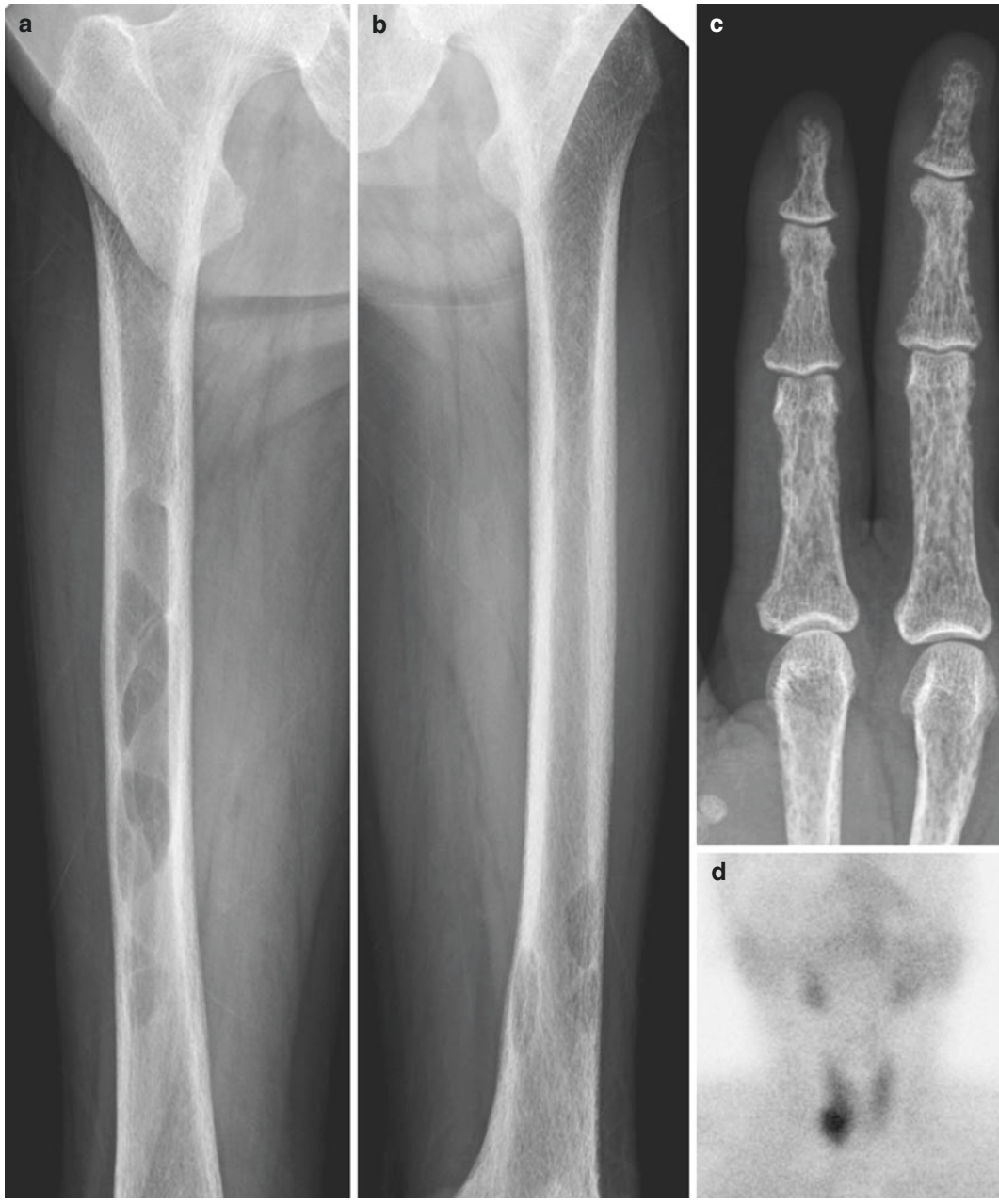

Fig. 8.24 Brown tumor. Anteroposterior radiograph of the right (**a**) and left (**b**) femora show multiple well-defined osteolytic lesions in the diaphysis. (**c**) Anteroposterior radiograph of the right hand shows characteristic subperiosteal bone resorption leading to the diagnosis of hyperparathyroidism. (**d**) Parathyroid scan shows increased uptake in the right parathyroid gland which was surgically proven to be parathyroid carcinoma. (**e**) Sagittal reformatted CT image shows a pathological fracture of the right femur. The cortex is markedly thinned by the osteolytic lesions (*arrows*). (**f**) Sagittal T2-weighted image, axial (**g**) T1-weighted image, (**h**) T2-weighted image, (**i**) contrast-enhanced T1-weighted fat-suppressed images are shown. The lesion shows mainly cystic nature and is scalloping and thinning the cortex. Fluid–fluid level is seen in some locules (*arrowheads*). The extensive soft tissue edema and enhancement around the femur are due to the pathological fracture

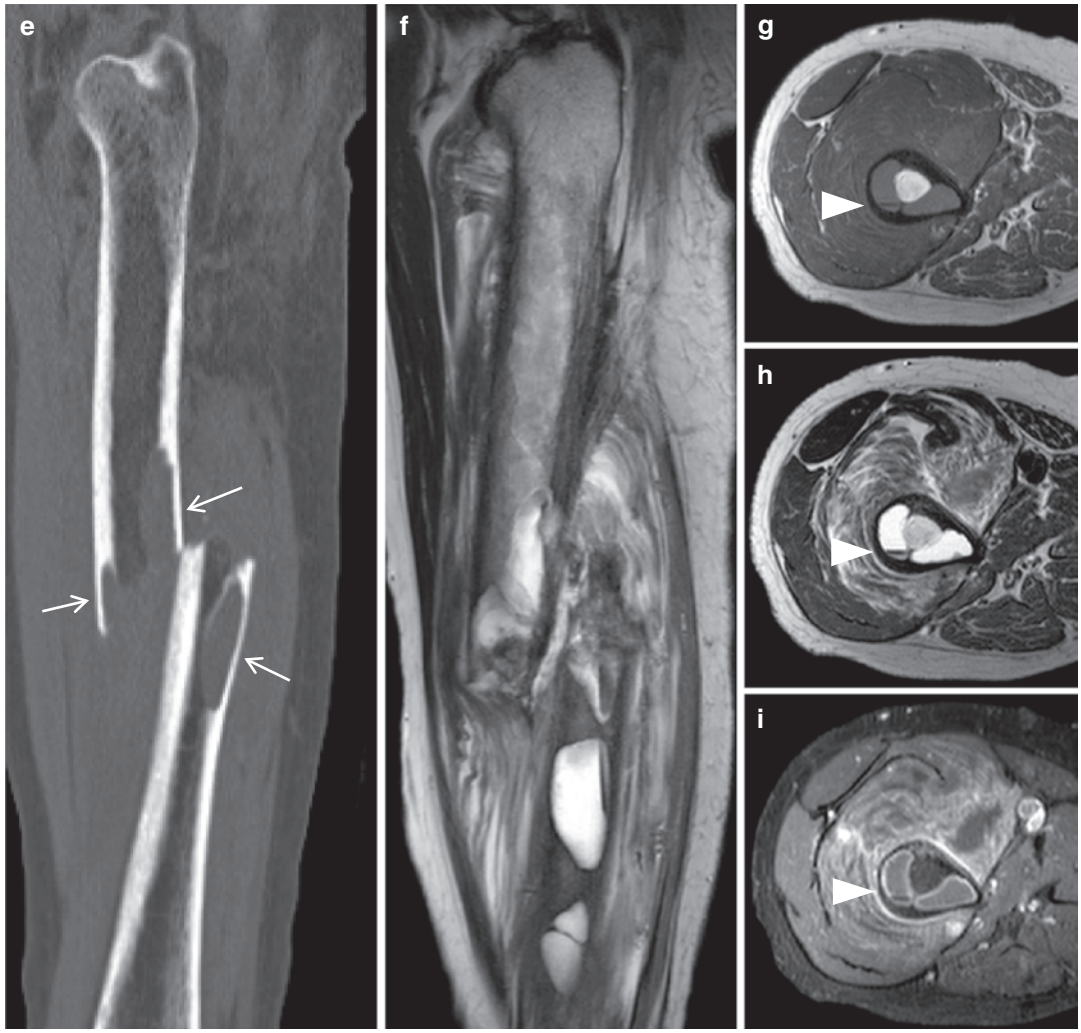

Fig. 8.24 (continued)

Suggested Reading

Simple Bone Cyst

Burr BA, Resnick D, Syklawer R, Haghighi P. Fluid-fluid levels in a unicameral bone cyst: CT and MR findings. J Comput Assist Tomogr. 1993;17:134–6.

Lokiec F, Wientroub S. Simple bone cyst: etiology, classification, pathology, and treatment modalities. J Pediatr Orthop B. 1998;7:262–73.

Margau R, Babyn P, Cole W, Smith C, Lee F. MR imaging of simple bone cysts in children: not so simple. Pediatr Radiol. 2000;30:551–7.

Struhl S, Edelson C, Pritzker H, Seimon LP, Dorfman HD. Solitary (unicameral) bone cyst. The fallen fragment sign revisited. Skeletal Radiol. 1989;18:261–5.

Wilkins RM. Unicameral bone cysts. J Am Acad Orthop Surg. 2000;8:217–24.

Aneurysmal Bone Cyst

Beltran J, Simon DC, Levy M, Herman L, Weis L, Mueller CF. Aneurysmal bone cysts: MR imaging at 1.5 T. Radiology. 1986;158:689–90.

Bonakdarpour A, Levy WM, Aegerter E. Primary and secondary aneurysmal bone cyst: a radiological study of 75 cases. Radiology. 1978;126:75–83.

Hudson TM. Fluid levels in aneurysmal bone cysts: a CT feature. AJR Am J Roentgenol. 1984;142:1001–4.

Hudson TM, Hamlin DJ, Fitzsimmons JR. Magnetic resonance imaging of fluid levels in an aneurysmal bone cyst and in anticoagulated human blood. Skelet Radiol. 1985;13:267–70.

Kransdorf MJ, Sweet DE. Aneurysmal bone cyst: concept, controversy, clinical presentation, and imaging. AJR Am J Roentgenol. 1995;164:573–80.

Levy WM, Miller AS, Bonakdarpour A, Aegerter E. Aneurysmal bone cyst secondary to other osseous lesions. Report of 57 cases. Am J Clin Pathol. 1975;63:1–8.

Mahnken AH, Nolte-Ernsting CC, Wildberger JE, et al. Aneurysmal bone cyst: value of MR imaging and conventional radiography. Eur Radiol. 2003;13:1118–24.

Munk PL, Helms CA, Holt RG, Johnston J, Steinbach L, Neumann C. MR imaging of aneurysmal bone cysts. AJR Am J Roentgenol. 1989;153:99–101.

Fibrous Dysplasia

Fitzpatrick KA, Taljanovic MS, Speer DP, et al. Imaging findings of fibrous dysplasia with histopathologic and intraoperative correlation. AJR Am J Roentgenol. 2004;182:1389–98.

Jee WH, Choi KH, Choe BY, Park JM, Shinn KS. Fibrous dysplasia: MR imaging characteristics with radiopathologic correlation. AJR Am J Roentgenol. 1996;167:1523–7.

Kransdorf MJ, Moser Jr RP, Gilkey FW. Fibrous dysplasia. Radiographics. 1990;10:519–37.

Kumar R, Madewell JE, Lindell MM, Swischuk LE. Fibrous lesions of bones. Radiographics. 1990;10:237–56.

Ozaki T, Sugihara M, Nakatsuka Y, Kawai A, Inoue H. Polyostotic fibrous dysplasia. A long-term follow up of 8 patients. Int Orthop. 1996;20:227–32.

Utz JA, Kransdorf MJ, Jelinek JS, Moser Jr RP, Berrey BH. MR appearance of fibrous dysplasia. J Comput Assist Tomogr. 1989;13:845–51.

Osteofibrous Dysplasia

Bethapudi S, Ritchie DA, Macduff E, Straiton J. Imaging in osteofibrous dysplasia, osteofibrous dysplasia-like adamantinoma, and classic adamantinoma. Clin Radiol. 2014;69:200–8.

Jung JY, Jee WH, Hong SH, et al. MR findings of the osteofibrous dysplasia. Korean J Radiol. 2014;15:114–22.

Kahn LB. Adamantinoma, osteofibrous dysplasia and differentiated adamantinoma. Skelet Radiol. 2003;32:245–58.

Khanna M, Delaney D, Tirabosco R, Saifuddin A. Osteofibrous dysplasia, osteofibrous dysplasia-like adamantinoma and adamantinoma: correlation of radiological imaging features with surgical histology and assessment of the use of radiology in contributing to needle biopsy diagnosis. Skelet Radiol. 2008;37:1077–84.

Levine SM, Lambiase RE, Petchprapa CN. Cortical lesions of the tibia: characteristic appearances at conventional radiography. Radiographics. 2003;23:157–77.

Langerhans Cell Histiocytosis

Azouz EM, Saigal G, Rodriguez MM, Podda A. Langerhans' cell histiocytosis: pathology, imaging and treatment of skeletal involvement. Pediatr Radiol. 2005;35:103–15.

Ghanem I, Tolo VT, D'Ambra P, Malogalowkin MH. Langerhans cell histiocytosis of bone in children and adolescents. J Pediatr Orthop. 2003;23:124–30.

Khung S, Budzik JF, Amzallag-Bellenger E, et al. Skeletal involvement in Langerhans cell histiocytosis. Insights Imaging. 2013;4:569–79.

Meyer JS, Harty MP, Mahboubi S, et al. Langerhans cell histiocytosis: presentation and evolution of radiologic findings with clinical correlation. Radiographics. 1995;15:1135–46.

Stull MA, Kransdorf MJ, Devaney KO. Langerhans cell histiocytosis of bone. Radiographics. 1992;12:801–23.
Song YS, Lee IS, Yi JH, Cho KH, Kim DK, Song JW. Radiologic findings of adult pelvis and appendicular skeletal Langerhans cell histiocytosis in nine patients. Skelet Radiol. 2011;40:1421–6.

Intraosseous Lipoma

Blacksin MF, Ende N, Benevenia J. Magnetic resonance imaging of intraosseous lipomas: a radiologic-pathologic correlation. Skelet Radiol. 1995;24:37–41.
Campbell RS, Grainger AJ, Mangham DC, Beggs I, Teh J, Davies AM. Intraosseous lipoma: report of 35 new cases and a review of the literature. Skelet Radiol. 2003;32:209–22.
Levin MF, Vellet AD, Munk PL, McLean CA. Intraosseous lipoma of the distal femur: MRI appearance. Skelet Radiol. 1996;25:82–4.
Murphey MD, Carroll JF, Flemming DJ, Pope TL, Gannon FH, Kransdorf MJ. From the archives of the AFIP: benign musculoskeletal lipomatous lesions. Radiographics. 2004;24:1433–66.
Propeck T, Bullard MA, Lin J, Doi K, Martel W. Radiologic-pathologic correlation of intraosseous lipomas. AJR Am J Roentgenol. 2000;175:673–8.
Reig-Boix V, Guinot-Tormo J, Risent-Martinez F, Aparisi-Rodriguez F, Ferrer-Jimenez R. Computed tomography of intraosseous lipoma of os calcis. Clin Orthop Relat Res. 1987;221:286–91.

Liposclerosing Myxofibrous Tumor

Corsi A, De Maio F, Ippolito E, et al. Monostotic fibrous dysplasia of the proximal femur and liposclerosing myxofibrous tumor: which one is which? J Bone Miner Res. 2006;21:1955–8.
Heim-Hall JM, Williams RP. Liposclerosing myxofibrous tumour: a traumatized variant of fibrous dysplasia? Report of four cases and review of the literature. Histopathology. 2004;45:369–76.
Kransdorf MJ, Murphey MD, Sweet DE. Liposclerosing myxofibrous tumor: a radiologic-pathologic-distinct fibro-osseous lesion of bone with a marked predilection for the intertrochanteric region of the femur. Radiology. 1999;212:693–8.
Murphey MD, Carroll JF, Flemming DJ, Pope TL, Gannon FH, Kransdorf MJ. From the archives of the AFIP: benign musculoskeletal lipomatous lesions. Radiographics. 2004;24:1433–66.

Adamantinoma

Bethapudi S, Ritchie DA, Macduff E, Straiton J. Imaging in osteofibrous dysplasia, osteofibrous dysplasia-like adamantinoma, and classic adamantinoma. Clin Radiol. 2014;69:200–8.
Kahn LB. Adamantinoma, osteofibrous dysplasia and differentiated adamantinoma. Skelet Radiol. 2003;32:245–58.
Khanna M, Delaney D, Tirabosco R, Saifuddin A. Osteofibrous dysplasia, osteofibrous dysplasia-like adamantinoma and adamantinoma: correlation of radiological imaging features with surgical histology and assessment of the use of radiology in contributing to needle biopsy diagnosis. Skelet Radiol. 2008;37:1077–84.
Levine SM, Lambiase RE, Petchprapa CN. Cortical lesions of the tibia: characteristic appearances at conventional radiography. Radiographics. 2003;23:157–77.

Brown Tumor

Chew FS, Huang-Hellinger F. Brown tumor. AJR Am J Roentgenol. 1993;160:752.
Davies AM, Evans N, Mangham DC, Grimer RJ. MR imaging of brown tumour with fluid-fluid levels: a report of three cases. Eur Radiol. 2001;11:1445–9.
Franco M, Bendini JC, Albano L, Barrillon D, Cassuto E, Bracco J. Radiographic follow-up of a phalangeal brown tumor. Joint Bone Spine. 2002;69:506–10.
Hong WS, Sung MS, Chun KA, et al. Emphasis on the MR imaging findings of brown tumor: a report of five cases. Skelet Radiol. 2011;205:205–13.
Hoshi M, Takami M, Kajikawa M, et al. A case of multiple skeletal lesions of brown tumors, mimicking carcinoma metastases. Arch Orthop Trauma Surg. 2008;128:149–54.
Jouan A, Zabraniecki L, Vincent V, Poix E, Fournie B. An unusual presentation of primary hyperparathyroidism: severe hypercalcemia and multiple brown tumors. Joint Bone Spine. 2008;75:209–11.

Tumor Syndromes

9

Contents

9.1 Enchondromatosis: Ollier Disease and Maffucci Syndrome

Enchondromatosis refers to nonhereditary sporadic skeletal disorders that present with multiple enchondromas. Ollier disease and Maffuci syndrome fall into this category. Ollier disease is a nonhereditary disorder characterized by multiple enchondromas, usually affecting the short and long tubular bones of the extremities (Figs. 9.1 and 9.2). Maffuci syndrome refers to enchondromatosis associated with multiple soft tissue hemangiomas in the soft tissue or viscera (Figs. 9.3 and 9.4). The diagnosis of enchondromatosis is made based on clinical features and characteristic imaging findings. Patients with enchondromatosis are at higher risk of developing secondary chondrosarcoma, compared to those with a solitary enchondroma, and are in need of regular follow-up.

H.S. Kang et al., *Oncologic Imaging: Bone Tumors*, DOI 10.1007/978-981-287-703-1_9

Fig. 9.1 Ollier disease. (**a**) Anteroposterior radiograph of the left hand shows multiple expansile osteolytic lesions in the phalanges of hand, with some showing chondroid mineralization. These lesions show typical features of chondroid matrix on magnetic resonance imaging. The lesions are isointense on T1-weighted image (**b**), hyperintense on T2-weighted fat-suppressed image (**c**), and show peripheral and septal enhancement (**d**)

Fig. 9.2 Ollier disease. Multiple enchondromas are noted at the right proximal femur (**a**), both proximal fibula (**b**), phalanges and metacarpal of hand (**c**), phalanges and metatarsal bones (**d**)

Fig. 9.3 Maffucci syndrome. (**a**) Anteroposterior radiograph of both hands show multiple enchondromas extensively involving the phalanges, metacarpal bones, and left distal radius and ulna. A magnified view of the left wrist shows a cluster of small round phleboliths (*arrows*), indicating the presence of soft tissue hemangiomatosis. (**b**) Coronal contrast-enhanced T1-weighted fat-suppressed image shows typical chondroid pattern of enhancement, peripheral and septal pattern with lobulated architecture. A soft tissue mass with intermediate signal intensity on T1-weighted image (**c**), bright hyperintensity on T2-weighted image (**d**), and strong enhancement on contrast-enhanced T1-weighted fat-suppressed image (**e**) is noted at the radial aspect of the left wrist. MR imaging findings are consistent with hemangioma

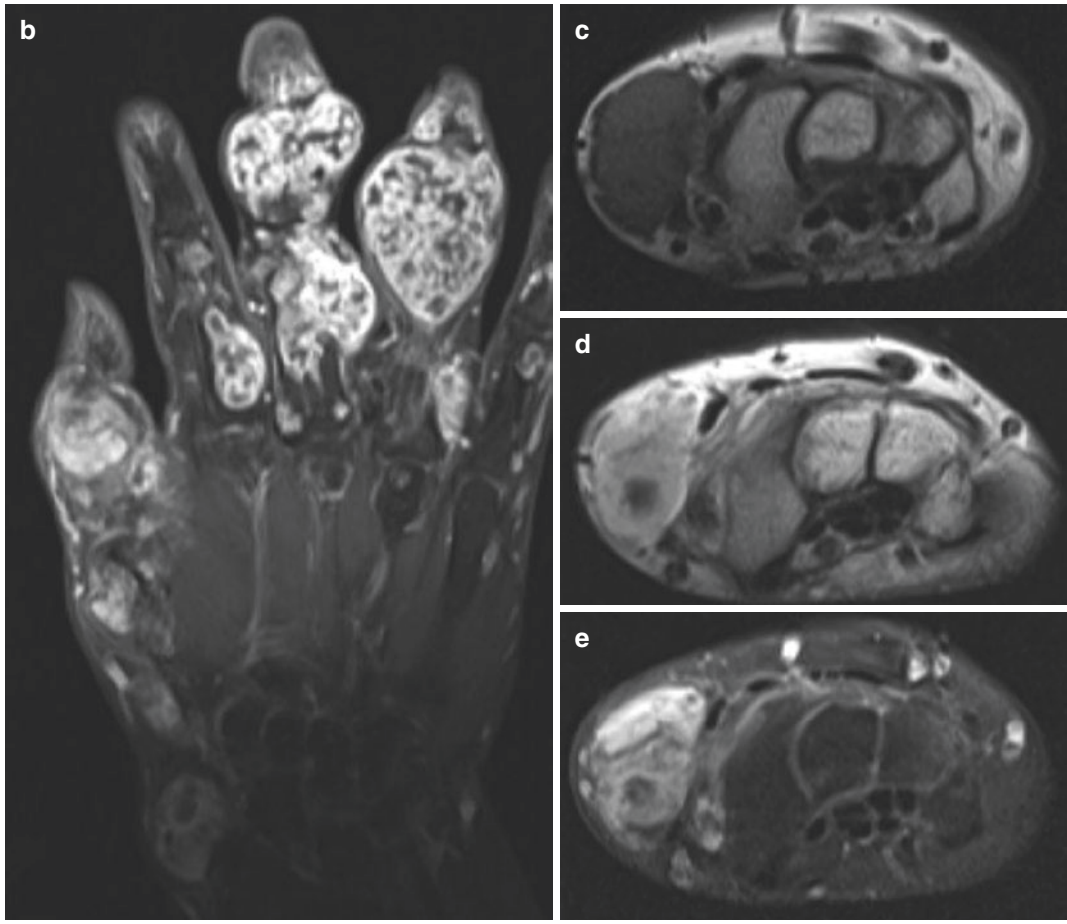

Fig. 9.3 (continued)

Fig. 9.4 Maffucci syndrome. Multiple enchondromas are present in the long bones and short tubular bones; multiple lesions in the tibia and fibula (**a**), phalanges, metatarsals and tarsal bones (**b**), radius and ulna (**c**) result in a skeletal deformity. (**d**) Characteristic phleboliths are noted along the radial side of the hand and along the thumb with prominent soft tissue shadow. The soft tissue lesion is consistent with hemangiomatosis on magnetic resonance imaging. (**e**) T1-weighted image shows soft tissue lesion with intermediate signal intensity intermixed with fat, and these lesions heterogeneously enhance on (**f**) contrast-enhanced T1-weighted fat-suppressed image (*arrows* on **e**, **f**)

Fig. 9.4 (continued)

9.2 Multiple Osteochondromas

(Synonyms: hereditary multiple exostoses, multiple cartilaginous exostoses, diaphyseal aclasis, osteochondromatosis).

Multiple osteochondromas (MO) is an autosomal dominant condition characterized by the development of two or more osteochondromas (Figs. 9.5 and 9.6). It is caused by a mutation in the tumor-suppressor genes *EXT1* or *EXT2*. Osteochondromas grow and ossify during skeletal development and stop growing after skeletal maturity. MO may be associated with bony deformity, short stature, restricted joint motion, early osteoarthritis, and compression of peripheral nerves. Malignant transformation of osteochondroma to secondary chondrosarcoma has been reported to occur in 0.5–5 % of MO cases. Malignant transformation should be suspected when there is (a) newly developed pain, (b) interval growth of an osteochondroma in a skeletally mature patient, (c) irregularity of the lesion surface, (d) focal lucent regions within the lesion (d) erosion or destruction of adjacent bone, or (e) a soft tissue mass with irregular calcifications.

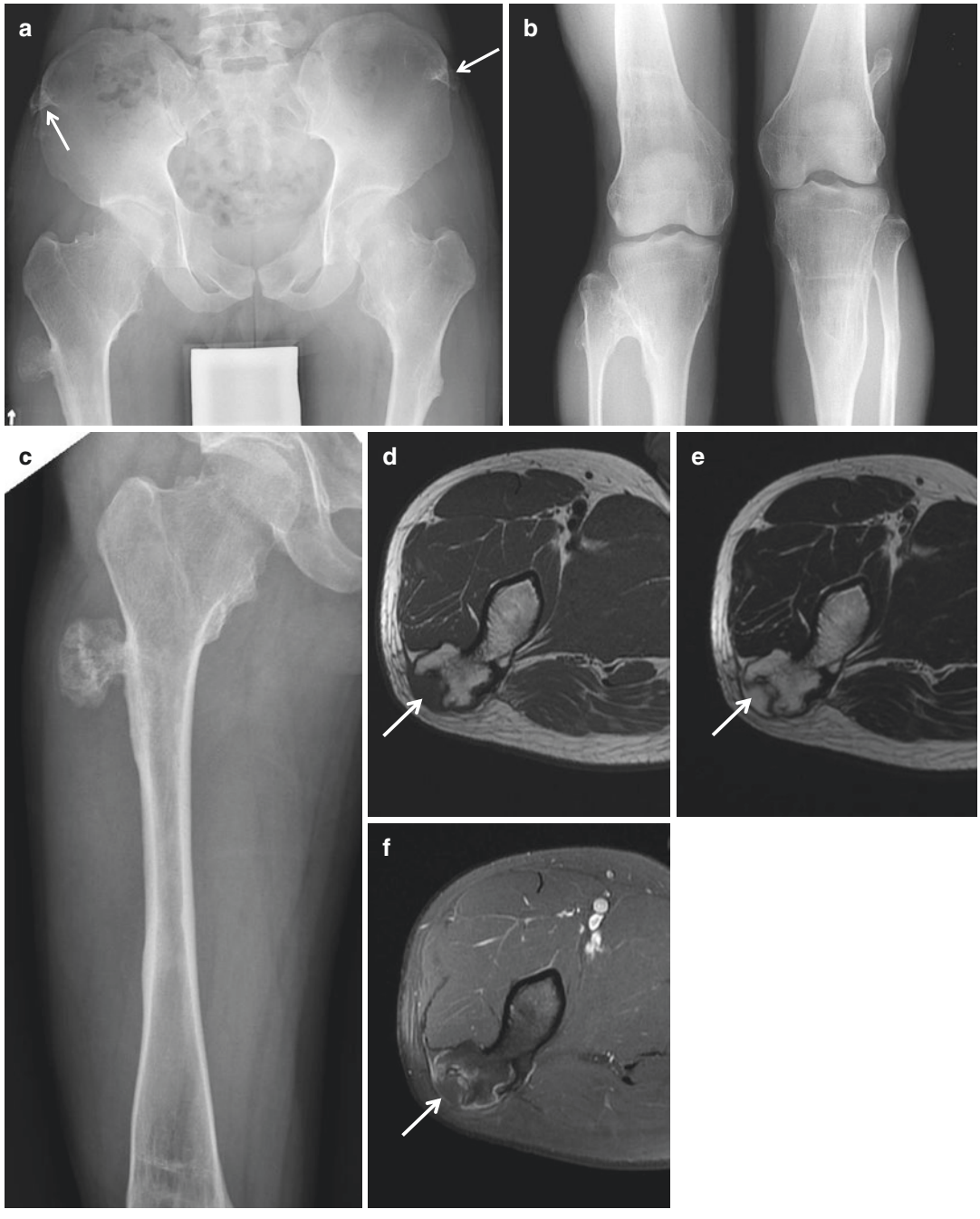

Fig. 9.5 Multiple osteochondromas. (**a**) Anteroposterior radiograph of the pelvis shows numerous sessile and pedunculated osteochondromas affecting the pelvic bone (*arrows*) and proximal femora. (**b**) Anteroposterior radiographs of both knee show numerous sessile and pedunculated osteochondromas affecting the distal femora, proximal tibia, and fibula. (**c**) A prominent pedunculated osteochondroma is noted at the proximal metaphysis of the femur. (**d**) Axial T1-weighted, (**e**) axial T2-weighted, and (**f**) axial contrast-enhanced T1-weighted fat-suppressed images are shown. The osteochondroma has medullary continuation with the mother bone, and has a cartilage cap (*arrows* in **d**–**f**) that is isointense on T1-weighted image, hyperintense on T2-weighted image

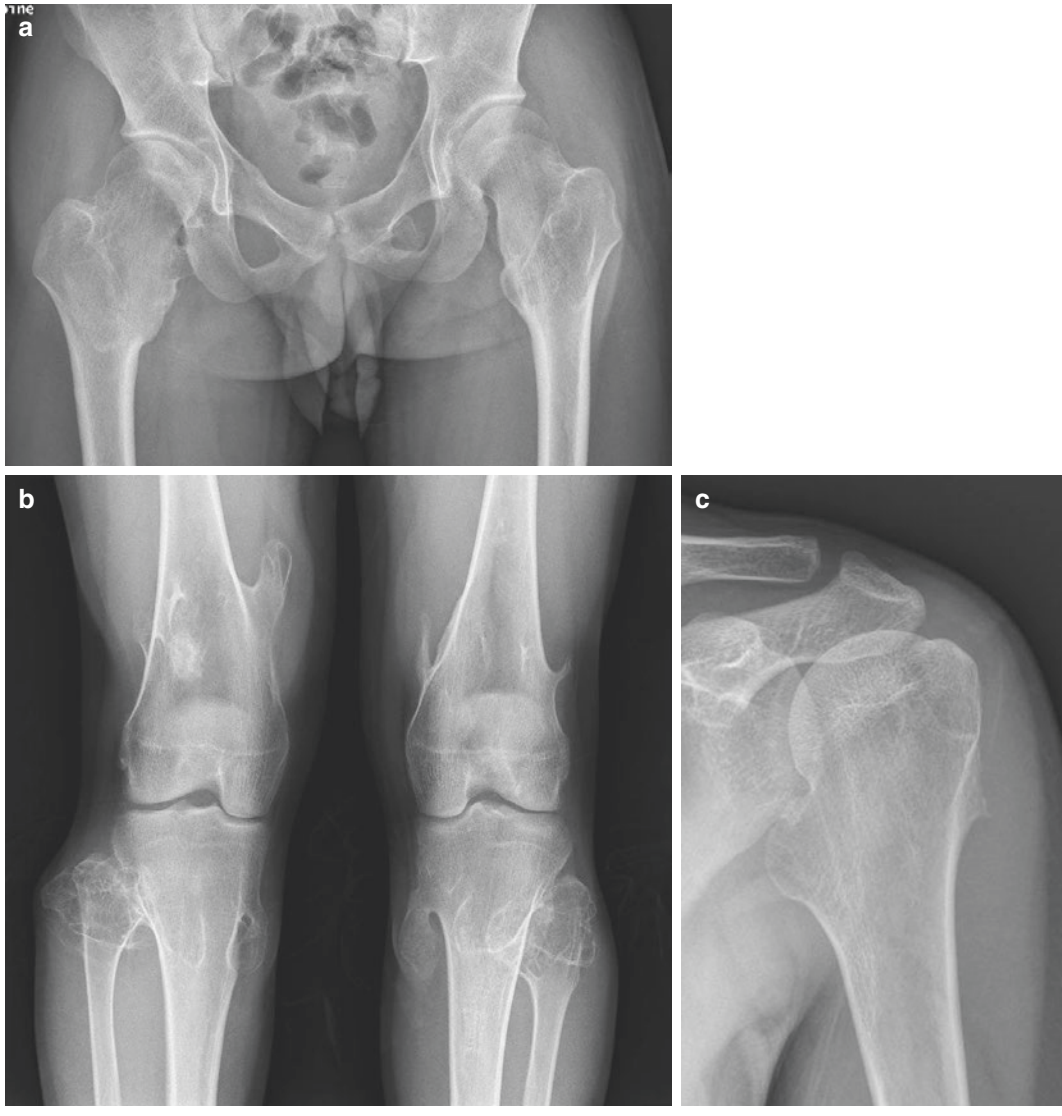

Fig. 9.6 Multiple osteochondromas. (**a**–**c**) Numerous sessile and pedunculated osteochondromas are noted at the proximal and distal metaphysis of both femora, proximal tibia and fibula, and left humerus

9.3 McCune-Albright Syndrome

McCune-Albright syndrome is a sporadic syndrome characterized by the triad of (i) polyostotic fibrous dysplasia (Fig. 9.7), (ii) café-au-lait skin lesions, and (iii) endocrine abnormalities. Various endocrine abnormalities may be present including precocious puberty, acromegaly, Cushing's disease, hyperprolactinemia, and hyperparathyroidism.

Fig. 9.7 McCune-Albright syndrome. (**a**) Anteroposterior radiograph of the hip shows polyostotic fibrous dysplasia involving the pelvic bone and both femora. The extensive involvement of both proximal femora results in a "shepherd crook" deformity. The lesions are of intermediate to low signal intensity on T1-weighted image (**b**), high signal intensity on T2-weighted image (**c**), and show heterogeneous enhancement after intravenous gadolinium administration (**d**). Bilateral femoral lesions include areas of cystic degeneration (*arrows* in **c**). The patient had a clinical history of precocious puberty, and café-au-lait skin lesions were present on physical examination, leading to the diagnosis of McCune-Albright syndrome

9.4 Mazabraud Syndrome

Mazabraud syndrome is a rare syndrome characterized by the presence of fibrous dysplasia and multiple soft tissue myxomas (Figs. 9.8 and 9.9). Soft tissue myxomas are more commonly associated with polyostotic fibrous dysplasia, but the association with monostotic form has been also reported. Soft tissue myxomas are usually present near the most severely affected bone.

Fig. 9.8 Mazabraud syndrome. (**a**) Anteroposterior radiograph of the hip shows a geographical ground-glass opacity lesion in both the ilium and left proximal femur (*arrows*). (**b**) Axial T1-weighted image, (**c**) axial T2-weighted image, (**d**) axial and (**e**) contrast-enhanced T1-weighted fat-suppressed images are shown. Intramedullary lesions involving both ilium and left proximal femur exhibit signal intensity characteristics consistent with fibrous dysplasia (*arrows* in **b**–**e**). A soft tissue mass is noted at the right ischiofemoral space, with fluid-like signal intensity and thin rim enhancement (*arrowheads* in **b**–**e**). This lesion was surgically proven as myxoma

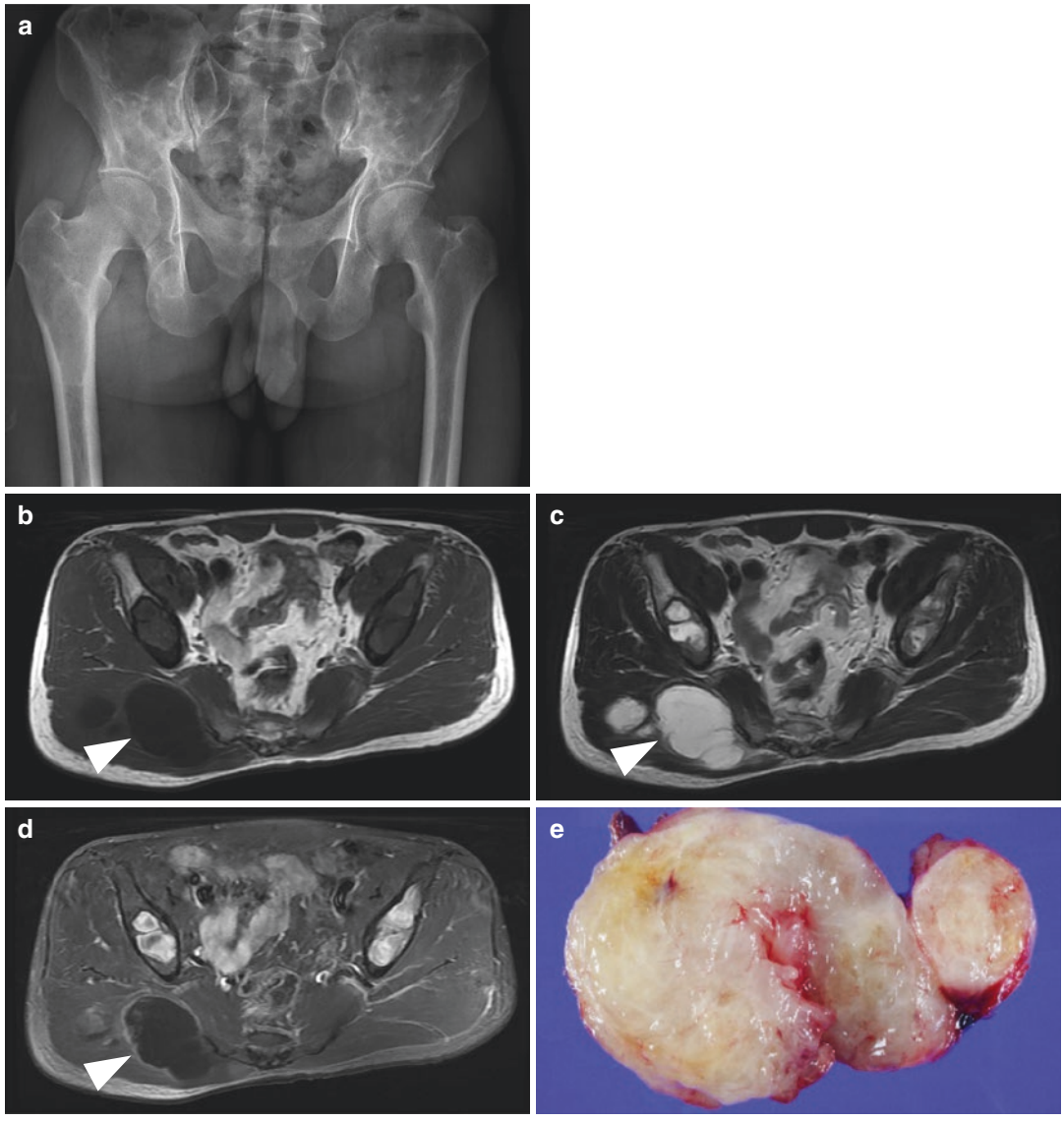

Fig. 9.9 Mazabraud syndrome. (**a**) Anteroposterior radiograph of the pelvis shows multiple ground-glass opacity lesions with thin sclerotic rims involving bilateral pelvic bones and right proximal femur; findings are consistent with polyostotic fibrous dysplasia. On magnetic resonance imaging, soft tissue masses with hypointensity on T1-weighted image (**b**), bright hyperintensity on T2-weighted image (**c**), rim enhancement on contrast-enhanced T1-weighted fat-suppressed image (**d**) were noted within the gluteus maximus muscle. (**d**) Surgical excision of this lesion revealed a whitish glistening mass, histologically proven to be a myxoma (**e**)

9.5 Jaffe-Campanacci Syndrome

Jaffe-Campanacci syndrome is a disorder characterized by multiple nonossifying fibromas, café-au-lait spots, intellectual disability, hypogonadism or cryptorchidism, and giant cell reparative granuloma of the jaw. Nonossifying fibromas in Jaffe-Campanacci syndrome affect the long bones (femur, tibia, and humerus), as well as the jaw.

Suggested Reading

Bovee JV. Multiple osteochondromas. Orphanet J Rare Dis. 2008;3:3.

Cabral CE, Guedes P, Fonseca T, Rezende JF, Cruz Junior LC, Smith J. Polyostotic fibrous dysplasia associated with intramuscular myxomas: Mazabraud's syndrome. Skelet Radiol. 1998;27:278–82.

Case DB, Chapman Jr CN, Freeman JK, Polga JP. Best cases from the AFIP: Atypical presentation of polyostotic fibrous dysplasia with myxoma (Mazabraud syndrome). Radiographics. 2010;30:827–32.

Chapurlat RD, Orcel P. Fibrous dysplasia of bone and McCune-Albright syndrome. Best Pract Res Clin Rheumatol. 2008;22:55–69.

Cherix S, Bilde Y, Becce F, Letovanec I, Rudiger HA. Multiple non-ossifying fibromas as a cause of pathological femoral fracture in Jaffe-Campanacci syndrome. BMC Musculoskelet Disord. 2014;15:218.

Dumitrescu CE, Collins MT. McCune-Albright syndrome. Orphanet J Rare Dis. 2008;3:12.

Foreman KL, Kransdorf MJ, O'Connor MI, Krishna M. AIRP best cases in radiologic-pathologic correlation: Maffucci syndrome. Radiographics. 2013;33: 861–8.

Hau MA, Fox EJ, Cates JM, Brigman BE, Mankin HJ. Jaffe-Campanacci syndrome. A case report and review of the literature. J Bone Joint Surg Am. 2002;84-A:634–8.

Iwasko N, Steinbach LS, Disler D, et al. Imaging findings in Mazabraud's syndrome: seven new cases. Skelet Radiol. 2002;31:81–7.

Karasick D, Schweitzer ME, Eschelman DJ. Symptomatic osteochondromas: imaging features. AJR Am J Roentgenol. 1997;168:1507–12.

Kransdorf MJ, Murphey MD. Diagnosis please. Case 12: Mazabraud syndrome. Radiology. 1999;212:129–32.

Lee KC, Davies AM, Cassar-Pullicino VN. Imaging the complications of osteochondromas. Clin Radiol. 2002;57:18–28.

Mellon CD, Carter JE, Owen DB. Ollier's disease and Maffucci's syndrome: distinct entities or a continuum. Case report: enchondromatosis complicated by an intracranial glioma. J Neurol. 1988;235:376–8.

Murphey MD, Choi JJ, Kransdorf MJ, Flemming DJ, Gannon FH. Imaging of osteochondroma: variants and complications with radiologic-pathologic correlation. Radiographics. 2000;20:1407–34.

Nguyen BD, Ram PC. Mazabraud's syndrome with sarcomatous transformation: scintigraphic and radiologic imaging. Clin Nucl Med. 2005;30:829–30.

Pannier S, Legeai-Mallet L. Hereditary multiple exostoses and enchondromatosis. Best Pract Res Clin Rheumatol. 2008;22:45–54.

Schwartz HS, Zimmerman NB, Simon MA, Wroble RR, Millar EA, Bonfiglio M. The malignant potential of enchondromatosis. J Bone Joint Surg. 1987;69-A: 269–74.

Silve C, Juppner H. Ollier disease. Orphanet J Rare Dis. 2006;1:37.

Stewart DR, Brems H, Gomes AG, et al. Jaffe-Campanacci syndrome, revisited: detailed clinical and molecular analyses determine whether patients have neurofibromatosis type 1, coincidental manifestations, or a distinct disorder. Genet Med. 2014;16:448–59.

Stieber JR, Dormans JP. Manifestations of hereditary multiple exostoses. J Am Acad Orthop Surg. 2005;13: 110–20.

Sundaram M, McDonald DJ, Merenda G. Intramuscular myxoma: a rare but important association with fibrous dysplasia of bone. AJR Am J Roentgenol. 1989;153: 107–8.

Vanhoenacker FM, Van Hul W, Wuyts W, Willems PJ, De Schepper AM. Hereditary multiple exostoses: from genetics to clinical syndrome and complications. Eur J Radiol. 2001;40:208–17.

Walker RE, Schwartz RK, Gale DR. Musculoskeletal case of the day. Mazabraud's syndrome (intramuscular myxomas associated with fibrous dysplasia of bone). AJR Am J Roentgenol. 1999;173:797.

Zwenneke Flach H, Ginai AZ, Wolter OJ. Best cases from the AFIP. Maffucci syndrome: radiologic and pathologic findings Armed Forces Institutes of Pathology. Radiographics. 2001;21:1311–6.

Part III

Practical Pearls in the Diagnosis of Bone Tumors

Radiographic Findings

10

Contents

10.1 Intramedullary Sclerotic Bone Lesions

Intramedullary sclerotic tumor and tumor-like bone lesions include, but are not limited to, bone islands (Fig. 10.1), bone infarction (Fig. 10.2), enchondroma, conventional osteosarcoma (Fig. 10.3), osteoblastic metastasis, mastocytosis (Fig. 10.4), and POEMS (polyneuropathy, organomegaly, endocrinopathy, monoclonal gammopathy, and skin changes) syndrome (Fig. 10.5).

Bone islands appear as homogeneously sclerotic foci with spiculation. Bone infarction can be characterized with peripheral sclerosis. Enchondroma contains central chondroid matrix. Conventional osteosarcoma appears as aggressive lesion with amorphous osteoid matrix and soft tissue mass. Osteoblastic metastasis may be radiographically indistinguishable from bone islands, and may show enhancement on the post-contrast MR images. Mastocytosis may appear as multiple scattered sclerotic foci involving the axial skeleton and long bones, similar to metastatic disease, and clinical manifestation of skin rash, episodic vomiting, and diarrhea could be diagnostic hints. POEMS syndrome shows as homogeneously sclerotic lesion, and clinical clues are polyneuropathy, organomegaly, endocrinopathy, monoclonal gammopathy, and skin changes.

H.S. Kang et al., *Oncologic Imaging: Bone Tumors*, DOI 10.1007/978-981-287-703-1_10

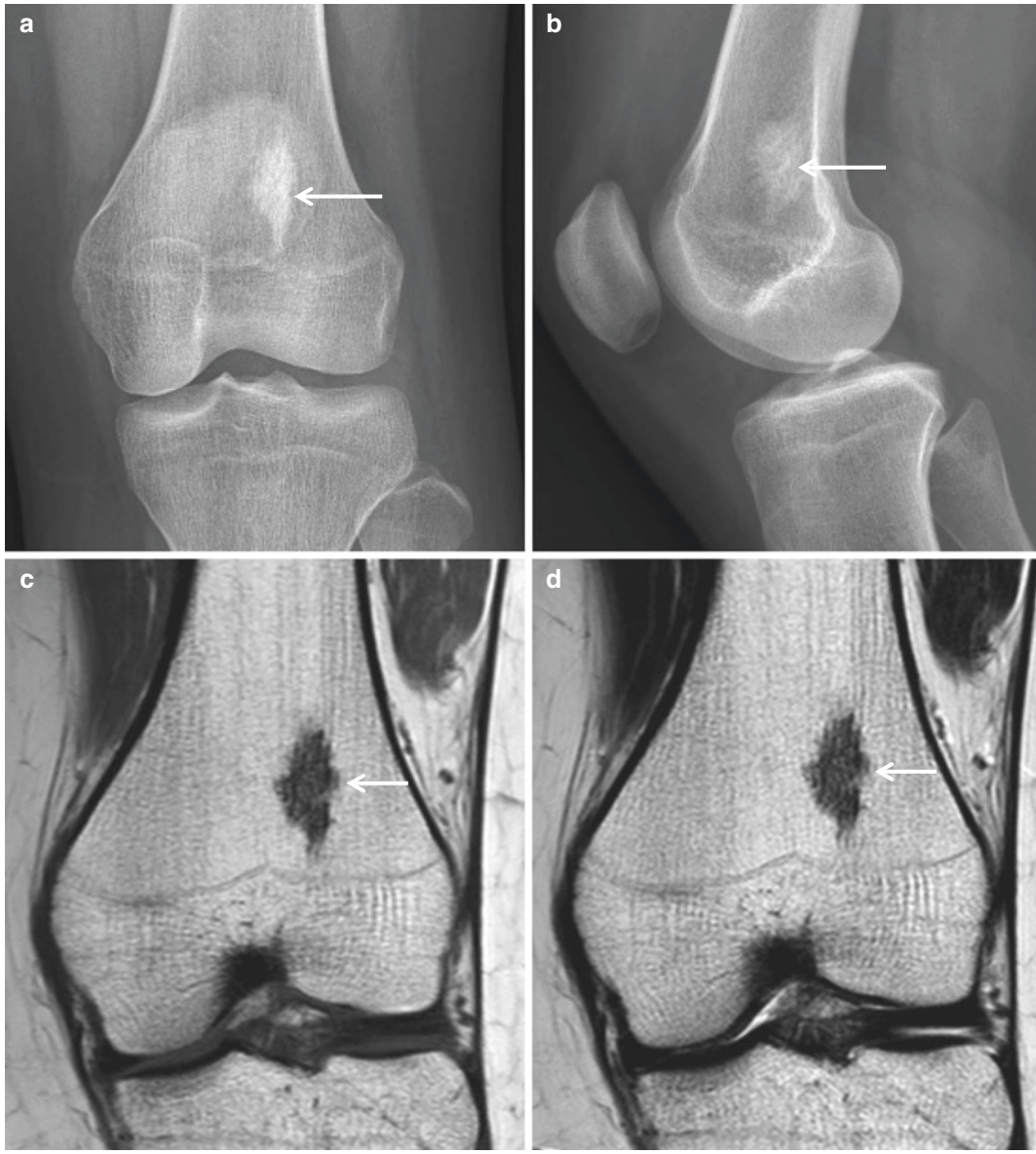

Fig. 10.1 Bone island. (**a**) Anteroposterior radiograph of the left femur shows a densely sclerotic intramedullary focus with thorny margin (*arrow*). The long axis of this focus is paralleling the long axis of the affected bone. (**b**) Lateral radiograph again shows a densely sclerotic focus with thorny margin (*arrow*). (**c**) Coronal T1-weighted MR image shows low signal intensity (*arrow*). (**d**) Coronal T2-weighted MR image again reveals low signal intensity (*arrow*)

Fig. 10.2 Bone infarction. Anteroposterior radiograph of the pelvis shows multiple sclerotic lesions with peripheral sclerosis (*arrows*) in the bilateral proximal femurs and bony pelvis

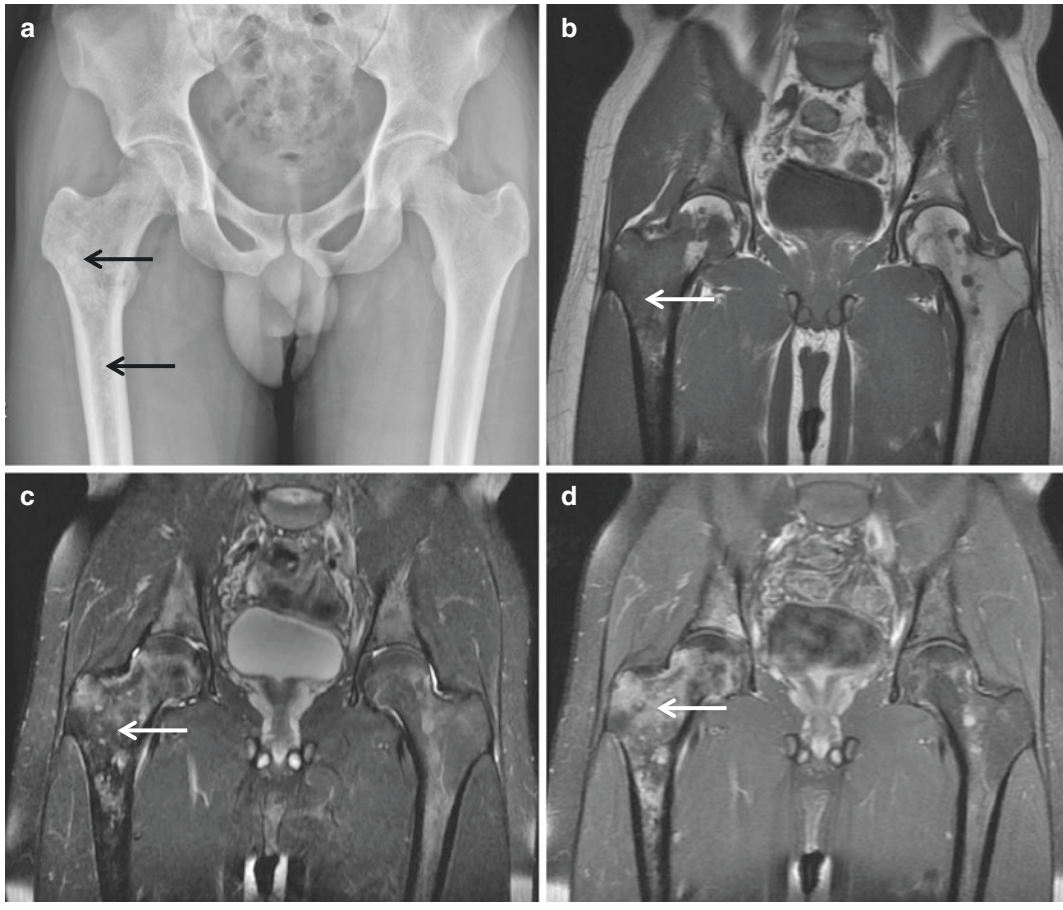

Fig. 10.3 Osteosarcoma. (**a**) Anteroposterior radiograph of the pelvis shows multiple sclerotic lesions in the right proximal femur (*arrows*). (**b**) Coronal T1-weighted MR image shows intramedullary low signal intensity (*arrow*). (**c**) Coronal fat-suppressed T2-weighted MR image shows intramedullary low-to-high signal intensity (*arrow*). (**d**) Coronal fat-suppressed contrast-enhanced T1-weighted MR image demonstrates heterogeneous enhancement (*arrow*)

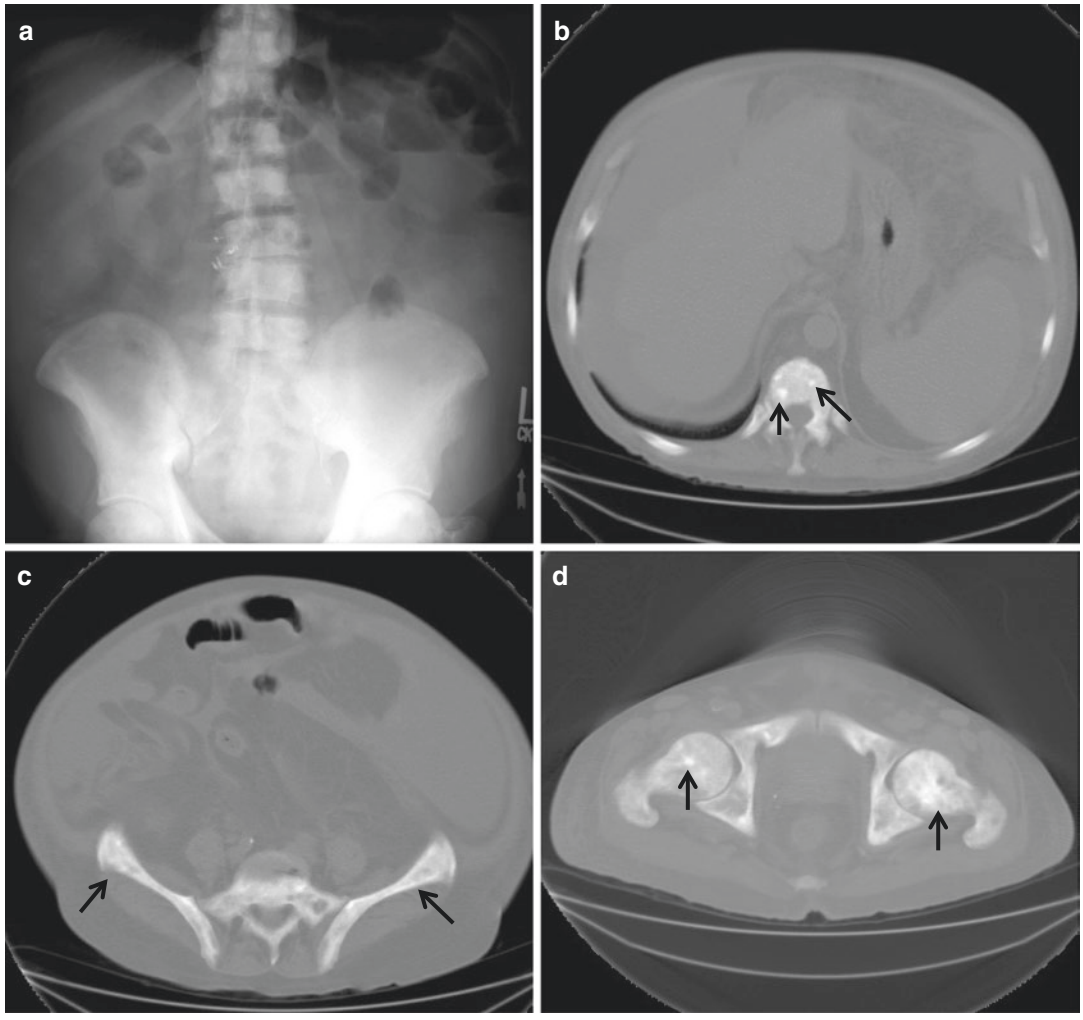

Fig. 10.4 Mastocytosis. (**a**) Anteroposterior radiograph of the abdomen shows multiple sclerotic lesions in the bony pelvis as well as the spinal column. (**b**–**d**) Axial CT scans show sclerotic foci in the vertebral body, bony pelvis, and bilateral femurs (*arrows*)

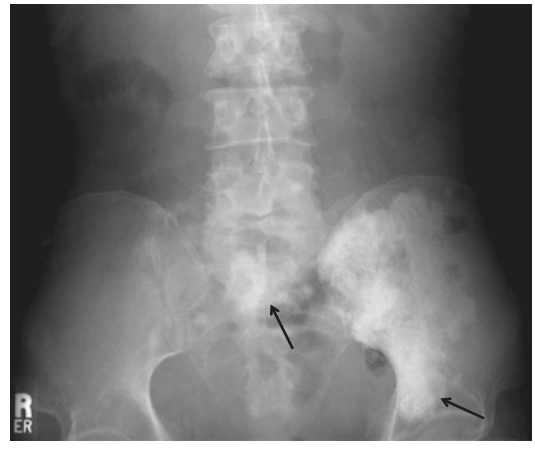

Fig. 10.5 POEMS syndrome (polyneuropathy, organomegaly, endocrinopathy, monoclonal gammopathy, and skin changes). Anteroposterior radiograph of the pelvis shows multiple sclerotic lesions in the left hemipelvis and sacrum (*arrows*)

10.2 Bone-Forming Surface Lesions

Osteoid osteoma is most commonly localized within the cortex of the bone, and is surrounded by thick sclerotic reactive bone. Osteoblastoma is most commonly located within the cancellous bone and characteristically does not demonstrate extensive reactive bone formation. Occasionally, osteoid osteoma and osteoblastoma may occur on the surface of the bone. The two conditions may overlap and may be described as either osteoid osteoma or osteoblastoma.

Parosteal osteoma has been used to describe a benign compact bone-forming lesion arising from the periosteum, and appears as a well-circumscribed dense, rounded, or lobulated mass with no associated soft tissue masses on radiographs. Parosteal osteomas have intensely homogeneous sclerotic appearance.

In contrast, parosteal osteosarcoma (Fig. 10.6) may show a zone of decreased density at the periphery and usually appears less dense and homogeneous than parosteal osteoma. However, radiographically, parosteal osteoma and parosteal osteosarcoma may have indistinguishable features.

Periosteal osteosarcoma is fusiform and firmly attached to the surface of the bone without a cleavage line. Periosteal osteosarcoma may erode and permeate the outer cortex. The lesion is covered by periosteum and demonstrates spiculated perpendicular periosteal reaction.

High-grade surface osteosarcoma usually arises on the surface of the bone along the midshaft and usually does not invade the medullary cavity.

Fig. 10.6 Parosteal osteosarcoma. (**a**) Anteroposterior radiograph of the right knee shows a juxtacortical ossific mass (*arrow*) in the right distal femur. (**b**) Lateral radiograph shows a juxtacortical ossific mass (*arrow*), which is separated by a radiolucent cleavage plane from the remaining cortical bone. (**c**) Axial T1-weighted MR image shows a lobulated and exophytic juxtacortical mass with heterogeneous signal intensity (*arrow*). (**d**) Axial T2-weighted fat-suppressed MR image demonstrates slightly increased signal intensity in the juxtacortical ossific mass (*arrow*)

10.3 Geographical Osteolytic Lesion, Sclerotic Border, No Intralesional Matrix

Lesions described as geographical show comparatively slow rates of growth and are typically less aggressive. These lesions may be subcategorized based on the radiographic appearance of their margins. Geographical osteolytic lesions with a sclerotic border show the slowest rate of growth and are generally considered benign. The slow rate of growth allows time for osteoblasts to form the reactive sclerotic rim that defines this category of lesions. Geographical osteolytic lesions with a sclerotic border and no intralesional matrix include subchondral cyst (Fig. 10.7), nonossifying fibroma, simple bone cyst (Fig. 10.8), Brodie abscess, intraosseous ganglion, intraosseous lipoma, and liposclerosing myxofibrous tumor (Fig. 10.9).

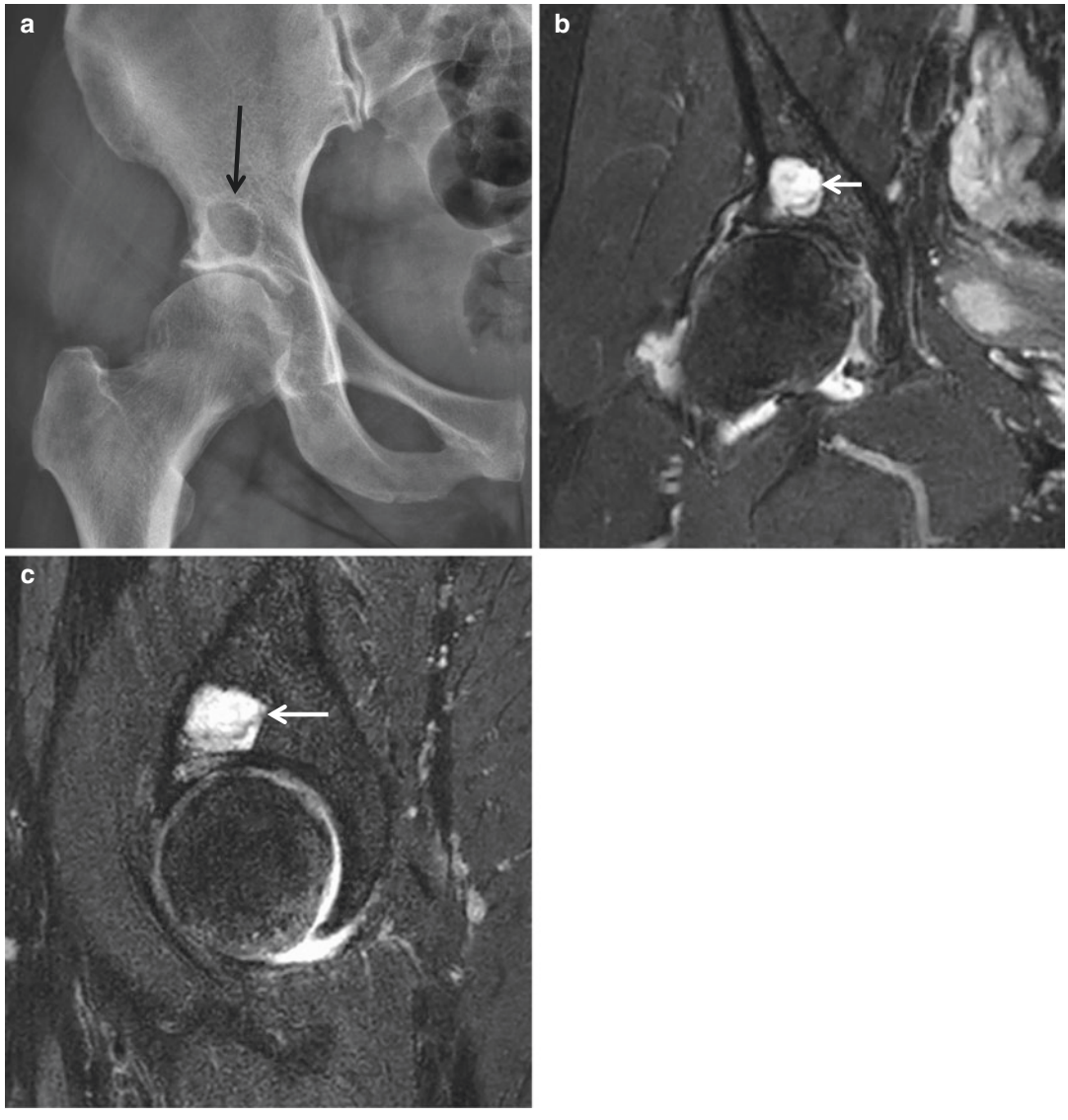

Fig. 10.7 Subchondral cyst. (**a**) Anteroposterior radiograph of the pelvis shows a well-defined radiolucent lesion (*arrow*) in the right supra-acetabular region. (**b**) Coronal fat-suppressed proton density-weighted MR image shows a periarticular cystic lesion (*arrow*). (**c**) Sagittal fat-suppressed proton density-weighted MR image again demonstrates a periarticular cystic lesion (*arrow*)

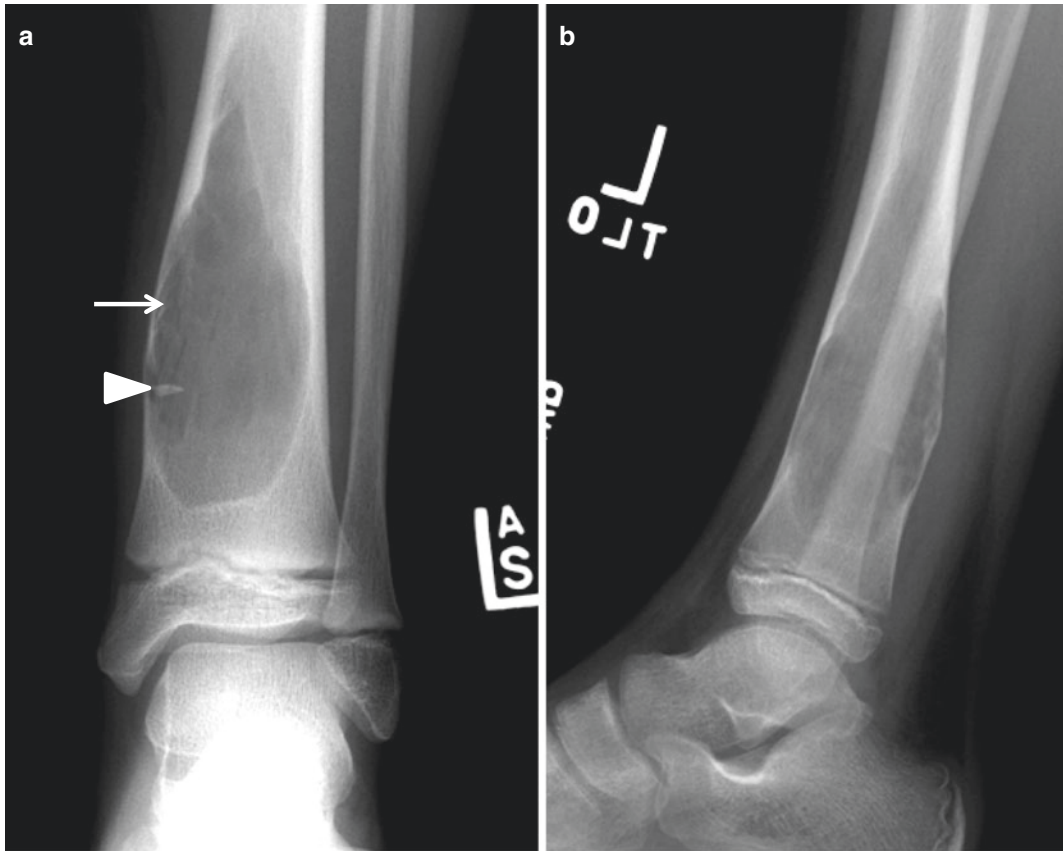

Fig. 10.8 Simple bone cyst. (**a**) Anteroposterior radiograph of the left lower leg shows a well-defined geographical osteolytic lesion (*arrow*) with a thin sclerotic rim and fallen fragment sign (*arrowhead*). (**b**) Lateral radiograph again shows a well-defined geographical osteolytic lesion with no matrix calcification

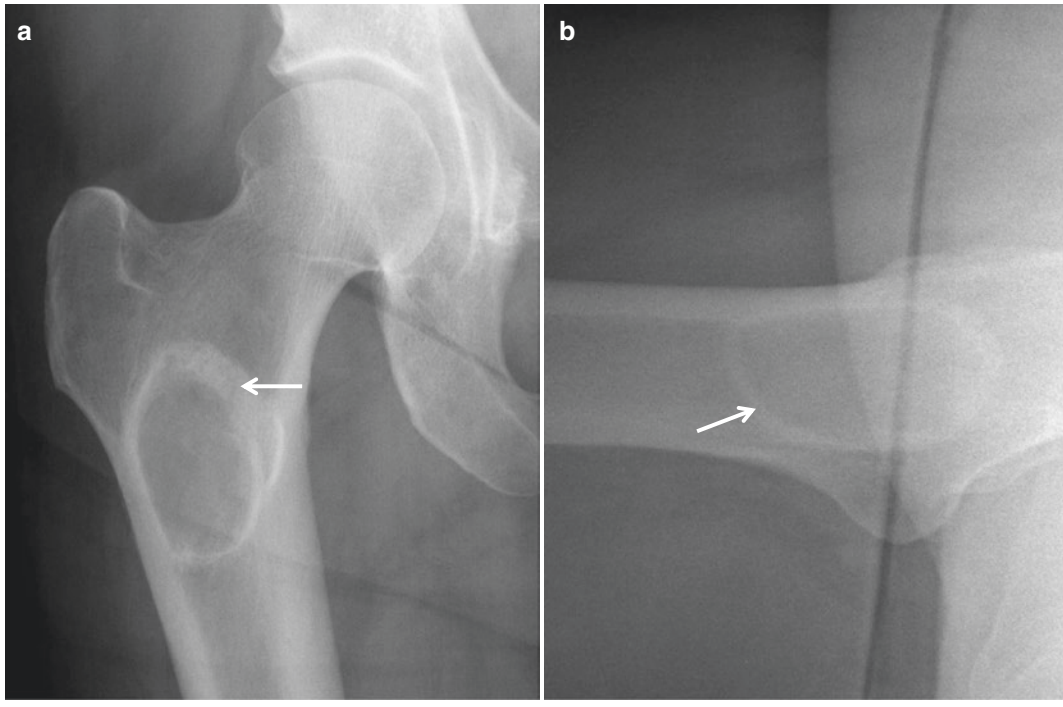

Fig. 10.9 Liposclerosing myxofibrous tumor. (**a**) antero-posterior and (**b**) translateral radiographs of the right hip show a well-defined geographic osteolytic lesion (*arrow*) with thick sclerotic rim. No mineralized matrix is noted within the lesion

10.4 Geographical, Osteolytic Lesion, No Sclerotic Border, No Intralesional Matrix

Trabeculae in normal unaffected bone may be seen extending to the edge of the lytic lesion, and the tumor cells rarely extend beyond this margin. Accordingly, these lesions are best detected in areas of cancellous bone because of the contrast provided by the adjacent trabeculae. If these lesions occur in the diaphysis, where the relative proportion of cancellous bone is lower, they may go undetected or show only endosteal scalloping. Examples of the geographical, osteolytic lesion with no sclerotic border and no intralesional matrix include benign lesion such as giant cell tumor (Fig. 10.10), Langerhans cell histiocytosis (Fig. 10.11), and fibrous dysplasia. However, the punched-out lesions of multiple myeloma (Fig. 10.12) and low-grade sarcoma may show similar appearance. Therefore, consideration of the patient's age and clinical presentation can help guide the differential diagnosis.

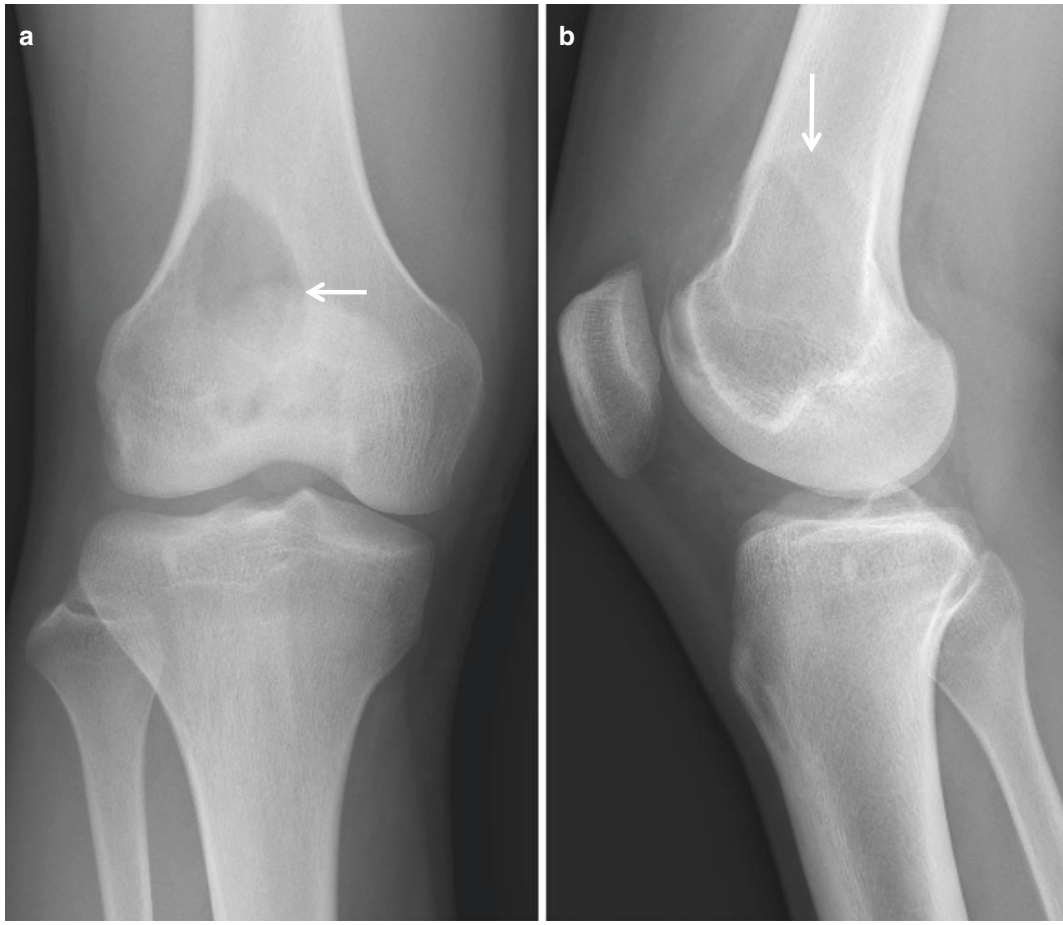

Fig. 10.10 Giant cell tumor. (**a**) Anteroposterior radiograph of the right knee shows an eccentric osteolytic lesion with a nonsclerotic well-defined border (*arrow*) at the metaepiphysis of the right distal femur. (**b**) Lateral radiograph demonstrates eccentric osteolytic lesion (*arrow*) with no periosteal reaction at the metaepiphysis of the right distal femur. No matrix mineralization is seen within the lesion

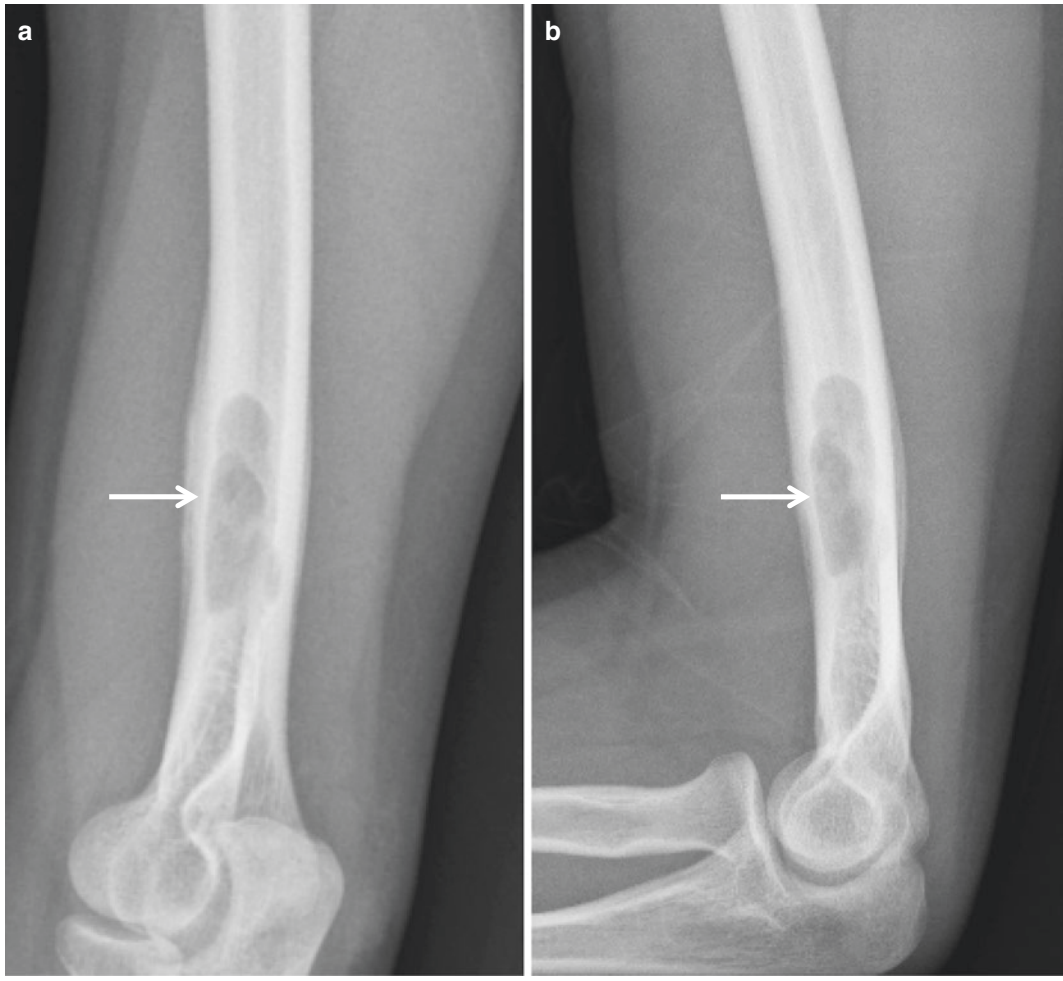

Fig. 10.11 Langerhans cell histiocytosis. (**a**) Oblique radiograph of the right humerus shows a well-defined osteolytic lesion (*arrow*) at an intramedullary location of the diaphysis with endosteal scalloping. (**b**) Lateral radiograph demonstrates a well-defined diaphyseal osteolytic lesion (*arrow*) with endosteal scalloping

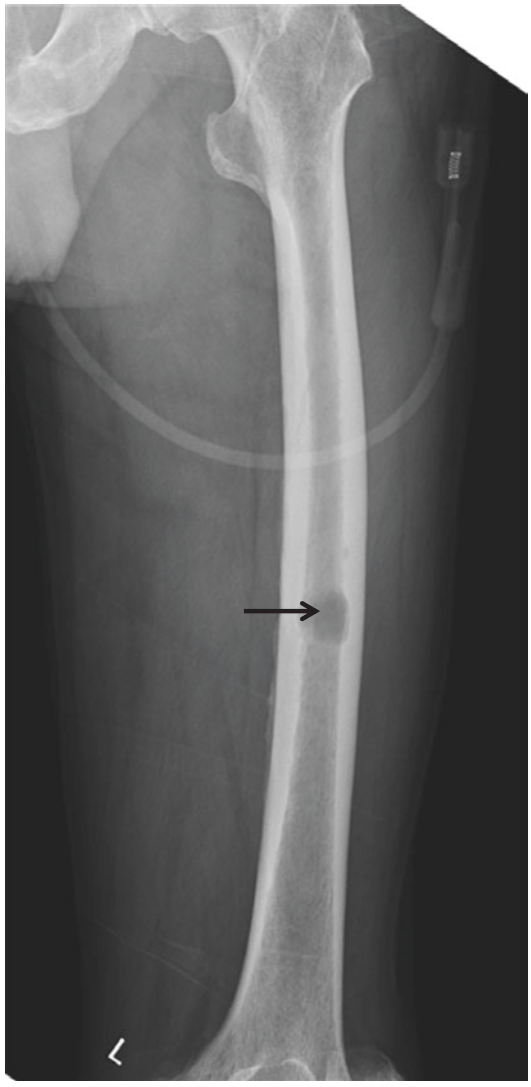

Fig. 10.12 Multiple myeloma. Anteroposterior radiograph of the left femur show an intramedullary well-defined diaphyseal osteolytic lesion (*arrow*) with endosteal scalloping

10.5 Expansive Osteolytic Lesion with Pseudotrabeculation (Soap-Bubble Appearance)

Bubbly lesions of bones are common findings on skeletal radiographs. Fibrous dysplasia, osteoblastoma, giant cell tumor, metastasis, myeloma, aneurysmal bone cyst, chondroblastoma, chondromyxoid fibroma, hyperparathyroidism, infection, nonossifying fibroma (Fig. 10.13), enchondroma, Langerhans cell histiocytosis, and simple bone cyst (Fig. 10.14) account for more than 95 % of the conditions that produce soap-bubble appearance.

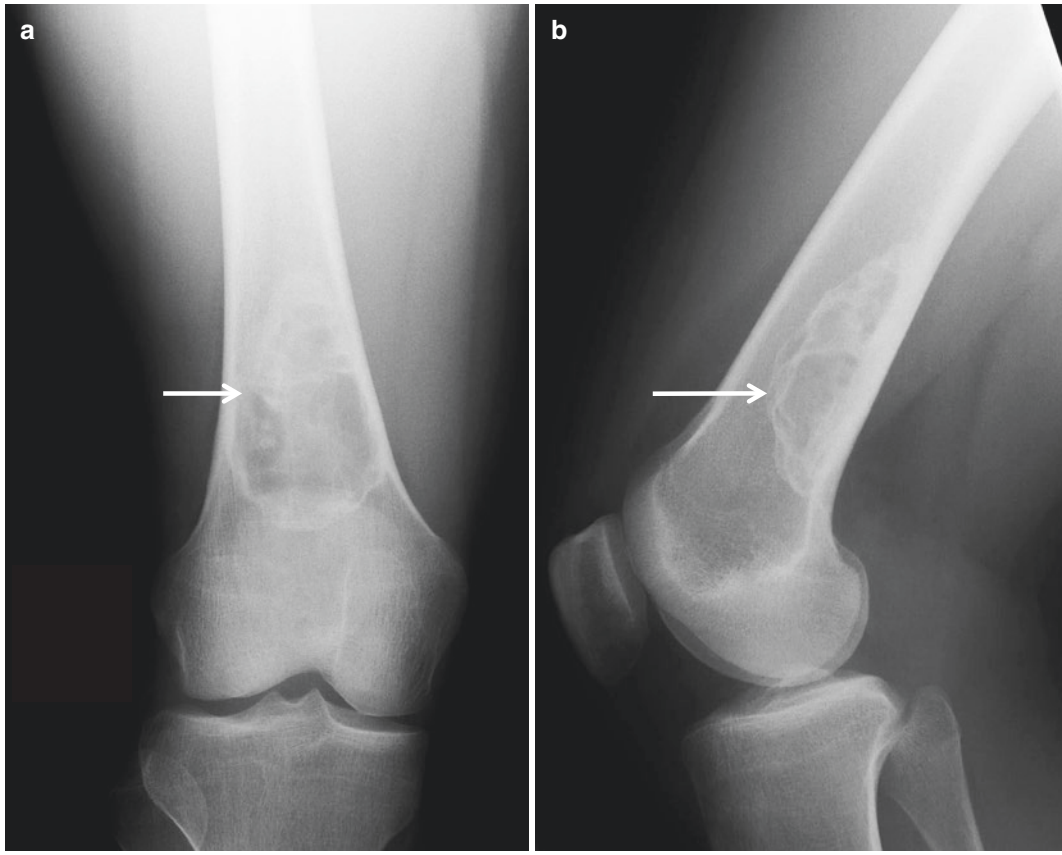

Fig. 10.13 Nonossifying fibroma. (**a**) Anteroposterior radiograph of the right knee shows a well-defined expansile bubbly geographical radiolucent lesion (*arrow*) with a sclerotic border. (**b**) Lateral radiograph demonstrates a well-defined cortically based bubbly radiolucent lesion (*arrow*)

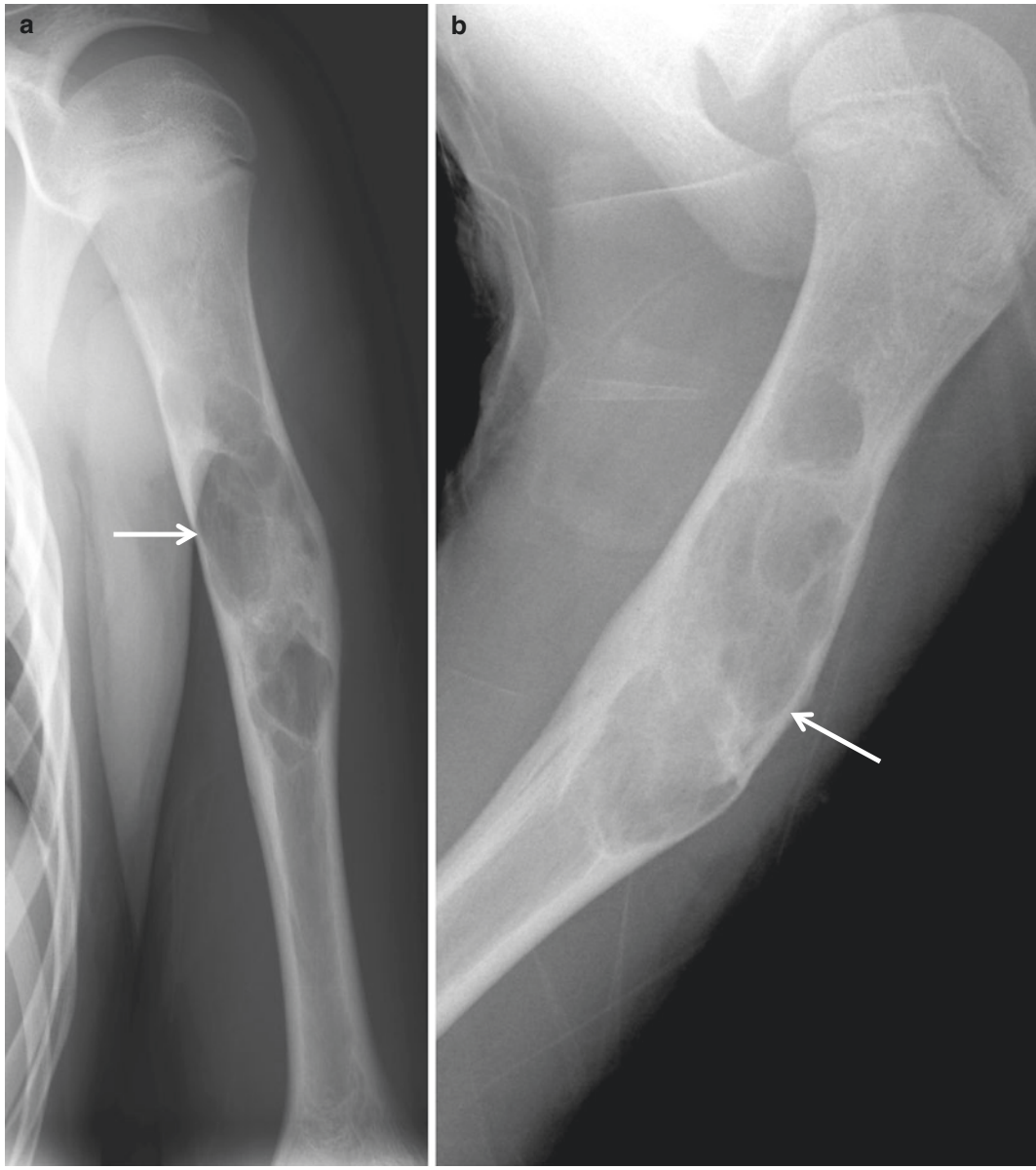

Fig. 10.14 Simple bone cyst. (**a**) Anteroposterior radiograph of the left humerus shows a well-defined expansile bubbly geographical radiolucent lesion (*arrow*) with osseous remodeling. (**b**) Lateral radiograph demonstrates a well-defined expansile bubbly radiolucent lesion (*arrow*) with osseous remodeling

10.6 Aggressive Osteolytic Lesions: Moth-Eaten/ Permeative Osteolytic Lesion

Aggressive pattern of bone destruction characterized by multiple small holes of varying sizes is coined moth-eaten. The multiple small lucencies combine to form a larger mass with poorly defined margins and a wide zone of transition. The lucent defects are frequently ovoid and parallel the long axis of the bone, measuring 2–5 mm in diameter. This pattern represents greater biological activity, with tumor cells infiltrating rapidly among normal cancellous trabeculae and resulting in indistinct endosteal scalloping. Pathologically, tumor frequently extends beyond the visible radiographic margins. Examples of moth-eaten lesions include metastasis, osteosarcoma (Fig. 10.15), multiple myeloma (Fig. 10.16), chondrosarcoma, lymphoma, osteomyelitis, and occasionally, Langerhans cell histiocytosis and giant cell tumor.

The permeative radiographic pattern is characterized by numerous small, <1 mm, and oval lucencies of relatively uniform morphology or lucent bands within the cortical bone, indicating the most aggressive pattern of bone destruction. The coalescent mass is poorly defined, with wide zones of transition. This pattern often denotes cortical destruction, and cross-sectional imaging frequently reveals an associated soft tissue mass. However, this pattern may be seen with osteomyelitis, metabolic bone diseases such as hyperparathyroidism, rapidly progressive osteoporosis, and malignant conditions. Examples of malignant lesions of permeative osteolytic lesion include metastasis, multiple myeloma, lymphoma, Ewing's sarcoma, osteosarcoma, and high-grade chondrosarcoma.

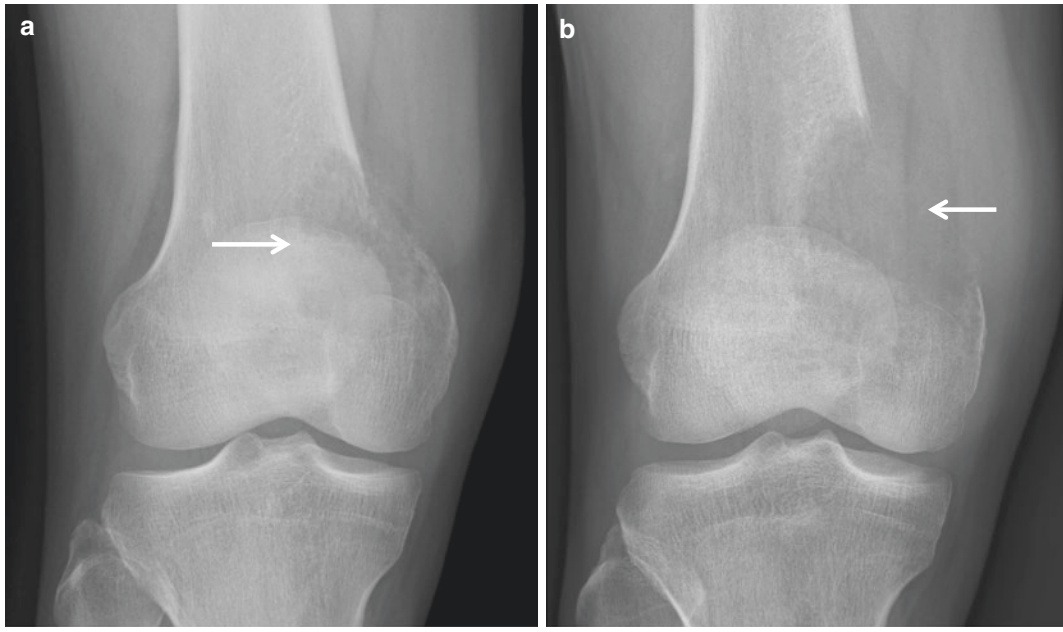

Fig. 10.15 Osteosarcoma. (**a**) Anteroposterior radiograph of the left knee shows an eccentric moth-eaten lesion (*arrow*) in the metaphysis of the right distal femur with interrupted periosteal reaction and cortical breaching. (**b**) One-month follow-up anteroposterior radiograph shows increased radiolucency (*arrow*) with progressive cortical destruction

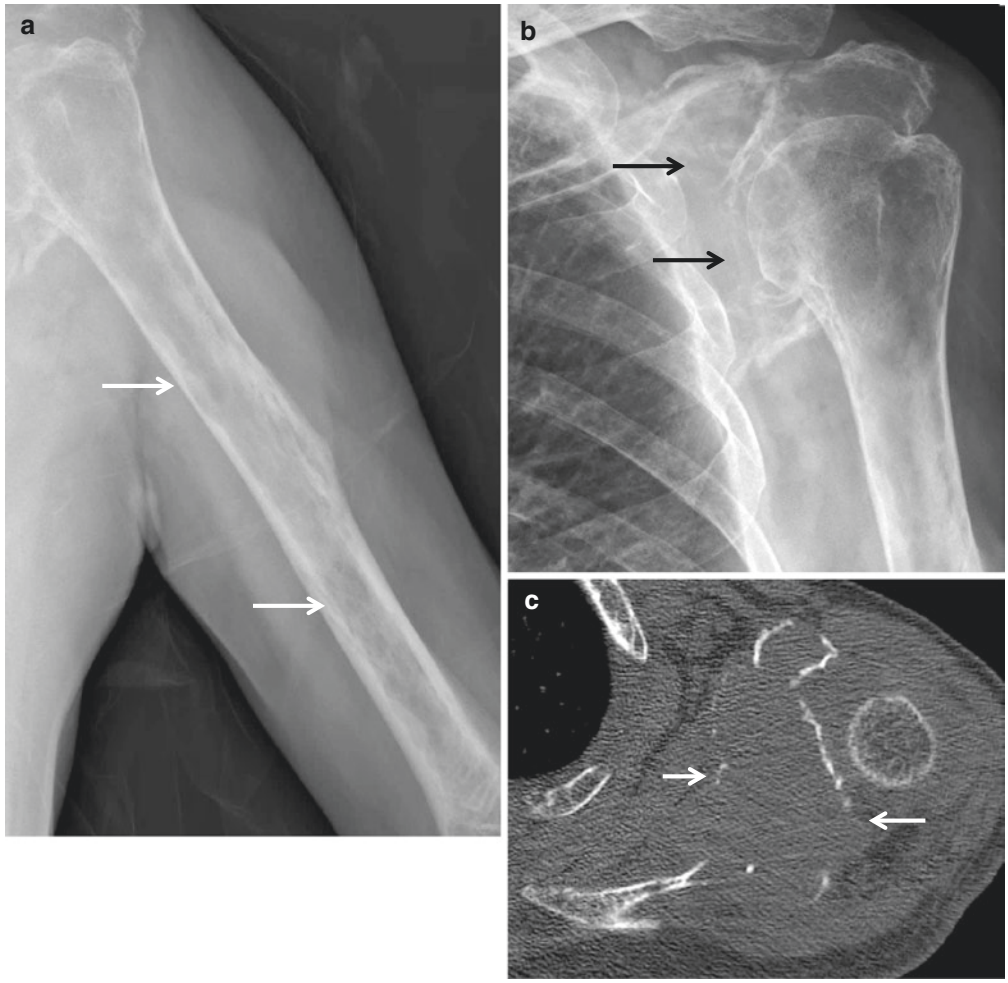

Fig. 10.16 Multiple myeloma. (**a**) Anteroposterior radiograph of the left humerus shows diffuse moth-eaten lesions (*arrows*) in the left humerus. (**b**) Anteroposterior radiograph of the left shoulder shows expansile moth-eaten lesion (*arrows*) in the left scapula. (**c**) Corresponding axial CT scan demonstrates expansile osteolytic lesion (*arrows*) in the left scapula

10.7 Mixed Lytic and Sclerotic Lesions

Osteoblastomas have variable radiographic presentation from purely lytic to mixed and sclerotic. The most common pattern of conventional osteosarcoma is mixed lytic and sclerotic lesion. Osseous metastases (Fig. 10.17) may present as lucent or sclerotic lesions. Fibrous dysplasia can present as either a lytic or a sclerotic lesion. Osteomyelitis has a wide variety of appearances, and can present as mixed lucency and sclerosis.

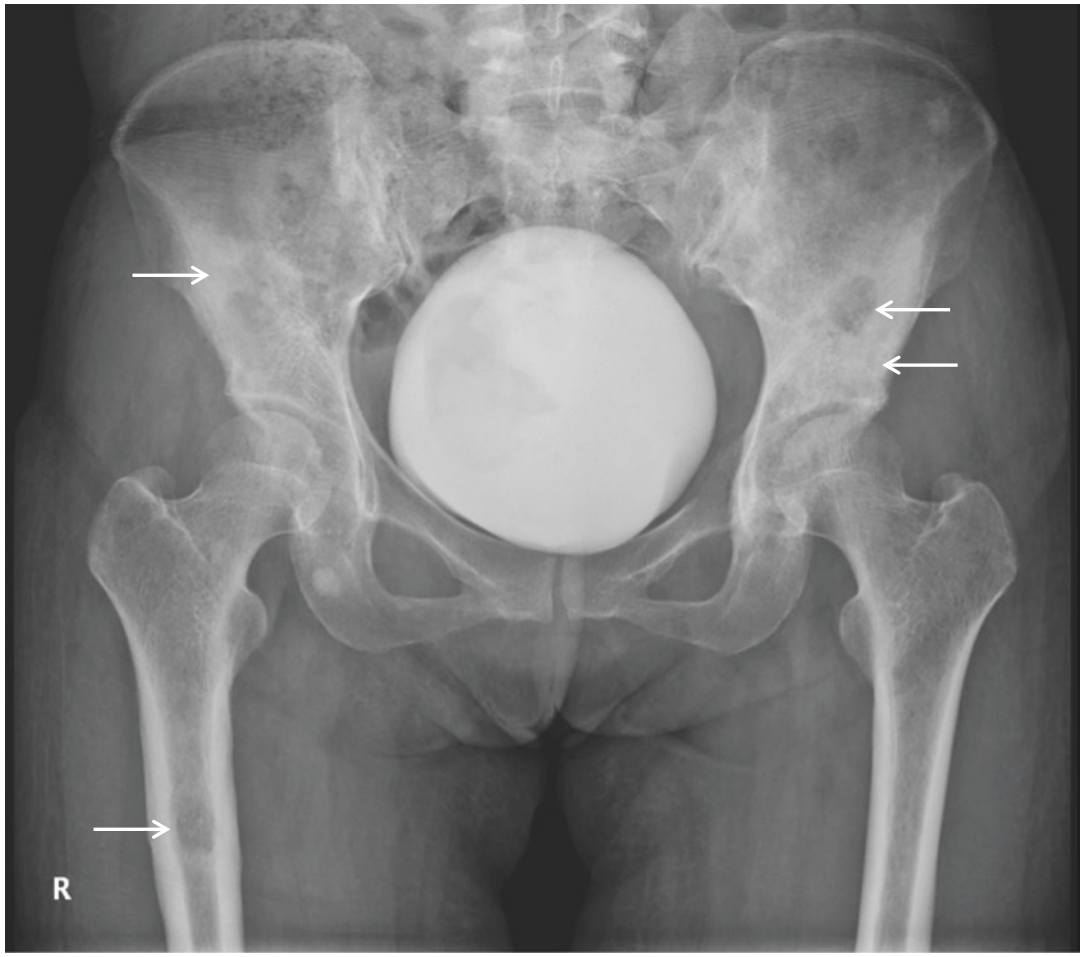

Fig. 10.17 Metastasis. Anteroposterior radiograph of the pelvis shows diffuse scattered mixed scattered lytic and sclerotic lesions (*arrows*) in the bony pelvis and the right proximal femur

10.8 Chondroid Matrix

Chondroid matrix is seen in lesions comprised of chondrocyte proliferation. The radiographic appearance can be described as ring-and-arc, punctate, curved, stippled, or coarser flocculent foci of calcification. The radiographic presence of chondroid matrix implies mature cartilage production; however, this may be seen in both benign and malignant lesions (Fig. 10.18). A benign enchondroma may be radiographically identical to a low-grade chondrosarcoma in the absence of aggressive features such as cortical destruction and soft tissue extension.

The location of the chondroid matrix within the bone and the age of the patient help narrow the differential diagnosis. A chondroid lesion in the epiphysis of a pediatric patient is almost certainly a chondroblastoma, whereas the same lesion in the third or fourth decades of life may represent a clear cell chondrosarcoma. An intramedullary lesion in the metaphysis of an adult patient may represent an enchondroma or chondrosarcoma. Occasionally, chondroid matrix may be occult on radiographs. A CT scan affords greater sensitivity for the detection of intralesional calcifications.

Fig. 10.18 Enchondroma and chondrosarcoma. (**a**) Enchondroma shows stippling, rings-and-arcs calcification (*arrow*). (**b**) Chondrosarcoma, grade 1, shows chondroid matrix (*arrow*) indistinguishable from that of an enchondroma. (**c**) Chondrosarcoma, grade 2, shows chondroid matrix with geographical pattern of destruction and cortical breaching (*arrow*). (**d**) Chondrosarcoma, grade 3, shows chondroid matrix with more aggressive bone destruction (*arrow*)

10.9 Osteoid Matrix

The matrix of a bone lesion refers to the acellular material produced by the mesenchymal cells composing the lesion. Although many bone lesions produce no matrix, its presence can indicate the predominant cell type of the lesion. An osseous matrix is the result of abnormal osteoid production by tumor cells. It is often described as amorphous, fluffy, cloud-like, solid, cotton-like, or ivory-like on radiographs. It appears as homogeneously increased density within the bone and adjacent soft tissues. The prototype lesion with an osseous matrix is osteosarcoma (Fig. 10.19). Osteosarcoma should be strongly considered if irregular, not fully mineralized, bone matrix (Fig. 10.20) is identified on the radiograph, as well as if cloud-like densities in the medullary cavity and neighboring soft tissue can be discerned.

In contrast, osteoblastomas have a variable radiographic presentation from purely lytic to mixed and sclerotic. This is explained by the histological evidence that the osteoid produced by osteoblastomas is occasionally not mineralized by calcium hydroxyapatite and other inorganic salts. The nidus of osteoid osteoma shows variable degrees of mineralization, often only appreciated on a CT scan.

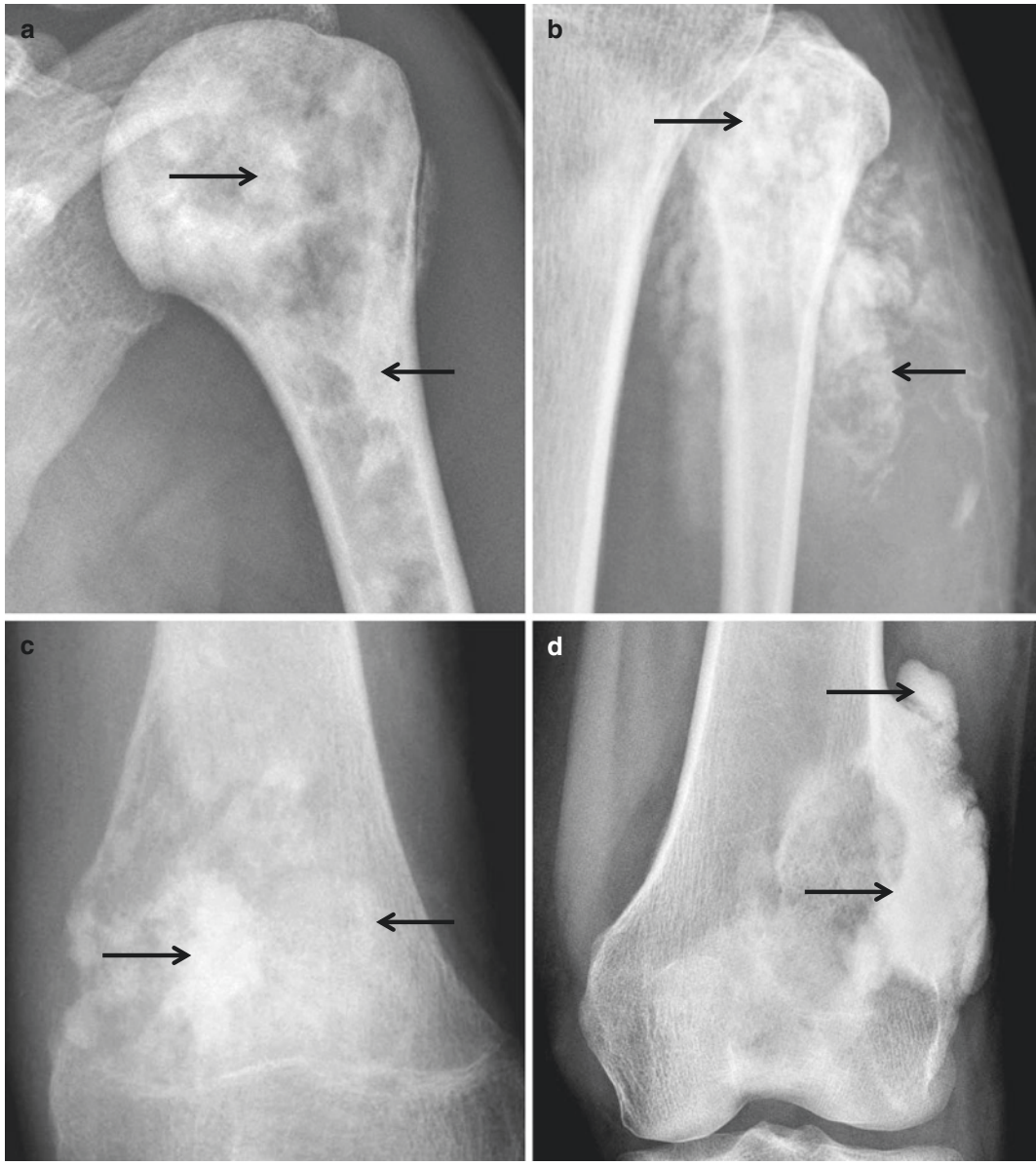

Fig. 10.19 Osteosarcoma. (**a**) Anteroposterior radiograph of the left humerus shows amorphous matrix calcification (*arrows*). (**b**) Anteroposterior radiograph of the left lower leg shows fluffy matrix calcification (*arrows*). (**c**) Anteroposterior radiograph of the left knee shows solid and cotton-like matrix calcification (*arrows*). (**d**) Anteroposterior radiograph of the left knee shows ivory-like matrix calcification (*arrows*)

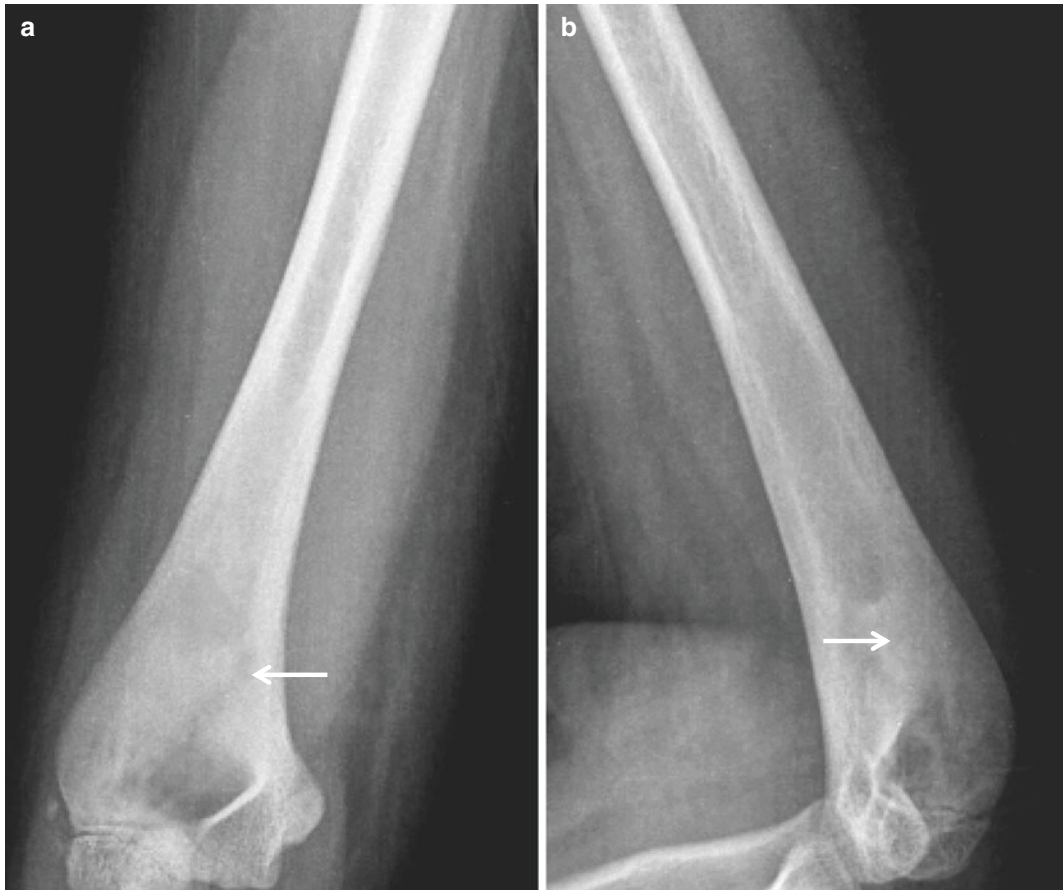

Fig. 10.20 Osteosarcoma. (**a**) Anteroposterior radiograph of the left humerus shows amorphous osseous mineralization (*arrow*) with expansile remodeling of bone. (**b**) Lateral radiographs show area of osseous mineralization (*arrow*) with remodeling of bone. Histopathology showed a well-differentiated osteosarcoma mimicking fibrous dysplasia

10.10 Pedunculated or Sessile Bony Excrescences

Osteochondroma may have either a broad sessile (Fig. 10.21) or a pedunculated stalk. The diagnostic feature of osteochondroma is corticomedullary continuity of a juxtacortical bone lesion with the adjacent bone, with or without a hyaline cartilage cap.

Mature bizarre parosteal osteochondromatous proliferation appears to be attached to the adjacent bone with a pedunculated or sessile base with no communication to the medullary cavity.

Subungual exostosis is a reactive nonneoplastic growth characterized by proliferating fibroblasts and cartilage metaplasia, which progresses to mature ossification. Subungual exostosis may show pedunculated ossific mass without corticomedullary continuity to the underlying bone.

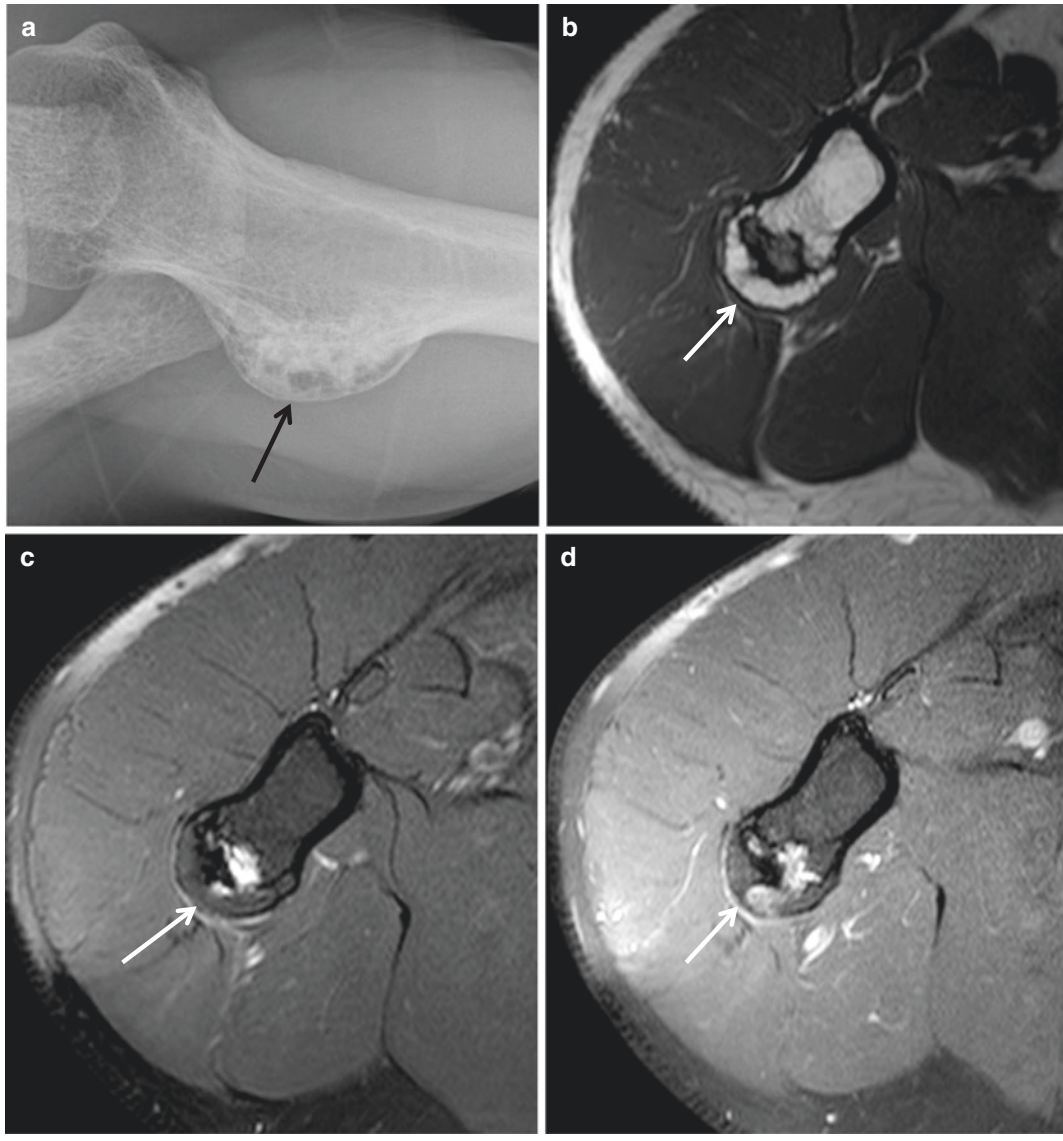

Fig. 10.21 Osteochondroma. (**a**) Axillary radiograph of the right humerus shows sessile osteochondroma (*arrow*). (**b**) Axial T1-weighted MR image shows a broad-based osseous protrusion (*arrow*) with internal low signal intensity. (**c**) Axial T2-weighted fat-suppressed MR image shows a broad-based osseous protrusion (*arrow*) with hyperintense areas. (**d**) Axial fat-suppressed contrast-enhanced T1-weighted MR image shows a broad-based osseous protrusion (*arrow*) with areas of nodular enhancement

10.11 Juxtacortical Lesions

The term "juxtacortical" is flexible and is applied to surface lesions of extracortical origin. Since in some lesions, the point of origin cannot be determined, the term "juxtacortical" is the most appropriate. A surface lesion of bone refers to an entity that arises within or on a portion of the bone that is external to the medullary cavity. However, the terminology can be confusing, and the terms parosteal and juxtacortical are used interchangeably by some authors.

An endosteal lesion is one that originates within the inner cortex of the bone, adjacent to the medullary cavity. An intracortical lesion is centered within the cortex. Cortical lesions (Fig. 10.22) should be included in the differential diagnosis of surface lesions, because they may break through the cortex to involve the subperiosteal space.

Subperiosteal process begins immediately beneath the periosteum and separates the periosteum from the cortex, resulting in subperiosteal bone formation. Most of subperiosteal lesions are not neoplastic. Traumatic lesions should be considered in the differential diagnosis of a juxtacortical lesion, especially in the young or athletic individual, as the posttraumatic reparative processes are the most frequent etiologies of the nonneoplastic conditions.

Periosteal lesions (Fig. 10.22) are defined as processes which originate from the deep layer of the periosteum. Periosteal lesions are firmly attached to the cortex with no cleavage line. In indolent lesions, such as periosteal chondroma, the peripheral periosteal reaction produces a solid wedge-shaped reaction (buttress). In aggressive lesions (Fig. 10.23), such as periosteal osteosarcoma, the peripheral periosteal reaction is lamellated.

Parosteal lesions are defined as processes which originate from the outer fibrous layer of the periosteum. These lesions are separated from the cortex by a thin radiolucent periosteal membrane; therefore, they do not elevate the cambium layer and do not demonstrate peripheral periosteal reaction.

Fig. 10.22 Osteoid osteoma. (**a**) Sagittal reformatted CT scan shows centrally calcified nidus (*arrow*) in the endosteal and intracortical location. (**b**) Additional sagittal reformatted CT scan shows a second nidus (*arrow*) in the periosteal or subperiosteal location. (**c**) Axial CT scan shows centrally calcified nidus (*arrow*) in the endosteal and intracortical location. (**d**) Additional axial CT scan shows a second nidus (*arrow*) in the periosteal or subperiosteal location

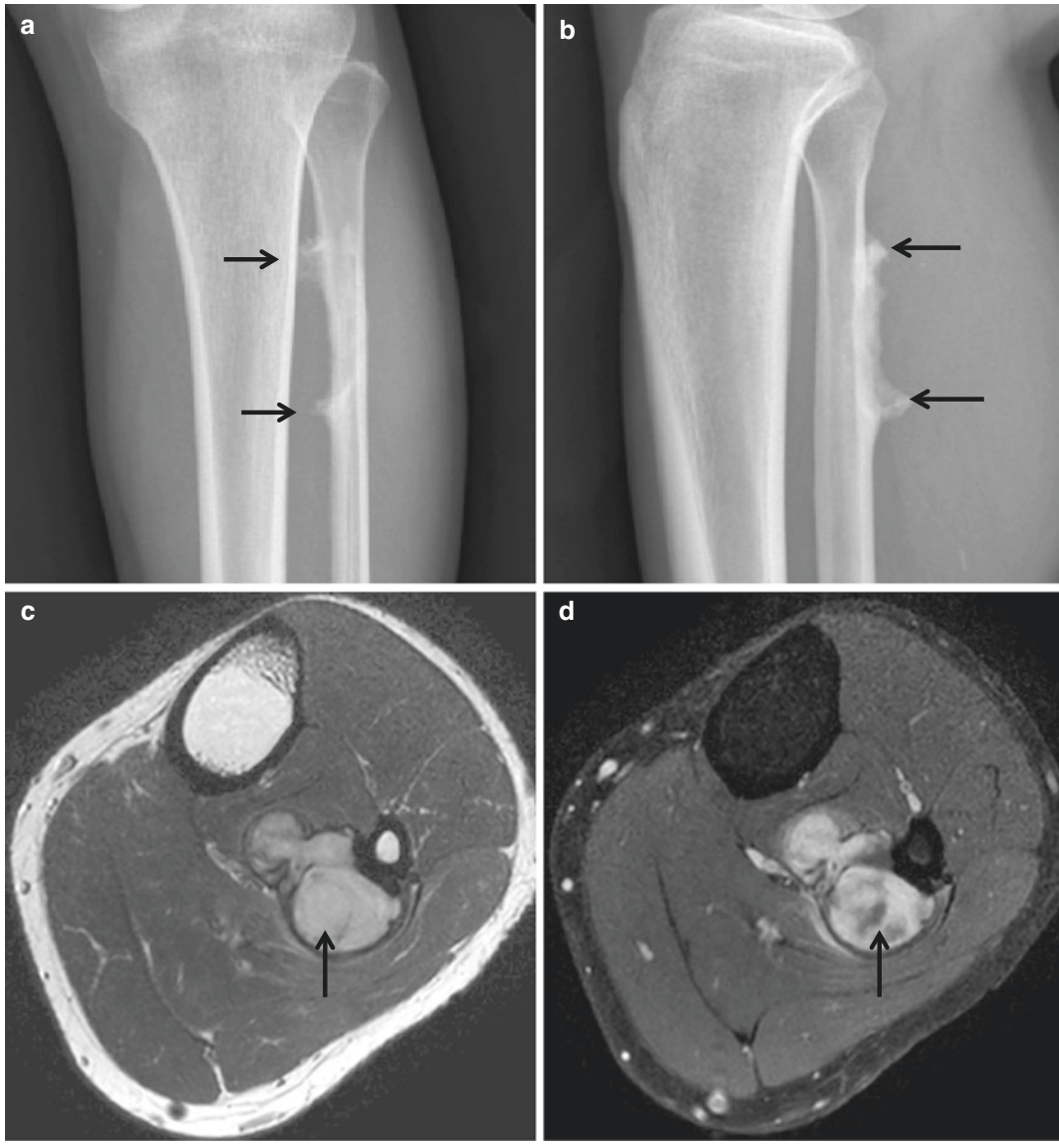

Fig. 10.23 Low-grade sarcoma. (**a**) Anteroposterior radiograph of the left lower leg shows ossific surface lesion with areas of perpendicular periosteal reaction (*arrows*). (**b**) Lateral radiograph again shows ossific surface lesion (*arrows*). Also noted is striated mineralization perpendicular to the cortex. (**c**) Axial T2-weighted MR image demonstrates a juxtacortical mass with high signal intensity (*arrow*). (**d**) Axial fat-suppressed contrast-enhanced T1-weighted MR image demonstrates an enhancing juxtacortical mass (*arrow*). Histopathology showed a low-grade sarcoma

References

Intramedullary Sclerotic Bone Lesions

Currie JW, Davis KW, Lafita VS, Blankenbaker DG, De Smet AA, Rosas H, Lee KS. Musculoskeletal mnemonics: differentiating features. Curr Probl Diagn Radiol. 2011;40:45–71.
Nichols RE, Dixon LB. Radiographic analysis of solitary bone lesions. Radiol Clin N Am. 2011;49:1095–114.

Bone-Forming Surface Lesions

Currie JW, Davis KW, Lafita VS, Blankenbaker DG, De Smet AA, Rosas H, Lee KS. Musculoskeletal mnemonics: differentiating features. Curr Probl Diagn Radiol. 2011;40:45–71.
Kenan S, Abdelwahab IF, Klein MJ, Hermann G, Lewis MM. Lesions of juxtacortical origin (surface lesions of bone). Skelet Radiol. 1993;22:337–57.
Kransdorf MJ, Murphey MD. Osseous tumors. In: Davies AM, Sundaram M, James SLJ, editors. Imaging of bone tumors and tumor-like lesions: techniques and applications. 1 ed. Berlin: Springer; 2009. p. 251–306.
Nichols RE, Dixon LB. Radiographic analysis of solitary bone lesions. Radiol Clin N Am. 2011;49:1095–114.
Seeger LL, Yao L, Eckardt JJ. Surface lesions of bone. Radiology. 1998;206:17–33.
Sundaram M, Falbo S, McDonald D, Janney C. Surface osteomas of the appendicular skeleton. AJR Am J Roentgenol. 1996;167:1529–33.

Geographic Osteolytic Lesion, Sclerotic Border, No Intralesional Matrix

Caracciolo JT, Temple HT, Letson GD, Kransdorf MJ. A modified Lodwick-Madewell grading system for the evaluation of lytic bone lesions. AJR Am J Roentgenol. 2016;207:150–6.
Cerase A, Priolo F. Skeletal benign bone-forming lesions. Eur J Radiol. 1998;27:S91–7.
Currie JW, Davis KW, Lafita VS, Blankenbaker DG, De Smet AA, Rosas H, Lee KS. Musculoskeletal mnemonics: differentiating features. Curr Probl Diagn Radiol. 2011;40:45–71.
Lodwick GS. Radiographic diagnosis and grading of bone tumors, with comments on computer evaluation. Proc Natl Cancer Conf. 1964;5:369–80.
Nichols RE, Dixon LB. Radiographic analysis of solitary bone lesions. Radiol Clin N Am. 2011;49:1095–114.
Priolo F, Cerase A. The current role of radiography in the assessment of skeletal tumors and tumor-like lesions. Eur J Radiol. 1998;27:S77–85.

Geographic, Osteolytic Lesion, No Sclerotic Border, No Intralesional Matrix

Caracciolo JT, Temple HT, Letson GD, Kransdorf MJ. A modified Lodwick-Madewell grading system for the evaluation of lytic bone lesions. AJR Am J Roentgenol. 2016;207:150–6.
Cerase A, Priolo F. Skeletal benign bone-forming lesions. Eur J Radiol. 1998;27:S91–7.
Currie JW, Davis KW, Lafita VS, Blankenbaker DG, De Smet AA, Rosas H, Lee KS. Musculoskeletal mnemonics: differentiating features. Curr Probl Diagn Radiol. 2011;40:45–71.
Lodwick GS. Radiographic diagnosis and grading of bone tumors, with comments on computer evaluation. Proc Natl Cancer Conf. 1964;5:369–80.
Nichols RE, Dixon LB. Radiographic analysis of solitary bone lesions. Radiol Clin N Am. 2011;49:1095–114.
Priolo F, Cerase A. The current role of radiography in the assessment of skeletal tumors and tumor-like lesions. Eur J Radiol. 1998;27:S77–85.

Expansive Osteolytic Lesion with Pseudotrabeculation (Soap-Bubble Appearance)

Currie JW, Davis KW, Lafita VS, Blankenbaker DG, De Smet AA, Rosas H, Lee KS. Musculoskeletal mnemonics: differentiating features. Curr Probl Diagn Radiol. 2011;40:45–71.
Eisenberg RL. Bubbly lesions of bone. AJR Am J Roentgenol. 2009;193:W79–94.
Nichols RE, Dixon LB. Radiographic analysis of solitary bone lesions. Radiol Clin N Am. 2011;49:1095–114.

Aggressive Osteolytic Lesions: Moth-Eaten/Permeative Osteolytic Lesion

Caracciolo JT, Temple HT, Letson GD, Kransdorf MJ. A modified Lodwick-Madewell grading system for the evaluation of lytic bone lesions. AJR Am J Roentgenol. 2016;207:150–6.

Currie JW, Davis KW, Lafita VS, Blankenbaker DG, De Smet AA, Rosas H, Lee KS. Musculoskeletal mnemonics: differentiating features. Curr Probl Diagn Radiol. 2011;40:45–71.
Lodwick GS. Radiographic diagnosis and grading of bone tumors, with comments on computer evaluation. Proc Natl Cancer Conf. 1964;5:369–80.
Nichols RE, Dixon LB. Radiographic analysis of solitary bone lesions. Radiol Clin N Am. 2011;49:1095–114.

Mixed Lytic and Sclerotic Lesions

Currie JW, Davis KW, Lafita VS, Blankenbaker DG, De Smet AA, Rosas H, Lee KS. Musculoskeletal mnemonics: differentiating features. Curr Probl Diagn Radiol. 2011;40:45–71.
Nichols RE, Dixon LB. Radiographic analysis of solitary bone lesions. Radiol Clin N Am. 2011;49:1095–114.

Chondroid Matrix

Currie JW, Davis KW, Lafita VS, Blankenbaker DG, De Smet AA, Rosas H, Lee KS. Musculoskeletal mnemonics: differentiating features. Curr Probl Diagn Radiol. 2011;40:45–71.
Nichols RE, Dixon LB. Radiographic analysis of solitary bone lesions. Radiol Clin N Am. 2011;49:1095–114.

Osteoid Matrix

Currie JW, Davis KW, Lafita VS, Blankenbaker DG, De Smet AA, Rosas H, Lee KS. Musculoskeletal mnemonics: differentiating features. Curr Probl Diagn Radiol. 2011;40:45–71.
Greenspan A, Borys D. Radiology and pathology correlation of bone tumors: a quick reference and review. 1 ed. Philadelphia: Wolters Kluwer; 2016. p. 1–31.
Nichols RE, Dixon LB. Radiographic analysis of solitary bone lesions. Radiol Clin N Am. 2011;49:1095–114.

Pedunculated or Sessile Bony Excrescences

Currie JW, Davis KW, Lafita VS, Blankenbaker DG, De Smet AA, Rosas H, Lee KS. Musculoskeletal mnemonics: differentiating features. Curr Probl Diagn Radiol. 2011;40:45–71.
Murphey MD, Choi JJ, Kransdorf MJ, Flemming DJ, Gannon FH. Imaging of osteochondroma: variants and complications with radiologic-pathologic correlation. Radiographics. 2000;20:1407–34.
Nichols RE, Dixon LB. Radiographic analysis of solitary bone lesions. Radiol Clin N Am. 2011;49:1095–114.
Seeger LL, Yao L, Eckardt JJ. Surface lesions of bone. Radiology. 1998;206:17–33.

Juxtacortical Lesions

Currie JW, Davis KW, Lafita VS, Blankenbaker DG, De Smet AA, Rosas H, Lee KS. Musculoskeletal mnemonics: differentiating features. Curr Probl Diagn Radiol. 2011;40:45–71.
Kenan S, Abdelwahab IF, Klein MJ, Hermann G, Lewis MM. Lesions of juxtacortical origin (surface lesions of bone). Skelet Radiol. 1993;22:337–57.
Nichols RE, Dixon LB. Radiographic analysis of solitary bone lesions. Radiol Clin N Am. 2011;49:1095–114.
Seeger LL, Yao L, Eckardt JJ. Surface lesions of bone. Radiology. 1998;206:17–33.

MRI Characteristics

11

Contents

11.1 Intralesional Feature

11.1.1 Fat-Containing Lesions

Imaging features of benign lipomatous lesions are often pathognomonic. Radiographs frequently reveal tissue with either diffuse or focal areas that are similar or identical to subcutaneous fat. These intrinsic features and lesion extent are best depicted with either CT or MR imaging.

Most bone lesions containing hyperintense fat signal on T1-weighted images are benign and include intraosseous lipoma (Fig. 11.1), hemangioma, parosteal lipoma, liposclerosing myxofibrous tumor, and nontumorous conditions such as medullary infarction.

The presence of focal normal fatty marrow or fat within a bone tumor is highly suggestive of a benign etiology. Osteosarcoma arising within a medullary infarct may have fat from the infarct and not within the osteosarcoma itself. Dedifferentiated chondrosarcoma or Paget sarcoma can show fat in the nonmalignant portion of the lesion.

H.S. Kang et al., *Oncologic Imaging: Bone Tumors*, DOI 10.1007/978-981-287-703-1_11

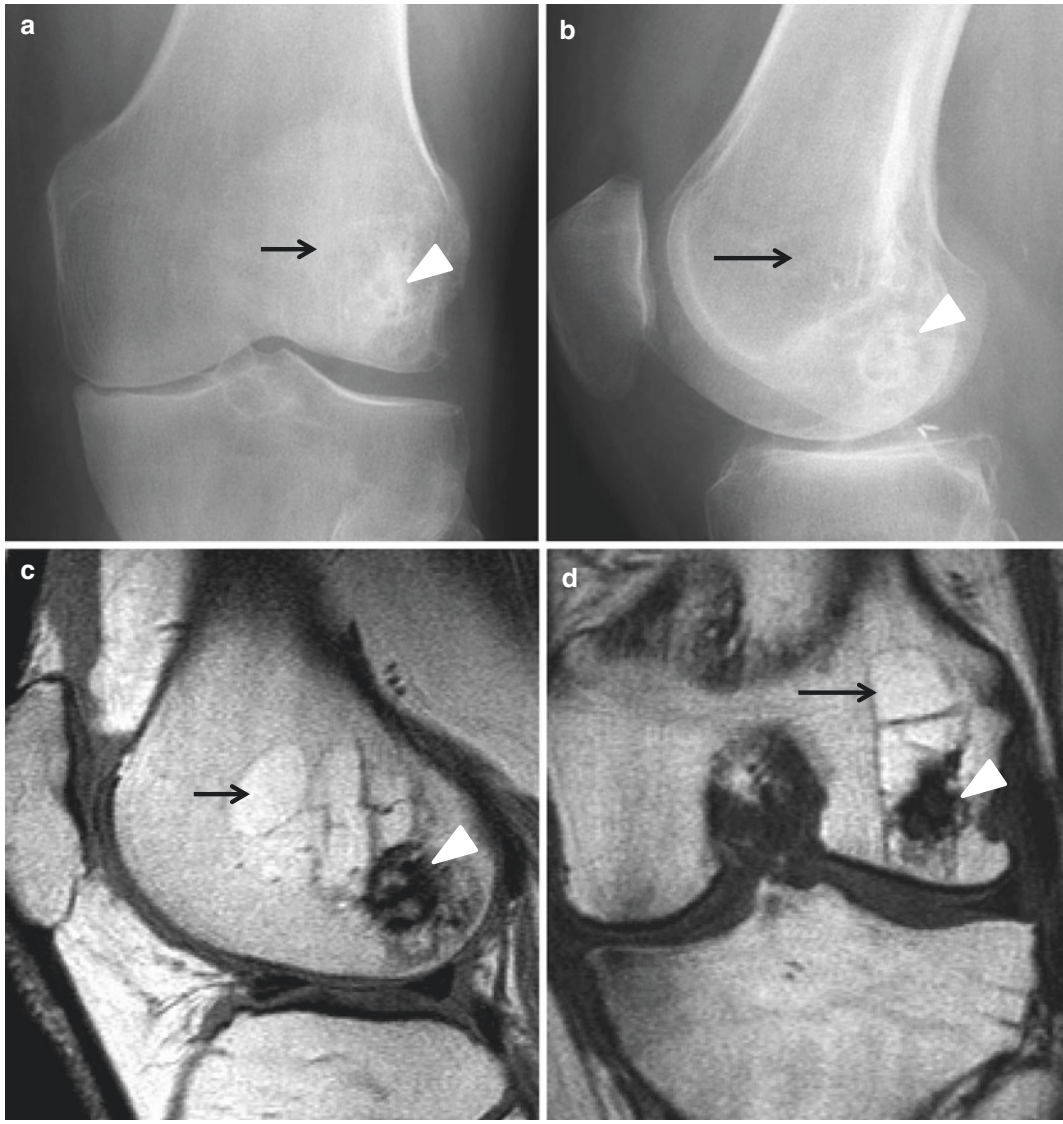

Fig. 11.1 Intraosseous lipoma. (**a**) Anteroposterior radiograph of the left knee shows an intramedullary radiolucent lesion (*arrow*) with thin sclerotic rim and foci of calcification (*arrowhead*) within the lesion. (**b**) Lateral radiograph again shows an intramedullary radiolucent lesion (*arrow*) with thin sclerotic rim and foci of calcification (*arrowhead*) within the lesion. (**c**) Sagittal proton density-weighted MR image demonstrates an intramedullary lesion (*arrow*) following the signal intensity of the fat, and foci of low signal intensity indicating calcification or ossification (*arrowhead*). (**d**) Coronal proton density-weighted MR image demonstrates an intraosseous adipose lesion (*arrow*) with foci of low signal intensity indicating calcification or ossification (*arrowhead*)

11.1.2 T2 Hypointense Tumor Matrix

The signal characteristics seen on MR imaging relate to the properties of the intralesional tissue. A majority of bone tumors are nonspecific, being isointense to skeletal muscle on T1-weighted images and of intermediate or increased signal intensity of T2-weighted images, as most bone tumors and tumor-like lesions have a significant chondroid or liquid component. However, there are primary lesions that can show partial or entire T2 hypointensity secondary to an immature chondroid matrix, hemosiderin, and calcification. This feature can be used for making the specific diagnosis.

A bone island is of low signal intensity on all pulse sequences.

Nonossifying fibroma is a cortical based lesion, which most commonly has low signal intensity on T1- and T2-weighted images related to its fibrous content. Signal intensity varies depending on the amount of hypercellular fibrous tissue, hemosiderin, and healing process.

Similarly, desmoplastic fibroma (Fig. 11.2) may demonstrate low-to-intermediate signal intensity on T2-weighted images secondary to T2 shortening of a nonsclerotic fibro-osseous lesion.

Giant cell tumor (Fig. 11.3) demonstrates peripheral low signal intensity on T1-weighted images and generalized hypointensity on T2-weighted images related to hemosiderin deposition from recurrent hemorrhage.

Brown tumor demonstrates low signal intensity on MR images, together with other manifestations of hyperparathyroidism.

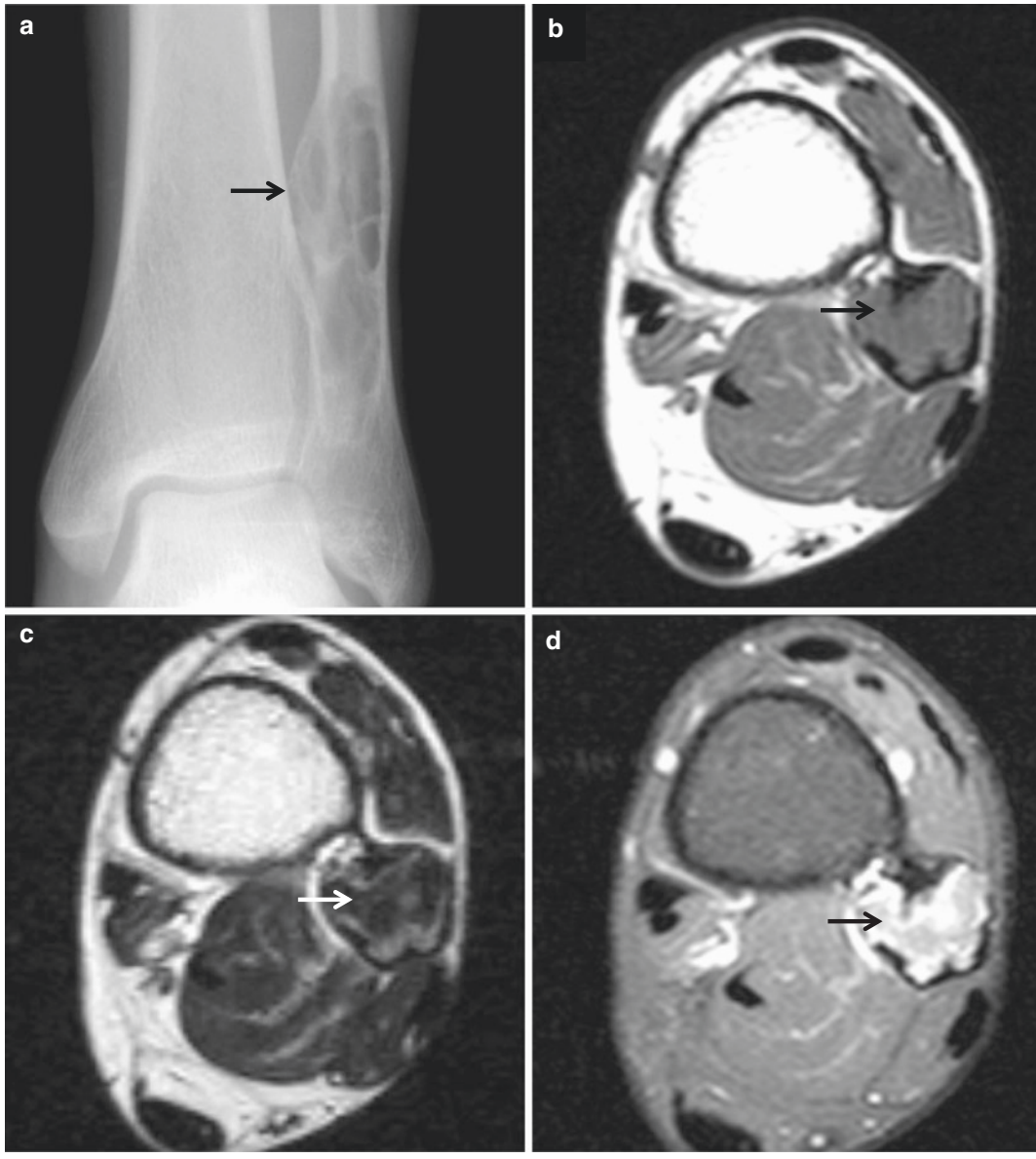

Fig. 11.2 Desmoplastic fibroma. (**a**) Anteroposterior radiograph of the left ankle shows a well-defined expansile osteolytic lesion (*arrow*) with a sclerotic border in the metadiaphysis of the left distal fibula. The internal trabeculation or ridges within the lesion give a soap-bubble appearance. (**b**) Axial T1-weighted MR image demonstrates diffuse intermediate signal intensity of the lesion (*arrow*). (**c**) Axial T2-weighted MR image demonstrates heterogeneous low-to-intermediate signal intensity of the lesion (*arrow*). The signal intensity of desmoplastic fibroma is attributable to its collagen content. (**d**) Axial fat-suppressed contrast-enhanced T1-weighted MR image demonstrates diffuse enhancement (*arrow*)

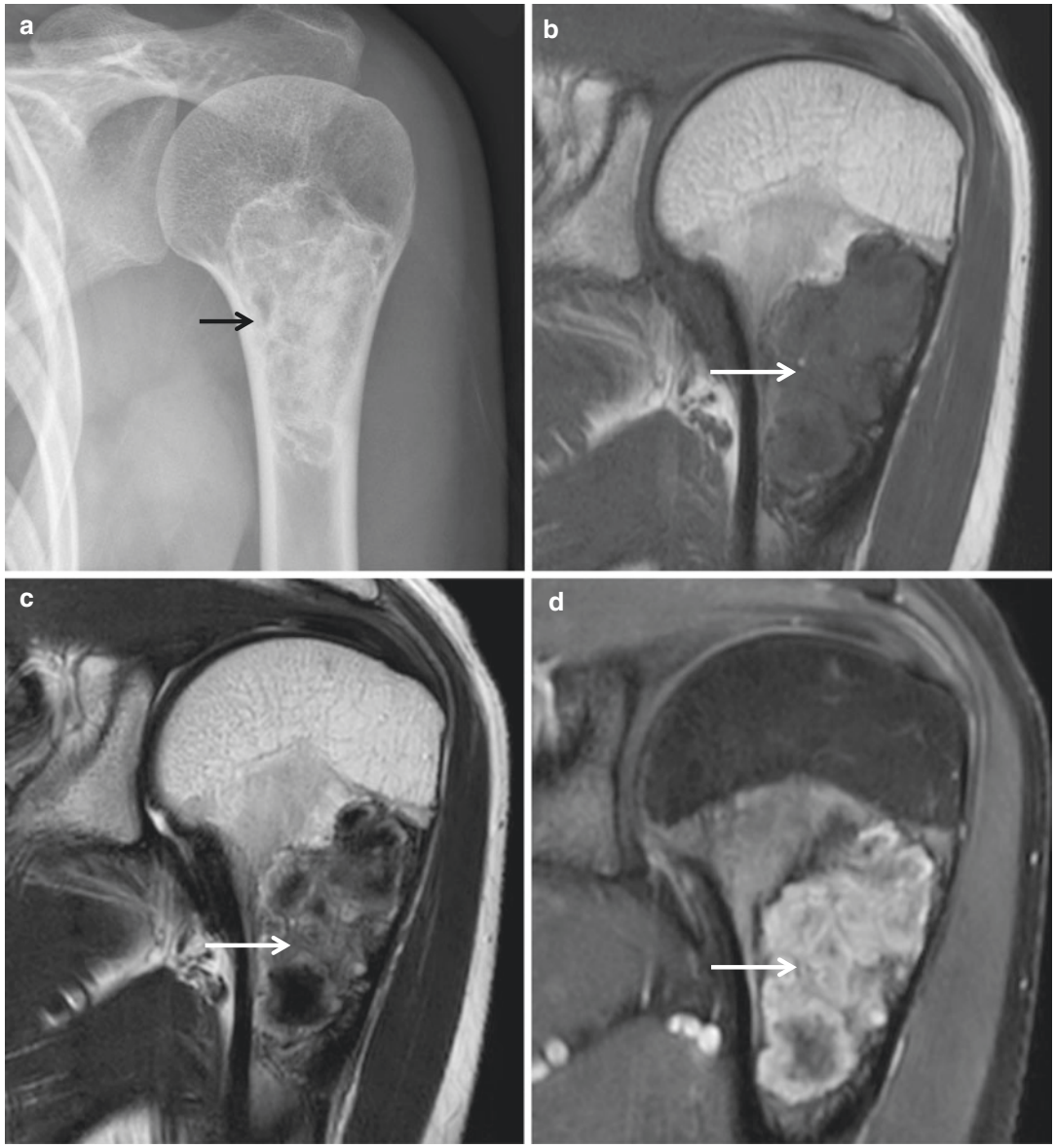

Fig. 11.3 Giant cell tumor. (**a**) Anteroposterior radiograph of the left shoulder shows a well-defined osteolytic lesion (*arrow*) with a sclerotic border in the metadiaphysis of the left proximal humerus. The internal ridges within the lesion give a soap-bubble appearance. (**b**) Coronal T1-weighted MR image demonstrates heterogeneous low-to-intermediate signal intensity of the lesion (*arrow*). (**c**) Coronal T2-weighted MR image demonstrates heterogeneous low-to-high signal intensity of the lesion (*arrow*). Giant cell tumor may demonstrate hypointensity on T2-weighted images related to hemosiderin deposition from recurrent hemorrhage. (**d**) Coronal fat-suppressed contrast-enhanced T1-weighted MR image demonstrates heterogeneous enhancement (*arrow*)

11.1.3 Fluid–Fluid Levels

CT or MR imaging may demonstrate a fluid–fluid level within a bone tumor. Fluid–fluid levels become apparent when a fluid collection containing substances of different density is allowed to settle and the plane of imaging is perpendicular to the fluid level. These levels usually represent blood–fluid levels, and typically indicate prior hemorrhage.

Although most commonly seen in aneurysmal bone cyst (Fig. 11.4), this level is relatively nonspecific and can be identified in a variety of lesions including simple bone cyst, fibrous dysplasia, osteoblastoma, chondroblastoma, giant cell tumor, telangiectatic osteosarcoma, conventional osteosarcoma, and undifferentiated pleomorphic sarcoma.

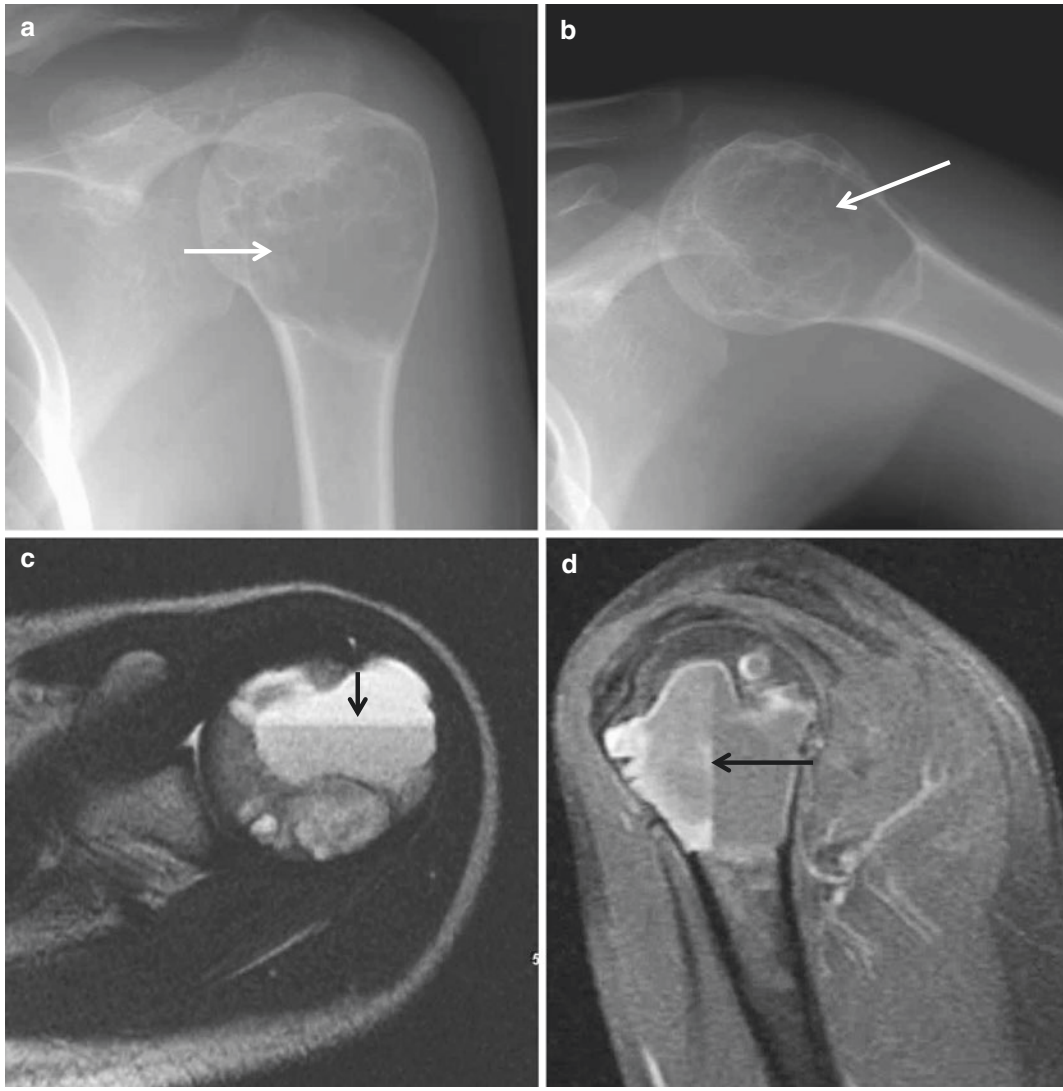

Fig. 11.4 Aneurysmal bone cyst. (**a**) Anteroposterior radiograph of the left shoulder shows a well-defined osteolytic lesion (*arrow*) with a sclerotic border in the left proximal humerus. The internal trabeculation within the lesion gives a soap-bubble appearance. (**b**) Lateral radiograph again shows a well-defined osteolytic lesion (*arrow*) with a sclerotic border in the left proximal humerus. The internal trabeculation within the lesion gives a soap-bubble appearance. (**c**) Axial T2-weighted MR image demonstrates a fluid–fluid level (*arrow*) within the lesion. (**d**) Sagittal fat-suppressed contrast-enhanced T1-weighted MR image again demonstrates a fluid–fluid level (*arrow*)

11.1.4 Flow Voids

Flow voids have been demonstrated in vascular tumors such as hemangioma and hemangioendothelioma. A single large osteolytic metastasis may appear as an expansive and trabeculated lesion, which is typically secondary to a hypervascular carcinoma of the kidney (Fig. 11.5) or thyroid. Renal cell and hepatocellular carcinoma metastases are known to exhibit flow voids on MR imaging. Flow voids can therefore be regarded as an additional diagnostic feature.

Fig. 11.5 Metastatic renal cell carcinoma. (**a**) Anteroposterior radiograph of the left knee shows a bubbly osteolytic lesion (*arrow*) with a sclerotic border and cortical breaching in the medial femoral condyle. (**b**) Lateral radiograph again shows a bubbly osteolytic lesion (*arrow*) in the medial femoral condyle. (**c**) Sagittal proton density-weighted MR image demonstrates an expansile mass with cortical breaching and flow voids (*arrows*) within the lesion. (**d**) Axial fat-suppressed T2-weighted MR image demonstrates an expansile mass with cortical breaching and flow voids (*arrows*) within the lesion

11.2 Ancillary Findings

11.2.1 Soft Tissue Extension

Although MR imaging contributes little additional information on the characterization of a bone tumor when compared with the radiographs in most cases, soft tissue extension should alert the radiologist to the presence of an aggressive lesion likely to be malignant, and further work-up should be initiated.

Typically, benign bone tumors are well defined and sharply demarcated from the adjacent normal tissue. Malignant lesions involve surrounding tissue to a greater extent. Giant cell tumor and osteosarcoma show frequent soft tissue extension. Soft tissue extension of the giant cell tumor typically occurs at the metaphyseal end of the lesion (Fig. 11.6), because the articular cartilage overlying the epiphyseal margin is a barrier to tumor extension. This also explains why joint involvement of the giant cell tumor is unusual, despite the subarticular spread of the giant cell tumor.

The presence of a soft tissue extension of bone tumor is an important predictor concerning a malignant lesion (Fig. 11.7). It may indicate a malignant degeneration of benign chondroid tumor and Paget disease. Tumors that often have a soft tissue component are osteosarcoma, Ewing's sarcoma, and lymphoma.

Although infectious etiologies such as osteomyelitis may have an aggressive appearance, they usually do not have an associated solid soft tissue mass.

Muscle edema shows a feathery appearance following fascial planes without mass effect, which contrasts with the mass effect typically seen with extraosseous tumor extension.

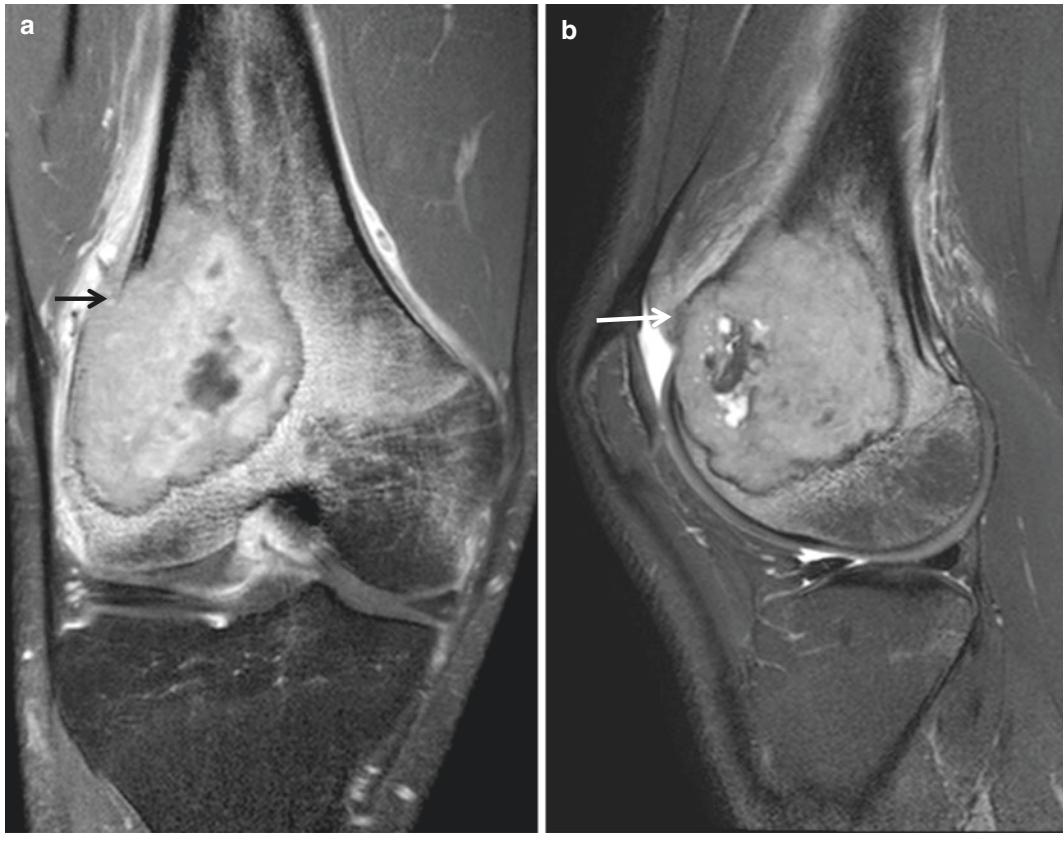

Fig. 11.6 Giant cell tumor. (**a**) Coronal fat-suppressed contrast-enhanced T1-weighted MR image demonstrates a soft tissue extension of the osseous lesion with lateral cortical breaching (*arrow*). (**b**) Sagittal fat-suppressed T2-weighted MR image demonstrates a soft tissue extension of the osseous lesion with anterior cortical breaching (*arrow*)

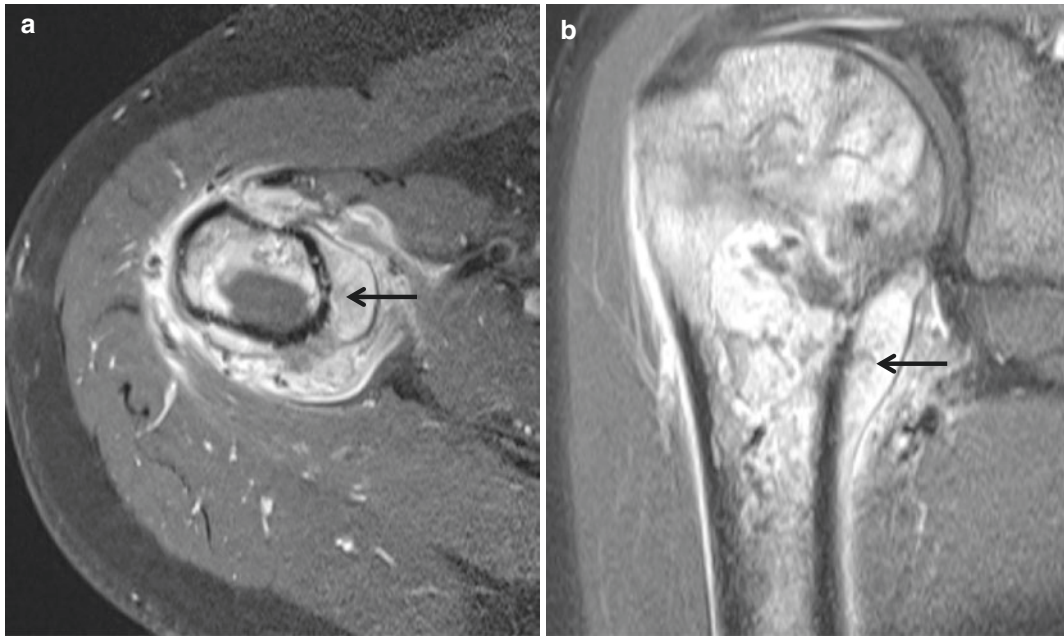

Fig. 11.7 Osteosarcoma. (**a**) Axial fat-suppressed contrast-enhanced T1-weighted MR image demonstrates a soft tissue extension of the osseous lesion (*arrow*). (**b**) Axial fat-suppressed contrast-enhanced T1-weighted MR image demonstrates a soft tissue extension of the osseous lesion (*arrow*)

11.2.2 Peritumoral Edema

Marrow edema is characterized by signal intensity on T1-weighted images between that of fat and skeletal muscle and hyperintensity on fluid-sensitive sequences. The presence of extensive bone marrow edema adjacent to a bone tumor can be an important diagnostic clue in the diagnoses of osteoid osteoma, osteoblastoma, chondroblastoma (Fig. 11.8), and Langerhans cell histiocytosis.

The reason for this extensive concomitant reaction is unclear, but it is unlikely to be explained simply as a stress reaction. Possible mechanisms generating peritumoral edema, such as increased permeability of tumor capillaries and osmotically active molecules, have been described, and the peritumoral edema represents a nonspecific response of tissue to a stimulus. Histological examination of these areas revealed edematous fluid together with inflammatory cells.

MR imaging may be misleading, as there is usually a significant amount of surrounding edema, which belies the benign nature of these benign bone tumors. Malignant lesions frequently surrounded by bone marrow edema include metastasis, osteosarcoma, chondrosarcoma, and Ewing's sarcoma.

Surrounding edema may cause a benign lesion to appear much larger on MR images than suspected from radiographic finding, or it may decrease the conspicuity of a lesion. As a rule of thumb, the more marked the marrow edema as compared with the size of the main lesion, the less likely it is to be malignant. MR imaging cannot always help distinguish tumor from peritumoral edema. Edema around a malignant bone tumor may contain viable tumor cells.

Marrow edema can lead to overestimation of the size of the tumors on fluid-sensitive sequences; therefore, assessment on T1-weighted images and fat-suppressed postcontrast images can be helpful.

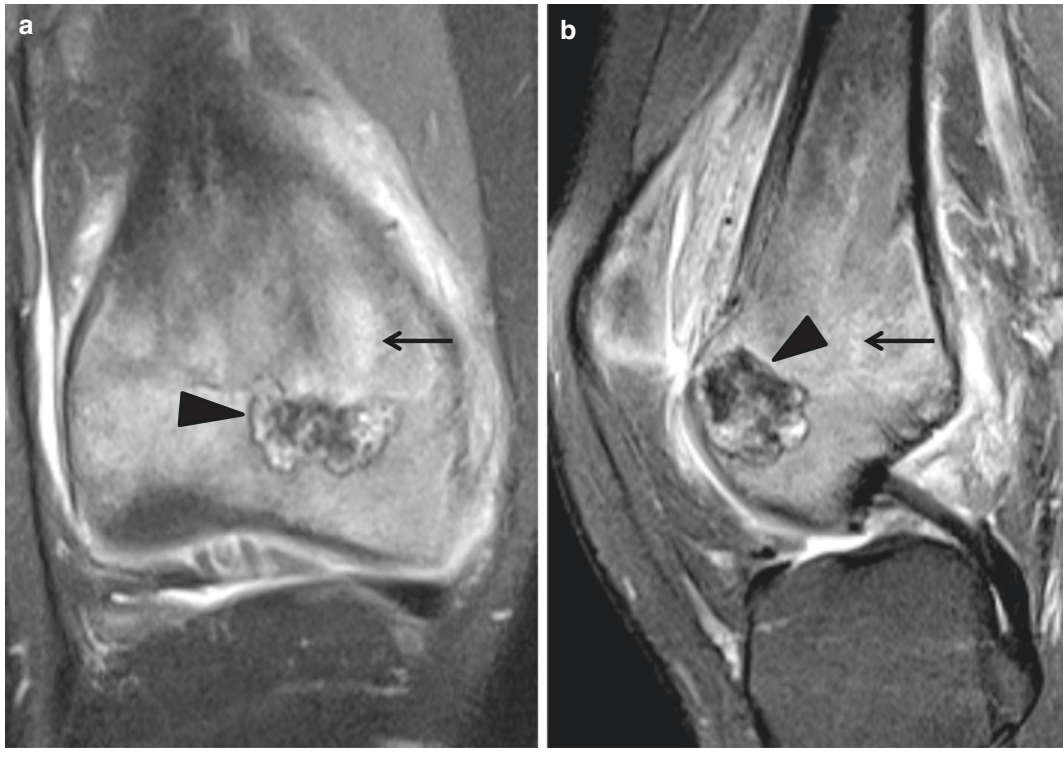

Fig. 11.8 Chondroblastoma. (**a**) Coronal fat-suppressed proton density-weighted MR image demonstrates a lesion with low-to-high signal intensity (*arrowhead*) and intense surrounding reactive edema (*arrow*). (**b**) Sagittal fat-suppressed proton density-weighted MR image demonstrates a lesion with low-to-high signal intensity (*arrowhead*) and intense surrounding reactive edema (*arrow*)

11.3 "Look Like Anything" Lesions

Five lesions – fibrous dysplasia, metastatic carcinoma, infection, chondroid tumors, and Langerhans cell histiocytosis – present in such a variable fashion that they can virtually "look like anything." These five lesions may well be considered in the differential diagnosis of most unknown bone lesions.

Fibrous dysplasia (Fig. 11.9) is typically a well-defined, expansive, and intramedullary lesion, but it can vary in its radiographic appearance. Although ground-glass matrix is classic, this finding is neither sensitive nor specific, because fibrous dysplasia can present as either a lytic or a sclerotic lesion.

Enchondroma is included in the differential diagnosis of lucent lesions, because it lacks matrix mineralization in the hands. However, enchondromas outside of the hands and feet often have a different radiographic appearance because of the calcified chondroid matrix.

Most lytic metastases (Fig. 11.10) are irregular and poorly defined. Multiple foci are the best clue to metastatic disease. However, a single large metastatic focus may occasionally appear as an expansive, trabeculated lesion.

Infection has a wide variety of appearance, and can present as either an ill-defined or a well-demarcated lucent lesion (Fig. 11.11). Brodie abscess may or may not be expansive, and may have a sclerotic or nonsclerotic border. Lytic lesion of infectious etiology often shows an oval configuration that is oriented along the long axis of the long bone and lucent tortuous channel extending toward the growth plate. Infectious process shows rapid interval changes.

The radiographic appearance of the Langerhans cell histiocytosis (Fig. 11.12) can be quite varied. Langerhans cell histiocytosis can present as a well-defined lytic lesion, as is typical in the skull, or as a permeative lesion, which is more typical in the long bones. Langerhans cell histiocytosis can even demonstrate sclerosis, particularly in the healing phase.

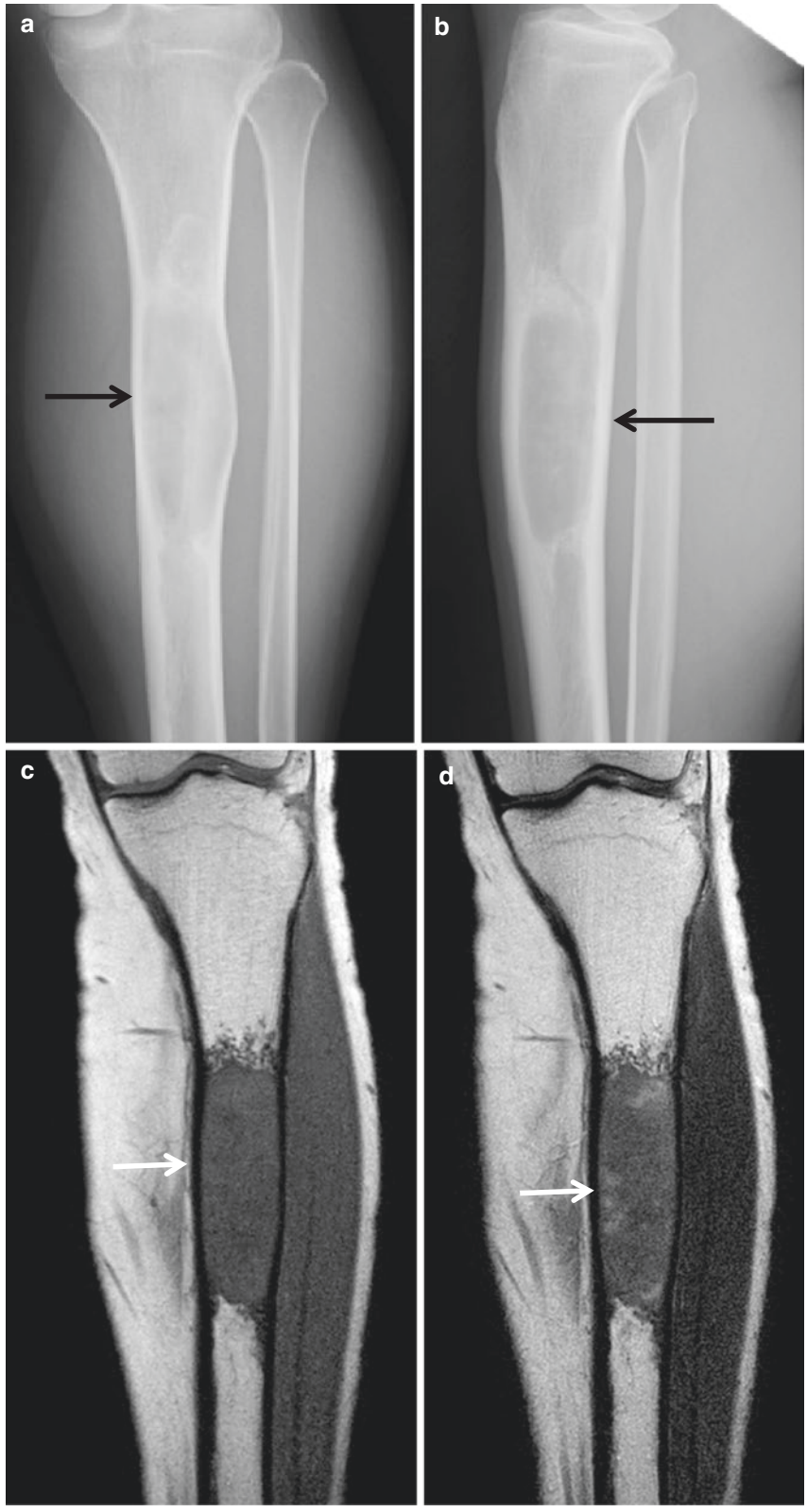
a
b
c
d

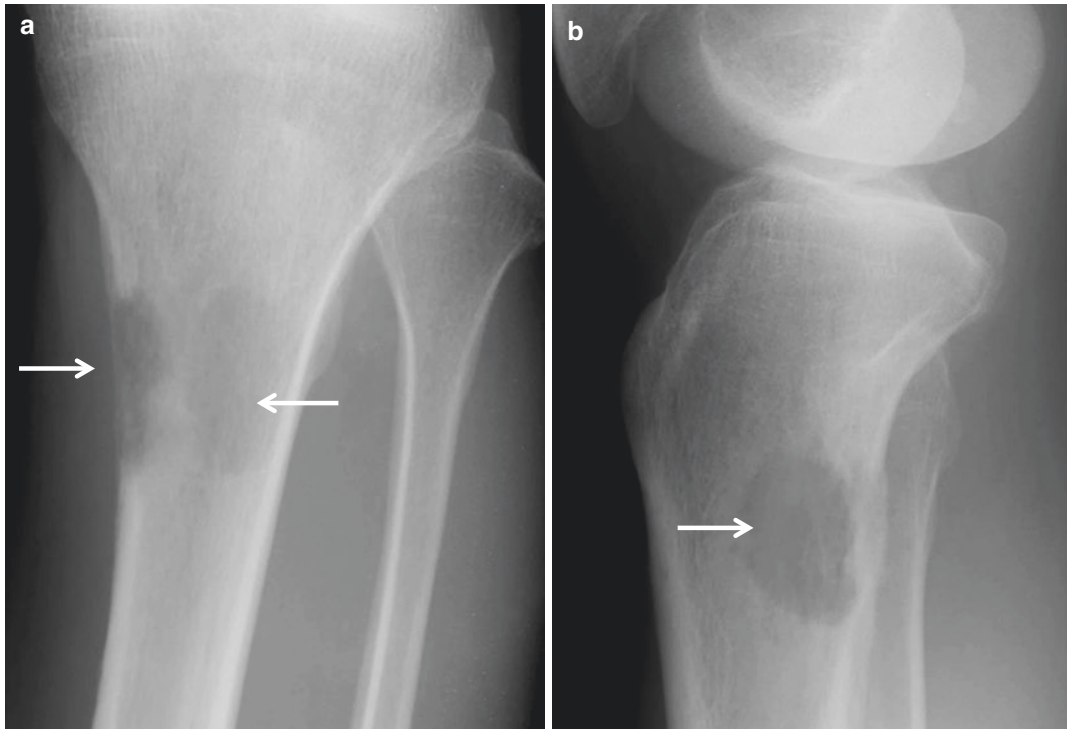

Fig. 11.10 Metastasis. (**a**) Anteroposterior radiograph of the left lower leg shows ill-defined osteolytic lesion (*arrow*) in the metadiaphysis of the left proximal tibia. (**b**) Lateral radiograph again shows ill-defined osteolytic lesion (*arrow*) with no mineralization

Fig. 11.9 Fibrous dysplasia. (**a**) Anteroposterior radiograph of the left lower leg shows a well-defined intramedullary lesion with ground-glass density (*arrow*). (**b**) Lateral radiograph again shows an expansile intramedullary lesion with ground-glass density (*arrow*). (**c**) Coronal T1-weighted MR image demonstrates an intramedullary lesion with low signal intensity (*arrow*). (**d**) Coronal T2-weighted MR image shows low signal intensity (*arrow*) of the lesion with foci of high signal intensity

Fig. 11.11 Tuberculosis. (**a**) Anteroposterior radiograph of the left forearm shows multiple rounded osteolytic lesions (*arrows*) in the shafts of the radius and ulna. Uninterrupted periosteal reaction is noticed in ulna. (**b**) Lateral radiograph again shows multiple rounded osteolytic lesions (*arrows*) and periosteal reaction

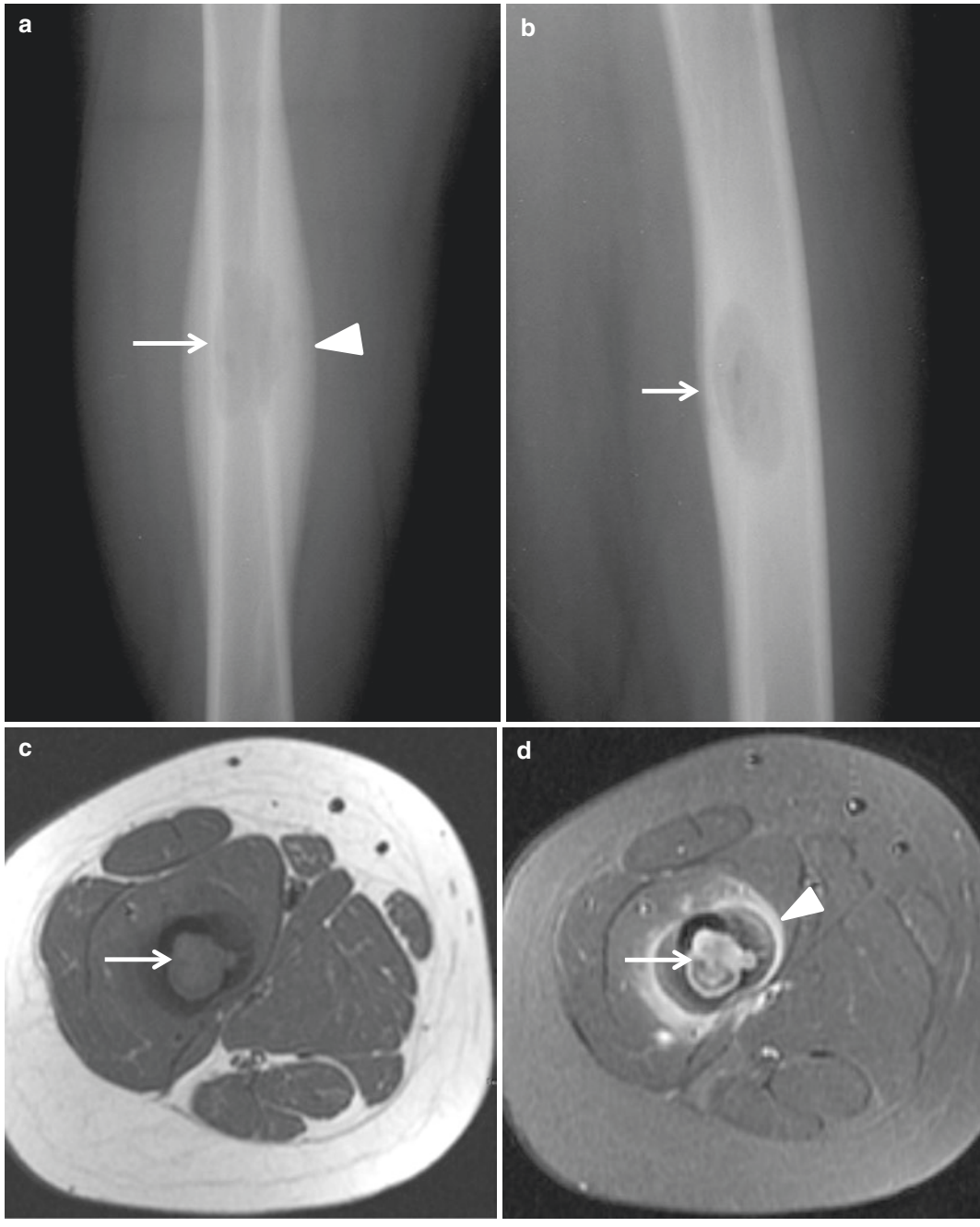

Fig. 11.12 Langerhans cell histiocytosis. (**a**) Anteroposterior radiograph of the right femur shows multiple intramedullary osteolytic lesions (*arrow*) with thick multilamellated periosteal reaction (*arrowhead*) in the shaft of the right femur. (**b**) Lateral radiograph again shows osteolytic lesion (*arrow*) with periosteal reaction. (**c**) Axial T1-weighted MR image demonstrates an intramedullary lesion with low signal intensity (*arrow*). (**d**) Axial fat-suppressed contrast-enhanced T1-weighted MR image demonstrates enhancement of the intramedullary lesion (*arrow*) and periosteum (*arrowhead*)

References

Intralesional Feature: Fat Containing Lesions

Alyas F, James SL, Davies AM, Saifuddin A. The role of MR imaging in the diagnostic characterisation of appendicular bone tumours and tumour-like conditions. Eur Radiol. 2007;17:2675–86.

Campbell RSD. Lipogenic tumours of bone. In: Davies AM, Sundaram M, James SLJ, editors. Imaging of bone tumors and tumor-like lesions: techniques and applications. 1 ed. Berlin: Springer; 2009. p. 401–10.

Davies AM, Cassar-Pullicino VN. Principles of detection and diagnosis. In: Davies AM, Sundaram M, James SLJ, editors. Imaging of bone tumors and tumor-like lesions: techniques and applications. 1st ed. Berlin: Springer; 2009. p. 112–37.

Murphey MD, Carroll JF, Flemming DJ, Pope TL, Gannon FH, Kransdorf MJ. From the archives of the AFIP: benign musculoskeletal lipomatous lesions. Radiographics. 2004;24:1433–66.

Nascimento D, Suchard G, Hatem M, de Abreu A. The role of magnetic resonance imaging in the evaluation of bone tumours and tumour-like lesions. Insights Imaging. 2014;5:419–40.

Simpfendorfer CS, Ilaslan H, Davies AM, James SL, Obuchowski NA, Sundaram M. Does the presence of focal normal marrow fat signal within a tumor on MRI exclude malignancy? An analysis of 184 histologically proven tumors of the pelvic and appendicular skeleton. Skelet Radiol. 2008;37:797–804.

Intralesional Feature: T2 Hypointense Tumor Matrix

Alyas F, James SL, Davies AM, Saifuddin A. The role of MR imaging in the diagnostic characterisation of appendicular bone tumours and tumour-like conditions. Eur Radiol. 2007;17:2675–86.

Frick MA, Sundaram M, Unni KK, Inwards CY, Fabbri N, Trentani F, Baccini P, Bertoni F. Imaging findings in desmoplastic fibroma of bone: distinctive T2 characteristics. AJR Am J Roentgenol. 2005;184:1762–7.

Nascimento D, Suchard G, Hatem M, de Abreu A. The role of magnetic resonance imaging in the evaluation of bone tumours and tumour-like lesions. Insights Imaging. 2014;5:419–40.

Intralesional Feature: Fluid-Fluid Levels

Davies AM, Cassar-Pullicino VN. Principles of detection and diagnosis. In: Davies AM, Sundaram M, James SLJ, editors. Imaging of bone tumors and tumor-like lesions: techniques and applications. 1st ed. Berlin: Springer; 2009. p. 112–37.

Nichols RE, Dixon LB. Radiographic analysis of solitary bone lesions. Radiol Clin N Am. 2011;49:1095–114.

Van Dyck P, Vanhoenacker FM, Vogel J, Venstermans C, Kroon HM, Gielen J, Parizel PM, Bloem JL, De Schepper AM. Prevalence, extension and characteristics of fluid-fluid levels in bone and soft tissue tumors. Eur Radiol. 2006;16:2644–51.

Yarmish G, Klein MJ, Landa J, Lefkowitz RA, Hwang S. Imaging characteristics of primary osteosarcoma: nonconventional subtypes. Radiographics. 2010;30:1653–72.

Intralesional Feature: Flow Voids

Alyas F, James SL, Davies AM, Saifuddin A. The role of MR imaging in the diagnostic characterisation of appendicular bone tumours and tumour-like conditions. Eur Radiol. 2007;17:2675–86.

Choi JA, Lee KH, Jun WS, Yi MG, Lee S, Kang HS. Osseous metastasis from renal cell carcinoma: "flow-void" sign at MR imaging. Radiology. 2003;228:629–34.

Nascimento D, Suchard G, Hatem M, de Abreu A. The role of magnetic resonance imaging in the evaluation of bone tumours and tumour-like lesions. Insights Imaging. 2014;5:419–40.

Ancillary Findings: Soft Tissue Extension

Alyas F, James SL, Davies AM, Saifuddin A. The role of MR imaging in the diagnostic characterisation of appendicular bone tumours and tumour-like conditions. Eur Radiol. 2007;17:2675–86.

Davies AM, Cassar-Pullicino VN. Principles of detection and diagnosis. In: Davies AM, Sundaram M, James SLJ, editors. Imaging of bone tumors and tumor-like lesions: techniques and applications. 1st ed. Berlin: Springer; 2009. p. 112–37.

Miller TT. Bone tumors and tumorlike conditions: analysis with conventional radiography. Radiology. 2008;246:662–74.

Murphey MD, Nomikos GC, Flemming DJ, Gannon FH, Temple HT, Kransdorf MJ. From the archives of AFIP. Imaging of giant cell tumor and giant cell reparative granuloma of bone: radiologic-pathologic correlation. Radiographics. 2001;21:1283–309.

Nascimento D, Suchard G, Hatem M, de Abreu A. The role of magnetic resonance imaging in the evaluation of bone tumours and tumour-like lesions. Insights Imaging. 2014;5:419–40.

Ancillary Findings: Peritumoral Edema

Alyas F, James SL, Davies AM, Saifuddin A. The role of MR imaging in the diagnostic characterisation of appendicular bone tumours and tumour-like conditions. Eur Radiol. 2007;17:2675–86.

Crim JR, Mirra JM, Eckardt JJ, Seeger LL. Widespread inflammatory response to osteoblastoma: the flare phenomenon. Radiology. 1990;177:835–6.

Currie JW, Davis KW, Lafita VS, Blankenbaker DG, De Smet AA, Rosas H, Lee KS. Musculoskeletal mnemonics: differentiating features. Curr Probl Diagn Radiol. 2011;40:45–71.

Davies AM, Cassar-Pullicino VN. Principles of detection and diagnosis. In: Davies AM, Sundaram M, James SLJ, editors. Imaging of bone tumors and tumor-like lesions: techniques and applications. 1st ed. Berlin: Springer; 2009. p. 112–37.

Hayes CW, Conway WF, Sundaram M. Misleading aggressive MR imaging appearance of some benign musculoskeletal lesions. Radiographics. 1992;12: 1119–34.

Hwang S, Panicek DM. Imaging techniques: magnetic resonance imaging. In: Davies AM, Sundaram M, James SLJ, editors. Imaging of bone tumors and tumor-like lesions: techniques and applications. 1 ed. Berlin: Springer; 2009. p. 31–52.

James SL, Hughes RJ, Ali KE, Saifuddin A. MRI of bone marrow oedema associated with focal bone lesions. Clin Radiol. 2006;61:1003–9.

James SL, Panicek DM, Davies AM. Bone marrow oedema associated with benign and malignant bone tumours. Eur J Radiol. 2008;67:11–21.

Kaim AH, Hügli R, Bonél HM, Jundt G. Chondroblastoma and clear cell chondrosarcoma: radiological and MRI characteristics with histopathological correlation. Skeletal Radiol. 2002;31:88–95.

Steen RG. Edema and tumor perfusion: characterization by quantitative 1H MR imaging. AJR Am J Roentgenol. 1992;158:259–64.

"Look Like Anything" Lesions

Currie JW, Davis KW, Lafita VS, Blankenbaker DG, De Smet AA, Rosas H, Lee KS. Musculoskeletal mnemonics: differentiating features. Curr Probl Diagn Radiol. 2011;40:45–71.

Nichols RE, Dixon LB. Radiographic analysis of solitary bone lesions. Radiol Clin N Am. 2011;49:1095–114.

Sanders TG, Parsons 3rd TW. Radiographic imaging of musculoskeletal neoplasia. Cancer Control. 2001;8: 221–31.

Part IV

Drill and Practice: Image Interpretation Session

Cases

12

H.S. Kang et al., *Oncologic Imaging: Bone Tumors*, DOI 10.1007/978-981-287-703-1_12

Case 1

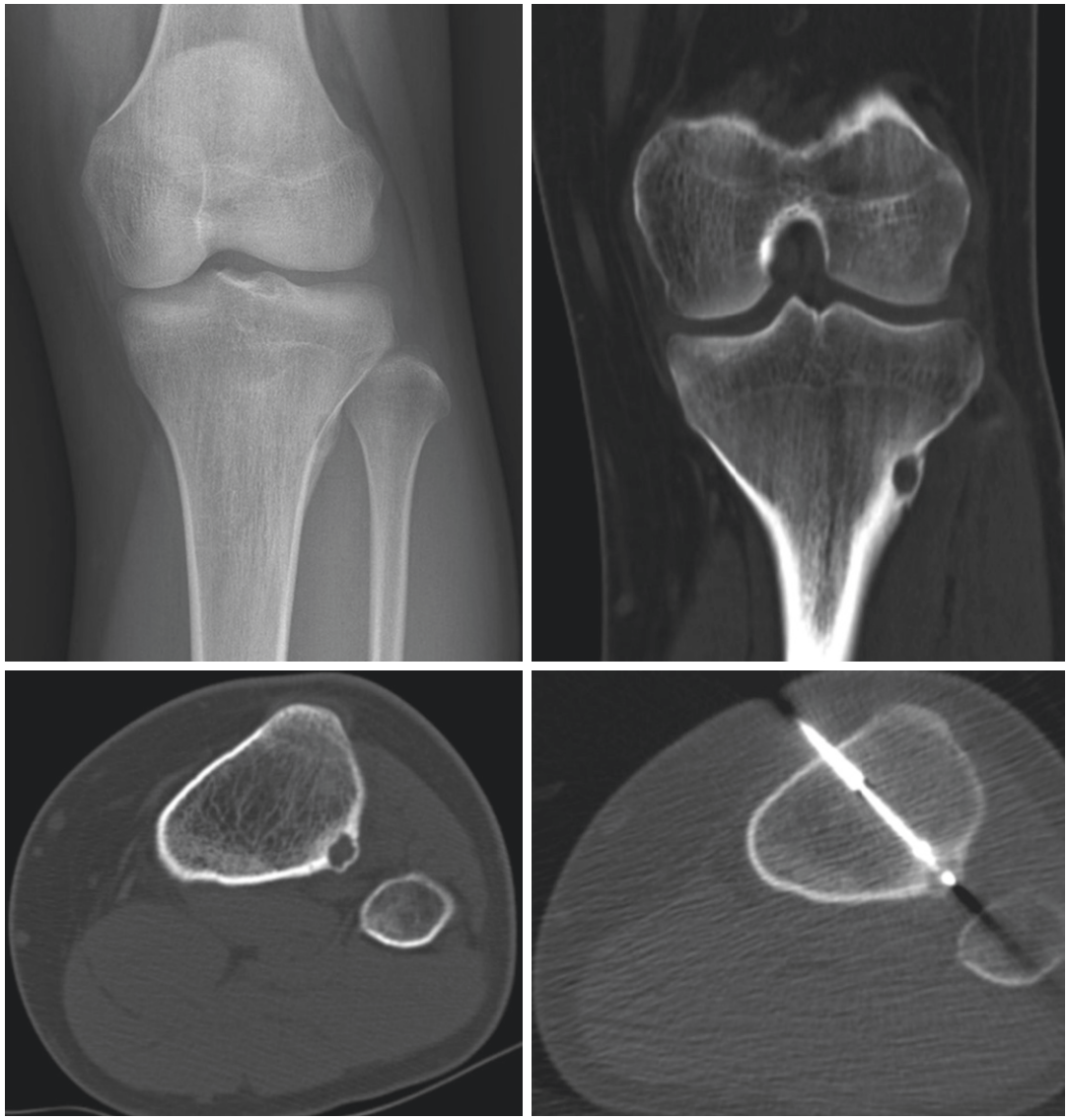

Fig. 12.1

1. List the differential diagnoses of this condition.
2. What is the most likely diagnosis?
3. How would you treat this patient?
4. What procedure does this patient have?
5. What are the advantages of the treatment methods you mentioned?
6. List the relative contraindications of this procedure.
7. What are the complications of this procedure?

Case 2

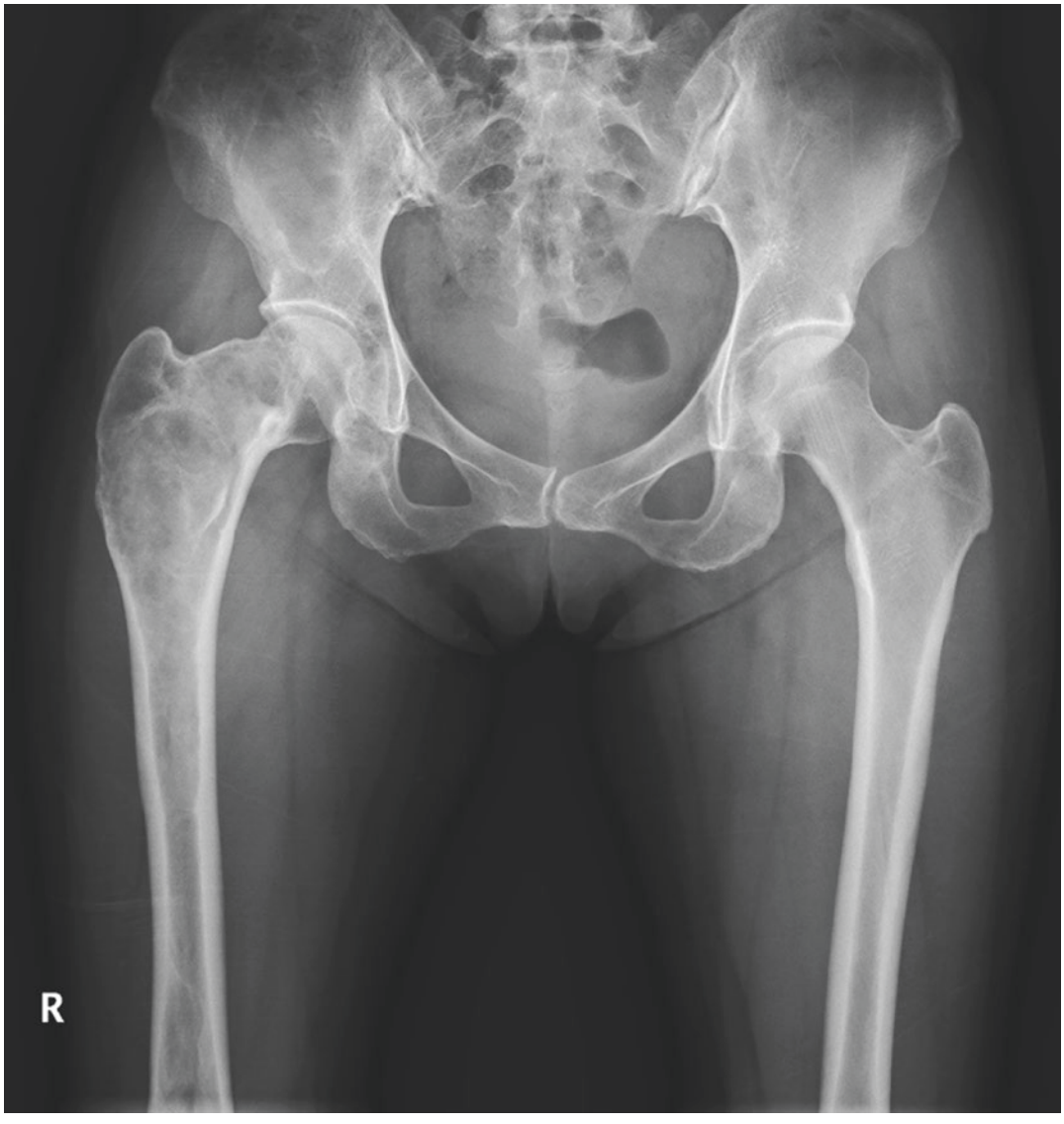

Fig. 12.2

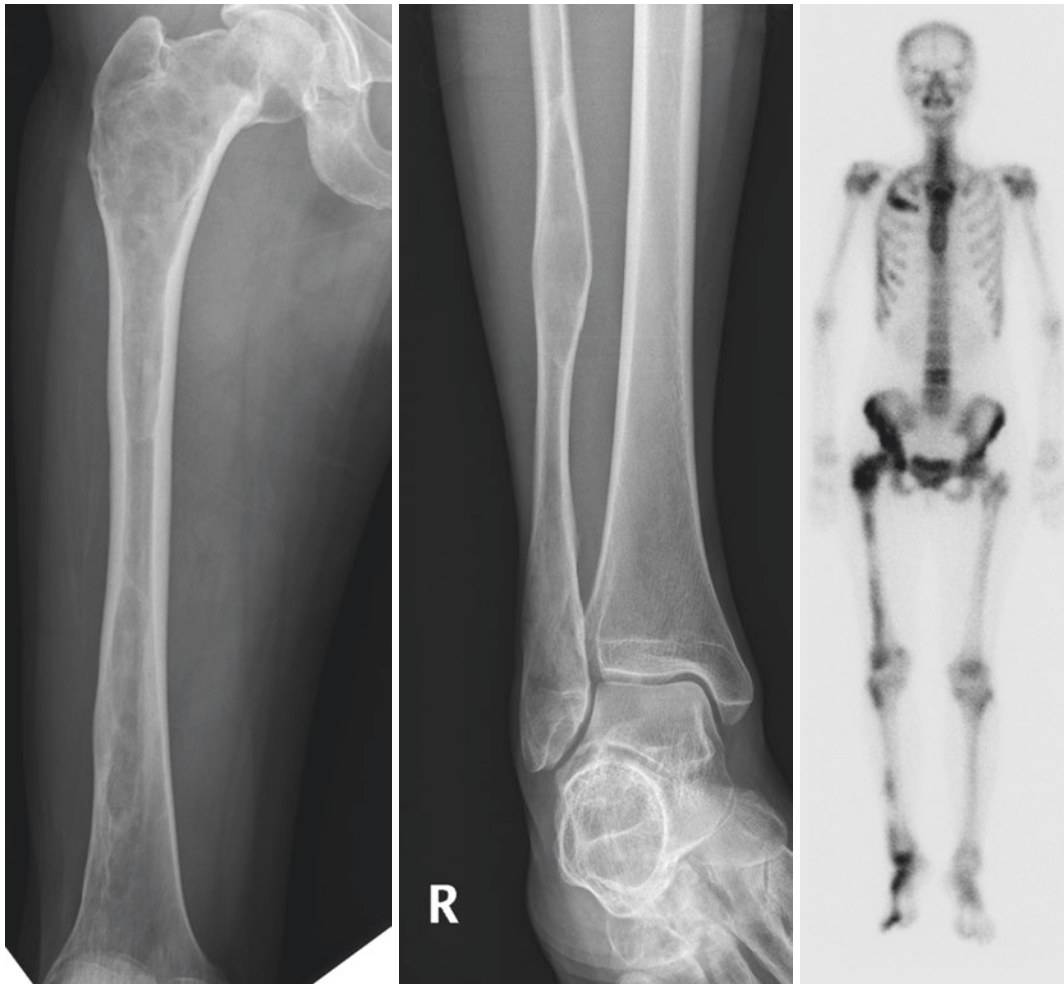

Fig. 12.2 (continued)

1. What is the likely diagnosis?
2. What is the McCune-Albright syndrome?
3. What is meant by a ground-glass appearance?
4. What is the diagnosis if this patient also has multiple soft tissue myxomas?
5. What is the most common cause of an expansile focal rib lesion?

Case 3

Fig. 12.3

1. What observation did you make?
2. What is the most common tumor of the hand?
3. Can enchondroma be purely lytic in appearance on radiographs?
4. What is the most likely diagnosis?

Case 4

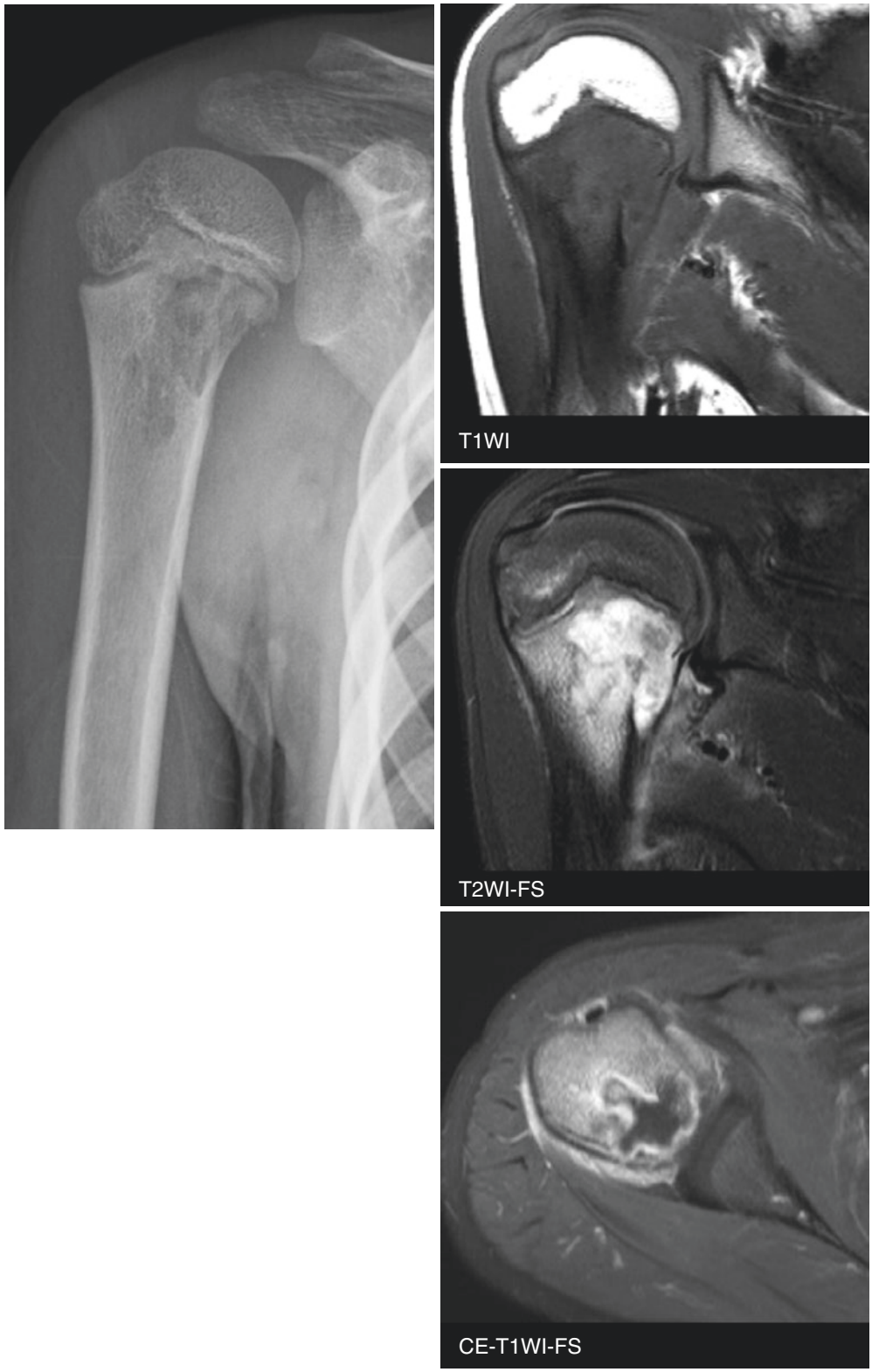

Fig. 12.4

1. List your differential diagnoses.
2. What is the most likely diagnosis?
3. Where are the common locations of this lesion?
4. At what age does this lesion occur?
5. List benign musculoskeletal lesions which may show misleading aggressive appearance.

Case 5

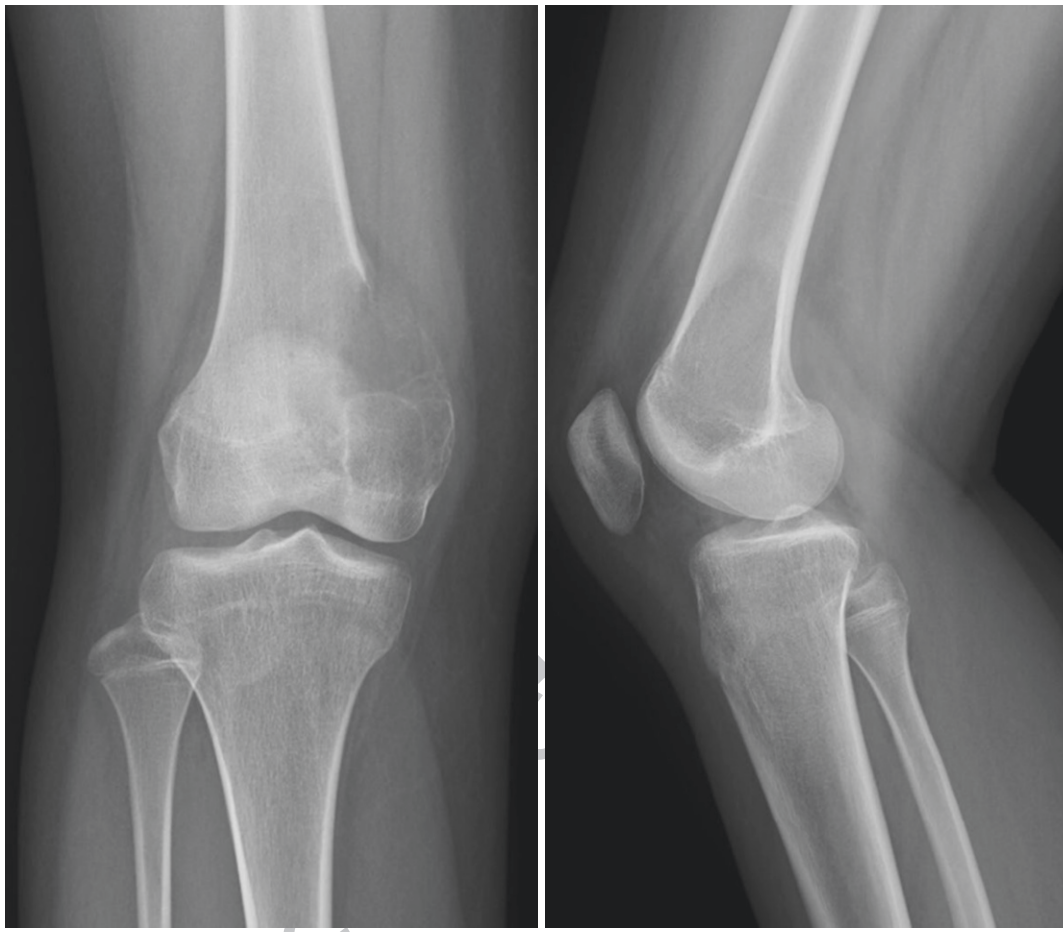

Fig. 12.5

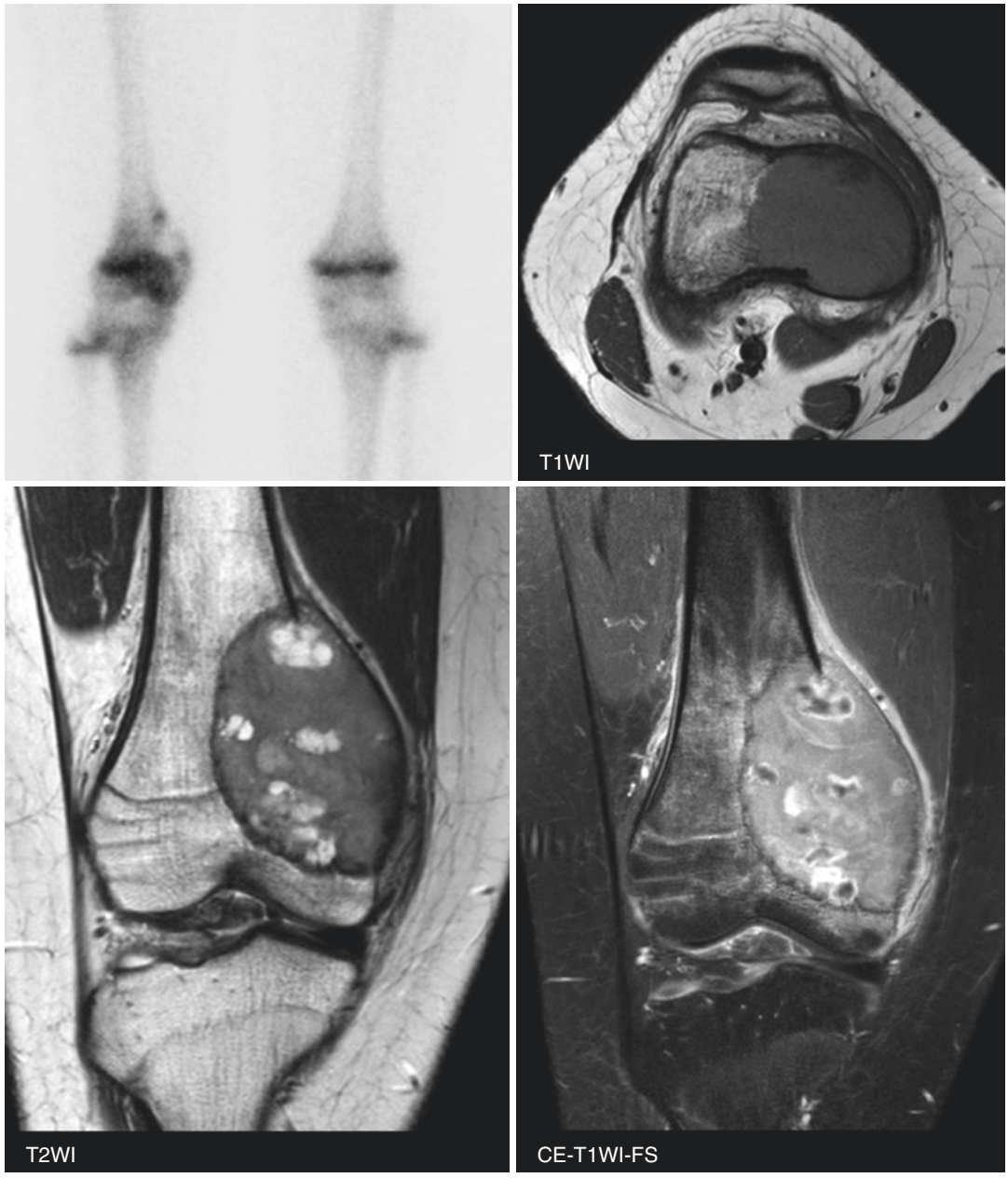

Fig. 12.5 (continued)

1. What is the likely diagnosis?
2. Most bone tumors show equal sex predilection or slight male predominance. List the tumors with female predilection.
3. What is the characteristic MR appearance on fluid-sensitive sequences?
4. List the osseous lesions with T2-hypointense tumor matrix.

Case 6

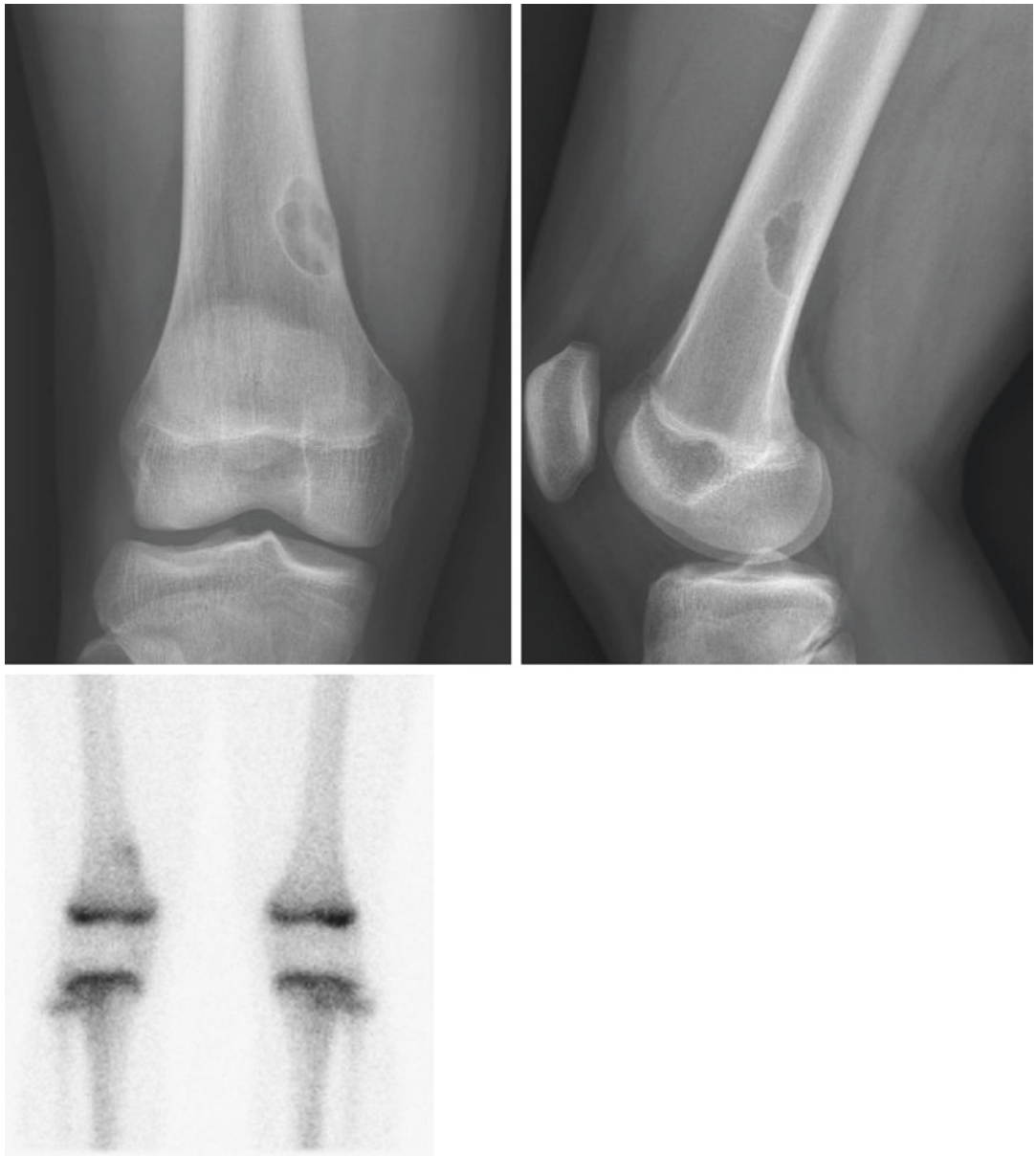

Fig. 12.6

1. List the bubbly lesions of bone.
2. What is the most likely diagnosis?
3. What is a finding that would represent a benign process?
4. Does the differential diagnosis include a nonossifying fibroma, if the patient is a 50-year-old man?
5. In which syndrome could the multiple nonossifying fibromas be seen?

Case 7

Fig. 12.7

1. What observation did you make on radiographs?
2. List the differential diagnoses.
3. What is the characteristic CT finding to help to distinguish this condition from an osteochondroma?
4. What is the most likely diagnosis?

Case 8

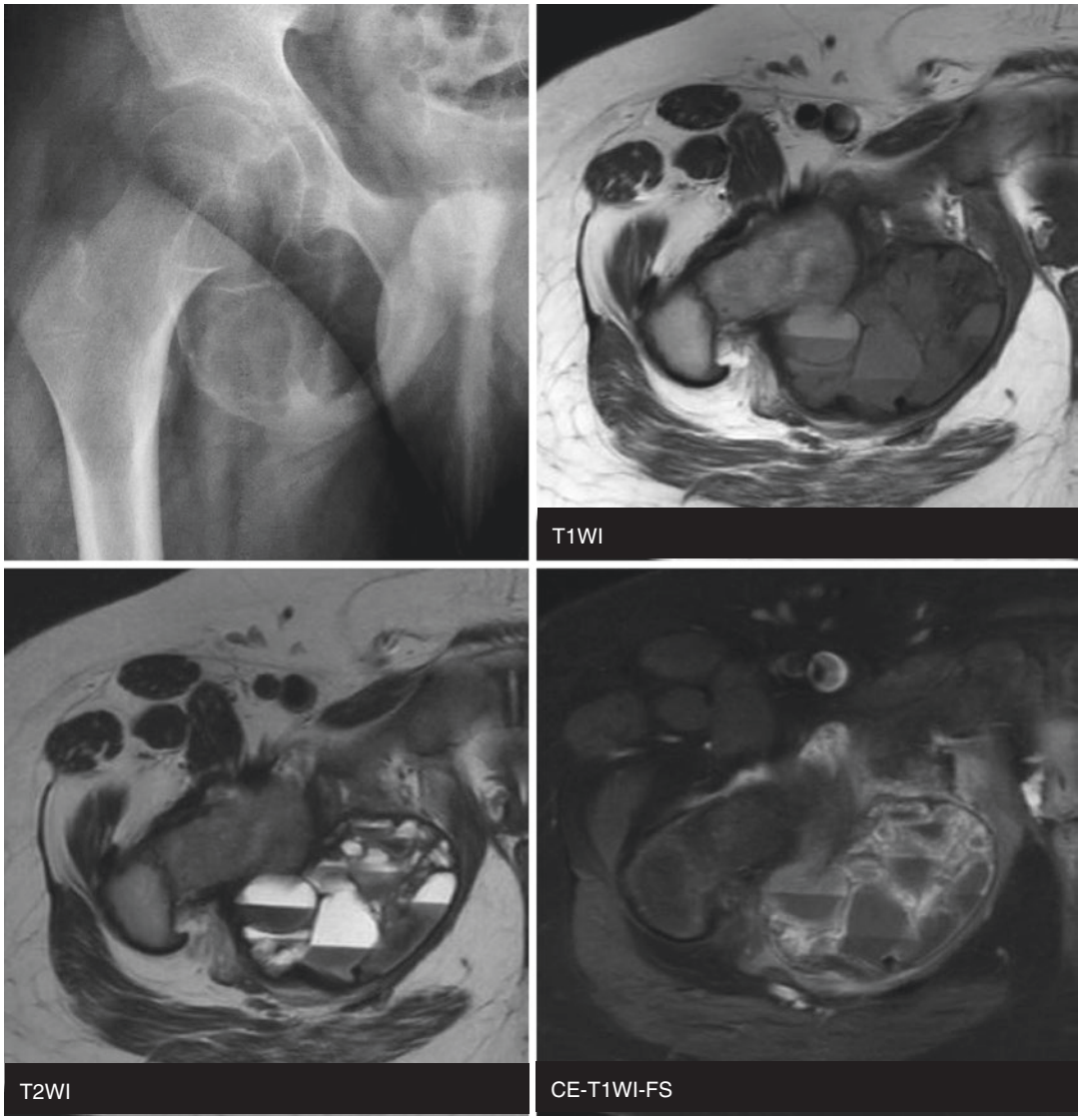

Fig. 12.8

1. What observation did you make on radiographs?
2. What are the characteristic observations on MR images?
3. What is the most likely diagnosis?
4. What is the definition of the secondary aneurysmal bone cyst?
5. What are the typical MR imaging findings of the primary aneurysmal bone cyst?

Case 9

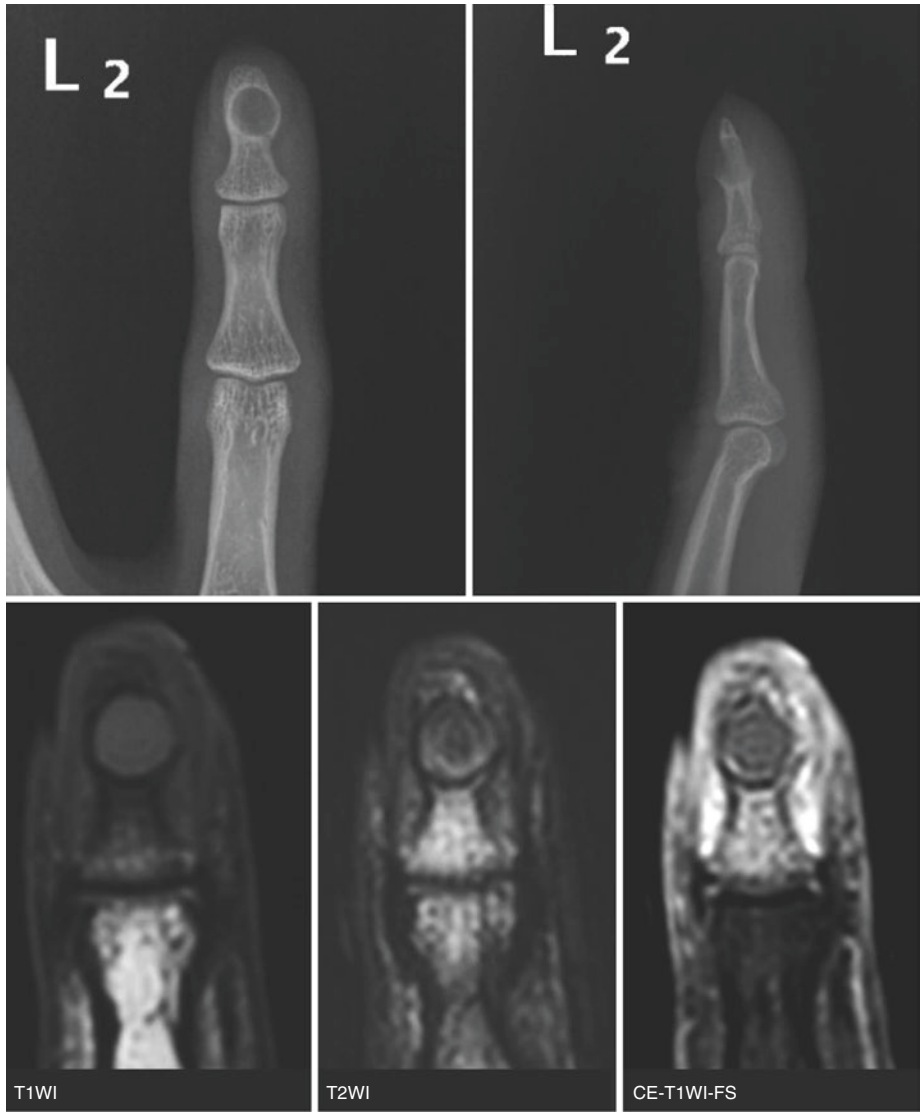

Fig. 12.9

1. What observation did you make on radiograph?
2. List your differential diagnoses.
3. What is the most likely diagnosis?
4. Which is the most common location for an epidermal inclusion cyst?
5. What MR imaging findings can distinguish this condition from a glomus tumor?

Case 10

Fig. 12.10

1. What are the findings?
2. What is the likely diagnosis?
3. Dose this disorder involve epiphysis?
4. Can this condition be unilateral?
5. List the differential diagnoses if this lesion involved a single bone.

Case 11

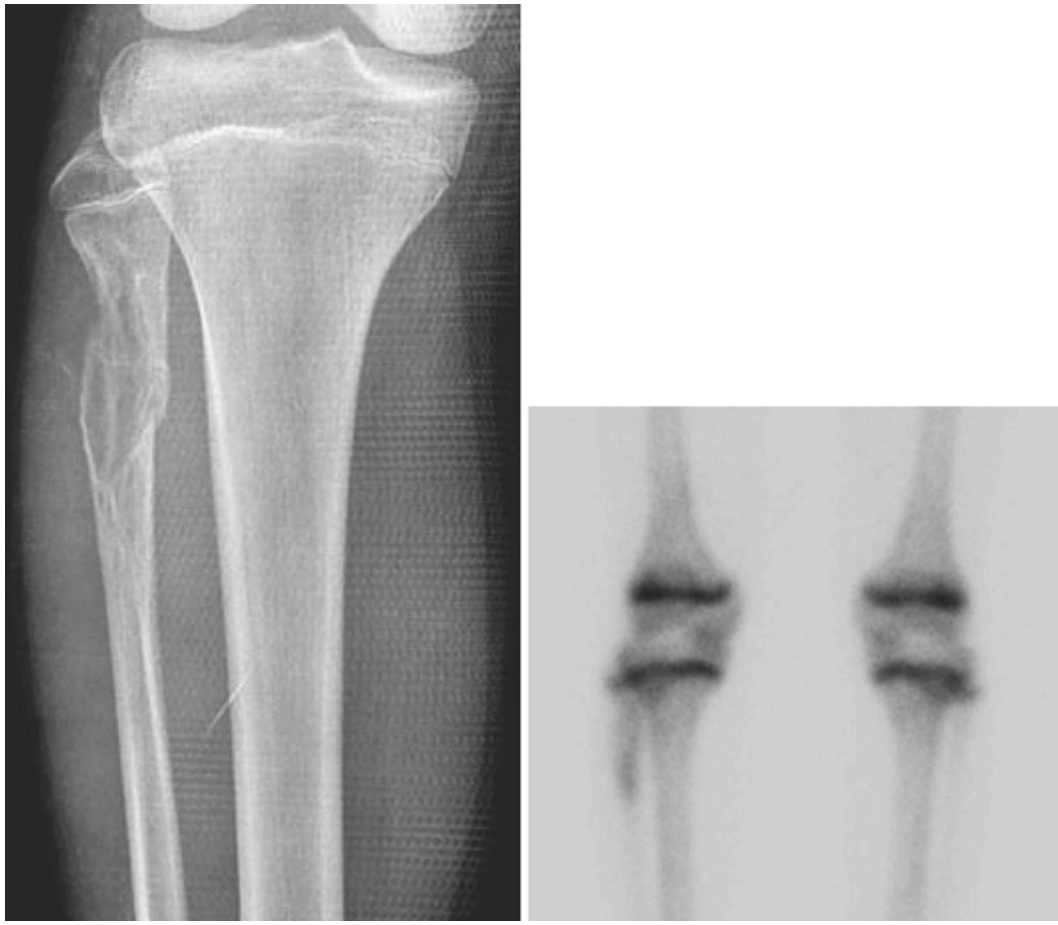

Fig. 12.11

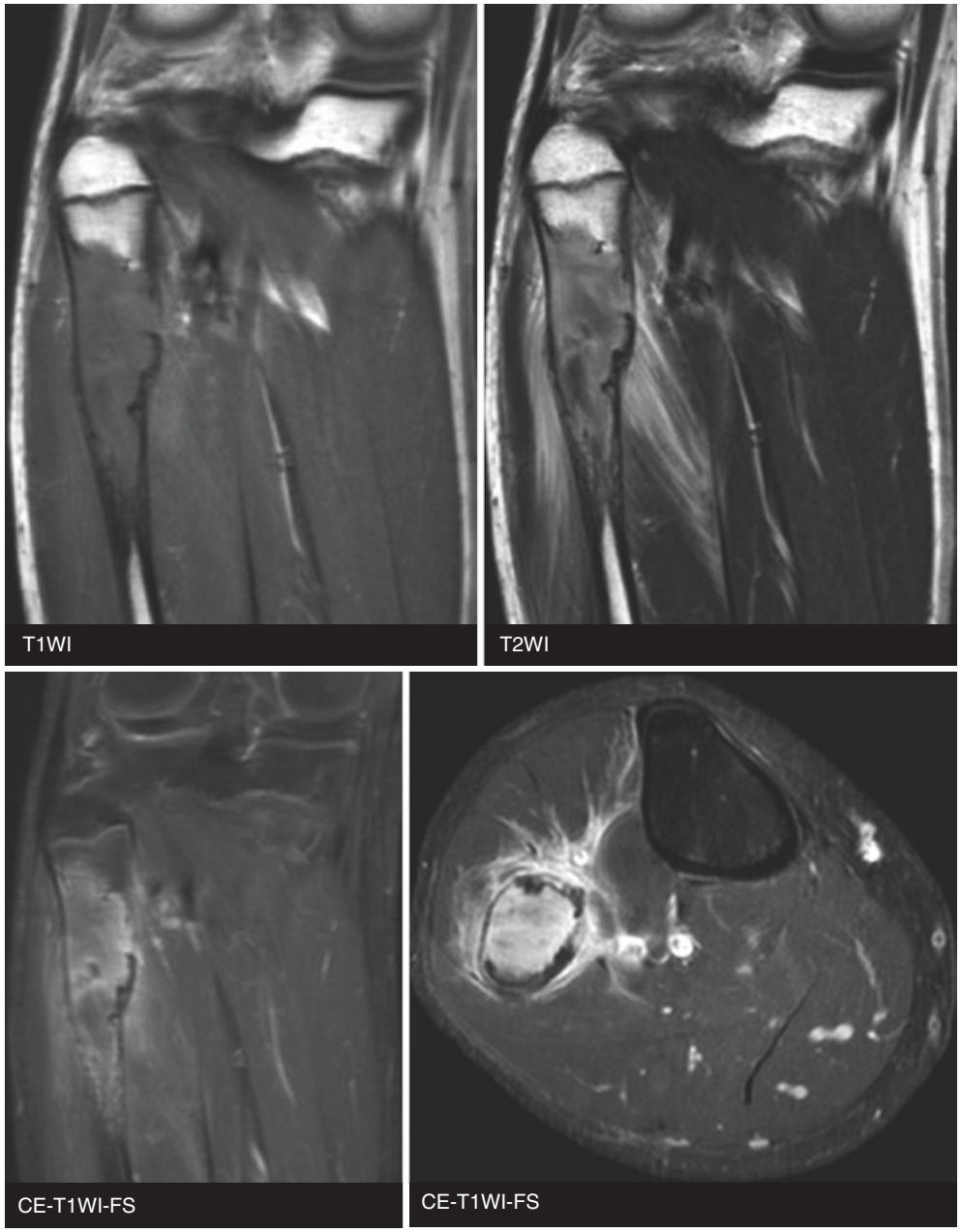

Fig. 12.11 (continued)

1. List the differential diagnoses on radiograph.
2. What are the radiographic findings that suggest aggressive tumor in this patient?
3. What is the likely diagnosis?
4. What radiographic finding can help to distinguish low-grade central osteosarcoma from conventional osteosarcoma?

Case 12

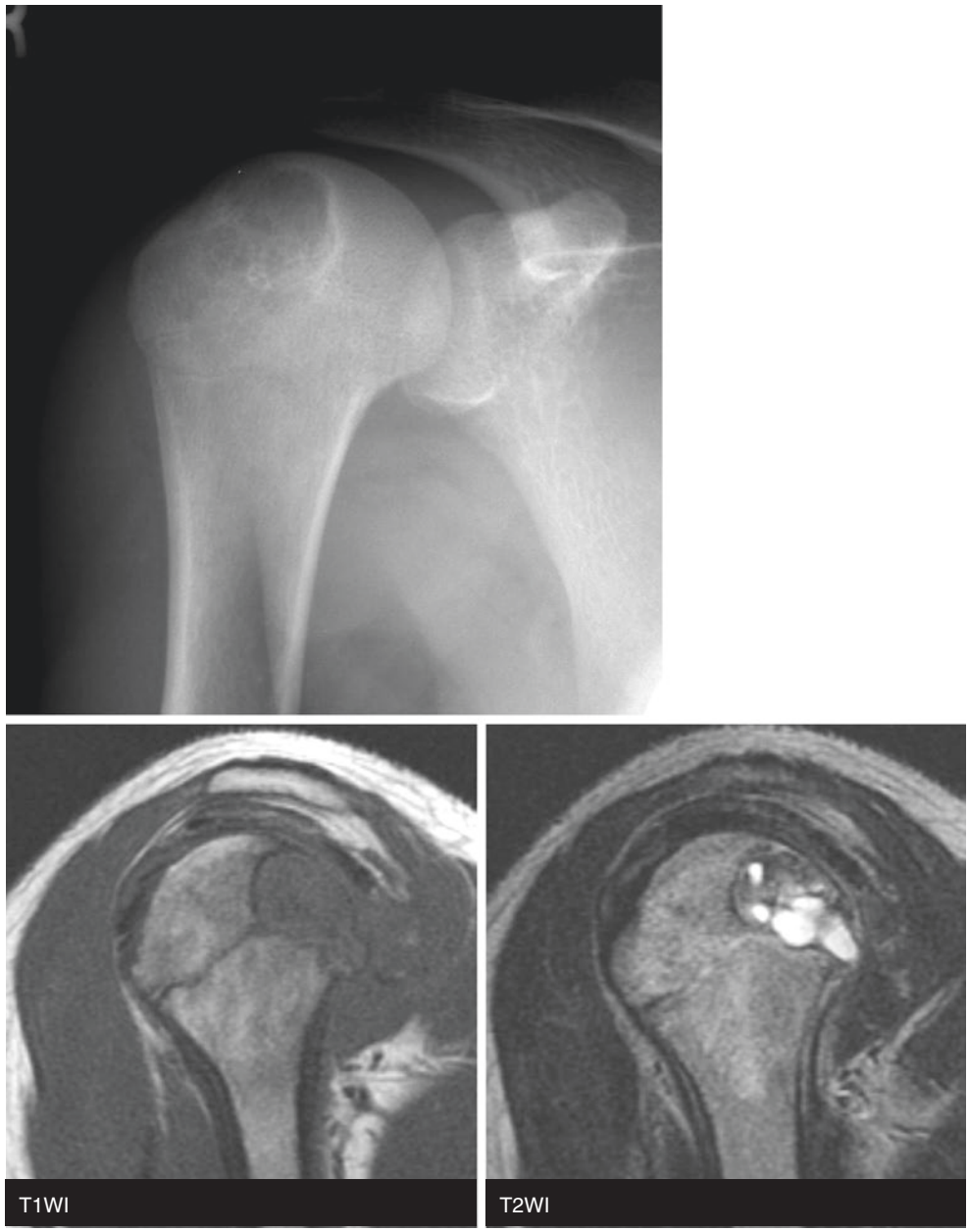

Fig. 12.12

1. List the differential diagnoses of this lesion.
2. What is the most likely diagnosis?
3. What is a characteristic observation on MR imaging?
4. Where are the preferred sites of this lesion in the feet?

Case 13

Fig. 12.13

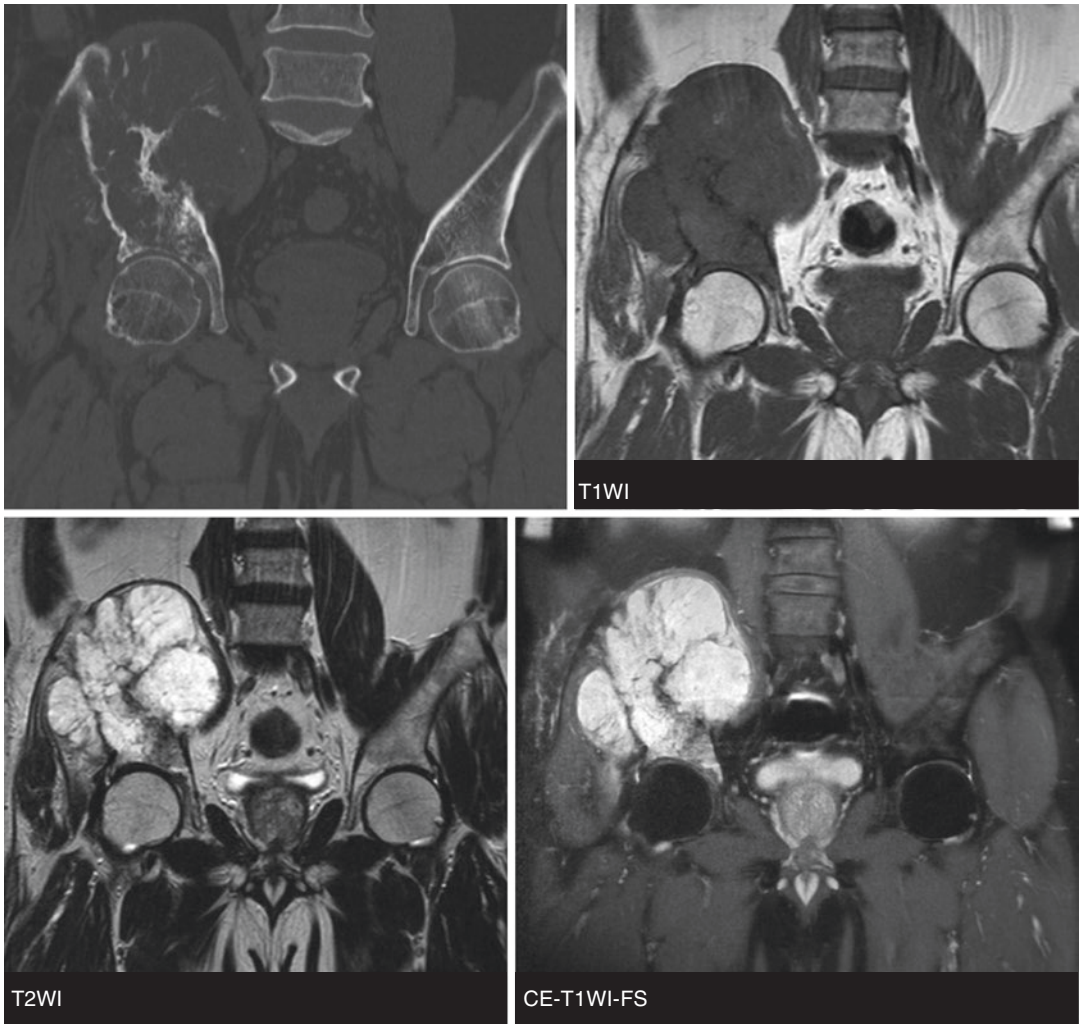

Fig. 12.13 (continued)

1. What observation did you make on CT?
2. What observation did you make on MR images?
3. What is the most likely diagnosis?
4. What radiographic findings in this condition would suggest high-grade lesion in histology?

Case 14

Fig. 12.14

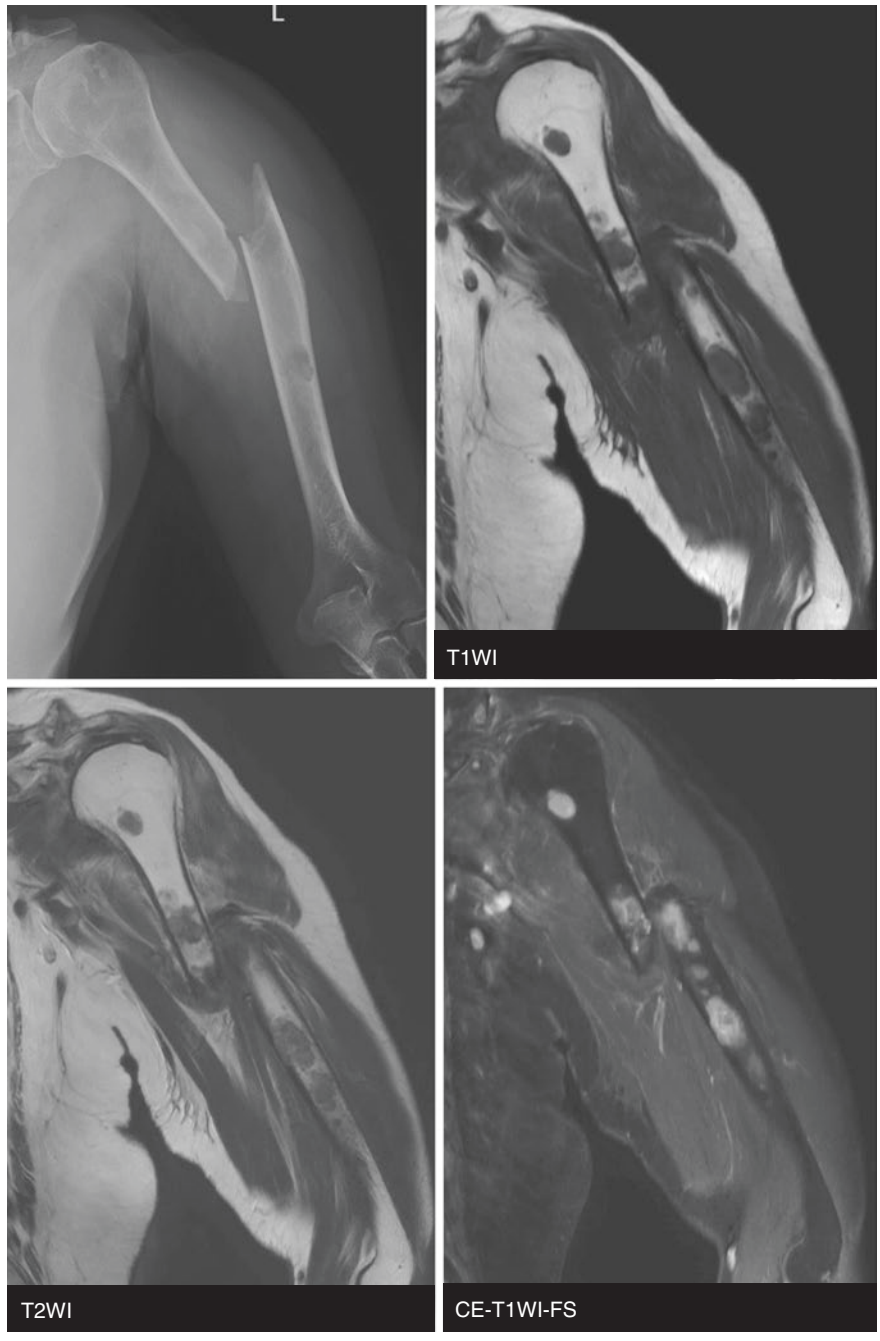

1. What is the likely diagnosis?
2. List the skeletal locations where multiple myeloma preferentially involves.
3. Explain the reason above.
4. Can multiple myeloma and plasmacytoma be sclerotic?
5. What does POEMS stand for?

Case 15

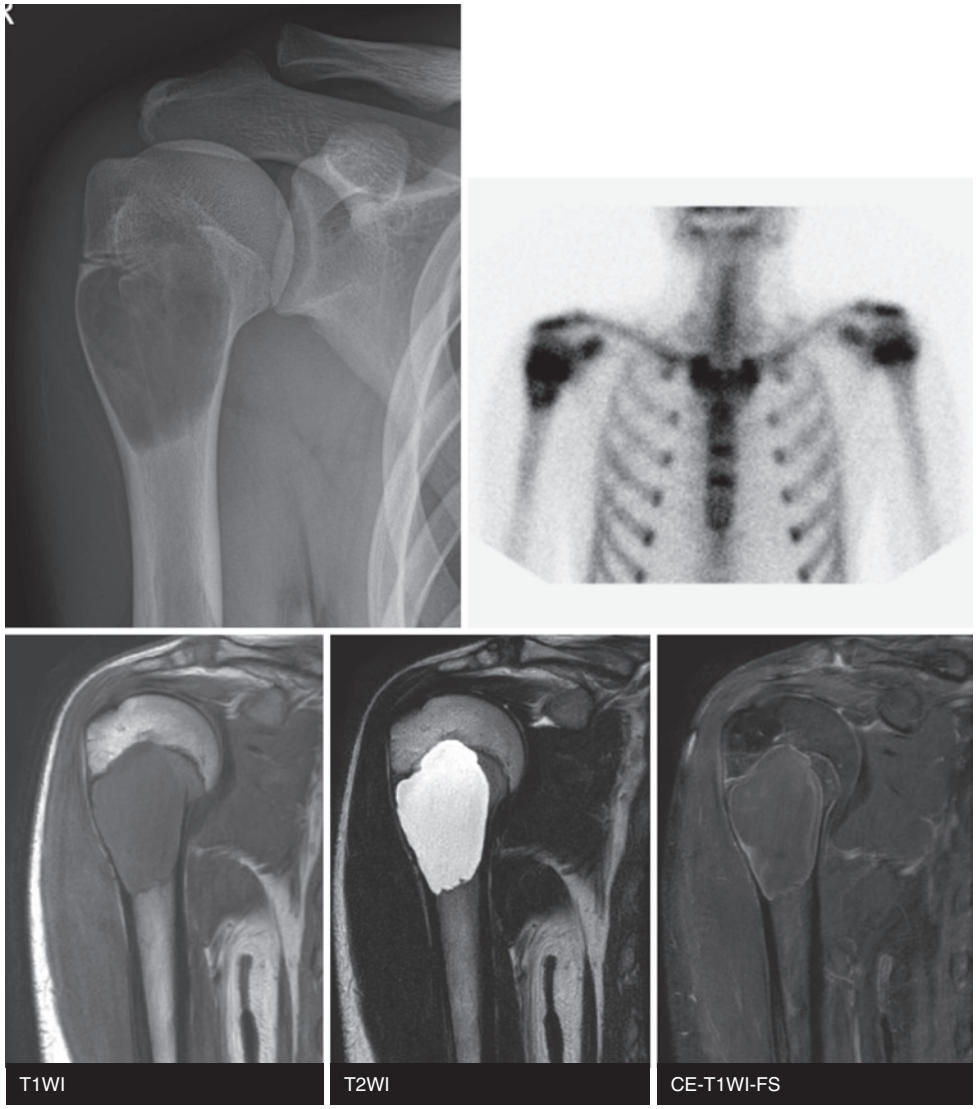

Fig. 12.15

1. What is the likely diagnosis?
2. Where is it most common?
3. What is a "fallen fragment sign"?
4. Could the fallen fragment sign be seen in fibrous dysplasia?
5. List a short differential diagnosis for a well-defined lucent lesion in the anterior aspect of the body of the calcaneus.

Case 16

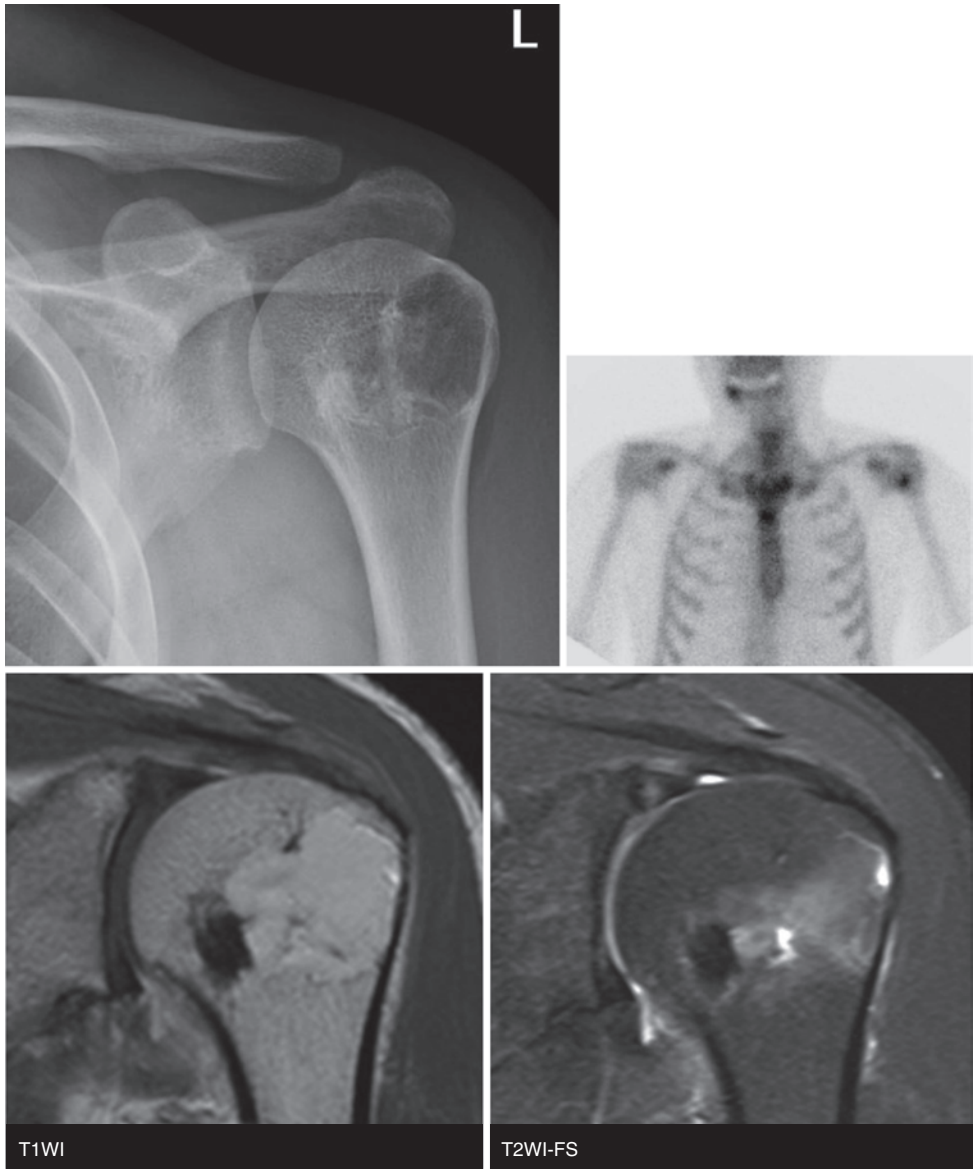

Fig. 12.16

1. What observation did you make on radiograph?
2. What observation did you make on MR images?
3. What is the pathogenesis of the associated ossification in this condition?
4. What is the likely diagnosis?

Case 17

Fig. 12.17

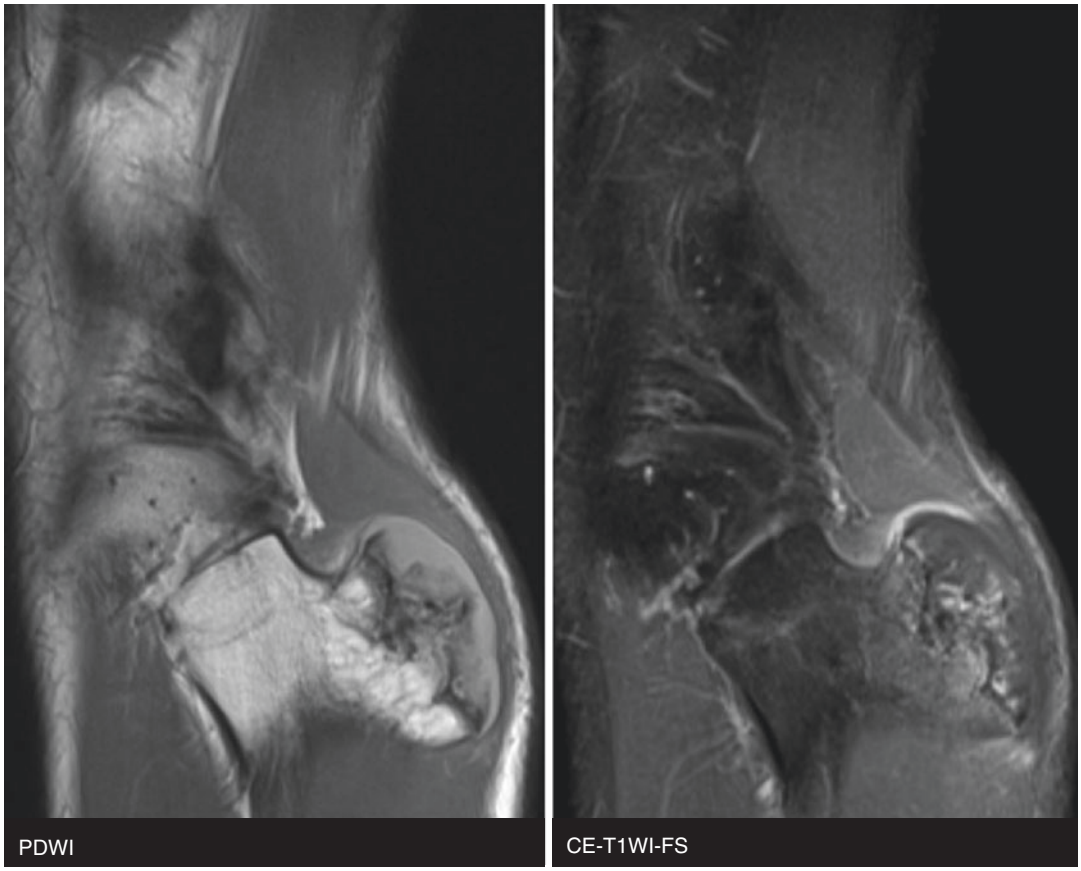

Fig. 12.17 (continued)

1. What are some characteristic findings of this lesion?
2. List the differential diagnoses.
3. What is the most likely diagnosis?
4. When does this lesion stop growing?

Case 18

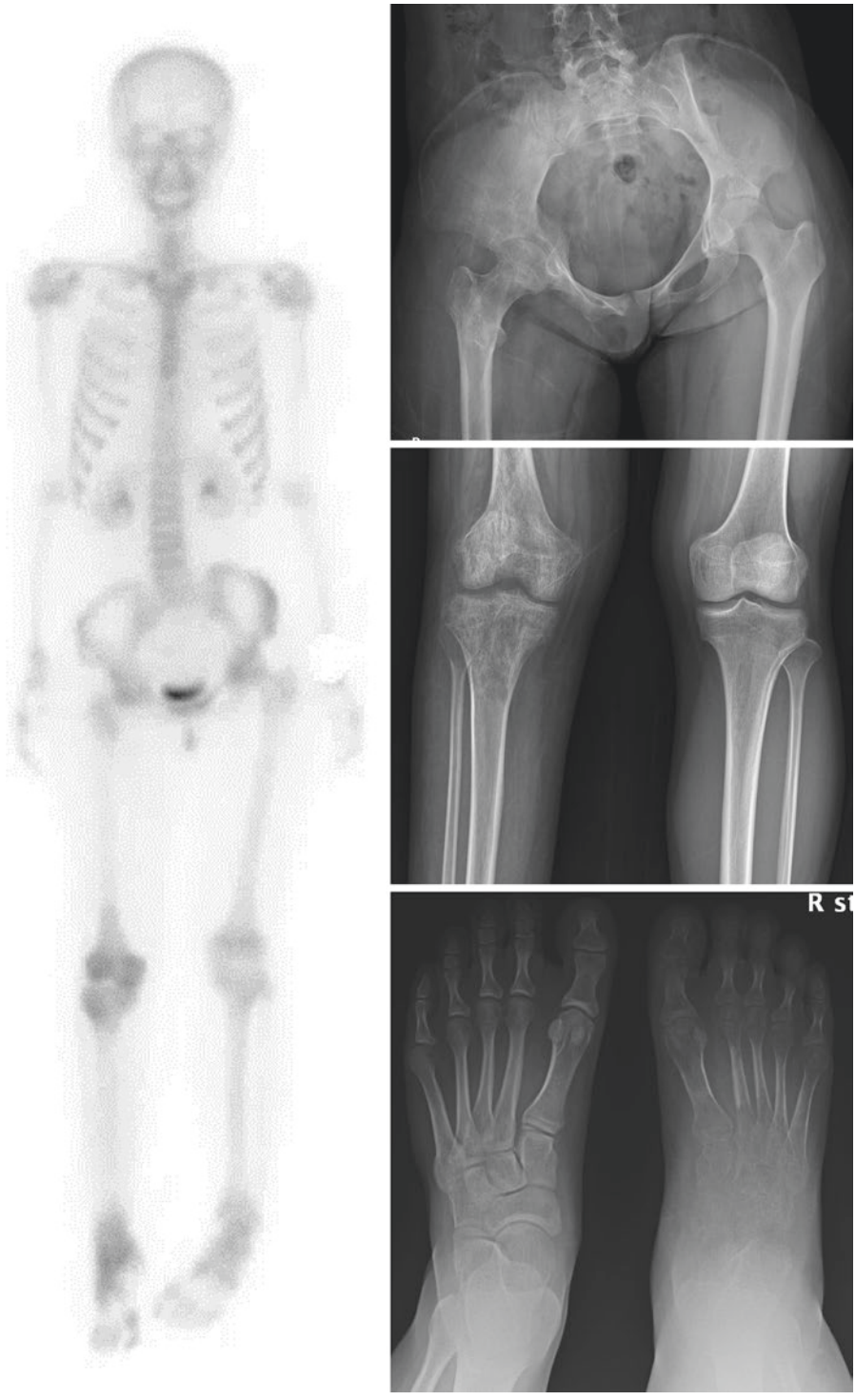

Fig. 12.18

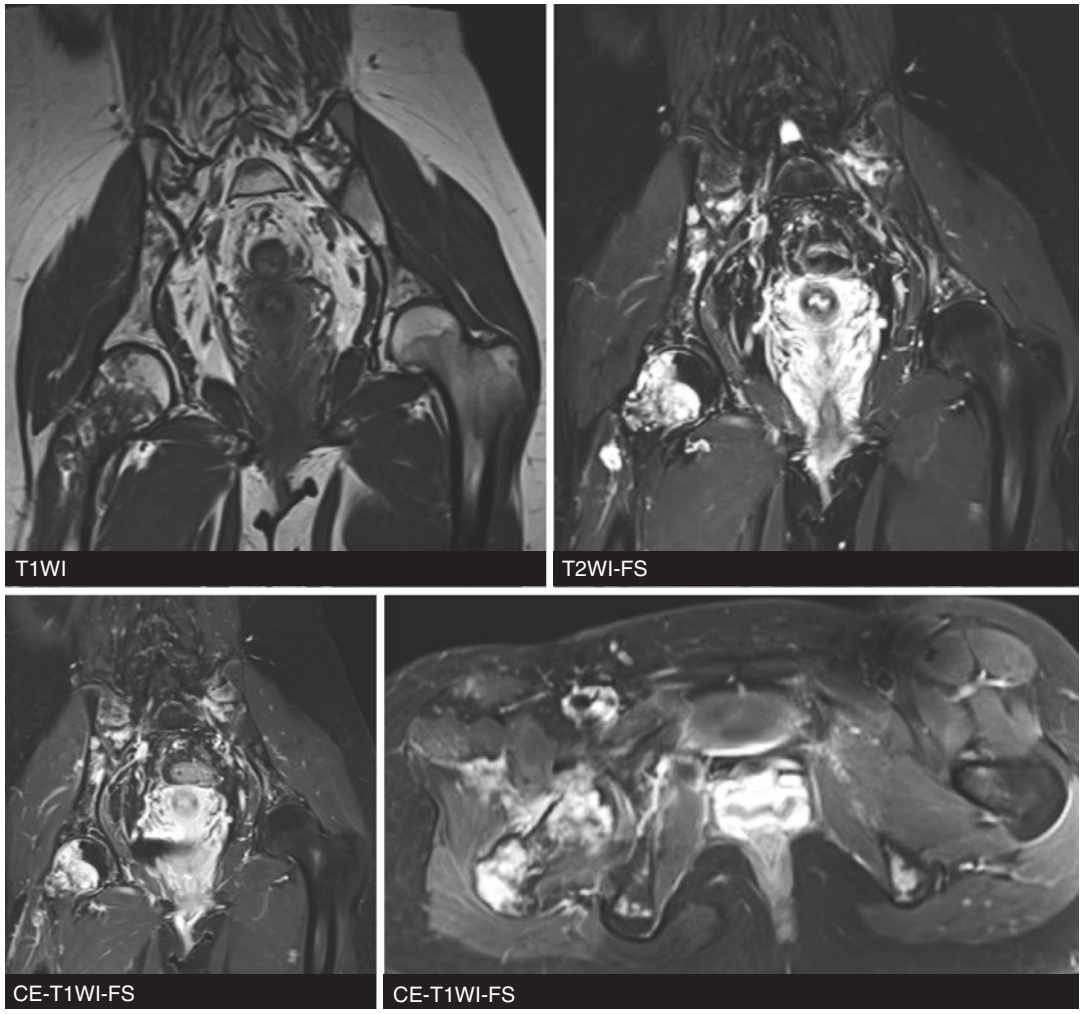

Fig. 12.18 (continued)

1. What observations did you make on radiographs?
2. What observations did you make on MR images?
3. List the differential diagnoses.
4. What is the likely diagnosis?

Case 19

Fig. 12.19

Fig. 12.19 (continued)

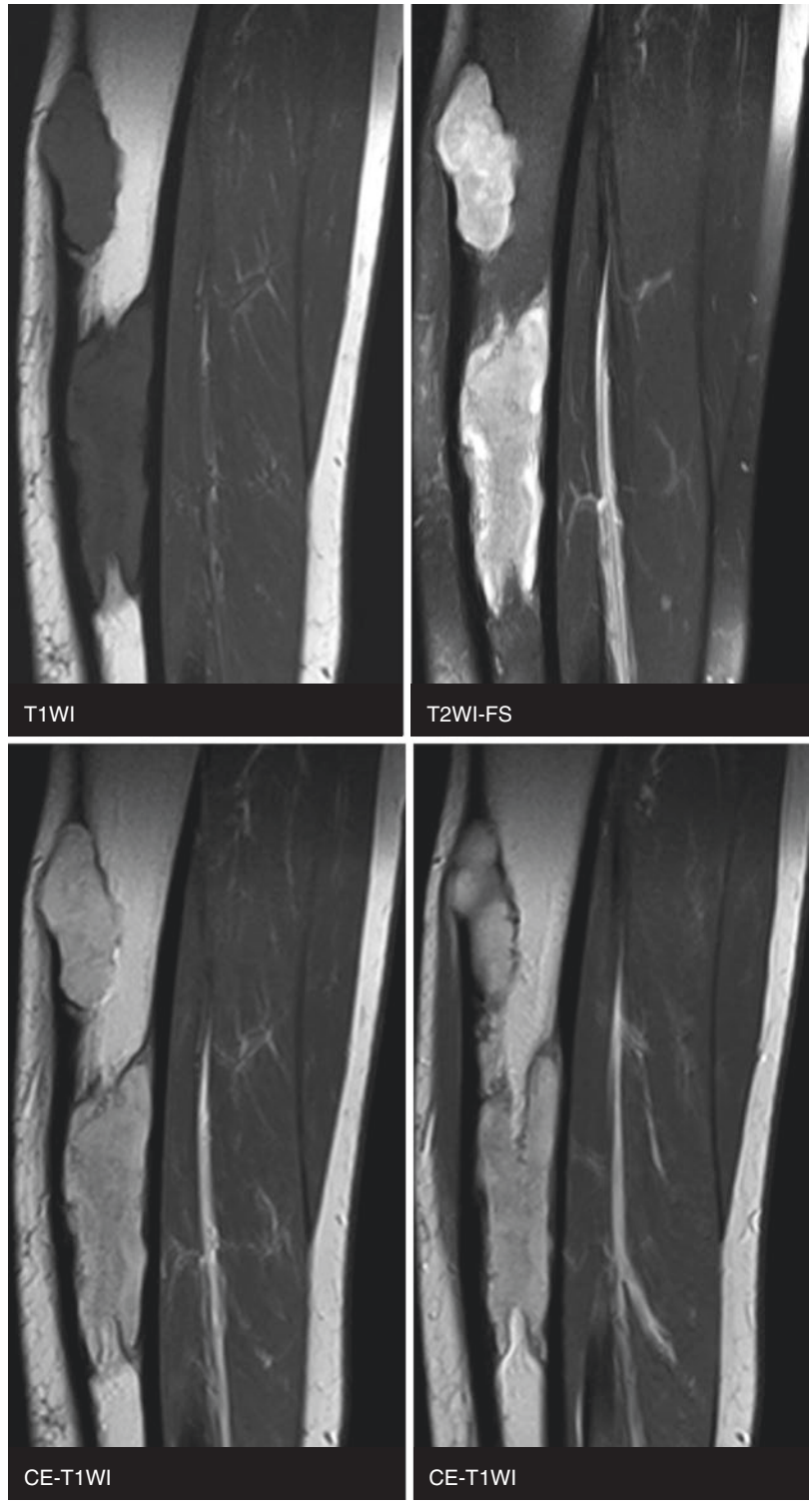

1. What are the differential diagnoses?
2. What is the most likely diagnosis?
3. Where is it most common?
4. What is the distinguishing feature between this condition and fibrous dysplasia in terms of location within a bone?

Case 20

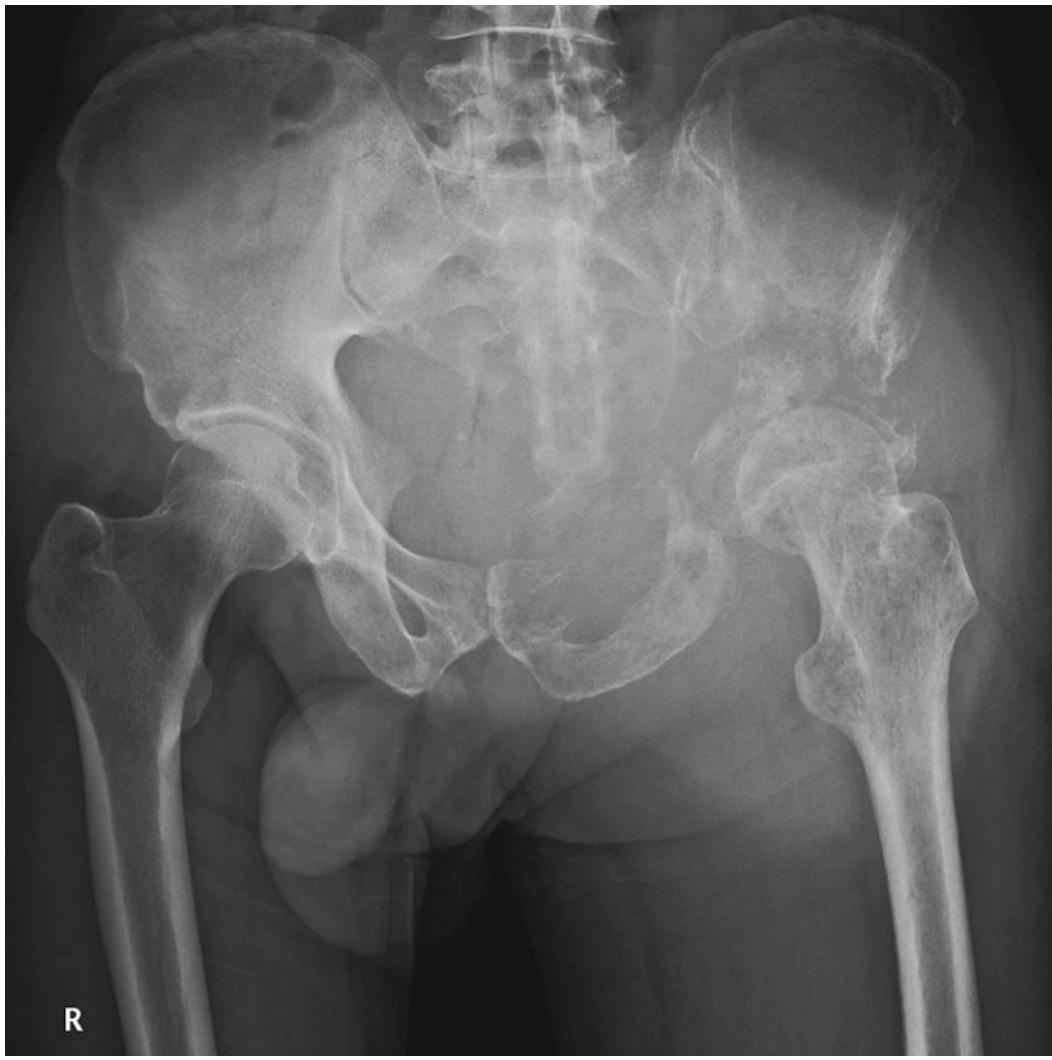

Fig. 12.20

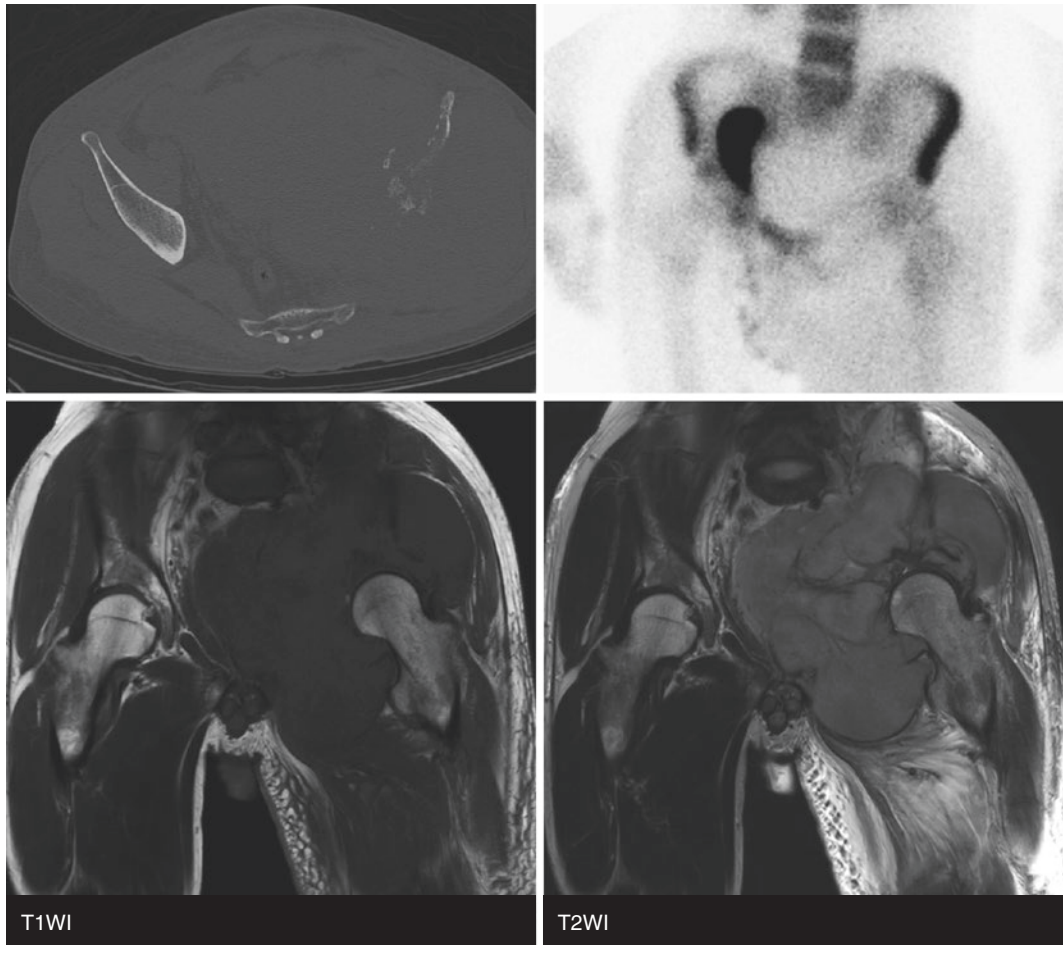

Fig. 12.20 (continued)

1. What is the characteristic appearance of this lesion on CT?
2. List the conditions that may produce radiographic image of sequestrum.
3. What is the signal intensity characteristic of this lesion on T2-weighted images?
4. What is the likely diagnosis?
5. Where are the typical locations of these lesions?
6. What is the definition of the primary lymphoma of the bone?

Case 21

Fig. 12.21

1. What is the most likely diagnosis?
2. Can this condition involve the soft tissues?
3. What is a radiographic hallmark of this condition?
4. Where is it most common?
5. Where does the deposition of the bone begin?

Case 22

Fig. 12.22

1. What observation did you make on radiographs?
2. Did you observe matrix calcification?
3. What is your differential diagnosis?
4. What is the likely diagnosis?
5. Is calcification common in chondromyxoid fibroma?

Case 23

Fig. 12.23

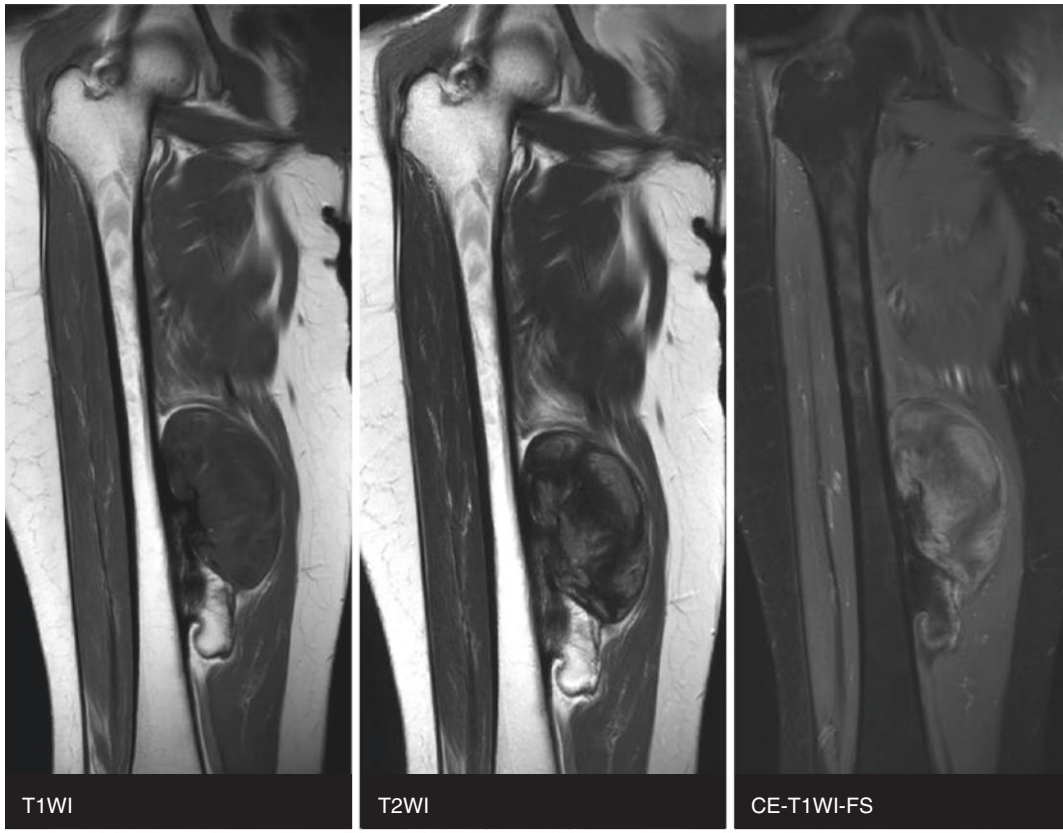

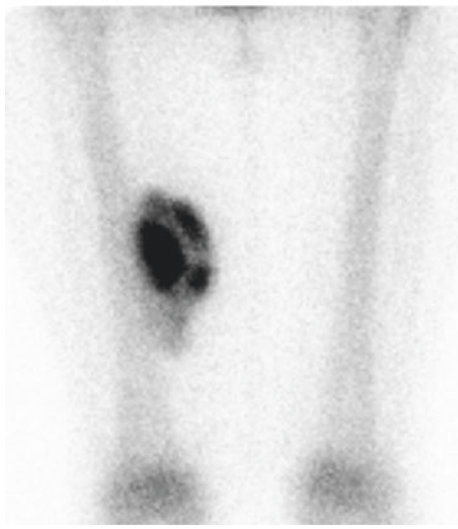

Fig. 12.23 (continued)

1. What observation did you make on radiographs?
2. What are the characteristic observations on MR images?
3. List the differential diagnoses.
4. What is the likely diagnosis?
5. What are the surface subtypes of the osteosarcoma?

Case 24

Fig. 12.24

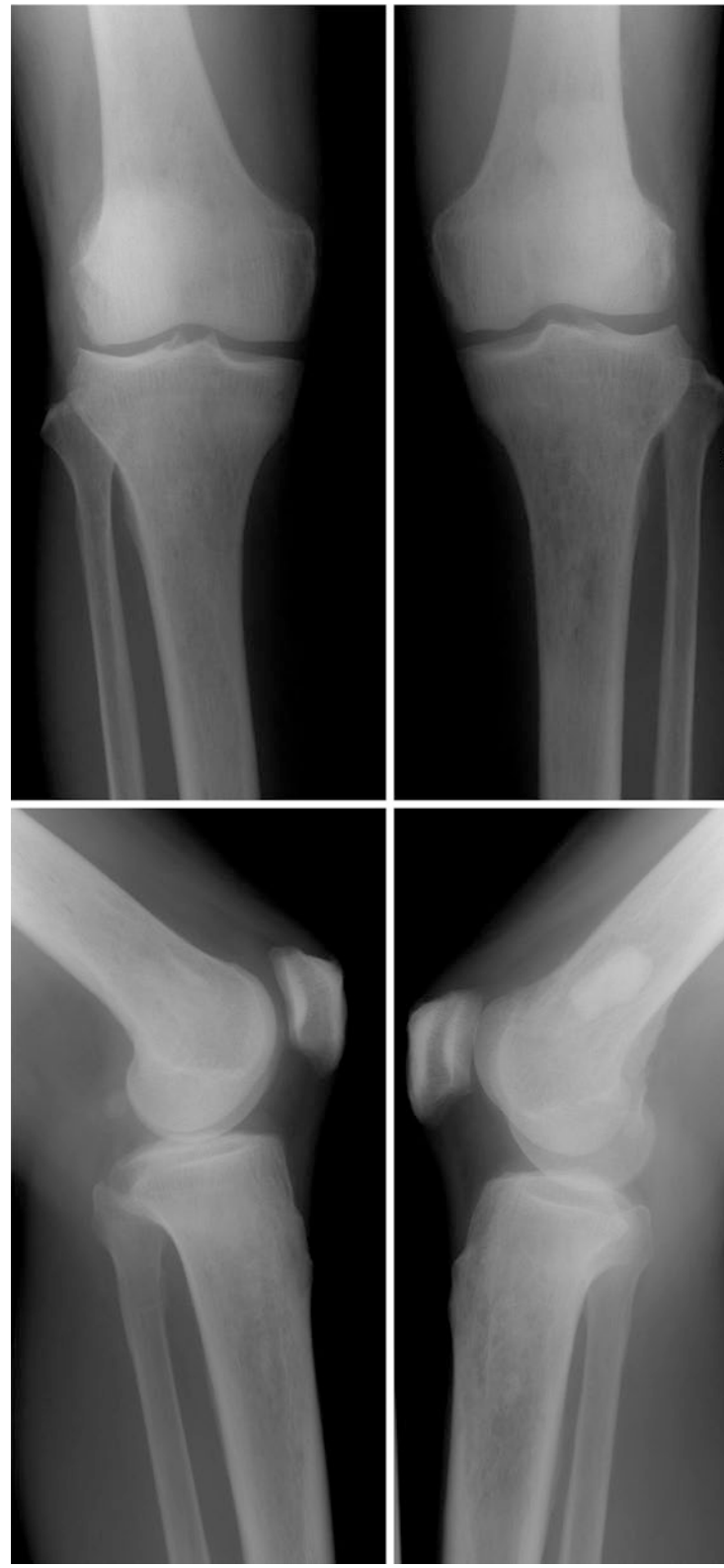

Fig. 12.24 (continued)

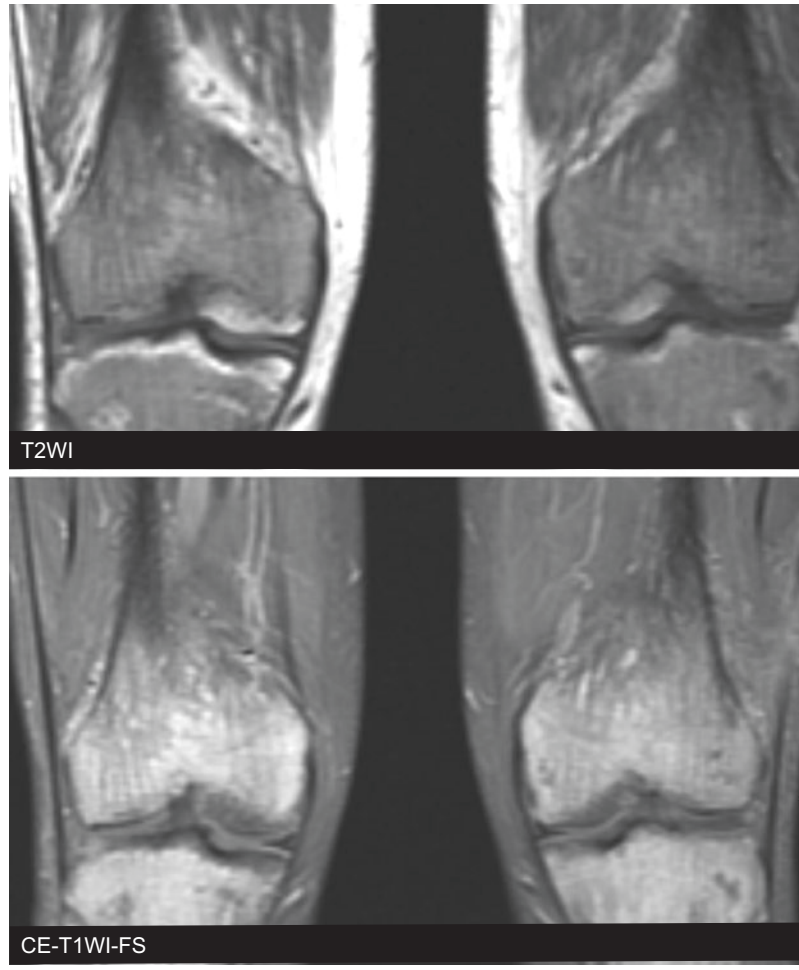

1. What observation did you make on radiographs?
2. What are the characteristic observations on MR images?
3. What is the likely diagnosis?
4. Where are the preferred sites of this lesion?
5. Does this disorder involve epiphysis?
6. What other clinical and extraosseous manifestations may occur in these patients?

Case 25

Fig. 12.25

1. What is the likely diagnosis?
2. Where is the most common location for a subungual exostosis?
3. Why does it occur in the dorsum of the phalanx and not on the volar side?
4. What is the etiology of this lesion?
5. Does this lesion show corticomedullary continuity?

Case 26

Fig. 12.26

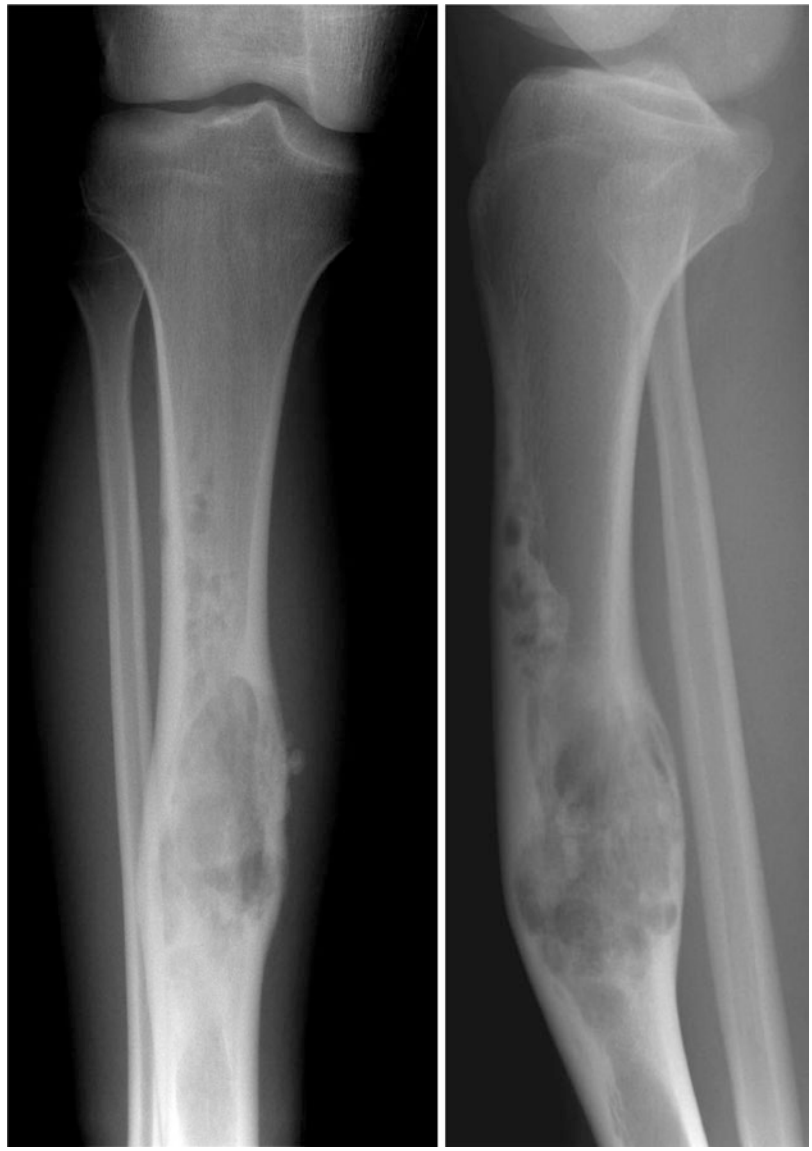

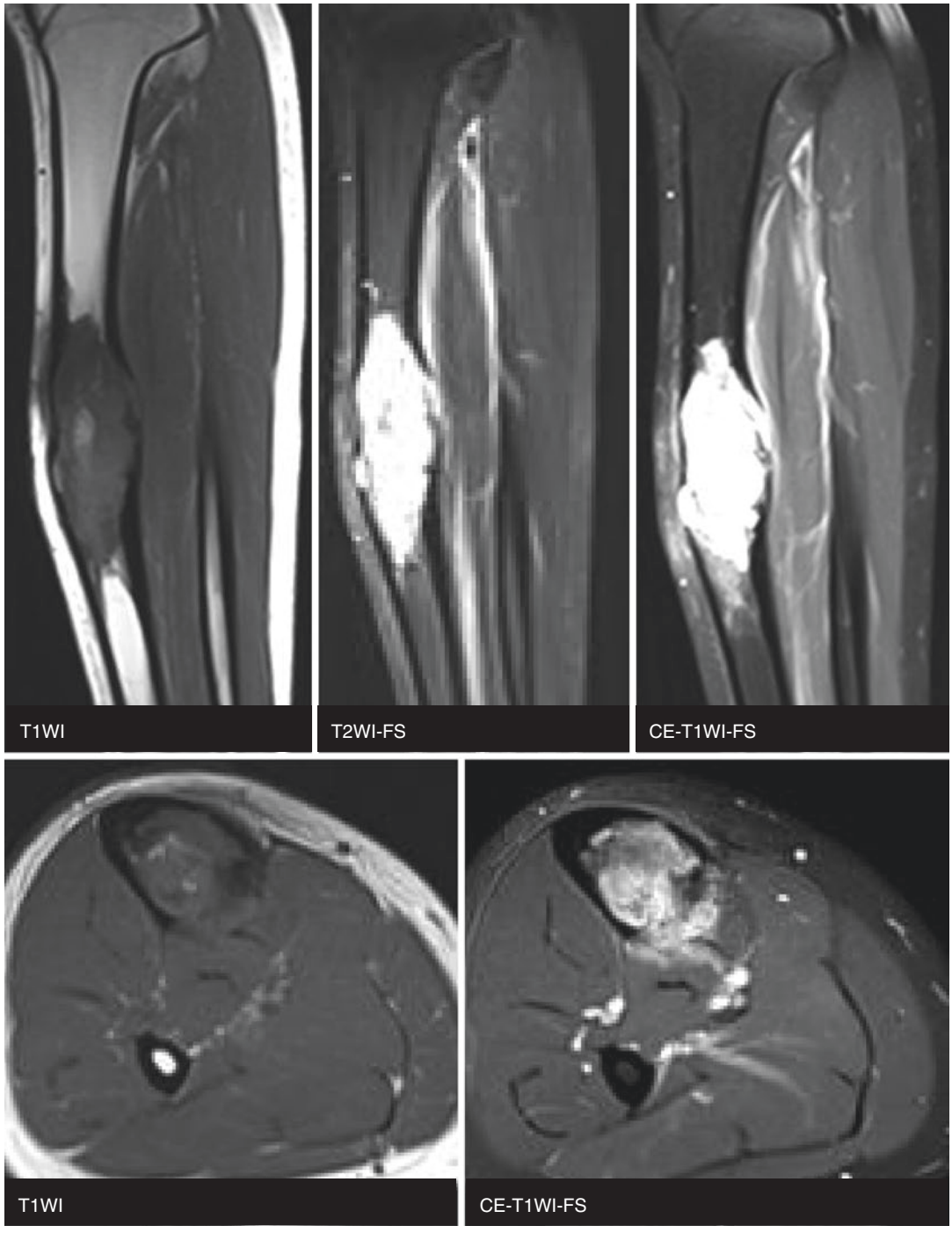

Fig. 12.26 (continued)

1. What observation did you make on radiographs?
2. What observation did you make on MR images?
3. What is your differential diagnosis?
4. What is the most likely diagnosis?
5. In which bone do most adamantinomas occur?

Case 27

Fig. 12.27

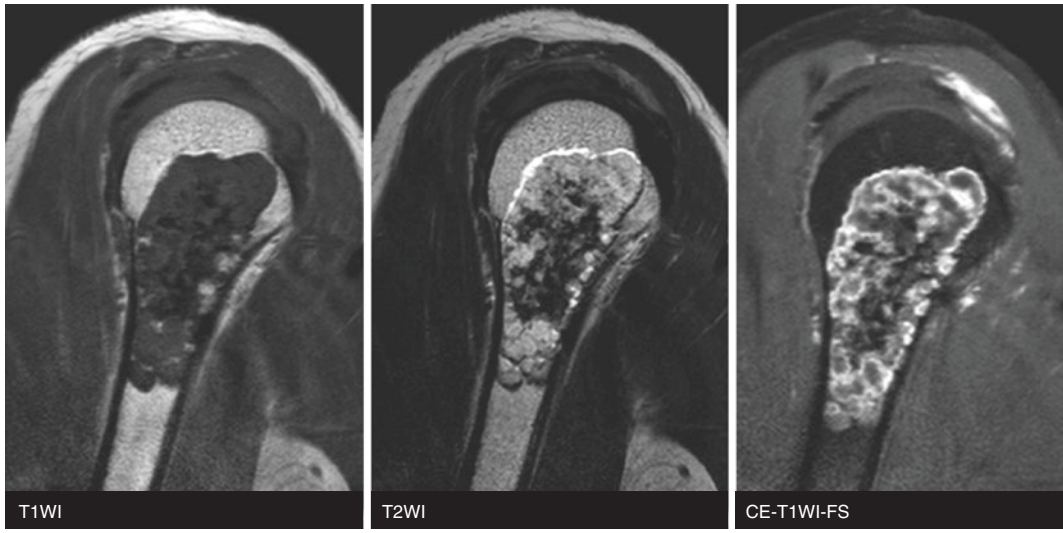

Fig. 12.27 (continued)

1. What observation enabled you to narrow your differential diagnosis?
2. What observation did you make on MR images?
3. What is the bone destruction pattern in this patient?
4. What is your differential diagnosis?
5. What is the most likely diagnosis?

Case 28

Fig. 12.28

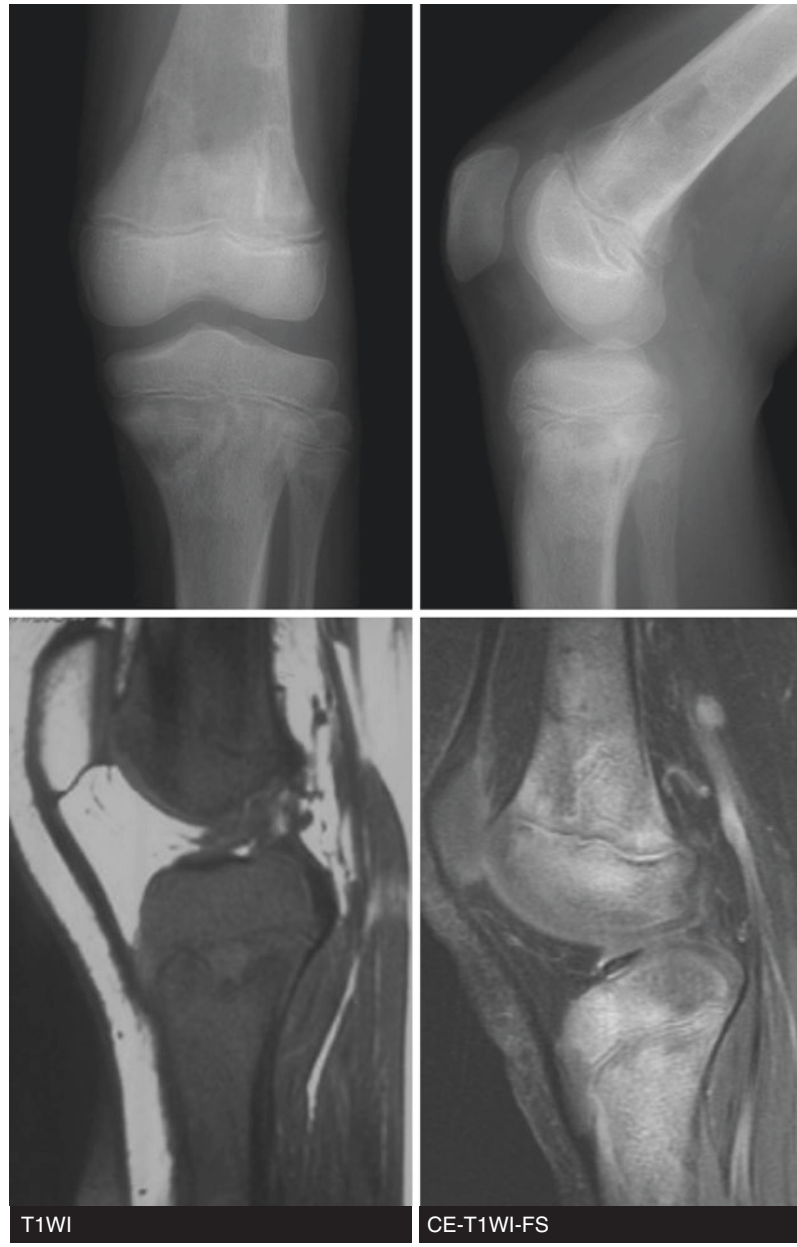

1. What observation did you make on radiographs?
2. What observation did you make on MR images?
3. What is the likely diagnosis?
4. What does the osteolytic lesion in patients with leukemia represent?

Case 29

Fig. 12.29

Fig. 12.29 (continued)

1. What observation did you make on radiographs?
2. What does the differential diagnosis include?
3. Did you observe a low signal intensity margin on MR images, representing either osseous sclerosis or a pseudocapsule, which is frequently noticed in a giant cell tumor?
4. Did you observe increased radiotracer uptake along the periphery of the lesion with central photopenia, which is typical appearance of giant cell tumor on bone scan?
5. What is the most likely diagnosis?

Case 30

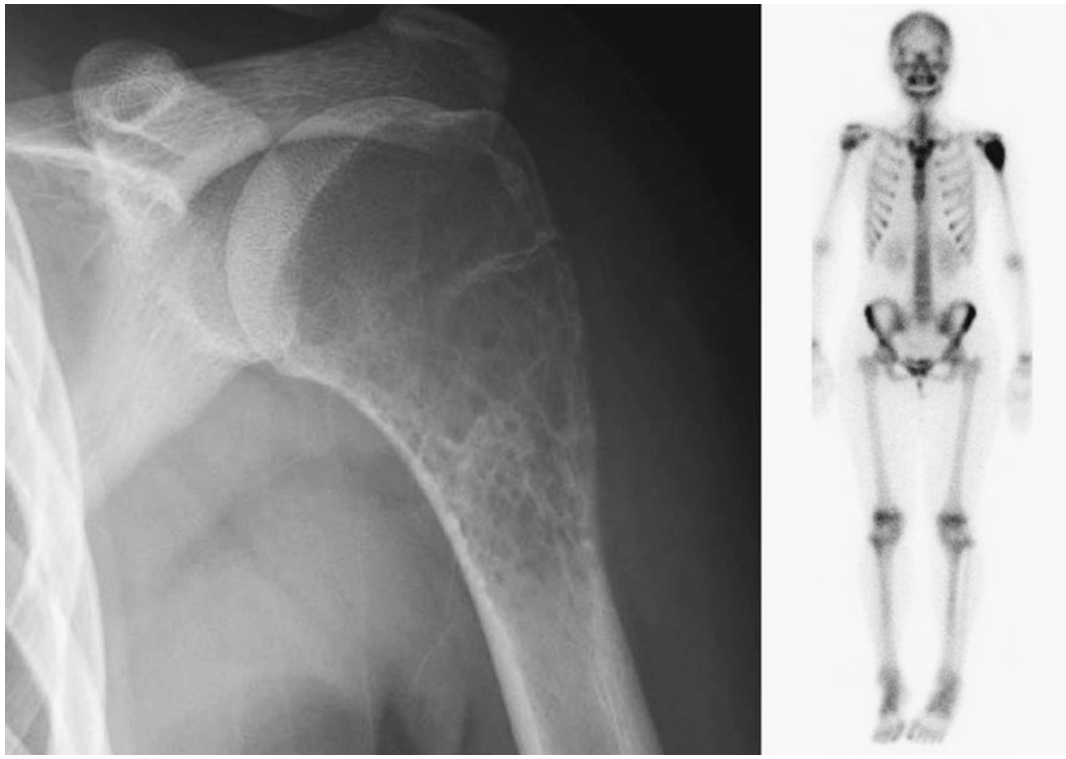

Fig. 12.30

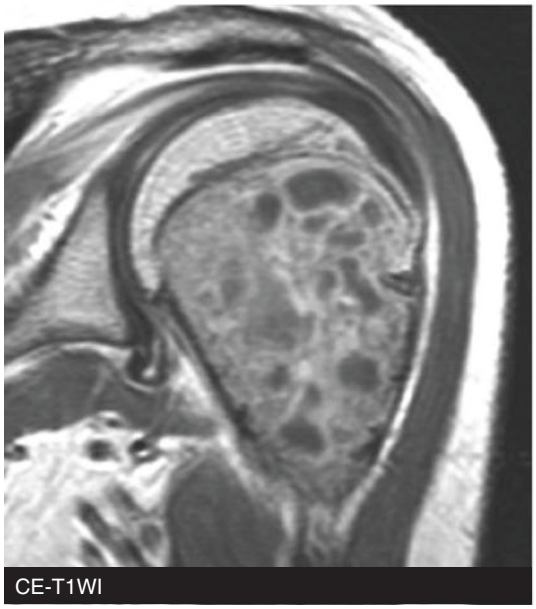

Fig. 12.30 (continued)

1. What observation did you make on radiographs?
2. What observation did you make on MR images?
3. List your differential diagnoses.
4. What is the most likely diagnosis?

12.1 Answers

Case 1

1. Osteoid osteoma, Brodie abscess, osteoblastoma
2. Osteoid osteoma
3. Radiofrequency ablation
4. Radiofrequency ablation
5. No incision scar, accurate targeting of the lesion, shorter hospital stay, and shorter recovery time
6. Location of the lesion in the hand or spine, cellulitis, pregnancy, sepsis, and coagulopathy
7. Skin burn with thermal necrosis, nerve injury, bleeding, and infection at the skin entry site

Case 2

1. Fibrous dysplasia
2. McCune-Albright syndrome consists of polyostotic fibrous dysplasia, café-au-lait skin pigmentation, and precocious puberty
3. A fibrous or fibro-osseous matrix is derived from the conversion of fibroblasts to osteoblasts, leading to mineralization of a fibrous lesion. The resultant bone is loosely organized, as it intercalates with the randomly distributed collagen fibers comprising the lesion. On radiographs, the matrix appears homogeneously hazy, described as ground glass, similar to opaque glass
4. Mazabraud syndrome
5. Fibrous dysplasia

Case 3

1. Well-defined slightly expansile osteolytic lesion in small bone
2. Enchondroma
3. Yes, there may not be a sufficient amount of mineralization to be detected on radiographs
4. Enchondroma

Case 4

1. Langerhans' cell histiocytosis, infection
2. Langerhans' cell histiocytosis
3. Skull, pelvis, femur, and spine
4. This condition almost always occurs before 30 years of age, and the most affected patients are under 20
5. Chondroblastoma, osteoid osteoma, Langerhans' cell histiocytosis, stress fracture

Case 5

1. Giant cell tumor
2. Giant cell tumor, enchondroma, fibrous dysplasia, and parosteal osteosarcoma
3. Heterogeneous low signal intensity in a whorled or uniform pattern from hemosiderin and collagen deposition, and high cellularity
4. Bone island, nonossifying fibroma, giant cell tumor, desmoplastic fibroma, and brown tumor

Case 6

1. Fibrous dysplasia, osteoblastoma, giant cell tumor, metastasis, myeloma, aneurysmal bone cyst, chondroblastoma, chondromyxoid fibroma, hyperparathyroidism, infection, nonossifying fibroma, enchondroma, Langerhans cell histiocytosis, and simple bone cyst
2. Nonossifying fibroma
3. The outer margin of the sclerotic rim seems sharper than the inner margin.
4. No. Nonossifying fibroma should not be the primary consideration in a patient >40 years of age, because nonossifying fibromas heal in and typically disappear before that age
5. Jaffe-Campanacci syndrome

Case 7

1. Calcified osseous mass arising from the cortex
2. Bizarre parosteal osteochondromatous proliferation, osteochondroma, parosteal osteosarcoma
3. No corticomedullary continuation
4. Bizarre parosteal osteochondromatous proliferation

Case 8

1. Well-defined metaphyseal eccentric expansive surface lesion surrounded by a shell of periosteal new bone

2. Surface cystic lesion with intraosseous and extraosseous expansion, peripheral hypointense rim, and internal fluid–fluid level
3. Aneurysmal bone cyst
4. Aneurysmal cystic changes superimposed on preexisting bone lesions
5. Blood-filled spaces with thin septae and usually no or minimal solid component

Case 9

1. A well-defined unilocular, osteolytic lesion with a sclerotic margin
2. Epidermal inclusion cyst, glomus tumor, enchondroma, metastasis
3. Epidermal inclusion cyst
4. Distal phalanx of the left middle finger
5. Most glomus tumors show high signal intensity on T2-weighted images and avid contrast enhancement. Epidermal inclusion cysts demonstrate high signal intensity background with variable low signal intensity components on T2-weighted images and peripheral rim enhancement.

Case 10

1. Circumferential endosteal and periosteal new bone formation along the shafts of long bones in the lower extremity
2. Ribbing disease (hereditary multiple diaphyseal sclerosis)
3. No, the epiphyses are spared
4. Yes, Ribbing disease is either unilateral or asymmetric and asynchronously bilateral
5. Stress fracture, osteoid osteoma, osteosarcoma, and osteomyelitis

Case 11

1. Low-grade central osteosarcoma, fibrous dysplasia, desmoplastic fibroma
2. Bone lysis, focally indistinct margin, cortical destruction
3. Low-grade central osteosarcoma
4. In contrast to conventional osteosarcoma, periosteal reaction is minimal or absent, the diaphysis may be extensively involved, and a coarse trabeculated pattern of ossification may be seen in low-grade central osteosarcoma

Case 12

1. Chondroblastoma, giant cell tumor, intraosseous ganglion, bone abscess, chondromyxoid fibroma
2. Chondroblastoma
3. Peritumoral edema, secondary to the hypervascularity
4. Talus and calcaneus

Case 13

1. Expansive osseous lesion, cortical destruction, and soft tissue mass
2. Lobulated pattern of T1 hypointensity and T2 hyperintensity with strong enhancement
3. Chondrosarcoma
4. Moth-eaten tumor with ill-defined margin, cortical destruction, and soft tissue mass

Case 14

1. Multiple myeloma
2. Skull, spine, scapula, sternum, ribs, pelvis, proximal femora, and proximal humeri
3. Hematopoietically active red marrow is predominantly distributed in the locations detailed above
4. Rarely, they can be sclerotic as in POEMS syndrome
5. Polyneuropathy, organomegaly, endocrinopathy, monoclonal gammopathy, and skin changes

Case 15

1. Simple bone cyst
2. Proximal humerus
3. The fallen fragment sign refers to the presence of osseous fracture fragments that are free to fall into the dependent portion of a fluid-filled cyst, unlike a bone tumor that has a firm tissue consistency
4. No. Fibrous dysplasia has a solid matrix and would not allow fragment migration into the dependent portion within the lesion
5. Simple bone cyst, intraosseous lipoma, and intraosseous ganglion

Case 16

1. A radiolucent lesion with sclerotic rim and adjacent focal region of calcification

2. Expansile osseous lesion of adipose signal intensity with a thin margin and focal region of persistent low signal intensity
3. Calcification in the ischemic fat necrosis, secondary to increased intramedullary pressure produced by enlargement of a lipoma in the enclosed space of the medullary canal, or inherent product of the mesenchymal cells
4. Intraosseous lipoma

Case 17

1. Continuity with the medullary space and typical orientation away from the adjacent joint
2. Osteochondroma, parosteal osteosarcoma, periosteal chondroma, chondrosarcoma
3. Osteochondroma
4. With closure of the physis

Case 18

1. Radiolucent foci in the intramedullary or subchondral regions resembling findings seen in patchy osteoporosis, and osseous and soft tissue atrophy
2. Foci of low signal intensity on T1-weighted images and increased signal intensity on T2-weighted images with enhancement after intravenous contrast administration
3. Skeletal angioma, angiosarcoma, essential osteolysis, hereditary osteolysis, osteomyelitis, and metastasis.
4. Gorham disease

Case 19

1. Osteofibrous dysplasia, adamantinoma, fibrous dysplasia
2. Osteofibrous dysplasia
3. Anterior cortex of the proximal or midshaft of tibia
4. Fibrous dysplasia is usually intramedullary, whereas osteofibrous dysplasia is intracortical.

Case 20

1. Sequestrum is radiologically defined as a piece of calcified tissue within a lucent lesion, completely separated from the surrounding bone
2. Osteomyelitis, skeletal tuberculosis, osteoid osteoma, osteoblastoma, chondroblastoma, Langerhans cell histiocytosis, primary lymphoma of bone, fibrosarcoma, and metastasis
3. Low or mildly increased signal intensity
4. Lymphoma
5. Diaphyses and metaphyses of long bones, and flat bones of axial skeleton
6. Lymphoma presenting within a bone without disease elsewhere for at least 6 months

Case 21

1. Melorheostosis
2. Yes, in more severe cases
3. Flowing candle wax (wax dripping down one side of a candle)
4. The lower extremity, especially the proximal femur
5. At the proximal end of the bone, and it proceeds distally

Case 22

1. Central expansile osteolytic lesion with coarse trabeculation, focal osseous defect, and scalloped medullary border
2. No, there is no evident matrix calcification
3. Chondromyxoid fibroma, enchondroma, and aneurysmal bone cyst
4. Chondromyxoid fibroma
5. No. Calcification is infrequent in the chondromyxoid fibroma, unlike chondroblastoma and other cartilaginous lesions

Case 23

1. Lobulated and exophytic juxtacortical ossific mass
2. Predominantly hypointense mass on T1-weighted and T2-weighted images
3. Parosteal osteosarcoma, appendicular osteoma, myositis ossificans, osteochondroma, periostitis ossificans
4. Parosteal osteosarcoma
5. Periosteal osteosarcoma, parosteal osteosarcoma, high-grade surface osteosarcoma

Case 24

1. Bilateral and symmetric osteosclerosis of the diaphysis of the long bones
2. Replacement of the normal fatty bone marrow by heterogeneous signal intensity with preserved subchondral fatty marrow

3. Erdheim-Chester disease
   Appendicular skeleton, with the lower extremities being involved more often and more severely than the upper extremities
4. No, the epiphyses are spared
5. Diabetes insipidus, bilateral exophthalmos, chronic renal failure, hydronephrosis, pulmonary fibrosis, and heart failure

Case 25

1. Subungual exostosis
2. Dorsal or dorsomedial aspect of the distal phalanx of the great toe
3. This location may be related to the loose periosteum in the dorsum, as opposed to the tightly adherent periosteum in the volar aspect of the toe and finger pads
4. The etiology is uncertain, although trauma, irritation, inflammation, and infection have been proposed
5. No. Corticomedullary continuity is typical finding of osteochondroma, which represents a different entity

Case 26

1. Well-defined intracortical osteolytic lesion at the anterior tibial cortex, with medullary extension
2. Intracortical lesion with medullary extension, which is hypointense on T1-weighted image and hyperintense on fluid-sensitive sequences, with moderate contrast enhancement
3. Adamantinoma, osteofibrous dysplasia, and fibrous dysplasia
4. Adamantinoma
5. Tibia

Case 27

1. Rings-and-arcs, punctate, flocculent foci calcification, representing chondroid matrix
2. Lobular pattern with low signal intensity on T1-weighted images and high signal intensity on T2-weighted images, and ring-and-arcs pattern of enhancement
3. Geographical lesion with ill-defined border
4. Low-grade chondrosarcoma, enchondroma
5. Low-grade chondrosarcoma

Case 28

1. Multiple osteolytic foci in the metaphysis of the femur and tibia with cortical thinning and periosteal reaction
2. Diffuse infiltrative low signal intensity on T1-weighted images and diffuse contrast enhancement
3. Leukemia
4. Leukemic infiltration, local hemorrhage, osteonecrosis secondary to vascular compromise

Case 29

1. Subtle radiolucent lesion with ill-defined margin
2. Metastasis, giant cell tumor, plasmacytoma
3. No, there is no low signal intensity margin in this patient
4. No, there is no central photopenia
5. Metastasis

Case 30

1. Geographical expansile osteolytic lesion without a sclerotic rim or matrix calcification, with areas of soap-bubble appearance, arising from the metaphysis of the proximal humerus, extending toward epiphysis and apophyses
2. Intramedullary mass with intermediate signal intensity on T1-weighted image, heterogeneous intermediate-to-high signal intensity with fluid–fluid levels on T2-weighted image, and rim and nodular enhancement after contrast administration
3. Giant cell tumor, aneurysmal bone cyst, and telangiectatic osteosarcoma
4. Giant cell tumor with secondary aneurysmal bone cyst